Pacific Northwest
NATIONAL LABORATORY

PNNL-38530, Rev. 0
DVZ-RPT-118, Rev. 0

200-DV-1 Treatability Testing: Final Results

January 2026

Hilary P Emerson
James E Szecsody
Amanda R Lawter
Shelby M Brooks
Nancy M Escobedo
Andrew E Plymale
Alex Kugler
Mariah Doughman
Suraj Pochampally
Jacqueline R Hager
Charles T Resch
Carolyn I Pearce
Sarah Saslow
Daria Boglaienko
Sabrina Hoyle
Danielle L Saunders
Melissa A Dieguez
Zoe G Vincent
Ean Arnold
Kelly L Rue
Rachel Anguish
Jenna M Schroeder
Minbum Kim
Bryan He
Christopher Bagwell
Katherine A Muller
Nicholas J Reichart
Jacob Morton
Aiden Henson
Ilana Szlamkowicz
Nabajit Lahiri
Steven R Baum
Ian I Leavy
Deanna Auberry
Nikolla P Qafoku
Inci Demirkanli
Rob Mackley

U.S. DEPARTMENT of ENERGY

Prepared for the U.S. Department of Energy
under Contract DE-AC05-76RL01830

DISCLAIMER

PACIFIC NORTHWEST NATIONAL LABORATORY
operated by
BATTELLE
for the
UNITED STATES DEPARTMENT OF ENERGY
under Contract DE-AC05-76RL01830

Printed in the United States of America

Available to DOE and DOE contractors from
the Office of Scientific and Technical Information,
P.O. Box 62, Oak Ridge, TN 37831-0062
www.osti.gov
ph: (865) 576-8401
fax: (865) 576-5728
email: reports@osti.gov

Available to the public from the National Technical Information Service
5301 Shawnee Rd., Alexandria, VA 22312
ph: (800) 553-NTIS (6847)
or (703) 605-6000
email: info@ntis.gov
Online ordering: http://www.ntis.gov

PNNL-38530, Rev. 0
DVZ-RPT-118, Rev. 0

0B200-DV-1 Treatability Testing: Final Results

January 2026

Hilary P Emerson
James E Szecsody
Amanda R Lawter
Shelby M Brooks
Nancy M Escobedo
Andrew E Plymale
Alex Kugler
Mariah Doughman
Suraj Pochampally
Jacqueline R Hager
Charles T Resch
Carolyn I Pearce
Sarah Saslow
Daria Boglaienko
Sabrina Hoyle
Danielle L Saunders
Melissa A Dieguez
Zoe G Vincent
Ean Arnold
Kelly L Rue
Rachel Anguish
Jenna M Schroeder
Minbum Kim
Bryan He
Christopher Bagwell
Katherine A Muller
Nicholas J Reichart
Jacob Morton
Aiden Henson
Ilana Szlamkowicz
Nabajit Lahiri
Steven R Baum
Ian I Leavy
Deanna Auberry
Nikolla P Qafoku
Inci Demirkanli
Rob Mackley

Prepared for
the U.S. Department of Energy
under Contract DE-AC05-76RL01830

Pacific Northwest National Laboratory
Richland, Washington 99354

Executive Summary

A laboratory treatability study has been completed to evaluate site-relevant performance for nine *in situ* technologies that may be used to treat subsurface contamination, focused on the 200-DV-1 Operable Unit (OU) within the Hanford Site's Central Plateau. This report presents the final results from the treatability study. While none of the potential vadose zone technologies are recommended for future feasibility study consideration, all six of the potential technologies for application in saturated zones met performance thresholds for at least one of the potential treatment scenarios (including direct treatment of perched water or formation of a permeable reactive barrier at the water table). For potential direct treatment of perched water (located beneath the B Complex, referred to as the 200-DV-1 OU perched water), particulate-phase chemical reduction and sequestration (sulfur modified iron with polyphosphate) was the top performer with potential for treatment of both technetium-99 (Tc-99) and uranium (U). For treatment with a permeable reactive barrier at the water table (located beneath the BY Cribs), liquid-phase bioreduction and chemical sequestration (molasses with polyphosphate) and liquid-phase chemical reduction and sequestration (calcium polysulfide with polyphosphate) performed well for both Tc-99 and U. Notably, particulate-phase chemical sequestration (bismuth subnitrate) outperformed all other amendments for U for treatment with a permeable reactive barrier at the water table, though it was ineffective for Tc-99.

Technologies were evaluated to support future development of a feasibility study for the 200-DV-1 OU with complex challenges for deep vadose zone remediation. Testing protocols were developed following a technology prescreening effort and are documented in a laboratory treatability study plan[1] (hereinafter referred to as the test plan). The test plan was developed to present a framework and overall guidance for detailed laboratory evaluations of each technology, focusing on the data gaps identified by the technology prescreening effort. The test plan identified potential amendments designed to immobilize or degrade the primary contaminants *in situ* within the subsurface (i.e., below ground, where they are located) based on the previous technology evaluation. The test plan was developed in phases based on a tiered approach:

- Phase 1: An initial assessment of technology bulk performance targeting technologies treating primary contaminants to at least 35% immobilized or transformed (i.e., proof-of-principle)
- Phase 2: A detailed evaluation of immobilization and transformation mechanisms
- Phase 3: A measurement of end product stability and longevity targeting a minimum of 50% immobilized or transformed

Down-selection of technologies involved expert decisions based on the experimental results and was applied between phases to eliminate technologies that did not perform well from further detailed evaluation. Recommendations were based on whether a technology showed (1) a significant decrease in contaminant mobility (>35% or 50% depending on phase) and (2) long-term stability over months as determined by measurement of low-solubility surface phases.

The technologies selected for treatability evaluation relied on various biogeochemical processes, with a combination of reduction and sequestration or sequestration alone, to immobilize contaminants into solid phases, rendering them less mobile in the subsurface, or to transform them into nontoxic end products, reducing continuing source contributions to the groundwater and helping to mitigate risk (Table ES.1). The primary contaminants targeted for this treatability study were waste site specific and included Tc-99 U, nitrate, and iodine-129 (I-129). Depending on the waste site, these contaminants may have significant potential mobility and persistence in the environment, higher inventories within the 200-DV-1 waste sites, and potential for adverse health effects if/when they reach groundwater. Additional co-contaminants,

[1] DOE/RL-2019-28, Rev. 0. 2019. *200-DV-1 Operable Unit Laboratory Treatability Study Test Plan*. U.S. Department of Energy, Richland Field Office, Richland, WA.

including hexavalent chromate, strontium, and ferrocyanide, were also included depending on the targeted waste sites for each technology.

The nine technologies evaluated are represented by three different groups based on their physical characteristics (Table ES.1): gaseous, particulate, and liquid amendments. The gas-phase technologies were selected for unsaturated vadose zone applications, while the liquid- and particulate-phase technologies were selected for saturated zone applications, potentially targeting direct treatment of contaminants in the perched water zone or in a water table application as a permeable reactive barrier. Each technology was evaluated based on its ability to transform or immobilize the primary contaminants of interest under the targeted application conditions, including the potential presence of co-contaminants. Of the nine technologies evaluated during Phase 1, eight were selected to advance to Phases 2 and 3 as part of the treatability study; gas-phase bioreduction and chemical sequestration of Tc-99 was eliminated due to poor performance.[1]

This document presents the technical approach and final results of laboratory-scale treatability evaluation of the eight remaining *in situ* remedial technologies in Phases 2 and 3 (Table ES.1) for their consideration in future feasibility studies for the 200-DV-1 OU. The primary objectives of Phases 2 and 3 testing were to further evaluate the performance of technologies advanced from Phase 1 testing[1] by assessing process-specific rates, extent, and longevity of contaminant transformation or immobilization. Laboratory testing was conducted primarily with columns to quantify changes in mobility of contaminants of interest in the presence of flow under site-specific conditions, though select experiments used batch systems with contaminant reaction times of up to 1 year with amendments. Based on these experiments, recommendations were made for which technologies may advance to support feasibility studies once specific sites have been identified.

The two gas-phase technologies tested in Phases 2 and 3 target different contaminants in the vadose zone: (1) chemical sequestration of I-129 by carbon dioxide gas and (2) bioreduction of nitrate by ethane. Both technologies for I-129 did not meet performance thresholds for sequestration and are not recommended for further feasibility study consideration. Chemical sequestration of I-129 was less successful under unsaturated conditions during leaching in columns than in the batch experiments conducted in Phase 1 testing. In addition, performance was dependent on sediments, likely due to availability of Ca. For bioreduction of nitrate, there was significant transformation at low nitrate concentrations (8 μg/g), but it was not significantly different than a nitrogen gas control, indicating that anoxic conditions may suffice for abiotic reduction at relatively low concentrations. Moreover, in higher nitrate concentrations, ranging from 100 to 10,000 mg/g, which represent more realistic site conditions and contamination, bioreduction showed little transformation.

[1] PNNL-3452. 2025. *200-DV-1 Laboratory Treatability Testing: Proof-of-Principle Results*. Pacific Northwest National Laboratory. Richland, WA.

The remaining six technologies were tested under two different scenarios for saturated zone applications: (1) as a permeable reactive barrier or (2) direct treatment of contamination in perched water. The best-performing technologies for the water table permeable reactive barrier scenario for Tc-99 were liquid-phase bioreduction and chemical sequestration (molasses with polyphosphate) and liquid-phase chemical reduction and sequestration (calcium polysulfide with polyphosphate). For U, particulate-phase chemical sequestration (bismuth subnitrate) outperformed all other amendments, though significant sequestration was also observed for three liquid-phase technologies: bioreduction and chemical sequestration (molasses with polyphosphate), chemical sequestration (calcium citrate phosphate), and chemical reduction and sequestration (calcium polysulfide with polyphosphate). Therefore, if U and Tc-99 are collocated, the liquid-phase reduction/sequestration technologies (calcium polysulfide or molasses in combination with polyphosphate) may effectively treat both primary contaminants. Co-contaminants significantly impacted Tc-99 and U sequestration for select technologies, likely due to (1) consumption of reduction capacity by Cr and nitrate (i.e., decreasing Tc-99 and U sequestration) and (2) potential co-precipitation of U with strontianite (i.e., increasing U sequestration).

The best-performing technologies for the perched water scenario for Tc-99 were particulate-phase chemical sequestration (tin-substituted apatite), particulate-phase chemical reduction and sequestration (sulfur modified iron with polyphosphate), and liquid-phase chemical reduction and sequestration (calcium polysulfide with polyphosphate). For U, particulate-phase sulfur modified iron with polyphosphate was the only technology that performed well. The presence of nitrate as a co-contaminant likely significantly impacted treatability for Tc-99 and U sequestration for select technologies under perched water conditions due to consumption of reduction capacity.

In general, no single technology is applicable for both saturated zone applications (as a permeable reactive barrier or direct treatment of contamination in perched water) due to differences in physical and geochemical sediment characteristics as well as chemical constituents released in the waste. Table ES.1 illustrates the technologies tested at different phases and their qualitative performance. The results from this laboratory treatability study will be used to further evaluate technology viability and potential additional feasibility study needs to support decision-making for the Central Plateau. The laboratory-scale testing results alone are not sufficient to determine the full-scale applicability of any of the tested technologies. Feasibility testing would provide additional information on potential effectiveness and long-term stability, implementability, and costs for evaluating these technologies for their site-specific application.

Table ES.1. Summary of final results and recommendations for the 200-DV-1 OU treatability testing.

Technology Process	Contaminants of Interest[a]	Phase 1 Amendments	Phase 1 Decision	Phase 2 and 3 Amendments	Potential 200-DV-1 OU Applications
Technologies for Unsaturated Zone Applications					
Gas-phase combined bioreduction and chemical sequestration	**Tc-99**, U, I-129, Cr(VI), CN^-, nitrate	Organic gases including ethane, butane, and butyl acetate for bioreduction CO_2 for sequestration	No-Go	None	Cr(VI)[b]
Gas-phase bioremediation	**Nitrate**, Cr(VI)	Organic gases including pentane, butyrate, ethane, and butane	Go	Ethane gas	None
Gas-phase chemical sequestration	**I-129**, U, Tc-99, Sr, Cr(VI)	CO_2 gas	Go	CO_2 gas	None
Technologies for Saturated Zone Applications[c]					
Particulate-phase chemical sequestration	**U**, **Tc-99**, Sr-90, Cr(VI), I-129, nitrate	Stannous apatite	Go	Stannous apatite	Perched water for Tc
Particulate-phase chemical sequestration	**U, Tc-99,** Sr-90, Cr(VI), I-129, nitrate	Bismuth oxyhydroxide and bismuth subnitrate	Go	Bismuth subnitrate	Water table PRB for U
Particulate-phase combined chemical reduction and sequestration	**U**, **Tc-99**, Sr-90, Cr(VI), I-129, nitrate	Zero valent iron and sulfur modified iron for reduction Polyphosphate solutions for sequestration	Go	Sulfur modified iron followed by polyphosphate	Perched water for Tc-99 and U
Liquid-phase chemical sequestration	**U**, **Tc-99**, Sr-90, Cr(VI), I-129, nitrate	Polyphosphate and citrate phosphate solutions	Go	Calcium citrate phosphate[d]	Water table PRB for U
Liquid-phase combined chemical reduction and sequestration	**U**, **Tc-99**, Sr-90, Cr(VI), I-129, nitrate	Calcium polysulfide for reduction Polyphosphate solutions for sequestration	Go	Calcium polysulfide followed by polyphosphate	Water table PRB for Tc-99 and U and perched water for Tc
Liquid-phase combined bioreduction and chemical sequestration	**U**, **Tc-99**, **nitrate**, Sr-90, Cr(VI), I-129	Organic liquids including emulsified oil substrate and blackstrap molasses for bioreduction Polyphosphate solutions for sequestration	Go	Molasses followed by polyphosphate	Water table PRB for Tc-99 and U

(a) The contaminants of interest shown in bold are primary known contaminant targets while others are potential co-contaminants to evaluate with primary contaminants.
(b) Despite demonstrating poor to moderate sequestration for the primary contaminant (Tc-99), organic gases followed by CO_2 gas treatment showed > 99% immobilization of Cr(VI).
(c) Water table permeable reactive barrier (PRB) and perched water applications represent some of the 200-DV-1 waste sites (see Section 1.2 for more information).
(d) Although calcium citrate phosphate was chosen for additional testing in the liquid-phase chemical sequestration technology, polyphosphate was chosen to advance as the sequestration step in the following technologies: particulate-phase combined chemical, liquid-phase combined chemical reduction and sequestration, and liquid-phase combined bioreduction and sequestration.

Acknowledgments

This document was prepared by the Deep Vadose Zone – Applied Field Research Initiative at Pacific Northwest National Laboratory. Funding was provided by the U.S. Department of Energy (DOE) Hanford Field Office. Pacific Northwest National Laboratory is operated by Battelle Memorial Institute for the DOE under Contract DE-AC05-76RL01830.

The authors acknowledge Christian Johnson, Christopher Thompson, and Matthew Wilburn for their attention to detail in data review and technical editing as well as Mike Perkins and Klaudio Peshtani for development of conceptual diagrams. Steve Eklund and Jamie Sachs are appreciated for their careful attention to detail and quality. The team also thanks the many technical reviewers who spent countless hours sifting through data and confirming calculations.

Pacific Northwest National Laboratory's Analytical Services Center and Christopher J. Thompson are appreciated for their expertise in analyzing the tremendous number of samples generated as part of this study. James B. Duncan is acknowledged for expert guidance on the synthesis of Sn(II)-PO_4.

Use of the Stanford Synchrotron Radiation Lightsource, SLAC National Accelerator Laboratory, is supported by the DOE Office of Science, Office of Basic Energy Sciences under Contract No. DE-AC02-76SF00515. The authors acknowledge Sam Webb for his help with X-ray microprobe mapping and spectroscopic analysis, and Ryan Davis for his help with bulk spectroscopic analysis.

Acronyms and Abbreviations

µXRF	microprobe X-ray fluorescence
ANOVA	analysis of variance (statistical test to compare means of two groups)
BET	Brunauer-Emmett-Teller (method of measuring surface area)
bgs	below ground surface
BOH	bismuth oxyhydroxide
BSN	bismuth subnitrate
Ca-Cit-PO_4	calcium-citrate, sodium phosphate solution used to precipitate apatite
CCug	Cold Creek unit gravel
CCu-PZsd	Cold Creek unit perching zone sand
CCV	Continuing Calibration Verification
CEC	cation exchange capacity
COI	contaminant of interest
CoCOI	co-contaminant of interest
CPS	calcium polysulfide
DI	deionized
DVZ	deep vadose zone
EOS	emulsified oil substrate
ESI	Elemental Scientific Incorporated
EXAFS	extended X-ray absorption fine structure
FIO	For Information Only
FS	feasibility study
GG	guar gum
HCN	hydrogen cyanide
HCV	High Calibration Verification
HEIS	Hanford Environmental Information System
Hf	Hanford formation
HSD	Tukey's honest significant difference test (to identify pairwise differences)
KCN	potassium cyanide
KPA	kinetic phosphorescence analyzer
ICP-MS	inductively coupled plasma mass spectrometer
ICP-OES	inductively coupled plasma optical emission spectrometer
ICV	Initial Calibration Verification
IDL	instrument detection limit
ISTD	internal standard
LCF	linear combination fit
LSC	liquid scintillation counting

NOM	natural organic matter
OU	operable unit
PCOI	primary contaminant of interest
PCR	polymerase chain reaction
PFBA	pentafluorobenzoic acid
PTFE	polytetrafluoroethylene
PNNL	Pacific Northwest National Laboratory
Poly-PO_4	sodium phosphate and sodium polyphosphate solution used to precipitate apatite
PRB	permeable reactive barrier
PUF	pressurized unsaturated flow (1-D column infiltration system)
PV	pore volume
qPCR	quantitative polymerase chain reaction
RFI	Resource Conservation and Recovery Act Facility Investigation
RFICS	Reagent-Free Ion Chromatography System
RMSE	root mean square error
SGW	synthetic groundwater
SMI	sulfur modified iron
Sn(II)-PO_4	tin(II)-substituted apatite
SPW	synthetic perched water
SSRL	Stanford Synchrotron Radiation Lightsource
TOC	total organic carbon
TMAH	tetramethylammonium hydroxide
TTER	treatability test evaluation report
UV	ultraviolet
VZ	vadose zone
WC	water content
WMA	waste management area
XANES	X-ray absorption near edge structure
XAS	X-ray absorption spectroscopy
XRD	X-ray diffraction
XRF	X-ray fluorescence
XMCD	X-ray magnetic circular dichroism
ZVI	zero valent iron

Contents

Figures

Tables

1.0 Introduction

This document summarizes and evaluates results of Phase 2 and 3 laboratory-scale treatability testing (with Phase 1 results in PNNL-35432) of eight *in situ* remedial technologies, as listed in Table 1.1, for their consideration in a future feasibility study (FS) for the 200-DV-1 Operable Unit (OU) at the U.S. Department of Energy Hanford Site. Eight technologies were initially identified through a prescreening effort that evaluated remedial technologies for the deep vadose zone (DVZ) contamination in the Hanford Site Central Plateau, as reported in the *Technology Evaluation and Treatability Studies Assessment for the Hanford Central Plateau Deep Vadose Zone* (DOE/RL-2017-58; hereinafter referred to as the treatability test evaluation report [TTER]). Another technology (bismuth subnitrate, BSN) was added to the treatability study based on new information from separate laboratory investigations and advanced to Phase 2 and 3 testing alongside the others. After Phase 1 testing, one technology was eliminated from further study based on performance (PNNL-35432)

The eight technologies identified in the TTER and one additional technology were selected for a laboratory treatability study to address site-specific data gaps (Table 1.1). These include gas-phase, particulate-phase, and liquid-phase technologies that would inject amendments into the subsurface to manipulate the biogeochemistry to induce sequestration of contaminants in solid phase. Gas-phase technologies were selected for unsaturated applications within the vadose zone (VZ) soil column and particulate- and liquid-phase technologies were selected for applications in saturated conditions, such as direct injection into the perched water zone (i.e., thin, saturated zone within the VZ due to geologic heterogeneities) and/or development of a permeable reactive barrier (PRB) at the water table. The main purpose of the treatability study is to assess the performance of each technology in a laboratory environment using simulated site-specific conditions. Evaluation of the results from the laboratory-scale testing will be used to support FS planning.

Following the recommendations of the TTER, a laboratory treatability study plan was developed for the original eight technologies: *200-DV-1 Operable Unit Laboratory Treatability Study Test Plan* (DOE/RL-2019-28, Rev. 0; hereinafter referred to as the test plan). The test plan presented a framework and overall guidance for detailed laboratory evaluations of each technology, focusing on the data gaps identified in the TTER. Based on existing knowledge and past experiences, the test plan identified potential amendments targeting reduction and/or sequestration to be tested for each technology, as appropriate (Table 1.1).

The evaluation approach presented in the test plan was developed to outline a tiered methodology with multiple incremental decision points throughout the study for each technology (Figure 1.1). The purpose of the tiered approach was to eliminate the technologies that did not meet minimum performance thresholds after the initial proof-of-principle step (Phase 1) from further detailed testing. While technology-specific testing objectives were identified for each phase (DOE/RL-2019-28) targeting specific contaminants, in general, the main components of the tiered testing approach included the following sequence of actions or phases:

- Phase 1: An initial assessment of bulk technology performance in ideal conditions (as a proof-of-principle step). The TTER recommended that this determination be based on an overall minimum success rate of 35% of contaminant transformation to immobile, temporarily immobile, or nontoxic end products.
- Phase 2: A detailed evaluation of process-specific rates and extent of reduction, degradation, and/or sequestration with an assessment of potential contaminant remobilization to determine if a minimum of 50% contaminant transformation to immobile, temporarily immobile, or nontoxic end products is achieved.

- Phase 3: Additional characterization to evaluate the end product stability (i.e., longevity) of a minimum of 50% immobilized contaminants as well as potential remobilization rates (based on the TTER recommendation).

This document presents the technical approach (Section 2.0) and final results (Section 3.0) of laboratory-scale treatability evaluation of the remaining (after Phase 1) eight *in situ* remedial technologies (Table 1.1) for their consideration to support a future FS for the 200-DV-1 OU. Phase 2 and 3 were conducted concurrently and are presented together here because additional characterization for Phase 3 was conducted primarily on samples generated from Phase 2 tests. Phase 1 results are presented in a previous report (PNNL-35432) and are briefly summarized in Section 1.3.

Table 1.1. Laboratory studies recommended by the TTER.

Technology Process	COI to Study	Phase 2 and 3 Amendments Selected for Testing	Examples of Potentially Applicable Waste Sites	
			200-DV-1	Other
Technologies for Unsaturated Zone Applications				
Gas-phase combined bioreduction and chemical sequestration	**Tc-99**, U, I-129, Cr, CN, nitrate	Technology did not meet criteria for further testing	Tc-99 and/or CN BY Cribs Nitrate, I-129, and Cr(VI) Unknown	Tc-99 BC Cribs/Trenches Cr(VI) 216-S-10 216-S-8 216-T-4a I-129 216-S-9 216-A-10 216-A-5 216-S-7 CN Unknown
Gas-phase bioreduction	**Nitrate**, Cr	Ethane		
Gas-phase chemical sequestration	**I-129**, U, Tc-99, Sr, Cr	CO_2 gas		
Technologies for Saturated Zone Applications[a]				
Particulate-phase chemical sequestration	**U**, **Tc-99**, nitrate, Sr-90, Cr, I-129	Stannous apatite	U and/or Tc-99 Perched water Below perched water Below BY Cribs	U and/or Tc-99 216-U-1&2 S-SX Tank Farm T-TX-TY Tank Farm C Tank Farm BC Cribs/Trenches Cr(VI) 216-S-10 216-S-8 216-T-4a I-129 216-A-10 216-A-5 216-S-7
Particulate-phase combined chemical reduction and sequestration	**U**, **Tc-99**, nitrate, Sr-90, Cr, I-129	Sulfur modified iron (SMI) for reduction Polyphosphate solution for sequestration		
Particulate-phase chemical sequestration (Bi)[b]	**U**, **Tc-99**, nitrate, Sr-90, Cr, I-129	Bismuth subnitrate		
Liquid-phase chemical sequestration	**U, Tc-99**, nitrate, Sr-90, Cr, I-129	Citrate phosphate solutions		
Liquid-phase combined chemical reduction and sequestration	**U**, **Tc-99**, nitrate, Sr-90, Cr, I-129	Calcium polysulfide for reduction Polyphosphate solution for sequestration		
Liquid-phase combined bioreduction and chemical sequestration	**U**, **Tc-99**, **nitrate**, Sr-90, Cr, I-129	Molasses for reduction Polyphosphate solution for sequestration		

Reference: DOE/RL-2017-58, Draft A, *Technology Evaluation and Treatability Studies Assessment for the Hanford Central Plateau Deep Vadose Zone.*

Notes: Laboratory quantification of performance is needed for use in combination with existing field-scale information from other sites to evaluate these technologies in an FS.

The primary contaminants of interest (PCOIs) shown in bold are primary known contaminant targets. The co-contaminants of interest (CoCOIs) are potential co-contaminants to evaluate with PCOIs.

(a) The saturated zone applications include 200-DV-1 perched water (located beneath the B Complex) and horizontal PRB at the water table (beneath the BY Cribs).

(b) The technical information about the potential applicability of this technology for DVZ remediation became available through bench-scale investigations after initiating the treatability study. Based on this information, the technology was added to the treatability study to evaluate its site-specific performance.

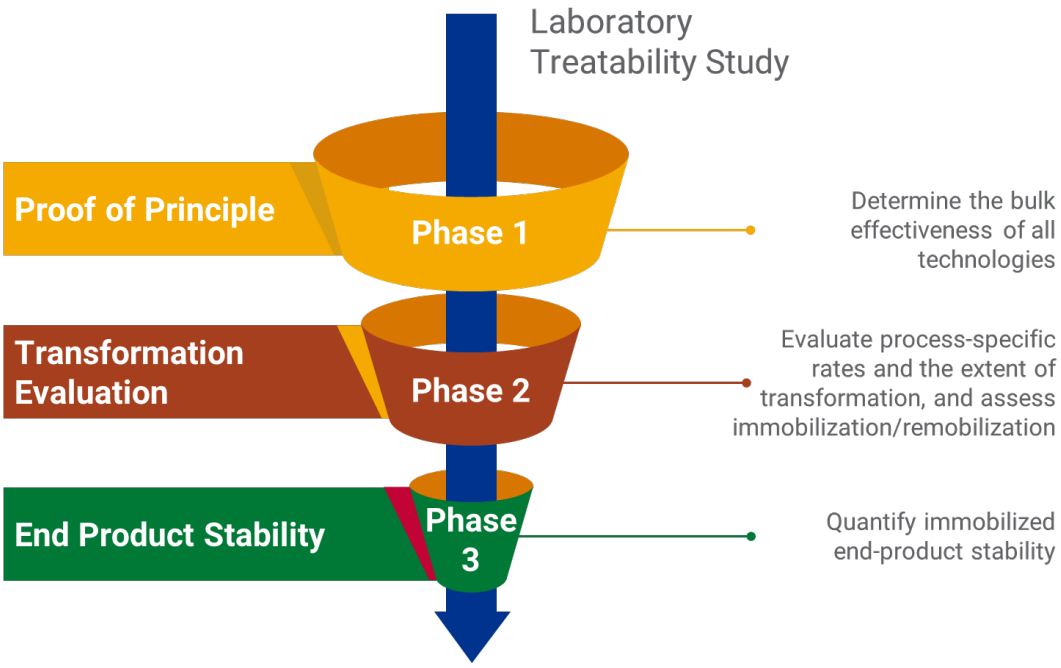

Figure 1.1. Tiered phases of the laboratory treatability testing approach for the 200-DV-1 OU.

To evaluate the performance of the technology, the project team used the thresholds determined in the test plan as an initial indicator of performance. However, these thresholds were not an absolute factor in determining the decision as the overall evaluation included a holistic evaluation of all results alongside expert judgement. The thresholds were based on transformation to immobile, temporarily immobile [e.g., TcO_4^- to TcO_2, $Ca_2UO_2(CO_3)_3$ to $Ca(UO_2)_2(PO_4)_2 \cdot 10\text{-}12H_2O$, or IO_3^- to IO_3 incorporated into $CaCO_3$], or nontoxic end products (e.g., NO_3^- to N_2 gas). A 35% transformation or immobilization threshold was considered for Phase 1, and a 50% immobilization threshold was considered for Phases 2 and 3 based on an increase in transformation or immobilization as compared to an appropriate control experiment (e.g., sediments and contaminants reacting in the absence of treatments).

1.1 200 DV-1 Operable Unit at the Hanford Site

The Hanford Site consists of an area of approximately 1,517 km^2 (586 mi^2) in the Columbia River Basin, Washington State. The Central Plateau is in the central portion of the Hanford Site and includes the 200 Areas, where historical chemical separation and waste management activities took place during the production era, resulting in nearly 1,100 waste sites, including ponds, cribs, ditches, trenches, tanks, and others. To support waste site remediation, more than 15 source OUs have been established in the Central Plateau (Figure 1.2). Some of the contaminants at these waste sites have migrated to the DVZ to depths where they continue to impact underlying groundwater and contribute to groundwater plumes and, therefore, require remedial action. The Central Plateau DVZ is defined as the soil located more than 4.6 m (15 ft) below ground surface (bgs) and above the water table, which is located approximately 76 m (250 ft) bgs in the western portion of the Central Plateau. .

The 200-DV-1 OU, located in the Central Plateau, was established in 2010 to address DVZ contamination at 43 waste sites based on (1) the unique remediation challenges of mobile contamination in the DVZ, (2) the complex technical and regulatory challenges of DVZ contamination (e.g., co-mingled plumes, determining nature and extent), and (3) the geographic proximity to waste management areas (WMAs) (DOE/RL-2011-102). These waste sites are primarily cribs and trenches associated with the single-shell

tank farms, B-BX-BY (B Complex), T-TX-TY (T Complex), and S-SX (S Complex) tank farm WMAs (PNNL-26208; PNNL-27524; PNNL-27846; PNNL-26266). The 200-DV-1 OU also includes a perched water zone below the B Complex (referred to as the 200-DV-1 OU perched water), located in the DVZ above a fine-grained unit (perching silt layer) that overlies the unconfined regional aquifer in the 200-BP-5 OU, near a depth of 69 m (225 ft) bgs, with saturated thickness of about 4 m (12 ft) at the highest location (PNNL-26208; PNNL-27846). It contains elevated levels of uranium (U), technetium-99 (Tc-99), nitrate (NO_3), and other contaminants of concern (PNNL-27524; PNNL-34340).

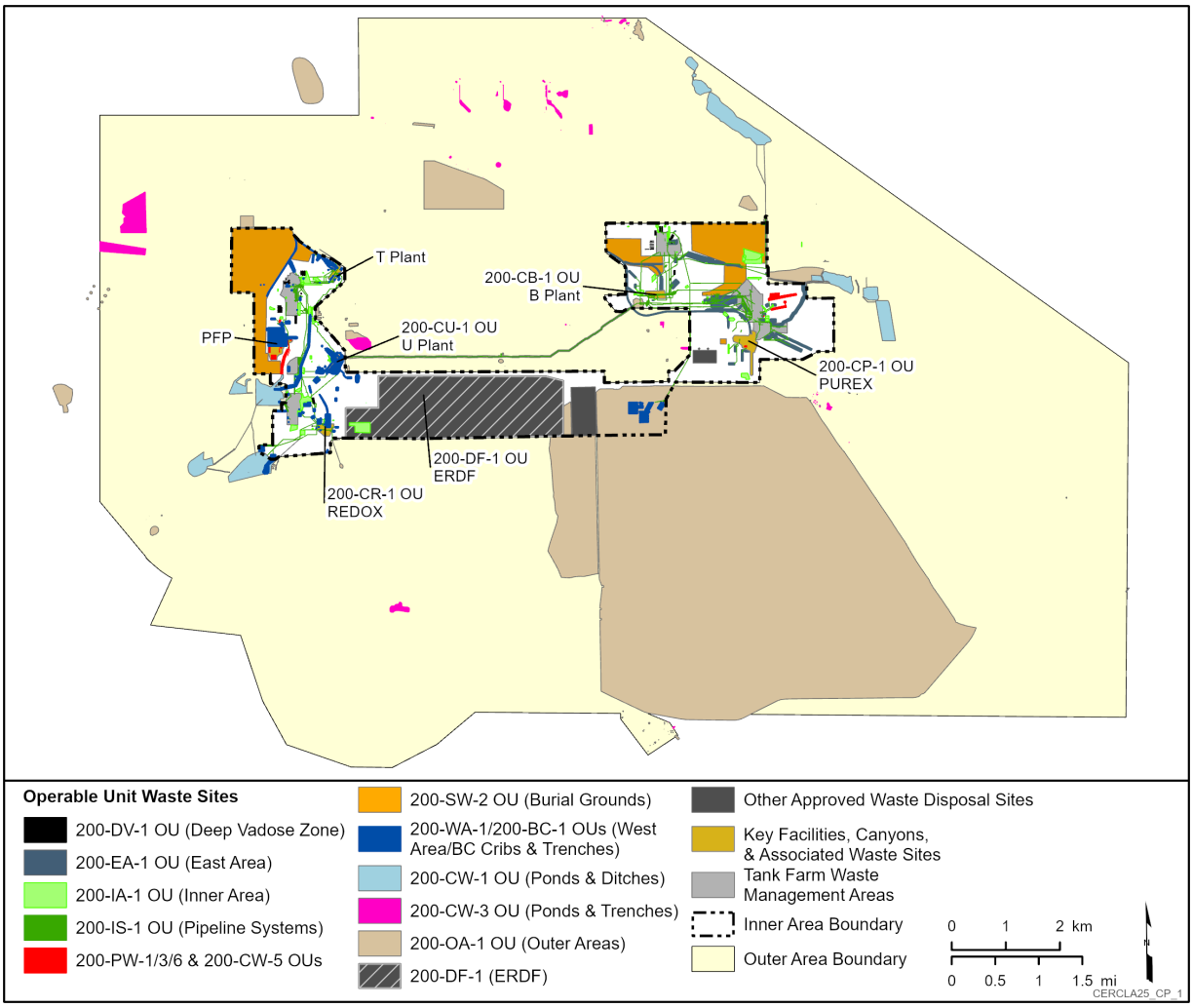

Figure 1.2. Source OUs in the Central Plateau.

The primary DVZ contaminants at the Central Plateau driving long-term risk are Tc-99 and U because of their potential adverse health effects, persistence in the environment, high inventory in the VZ, mobility, complex subsurface behavior, and long half-lives (DOE/RL-2011-102). Additional contaminants of interest (COIs) in the VZ include iodine-129 (I-129), chromium (Cr, as chromate), NO_3, and cyanide (CN) due to their mobility and historical discharges (DOE/RL-2017-58; PNNL-35432; PNNL-26208; PNNL-27524).

1.2 Remediation Technologies for Treatability Testing

The following sections present each of the technologies selected for Phases 2 and 3 of testing as part of the treatability study (Table 1.1), including gas-phase technologies (Sections 1.2.1 and 1.2.1.2), particulate-phase technologies (Sections 1.2.2.1 through 1.2.2.3), and liquid-phase technologies (Sections 1.2.2.4, through 1.2.2.6). For each technology, the chosen amendments are described, including the targeted mechanisms and processes for reduction and sequestration, the potential locations of application, and the PCOIs and CoCOIs.

1.2.1 Vadose Zone Technologies

These gas-phase technologies were evaluated in Phases 2 and 3 of the treatability study for VZ remediation. Gas-phase amendments can be delivered to the VZ without injection of additional liquids that may mobilize contaminants and may have physical properties that allow for more uniform delivery (WSRC-MS-2005-00589; Muller et al. 2021a).

1.2.1.1 Gas-Phase Sequestration – Carbon Dioxide

This technology is focused on gas-phase chemical sequestration of I-129 as the PCOI using CO_2 gas with U, Sr, Tc-99, and Cr as CoCOIs. The mechanism for sequestration requires carbon dioxide (CO_2) gas partitioning into VZ sediment pore water, increasing dissolved carbonate, and eventually precipitating calcite (Figure 1.3). Calcite can incorporate some iodate (IO_3^-) into the structure during precipitation. While CO_2 supplies sufficient carbonate ions, the calcium needs to come from ion exchange sites on sediments. This treatment is targeting unsaturated zones, for example, under the 216-S-9 waste site. Sites that received significant acidic waste, such as 216-U-8 Crib (PNNL-29650; Szecsody et al. 2013), may be depleted in calcium and carbonate, as acids have dissolved and flushed ions to greater depth (Szecsody et al. 2013), making these sites less amenable to this technology. Potential secondary treatment zones include the 216-A-10, 216-A-5, and 216-S-7 waste sites.

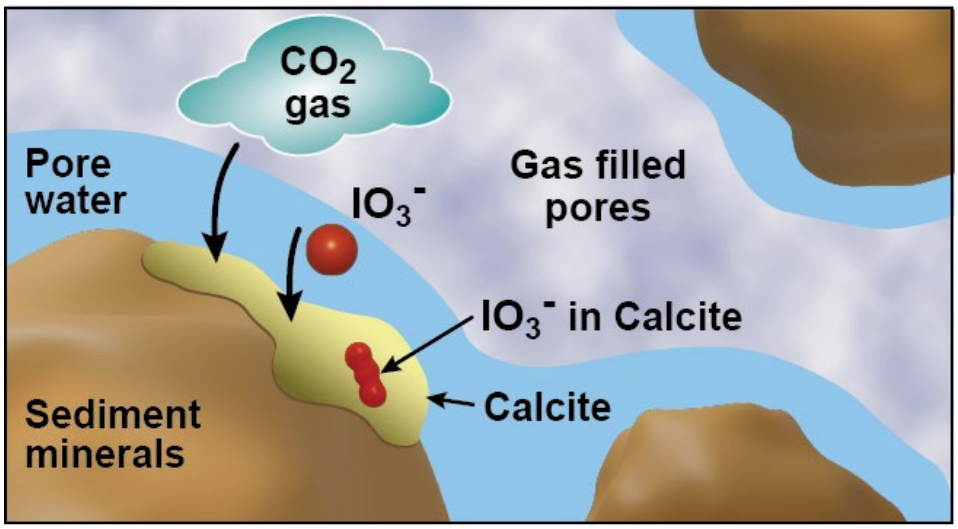

Figure 1.3. Conceptual diagram of I-129 sequestration in VZ pore water as a result of CO_2 gas injection, partitioning of carbonate into pore water, and subsequent calcite precipitation with simultaneous incorporation of aqueous IO_3^- and coating of adsorbed I species.

A recent evaluation of IO_3^- incorporation into precipitating calcite showed that a small fraction of IO_3^- (starting concentration 100 to 500 µg/L) was removed during precipitation of calcite (from 0.28 to 1.6 µg/g depending on the initial iodate aqueous concentration): (1) 100 µg/L IO_3^- initially, 0.28 µg/g in calcite; (2) 250 µg/L IO_3^- initially, 0.69 µg/g in calcite; and (3) 500 µg/L IO_3^- initially, 1.38 µg/g in calcite (PNNL-28064). Another study showed CO_2 gas injection successfully decreased uranium mobility (i.e., presumed to be co-precipitation of uranium in calcite) in unsaturated sediments at 4 and 16 wt% water content (WC) (Szecsody et al. 2012). However, in batch experiments, the CO_2 gas treatment resulted in 25% to 60% of IO_3^- incorporation into precipitating calcite (McElroy et al. 2020). Different aspects of iodate interaction with calcium carbonate minerals (including calcite) are further covered in a series of recent publications (Katsenovich et al. 2021; Kerisit et al. 2018; Saslow et al. 2019; Qafoku et al. 2022).

The objectives of this study were to quantify (1) the extent and rate of sequestration of I-129 by CO_2 gas treatment via co-precipitation with calcite, and (2) the stability of end products (i.e., I-129 immobilization). Batch and variably saturated columns were conducted with an uncontaminated Hanford formation (Hf, described in Section 2.1) sediment and a contaminated vadose sediment from under the 216-S-9 Crib (primary treatment target).

1.2.1.2 Gas-Phase Bioreduction – Organic gases

This technology is focused on gas-phase bioreduction by stimulating microbial activity in VZ sediments with ethane to reduce concentrations of NO_3^-. In this approach, NO_3^- reduction is coupled to the oxidation of ethane, which acts as a gaseous electron donor. Additionally, this technology includes the presence of Cr as chromate [Cr(VI)] as a CoCOI to understand its potential impact on the efficiency of this reduction. Microbial NO_3^- reduction, or denitrification, is an anaerobic respiratory process where NO_3^- is sequentially reduced to gaseous nitrogen products, primarily non-toxic dinitrogen gas (N_2) as shown in Figure 1.4.

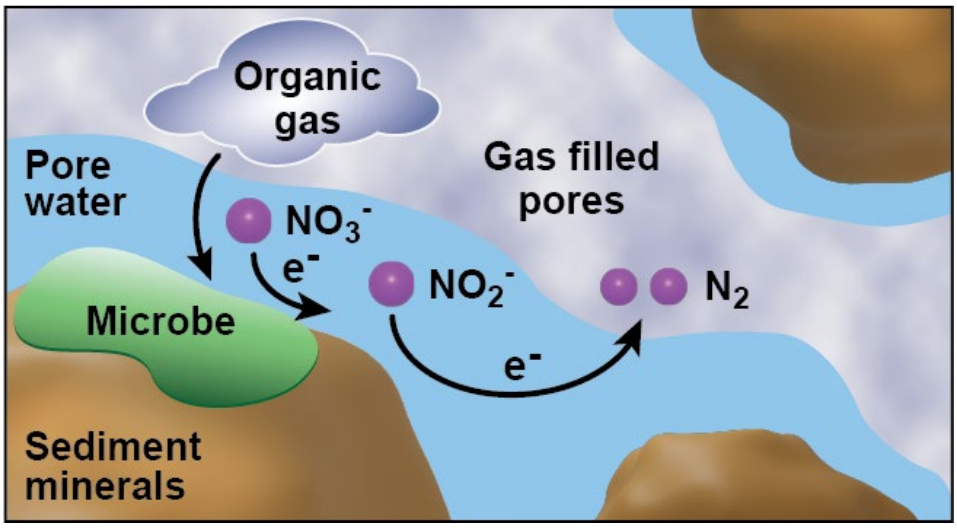

Figure 1.4. Conceptual diagram of bioreduction of aqueous NO_3^- in VZ pore water following the introduction of an organic gas to stimulate microbial activity and generate reducing conditions to turn NO_3^- into gaseous nitrogenous end products.

A competing pathway, dissimilatory NO_3^- reduction to ammonium (DNRA), produces ammonium (NH_4^+) instead. This pathway is unlikely to be present in unsaturated zones treated with organic gases, as these conditions typically do not have the levels of organic carbon (i.e., electron donors) required to sustain microbial growth (van den Berg et al. 2017). Additionally, Cr(VI) may inhibit DNRA more strongly than denitrification due to differences in redox potential (Wu et al. 2024).

Gas-phase carbon amendments have been successfully applied to stimulate subsurface microbial communities for bioremediation of organic and inorganic contaminants in the VZ (Evans et al. 2011; Evans and Trute 2006; WSRC-MS-94-0323). For Hanford Site applications, scoping tests and bench-scale studies have demonstrated that the VZ has sufficient nutrients and microbial communities to support *in situ* bioremediation, with gas-phase hydrocarbons successfully stimulating microbial activity to reduce NO_3^- and immobilize Cr (PNNL-28055; PNNL-14535). Target treatment areas within the 200-DV-1 OU include unsaturated zones such as the S and T Cribs (e.g., 216-S-10 affected by Cr) and BY Cribs (affected by Tc-99, U, and cyanide). These previous studies suggest that the use of gaseous hydrocarbons to increase microbial activity may be viable for *in situ* treatment for Hanford Site DVZ sediments, including for the 200-DV-1 OU.

The objectives of Phase 2 of the treatability study are to (1) evaluate the rate and extent of NO_3^- transformation into non-toxic end products using ethane as the gas treatment and (2) compare these results to samples treated with nitrogen gas under identical conditions. These conditions include varying initial contaminant concentrations, sediments from the S Cribs, and different levels of water saturation, both with and without CoCOIs (Cr).

1.2.1.3 Gas-Phase Bioreduction and Chemical Sequestration

This technology is focused on gas-phase bioreduction and chemical sequestration of Tc-99 through an initial reductive precipitation step followed by coating with calcite minerals (Figure 1.5). CoCOIs included U, Sr, I, Cr, and nitrate. The first step is injection of a nontoxic organic gas (ethane, butane, or butyl acetate) to stimulate natural microbes in sediments to generate conditions for reduction of Tc-99, followed by injection of a second gas (carbon dioxide, CO_2) to precipitate calcite on Tc-99 precipitates. This second step is needed because Tc(IV) precipitates may be oxidized and remobilized. This technology uses sequential gas treatment for reductive Tc-99 precipitation [i.e., $Tc(IV)O_2$ precipitate] followed by calcite coating via precipitation from CO_2 gas treatment. This concept is based on a previously tested sequential gas technology using H_2S gas, which reduced most of the Tc-99, followed by NH_3 gas, which resulted in aluminosilicate precipitate coatings on surfaces (Szecsody et al. 2012). Because of concerns about using a toxic reductive gas (H_2S) at field scale, this current study evaluated the use of nontoxic, organic gases (ethane, butane, and butyl acetate) to generate reducing conditions from biostimulation.

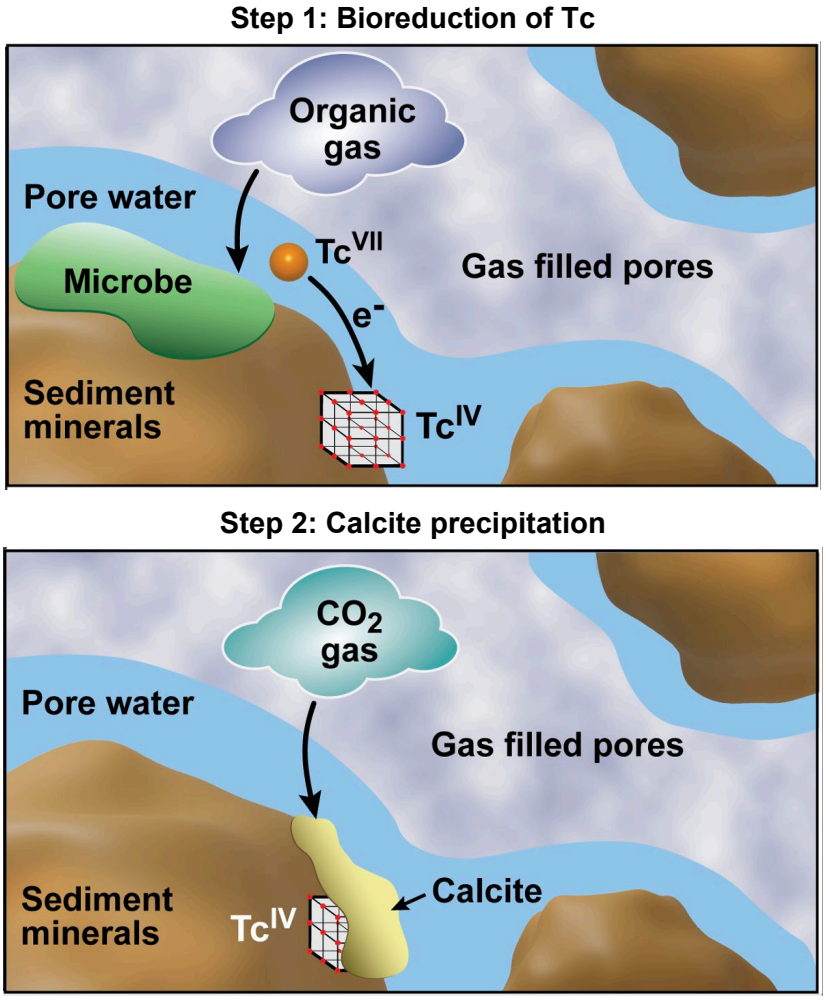

Figure 1.5. Conceptual diagram of bioreduction of aqueous Tc-99 using an organic gas (Step 1) followed by calcite precipitation using CO_2 gas (Step 2).

1.2.2 Water-Saturated Technologies

Technologies have been identified for *in situ* remedy applications in water-saturated areas, with primary treatment zones in the 200-DV-1 OU including direct injection to a perched water zone below the B Complex area and/or the development of a PRB at the water table beneath the BY Cribs. Secondary treatment zones in the Central Plateau may include 216-U-1&2, S-SX Tank Farm, C Tank Farm, and BC Cribs and Trenches, where U and/or Tc-99 are also PCOIs. A previously developed conceptual model suggests significant U and Tc-99 contamination in the VZ below the B Complex within 6 m (20 ft) of the water table, which may influence ultimate remedial decisions (PNNL-19277).

Amendment delivery is not the focus of this treatability study, though it may impact whether these technologies move to FS. Guidance for amendment delivery has been outlined previously by the Interstate Technology Regulatory Council (ITRC 2017). Moreover, a recent review summarizes delivery options and challenges for remedial amendments, including needs for field-tested approaches for perched water and low-permeability zones – especially in relatively deep formations with low hydraulic conductivity (< 1.5 m/day or < 5 ft/day) (Muller et al. 2021a). Particulate technologies function via injection of a solid phase amendment [e.g., 1- to 5-µm particle sized zero valent iron (ZVI) or SMI], likely with a

high-viscosity, shear-thinning delivery fluid (e.g., xanthan) to advect reactive particulates into sediments from an injection well.

Materials may also be jet-injected, as was done previously for a treatability study where solid phase apatite was successfully jet-injected in the field at 100-NR-2 OU for sequestration of strontium-90 (SGW-47062). In this case, the pre-formed apatite was a powdered fishbone, Na-PO_4, or a mixture of both materials that was jet-injected a few feet into the subsurface using water as a delivery fluid. PRB walls of ZVI have also been created using a trenchless technique of vertically slotted wells and high-pressure injection of ZVI using guar gum as the delivery agent. These can extend 5 m (15 ft) from the injection well (azimuth oriented vertical hydraulic fracturing and vertical inclusion propagation) (McElroy et al. 2003).

1.2.2.1 Particulate-Phase Sequestration – Tin Apatite

This technology is focused on chemical sequestration, including U and Tc-99 as PCOIs and Sr, I-129, Cr, and nitrate as potential CoCOIs, via injection of a solid phase particulate amendment [i.e., Sn(II) apatite]. Conceptually, Tc-99 and U are reduced in the presence of the tin(II)-substituted apatite [Sn(II)-PO_4], then potentially slowly incorporated into apatite (Figure 1.6). Once sequestered on or within apatite, contaminants would be immobilized as particles are not expected to move within pore spaces due to their size and density.

Laboratory testing using solid phase Sn(II)-PO_4 conducted in the past has shown potential for recovery and sequestration of Tc-99 from low-activity waste simulants and for getters in cementitious waste forms over a wide pH range (0 to 14) and high ionic strength (Asmussen et al. 2016, 2018; RPP-53855). The mechanisms involved in contaminant sequestration were (1) adsorption and incorporation into hydroxyapatite and (2) reduction via Sn(II) [reduction potential of Sn(IV) to Sn(II) is 0.384 V]. Although testing has not been conducted under Central Plateau subsurface conditions, similar mechanisms are expected. It is unclear if the reduction is direct (electron transfer from Sn to the contaminant at the surface) or indirect (via a secondary species).

In addition, Sn(II) apatite has not been directly tested for U sequestration; however, apatite (with no Sn substitution) has been used to sequester U (Wellman et al. 2005). Moreover, it is expected that the Sn(II)-PO_4 will also sequester U, although the stannous tin may reduce U(VI) aqueous phases and, therefore, slow precipitation of U(VI)-PO_4 precipitates. Sn(II) apatite also has yet to be demonstrated for sequestration of U and Tc-99 in the presence of CoCOIs and for sequestration of CoCOIs. It is anticipated that redox-sensitive CoCOIs will decrease Sn(II)-PO_4 reactivity for $Tc(VII)O_4^-$ and may increase the mobility of iodine-129 as a result of potential iodate reduction to iodide.

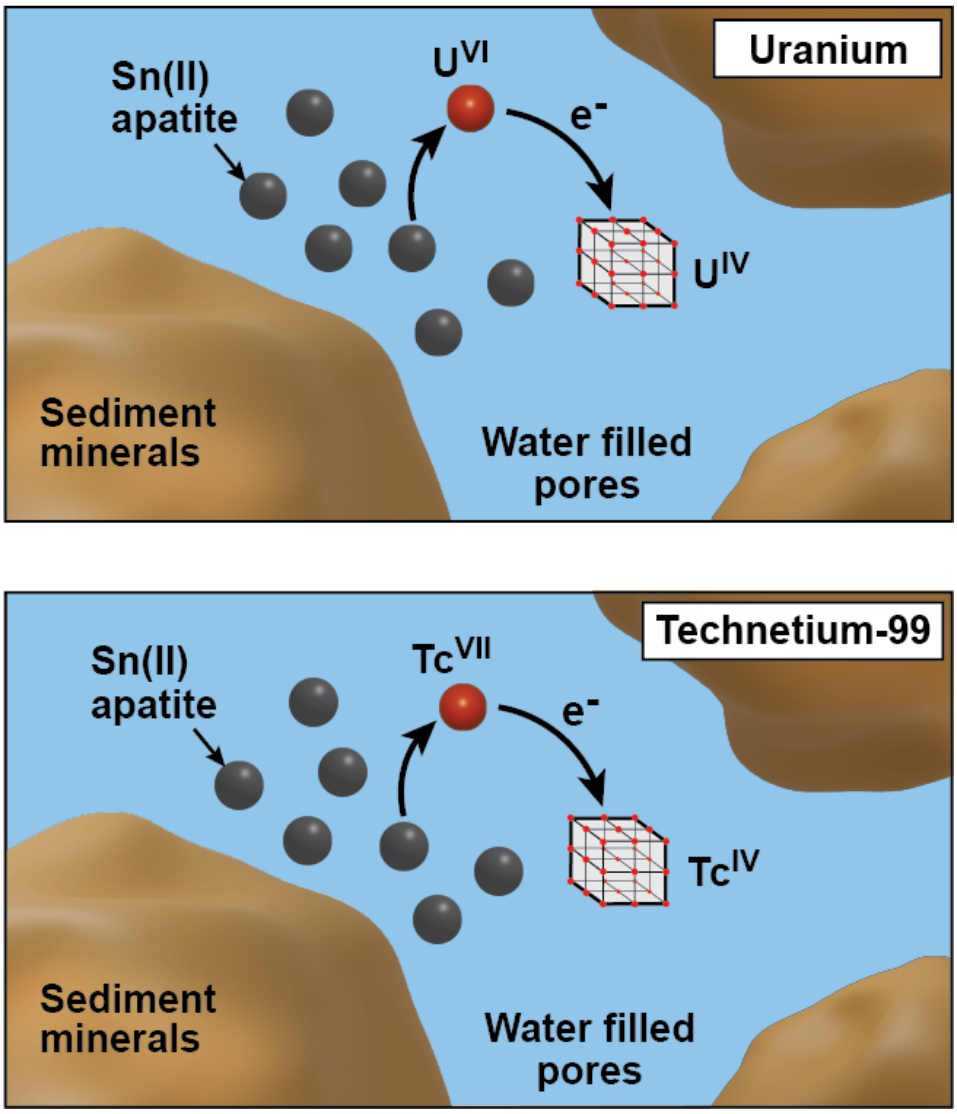

Figure 1.6. Conceptual diagram of sequestration of U (*top*) and Tc-99 (*bottom*) Sn(II) apatite: U(VI) or $Tc(VII)O_4^-$ reduction and precipitation of U(IV)/Tc(IV); the reduction step is likely followed by a second, more permanent mechanism such as subsequent coating of the U(IV) or Tc(IV) by apatite or incorporation of U or Tc-99 in the apatite structure, but this mechanism is currently unknown.

The objectives of this study were to quantify (1) the extent and rate of U (via adsorption and incorporation) and Tc-99 (via reduction with subsequent adsorption and incorporation) sequestration by Sn(II) apatite and (2) the stability of end products (i.e., the newly formed solid phases).

1.2.2.2 Particulate-Phase Reduction and Sequestration – Sulfur Modified Iron and Polyphosphate

This technology is focused on a two-step particulate-phase reduction (with ZVI or SMI in Phase 1 studies, down-selected to SMI in Phases 2 and 3) followed by liquid-phase sequestration with Poly-PO_4 (i.e., sodium phosphate and sodium polyphosphate solution), which precipitates apatite (Figure 1.7 and Figure 1.8 for Tc-99 and U, respectively).

This technology is targeting two PCOIs (Tc-99 and U) as well as Sr, I-129, nitrate, and Cr as potential CoCOIs. Once emplaced, the ZVI/SMI temporarily reduces/precipitates contaminants if reduction can occur within the residence time of contaminants in the relatively thin ZVI/SMI wall.

Following reaction of ZVI or SMI, which serve as electron donors reducing Tc-99 and U, Poly-PO_4 is added, which may either incorporate contaminants or coat precipitated contaminants. The subsequent addition of Poly-PO_4 results in precipitation of apatite, which can incorporate $U(VI)O_2^{2+}$ and precipitate on top of (i.e., coat) reduced Tc(IV) and U(IV) species. Initial ZVI reactivity is slow due to an intrinsic passive (i.e., Fe oxide) layer on the ZVI surface, which can be eliminated by pretreatment before deployment (Guan et al. 2015). Moreover, there is a loss in ZVI reactivity over time as metal hydroxides and metal carbonates precipitate on the ZVI surface. As metallic iron (Fe^0) corrodes (oxidizes), ferrous iron (Fe^{+2}) is created, which can adsorb to sediment minerals, form ferrous iron phases such as magnetite or green rust, or further oxidize to ferric (Fe^{3+}) minerals (Boglaienko et al. 2019, 2020; Emerson et al. 2020). Depending on the contaminant, reduction may be direct (electron transfer from the ZVI surface) or indirect (via a secondary species like iron oxides or hydrogen).

While initial oxidation of Fe^0 is expected under aerobic conditions, anaerobic conditions will likely be established within the first few days, likely allowing for oxidation by water or H^+ (de Lima Perini and Nogueira 2017). Further oxidation of resulting ferrous iron phases results in ferric oxides and hydroxides such as hematite, depending on the pH and available ions. Moreover, the presence of trace sulfur in SMI has been shown to promote electron transfer and Fe^0 corrosion, including reduction of mineral surface Fe^{3+} by Fe^0 to Fe^{2+} (Shao et al. 2018). Oxidation of sulfide also consumes significant hydroxide, which may be confirmed by measuring the pH over time.

A recent evaluation of the combined ZVI/SMI treatment followed by Poly-PO_4 treatment showed that the initial reduction step effectively decreased the aqueous concentration of Tc-99 and U, and the second apatite precipitation step may decrease Tc-99, U, and nitrate remobilization as the system oxidizes (PNNL-31959). Because that study was conducted in groundwater with no other contaminants, the effect of additional CoCOIs, which use ZVI/SMI reductive capacity, is not well understood. The impact of CoCOIs on reduction will likely be important based on previous research (Xin et al. 2020).

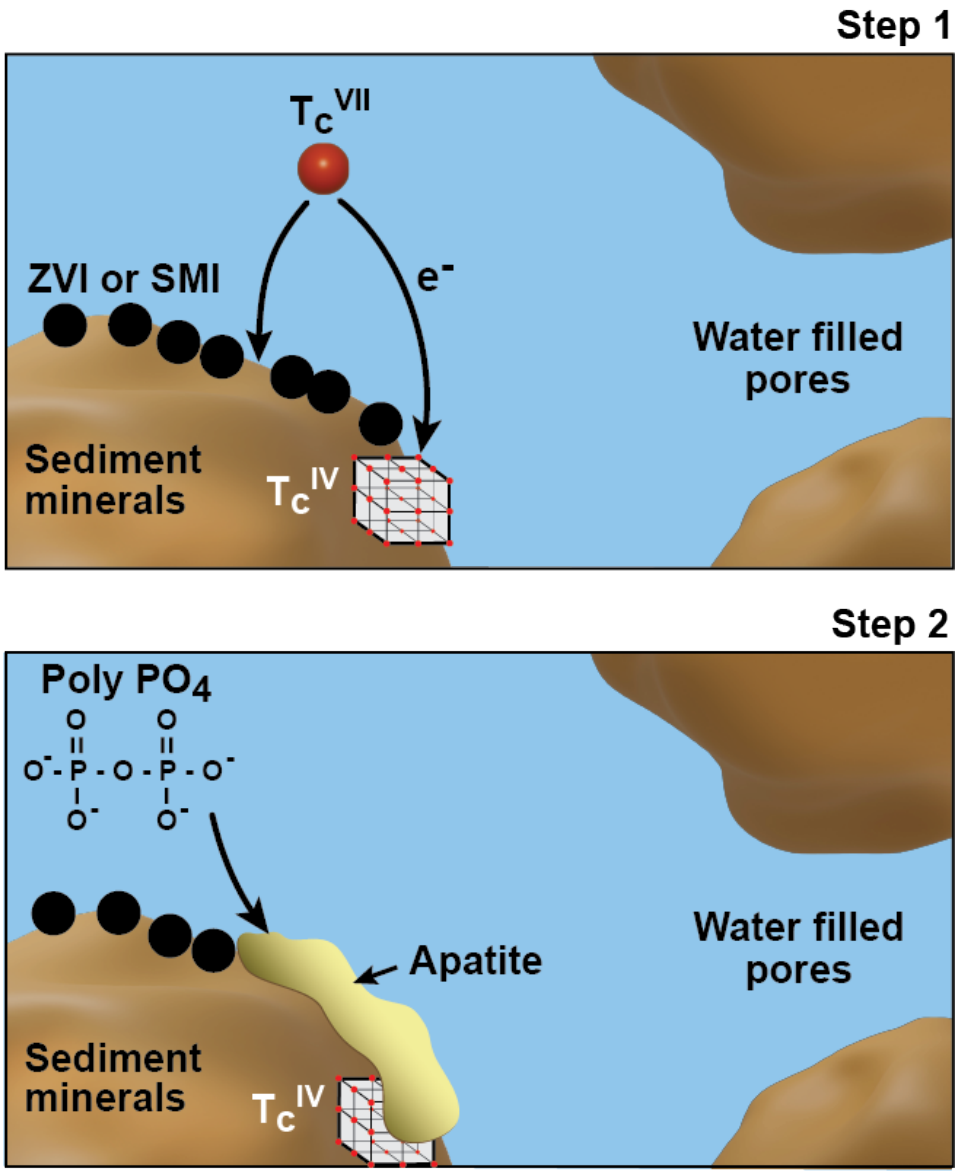

Figure 1.7. Conceptual diagram of sequestration of Tc-99 in the saturated zone by treatment with ZVI or SMI particles to stimulate reducing conditions followed by Poly-PO_4 (*top*) aqueous $Tc(VII)O_4^-$ reduction and precipitation as Tc(IV) with ZVI or SMI and (*bottom*) subsequent coating of Tc(IV) by apatite following treatment with Poly-PO_4.

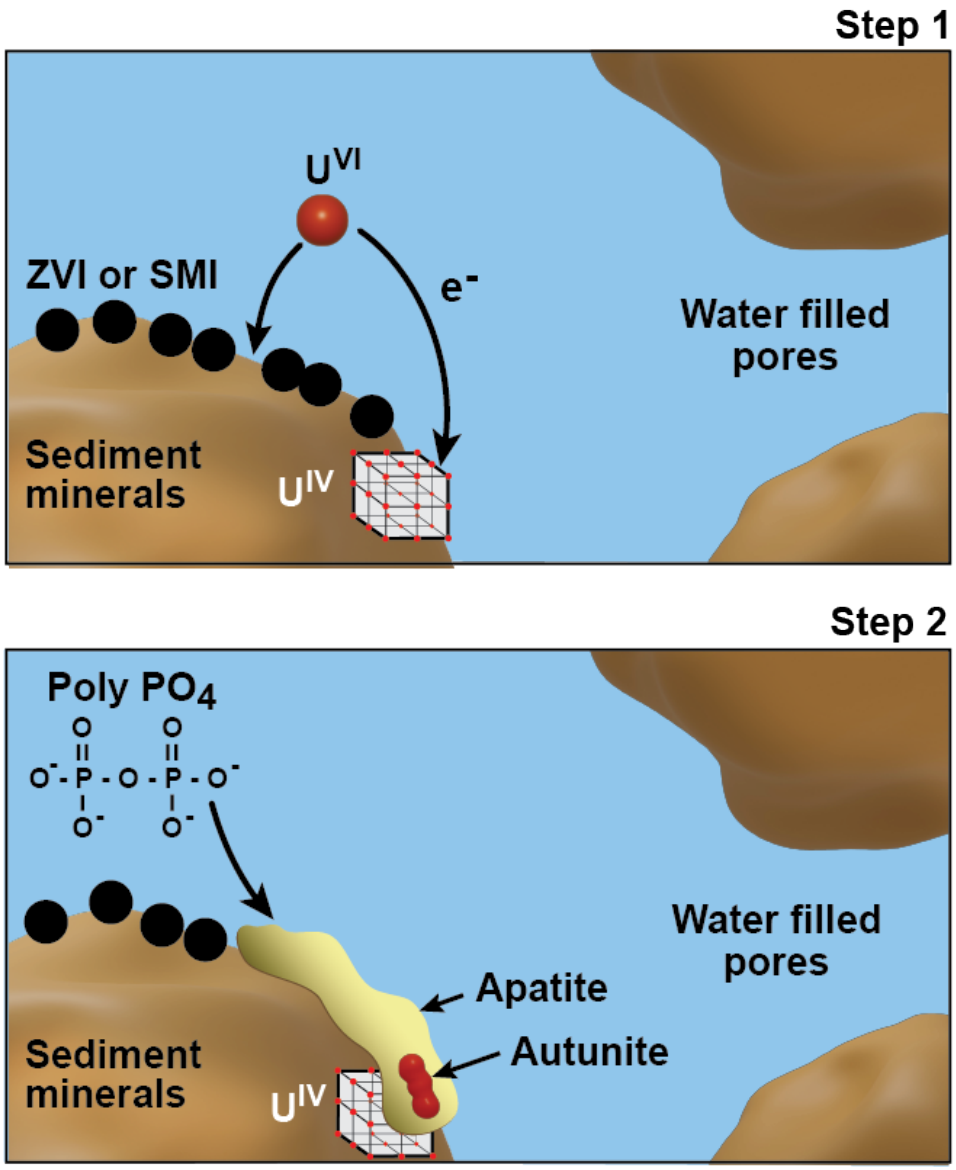

Figure 1.8. Conceptual diagram of sequestration of U in the saturated zone by treatment with ZVI or SMI particles followed by Poly-PO_4 (*top*) reduction of aqueous and adsorbed U(VI) species and precipitation of U(IV) following reaction with ZVI or SMI and (*bottom*) subsequent coating of U(IV) by apatite and/or incorporation of U(VI) species in apatite and autunite following treatment with Poly-PO_4.

The objectives of this study were to quantify (1) the extent and rate of sequestration of U (primarily via adsorption, co-precipitation, and coating) and Tc-99 (by reductive precipitation and coating) by SMI and Poly-PO_4, and (2) the stability of end products following Poly-PO_4 treatment.

1.2.2.3 Particulate-Phase Sequestration – Bismuth

This technology is focused on chemical sequestration, including U and Tc-99 as PCOIs and Sr, I-129, Cr, and nitrate as potential CoCOIs, via injection of bismuth (Bi)-based solid phase particulate amendments [i.e., bismuth oxyhydroxide (BOH) or BSN] (Boglaienko et al. 2024; Pearce et al. 2025; Lawter et al. 2021) as shown in Figure 1.9.

Bi-based materials can form a variety of layered and cluster structures that can accommodate a wide variety of cations and anions (Levitskaia et al. 2022; Perumal et al. 2022). Bismuth materials have been shown to remove contaminants, including U as uranyl carbonate complexes [e.g., at pH 8, $Ca_2UO_2(CO_3)_3$ and $CaUO_2(CO_3)_3^{2-}$], Tc-99 as TcO_4^-, Cr as chromate (CrO_4^{2-}), and I as iodate (IO_3^-), from a variety of geochemical environments (Lawter et al. 2021; Moore et al. 2020; Pearce et al. 2020, 2025). Figure 1.9 shows the sequestration of Tc-99 and U by BSN or BOH, with adsorption of Tc-99 as $Tc(VII)O_4^-$ and incorporation of U(VI) into interlayers of the Bi materials, which are both expected to transform to bismutite ($Bi_2CO_3O_2$) under the expected geochemical conditions. Once sequestered on or within Bi-based materials, contaminants would be immobilized as particles are not expected to move within pore spaces due to their size and density (BOH density 9.78 g/cm^3).

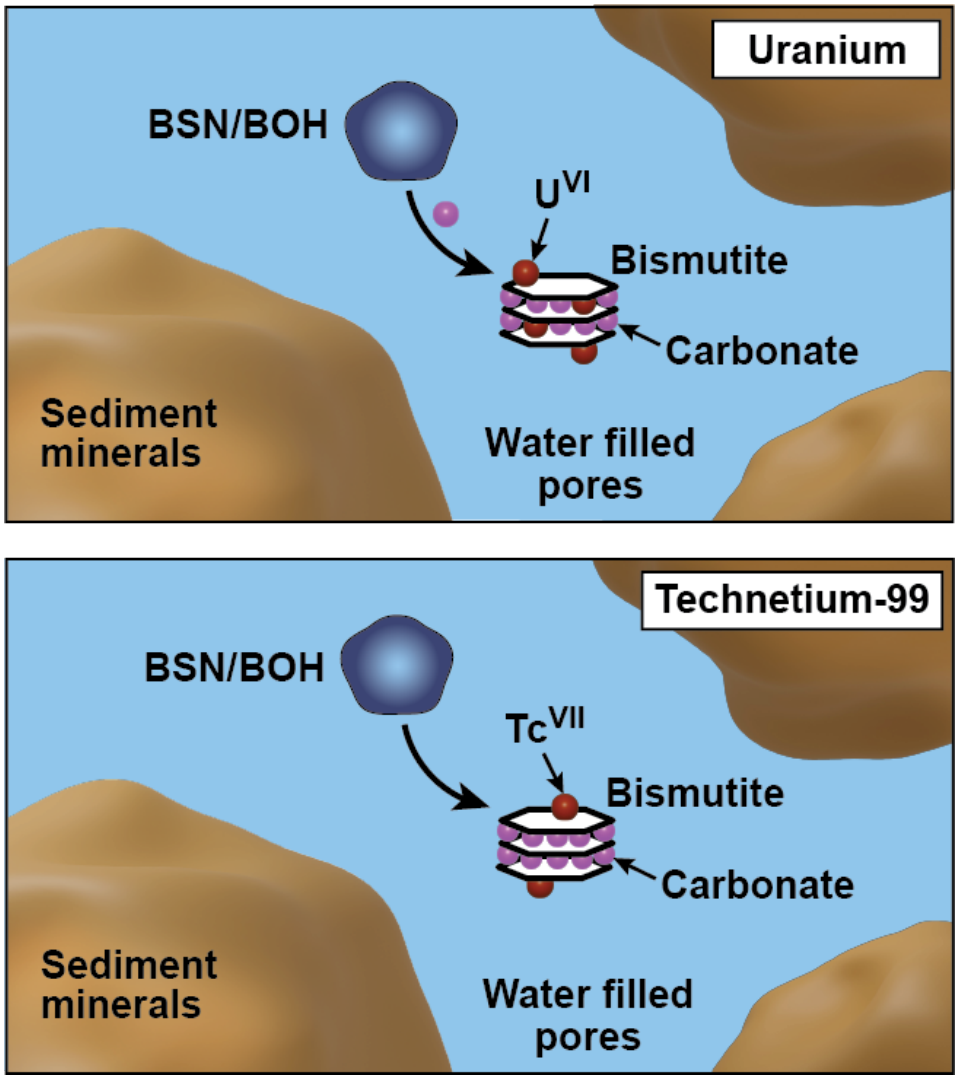

Figure 1.9. Sequestration of U (*top*) and Tc-99 (*bottom*) by Bi materials (BSN or BOH): transformation of BSN or BOH to bismutite and subsequent incorporation of U(VI) into the bismutite layers, or adsorption of U(VI) or $Tc(VII)O_4^-$ to the surface of the bismutite.

Laboratory research using solid phase BOH and BSN has shown potential for U and Tc-99 recovery and sequestration from solution in a variety of geochemical environments (Boglaienko et al. 2024; Lawter et al. 2021), but these materials have not been evaluated for U or Tc-99 sequestration under the targeted conditions for the 200-DV-1 OU (e.g., specific sediment and contaminant mixtures). In addition, BOH

has not been evaluated with delivery fluids. BSN has been evaluated for reactivity and suspendability (Muller et al. 2021b), but Cr was the only contaminant tested. The effects of site-specific conditions (e.g., sediment type and contaminant mixtures) as well as delivery fluid compatibility have yet to be tested for Bi-based materials.

The objectives of this study were to quantify (1) the extent and rate of sequestration of U and Tc-99 by adsorption and incorporation into BSN and (2) the stability of end products.

1.2.2.4 Liquid-Phase Sequestration – Calcium Citrate Phosphate and Polyphosphate

This technology is focused on chemical sequestration of U and Tc-99 as PCOIs and I-129, Sr, Cr, and nitrate as potential CoCOIs via injection of a liquid-phase amendment to form precipitates of calcium phosphate. Two formulations were selected for the initial phase of testing for this technology: (1) calcium-citrate/sodium-phosphate, Ca-Cit-PO_4; and (2) sodium-phosphate/polyphosphate, Poly-PO_4. These liquid phosphate amendments aim to sequester contaminants through a combination of adsorption, reduction, precipitation, and coating processes. Once sequestered on or within calcium phosphate precipitates (e.g., apatite), contaminants would be immobilized as particles are not expected to move within pore spaces due to their size and potential to coat sediment particles.

While both amendments slowly precipitate calcium phosphates following injection into the subsurface, they differ slightly in the biogeochemical reactions that lead to precipitation. Ca-Cit-PO_4 slowly precipitates apatite after biodegradation of citrate. Citrate is added because it strongly complexes with Ca, keeping it soluble during delivery of the amendment to the subsurface. Once the citrate is degraded, Ca is available to precipitate with PO_4 and form calcium phosphates. Citrate biodegradation also results in mild reducing conditions, which may reduce Tc-99 [Tc(VII) as TcO_4^-] and U(VI) aqueous species, leading to formation of low-solubility solid phases (+4 oxidation state as TcO_2 and UO_2). During subsequent precipitation, reduced Tc-99 and U phases may be adsorbed or coated by calcium phosphates, with remaining U(VI) also potentially being incorporated into calcium phosphates and/or forming autunite as depicted for Ca-Cit-PO_4 in Figure 1.10.

Poly-PO_4 reacts differently than Ca-Cit-PO_4 and slowly precipitates after PO_4 chains break apart and precipitate with Ca, as depicted in Figure 1.11. The PO_4 chains allow for delivery of the amendment to the subsurface before precipitation. The major difference between the two amendments is the mildly reducing conditions that form with Ca-Cit-PO_4 but not Poly-PO_4, which potentially enhances removal from the aqueous phase and sequestration of oxidized species of the PCOIs [e.g., Tc(VII)O_4^- and U(VI) carbonate species].

Chemical sequestration using these liquid-phase amendments has been successfully demonstrated previously in the field along the river corridor at the Hanford Site for both U and Sr via Ca-Cit-PO_4 and for U via Poly-PO_4 (PNNL-19524; PNNL-29650; PNNL-18529; Vermeul et al. 2014; SGW-47062; SGW-59614; SGW-63113). Other sites have also implemented these technologies for U sequestration (PNNL-25303; Lammers et al. 2017; Fuller et al. 2003). In addition, treatment via Poly-PO_4 and dihydrogen phosphate (NaH_2PO_4) has been shown to perform well in water-saturated Hf sediments for U at the laboratory scale (PNNL-65124; Pan et al. 2016). Ca-Cit-PO_4 also performed well at the laboratory scale for Sr (Robinson et al. 2023). However, these technologies have not been implemented at the field scale in the presence of the other PCOI (Tc-99) or CoCOIs (except Sr). Moreover, there is only limited data showing (1) Tc-99 is not removed from solution during apatite formation without a reductant and (2) there is potential for substitution of C-14 into the apatite structure via carbonation at the laboratory scale (PNNL-28054; Heslop et al. 2005).

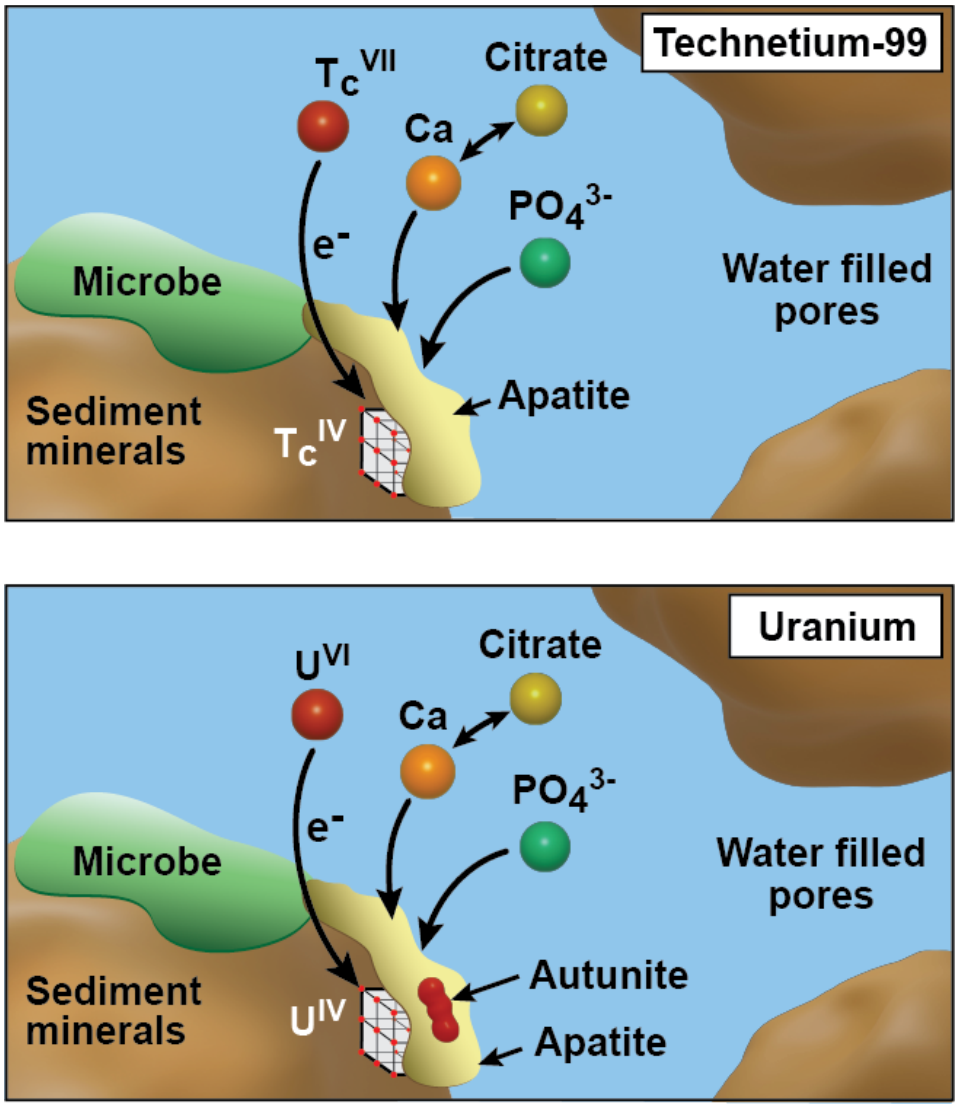

Figure 1.10. Sequestration of Tc-99 (*top*) and U (*bottom*) in the saturated zone by treatment with a solution of Ca-Cit-PO_4 occurs simultaneously via the following processes: citrate biodegradation to generate conditions for aqueous $Tc(VII)O_4^-$ and U(VI) reduction and precipitation as Tc(IV) and U(IV), citrate degradation leaving Ca available to precipitate with PO_4 and form apatite, leading to coating of Tc(IV) and U(IV) by apatite as well as incorporation of U(VI) into autunite and apatite phases.

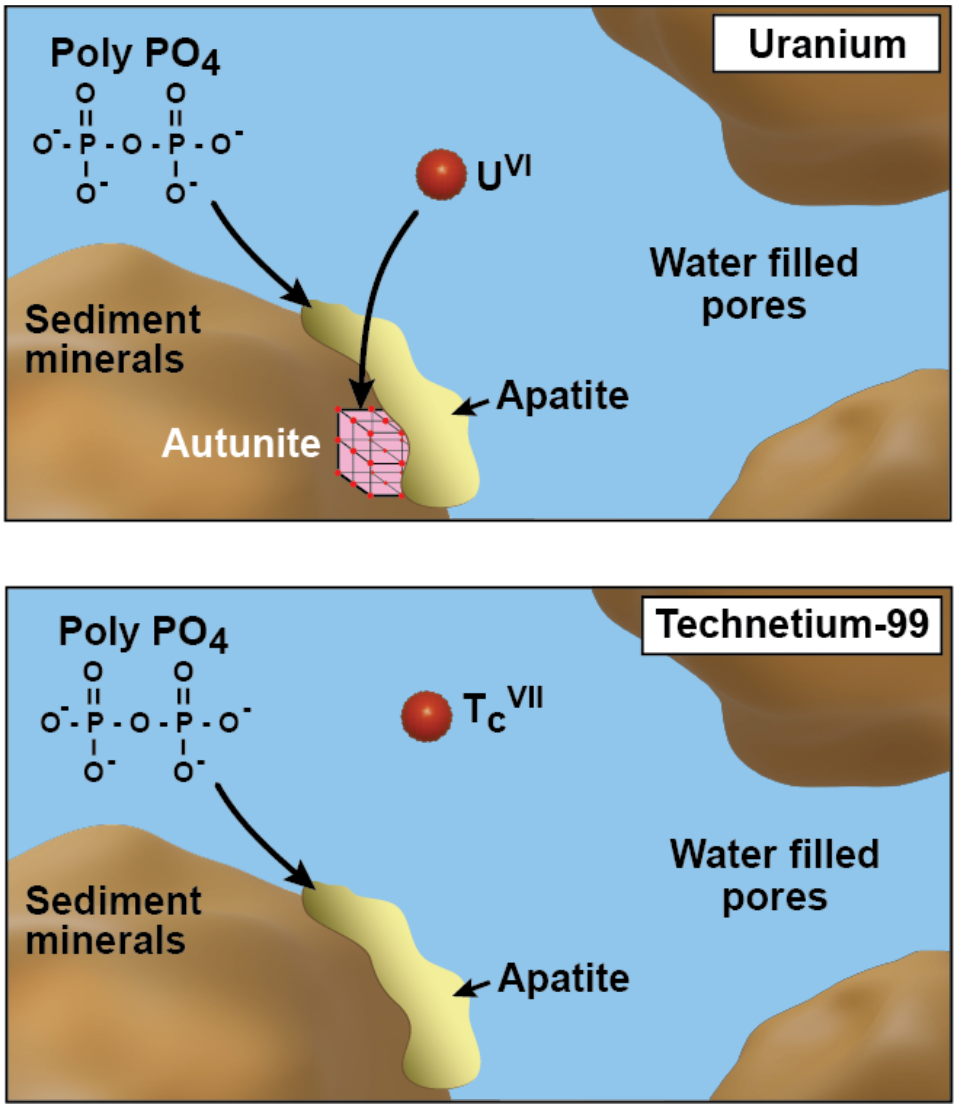

Figure 1.11. Sequestration of U (*top*) and Tc-99 (*bottom*) in the saturated zone by treatment with a Poly-PO_4 solution via the following processes: aqueous U(VI) incorporation into apatite and formation of autunite precipitates along with coating of adsorbed and precipitated U(VI) by apatite and limited adsorption of aqueous TcO_4^- to sediments with coating by apatite.

The objectives of this study were to quantify (1) the extent and rate of sequestration of U (primarily via adsorption, co-precipitation, and coating) and Tc-99 (via reductive precipitation and coating) by Ca-Cit-PO_4 and (2) the stability of end products. Although Ca-Cit-PO_4 was chosen for additional testing in the liquid-phase chemical sequestration technology, Poly-PO_4 was chosen to advance as the sequestration step in the following technologies: particulate-phase combined chemical, liquid-phase combined chemical reduction and sequestration, and liquid-phase combined bioreduction and sequestration. The formulations for Ca-Cit-PO_4 and Poly-PO_4 are based on previous optimization for injection in the Hanford Site's 100 Area and 300 Area, respectively (PNNL-19524; PNNL-29650; PNNL-18529; Vermeul et al. 2014; SGW-47062; SGW-59614; SGW-63113).

1.2.2.5 Liquid-Phase Chemical Reduction and Sequestration – Calcium Polysulfide and Polyphosphate

This technology is focused on a two-step chemical reduction and sequestration of PCOIs including U and Tc-99 alongside I-129, Sr, Cr, and nitrate as potential CoCOIs via sequential injection of two liquid-phase amendments, including calcium polysulfide (CPS) to initiate reducing conditions followed by Poly-PO_4 to form apatite (Figure 1.12 and Figure 1.13 for Tc-99 and U, respectively). The CPS amendment is added to initially reduce PCOIs to lower solubility oxidation states. Reduction may be direct (electron transfer from the polysulfide) or indirect (via secondary species like iron sulfides). Next, the Poly-PO_4 is added to sequester contaminants for the long-term via a combination of processes including adsorption, precipitation, and coating. This technology differs from the Ca-Cit-PO_4 technology in that sequential injections of CPS and then Poly-PO_4 are performed for this technology, while the Ca-Cit-PO_4 is added altogether and initiates mildly reducing conditions during apatite precipitation due to the natural microbes consuming available oxygen. The concentration of the CPS can also be changed based on PCOI and CoCOI concentrations, whereas with the Ca-Cit-PO_4 technology, the generation of reducing conditions is dependent on natural microbes that consume oxygen during respiration while degrading the citrate.

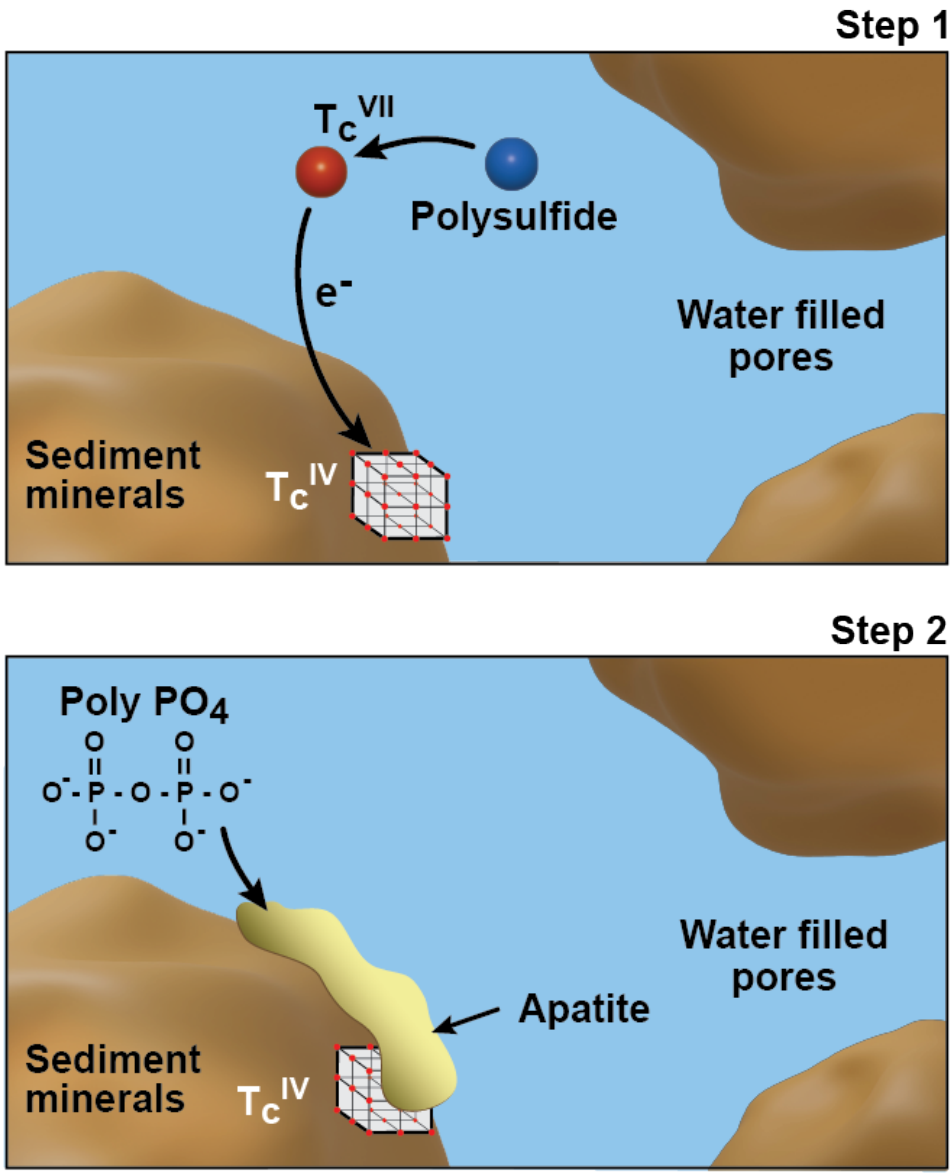

Figure 1.12. Sequestration of Tc-99 in the saturated zone via treatment with sequential solutions of CPS followed by sodium Poly-PO_4 via the following processes: (step 1, *top*) aqueous $Tc(VII)O_4^-$ reduction by sulfide followed by reductive precipitation as Tc(IV) with (step 2, *bottom*) subsequent injection of Poly-PO_4 for coating of Tc(IV) by apatite.

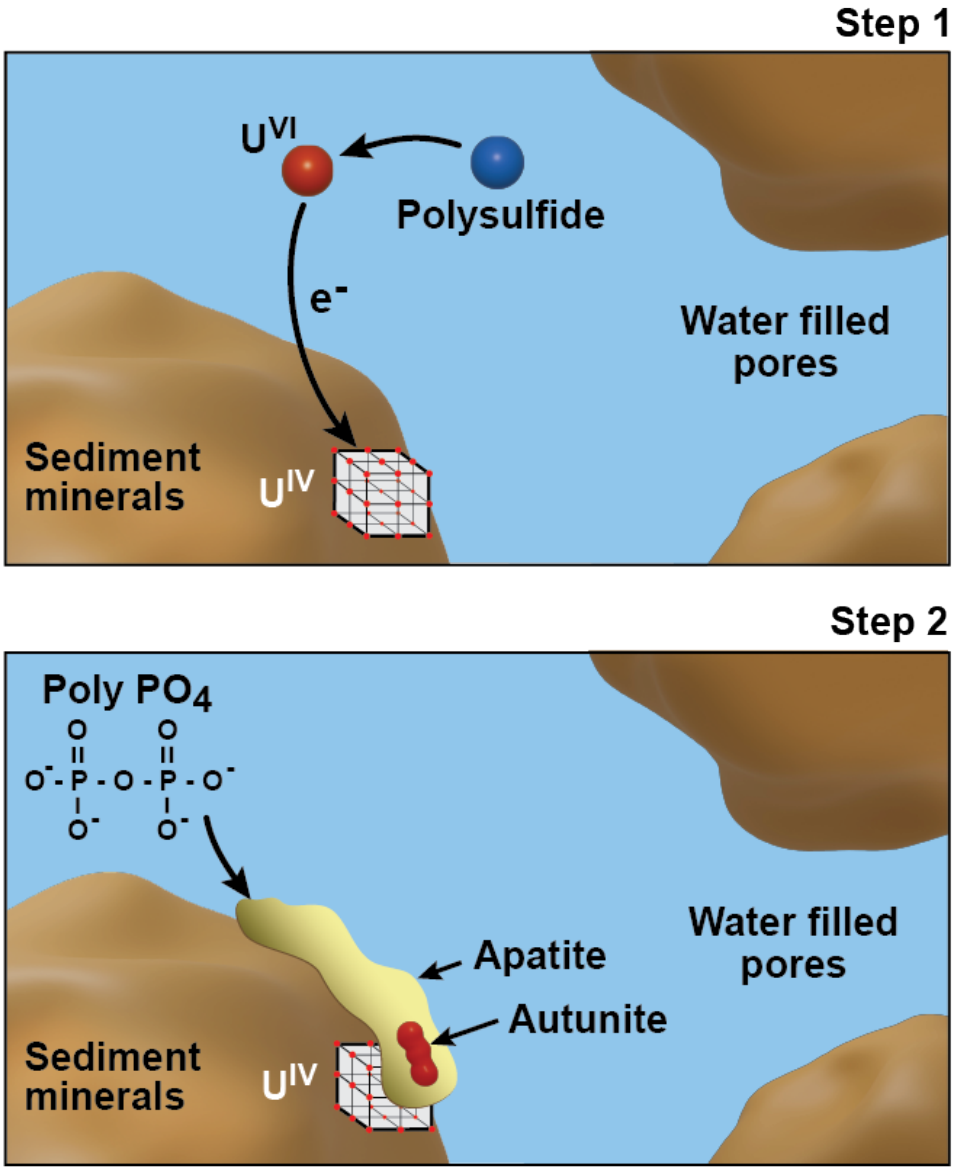

Figure 1.13. Sequestration of U in the saturated zone via treatment with sequential solutions of CPS followed by Poly-PO_4 via the following processes (step 1, *top*) injection of CPS for reduction of aqueous and adsorbed U(VI) species by sulfide and precipitation of U(IV) followed by (step 2, *bottom*) subsequent coating of precipitated U(IV) and adsorbed U(VI) by apatite and/or incorporation of U(VI) species in apatite and autunite.

Chemical reduction using CPS has been demonstrated previously for Cr (Zhang et al. 2020; Chrysochoou et al. 2010), with some testing for Tc-99 and U with CPS followed by a second apatite chemical sequestration step at the laboratory scale, including preliminary testing with Hanford Site sediments (PNNL-31959; PNNL-17674). However, these technologies have yet to be used in tandem at the field scale. Chemical sequestration using liquid-phase Poly-PO_4 has been demonstrated previously by itself in the field along the river corridor at the Hanford Site for both U and Sr (SGW-59614; SGW-63113; PNNL-19524; PNNL-29650), and other sites have implemented it for U sequestration (Lammers et al. 2017; Fuller et al. 2003; PNNL-25303). In addition, treatment performed well in water-saturated Hf sediments for U at the laboratory scale (Pan et al. 2016; PNNL-65124). However, the sequestration technology has not been implemented at the field scale in the presence of the other PCOI (Tc-99) or

CoCOIs (except Sr). Moreover, there is only limited data showing (1) Tc-99 is not removed from solution during apatite formation without a reductant and (2) there is potential for substitution of carbonate into the apatite structure via carbonation at the laboratory scale (Heslop et al. 2005; PNNL-28054).

The objectives of this study were to quantify (1) the extent and rate of sequestration of Tc-99 (via reductive precipitation and coating) and U (primarily via adsorption, co-precipitation, and coating) by CPS and Poly-PO_4 and (2) the stability of end products.

1.2.2.6 Liquid-Phase Bioreduction and Sequestration – Molasses and Polyphosphate

This technology is focused on a two-step bioreduction and chemical sequestration of PCOIs U, Tc-99, and nitrate, alongside I, Sr, and Cr as potential CoCOIs via injection of two liquid-phase amendments. This technology begins with the introduction of an organic substrate into the treatment zone to sustain anaerobic microbial activity and dissimilatory reductive processes, which catalyze the reduction of soluble, oxidized contaminant species to less mobile forms of U and Tc-99, or gaseous, non-toxic forms for nitrate (e.g., formation of N_2 or NH_3 from NO_3^-). This is followed by the application of a Poly-PO_4 solution for sequestration as described in Section 1.2.2.4. Figure 1.14 and Figure 1.15 present conceptual diagrams of these steps for Tc-99 and U, respectively.

In situ bioremediation by injecting a readily available carbon/energy source (i.e., organic electron donor) is an effective means of decreasing aqueous concentrations of inorganic contaminants in the subsurface. Organic carbon supplies in the subsurface are generally present at low concentrations (< 4 mg/L) (Regan et al. 2017; Konopka et al. 2013); therefore, alleviating this limitation rapidly stimulates indigenous microbial metabolism and growth. Numerous studies have validated this remedial approach by coupling substrate oxidation with respiratory reduction of inorganic contaminants to less soluble species (Newsome et al. 2014). Successful demonstrations have been performed for U at the Old Rifle Processing Site (CO, USA) – though reducing conditions were not maintained long term (Williams et al. 2011), and for U, Tc-99, and nitrate at the Oak Ridge Reservation (TN, USA) (Istok et al. 2004). Unlike Cr(VI), which reduces to highly stable, insoluble Cr(III) (Rahman and Thomas 2021), U and Tc-99 are challenging because reduced species can rapidly re-oxidize and remobilize if the system returns to oxic conditions (e.g., Komlos et al. 2008; Newsome et al. 2014). Therefore, stabilization of Tc-99 and U may require an additional treatment step post-reduction to coat or incorporate these reduced species into a stable form (e.g., phosphate minerals).

Chemical sequestration using liquid-phase Poly-PO_4 has been successfully demonstrated previously by itself in the field along the river corridor at the Hanford Site for both U and Sr (SGW-59614; SGW-63113; PNNL-19524; PNNL-29650), and other sites have implemented it for U sequestration (Lammers et al. 2017; Fuller et al. 2003; PNNL-25303). Poly-PO_4 treatment has been shown to perform well in water-saturated Hf sediments for U at the laboratory scale (Pan et al. 2016; PNNL-65124). However, the sequestration technology has not been implemented at the field scale in the presence of other PCOIs and CoCOIs (e.g., Tc-99, I, Cr, NO_3). Moreover, there is only limited data showing (1) Tc-99 is not removed from solution during apatite formation without a reductant and (2) there is potential for substitution of carbonate into the apatite structure via carbonation at the laboratory scale (Heslop et al. 2005; PNNL-28054). Notably, these two remediation methods have not been previously tested in combination.

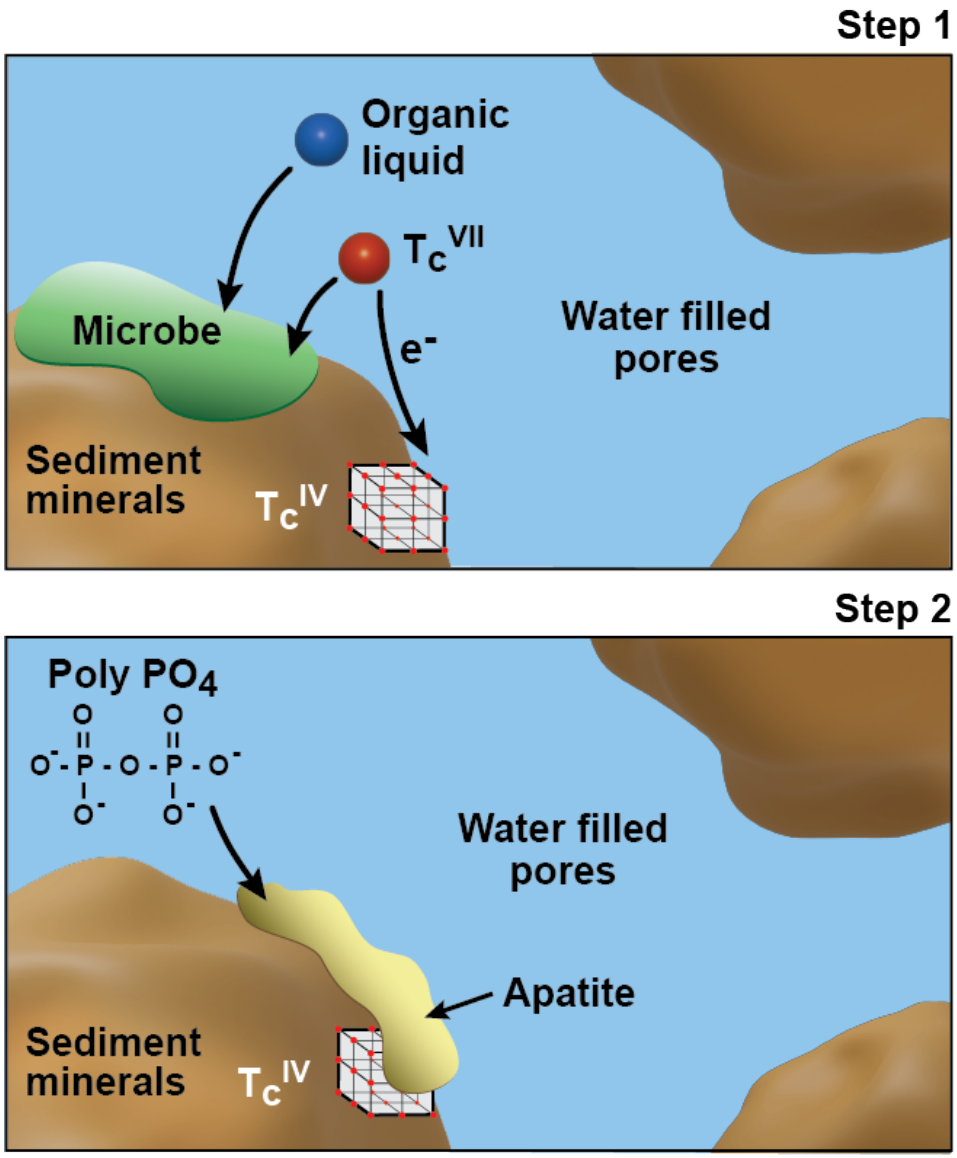

Figure 1.14. Sequestration of Tc-99 in the saturated zone via sequential solutions of an organic substrate followed by Poly-PO_4 where (step 1, *top*) an organic substrate is injected and stimulates microbial activity to generate reducing conditions to reductively precipitate aqueous $Tc(VII)O_4^-$ as Tc(IV) followed by (step 2, *bottom*) injection of Poly-PO_4 solutions for subsequent coating of Tc(IV) by apatite.

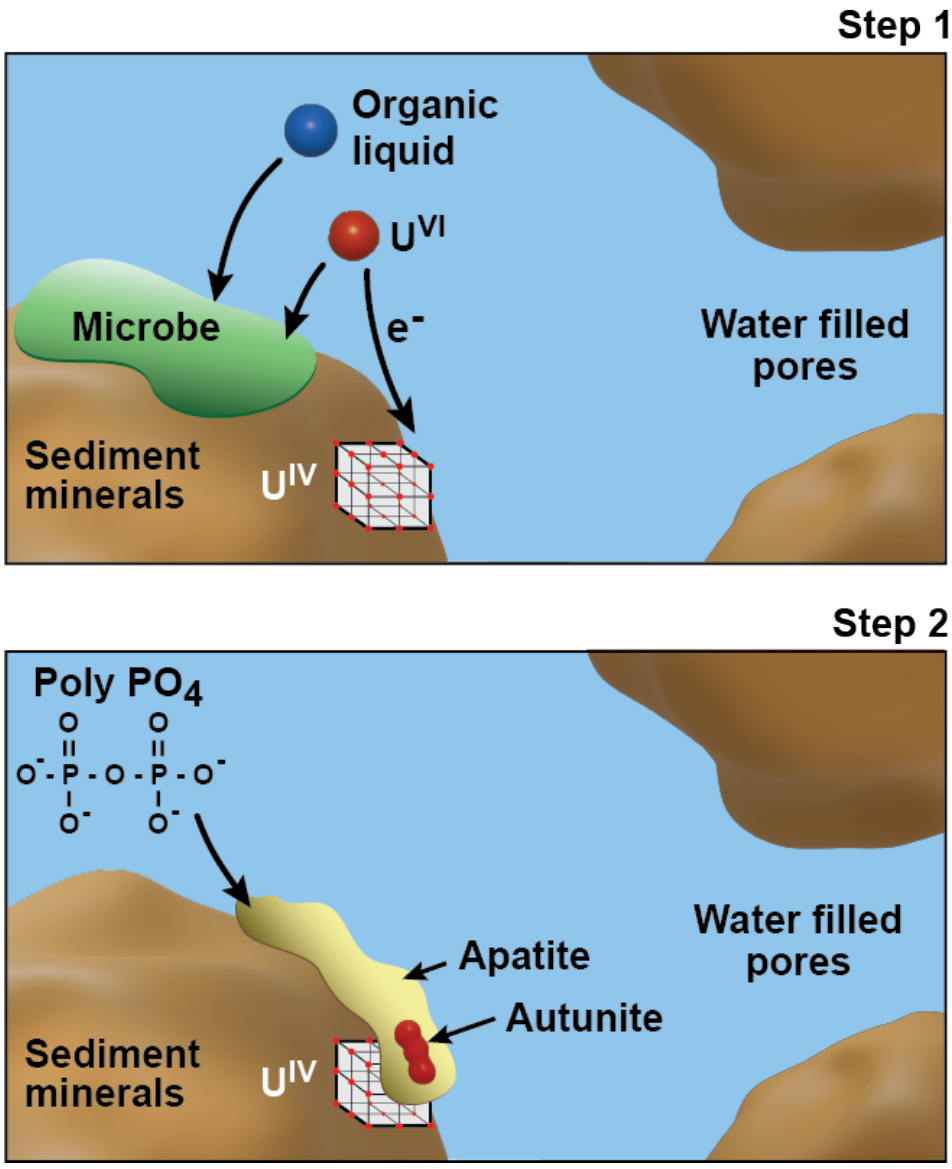

Figure 1.15. Sequestration of U in the saturated zone via sequential solutions of an organic substrate followed by Poly-PO_4 where (step 1, *top*) an organic substrate is injected and stimulates microbial activity to generate reducing conditions to reductively precipitate aqueous U(VI) as U(IV) followed by (step 2, *bottom*) injection of Poly-PO_4 solutions for subsequent coating of precipitated U(IV) and adsorbed U(VI) by apatite and/or incorporation of U(VI) species in apatite and autunite.

The objectives of this study were to quantify (1) the extent and rate of reduction and sequestration of U and Tc-99 and transformation of NO_3^- via biostimulation with organic liquids and (2) the stability of end products (for U and Tc-99).

1.3 Summary of Phase 1 Conclusions and Recommendations

The project team evaluated the results of Phase 1 testing (PNNL-35432) to assess the nine different technologies. To evaluate each technology, the project team used a threshold of 35% transformation to immobile or nontoxic end products as an initial indicator of performance. However, these thresholds were not an absolute factor in determining the decision as the overall evaluation included a holistic evaluation of all results alongside expert judgement to determine whether they were recommended for Phase 2 and 3 testing of the treatability studies. The following discussion summarizes the conclusions and recommendations for each technology.

The three gas-phase technologies targeted different contaminants in the VZ:

1. **Combined bioreduction and sequestration of Tc-99 by sequential treatment with organic gas followed by CO_2 gas**: Technology did not meet treatment criteria for further testing, though some sequestration of Tc-99 was observed. High (66-88%) sequestration of a CoCOI (Cr) was observed for butane, ethane, and butyl acetate treatments.
2. **Bioreduction of nitrate by organic gases**: Technology met 35% minimum transformation to temporarily immobile, immobile, or nontoxic end products and will advance to Phase 2 and 3 testing. Butyrate and ethane gas amendments were recommended because they showed superior performance to butane and pentane. Butyrate was not used for Phase 2 and 3 experiments due to very low volatility (i.e., inability to inject sufficient gas mass).
3. **Sequestration of I-129 by CO_2 gas**: Technology met 35% minimum transformation to temporarily immobile, immobile, or nontoxic end products and will advance to Phase 2 and 3 testing.

The three particulate-phase technologies are recommended for Phase 2 and 3 testing, including:

1. Chemical sequestration by Sn(II)-PO_4
2. Chemical sequestration by BOH or BSN with down-selection to BSN (due to its superior performance for Tc-99)
3. Combined chemical reduction and sequestration by ZVI or SMI (with down-selection to SMI due to its faster reduction of Tc-99) followed by treatment with apatite-forming solutions (as Poly-PO_4)

The three liquid-phase technologies are all recommended for Phase 2 and 3 testing, including:

1. Chemical sequestration by Poly-PO_4 or Ca-Cit-PO_4 solutions with down-selection to Ca-Cit-PO_4 (due to its superior performance for Tc-99)
2. Combined chemical reduction and sequestration by CPS followed by treatment with apatite-forming solutions (as Poly-PO_4)
3. Combined bioreduction and sequestration by organic liquids (with down-selection to molasses) followed by treatment with apatite-forming solutions (as Poly-PO_4)

Each amendment was tested with the PCOIs, including Tc-99 and U, and with and without potential CoCOIs, including Sr-90, I-129, Cr, and nitrate. All of these technologies are recommended to advance to Phase 2 and 3 testing. The Poly-PO_4 technology will continue to be the sequestration step for all reduction/sequestration technologies due to its performance for sequestration of U.

These results were used to inform testing for Phases 2 and 3 of this treatability study for further evaluation of selected technologies. The final results from the treatability study, following the completion of remaining experimental phases, were used to determine whether the technologies tested can be appropriately evaluated in an FS to expand on the limited number of viable DVZ remediation technologies. Recommendations are summarized in Section 4.0. After completion of the laboratory treatability study and the 200 DV-1 OU remedial investigation and RFI of the waste sites, results will be evaluated to determine whether field studies are needed to provide additional information on performance, implementability, or costs for evaluating these technologies in the FS for their site-specific application.

2.0 Materials and Methods

2.1 Sediments

Three groups of sediments were used for this work: (1) VZ sediments from specific cores, (2) composite sediments representing saturated locations (i.e., BY Cribs water table and perched water below the B Complex), and (3) an uncontaminated Hf sediment. The sediments were analyzed for particle size distribution (Table 2.1), mineralogy by X-ray diffraction (XRD) (Table 2.2), and surface area (Table 2.3) based on the Brunauer-Emmett-Teller (BET) method (Brunauer et al. 1938). Additional information about analysis methods and the characterization data is summarized in Appendix A of the Phase 1 report (PNNL-35432).

The VZ sediments – collected from BY Cribs at 32-m (106-ft) depth and 216-S-9 Cribs at 20-m (64-ft) and 38- to 39-m (125- to 127-ft) depths – were used for the majority of the testing conducted under unsaturated conditions. These sediments were chosen because they were collected from DV-1 sites of interest for these technologies and included representative contamination, as summarized previously (PNNL-35432). Initial characterization of cores from the same boreholes at similar depths is included in additional reports and is consistent with data for these specific core depths (PNNL-27524; PNNL-24709). Sediment from the 216-S-9 Crib was obtained from borehole C9512 (64 to 65 ft, Hf H1/H2 and 125 to 127 ft bgs, H2 and Cold Creek unit silt transition, PNNL-24709).

Two composite sediments – Cold Creek Unit gravel (CCug) and perching zone sand (CCu-PZsd) – were used for the majority of testing for water-saturated conditions as described in Section 2.4. These two composite sediments were generated to represent the two formations targeted for saturated areas of the subsurface, based on the locations of the BY Cribs water table and perched water below the B Complex. The sediment was homogenized from cores within those layers (which are included within the Hf) from previous DV-1 characterization campaigns for the D0112 borehole (SGW-67996; PNNL-35432).

An uncontaminated Hf sediment was procured from a gravel pit in Pasco, WA. This sediment was used for select experiments for all technologies as it is representative of the Hf, which covers a significant portion of the VZ in the Central Plateau subsurface and represents similar mineralogy across the different formations within the saturated zones. The Hf sediments are coarse-textured silty-sandy-gravels consisting of approximately 50% gravel, 40% sand, and 10% silt (DOE/RL-88-09) and are composed primarily of quartz, feldspars, and ferromagnesian minerals (DOE/RL-92-24). These compositions are consistent with the characterization of sediments used for this testing to represent the Hf.

All sediments were stored double-bagged in a cool, climate-controlled environment until use. All experiments used the < 2-mm size fraction, unless otherwise noted.

Table 2.1. Wentworth particle size distribution based on laser particle size analysis (of the < 2-mm size fraction from sieving) (Wentworth 1922).

Classification	Hf	CCug	CCu-PZsd	216-S-9 (B)[a]	216-S-9 (C)[a]	BY
Gravel (> 2 mm)	3.6	6.4	0	0	0	3.3
Sand (2 mm to 63 µm)	96.2	78.4	38.3	56.8	68.3	86.7
Silt/Clay (< 63 µm)	0.2	15.2	61.7	43.2	31.7	9.9

(a) Two cores were opened from 216-S-9; Batch "B" was used for CO_2 experiments, and batch "C" was used for NO_3 columns.

Table 2.2. X-ray diffraction of the < 2-mm size fraction of sediments. Note: Amorphous fraction subtracted from total to estimate crystalline mineral fractions. These data are For Information Only.

Mineral Name	Hf	CCu-PZsd	CCug	216-S-9 (B)[a]	216-S-9 (C)[a]	BY
Quartz	32.7%	39.5%	31.8%	40.8%	35.5%	34.7%
Feldspar	49.5%	40.1%	48.4%	40.9%	47.4%	48.8%
Mica	5.0%	7.8%	6.7%	6.9%	8.3%	6.3%
Amphibole	4.0%	4.9%	2.5%	5.3%	2.2%	3.8%
Pyroxene	5.9%	1.7%	6.4%	1.9%	2.6%	1.3%
Chlorite	2.9%	6.0%	4.2%	4.1%	3.9%	4.9%

(a) Two cores were opened from 216-S-9; Batch "B" was used for CO_2 experiments, and batch "C" was used for NO_3 columns.

Table 2.3. BET surface area measurements on the < 2-mm size fraction of sediments. Note: These data are For Information Only.

Sediment	Surface Area (m^2/g)
Hf	11.4 ± 2.0
CCug	7.2 ± 1.6
CCu-PZsd	8.0 ± 0.2
216-S-9 (B)[a]	6.0 ± 0.1
216-S-9 (C)[a]	7.5 ± 0.5
BY	2.6 ± 0.7

(a) Two cores were opened from 216-S-9; batch "B" was used for batch experiments, and batch "C" was used for static columns.

2.2 Background Solutions

Synthetic groundwater (SGW), synthetic perched water (SPW), and artificial pore water were prepared based on relevant historical monitoring data from the Central Plateau (PNNL-28054; Lawter et al. 2021). Targeted contaminant concentrations were also based on historical data. These site-specific simulants were used for testing each technology based on the targeted treatment locations (i.e., groundwater,

perched water, or VZ for pore water). During technology testing, not all contaminants were included and/or were adjusted based on specific testing needs for each scenario, with any deviations noted in the experimental methods for the individual technology. For example, in the case of Tc-99, specific contaminant solid-phase concentrations were targeted (i.e., µg/g Tc-99), and higher concentrations of aqueous Tc-99 were needed in unsaturated experiments [i.e., at 4 wt% water content (WC) or 0.04 mL/g] compared to water-saturated experiments, which had 2 mL/g of sediment.

The artificial pore water used for unsaturated experiments approximates the composition of Hanford Site 200 Area VZ pore water based on cation and anion averages of pore water extractions from sediments (Table 2.4) (PNNL-24297). The representative SGW is based on cation and anion averages of 54 well samples from the 200-UP-1 and 200-ZP-1 OUs from 2010 to 2018 (Lawter et al. 2021) (Table 2.5), and the SPW is based on cation and anion data from monitoring wells (299-E33-18, 299-E33-205, and 299-E33-341 to 345) in the 200-BP-5 OU for the period from 2010 to 2015 (PNNL-28054) (Table 2.6).

Table 2.4. Artificial pore water with pH adjustment to pH 7.0 to 7.2.

Constituent	Concentration (mmol/L)
$CaSO_4$	12
NaCl	1.7
$NaHCO_3$	0.4
$NaNO_3$	3.4
$MgSO_4$	2.6
$MgCl_2$	2.4
KCl	0.7

Table 2.5. Synthetic groundwater with pH adjustment to approximately 7.8.

Constituent	Concentration (mmol/L)
$MgSO_4$	0.37
$MgCl_2$	0.25
$CaCl_2$	1.07
$KHCO_3$	0.12
$NaHCO_3$	1.59

Table 2.6. Synthetic perched water with pH adjustment to approximately 8.2.

Constituent	Concentration (mmol/L)
$CaSO_4$	0.56
$MgSO_4$	2.7
Na_2SO_4	1.74
NaCl	3.30
$NaHCO_3$	10.71
$KHCO_3$	0.31

2.3 Vadose Zone Experiments

Phase 2 and 3 laboratory-scale experiments for immobilization and/or transformation of PCOIs and CoCOIs with technologies targeting VZ (unsaturated) conditions were conducted primarily with columns. Gas-phase amendments were injected into columns containing sediment at low WC (1% to 8%). The change in contaminant mobility after 1 to 150 days of reaction time was evaluated by sequential extractions, water-saturated leach, infiltrated leach (moderate water saturation), and pressurized unsaturated flow (PUF) experiments (Figure 2.1). Each type of experiment tests different conditions in which amendments may interact with sediments and PCOIs (with and without CoCOIs) under VZ conditions with differences in WC and reaction time based on water flux rates. For additional experimental details, see Appendix D and Appendix E. Control columns without treatment but with PCOIs (with and without CoCOIs) were also conducted for each technology. All amendment (treated) column and batch experiments were conducted in duplicate unless otherwise noted.

Although these experiments were conducted under site-specific conditions (including field sediments and SGW and contaminant concentrations based on site conditions), contaminant partitioning and rates of immobilization and/or transformation were not directly translatable to the field due to potential differences in scale, heterogeneity, and fluctuations in flow and contaminant concentrations. Additional batch experiments (lasting up to approximately 1 year) were conducted to qualitatively examine the sequestration of PCOIs with variable contact times with amendments, which may fluctuate significantly depending on the vertical and horizontal movement of water in the VZ as well as the volume of the subsurface that could be treated.

The WC used in experiments for VZ technologies (4 and 8 wt%) was based on the average field WC of B-, S-, and T-Complex VZ sediments (4.28 ± 1.68 wt%, based on 17 sediments) previously evaluated (PNNL-26208; PNNL-27524). Finer grained zones are at higher field WC. (VZ sediments have been measured as high as 15 wt%, and water saturation varied from 18 to 21 wt%.) Therefore, for some technologies, an additional 8 wt% WC was used. Similarly, units with significant amounts of gravel have lower water contents (as low as 2.1 wt% WC), so for some technologies, 2 wt% WC was used for selected experiments.

2.3.1 Gas-Phase Chemical Sequestration

The approach for the gas-phase chemical sequestration technology is to inject CO_2 gas into the VZ. The injected CO_2 gas subsequently partitions into VZ pore water and precipitates calcite, which can incorporate some contaminants such as I-129 (as iodate), U, and Cr (as chromate). Although the CO_2 gas supplies carbonate, the calcium needs to be provided by ion exchange sites on sediments and/or dissolving carbonate phases. Waste sites that were exposed to significant acidic CoCOIs, such as 216-U-8 Crib, can be somewhat to significantly depleted in calcium as well as carbonate because the acids may have dissolved and flushed ions to greater depths.

In laboratory experiments in this study, Hf and 216-S-9 sediments with 2 wt% WC (coarser sediment zones), 4 wt% WC (VZ average), and 8 wt% WC (higher WC characteristic of finer grain zones) were packed into columns 1.3- to 2.6-cm (0.5- to 1-in.) diameter by 16-cm (6.3-in.) long. Each column was injected with 10 to 30 pore volumes (PVs, depending on water content) of 100% CO_2 gas over the course of 5 minutes. Using Henry's law partition coefficient for CO_2, the retardation factor (R_f) of CO_2 gas is 1.26 at 4 wt% WC and R_f = 1.74 at 8 wt% WC. The volume of gas injected (10 PVs for 4 wt% WC and 30 PVs for 8 wt% WC sediments) was chosen to ensure gas-pore water equilibrium was achieved in all of the sediment. Column ends were then sealed, and no flow occurred for 60 days to allow calcite to precipitate.

At 60 days, 10 to 30 PVs of air was injected into the columns to simulate return to natural pore water pH conditions. Columns were sealed again and had no flow for an additional 90 days. After this, batch sequential extractions were conducted for some sediments, and three different types of columns were conducted to evaluate the change in contaminant mobility from the treatment (Figure 2.1: (1) water-saturated leach, (2) infiltration leach, and (3) pressurized unsaturated flow (PUF) infiltration leach as depicted in Figure 2.1 with the experimental matrix in Table 2.7. Additional experimental details are presented in Appendix D, Section D.1.

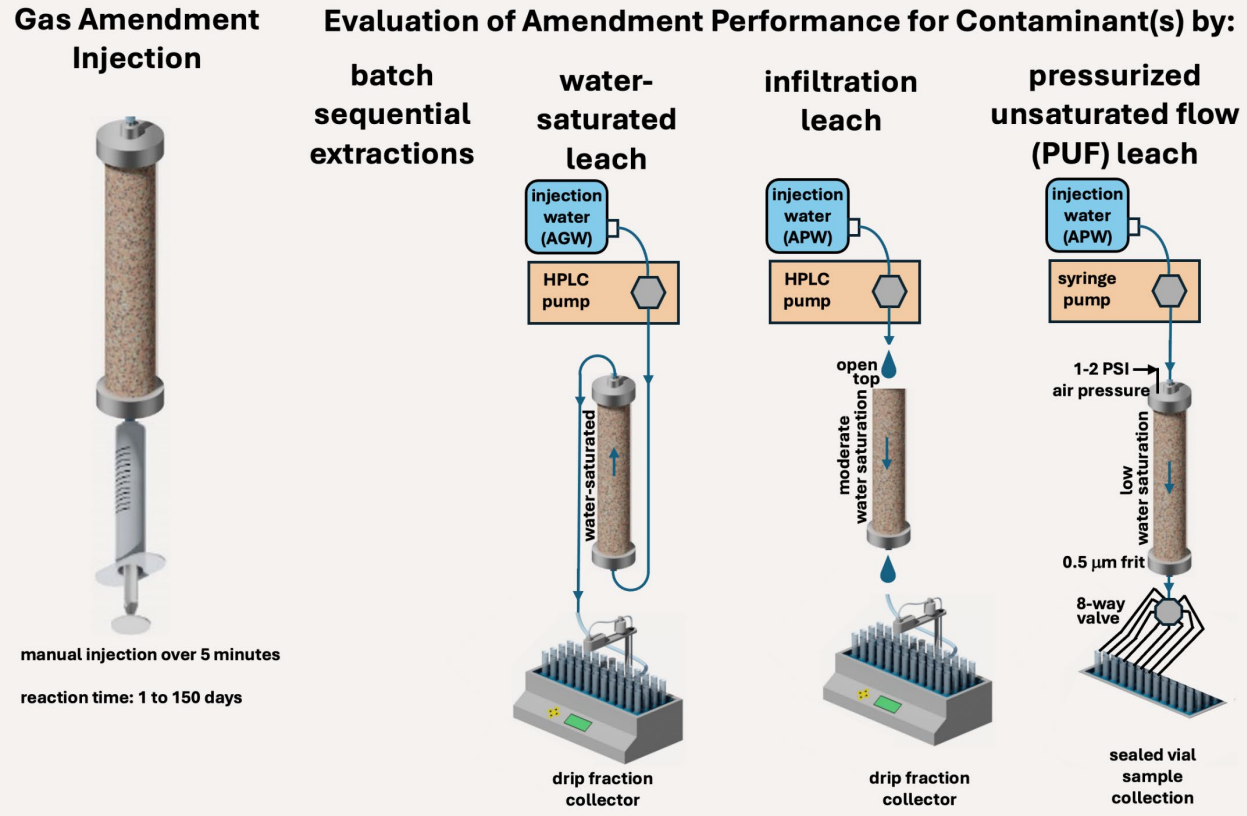

Figure 2.1. Conceptual diagram of experimental setup for unsaturated column testing, including gas injection (*left*) and performance evaluation (*right*) by sequential extractions or leaching in columns at different water content.

Table 2.7. Batch and column experiments conducted with CO_2 gas.

Sediment	Type	WC (%)	Treatment	Sequestration Evaluation
Hf	Batch	8	No treatment control[(a)]	Sequential extractions (150 days)
	Batch	8	60 days CO_2, 90 days air	Sequential extractions (30, 60, 150 days)
	Column	4	No treatment control[(a)]	Water-saturated leach
	Column	4	60 days CO_2, 90 days air	Water-saturated leach
216-S-9	Batch	8	No treatment control[(a)]	Sequential extractions (150 days)
	Batch	8	60 days CO_2, 90 days air	Sequential extractions (30, 60, 150 days)
	Batch	2	No treatment control[(a)]	Sequential extractions (150 days)
	Batch	2	60 days CO_2, 90 days air	Sequential extractions (up to 150 days)
	Column	4	No treatment control[(a)]	Water-saturated leach
	Column	4	60 days CO_2, 90 days air	Water-saturated leach
	Column	4	No treatment control[(a)]	Infiltration leach
	Column	4	60 days CO_2, 90 days air	Infiltration leach
	Column	4	No treatment control[(a)]	PUF leach
	Column	4	60 days CO_2, 90 days air	PUF leach

(a) No gas addition, controls contain air.

2.3.2 Gas-Phase Bioreduction

The strategy for gas-phase bioreduction is to inject an organic gas into unsaturated sediments (4 and 8 wt% WC) to stimulate microbe activity that will subsequently transform nitrate into gaseous nontoxic end products (e.g., N_2O, N_2, NH_3 in order of increasing reduction). Testing evaluated NO_3^- transformation under varying conditions, including different nitrate concentrations, water saturation levels, and the presence of a CoCOI (i.e., Cr). Measurements of NO_3^- and potential intermediate species (e.g., NH_4^+) were used to quantify the magnitude of removal or transformation of NO_3^-. Ethane was selected over butyrate as the primary gas for Phase 2 and 3 testing because ethane's higher volatility and lower solubility make it more suitable for delivering large volumes to the subsurface during a field application.

Batch experiments were designed to investigate NO_3^- transformation across a wide range of concentrations, while static columns focused on constant nitrate concentrations with and without the addition of Cr as a CoCOI (Figure 2.2). The starting concentrations for NO_3^- and Cr were selected based on values relevant to the VZ sediments at the Hanford Site (PNNL-35629; Szecsody et al. 2023). For the static columns, the average values were used to reflect typical site conditions. The average NO_3^- concentration in the 200 Area VZ sediments is ~100 µg/g NO_3^-. For Cr, the starting concentration in the experiments was 1.6 µg/g, which represents the average leachable Cr. There is only a small fraction of natural Cr in 100-D and 200 East Areas of the VZ that is leachable. In contrast, batch experiments focused solely on NO_3^- encompassed both the lowest (background NO_3^-) and highest (10,000 µg/g) concentrations observed at the site.

A detailed experimental design and methodology for this technology is summarized in Appendix E, Section E.1. All experiments were conducted in duplicate using VZ sediments from 216-S-9 Crib (C9512) utilizing cores from 38 to 39 m (125 to 127 ft) bgs, except for timepoint 0 for batch experiments that included triplicate measurements. 216-S-9 sediment was subsampled directly from bulk core material without sieving to maintain representative native microbiological complexity. Initially, sediments were spiked with the PCOIs (with and without CoCOIs) at variable concentrations and mixed thoroughly. Then, sediments were allowed to dry until reaching the final WC of either 4 or 8 wt%. All testing was conducted in glass serum vials with butyl rubber septa and aluminum crimps. Since this technology is intended to analyze microbial processes that directly impact the chemical forms of contaminants, all experiments were carefully conducted using strict aseptic techniques to prevent external contamination. Additionally, all experiments were conducted in the absence of oxygen after sealing contaminated

sediments into vials, where controls were injected with N_2 gas and treated experiments were injected with various concentrations of ethane gas. Ethane concentrations differed between batch and column experiments, with batch experiments receiving a mix of 24% ethane and 76% nitrogen gas while columns were initially spiked with 41% ethane and 59% nitrogen gas, followed by incremental additions leading to a total concentration of 82% ethane over time.

Samples were analyzed at variable time points up to 129 days (static column) and 195 days (batch) to measure the potential transformation of NO_3^- and change in mobility of Cr. Table 2.8 summarizes the experimental matrix for the static column and batch experiments. Select results are presented in Section 3.1.2, while supplemental results for CoCOI (Cr) are presented in Appendix E, Section E.2. Microbial characterization analysis was conducted to investigate how native Hf sediment microbial communities with potential for bioremediation processes, such as nitrate and metal reduction, change before and after gas treatments. By combining DNA sequencing and quantitative polymerase chain reaction, the project team aimed to identify key microbial taxa and gain insights into microbial ecology and related processes driving contaminant transformation. These results are presented in Section E.3. Ammonia concentrations were measured; however, the results for most samples were below the detection limit and therefore are not included. Sediment pH was measured and results are presented in Section E.4; however, no significant changes were observed over the course of the experiment.

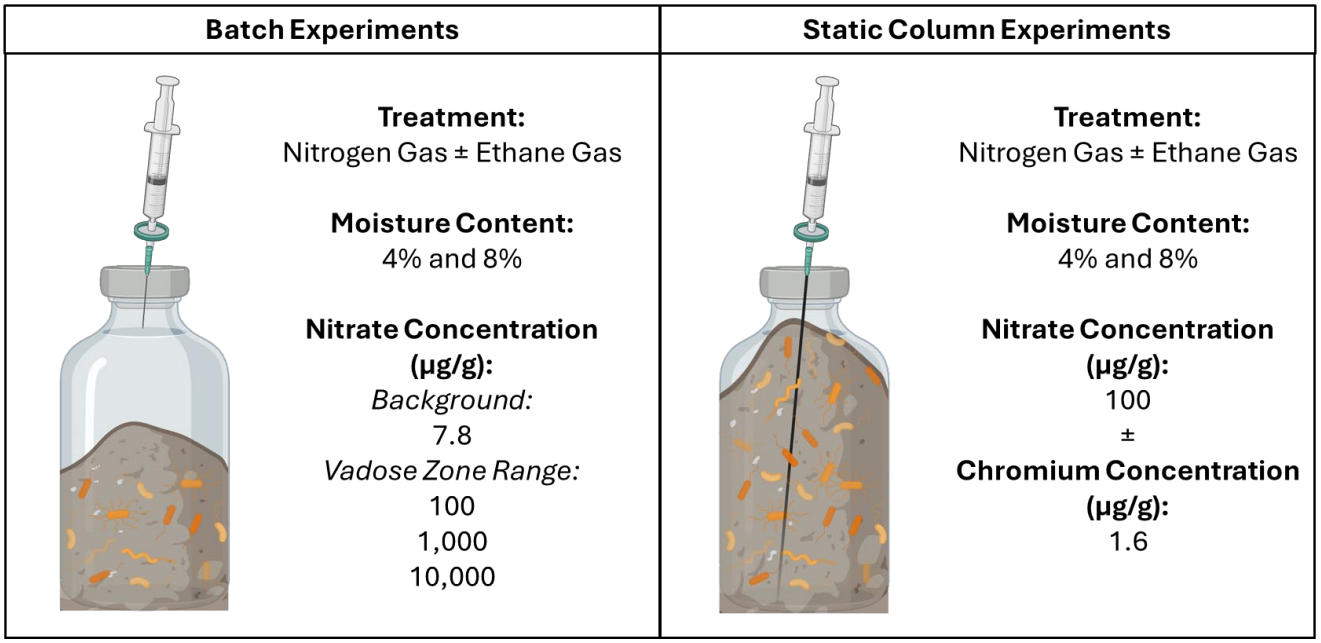

Figure 2.2. Conceptual diagram of experimental setup for gas-phase batch and static column bioremediation experiments. Batch experiments (*left*) and static column experiments (*right*) were conducted to evaluate the transformation of nitrate under various conditions. Orange objects represent native microbial activity in the S-9 sediment.

Table 2.8. Experimental overview for batch and static column experiments.

WC (wt%)	Gas Treatment	NO_3^- (µg/g)[(a)]	Cr (µg/g)[(a)]
Static Column Conditions			
4	N_2	100	0
4	Ethane	100	1.6
8	N_2	100	0
8	Ethane	100	1.6
Batch Conditions			
4	N_2	7.8 (Background) 100 1,000 10,000	0
4	Ethane	7.8 (Background) 100 1,000 10,000	0
8	N_2	7.8 (Background) 100 1,000 10,000	0
8	Ethane	7.8 (Background) 100 1,000 10,000	0

(a) Concentration represents the total concentration of PCOI or CoCOI added to experiment. Aqueous background concentrations of NO_3^- in the 216-S-9 sediment were determined to be 7.8 and 7.5 µg/g for the batch and static column experiments, respectively. Aqueous Cr was below detection limit (0.02 µg/g). Note that nitrogen gas was used as a control, not as an organic gas treatment.

2.4 Water-Saturated Experiments

The approach for technologies for water-saturated conditions, including direct treatment of perched water below the B Complex and formation of a PRB at the BY Cribs water table, was to quantify the following for PCOIs:

1. Initial immobilization or transformation
2. Long-term leaching or end product stability

Testing was conducted primarily with columns (Figure 2.3) to quantify changes in mobility of PCOIs in the presence of flow under site-specific conditions. Columns allow for quantification of the mass of PCOIs sequestered or transformed and leaching rates over time with and without addition of an amendment. Although these experiments were conducted under site-specific conditions (including field sediments and SGW and contaminant concentrations based on site conditions), contaminant partitioning and rates of immobilization and/or transformation were not directly translatable to the field due to potential impacts of scale, heterogeneity, and fluctuations in flow and contaminant concentrations. Additional long-term batch experiments (up to approximately 1 year, details in Appendix A, Section A.2.1) were conducted to qualitatively examine the sequestration of PCOIs with variable contact times with amendments. The batch-type experiments are especially relevant for the conditions for perched water

where the flow of water will likely be significantly slower, leading to longer contact times of PCOIs with amendments.

Starting conditions for experiments were similar for each of the technologies prior to addition of amendments, and control columns were run in the same manner for each technology. Table 2.9 outlines the testing conditions for each of the experiments (both column and batch). Sections 2.4.1 and 2.4.2 summarize methods for conditions for perched water and water table conditions, respectively. Long-term batch experiments are described in Appendix A, Section A.2.1. Additional amendment-specific methods are summarized in their respective appendices. The general experimental setup for column testing is shown in Figure 2.3, where solutions were injected into the bottom of the column. Then, effluent from the top of the column was collected via a timed fraction collector to monitor contaminant movement through columns over time with analysis of PCOIs and CoCOIs as described in Appendix A, Section A.1.

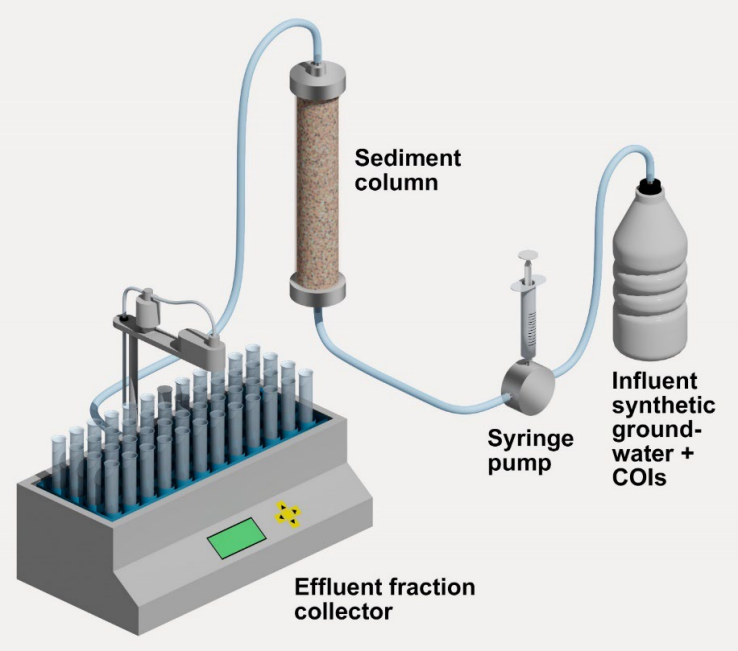

Figure 2.3. Conceptual diagram of experimental setup for saturated column testing.

Table 2.9. Summary of treatment conditions for technologies targeting saturated conditions.

Technology	Amendment	Ground-water	Sediment	Treatment Conditions
Perched Water below the B Complex[a]				
Particulate-phase chemical sequestration	Sn(II)-PO_4	SPW	CCu-PZsd	0.5 wt% Sn(II)-PO_4 mixed with sediment, prior to column packing
Particulate-phase combined chemical reduction and sequestration	SMI + Poly-PO_4	SPW	CCu-PZsd	0.1 wt% SMI mixed with sediment, then after 7 days treated with Poly-PO_4 with 35 mM total PO_4 in pore water, prior to packing into columns
Particulate-phase chemical sequestration (Bi)	BSN	SPW	CCu-PZsd	1.5 wt% BSN mixed with sediment, prior to column packing
Liquid-phase chemical sequestration	Ca-Cit-PO_4	SPW	CCu-PZsd	Pore water filled with Ca-Cit-PO_4 with 35 mM total PO_4, prior to column packing
Liquid-phase combined chemical reduction and sequestration	CPS + Poly-PO_4	SPW	CCu-PZsd	Pore water filled with 0.725 vol% CPS and Poly-PO_4 with 35 mM total PO_4, prior to column packing
Liquid-phase combined bioreduction and chemical sequestration	Molasses + Poly-PO_4	SPW	CCu-PZsd	Pore water filled with 0.625 g/L total organic carbon (TOC) from molasses, equilibrated approximately 1 month, then pore water filled with Poly-PO_4 with 35 mM total PO_4, prior to column packing
BY Cribs Groundwater[b]				
Particulate-phase chemical sequestration	Sn(II)-PO_4	SGW	CCug	0.5 wt% Sn(II)-PO_4 mixed with sediment, prior to column packing
Particulate-phase combined chemical reduction and sequestration	SMI + Poly-PO_4	SGW	CCug	0.1 wt% SMI mixed with sediment, then after 7 days treated with Poly-PO_4 with 35 mM total PO_4 in pore water, prior to packing into columns
Particulate-phase chemical sequestration (Bi)	BSN	SGW	CCug	1.5 wt% BSN mixed with sediment, prior to column packing
Liquid-phase chemical sequestration	Ca-Cit-PO_4	SGW	CCug	Sediments packed into column, then approximately three PVs of Ca-Cit-PO_4 with 35 mM total PO_4 injected, equilibrated approximately 6 weeks prior to PCOI (with and without CoCOIs) injection
Liquid-phase combined chemical reduction and sequestration	CPS + Poly-PO_4	SGW	CCug	Sediments packed into column, then two step injections of 1.5 vol% CPS followed by Poly-PO_4 with 70 mM total PO_4 injected approximately 1.5 PVs of solutions, equilibrated approximately 6 weeks prior to PCOIs (with and without CoCOIs) injection
Liquid-phase combined bioreduction and chemical sequestration[c]	Molasses + Poly-PO_4	SGW	CCug	Pore water filled with 0.625 g/L TOC from molasses, equilibrated approximately 1 month, then pore water filled with Poly-PO_4 with 35 mM total PO_4, prior to column packing

(a) Perched water conditions below the B Complex included all PCOIs and CoCOI (U, Tc-99, and NO_3 for all conditions).
(b) BY Cribs groundwater conditions included one set of experiments with only PCOIs (U and Tc-99) and one set with both PCOIs and CoCOIs (NO_3, I, Cr, and Sr).
(c) For the liquid-phase combined bioreduction and chemical sequestration technology, NO_3 is a PCOI and was always present.

2.4.1 Column Leaching Experiments for Perched Water

For testing of technologies under conditions for perched water, COIs were added directly to the sediments at the concentrations described in Table 2.10 approximately 3 to 5 days before sediments were treated with the amendment concentrations and conditions as described in Table 2.9. All experiments were conducted in the presence of nitrate because of its prevalence in perched water conditions. Concentrations of PCOIs and CoCOI (including Tc-99, U, and nitrate) were chosen to approximate field concentrations, although Tc-99 concentrations were elevated with respect to contamination levels to improve the minimum fraction detectable in the aqueous phase (i.e., targeted detection of < 1% remaining in the aqueous phase). U and nitrate concentrations were based on perched water extraction well data from the pump-and-treat facility (i.e., wells 299-E33-344, 299-E33-350, 299-E33-351) from 2019 through 2021, which includes 43 to 88 measurements, depending on the PCOI or CoCOI. Nitrate data from the perched water extraction wells were also similar to previous extractions for B Complex cores (PNNL-31959;PNNL-27524). Tc-99 concentrations for perched water conditions were kept the same for water table conditions to improve the minimum fraction detectable in the aqueous phase. The maximum concentration measured in the perched water extraction wells under the B Complex was for well 299-E33-350 (82,400 pCi/L or 4.8 µg/L).

Table 2.10. COI concentrations added to sediments prior to treatment for the columns for conditions representing perched water below the B Complex.

Contaminant		Added as
Perched Water Conditions below the B Complex (µg/g)		
Tc	0.2	NH_4TcO_4
U[(a)]	100	$UO_2(NO_3)_2$
NO_3	1,600	$NaNO_3$

(a) 33 µg/g of U added based on background U already present in sediments.

Columns [2.43-cm (0.96-in.) inner diameter by 15.24-cm (6-in.) long, clear Schedule 40 PVC plastic, with hydrophilic plastic frits, 90-µm pore size and 0.16-cm (1/16-in.) thickness, Porex] were packed with moist, contaminated sediment following reaction with amendments for approximately 6 weeks. Select columns had additional monitoring with dissolved oxygen spots (as described in Appendix A, Section A.1.3). The columns were saturated with SPW (Table 2.9) that previously had been equilibrated with air (and O_2). Fluid was pumped into the bottom of the column at a constant flow rate of 0.6 m/day (2 ft/day) (via Kloehn syringe pumps, resulting in a residence time in column experiments of approximately 6 hours). The relatively slow flow rate is representative of groundwater flow rates in the Central Plateau for the B-BX-BY, C, A-AX, and S-SX WMAs, where average linear velocities ranged from 0.2 to 1.7 m/day (0.75 to 5.6 ft/day) in 2021 (DOE/RL-2022-40).

At the top (effluent end) of the column, effluent samples were collected to measure the change in concentration of the PCOIs over time. These samples were automatically collected using a timed fraction collector (Isco Foxy 200 or similar), which contained tubes to collect effluent aliquots over time. PCOIs typically leach from the sediment at a high initial rate (i.e., at high initial concentration, which decreases over time), and the leaching rate decreases as more PVs of fluid are passed through the column. Because of this general “breakthrough curve” behavior, more effluent samples are analyzed in the first two PVs, with less frequent analysis for subsequent PVs.

Stop flow events up to approximately 500 hours in duration were also conducted to quantify rates of leaching of PCOIs under no-flow conditions. Similar stop flows have been used in previous testing for U (PNNL-29650). These events provided time for contaminants present in one or more surface phases on the sediment to partition into pore water (i.e., via diffusion from intraparticle pore space or dissolution of precipitate phases or slow desorption). The stop flow events were approximately 16 hours (at 2.5 PVs), 48 hours (at 10 PVs), and 480 hours (at 100 PVs), unless otherwise indicated for specific technologies.

A bromide (Br^-, referred to in the text as Br) tracer test was also conducted at the end of the column tests, where 2 to 3 PVs of SPW with 80 mg/L Br were injected at the same flow rate used for the leaching experiment. Then, the solutions were switched back to SPW for subsequent flushing of Br over approximately 3 to 5 PVs. For BSN columns, pentafluorobenzoic acid (PFBA) was used as the nonreactive tracer instead of Br due to Br-BSN interactions. After solution injection was complete, the columns were sectioned in approximately 2.5-cm (1-in.) increments, with each increment homogenized. One aliquot of sediment from each section was treated with 8 M HNO_3 per Extraction 5 (as described in Appendix A, Section A.2.3) conditions to measure remaining PCOIs and CoCOIs in sediments across the columns. Remaining sediments (not subjected to extractions) were archived for additional solid phase characterization (Appendix B).

2.4.2 Column Loading and Leaching Experiments for Groundwater

Sediments were packed into columns after addition of amendments for most experiments, though deviations are noted in Table 2.9. During packing, at approximately 1-cm intervals, sediments were tamped down with a plastic rod and the surface scraped lightly to achieve a tight, homogenous packing that was more representative of subsurface porosity. Then, SGW with PCOIs (with and without CoCOIs) was injected into columns. The PCOI and CoCOI concentrations, summarized in Table 2.11, for groundwater conditions were based on previously measured concentrations from the Hanford Environmental Information System (HEIS) database, including data up to December 2021, for the BY Tank Farm, located in the 200 West Area of the Central Plateau. Because data were limited, core concentrations from both saturated and unsaturated depths were combined based on reported solid phase concentrations (in μg/g) and then converted to porewater concentrations based on the experimental conditions.

PCOI and CoCOI concentrations for the BY Cribs were based on 35 to 70 measurements for each element in sediments for groundwater table conditions. Amounts of U, CN^-, and Cr were based on the maximum solid-phase concentrations measured in BY Tank Area cores as reported in HEIS. The nitrate level was based on average solid phase concentrations (instead of maximum) measured in BY Tank Area cores as reported in HEIS, because higher nitrate concentrations were considered for the perched water below the B Complex. Iodine was added as I-127 based on previous literature measuring background, natural iodine in Hanford Site groundwater (Zhang et al. 2013; Kimmig et al. 2021), as these treatments are not isotope specific, and the concentration of natural/anthropogenic I-127 is significantly greater than that of I-129. The maximum I-129 concentration reported in HEIS for the BY Tank Area was 0.03 μg/g and the maximum I-127 concentration measured at a 104-ft depth under BY Cribs was 2.0 μg/g.

Sr was also added based on total maximum natural Sr concentrations in the BY Cribs and BY Tank Areas. Because concentrations of natural Sr (Sr-87) are significantly greater than Sr-90, concentrations represent natural Sr concentrations instead of Sr-90. The maximum Sr-90 measured in the BY Tank Area was 5.7×10^{-9} μg/g as compared to 125 μg/g of total Sr. Moreover, in experiments, natural Sr was used. Unlike the other PCOIs and CoCOIs, the concentration of Tc-99 used was higher than that observed in relevant field sediments (BY Tank Area: 0.006 μg/g) to improve detection of Tc-99 in the aqueous phase.

Table 2.11. COI concentrations injected during loading for columns for the BY Cribs groundwater conditions.

Contaminant		Added as
Groundwater Conditions (µg/L)		
Tc	100	NH_4TcO_4
U	1,000	$UO_2(NO_3)_2$
I-127	150	$NaIO_3$
Cr	17,500	Na_2CrO_4
Sr	25,000	$Sr(NO_3)_2$
NO_3[1]	50,000	$NaNO_3$

(a) 15,000 µg/L of NO_3 added based on NO_3 added from other contaminant salts.

Sequestration and leaching of PCOIs was measured through initial injection of SGW with PCOIs (with and without CoCOIs) followed by leaching with SGW as described in Section 2.4.1. The initial sequestration step included continuous injection of PCOIs (with and without CoCOIs) mixed with SGW until complete breakthrough (e.g., effluent PCOI concentrations equaled influent PCOI concentrations). Notably, some experiments did not reach complete breakthrough with over 300 PVs of solution injection and therefore were moved to the leaching step without fully saturating the system with contaminants. To exclude the impact of oxygen on reductant consumption during the initial sequestration phase, SGW solutions were prepared from de-gassed ultrapure water (i.e., equilibrated with N_2 gas instead of air). However, for reducing technologies, the impact of oxygen during sequestration would need to be factored into the amount of reductant added to the system.

3.0 Results

3.1 Vadose Zone Treatment

Two gas-phase technologies were evaluated for sequestration of contaminants in the VZ to decrease long-term contaminant flux to perched water or the water table:

1. **Gas-phase chemical sequestration**: CO_2 gas for I-129 sequestration
2. **Gas-phase bioreduction**: Organic gas (ethane) for nitrate

One technology was eliminated during Phase 1 testing: combined gas-phase bioreduction and chemical sequestration for Tc-99.

Evaluation of Gas-Phase Technologies

- Significant chemical sequestration with CO_2 gas was not observed for iodine or the following CoCOIs: U, Sr, Tc-99, and Cr.
- Bioreduction with ethane gas did not significantly transform nitrate at the elevated concentrations expected in the DV-1 OU waste sites.
- Ethane or nitrogen gas may reduce nitrate at lower amounts closer to expected sediment background concentrations.

3.1.1 Gas-Phase Chemical Sequestration – Carbon Dioxide

The gas-phase chemical sequestration technology injected CO_2 gas into VZ sediments in columns to increase pore water carbonate concentrations with subsequent calcite precipitation, which may incorporate I-129 (as iodate) as well as other elements. Testing was conducted to determine (1) initial immobilization or transformation of PCOIs, (2) long-term leaching or end product stability of PCOIs, and (3) controls on CO_2 movement in sediments; results are summarized in subsequent sections.

Evaluation of Iodate Sequestration by CO_2 Gas

- Significant chemical sequestration with CO_2 gas was not observed for iodate under variably saturated conditions in column testing with flow – decreasing in performance with decreasing WC.
- Chemical sequestration with CO_2 gas was dependent on sediments, potentially due to availability of Ca.

3.1.1.1 I-127 Sequestration by CO_2

All sediments used in column tests were saturated at VZ WCs (2, 4, or 8 wt%) and treated in columns by 100% CO_2 gas injection (10 PVs) followed by 60 days of reaction time (i.e., no injection), then 10 PVs of air injection followed by 90 days of reaction time to neutralize pH and accelerate calcite precipitation and subsequent contaminant incorporation. Then, sediments were subjected to sequential liquid extractions (in batch experiments) or one of three variably saturated leach tests (in column configurations): (1) 100% water saturation, (2) unsaturated infiltration, and (3) PUF leaching.

Based on the batch and column tests conducted in Phase 2 [and batch experiments in Phase 1 (PNNL-35432)], I-127 mobility with CO_2 gas treatment was inconsistent as batch extractions with Hf and 216-S-9 sediments showed variable results with a 0% to 60% decrease in I-127 mobility (based on sequential extractions), suggesting an increase in precipitate phases, while results for column leach experiments at different water content were inconclusive. Column tests were conducted under water-saturated (100% water saturation), infiltration (80% water saturation), and PUF systems (47% water saturation). CO_2 treatment resulted in anywhere from 14% more to 13% less I-127 sequestration compared to untreated (control) tests.

Generally, sequestration of iodate decreased with decreasing WC. For example, for the 216-S-9 sediment under water-saturated leach conditions, CO_2 treatment showed 6% to 14% more I-127 sequestered than without treatment (Figure 3.1). In contrast, infiltration columns with the 216-S-9 sediment at 82% water saturation (and 6-hour residence time) showed 13% less I-127 sequestered compared to without treatment. Finally, in conditions most representative of leaching in the VZ, PUF infiltration experiments at 56% water saturation and a 33- to 51-hour residence time showed no difference in I-127 sequestered with CO_2 treatment (Figure 3.1, right-most bars, and Figure 3.2).

Although inconclusive in column testing, the Phase 1 batch extraction results from testing a wider range of water content suggested that iodate sequestration was also dependent on sediment and CoCOIs. Testing with the Hf sediment showed greater sequestration of iodate than 216-S-9 sediment in batch extractions at variable water saturation. Although the two sediments were mineralogically similar, the Hf sediment was uncontaminated and the 216-S-9 sediment contained significant co-contaminants (high nitrate, low Cr). This may have contributed to less calcite precipitation in the 216-S-9 sediment. In column testing, Hf sediments showed slightly more iodate sequestration, similar to Phase 1 testing, as shown in Figure 3.1. However, these results are based on comparison of one to two column tests and are likely not statistically different.

There are significant differences between batch extraction and column leach results however, highlighting differences in iodate mobility under different conditions, including (1) in the presence and absence of flow and (2) with variable reaction times. Column testing took place over a longer period (i.e., 100 hours for water-saturated leach experiments, 2,000+ hours for the 47% water-saturated leach experiments) than batch extractions (5 days or 120 hours) and better reflected field conditions based on hydrological conditions (i.e., advection of water and PCOIs through sediments and field-relevant sediment-to-solution ratio). Notably, a comparison of tracer (bromide) breakthrough in unsaturated vs. water-saturated experiments showed greater tailing in unsaturated experiments, likely due to water migrating primarily through larger pores and less to no water movement through smaller pores when water migration was controlled by gravity and capillary forces (i.e., unsaturated flow) vs. pressure (i.e., saturated flow). These results are summarized in Appendix A, Section A.3.1, and Appendix D, Section D.3.4.

Shortly after injection, CO_2 gas partitions into pore water based on the measured decrease in pH after CO_2 gas injections observed in Phase 1 testing (PNNL-35432). However, there is no direct evidence that calcite precipitates under the conditions of these experiments. Under different conditions, other authors have reported iodate incorporation into calcite (Zhang et al. 2013) and adsorption (McElroy et al. 2020; Qafoku et al. 2022). Measurements of solid phase inorganic carbon concentrations before and after CO_2 gas treatment for two sediments (Hf and 216-S-9) were inconclusive. The Hf sediment showed an increase in solid phase inorganic carbon (0.00% for untreated vs. 0.057% for CO_2-treated, detection limits 0.02%). The 216-S-9 sediment, which likely had acidic co-contaminants that may have decreased ion exchangeable Ca^{2+}, showed a decrease in solid phase inorganic carbon (0.28% for untreated vs. 0.00% for CO_2-treated).

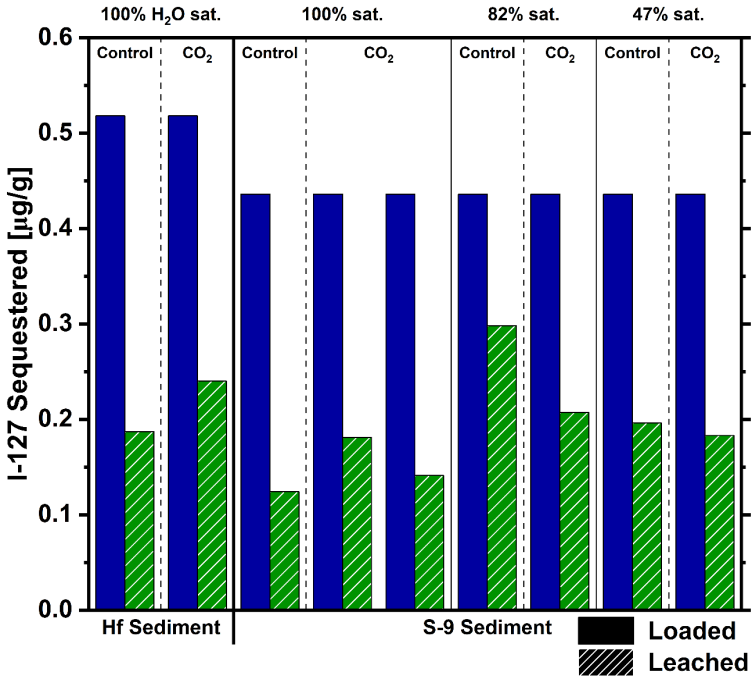

Figure 3.1. I-127 mass sequestered (µg/g) after loading and leaching phases of testing in variably saturated column testing compared with no treatment and CO_2 treatment of Hf or 216-S-9 sediments. Note: I-127 added as IO_3^-, percentage along the top represents water saturation.

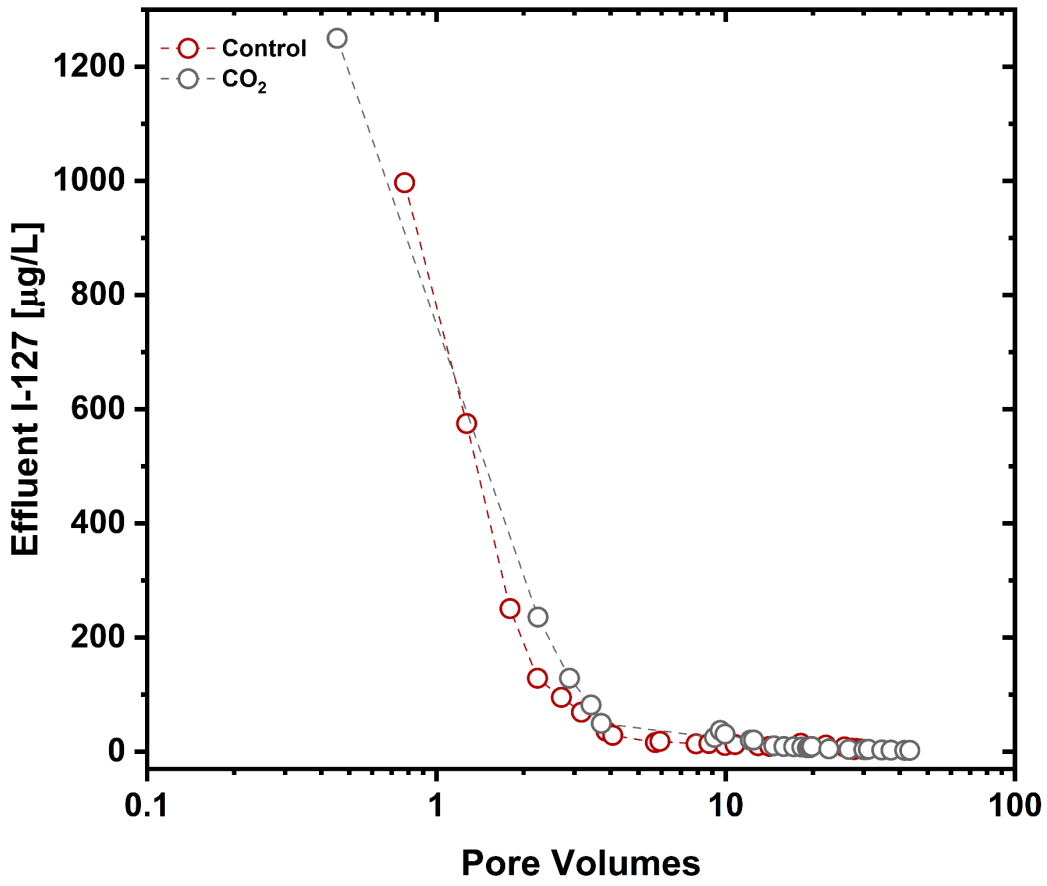

Figure 3.2. Comparison of I-127 (as iodate) leaching in untreated and CO_2-treated 216-S-9 sediment in PUF columns. Note: The residence time (i.e., 1 PV) was 50.6 hours for the untreated column and 33.0 hours for the CO_2-treated column.

3.1.1.2 CoCOI Sequestration by CO_2

Testing was also conducted with CoCOIs, including Tc-99, Sr, Cr, and U. Overall, there was no significant sequestration of Sr or U (as shown for U for column testing in Figure 3.4), but there was a relatively small amount of Tc-99 and Cr sequestered. Batch experiments showed a 3% to 35% increase in sequestration of Tc-99 (Appendix D, Section D.2). Similar results were observed in column testing, where CO_2 treatment of Hf and 216-S-9 sediment resulted in a weak to moderate increase (7% to 28%) or an 8% decrease in one case in Tc-99 sequestration (Figure 3.3).

Cr sequestration increased from 0.7% to 8.4% with CO_2 gas treatment. Treatment with CO_2 gas may result in formation of anoxic conditions due to removal of O_2, which could potentially reductively precipitate Cr. However, because Cr (as chromate) is more easily reduced than Tc-99 (as pertechnetate) and less Cr was sequestered than Tc-99, it is unlikely that reducing conditions were generated. However, previous research has shown this is possible for Tc-99 on other sediments from the Hf, where select minerals (magnetite, biotite) were able to slowly reduce compounds (Szecsody et al. 2014).

CO_2 gas treatment did not perform well for U and Sr considering both can incorporate into calcite (Qafoku et al. 2022). Batch experiments with both sediments at two WCs showed no difference in U and a 0% to 1.3% increase in sequestration for Sr. In column leach studies, CO_2 treatment of Hf and 216-S-9 sediment showed high variability in sequestration, ranging from a 13% decrease to a 20% increase in U sequestration with no correlation with sediment or WC (Figure 3.4). Batch experiments with two sediments at two WCs showed 0% to 1.3% more Sr sequestration with CO_2 treatment, which was significantly less than previous in batch experiments at a 2:1 solid-to-liquid ratio in Phase 1 testing (PNNL-35432).

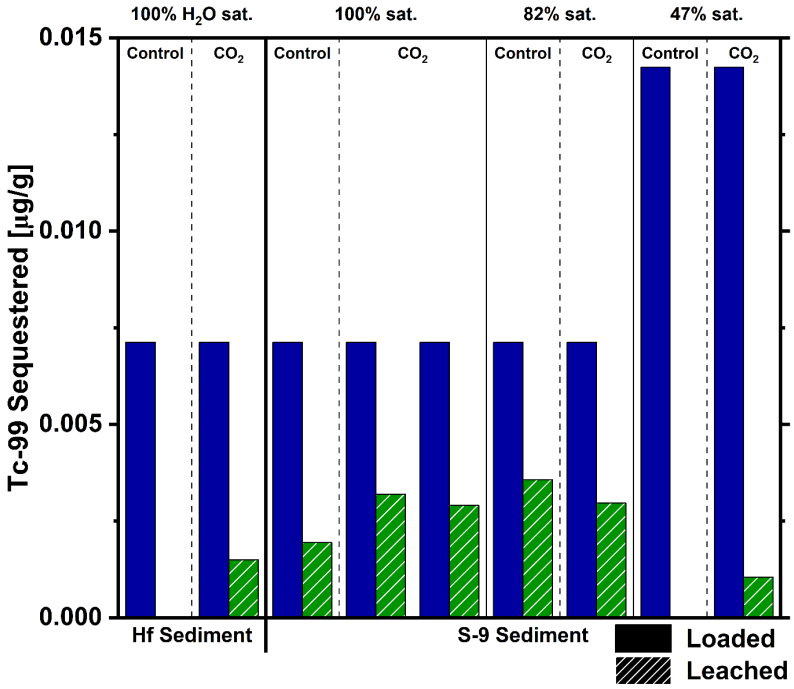

Figure 3.3. Tc-99 mass sequestered (µg/g) after loading and leaching phases of testing in variably saturated column testing compared with no treatment and CO_2 treatment of Hf or 216-S-9 sediments. Note: Percentage along the top represents water saturation.

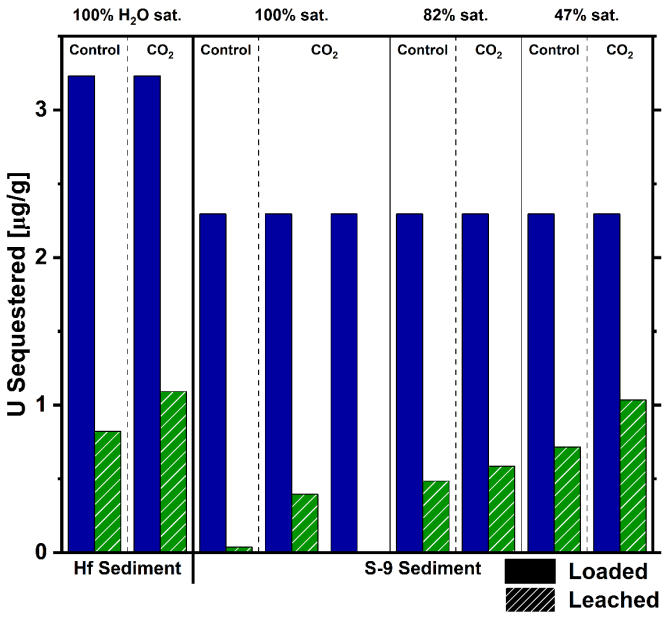

Figure 3.4. U mass sequestered (µg/g) after loading and leaching phases of testing in variably saturated column testing compared with no treatment and CO_2 treatment of Hf or 216-S-9 sediments. Note: Percentage along the top represents water saturation.

3.1.1.3 CO_2 Gas Mobility

For field-scale injection of CO_2 gas into VZ sediments, the two processes that primarily control CO_2 gas migration are (1) gas-to-liquid partitioning and (2) CO_2 density.

Laboratory CO_2 gas injection experiments have confirmed gas-to-liquid partitioning of a small retardation as predicted by Henry's law ($R_f = 1.26$ at 4% WC, $R_f = 1.74$ at 8% WC) as summarized in Appendix D, Section D.4. The high density of the CO_2 gas (1.839 kg/m^3) relative to air (1.205 kg/m^3) causes significant density sinking, which was observed in laboratory CO_2 gas injection experiments into vertical vs. horizontal columns. The density sinking effect could be controlled by CO_2 gas injections above a confining layer or using recirculation.

3.1.2 Gas-Phase Bioreduction – Ethane

The gas-phase bioreduction technology evaluated ethane gas treatment for enhancing bioreduction of nitrate in 216-S-9 sediments under anoxic conditions for potential VZ source remediation. This section discusses the transformation of aqueous nitrate in experiments with and without Cr as a CoCOI. Reduction of nitrate to nontoxic end products was determined based on the concentration of aqueous NO_3^- and NO_2^- assuming the remaining N was fully reduced to N_2, a gaseous nontoxic end product. Appendix E presents detailed results on microbial characterization, pH, aqueous total Cr, aqueous chromate (CrO_4^{-2}), solid-phase Cr reduction rates, and kinetic reduction rates.

Evaluation of Nitrate Bioreduction without Co-contaminants

- Nitrate reduction was observed across all concentrations for both ethane gas and nitrogen gas treatments.
- No nitrate reduction enhancement was observed from ethane gas treatment compared to nitrogen gas control.
- Nitrite formation may be more pronounced at lower nitrate concentrations.
- Increased WC did not increase nitrate reduction.

Evaluation of Nitrate Bioreduction with Co-contaminants

- Nitrate reduction was observed both with and without the addition of Cr for both ethane gas and nitrogen gas treatments.
- No nitrate reduction enhancement was observed from ethane gas treatment compared to nitrogen gas control.
- Nitrite formation was suppressed with the addition of Cr.
- Increased WC did not increase nitrate reduction.

Overall, these results show that the addition of ethane did not lead to bioreduction of nitrate as it failed to reach 50% or more reduction compared to the nitrogen gas control; therefore, the technology is not recommended to advance.

Results from both batch and static column experiments indicate that abiotic pathways, such as ferrous iron-facilitated nitrate reduction and nitrite suppression, are likely the dominant mechanisms driving nitrate reduction under the tested conditions. Microbial analyses revealed no significant changes in denitrification genes over time (Appendix E, Section E.3). Additionally, the inability to recover sequencing data in 216-S-9 sediment further supports the hypothesis that abiotic processes are the primary driver. Nitrite formation occurred at lower nitrate concentrations but was suppressed at higher concentrations and in the presence of Cr. While lower pH was recorded at higher nitrate concentrations (Section E.4), the system was not strongly acidic and the exact role of pH in nitrite suppression remains unclear. The presence of Cr neither inhibited nitrate reduction nor impacted ethane gas-treated samples compared to nitrogen gas controls; however, Cr may have acted as an alternative electron acceptor, affecting nitrite formation and recovery.

Increased WC did not enhance nitrate reduction, reinforcing the hypothesis that abiotic processes are governing nitrate transformation, as higher water levels typically stimulate microbial activity. Ethane gas treatments demonstrated no significant enhancement in nitrate reduction compared to nitrogen gas controls, and high ethane concentrations in static columns failed to increase nitrate reduction. Notably, nitrate reduction in 4 wt% WC systems performed better in static columns compared to batch setups, whereas 8 wt% WC systems showed comparable rates across experimental designs, suggesting that lower WC may promote nitrate reduction via abiotic processes.

3.1.2.1 Objective 1: Quantify NO_3^- Transformation via Treatment with Ethane Gas without Cr

Batch experiments were designed to evaluate the nitrate reduction capacity at various concentrations representative of those found in the VZ (from sediment background at 7.8 μg/g to 10,000 μg/g).

For the 4 wt% WC experiments, nitrate reduction was observed across all concentrations for both ethane gas and nitrogen gas treatments (Figure 3.5). Background nitrate showed the most significant reduction, decreasing to approximately 6% for both treatments within 55 days. At 100 μg/g, nitrate decreased to around 80% with ethane treatment and 70% with nitrogen treatment. Similarly, at 1,000 μg/g, nitrate decreased to 72% with ethane and 62% with nitrogen. At the highest concentration (10,000 μg/g), nitrate reduction was similar for both treatments, decreasing to approximately 64%. These results indicate consistent nitrate transformation, with ethane gas treatment showing no significant enhancement compared to nitrogen gas.

Nitrite concentrations showed varying patterns depending on nitrate levels and the type of gas treatment. For background nitrate, nitrite increased from 0% to 8% with ethane gas and from 0% to 31% with nitrogen gas. At 100 μg/g nitrate, nitrite rose from 0% to 10% with ethane and from 0% to 15% with nitrogen gas. However, at higher nitrate concentrations of 1,000 μg/g and 10,000 μg/g, no measurable nitrite accumulation (remaining at 0%) was observed for either treatment. These results suggest that nitrite formation may be more pronounced at lower (background and 100 μg/g) nitrate concentrations when compared to higher concentrations (1,000 and 10,000 μg/g).

At 8 wt% WC, nitrate reduction was observed across all concentrations for both ethane gas and nitrogen gas treatments (Figure 3.6). Background (7.8 μg/g) nitrate levels showed significant reduction, decreasing to 11% with ethane and 5% with nitrogen gas. At higher nitrate concentrations (100, 1,000, and 10,000 μg/g), reductions were less pronounced but relatively similar between treatments. For 100 μg/g, nitrate decreased to 77% with ethane and 74% with nitrogen; for 1,000 μg/g, reduction reached 96% with ethane and 94% with nitrogen; and for 10,000 μg/g, nitrate decreased to 82% with ethane and 79% with nitrogen gas. These results indicate consistent nitrate transformation, with ethane gas treatment showing no significant enhancement compared to nitrogen gas. Note that a plume of nitrate in the vadose zone could possibly be treated by this technology to decrease downward nitrate migration if implemented for a lower nitrate sediment concentration deep in the VZ (i.e., lower breakthrough front of a plume).

At 8 wt% WC, nitrite concentrations varied based on nitrate levels and gas treatments. For background nitrate, nitrite increased from 0% to 18% with ethane gas treatment and from 0% to 8% with nitrogen gas treatment. At 100 μg/g nitrate, nitrite rose slightly, from 0% to 2% with ethane and 0% to 5% with nitrogen gas. For higher nitrate concentrations (1,000 μg/g and 10,000 μg/g), nitrite accumulation was minimal. These results indicate that nitrite production may be more prominent at lower nitrate concentrations.

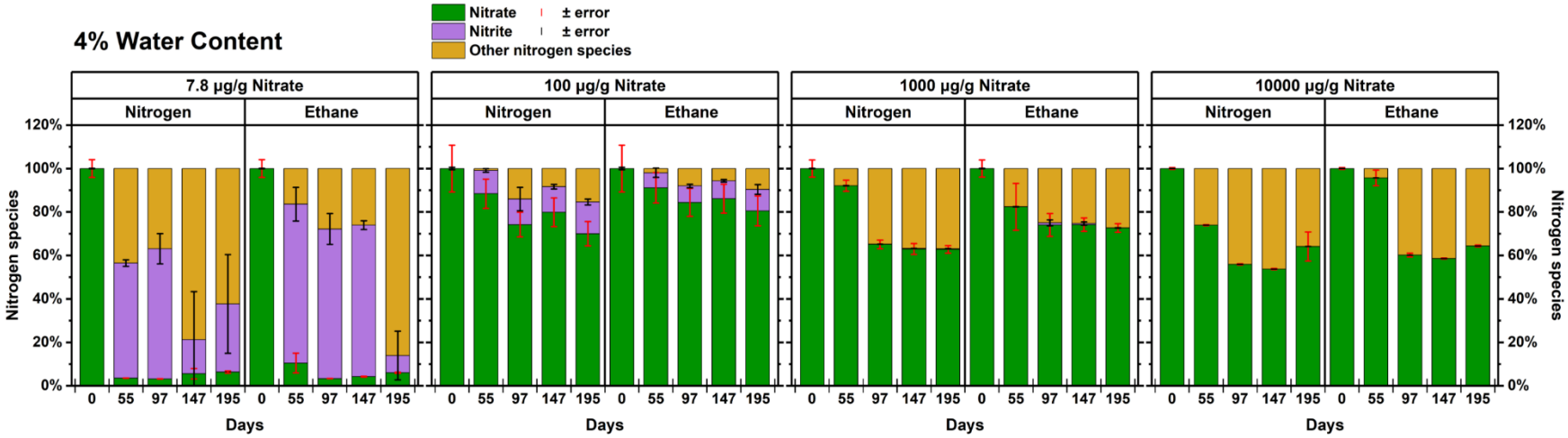

Figure 3.5. Aqueous nitrate, nitrate, and other nitrogen species [y-axis indicates % nitrogen species calculated from total nitrate (mMol/L) added] after 195 days of incubation in 4 wt% WC 216-S-9 sediment batch experiments treated with nitrogen gas +- 24% ethane. Starting concentrations of nitrate ranged from background (7.8 µg/g) to 10,000 µg/g. Note that nitrogen gas is used as a control, not as a carbon source. Error bars are one standard deviation.

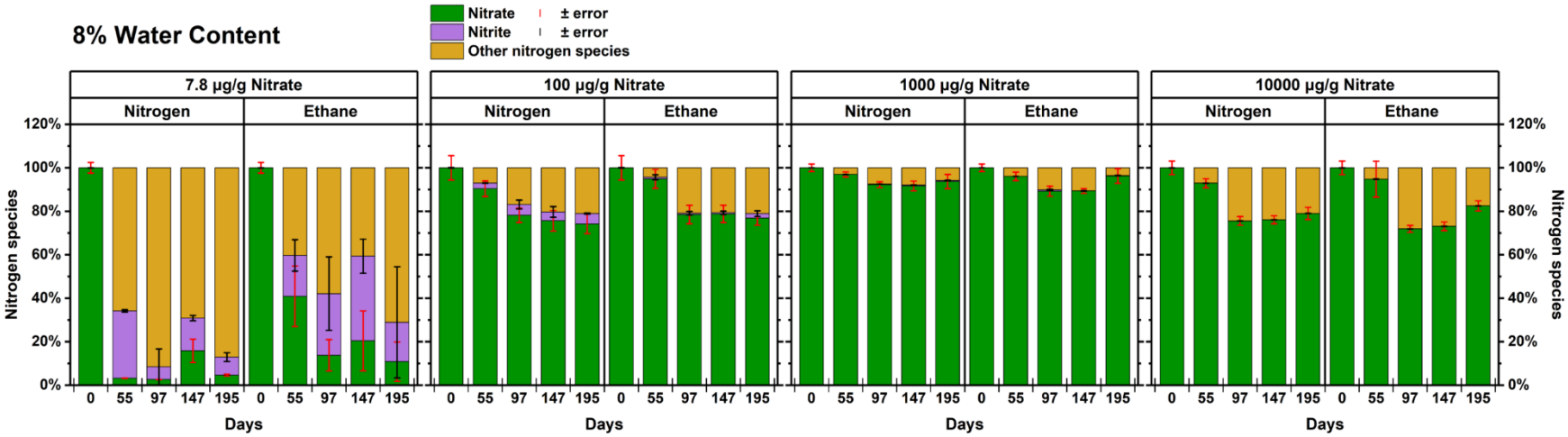

Figure 3.6. Aqueous nitrate, nitrate, and other nitrogen species (y-axis indicates % nitrogen species calculated from total nitrate added) after 195 days of incubation in 8 wt% WC 216-S-9 sediment batch experiments treated with nitrogen gas +- ethane. Note that nitrogen gas is used as a control, not as a carbon source. Starting concentrations of nitrate ranged from background (7.8 µg/g) to 10,000 µg/g. Error bars are one standard deviation.

3.1.2.2 Objective 2: Quantify NO_3^- Transformation via Treatment with Ethane Gas with Cr

Static columns focused on assessing the reduction capacity for nitrate (100 µg/g) in the presence of a CoCOI, Cr (1.6 µg/g). For the static columns with 4 wt% WC, nitrate reduction was observed in both ethane and nitrogen gas treatments (Figure 3.7), with reductions to 50% and 62%, respectively, in the absence of Cr. When Cr was present, nitrate reductions were similar, with final levels of 60% for ethane and 61% for nitrogen gas treatments. Nitrite concentrations at 4 wt% WC showed a small increase from 0% to 9% for ethane and from 0% to 3% for nitrogen gas in the absence of Cr, while no nitrite accumulation was observed in the presence of Cr for either treatment. At 8 wt% WC, nitrate reduction was less pronounced, with reductions to 86% for ethane and to 81% for nitrogen gas in the absence of Cr. With Cr present, nitrate decreased to 78% in both treatments. Nitrite accumulation at 8 wt% WC was minimal, with increases from 0% to 1% and 4% for ethane and nitrogen gas, respectively, in the absence of Cr, and no nitrite was detected when Cr was present. These results suggest that nitrate reduction is consistent across gas treatments but is slightly influenced by WC and the presence of Cr, with nitrite accumulation generally suppressed when Cr is present.

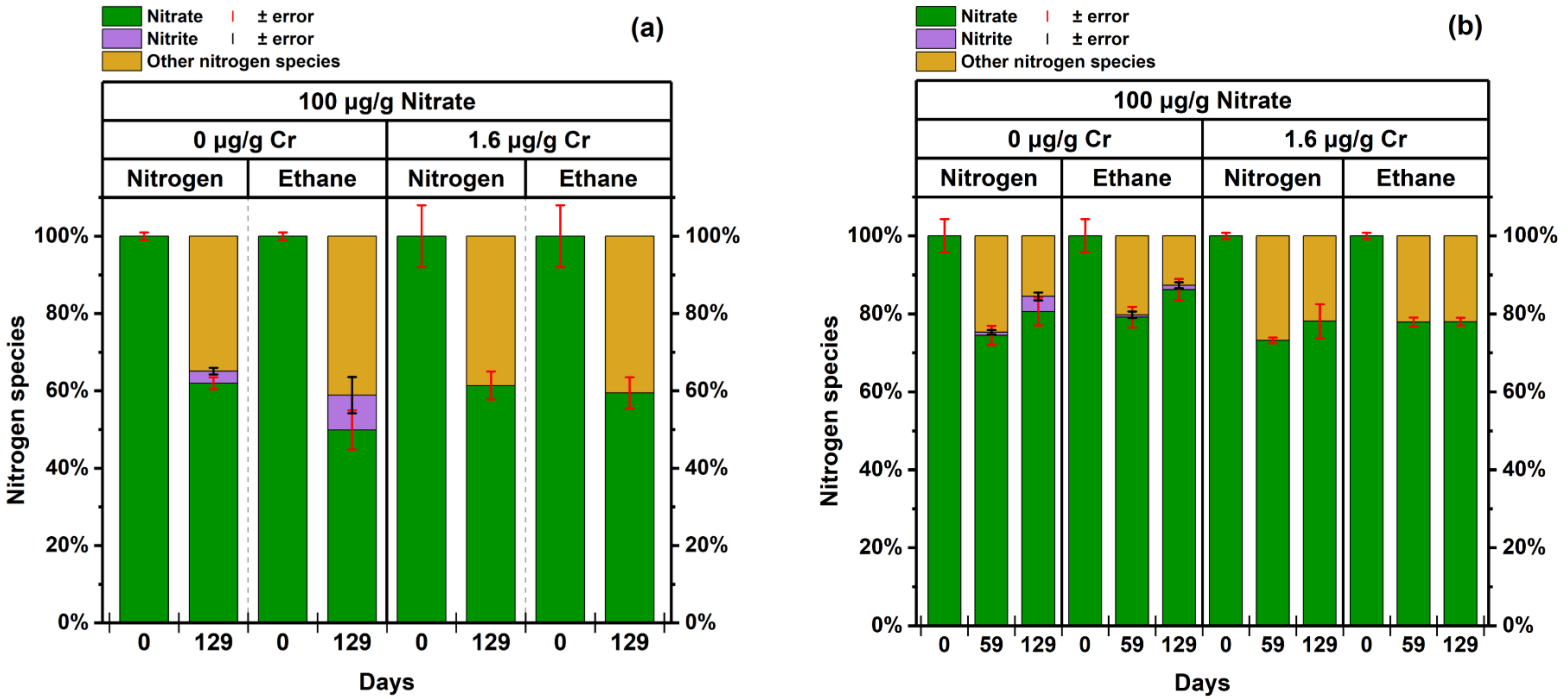

Figure 3.7. Aqueous nitrate, nitrate, and other nitrogen species (y-axis indicates % nitrogen species calculated from total nitrate added) after 125 days of incubation in 4 wt% (left) and 8 wt% (right) WC 216-S-9 sediment columns treated with nitrogen gas +- ethane. Note that nitrogen gas is used as a control, not as a carbon source. Starting concentrations of nitrate were 100 µg/g. Cr was added as a CoCOI at a concentration of 1.6 µg/g. Error bars are one standard deviation.

3.2 Water-Saturated Zone Treatment

Six technologies were tested for treatment under water-saturated conditions for two different scenarios representative of direct injection in the perched water zone beneath the B Complex and development of a PRB at the water table beneath the BY Cribs. This section summarizes and compares the results for these six technologies. Amendment performance was highly dependent on the conditions (based on perched or groundwater conditions with and without CoCOIs) and PCOIs. Results are summarized for PCOIs (Tc-99 and U) and select CoCOIs under the most relevant field conditions tested (i.e., with all potential CoCOIs), based on the objective to measure (1) initial sequestration or transformation and (2) long-term leaching or end product stability.

Evaluation of Technologies under Perched Water Conditions below the B Complex

- Particulate SMI+Poly-PO_4 sequestered both Tc-99 and U, meeting the 50% performance threshold for sequestration.
- Particulate Sn(II)-PO_4 performance was comparable to particulate SMI+PO_4, while liquid CPS+Poly-PO_4 was less effective but still met the threshold for sequestration of Tc-99.
- None of the other five technologies performed well for U sequestration; only SMI+Poly-PO_4 met the performance threshold.
- Technology performance was highly impacted by the relatively high ionic strength, presence of nitrate, and elevated U concentrations under these conditions.

Evaluation of Technologies under BY Cribs Groundwater Conditions

- Liquid molasses+Poly-PO_4 outperformed five other amendments for sequestration of Tc-99.
- Two technologies met the 50% performance threshold for sequestration of Tc-99 (molasses+Poly-PO_4 and CPS+Poly-PO_4).
- Particulate BSN outperformed all other amendments for U sequestration, though significant sequestration was also observed for liquid CPS+Poly-PO_4, Ca-Cit-PO_4, and molasses+Poly-PO_4.

This text serves as a primer outlining the types of measurements used to assess the initial immobilization or transformation of PCOIs and their long-term leaching or end product stability in saturated column-type testing. The results for water-saturated conditions are compared with a control (no treatment scenario with either SPW or SGW, respectively) using the following parameters, which are measured for each PCOI:

1. Time of initial breakthrough (for development of a PRB at the water table only)
2. Mass sequestered during loading and leaching (for direct injection into perched water and development of a PRB at the water table)
3. Rates of leaching with time (for direct injection into perched water and development of a PRB at the water table; see technology-specific appendices)
4. Surface phase characterization identifying sequestered Tc-99 and U precipitates

These parameters allow for determination of whether each technology meets performance metrics (i.e., > 50% increase in sequestration as compared to a control) and help facilitate cross-comparison of technologies to identify the top-performers based on an evaluation of the extent of immobilization or

transformation and the long-term stability of the end product. However, other factors are considered, including amendment loading in experiments as compared to potential field loadings and general feasibility for field implementation.

The time of breakthrough provides insight into how quickly a contaminant is transported through the porous medium packed in the column. It reflects the potential of the sediment or amendment in retaining, reducing, or transforming the contaminant over time. Breakthrough is typically monitored by analyzing the concentration of the contaminant in effluent water as a function of time or PVs. If the curve exhibits breakthrough (effluent concentration is increasing up to influent injection concentration) within a few PVs, there is minimal interaction of the contaminant with the sediments and/or amendment. However, if the breakthrough is significantly delayed in the effluent, results indicate that there is strong retention in the sediments due to processes like adsorption, precipitation, reduction, or coating by another precipitate. The slope of the breakthrough may also indicate kinetics of sequestration and release of PCOIs. For example, if the slope is rapidly increasing during injection of PCOIs (with and without CoCOIs), there may be minimal interaction with sediments and amendments. Alternatively, if the slope is gradually increasing, then significant slow interaction may be occurring (e.g., adsorption or precipitation).

The initial retardation of PCOIs within the sediment columns is assessed by estimating the PV at breakthrough (defined as the point where effluent concentration is 0.5× the influent concentration). A conservative tracer (e.g., bromide or tritium representing a nonreactive tracer), which does not undergo any geochemical reactions, would exhibit a breakthrough near 1.0, indicating it travels at the same velocity as water. In contrast, a solute subjected to geochemical reactions would experience slower transport and breakthrough at a PV greater than 1.0. In this case, the breakthrough PV reflects the effect or effects of geochemical reactions such as reduction, precipitation, and adsorption – which may increase in extent and rate by the added amendments. Therefore, the breakthrough PV for each technology is compared to the control (untreated) breakthrough PV. Additional details on how these values were calculated are presented in Appendix A, Section A.3.3. Because the tests for perched water conditions were initiated with PCOIs and CoCOIs in sediments, as is expected under field conditions, initial retardation could not be measured.

The mass of PCOIs and CoCOIs sequestered in the sediments is monitored based on effluent analysis during loading (with SGW solutions with PCOIs and with or without CoCOIs) and leaching (with SGW or SPW solutions) with subsequent solid phase analysis post-experiment. These data allow for (1) determination of 50% threshold criteria for sequestration by each technology as compared to the control and (2) comparisons of PCOI retention at different points in time across technologies. The threshold criteria are compared based on the total sequestered mass after leaching with SGW or SPW for approximately 100 PVs. It is important to note that the measured mass sequestered may not represent a permanent immobilization of PCOIs, depending on the mechanisms of sequestration (e.g., reduction, precipitation, adsorption). To illustrate these phenomena, the sequestered mass is shown over time across different phases of experiments (e.g., loading and leaching). Moreover, variations in the mass of amendment per gram of sediment across technologies arise due to differences in methods of emplacement and delivery depending on amendment type (i.e., liquid or particulate) and other factors in these experiments. However, each technology was evaluated under optimal laboratory conditions to maximize its performance potential. In field applications, varying loadings and distributions of amendments are anticipated based on the method of delivery; however, these factors are beyond the scope of this analysis.

Sections 3.2.1 and 3.2.2 summarize the treatment conditions for each of the technologies tested for direct injection into perched water and development of a PRB at the water table, respectively. Relatively similar amendment concentrations were used for each of the sequestration steps with Poly-PO_4 in the multi-step technologies, though injection concentrations were higher for the liquid-phase chemical reduction and sequestration technology (CPS+Poly-PO_4) in an attempt to produce Ca:P ratios that were closer to apatite

(5:3). Moreover, the liquid-phase chemical sequestration technology (Ca-Cit-PO_4) has a lower P concentration due to solubility limitations. For example, particulate amendments were mixed directly with sediments prior to column packing and ranged from 0.001 to 0.015 g/g of sediment, while liquid-apatite forming solutions were either directly mixed with sediments or injected into columns and varied from 160 to 600 µg P/g (or 0.0006 to 0.00016 g/g).

In addition, some amendments have different amounts of reductant added, though they are relatively comparable across most of the inorganic reductants [i.e., Sn(II)-PO_4, SMI, and CPS, see Table 3.1]. Both the amendment loading concentration in sediments and the resulting reduction capacity added are included for comparison. Reduction capacity was not quantified for bioreduction technologies, such as molasses, due to the complexities (i.e., direct microbial reductive capacity changes with microbial population, growth, death, and pathways, and subsequent microbial reduction of Fe and Mn oxides also increases abiotic reductive capacity), though some inferences are made based on energetics (favorability) and theoretical e^- generation from different pathways. Kinetic leaching rates for each technology are summarized in the associated appendices but are only qualitatively compared within this section because of the significant variability in amendment loading and PCOI (and CoCOI) retention across testing timelines for each technology.

Table 3.1. Summary of treatment conditions for technologies targeting perched water.

Technology	Amendment	Ground-water	Sediment	Amendment Loading[a]
Perched Water Conditions below the B Complex[b]				
Particulate-phase chemical sequestration	Sn(II)-PO_4	SPW	CCu-PZsd	0.005 g/g Sn(II)-PO_4 (0.02 meq e^-/g)[c] + 186 µg P/g as Poly-PO_4
Particulate-phase combined chemical reduction and sequestration	SMI + Poly-PO_4	SPW	CCu-PZsd	0.001 g/g SMI (0.06 meq e^-/g) + 220 µg P/g as Poly-PO_4
Particulate-phase chemical sequestration (Bi)	BSN	SPW	CCu-PZsd	0.015 g/g BSN
Liquid-phase chemical sequestration	Ca-Cit-PO_4	SPW	CCu-PZsd	300 µg P/g as Ca-Cit-PO_4 (2,900 µg TOC/g from citrate)
Liquid-phase combined chemical reduction and sequestration	CPS + Poly-PO_4	SPW	CCu-PZsd	6,100 µg S/g as CPS (0.22 meq e^-/g) + 600 µg P/g as Poly-PO_4
Liquid-phase combined bioreduction and chemical sequestration	Molasses + Poly-PO_4	SPW	CCu-PZsd	234 µg/g TOC as molasses + 220 µg P/g as Poly-PO_4

(a) For technologies, amendment concentrations added are per gram of sediment and may be greater for perched water conditions below the B Complex than BY Cribs groundwater conditions due to additional reduction capacity requirements. For reducing amendments, reduction capacity is shown in parenthesis in meq e^- per gram of sediment.
(b) Perched water conditions below the B Complex included all PCOIs and CoCOIs (U, Tc-99, and NO_3 for all conditions).
(c) Based on the reductive capacity, 0.12% Sn/Sn-apatite was calculated (g/g) or 9.98 mol Ca and 0.012 mol Sn in apatite [$Ca_{10}(PO_4)_6(OH)_2$].

Table 3.2. Summary of treatment conditions for technologies targeting BY Cribs groundwater conditions.

Technology	Amendment	Ground-water	Sediment	Amendment Loading[a]
BY Cribs Groundwater Conditions[b]				
Particulate-phase chemical sequestration	Sn(II)-PO_4	SGW	CCug	0.005 g Sn(II)-PO_4/g (0.02 meq e^-/g) + 185 µg P/g as Poly-PO_4
Particulate-phase combined chemical reduction and sequestration	SMI + Poly-PO_4	SGW	CCug	0.001 g/g SMI (0.06 meq e^-/g) + 220 µg/g PO_4 as Poly-PO_4
Particulate-phase chemical sequestration (Bi)	BSN	SGW	CCug	0.015 g BSN/g
Liquid-phase chemical sequestration	Ca-Cit-PO_4	SGW	CCug	Bioreduction from citrate (1.55 mg C/g) + 160 µg P/g as Ca-Cit-PO_4
Liquid-phase combined chemical reduction and sequestration	CPS + Poly-PO_4	SGW	CCug	600 µg S/g as CPS (0.048 meq e^-/g) + 260 µg P/g as Poly-PO_4
Liquid-phase combined bioreduction and chemical sequestration[c]	Molasses + Poly-PO_4	SGW	CCug	854 µg/g TOC as molasses + 220 µg/g PO_4 as Poly-PO_4

(a) For technologies, amendment concentrations added are per gram of sediment. For reducing amendments, reduction capacity is shown in parenthesis in meq e^- per gram of sediment.
(b) BY Cribs groundwater conditions included one set of experiments with only PCOIs (U and Tc-99) and one with both PCOIs and CoCOIs (NO_3, I, Cr, and Sr).
(c) For the liquid-phase combined bioreduction and chemical sequestration technology, NO_3 is a PCOI and was always present.

3.2.1 B Complex Perched Water

3.2.1.1 Technetium

For Tc-99, particulate reductants performed well for perched water conditions, including Sn(II)-PO_4 and SMI+Poly-PO_4, with > 75% of Tc-99 retained in sediments. CPS+Poly-PO_4 also sequestered a significant amount of Tc-99 following leaching (~36%). These three technologies [Sn(II)-PO_4, SMI+Poly-PO_4, and CPS+Poly-PO_4] met the performance threshold with a > 50% increase in sequestered Tc-99 as compared to the control (<10% retained after leaching). Ca-Cit-PO_4, BSN, and molasses+Poly-PO_4 did not meet performance metrics and released most of the Tc-99 by the end of the leaching phase.

Particulate reductants performed well for perched water conditions, including Sn(II)-PO_4 and SMI+Poly-PO_4, based on leaching experiments conducted after initial equilibration of sediments, amendments, and PCOIs and CoCOIs for approximately 6 weeks (additional details in Section 2.4.2). This is potentially due to the presence of an immobile reductant (as compared to liquid reductants that flush out over time). More than 75% of Tc-99 was sequestered after 100 PVs of leaching for both technologies as compared to < 10% for the control column [with > 0.2 µg of Tc/g of sediment sequestered for Sn(II)-PO_4 after leaching. Note: Approximately 10× less Tc-99 was added for SMI+Poly-PO_4, so total mass sequestered cannot be compared]. However, CPS+Poly-PO_4 also met the performance threshold of > 50% increase in sequestered Tc-99 as compared to the control conditions with 34% of Tc-99 sequestered after 100 PVs of leaching (or 0.09 µg/g sequestered as compared to 0.02 µg/g for the control column).

Figure 3.8 and Figure 3.9 summarize initial leaching and mass sequestered, respectively. Figure 3.8 shows the amount of Tc-99 leaching over time, while Figure 3.9 shows the mass of Tc-99 sequestered over time (as PVs) in (a) with the total fraction sequestered after 100 PVs of leaching in (b). Overall, approximately 75% of Tc-99 was retained after > 100 PVs of leaching for both Sn(II)-PO_4 and SMI+Poly-PO_4.

The two particulate reductant technologies, Sn(II)-PO_4 and SMI+Poly-PO_4, performed well under the perched water conditions with approximately 6 weeks of reaction time prior to leaching. These reaction times should be sufficient as initial sequestration (via reductive precipitation) was observed in batch experiments within hours for Sn(II)-PO_4 and days for SMI+Poly-PO_4, as reported in the Phase 1 report (PNNL-35432). Similar results were observed for both amendments, despite them being added at significantly different reduction capacities [summarized in Table 3.1, 0.02 and 0.06 meq e^-/g for Sn(II)-PO_4 and SMI+Poly-PO_4, respectively], suggesting that both amendments may have a higher capacity for reduction of Tc-99. For CPS+Poly-PO_4, initial sequestration was also relatively fast, on the order of hours (PNNL-35432).

In the field, amendment reaction times would likely be greater than in a confined aquifer due to the movement of pore water through low-permeability zones, assuming the amendments could be delivered to these zones. Long-term batch studies were conducted to evaluate contaminant remobilization potential (via sequential extractions) with longer reaction times with amendments (up to 300 days), as described in Appendix F for Sn(II)-PO_4, Appendix G for SMI+Poly-PO_4, and Appendix J for CPS+Poly-PO_4. Sn(II)-PO_4 and CPS+Poly-PO_4 showed very little remobilization of Tc-99 [> 90% and > 75% for Sn(II)-PO_4 and CPS+Poly-PO_4, respectively] after reaction for > 270 days. However, SMI+Poly-PO_4 showed more substantial Tc-99 remobilization by 300 days (~50% as compared to ~20% immobilized in the control). These results suggest different potential mechanisms of sequestration for each technology, even though each initially met the targeted reduction fraction.

The results for both particulate amendments [Sn(II)-PO_4 and SMI+Poly-PO_4] suggest that Tc-99 is predominantly reduced to a low-solubility TcO_2-like phase coordinated with the amendment – phosphate in the case of Sn(II)-PO_4 and iron in the case of SMI+Poly-PO_4 (Pearce et al. 2018; Plymale et al. 2011). This is consistent with X-ray absorption spectroscopy (XAS) results summarized for batch experiments with (1) SMI+Poly-PO_4 in Figure 3.10 and Appendix G, Section G.1, where most Tc-99 was measured in the +4 oxidation state as TcO_2 coordinated with Fe oxide on the surface of SMI; and (2) Sn(II)-PO_4 in Appendix F, Section F.3.3, where most Tc-99 was measured in the +4 oxidation state as TcO_2 with evidence for Tc-P bonding, suggesting coordination with phosphate. For SMI+Poly-PO_4, Tc-99 remained immobilized on the surface even after 120 PVs of oxidation during leaching. However, this phase may still be susceptible to reoxidation, depending on the number of TcO_2 units in the chain attached to an Fe oxide surface (likely magnetite), with longer chains more likely to be oxidized. Subsequent precipitation of an additional phase (i.e., calcium phosphate) could limit the extent of reoxidation. With Sn(II)-PO_4, the presence of a Tc-P bond suggests a more direct interaction with phosphate, once the Tc-99 has been reduced by Sn(II). Preliminary research has suggested a more specific reduction pathway for Tc-99 with Sn(II)-PO_4 (Asmussen et al. 2016, 2018; RPP-53855). Effluent monitoring results suggest that significant nitrate reduction did not occur in the presence of Sn(II)-PO_4 under these conditions (Section 3.2.1.3, Figure 3.14). If confirmed, Sn(II)-PO_4 may perform better than some other reductants, as the reaction may be more specific to Tc-99 and subsequent coordination with P may allow for less remobilization over time.

Treatment with CPS (with or without Poly-PO_4, as described in Appendix J, Section J.3.2) was the next best performer with relatively similar leaching trends, though greater leaching overall was observed with approximately 34% remaining after leaching. Solid phase characterization (Section J.3.3) shows that Tc-99 visually correlated with S and P in elemental maps (via X-ray fluorescence) and was nearly

completely reduced (+4) in the solid phase. Therefore, it is likely that any Tc-99 leached from the solid phase was oxidized to TcO_4^-. Previous research has shown that Tc-sulfides (primarily TcS_2 or Tc_2S_7) have a low solubility (< TcO_2) and may resist reoxidation (Pearce et al. 2018). The potential for formation of Tc-sulfides may explain the lower remobilization of Tc-99 as compared to SMI+Poly-PO_4, because S content in SMI was likely significantly lower than CPS. In addition, Poly-PO_4 may form calcium phosphate phases (e.g., apatite) that may coat Tc-99 phases and decrease release. However, there was still relatively significant remobilization of Tc-99 with time, suggesting that low-solubility apatite may not have formed in these conditions (additional details in Section J.3.2). Moreover, the lesser success with the CPS+Poly-PO_4 amendments suggests that the reduced S from CPS was likely advected out of the sediment columns, as opposed to SMI+Poly-PO_4, where S was more likely to remain in the solid phase, allowing for heterogeneous reduction of Tc-99 (Peretyazhko et al. 2008; Technical Report 96-03). The fast release of S for CPS+Poly-PO_4 is shown in Section J.5.2, where effluent S was initially an order of magnitude higher for treated columns and reached similar concentrations by approximately 20 PVs.

BSN, molasses+Poly-PO_4, and Ca-Cit-PO_4 performed the worst, with leaching curves mirroring the control column without treatment as shown in Figure 3.8 (with < 11% or 0.03 µg/g of Tc-99 sequestered after leaching). After equilibration of amendments with PCOIs (and CoCOIs) in sediments over several weeks, neither amendment retained significantly more Tc-99 than the untreated control column (0.022 µg/g Tc-99). For BSN, Tc-99 sequestration may have been inhibited due to the high ionic strength of the SPW, leading to release of Tc-99, since previous research suggests that Tc-99 uptake by BSN was likely via anion exchange or outer sphere (electrostatic) complexation (Pearce et al. 2025). Both sequestration mechanisms would be very sensitive to solution ionic strength as elevated solution ionic strength will (1) add ions that compete for ion exchange sites and (2) compress the electrical double layer around charged surfaces, decreasing the capacity for outer sphere complexation (Sposito 1994).

The molasses+Poly-PO_4 may also have been impacted by the increased solution ionic strength as it may have inhibited microbiological activity. In addition, excess nitrate under these conditions likely consumed reduction capacity generated by microbes prior to reducing Tc-99, due to its relatively higher reduction potential (PNNL-18139), additional details in Appendix K, Section K.5.2. Similarly, for Ca-Cit-PO_4, the significant reduction of nitrate observed (Figure 3.14) suggests only partial reduction of Tc-99. However, it is also possible that whatever fraction of Tc-99 initially reduced was quickly oxidized and advected out of the column. For molasses+Poly-PO_4 and Ca-Cit-PO_4, a significant fraction was removed during the 100 PV leach (> 80% and > 90%, respectively).

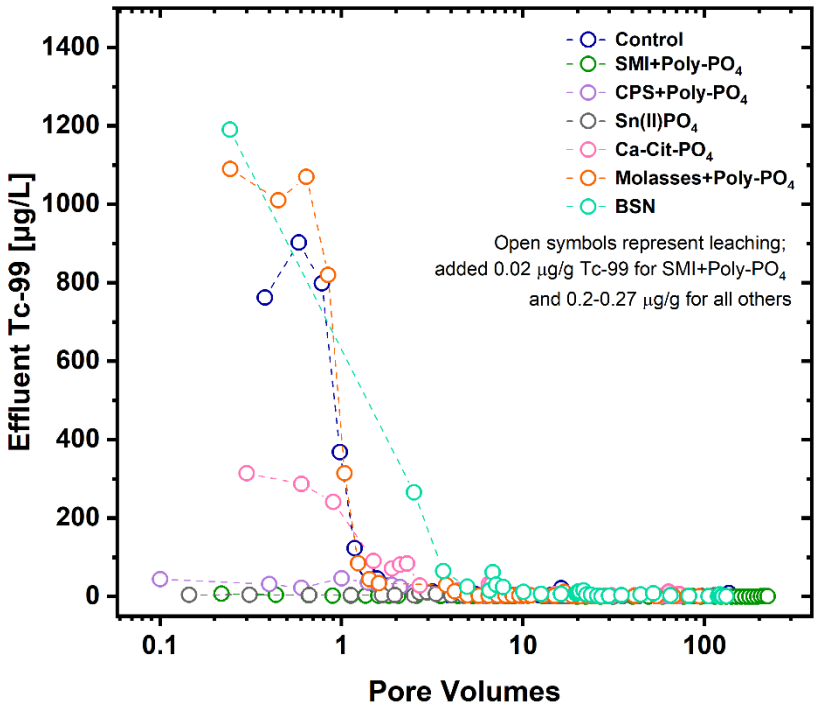

Figure 3.8. Tc-99 mobilization during leaching from sediments in columns via constant injection, with SPW represented as aqueous Tc-99 measured in the effluent in µg/L over time as indicated by the number of PVs of solution injected on the x-axis.

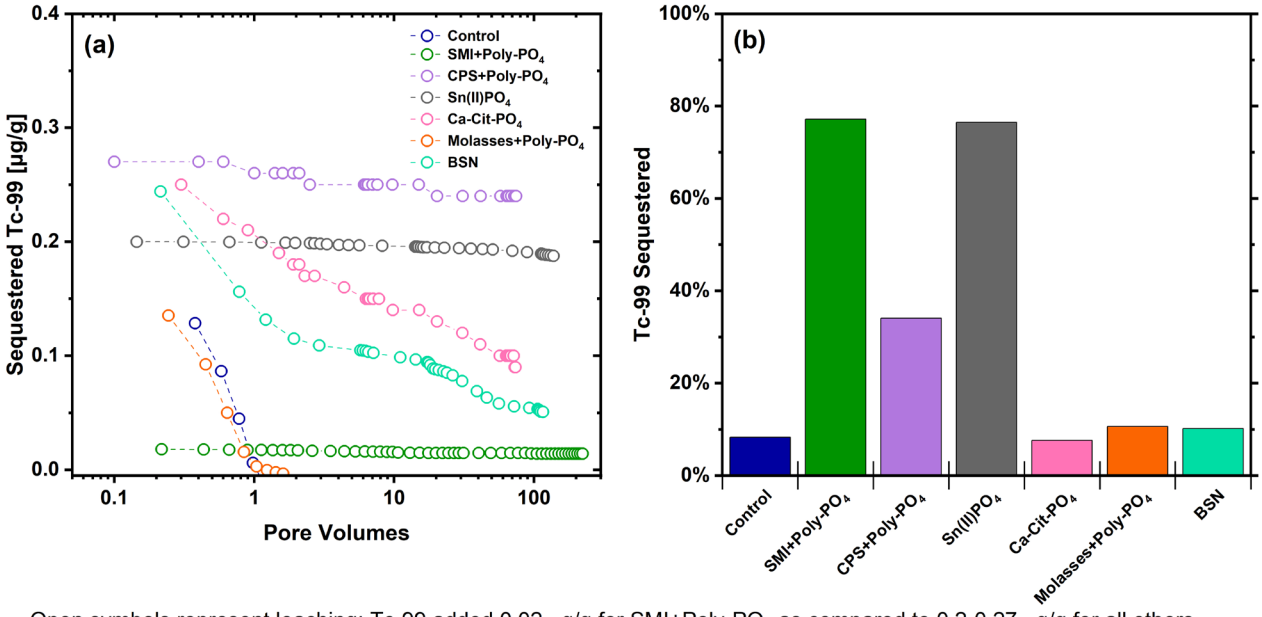

Figure 3.9. Tc-99 mass sequestered after leaching from sediments in columns, where (a) represents the mass of Tc-99 in sediments in µg/g over time, as indicated by the number of PVs of solution injected on the x-axis during leaching (*open symbols*), and (b) shows sequestered Tc-99 as % of initial mass loaded that remains after leaching.

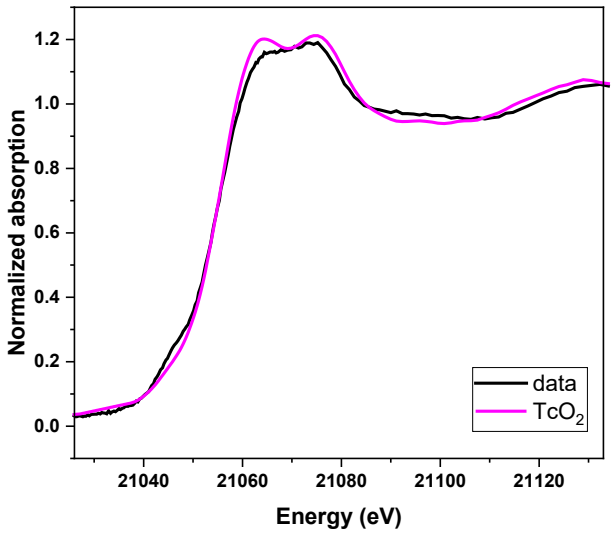

Figure 3.10. Tc-99 K-edge X-ray absorption near edge structure (XANES) for CCu-PZsd sediment reacted with SMI-PO_4 in a batch as compared to a TcO_2 standard showing that Tc-99 is reduced to +4 in the solid phase.

3.2.1.2 Uranium

For U, SMI+Poly-PO_4 performed well with relatively low and constant effluent leaching concentrations and sequestration of ~150 µg U/g after leaching. All other amendments resulted in significant leaching with final U concentrations below the background concentrations in sediments.

For U, SMI+Poly-PO_4 performed well, while all other amendments led to significant mobilization of U during leaching. Figure 3.11 and Figure 3.12 summarize initial leaching and mass sequestered, respectively. Figure 3.11 shows the amount of U leaching over time based on effluent concentrations, while Figure 3.12 shows the mass of U sequestered over time (as PVs) in (a) with the fraction of mass sequestered after leaching in (b). The performance threshold targeting > 50% increase in sequestration as compared to the control was challenging to set due to fluctuations in background U (shown by effluent breakthrough in Appendix A, Figure A.5), likely due to heterogeneity in sediments. Therefore, success for U in perched water conditions was determined by examining all types of data collected, including the mass sequestered after leaching and the rates of release.

For SMI+Poly-PO_4, relatively low and consistent release of U was observed across the leaching phase (effluent concentrations < 600 µg/L, leaving > 90% or 150 µg/g of U sequestered after 220 PVs of leaching), as compared to significantly higher release in the control column (< 5 µg/g of U remaining sequestered) and for all other amendments (next highest for BSN with ~50% or 50 µg/g of U sequestered), as shown in Figure 3.11. Notably, all other amendments resulted in significant leaching, with the final U concentrations in sediments falling below the initial background concentrations in some tests [~70.3 µg/g – based on 8 M HNO_3 acid extractions summarized in Appendix A, Section A.7, of the Phase 1 report (PNNL-35432)]. The release of U from sediments was much faster for all other amendments, as summarized in Figure 3.12a. Ca-Cit-PO_4 performed the worst, with the fastest release observed, similar to the untreated control column, though the ultimate differences between all other amendments were not significant.

For technologies targeting reduction [SMI+Poly-PO_4, CPS+Poly-PO_4, Sn(II)-PO_4, and molasses+Poly-PO_4], nitrate was present as the largest electron acceptor and likely consumed significant reduction potential prior to reducing U in most cases (i.e., note that nitrate was not reduced by SMI). Moreover, nitrate has been strongly correlated with U contamination in groundwater, with the potential to mobilize U due to oxidative dissolution (Nolan and Weber 2015). However, it is also possible that reduced sulfur species will be oxidized prior to U reduction, when nitrate-reducing conditions are present. This has been observed for microbial reduction in a shallow groundwater system (Paradis et al. 2016). Therefore, the presence of reduced sulfur in the SMI+Poly-PO_4 amendment may allow for longer term sequestration of U, especially as Poly-PO_4 may precipitate and coat U with apatite phases. Notably, U in batch experiments was primarily present as U(VI), as shown in Figure 3.13; therefore, reduction is likely not the primary sequestration mechanism. The fast release of S for CPS+Poly-PO_4 is shown in Appendix J, Section J.5.2, where effluent S was initially an order of magnitude higher for treated columns and reached similar concentrations by approximately 20 PVs.

For technologies targeting *in situ* precipitation of apatite (SMI+Poly-PO_4, CPS+Poly-PO_4, and Ca-Cit-PO_4), the presence of high ionic strength and alkalinity may have led to formation of higher solubility calcium phosphate phases (e.g., orthophosphates) as opposed to apatite (Rakovan 2002). If formed, many heavy metal phosphates have a higher solubility than apatite, though their solubility tends to decrease with increasing calcium substitution (Ayati and Madsen 2000). In addition, carbonated apatites have been previously shown to form in the presence of elevated carbonate concentrations, exhibiting lower crystallinity and higher solubility (Hughes and Rakovan 2015; Heslop et al. 2005). Therefore, it is likely that conditions for formation of low-solubility apatite and incorporation of U were not favored under these high ionic strength conditions due to a multitude of factors. Finally, the reaction time of approximately 6 weeks may not have been sufficient for transformation of initial amorphous Ca-PO_4 precipitate to crystalline apatite under these complex conditions and may not represent field reaction times, depending on groundwater flow rates and treatment volumes.

However, the perched water conditions, with relatively high ionic strength, nitrate, and mass loading of U, made it exceptionally difficult to sequester U. In addition, the alkaline pH and elevated carbonate concentrations commonly observed within the Hanford Site, including perched water (PNNL-28054; PNNL-35432), are known to form neutral and negatively charged U-carbonates that are highly mobile (Dong et al. 2005; Dong and Brooks 2006; Zhou and Gu 2005; PNNL-17031). However, it is possible that longer reaction times with amendments could result in greater sequestration. Previous field characterization in the 300 Area reported significant sequestration of U approximately 6 months after injection (PNNL-29650). Moreover, long-term batch experiments showed that after 270 days of reaction, significant sequestration of U occurred [> 60% for Sn(II)+PO_4, > 80% for CPS+Poly-PO_4, and > 90% for SMI+Poly-PO_4]. This may be the result of U sequestration mainly by PO_4 (i.e., autunite precipitation, incorporation into apatite, U adsorption to apatite) rather than U reduction and precipitation.

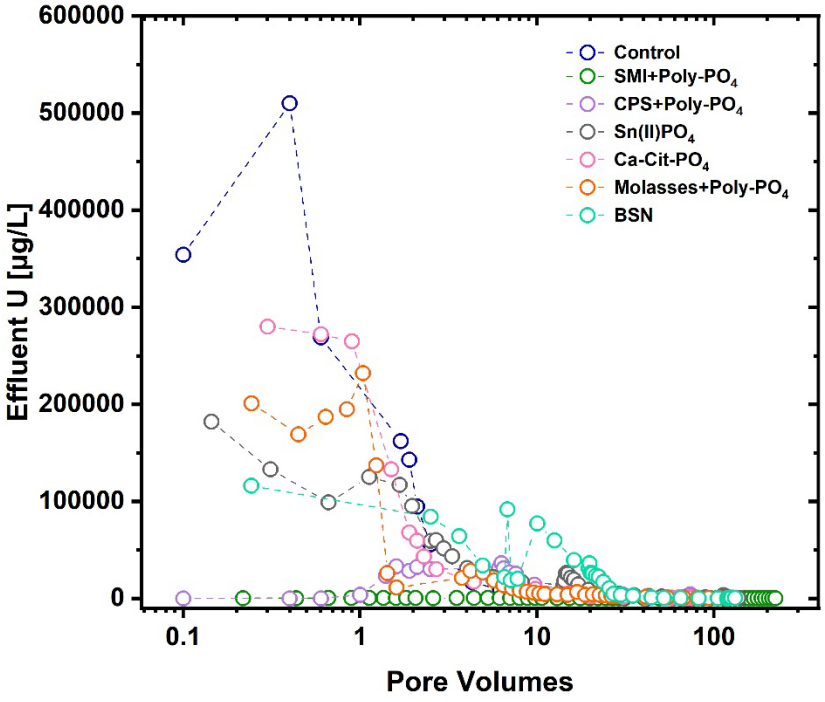

Figure 3.11. U mobilization during leaching from sediments in columns via constant injection with SPW represented as aqueous U measured in the effluent in µg/L over time, as indicated by the number of PVs of solution injected on the x-axis.

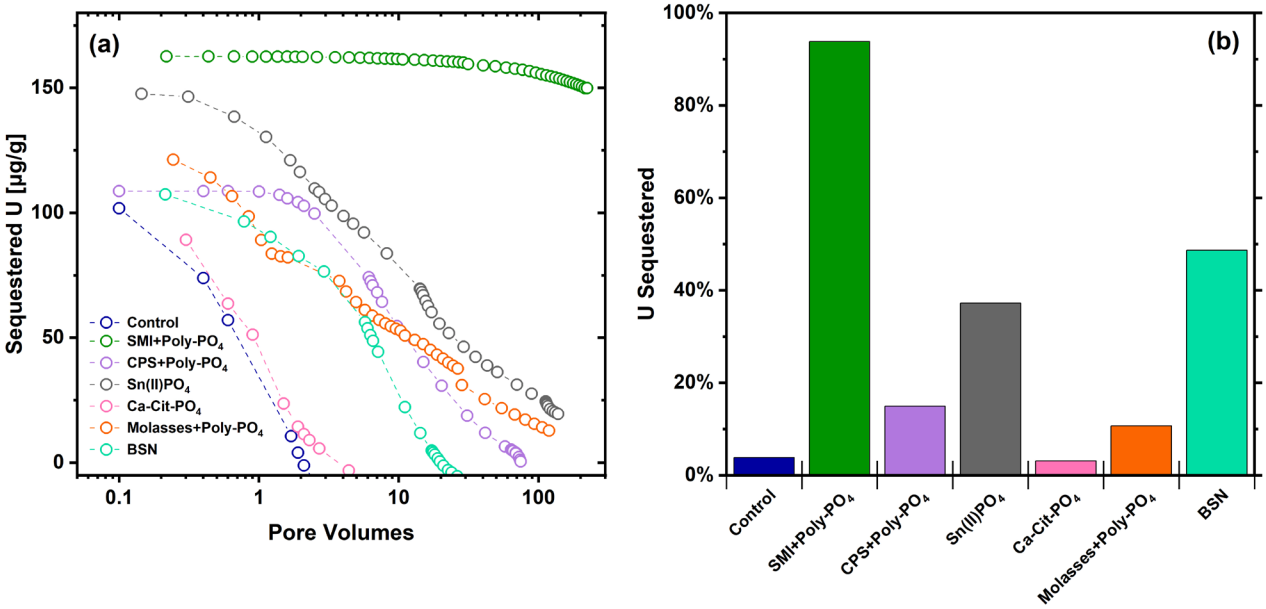

Figure 3.12. U mass sequestered after leaching from sediments in columns, where (a) represents the mass of U in sediments in µg/g over time as indicated by the number of PVs of solution injected on the x-axis during leaching (*open symbols*) and (b) shows sequestered Tc-99 as a percentage of initial mass loaded that remains after leaching.

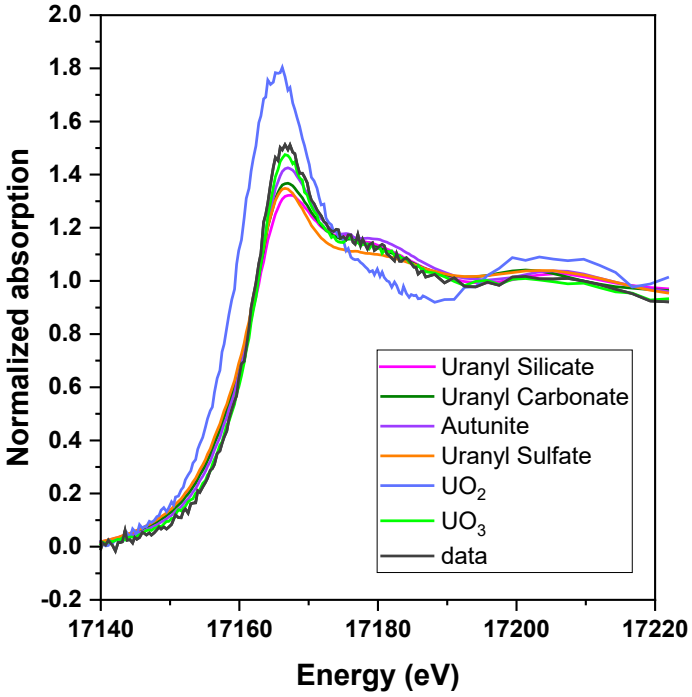

Figure 3.13. U L3-edge XANES for U in CCu-PZsd sediment reacted with SMI+Poly-PO_4 for approximately 1 week in a batch.

3.2.1.3 Nitrate

Figure 3.14 shows nitrate release from CCu-PZsd sediment columns during approximately 100 PVs of leaching based on effluent concentrations. Some nitrate reduction was observed for select technologies; however, significant nitrate remained across all technologies. The lowest nitrate concentrations were measured in the Ca-Cit-PO_4 columns, suggesting that citrate was oxidized to CO_2 rather than being fermented to hydrogen (as this is more energetically favorable when nitrate concentrations are high). Results for molasses+Poly-PO_4 and SMI+Poly-PO_4 show a decrease in effluent concentrations as compared to the control, suggesting nitrate reduction also occurred to a lesser extent under these conditions. However, for CPS+Poly-PO_4 and Sn(II)-PO_4, significant reduction of nitrate is not observed as compared to the control. Finally, the highest effluent concentrations were measured for BSN, likely due to exchange of nitrate on surfaces for aqueous carbonate during initial solution injection, leading to the observed delay in nitrate release as compared to other conditions.

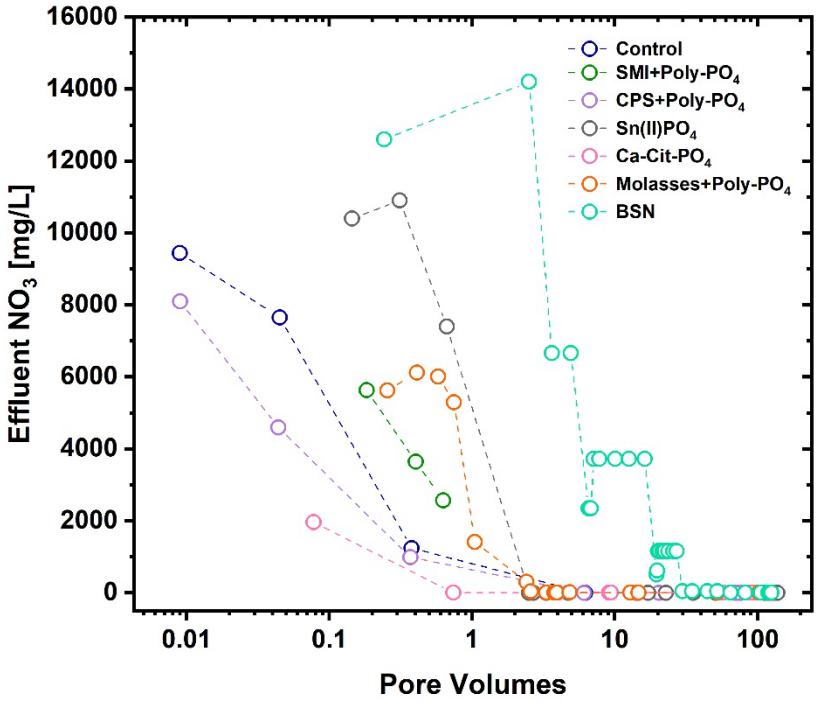

Figure 3.14. Nitrate mobilization during leaching from columns via constant injection with SPW represented as aqueous nitrate measured in the effluent in mg/L over time, as indicated by the number of PVs of solution injected on the x-axis.

3.2.2 BY Cribs Groundwater

3.2.2.1 Technetium

For Tc-99, treatment with molasses+Poly-PO_4 outperformed five other amendments when CoCOIs were present based on two parameters: breakthrough PV and the total amount of sequestered Tc-99. However, the 50% sequestration threshold was also met for CPS+Poly-PO_4. Without CoCOIs, CPS+Poly-PO_4, SMI+Poly-PO_4, and Sn(II)-PO_4 performed similarly to molasses+Poly-PO_4 with breakthrough PVs > 90. In addition, Sn(II)-PO_4 and CPS+Poly-PO_4 had the highest amounts sequestered, with release of Tc-99 from Sn(II)-PO_4 being negligible after leaching. The 50% threshold was met for molasses+Poly-PO_4, CPS+Poly-PO_4, Ca-Cit-PO_4, and Sn(II)-PO_4. The Ca-Cit-PO_4, SMI+Poly-PO_4, and Sn(II)-PO_4 treatments were especially impacted by the presence of CoCOIs, and BSN treatment showed relatively poor retardation and sequestration with breakthrough PVs < 10 for all conditions with and without CoCOIs.

Under the most relevant field conditions, when CoCOIs were present in the injection solution, molasses+Poly-PO_4 outperformed all other technologies for Tc-99 (Figure 3.15 and Figure 3.16) (additional details are included in Appendix K, Section K.4.1), with 80% sequestered after 100 PVs of leaching or 0.65 µg/g Tc-99 (> 50% more than the control). However, the 50% performance metric was also met for CPS+Poly-PO_4 and Ca-Cit-PO_4 (with 0.28 and 0.029 µg/g of Tc-99 sequestered after leaching, respectively). Tc-99 breakthrough PVs are compared across technologies and in the presence or absence of CoCOIs (Figure 3.15b and d). Changes in Tc-99 effluent (as C/C_0 or effluent concentration divided by influent concentration) as a function of PVs are also presented (Figure 3.15a and c). In Figure 3.16, long-term sequestration of Tc-99 is measured, where sequestered Tc-99 over time is shown

alongside the total fraction of sequestered Tc-99 after loading and leaching to illustrate the potential for long-term sequestration. Tc-99 effluent concentrations were below detection limits (0.37 µg/L) until approximately 50 PVs for the molasses+Poly-PO_4 treatment, whereas all other technologies detected Tc-99 in effluents within three PVs. For technologies that require native microbial populations (e.g., molasses+Poly-PO_4) to generate reducing conditions, different subsurface systems or conditions may have differing microbe populations available to consume the amendments and generate reducing conditions. Therefore, core characterization and testing should be conducted prior to implementation for each potential site.

The breakthrough PV for molasses+Poly-PO_4 is the largest measured in the presence of CoCOIs by more than double, with breakthrough occurring near 70 PVs. Complete Tc-99 breakthrough (i.e., $C/C_0 = 1$) was reached for all technologies, confirming that maximum uptake capacity was reached under these experimental conditions in the presence of CoCOIs. The performance of molasses compared with other technologies, particularly in the presence of Cr, may be partially due to the presence of natural organic matter (NOM) in molasses. NOM may act as both (1) an electron shuttle to promote reduction of sedimentary Fe(III) and other electron acceptors including Cr(VI) (Field et al. 2013; Yang et al. 2022; Gerlach et al. 2011) and (2) a direct reductant of Cr(VI) in the absence of biotic activity (Field et al. 2013; Chen et al. 2015). In addition, the potential inhibition of biological activity by Cr(VI) may have been ameliorated by the Cr-NOM complexation (or other organics in the molasses or subsequent metabolites) (Konopka et al. 2013; Kourtev et al. 2009; Yang et al. 2022). Also, reduction of TcO_4^- by biogenic Fe(II) can lead to Tc(IV)-Fe phases in which the solubility of Tc-99 is lower than the literature value for the solubility of TcO_2 (Plymale et al. 2011).

Treatment with CPS (with or without Poly-PO_4, as described in Appendix J) was the next best performer (approximately 0.28 µg/g of Tc-99 sequestered after leaching and breakthrough occurring near 40 PVs), although reduction capacity was likely consumed prior to switching to the contaminant-free leaching solution based on the significant Tc-99 release observed in the effluent – reaching $C/C_0 > 1.4$ before switching to leaching. Figure 3.15c and Figure 3.16c include effluent C/C_0 and sequestered Tc-99 masses per gram of sediment, respectively. Previous research has shown that Tc-sulfides (primarily TcS_2 or Tc_2S_7) have a low solubility (< TcO_2) and may resist reoxidation (Pearce et al. 2018). In addition, Poly-PO_4 may form calcium phosphate phases (e.g., apatite) that may coat Tc-99 phases and decrease release. However, Poly-PO_4 did not significantly improve sequestration of Tc-99 in experiments (Figure 3.16 and Appendix J, Section J.3). In long-term batch experiments (up to 300 days), Poly-PO_4 (added with CPS) improved sequestration of Tc-99 compared to the CPS treatment (Appendix J, Section J.2.1), which suggests that coating with calcium phosphate may occur if flow rates are lower or reaction times are longer with Poly-PO_4 allowing for Tc-sulfides to form.

If additional amendment was delivered for the inorganic reductants (SMI+Poly-PO_4, Sn(II)-PO_4, and CPS+Poly-PO_4), they may perform similarly to or better than molasses+Poly-PO_4. However, SMI (with or without Poly-PO_4, as described in Appendix G) breakthrough occurred much faster than CPS (on the order of tens of PVs). It is possible that the liquid reductant (CPS) reduced Tc-99 more quickly than the particulate reductant (SMI), potentially because the polysulfide directly reduced Tc-99 in solution (homogenous reduction), as relatively similar amounts of reductant were added (Table 3.2) with significantly greater reduction observed for liquid CPS. Literature has not directly compared the liquid polysulfide reductant with SMI, with the exception of preliminary testing for this work (PNNL-35432; PNNL-31959), which did not consider kinetics. However, previous research has reported differing rates for Tc-99 reduction by dissolved iron (homogenous reduction) as compared to particulate iron (heterogeneous reduction) (PNNL-17031; Peretyazhko et al. 2008; Bae and Hanna 2015). Note, however, that SMI may perform better in the field, where a larger volume of the subsurface is treated, as residence times would be significantly greater than in these columns [targeting groundwater flux of 0.6 m/day (2 ft/day) or a 6-hour residence time within columns], decreasing the importance of kinetics. However, SMI

and CPS cannot be directly compared because of the difference in injection solution concentrations of Tc-99 during the loading phase (injection of 4.7 vs. 100 µg/L for SMI and CPS, respectively).

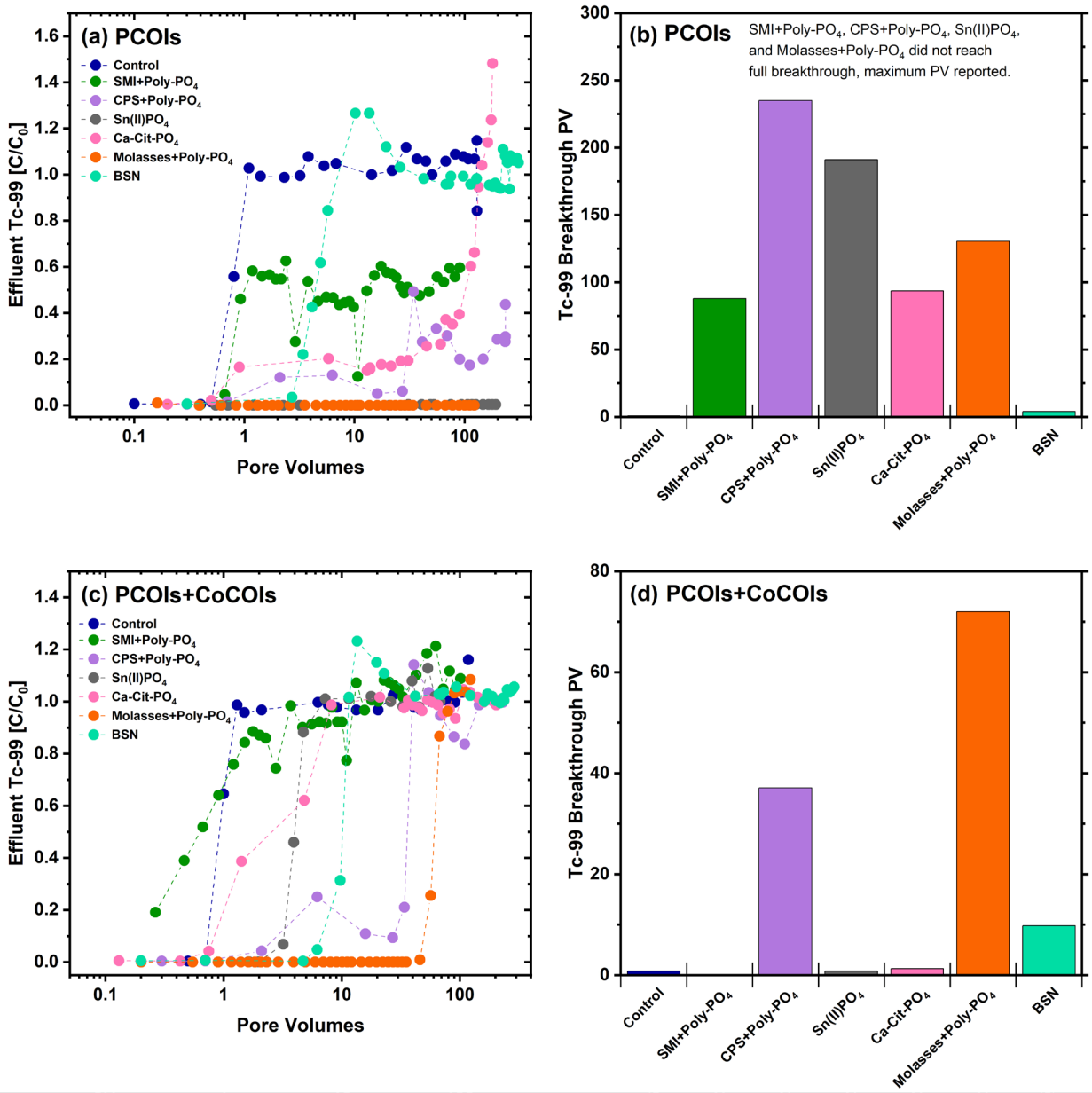

Figure 3.15. Tc-99 retardation during loading into columns via constant injection with SGW, where (a) and (c) represent aqueous Tc-99 as C/C_0, equivalent to effluent concentration divided by influent concentration, over time as indicated by the number of PVs of solution injected on the x-axis without and with CoCOIs, respectively, and (b) and (d) show breakthrough PV for Tc-99 in (a) and (c) without and with CoCOIs, respectively.

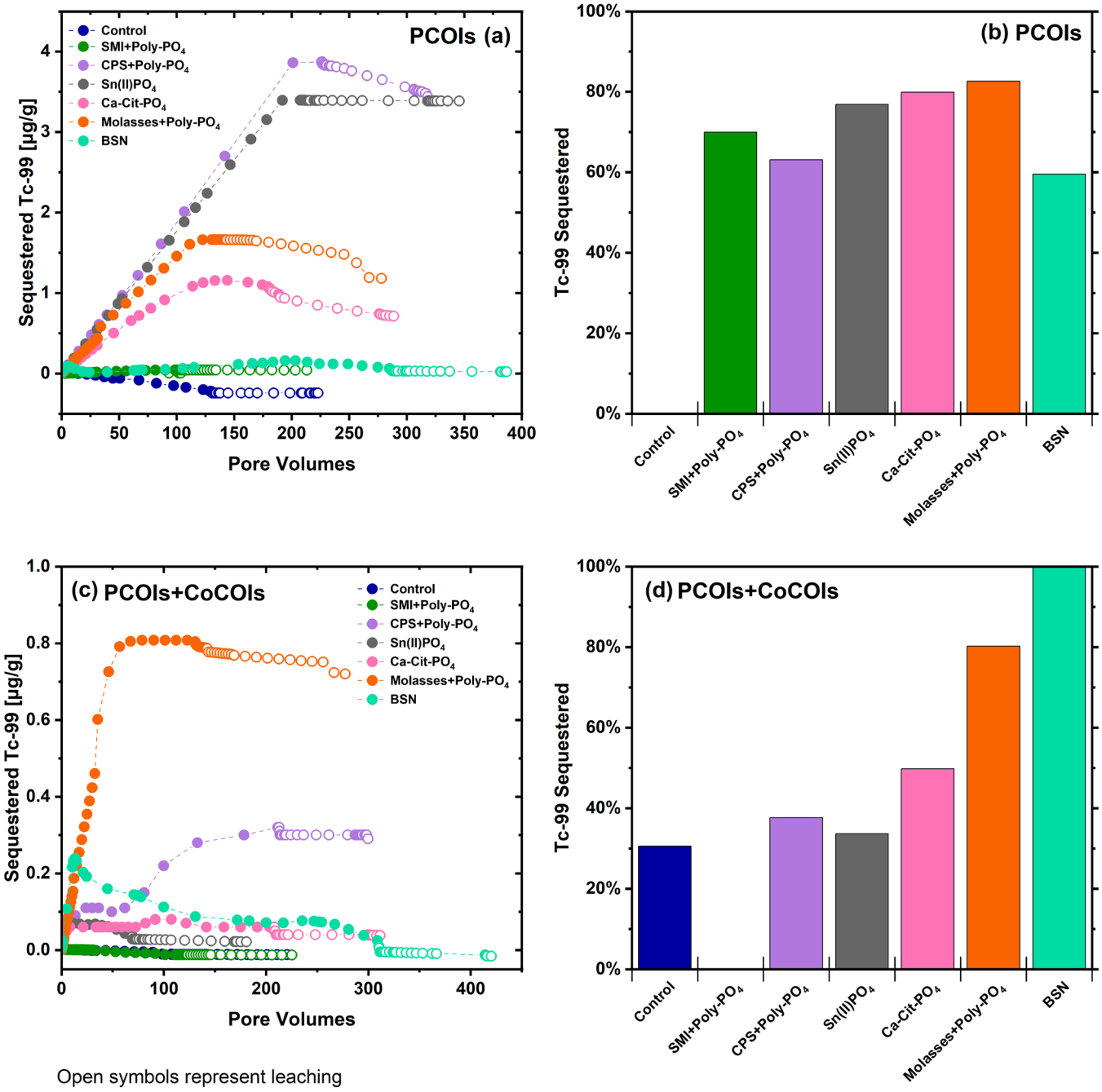

Figure 3.16. Tc-99 mass sequestered after loading and leaching in columns, where (a) and (c) represent the mass of Tc-99 in sediments in µg/g over time as indicated by the number of PVs of solution injected on the x-axis during loading (*solid symbols*) and leaching (*open symbols*) without and with CoCOIs, respectively, and (b) and (d) show sequestered fraction of Tc-99 mass remaining after 100 PVs of leaching divided by the mass sequestered during loading, without and with CoCOIs, respectively. Note: Y-axis scales are different for (a) and (c). Without CoCOIs, the control column sequestered 0% Tc-99.

In addition, for conditions including CoCOIs, there is value in comparing Tc-99 breakthrough for the two inorganic reductants (SMI and CPS) separately for treatment with only the reductants and with Poly-PO_4 (see Appendix G and Appendix J). There is a repeatable decrease in breakthrough PVs and total amounts sequestered after leaching for tests where Poly-PO_4 was added as compared to those where it was not added (e.g., 0.7 vs. 0.3 µg/g of Tc-99 sequestered after leaching for CPS as compared to CPS+Poly-PO_4). These results are consistent with preliminary testing (PNNL-31959) and results in Section 4.8.4 of the Phase 1 report (PNNL-35432). The additional salts added from the Poly-PO_4 may have led to desorption of reducible anions (e.g., NO_3^-) that consumed some of the available reduction capacity. Although performance was slightly reduced with the addition of Poly-PO_4, the dual amendment addition allows for potential to better sequester other PCOIs and CoCOIs (e.g., U and Sr). Therefore, the two-step reduction/sequestration amendment approach (via CPS+Poly-PO_4 or SMI+Poly-PO_4) needs to consider all potential PCOIs and CoCOIs present before being chosen.

However, under the conditions for these experiments, Ca-Cit-PO_4, BSN, and Sn(II)-PO_4 did not perform well – the amount of Tc-99 sequestered after loading and leaching was relatively similar to the control columns without treatment [0.015 µg/g Tc-99 sequestered for the control as compared to < 0.035 µg/g for Ca-Cit-PO_4, BSN, and Sn(II)-PO_4]. Therefore, these three technologies are not recommended unless injection amounts can be significantly increased. Note that, for Ca-Cit-PO_4, additional amendment could not be delivered by increasing concentrations due to limitations with the solubility of citrate (Baysinger et al. 2015), though multiple injections could be conducted in series.

For BSN, significant release of Tc-99 occurred during the loading phase of experiments (around 10 PVs with a maximum of 0.16 µg/g of Tc-99 around 10 PVs during loading, 0.065 µg/g of Tc-99 remaining at the end of loading, and 0.04 µg/g post-leaching), indicating failure to sequester Tc-99 before leaching was initiated. Previous batch testing has shown significant uptake of Tc-99 without release for up to 2 months (Boglaienko et al. 2024). However, it is possible that BSN transformed to phases that could not uptake Tc-99 [e.g., daubreeite related structures, lay-BiO(OH,Cl)] and/or pH and carbonate fluctuations occurred, impacting uptake. Previous research conducted in the presence of sediments showed some release over time depending on background solutions (Lawter et al. 2021). This is likely due to formation of different secondary phases (like bismutite, which has superior uptake of U) that did not uptake Tc-99 as in the absence of sediments. Moreover, additional research showed that Tc-99 uptake by BSN was likely via anion exchange or outer-sphere complexation, which would be impacted significantly by changes in solution chemistry over time (Pearce et al. 2025).

Sn(II)-PO_4 performed significantly better without CoCOIs present (2.65 vs. 0.02 µg/g of Tc-99 sequestered of > 75% vs. 33% retained from loading after 100 PVs of leaching). The solid phase characterization results for Sn(II)-PO_4 suggest that Tc-99 is predominantly reduced to a low-solubility TcO_2-like phase coordinated with P (Pearce et al. 2018). This is consistent with XAS results summarized for batch experiments in Appendix F, Section F.3.3, where most Tc-99 was measured in the +4 oxidation state as TcO_2 with evidence for Tc-P bonding, suggesting coordination with phosphate. The presence of a Tc-P bond suggests a more direct interaction with phosphate, once the Tc-99 has been reduced by Sn(II). Preliminary research has suggested a more specific reduction pathway for Tc-99 with Sn(II)-PO_4 (Asmussen et al. 2016, 2018; RPP-53855). If confirmed, Sn(II)-PO_4 may perform better than some other reductants, as the coordination with P may allow for less remobilization over time. However, the significant difference in Tc-99 sequestration with or without CoCOIs suggests that either reduction capacity was consumed or geochemical conditions altered the reaction mechanism (e.g., secondary precipitation on surfaces, potentially via formation of $SrCO_3$, or a shift in pH, less than 0.5 unit change observed – details in Appendix F, Sections F.4 and F.5).

In the absence of CoCOIs, most technologies performed better for Tc-99 because the CoCOIs include elements that are more readily reduced than Tc-99, including hexavalent Cr and nitrate (PNNL-18139). Molasses+Poly-PO_4, CPS+Poly-PO_4, SMI+Poly-PO_4, Sn(II)-PO_4, and Ca-Cit-PO_4 all performed well in the absence of CoCOIs – meeting the performance threshold of a minimum 50% increase in sequestration as compared to the control conditions (additional details for molasses+Poly-PO_4 in Appendix K, CPS+Poly-PO_4 in Appendix J, Sn(II)-PO_4 in Appendix F, Ca-Cit-PO_4 in Appendix I, and SMI+Poly-PO_4 in Appendix G).

These four amendments are challenging to compare under these conditions because none of them reached full breakthrough after injection of > 150 PVs. Similar total masses are sequestered; however, for Sn(II)-PO_4, there is a lack of measurable breakthrough of Tc-99 during injection (< detection limit of 0.37 µg/L). Moreover, during injection, CPS+Poly-PO_4 and SMI+Poly-PO_4 are both beginning to increase near the end of the experiment. Therefore, after comparison of breakthrough curves and effluent concentrations, Sn(II)-PO_4 is likely the highest performing in the absence of CoCOIs. Molasses+Poly-PO_4 is a close second under these conditions, followed by SMI+Poly-PO_4 and CPS+Poly-PO_4. Ca-Cit-PO_4 performed relatively well, with breakthrough occurring at > 90 PVs, though breakthrough does occur relatively quickly once it begins, likely due to consumption of all available reduction capacity faster than bacteria are able to replenish (i.e., oxidative dissolution of Tc-99). BSN performed poorly for Tc-99 both with and without CoCOIs present.

3.2.2.2 Uranium

For U, BSN significantly outperformed all other amendments when CoCOIs were present based on initial mobility, retardation, and long-term leaching, although breakthrough PVs > 130 were observed for BSN, Ca-Cit-PO_4, and CPS+Poly-PO_4. Similar uptake trends were observed for molasses+Poly-PO_4 as compared to Ca-Cit-PO_4 and CPS+Poly-PO_4. The poorest performers were SMI+Poly-PO_4 and Sn(II)-PO_4 when CoCOIs were present, highlighting the difficulty in sequestering U via reduction when other reducible CoCOIs are present. Without CoCOIs, results are less conclusive as breakthrough of U was not observed for several technologies, though BSN, Sn(II)-PO_4, and CPS+Poly-PO_4 sequestered the greatest amounts of U after leaching, and breakthrough was not observed for molasses+Poly-PO_4 .

Under the most relevant field conditions, when CoCOIs were present, BSN performed the best, as shown in panels c and d in both Figure 3.17 and Figure 3.18. Additional details on BSN performance are summarized in Appendix H. In Figure 3.17c, effluent U is plotted as C/C_0 (or effluent concentration divided by influent concentrations). U concentrations for BSN in effluent were < 3 µg/L until > 250 PVs were injected (Figure 3.17d), and full breakthrough was not reached. In addition, U was not mobilized during the initial PVs whereas other technologies mobilized background U (e.g., Ca-Cit-PO_4 and CPS+Poly-PO_4). For long-term sequestration of U, significantly greater masses were retained in the sediments after leaching (Figure 3.18c and d) with > 40 µg/g of U remaining sequestered. These results are consistent with previously observed strong retention of U in BSN (see Figure 3.19), likely via inner-sphere adsorption and incorporation as uranyl carbonate – especially if BSN is transforming to bismutite.

Alongside the strong performance of BSN, Ca-Cit-PO_4, and CPS+Poly-PO_4 also performed well, with breakthrough PVs > 130, indicating strong initial retardation of U in sediments as compared to the untreated sediments with a breakthrough PV of approximately 20. Significant delay in breakthrough of molasses+Poly-PO_4 (at PV=120) was also observed, though greater release also occurred during the leaching phase. Moreover, BSN, CPS+Poly-PO_4, and CPS+Poly-PO_4 amendments did not reach complete breakthrough and therefore likely could have sequestered more U in the initial loading phase. When

looking at longer term sequestration, BSN outperformed Ca-Cit-PO_4 and CPS+Poly-PO_4 with the largest retained mass after leaching (> 40 µg/g or 60% of the mass initially loaded, Figure 3.18d). However, Ca-Cit-PO_4 and CPS+Poly-PO_4 each retained approximately 16 and 12 µg/g of U, respectively. For CPS+Poly-PO_4, approximately 30% remained after leaching, while Ca-Cit-PO_4 retained approximately 50%, potentially suggesting more efficient apatite formation and/or incorporation of U in the Ca-Cit-PO_4 treatment.

Notably, all technologies resulted in significantly more U sequestered as compared to the control (with approximately 1 µg/g of U remaining after leaching), exceeding the 50% performance threshold. Ca-Cit-PO_4, CPS+Poly-PO_4, SMI+Poly-PO_4, and molasses+Poly-PO_4 all sequestered > 5 µg/g after leaching. However, because differing amounts of U were sequestered during loading, the fraction of U sequestered after leaching may provide a better comparison. These results highlight the potential for liquid phosphate amendments developed previously (Wellman et al. 2011; Heslop et al. 2005; Lammers et al. 2017), which have been used for U along the river corridor at the Hanford Site and the Old Rifle Processing site in Rifle, CO (PNNL-25303; PNNL-29650), as all technologies use phosphate, with the exception of BSN. Moreover, researchers have reported the potential to form low-solubility U phases including U orthophosphate and autunite [$Ca(UO_2)_2(PO_4)_2 \cdot 10\text{-}12H_2O$] (Robinson et al. 2025; PNNL-29650; Wellman et al. 2005).

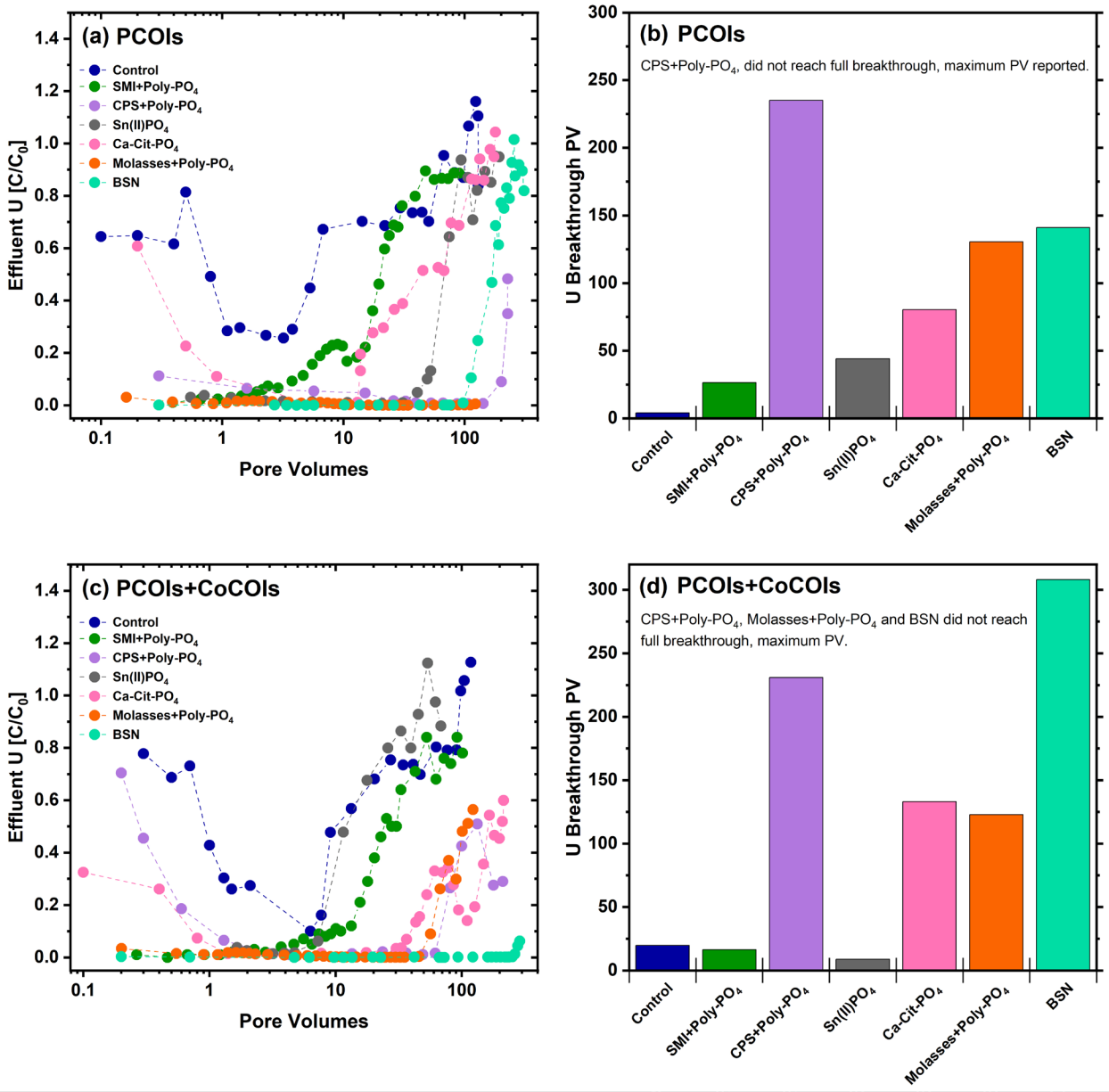

Figure 3.17. U retardation during loading into columns via constant injection with SGW, where (a) and (c) represent aqueous U as C/C_0, equivalent to effluent concentration divided by influent concentration, over time as indicated by the number of PVs of solution injected on the x-axis without and with CoCOIs, respectively, and (b) and (d) show breakthrough PV for U in (a) and (c) without and with CoCOIs, respectively.

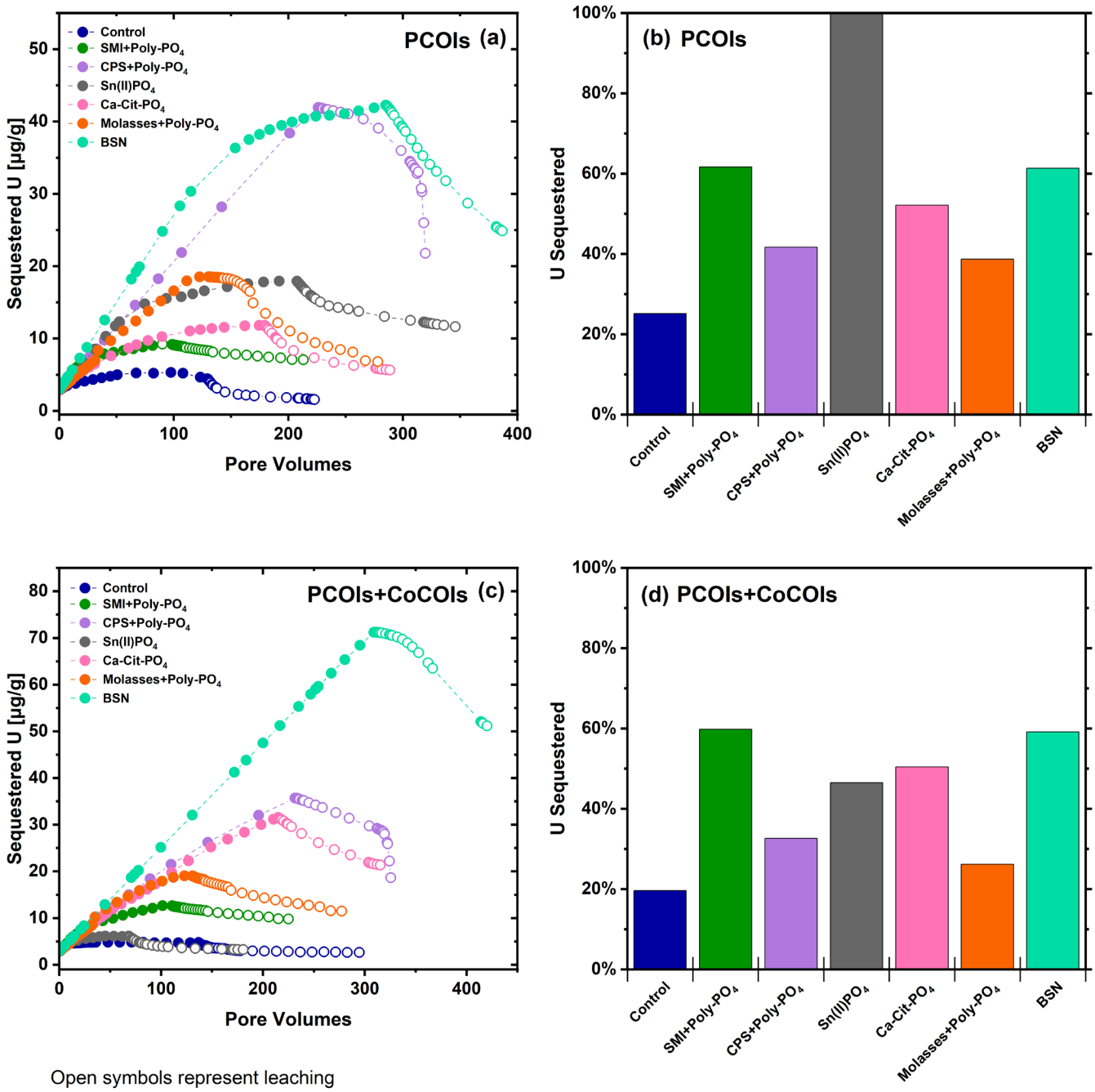

Figure 3.18. U mass sequestered after loading and leaching in columns, where (a) and (c) represent the mass of U in sediments in µg/g over time as indicated by the number of PVs of solution injected on the x-axis during loading (*solid symbols*) and leaching (*open symbols*) without and with CoCOIs, respectively, and (b) and (d) show sequestered fraction of Tc-99 mass remaining after 100 PVs of leaching divided by the mass sequestered during loading, without and with CoCOIs, respectively

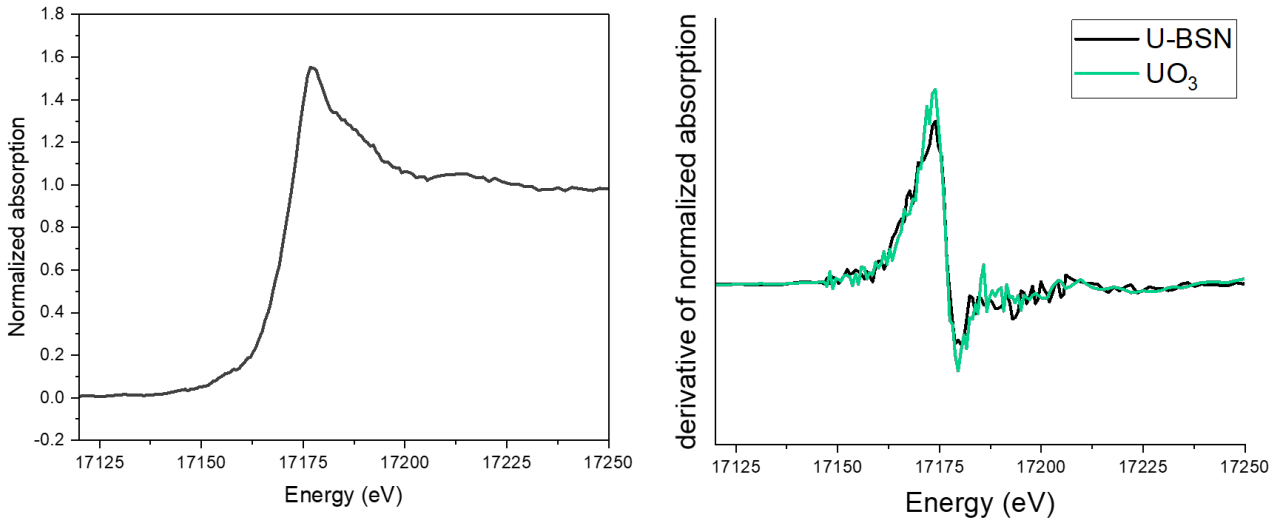

Figure 3.19. U L3-edge XANES (*left*) for U associated with BSN and comparison of the corresponding derivative with UO_3 standard (*right*), adapted from Pearce et al. 2025, showing U is present as U(VI) in association with BSN.

The poorest performers with CoCOIs were SMI+Poly-PO_4 and Sn(II)-PO_4, where much of the sequestered U was remobilized during the leaching phase. Molasses+Poly-PO_4 exhibited similar leaching behavior, though initial retardation of U was greater. These three technologies are not recommended for U if significant amounts are present. Additional work may be valuable to identify calcium phosphate phases forming for the systems with addition of Poly-PO_4 (molasses, SMI, CPS, and Ca-Cit-PO_4), since a significant fraction of U was remobilized during leaching, especially for molasses and SMI treatments. It is possible that the Ca:P ratios were insufficient for apatite formation or significant heavy metals or carbonates were incorporated, leading to formation of higher solubility phases (Heslop et al. 2005; Ayati and Madsen 2000).

Many technologies rely on aqueous and adsorbed or exchanged Ca in the sediment to reach ratios sufficient for apatite formation. For Ca-Cit-PO_4, ratios were close to 5:3 for Ca:P for apatite formation [$Ca_5(PO_4)_3OH$] or 1.67× more Ca. For CPS+Poly-PO_4, there was greater Ca due to the addition of polysulfide as CPS (2.78× more Ca). However, additional Ca was not added for SMI+Poly-PO_4 or molasses+Poly-PO_4. With the relatively small treated volume of sediments within the column, there may not have been sufficient Ca for apatite formation or other (more soluble) phosphate phases may have been formed. Although aqueous and adsorbed Ca^{2+} was not measured in the CCug sediment, measurements in the Hf sediment indicated sufficient aqueous and adsorbed Ca^{2+} to support precipitation of < 35 mmol/L apatite (Appendix D, Figure D.3a). Finally, the reaction time of approximately 6 weeks may not have been sufficient for apatite crystallization under these complex conditions and may not represent field reaction times, depending on groundwater flow rates and treatment volumes. Previous field characterization in the 300 Area reported significant sequestration of U approximately 6 months after injection (PNNL-29650).

Results in the absence of CoCOIs are less conclusive. BSN and CPS+Poly-PO_4 reported breakthrough PVs > 140 without CoCOIs, and molasses+Poly-PO_4 did not reach breakthrough after injection of > 130 PVs. Retardation of U in control (untreated) experiments resulted in a breakthrough PV of approximately 4. BSN and Sn(II)-PO_4 had the greatest sequestration of U following leaching without CoCOIs, with no measurable leaching for Sn(II)-PO_4 (though the breakthrough PV was lower, near 40). CPS+Poly-PO_4 followed closely behind, though significant remobilization of U was observed during leaching (approximately 70%). In addition, there are two peaks in U breakthrough curves (Figure 3.17a),

potentially due to small fluctuations in the pH and carbonate concentrations within columns over time. Appendix A, Section A.3.1 compares the U effluent breakthrough curves for all conditions, highlighting the relatively significant variability in U adsorption to sediments without treatment, further complicating interpretation of results. Appendix A, Figure A.6 summarizes the major minerals near solubility limits in SGW and the expected speciation of U. U speciation and subsequent sequestration are highly impacted by pH and carbonate (Qafoku and Icenhower 2008; Dong et al. 2005; Dong and Brooks 2006; Zhou and Gu 2005; PNNL-17031).

3.2.2.3 Additional Co-contaminants

The behavior of CoCOIs was also monitored during loading and leaching phases in select column experiments, including cyanide, nitrate, Cr, Sr, and I.

Cyanide

- Ferrocyanide was highly stable under the tested conditions without significant transformation to free cyanide, even when amendments [BSN, SMI+Poly-PO_4, and Sn(II)-PO_4] were present.
- BSN and SMI showed strong retention of ferrocyanide (> 90%), highlighting their potential for sequestration of cyanide, if needed.

Nitrate

- Molasses+Poly-PO_4, Sn(II)-PO_4, and Ca-Cit-PO_4 were reduced during the loading phase, consistent with generation of nitrate-reducing conditions.
- Significantly greater Tc-99 reduction was observed for molasses+Poly-PO_4, Sn(II)-PO_4, and Ca-Cit-PO_4, potentially due to kinetic limitations.

Chromium

- Cr reduction was observed for reducing amendments ranging from 10 to 50 PVs, including for molasses+Poly-PO_4, Sn(II)-PO_4, SMI+Poly-PO_4, CPS+Poly-PO_4, and Ca-Cit-PO_4.
- Tc-99 reduction may be inhibited in SMI+Poly-PO_4 due to passivation of SMI by the presence of high Cr.

Strontium

- Significant sequestration of Sr was observed for all conditions (with and without treatment), likely due to precipitation of $SrCO_3$.
- Leaching results suggest kinetically-limited dissolution of an Sr precipitate.

Iodine

- No significant sequestration of I was observed for any of the six technologies.
- Minimal sequestration of I was observed for CPS+Poly-PO_4, although further study is necessary.

Cyanide

Testing for the transformation of ferrocyanide, which is the most likely the form of cyanide to be encountered based on field conditions, into free cyanide, was conducted primarily via columns to quantify the potential for cyanide transformation by the technologies. Free cyanide (CN^- and HCN) is highly toxic,

bioavailable, and mobile, while complexed cyanide [e.g., ferrocyanide ($[Fe(CN)_6]^{4-}$) and ferricyanide ($[Fe(CN)_6]^{3-}$)] is significantly less hazardous. In EPA 815-B-16-012, *Cyanide Clarification of Free and Total Cyanide Analysis for Safe Drinking Water Act (SDWA) Compliance*, the U.S. Environmental Protection Agency clarifies that total cyanide methods are allowed, but cyanide is regulated as free cyanide.

The technologies selected for these experiments were based in part on the potential for interaction and in part informed by batch experiments conducted prior to column leach experiments (Appendix L). Sediments treated with BSN, Sn(II)-apatite, and SMI were prepared, packed into columns, and leached (described in Sections 2.4 and L.1.2), using H_f sediments amended with non-radiological CoCOIs (Sr and NO_3) and ferrocyanide at a targeted concentration of 10 µg/g. A control column was also prepared, which was loaded with ferrocyanide and CoCOIs but was not amended with any technology. Columns were leached with SGW and monitored for free cyanide, total cyanide, and pH.

The leached columns had predominantly stable pH levels between 8 and 8.5 except for BSN (Figure 3.20c). The first 10 PVs of leachate showed a marked decrease in pH, consistent with the known hydrolysis behavior of BSN. BSN is not fully hydrolyzed during the synthesis process, which leads to additional hydrolysis in the initial few PVs (Christensen et al. 2000). Hydrolysis of the bismuth nitrate forms additional BSN, which drives the pH down temporarily as the column leaches, flushing out the acidified solution. Once this initial hydrolyzation is completed, the phase stabilizes. Combined with the use of the H_f sediment, this led to a 2 pH unit decrease for the first 5 PVs before finally stabilizing again throughout the rest of the leach. A sudden decrease in pH may be relevant for the mobilization of cyanide species; however, a decrease to a pH of 6 does not risk freeing cyanide from a strong metal complex of ferrocyanide (Miltzarek et al. 2002), which is further reflected in the free cyanide data presented below.

Figure 3.20a,b shows the cumulative total and free cyanide leached from the columns, along with the initial concentration of ferrocyanide added as a potassium salt to the sediment prior to leaching, as a dotted red line. The no-treatment column reacted as expected with excess ferrocyanide, totaling 4 µg/g, being washed from the column quickly, as ferrocyanide is soluble in water. This indicates that nearly two-thirds of the starting ferrocyanide was sorbed to the sediments or otherwise bound to the stationary phase (e.g., as precipitates). Sn(II)-apatite slowed the overall release of ferrocyanide into the leachate, but ultimately reached the same, or possibly higher, breakthrough as the sediment alone by approximately 15 PV. The SMI retained nearly all the ferrocyanide, with less than 10% of the total amount added cumulatively leaching. Notably, the BSN retained all the ferrocyanide in the sediment. This was likely caused by the strong affinity of BSN for anions, as demonstrated by the technology through this and the previous Phase 1 report (Lawter et al. 2021; Pearce et al. 2025; PNNL-35432). Figure 3.20d shows the total fractions of cyanide measured as free and total cyanide in the aqueous and solid phases. While the sediment alone and treated with Sn(II)-apatite did retain a significant portion of the cyanide, much more was retained to the sediment when treated with SMI or BSN. None of these treatments generated significant amounts of free cyanide, with most measurements near or below the limit of detection (1 µg/L).

These leach experiments support the assumption that ferrocyanide is a highly stable coordination complex that will not change to free cyanide in groundwater even in the presence of the tested technologies. While a mass balance was not completed with solid phase analysis, it is unlikely that large quantities of HCN gas were generated during the equilibration or leaching process. Ferrocyanide can sorb to various mineral surfaces, including aluminum and iron oxides (e.g., goethite, ferrihydrite), clay minerals (e.g., kaolinite, montmorillonite, illite), and manganese oxides (e.g., pyrolusite). Sorption to sand and gravel at neutral pH is limited. Ferrocyanide can also precipitate with ferric compounds to form highly stable Prussian blue (Rennert and Mansfeldt 2002). The thermodynamic stability of the Fe-CN bond is quite high due to the low-spin d^6 configuration of the Fe^{2+} center. This prevents the complex from dissociating readily in water,

which would be required for the generation of free cyanide, and will only dissociate at low pH (i.e., pH < 2). It is possible that ferrocyanide ($[Fe(CN)_6]^{4-}$) will oxidize over long periods into ferricyanide ($[Fe(CN)_6]^{3-}$); however, the opposite is true in highly reducing conditions (e.g., those conditions likely to be found during technology application), though both are unlikely to release free cyanide.

The reported stability formation constants, $\log K_f$, for $[Fe(CN)_6]^{4-}$ and $[Fe(CN)_6]^{3-}$, are 36.9 and 43.9, respectively, which are both extremely high values reflecting the high thermodynamic stability of the complexes in aqueous solution (Beck 1987). The reducing conditions tested in the column leaches showed minimal effect on this system. While the studies were not long term or comprehensive of every technology, these data suggest that ferrocyanide in groundwater will be minimally impacted by the technologies described herein. The supporting batch experiments (Appendix L) suggest the same would be true of ferrocyanide and free cyanide. Also note that, due to the retention of ferrocyanide in the columns, BSN and SMI may be valuable technologies for remediation of cyanide complexes should the need arise.

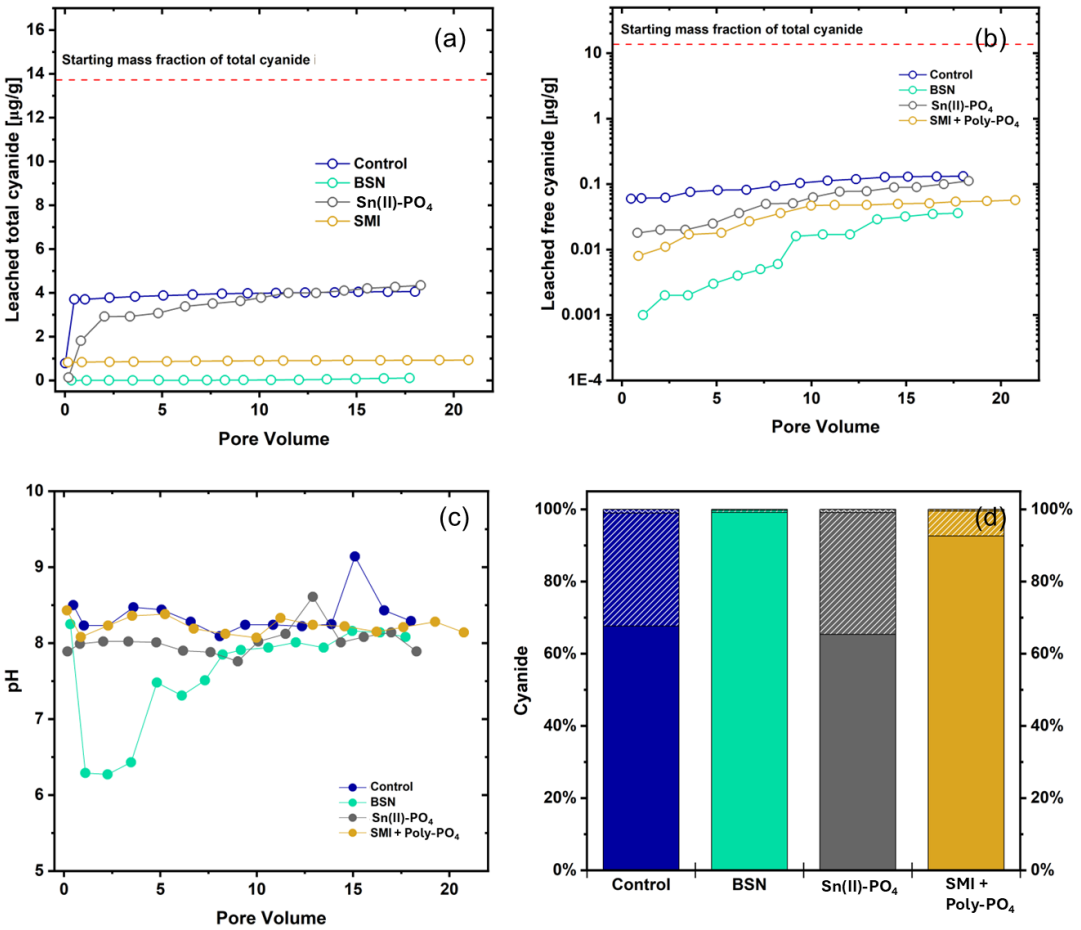

Figure 3.20. Cyanide mass sequestered after loading and leaching in columns, where (a) and (b) represent the mass of total and free cyanide leached µg/g over time as indicated by the number of PVs of solution injected on the x-axis during leaching with CoCOIs; (c) shows pH over time; and (d) shows sequestered mass of cyanide in the solid phase (*solid*), aqueous phase complexed cyanide (*diagonal*), and aqueous free cyanide (*cross hatched*), respectively. Note: The fraction of free cyanide measured (*cross-hatched*) was below detection limits and is reported as the limit of detection (<1%).

Nitrate

As shown in Figure 3.21, significant nitrate reduction was observed for select technologies, including molasses+Poly-PO_4 (*orange*), Sn(II)-PO_4 (*gray*), and Ca-Cit-PO_4 (*pink*). Additional discussion for molasses+Poly-PO_4 is included in Appendix K, Section K.4.3. The significant initial transformation of nitrate (for > 100 PVs) is consistent with generation of nitrate-reducing conditions. However, greater reduction of Tc-99 was observed for these technologies, suggesting potential kinetic limitations. These limitations may be due to the significantly greater nitrate concentration as opposed to Tc-99 or the consumption of more e^- for nitrate than Tc-99 (3 for Tc-99 vs. 5-8 depending on secondary N species), although different pathways may also be responsible for reduction of Tc-99 vs. nitrate [e.g., direct enzymatic reduction by microbes vs. abiotic reduction by Fe(II)]. Significant reduction was not observed for SMI+Poly-PO_4 (*green*). Although nitrate was not measured for CPS+Poly-PO_4 under these conditions, significant reduction was not observed under the perched water conditions (Section 3.2.1.3), likely due to advection of the CPS reductant out of the columns during injection with the loading phase. For BSN, significant release of nitrate from the amendment likely occurred during the first few PVs, as was observed for the perched water conditions (Section 3.2.1.3). However, nitrate was not measured for BSN-treated columns under the water table conditions.

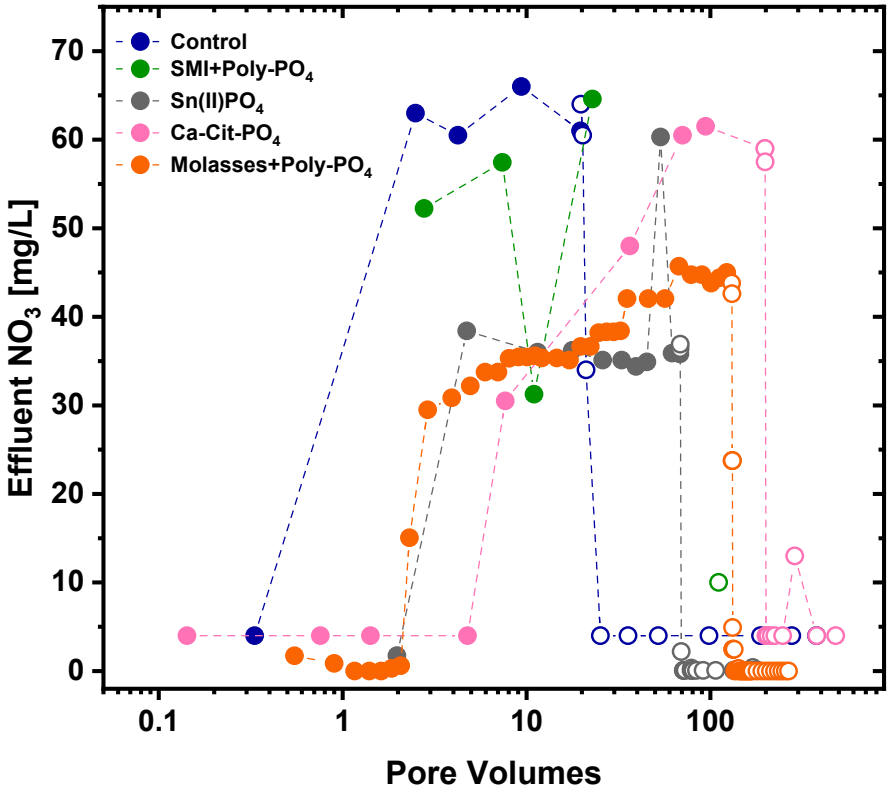

Figure 3.21. Nitrate transformation during loading and subsequent leaching from columns under water table conditions represented as aqueous nitrate measured in the effluent in mg/L over time as indicated by the number of PVs of solution injected on the x-axis. Note: Open symbols indicate effluent nitrate during leaching.

Chromium

Cr breakthrough was delayed with SMI+Poly-PO_4, Ca-Cit-PO_4, Sn(II)-PO_4, molasses+Poly-PO_4, and CPS+Poly-PO_4 treatment, but only for the first 10-50 PVs, likely due to reduction/precipitation. In

addition, significant loading of Cr was observed in 8 M HNO_3 extractions after leaching for Ca-Cit-PO_4 and CPS+Poly-PO_4 (> 10× background) as described in Appendix I, Section I.3.1, and Appendix J, Section J.2.2.1, respectively.

There is potential for secondary impacts from Cr on the SMI+Poly-PO_4 technology. The presence of Cr as chromate (CrO_4^{2-}) highly impacted Tc-99 and U treatment by 20 PVs for SMI+Poly-PO_4 (Appendix G, Figure G.19f). Cr has been shown previously to passivate ZVI surfaces, reducing corrosion, which can inhibit reduction of Tc-99 (Cartledge 1966; Guan et al. 2015; de Lima Perini and Nogueira 2017; Williams et al. 2024). Notably, recent research has shown that when the Fe^0:(Tc+Cr) molar ratio decreases to less than 100, ZVI may no longer reduce Tc-99 and Cr (Williams et al. 2024). Therefore, it is possible that the full reduction capacity of the SMI was unavailable after 20 PVs, although an e^- balance suggests that full reduction capacity would have been consumed by 35 PVs (Section G.4.4).

Strontium

Sr breakthrough in effluent was significantly delayed without treatment (i.e., in control columns), with breakthrough reached near 100 PVs in most experiments. Sn(II)-PO_4, SMI+Poly-PO_4, CPS+Poly-PO_4, BSN, molasses+Poly-PO_4, and Ca-Cit-PO_4 did not significantly change Sr mobility as compared to the controls. Results from both treated and untreated columns from Appendix H (BSN) suggest potential precipitation of Sr (see Appendix A, Section A.3.1 for speciation modeling indicating potential for strontianite, $SrCO_3$) with minimal breakthrough observed throughout the loading phase (as described in Section H.4.1).

Moreover, the relatively high Sr leaching observed confirms the likelihood of dissolution of a Sr precipitate both with and without CPS+Poly-PO_4 (Appendix J, Section J.4), with increased dissolution with longer stop flows suggesting kinetic limitations based on the flux through the columns. Strontianite ($SrCO_3$) may have also impacted PCOI and CoCOI stability by partially coating contaminant surface precipitates or incorporating other contaminants into the strontianite, thus limiting or decreasing their rate of dissolution. For example, U incorporation may have increased sequestration by SMI in the presence of CoCOIs (Appendix G, Figure G.15).

Iodine

Significant sequestration of iodine (initially as iodate) was not observed for BSN, SMI+Poly-PO_4, Sn(II)-PO_4, or Ca-Cit-PO_4. However, some I sequestration was observed for CPS+Poly-PO_4, suggesting that there could be some immobilization with Poly-PO_4, depending on conditions. Note that iodine breakthrough was not monitored for the molasses+Poly-PO_4 testing. Additional testing would be suggested for iodine with the CPS+Poly-PO_4 and molasses+Poly-PO_4 technology, if present in the field, as speciation may play an important role.

Iodine is generally present as iodate in groundwater and may be present as iodide in VZ porewater at the Hanford Site, depending on conditions (Kimmig et al. 2021; Zhang et al. 2013; PNNL-28064). Specifically, the reduction of iodate (IO_3^-) to iodide (I^-) has been shown to increase mobility due to reduced sorption potential (Hu et al. 2005; Kaplan et al. 2000, 2014). Therefore, iodine speciation should be understood prior to the addition of strong reductants to the subsurface. In addition, the addition of organic carbon from amendments may also form organo-iodine species whose mobility is much less understood (Schwehr et al. 2009).

A previous study of various remediation technologies did not identify any with potential for application at the Hanford Site (PNNL-28064). However, for dilute plumes, there is potential for monitored natural attenuation, depending on the mechanisms controlling species-specific sequestration (PNNL-35432).

4.0 Conclusions and Recommendations

Nine remedial technologies were tested at the laboratory-scale to assess their performance as *in situ* remedial applications at 200-DV-1 OU waste sites for direct VZ treatment of contaminants, saturated zone applications at the B Complex perched water zone or water table PRB applications beneath BY Cribs. The assessment included initial sequestration (during contaminant uptake), transformation, and long-term leaching of U, Tc-99, nitrate, Cr, Sr, and I.

For unsaturated VZ conditions, three technologies were tested: (1) gas-phase chemical sequestration of I with CO_2, (2) gas-phase bioreduction of nitrate with ethane, and (3) sequential gas-phase bioreduction then chemical sequestration of Tc-99 using an organic gas followed by CO_2 gas. However, no gas-phase technologies were suitable for further FS consideration. For saturated conditions, six technologies were tested for their potential to sequester PCOIs and CoCOIs under conditions representing the BY Cribs groundwater (targeting formation of a PRB as a contaminant flux barrier near the top of the unconfined aquifer) and direct treatment of contamination in the B Complex perched water zone (representing continuing sources to interconnected groundwater). These saturated zone technologies included three particulate-phase amendments [Sn(II)-PO_4, SMI+Poly-PO_4, and BSN] and three liquid-phase amendments (Ca-Cit-PO_4, CPS+Poly-PO_4, and molasses+Poly-PO_4). No single technology performed well for all conditions and contaminants. However, each technology may have viability for specific conditions and/or contaminants and is therefore recommended for further FS consideration.

Conclusions and recommendations are summarized in the following sections for each of the potential treatment conditions (Section 4.1 for VZ, Section 4.2.1 for perched water, and Section 4.2.2 for water table), followed by a summary of future considerations for FS as specific locations in Section 4.3. Breakout boxes provide high-level conclusions and are followed by expanded discussion. All recommendations for further FS consideration are based on whether the technology met performance thresholds for a greater than 50% increase in contaminant mass sequestered, as laid out in the test plan (DOE/RL-2019-28), alongside a comprehensive evaluation considering timing for initial contaminant breakthrough, rates of leaching over time, and surface phase characterization as indicators of long-term solubility and mobility.

4.1 Vadose Zone Treatment

Overall technology recommendations, considerations, and challenges for the VZ are summarized in Table 4.1 with additional details for gas-phase chemical sequestration in Section 4.1.1, gas-phase bioreduction in Section 4.1.2, and sequential gas-phase bioreduction and chemical sequestration in Section 4.1.3. However, no gas-phase technologies were suitable for further FS for the VZ. Future site-specific characterization could be conducted to (1) measure the concentrations of reducible contaminants (including but not limited to nitrate and Cr) and dissolved oxygen within the treatment area to optimize performance for reducing technologies, (2) survey microbial populations for potential impacts to potential remediation technologies (either for augmentation or reduction in performance), and (3) measure Ca and Mg concentrations for potential to form carbonate minerals from CO_2 gas injection.

No gas-phase technologies were suitable for further feasibility study consideration.

- Chemical sequestration with CO_2 gas was not observed for iodine (PCOI) or the following CoCOIs: U, Sr, Tc-99, and Cr.
- Bioreduction with ethane gas did not significantly transform nitrate (PCOI) at the elevated concentrations expected in the 200-DV-1 OU.
- Ethane or nitrogen gas reduces lower nitrate concentrations closer to expected sediment background concentrations.
- The sequential bioreduction then chemical sequestration technology did not perform well for Tc-99 (PCOI) or CoCOIs U, Sr, CN, and nitrate – but CoCOI Cr was sequestered.

Table 4.1. Summary of technology performance, considerations, and upscaling or implementation challenges for gas-phase technologies for the vadose zone. None of these technologies met thresholds for PCOIs, and they are not suitable for additional FS consideration.

PCOI/Technology	PCOI Performance	CoCOI Performance	Additional Considerations	Implementation Challenges
Nitrate/bioreduction with ethane gas	Not viable; reduction at low NO_3 concentration only	Cr reduction observed	Anoxic conditions using N_2 also performed at low NO_3 concentration	Gases could be relatively readily injected in low water content zones, but zones may need to be maintained via recirculation or other methods
I-129/chemical sequestration with CO_2 gas	Not viable; no I treatment	Minimal for Tc-99, Insignificant for U, Cr, Sr	Technology requires available Ca^{2+} in sediment	
Tc/sequential bioreduction and chemical sequestration[(a)]	Not viable; No Tc-99 sequestration	High Cr reduction (66-88%) observed with butane, ethane, and butyl acetate	Slow Tc-99 bioreduction (hundreds of hours)	

(a) Technology did not meet initial performance threshold for Phase 1 of testing; additional testing was not conducted as part of Phases 2 and 3.

4.1.1 Gas-Phase Chemical Sequestration – Carbon Dioxide

The gas-phase chemical sequestration technology used CO_2 gas for *in situ* sequestration of iodine via incorporation into calcite with and in the absence of U, Tc-99, Sr, Cr, and nitrate in unsaturated conditions. Variably saturated column (Section 3.1.1.1) and batch (Appendix D, Section D.2) experiments demonstrated that I sequestration via CO_2 treatment was not sufficient to meet the targeted 50% threshold. Batch extraction results showed that I mobility decreased to less than 15%. Variably saturated sediment column results (47% to 100% water saturation) did not show a significant increase in I sequestration with treatment. Therefore, this technology is not recommended for I-129 under these conditions. If this technology were considered for other contaminants (i.e., minimal treatment for CoCOI Tc-99), characterization of available Ca^{2+} in the sediment would be needed to confirm availability to precipitate calcite. As an example, acid-impacted sites may have low aqueous and adsorbed Ca^{2+} that would be insufficient for precipitation of calcite after delivery of CO_2.

4.1.2 Gas-Phase Bioreduction – Ethane

The gas-phase bioreduction technology evaluated ethane as an organic gas for *in situ* bioreduction of nitrate, both with and without Cr, in unsaturated conditions. Both batch (Section 3.1.2.1) and static column experiments (Section 3.1.2.2) demonstrated nitrate reduction, in some cases greater than 50% (i.e., low nitrate concentrations), but neither showed significant enhancement from using ethane gas as a treatment when compared to nitrogen gas. Therefore, anoxic conditions alone may suffice for nitrate reduction without additional gas additives, depending on total nitrate concentrations. Given these results, this technology is not recommended for further FS consideration. If this technology were considered for other contaminants such as Cr, site-specific microbial characterization should be conducted to optimize the carbon amendment addition and type for the native populations.

4.1.3 Gas-Phase Bioreduction and Chemical Sequestration

Two-step gas-phase bioreduction and chemical sequestration for Tc-99 is described in the Phase 1 report (PNNL-35432). PCOI (Tc-99) sequestration was low (0% to 6% for ethane, 4% to 12% for butane, and 0% to 2% for butyl acetate), so Phase 2 and 3 experiments were not conducted, and this technology is not recommended for further FS consideration for Tc-99 remediation. However, treatments performed well for a CoCOI (Cr), with approximately 66% sequestration using butyl acetate, 79% for ethane, and 88% for butane. If this technology were considered for other contaminants (e.g., Cr), because reduction is microbially controlled, site-specific microbial characterization should be conducted to optimize the carbon amendment for native populations.

4.2 Water-Saturated Zone Treatment

Overall technology recommendations, considerations, and challenges are summarized in Table 4.2 with additional details for the two treatment scenarios, including direct treatment of the perched water beneath the B Complex (also referred to as the 200-DV-1 OU perched water) in Section 4.2.1 and formation of a PRB at the BY Cribs water table in Section 4.2.2. No single technology performed well for all saturated zone conditions and contaminants. However, each technology may have viability for specific conditions and/or contaminants and is, therefore, recommended for further FS consideration.

No single technology performed well for all conditions and contaminants. Each of the technologies may have viability for specific conditions and/or contaminants.

Evaluation of Technologies under B Complex Perched Water Conditions

- Particulate SMI+Poly-PO_4 performed best for both Tc-99 and U, meeting the 50% performance threshold for sequestration.
- Particulate Sn(II)-PO_4 was comparable to particulate SMI+PO_4 for Tc-99, while liquid CPS+Poly-PO_4 was less effective but still met the threshold for sequestration of Tc-99.
- None of the other five technologies performed well for U sequestration; only SMI+Poly-PO_4 met the performance threshold.
- Technology performance was highly impacted by the relatively high ionic strength, presence of nitrate, and elevated U concentrations under these conditions.

Evaluation of Technologies under BY Cribs Groundwater Conditions with CoCOIs

- Liquid molasses+Poly-PO_4 outperformed five other amendments for sequestration of Tc-99.
- Two technologies met the 50% performance threshold for sequestration of Tc-99 (liquid molasses+Poly-PO_4 and CPS+Poly-PO_4).
- Particulate BSN outperformed all other amendments for U sequestration, though significant sequestration was also observed for liquid CPS+Poly-PO_4, Ca-Cit-PO_4 and molasses+Poly-PO_4.

Table 4.2. Summary of viable technologies for further FS consideration with a PRB in the BY Cribs water table or B Complex perched water. All technologies listed met the 50% performance threshold.

Subsurface Conditions	Viable Technologies for Tc[a]	Viable Technologies for U[a]	Viable Technologies for CoCOIs[a,b]	Additional Considerations	Implementation Challenges
BY Cribs groundwater	Molasses+Poly-PO_4 ≈ SMI+Poly-PO_4 ≈ CPS+Poly-PO_4 ≈ Sn(II)-PO_4	BSN ≈ Molasses+Poly-PO_4 ≈ CPS+Poly-PO_4 ≈ Sn(II)-PO_4	N/A	• Leachability was lowest for Tc-99 with Sn(II)-PO_4 treatment.	• Particulate-phase[a] amendments are more challenging to deliver to large volumes and require further optimization. • Reduction/sequestration amendments[c] may need additional optimization. • If PCOIs and CoCOIs are in low-permeability zones, delivery may be challenging. • Most technologies that involve reduction will be more readily oxidized in field zones with high oxygen (i.e., perched water or groundwater). • SMI and Sn(II)-PO_4 may retain some reductive capacity in oxidizing conditions. BSN performance is unaffected by oxidizing conditions.
BY Cribs groundwater + CoCOIs[b]	Molasses+Poly-PO_4 > CPS+Poly-PO_4	BSN > Ca-Cit-PO_4 ≈ CPS+Poly-PO_4 ≈ Molasses+Poly-PO_4	(for *Cyanide*) BSN, SMI+Poly-PO_4 (for *Nitrate*) Molasses+Poly-PO_4, Sn(II)-PO_4, and Ca-Cit-PO_4 (for *Cr*) Molasses+Poly-PO_4, Sn(II)-PO_4, SMI+Poly-PO_4, CPS+Poly-PO_4, and Ca-Cit-PO_4 (for *Iodine*) None	• U sequestration was greater in the presence of CoCOIs,[b] potentially due to incorporation of U into $SrCO_3$. • Cr may inhibit reduction via SMI at high concentrations.	
Perched water beneath the B Complex	Sn(II)-PO_4 ≈ SMI+Poly-PO_4 > CPS+Poly-PO_4	SMI+Poly-PO_4	(for *Nitrate*) Ca-Cit-PO_4, Molasses+Poly-PO_4	• Significant nitrate reduction not observed for Sn(II)-PO_4, suggesting some selectivity in reduction. • No other technologies performed well for U, likely due to conditions of perched water.	

(a) Particulate-phase technologies include Sn(II)-PO_4, BSN, and SMI+Poly-PO_4, and liquid-phase technologies include molasses+Poly-PO_4, CPS+Poly-PO_4, and Ca-Cit-PO_4. Note that ≈ means technologies have similar performance. Technologies: molasses+Poly-PO_4 is molasses bioreduction followed by Poly-PO_4, SMI+Poly-PO_4 is sulfur modified iron reduction followed by Poly-PO_4, CPS+Poly-PO_4 is calcium polysulfide reduction followed by Poly-PO_4, Sn(II)-PO_4 is tin(II) phosphate precipitate, BSN is bismuth subnitrate, and Ca-cit-PO_4 is calcium citrate and sodium phosphate.

(b) CoCOIs for the BY Cribs groundwater conditions included Sr, Cr, I, nitrate, and CN (for select testing) with testing conducted with and without CoCOIs. For perched water beneath the B Complex, all testing included the CoCOI nitrate because it was present in all waste released in this area.

(c) Reduction/sequestration amendments include SMI+Poly-PO_4, molasses+Poly-PO_4, and CPS+Poly-PO_4. Amendments were added sequentially in this testing but were not optimized for delivery.

4.2.1 B Complex Perched Water

Of the six technologies considered, the particulate-phase chemical reduction and sequestration technology, SMI+Poly-PO_4, performed the best at sequestering both Tc-99 and U, meeting the 50% performance threshold. Although no other technologies performed well for U, particulate-phase chemical sequestration with Sn(II)-PO_4 performed relatively similarly to SMI+Poly-PO_4 for Tc-99, and liquid-phase chemical reduction and sequestration with CPS+Poly-PO_4 also met the performance threshold for Tc-99. Therefore, particulate-phase chemical reduction and sequestration with SMI+Poly-PO_4 is recommended for feasibility testing for locations with Tc-99 and U contamination. If a location has regions primarily with Tc-99 contamination, SMI+Poly-PO_4, Sn(II)-PO_4, and CPS+Poly-PO_4 would all be recommended technologies for further FS consideration. Although nitrate was not a PCOI for most technologies (except molasses+Poly-PO_4), the relatively high nitrate concentrations expected under perched water conditions beneath the B Complex make reduction of other contaminants via reduction mechanisms challenging. Some nitrate was reduced for both of the technologies generating bioreducing conditions (Ca-Cit-PO_4 and molasses+Poly-PO_4), though significant nitrate remained with all technologies. Results are summarized in more detail for Tc-99 in Section 3.2.1.1, U in Section 3.2.1.2, and nitrate in Section 3.2.1.3.

The B Complex perched water conditions were challenging for contaminant sequestration. For example, the relatively high expected nitrate concentrations made it challenging to treat other contaminants via reduction mechanisms. In addition, the elevated ionic strength and carbonate likely impacted U co-precipitation and apatite formation processes. Therefore, site-specific characterization should be conducted to measure the concentrations of reducible contaminants (including but not limited to nitrate and Cr) and dissolved oxygen within the treatment area to optimize performance for reducing technologies. In addition, technologies that are more specific to the PCOIs [e.g., Sn(II)-PO_4 may be more selective for Tc] could be targeted for additional testing. Alternatively, some technologies performed better for transformation of nitrate (e.g., Ca-Cit-PO_4 and molasses+Poly-PO_4 but not SMI+Poly-PO_4) than others and could be used alone for nitrate or in combination with other technologies for areas with collocated, reducible contaminants (e.g., nitrate and Tc-99).

4.2.2 BY Cribs Groundwater

Of the six technologies considered, two liquid-phase technologies – molasses+Poly-PO_4 and CPS+Poly-PO_4 – met the 50% performance threshold for sequestration of Tc-99 and are recommended for future consideration for FS. For U, particulate-phase chemical sequestration with BSN outperformed all other amendments, though significant sequestration was also observed for three of the liquid-phase technologies: CPS+Poly-PO_4, molasses+Poly-PO_4, and Ca-Cit-PO_4. Thus, under the BY Cribs groundwater conditions, there are several potential technologies available for treatment of Tc-99 and U. However, if Tc-99 and U are collocated, CPS+Poly-PO_4 and molasses+Poly-PO_4 are recommended for further FS consideration. Results are summarized in more detail for Tc-99 in Section 3.2.2.1, U in Section 3.2.2.2, and other potential co-contaminants in Section 3.2.2.3.

Testing included experiments with and without potential CoCOIs, including I, Cr, Sr, and nitrate. For some technologies, the presence of these CoCOIs significantly impacted the potential for sequestration of the primary contaminants, Tc-99 and U. The technologies most impacted by CoCOIs included Ca-Cit-PO_4 and Sn(II)-PO_4 for both Tc-99 and U sequestration, likely due to faster consumption of reduction capacity and the occurrence of secondary precipitation processes. Cr, I, and nitrate were reduced at varying levels depending on the technology (as described in Section 3.2.2.3), consuming capacity targeted for reductive precipitation of Tc-99. Therefore, the amount of reductant added to the subsurface may need to be optimized after initial characterization of a potential treatment site. In addition, secondary precipitation of CoCOIs, such as Sr as strontianite, may impact the potential for treatment of other

contaminants (e.g., U) due to both incorporation of U into strontianite and coating of other U phases (e.g., adsorbed U or U precipitated with PO_4) with strontianite.

4.3 Considerations for Technology Implementation

As the recommended technologies potentially advance for FS, there are additional considerations, including (1) preliminary site characterization, (2) amendment sourcing, and (3) site-specific amendment selection and implementation.

4.3.1 Site Characterization Needs

For preliminary site characterization, in addition to hydrogeologic measurements (i.e., hydrogeologic formations, permeability, anisotropy, grain size distribution), some additional characterization is needed to optimize technologies for site-specific conditions, including measuring (1) contaminant concentrations and speciation and (2) microbial populations.

Because of the complexity of sequestration mechanisms for each of the potential remediation technologies, it is important to quantify contaminant concentrations and speciation. Methods for characterization of concentrations include microwave digestion with analysis of solutions or direct measurement of solid phase materials via X-ray fluorescence and energy-dispersive X-ray spectroscopy. For speciation in solution, techniques like ion chromatography and ion exchange separations can be used. For speciation in the solid phase, depending on the concentrations of contaminants, XRD and XAS techniques may be used for elevated concentrations and sequential extractions are effective as indirect measures of speciation at trace concentrations (< μg/g). For example, U speciation and subsequent sequestration are highly impacted by pH and carbonate, as summarized in Figure A.6 in Appendix A.

Additional characterization of site-specific microbial populations, including quantification of species and biomass population, is needed for technologies targeting bioreduction (Ca-Cit-PO_4 and molasses+Poly-PO_4). This is necessary to confirm that the naturally present bacteria can consume the provided carbon sources and optimize dosage based on whether they can directly reduce (i.e., metabolize) or reduce other metals (i.e., Fe) that then indirectly reduce the PCOIs. There is value in understanding local microbial populations for each of the technologies (including those not targeting bioreduction), because there may be an impact on remediation success. For example, specific bacteria (*Geobacter spp.* or *Desulfovibrio spp.*) have been shown to improve Cr reduction efficiency of ZVI (Shi 2019).

4.3.2 Technology Implementation

Alongside the technology performance described in this report, there are additional considerations outside of the scope of these studies for the technologies evaluated, including (1) the ability to source the amendment at the appropriate volumes and purity and (2) delivery potential of liquid and particulate amendments into the contaminated formation. In addition, the testing described herein approximated potential field conditions. However, prior to field injections, the technology's performance should be considered under site-specific conditions for the potential injection area.

Since field-scale remediation requires significant amounts of amendments, there is a need to identify manufacturers of the chosen amendments that can meet specific requirements, including mass, purity (for liquid, gas, and particulate amendments), synthesis method (for particulate amendments), particle size (for particulate amendments), and storage and delivery conditions. For example, different ZVI materials manufactured via different methods with different particle sizes and impurities have been shown to have significantly different treatment performance for Tc-99 (Boglaienko et al. 2019). For more novel amendments like BSN, the number of potential suppliers for large-scale quantities may be limited. In

addition, the transport and storage conditions of amendments must be carefully stipulated to avoid significant changes in geochemical conditions during amendment delivery based on chemical shelf-life and stability. For example, if basic solutions (e.g., KOH) that are used for synthesis of Poly-PO_4 are left open to the atmosphere, carbonate concentrations will increase significantly, as has been observed previously (PNNL-29650), and this change may impact the performance of apatite formation and subsequent sequestration of contaminants.

For all amendments that result in precipitation (i.e., phosphates and carbonates) and solid phase amendments [i.e., BSN, Sn(II)-PO_4, SMI], the mass loading relative to the pore space occupied by the precipitate (and hydraulic conductivity reduction) needs to be considered. In previous field injection of Ca-Cit-PO_4, it was calculated that a mass loading of 1 mg apatite per gram of sediment should result in an approximate 7.8% decrease in porosity (i.e., 20% field porosity decreases to 18.4%; PNNL-23367). Higher loadings of solid phase amendments used in this laboratory study [i.e., 1 mg SMI/g sediment, 5 mg/g Sn(II)-PO_4/g sediment, and 15 mg BSN/g sediment] would likely occupy a higher fraction of the pore space (decreasing hydraulic conductivity), so lower mass loadings would need to be considered in a site-specific study to have minimal impacts on hydraulic conductivity.

The ease of delivery of amendments to the subsurface varies with the physical state of the amendment(s) (i.e., gas, liquid, solid, or combination) and the current state of development of the technology, including previous field-scale injections (Table 4.3). Because no gas-phase technologies were recommended for further FS consideration for the VZ, this discussion is focused on liquid and particulate amendments for saturated conditions. Two remediation scenarios were considered for saturated subsurface environments: (1) direct treatment of contaminated subsurface (e.g., perched water as a secondary source for contaminants) and (2) creation of a PRB at the water table to treat contaminants as they move through the VZ and into groundwater. Implementation would differ between these scenarios because the perched water application is source area treatment of high contaminant concentrations whereas groundwater application is a PRB in the top portion (i.e., contaminated zone) of the unconfined aquifer with generally low to moderate contaminant concentrations.

Table 4.3. Technology development needs before field-scale deployment

Technology	State	Injection Status	Development Needs before Field-Scale Deployment
CO_2 gas	Gas	Routinely injected at field scale elsewhere	Measure field-scale gas permeability and anisotropy
Ethane gas	Gas	Only at laboratory scale	Laboratory-scale retardation at different water content, field-scale gas permeability and anisotropy
Ethane, propane, butyl acetate + CO_2 gas	Gas	Organic gases only at laboratory scale	Laboratory-scale retardation at different water content, field-scale gas permeability and anisotropy
Ca-Cit-PO_4	Liquid	Injected at 100-N, Rifle, CO, UMTRA site	Site-specific sediment cation exchange capacity (CEC), ion exchangeable Ca^{+2} and Mg^{+2}, citrate biodegradation rate
CPS + Poly-PO_4	Liquid	CPS injected at 100-K, Poly-PO_4 at 300A	Site-specific CEC, ion exchangeable Ca^{+2} and Mg^{+2}, CPS injection mass/rate optimization to reduce precipitation and permeability reduction
Molasses + Poly-PO_4	Liquid	Molasses routinely injected at field scale elsewhere, not in combination with Poly-PO_4	Site-specific CEC, ion exchangeable Ca^{+2} and Mg^{+2}, microbial population, molasses injection mass/rate/pulse optimization to reduce precipitation and permeability reduction
SMI + Poly-PO_4	Particulate + liquid	SMI and ZVI injected at field scale, not in combination with Poly-PO_4	Delivery optimization for SMI (mass, particle size, rate, and carrier fluid) for area extent, density effects, permeability reduction
Sn(II)-PO_4	Solid	Only at laboratory scale	Delivery optimization for Sn(II)-PO_4 (mass, particle size, rate, and carrier fluid) for area extent, density effects, permeability reduction
BSN	Solid	Only at laboratory scale	Delivery optimization for BSN (mass, particle size, rate, and carrier fluid) for area extent, density effects, permeability reduction

Note that five technologies involve reduction and could be oxidized by all electron accepters present (i.e., PCOIs, CoCOIs, and dissolved oxygen). In contrast, contaminant sequestration with BSN does not involve reduction and thus may perform longer at the water table, though the ions present do impact the secondary phase transformations and subsequent treatability for different contaminants. Notably, amendment delivery may result in some initial mobilization of contaminants in treatment zones where the materials are delivered (as was observed in the 300 Area during Poly-PO_4 injection for U and 100-N Area for Ca-Cit-PO_4 injections for Sr-90) (PNNL-19524; PNNL-29650).

Source area treatment requires injection of liquid and/or solid phase amendments into a relatively thin perched zone with underlying low-permeability zones and mixing with contaminants. Moreover, there may be lower permeability zones complicating delivery and requiring other approaches, such as shear-thinning fluids (Muller et al. 2021a). It may be easier to inject amendments if contaminants have a moderate to high retardation factor (i.e., > 5), which would limit contaminant displacement during amendment injection. Highly mobile contaminants, such as Tc-99, Cr, and nitrate (Rf ~ 1.0), can still be treated with source area amendment injection, but this requires a more complex injection strategy to mix amendments with contaminants. For example, previous research designed a process called engineered injection and extraction to improve mixing (Piscopo et al. 2013). In addition, multiple injections could be employed to increase amendment concentrations as has been done previously, including for re-generation of bioreducing conditions. Previous research reported that organic amendments were more likely to require repeat injections to maintain performance (Madejón et al. 2010).

The type of amendment will also be significant in determining delivery potential as particulate-phase and liquid-phase amendments may face different challenges, including potential safety considerations (as is expected for CPS). Although liquid amendments are more easily injected, particulate amendments can

also be injected but often require an additional high-viscosity fluid to keep particulates in suspension during injection. There may be additional reaction and flow considerations associated with this delivery fluid (i.e., guar or xanthan). The resulting radius of particulate amendment delivery may be less and will be needed to determine well spacing. For liquid-phase technologies, amendment fluid density also influences field emplacement due to sinking of the dense amendment injection solution. In addition, repeat or sequential injections may be required for longevity of single amendments or two-step (reduction/sequestration) technologies. However, step injections of liquid-phase amendments have been conducted in the field, including injection of dithionite followed by acetate (Reimus et al. 2022), low- then high-concentration Ca-Cit-PO_4 injections at the Hanford 100-N Area (PNNL-19524), and repeated injections of amendments to re-establish reducing conditions (Madejón et al. 2010).

As the team moves closer to FS and field-scale implementation, these considerations should be used to optimize and scale up the recommended technologies for contaminant sequestration.

5.0 References

Alowitz, M. J., and M. M. Scherer. 2002. "Kinetics of Nitrate, Nitrite, and Cr(VI) Reduction by Iron Metal." *Environmental Science and Technology* 36 (3): 299-306.

Arenholz, E., and S. O. Prestemon. 2005. "Design and Performance of an Eight-Pole Resistive Magnet for Soft X-Ray Magnetic Dichroism Measurements." *Review of Scientific Instruments* 76 (8).

Asmussen, R. M., C. I. Pearce, B. W. Miller, A. R. Lawter, J. J. Neeway, W. W. Lukens, M. E. Bowden, M. A. Miller, E. C. Buck, and R. J. Serne. 2018. "Getters for Improved Technetium Containment in Cementitious Waste Forms." *Journal of Hazardous Materials* 341: 238-247.

Asmussen, R. M., J. J. Neeway, A. R. Lawter, T. G. Levitskaia, W. W. Lukens, and N. P. Qafoku. 2016. "The Function of Sn (II)-Apatite as a Tc-99 Immobilizing Agent." *Journal of Nuclear Materials* 480: 393-402.

ASTM D2216-19. 2019. *Standard Test Methods for Laboratory Determination of Water (Moisture) Content of Soil and Rock by Mass.* West Conshohocken, PA: ASTM International.

ASTM D2482-15.. 2022. *Standard Test Method for Determination of Free Cyanide in Water and Wastewater by Microdiffusion.* West Conshohocken, PA: ASTM International.

Ayati, M., and H. E. L. Madsen. 2000. "Crystallization of Some Heavy-Metal Phosphates Alone and in the Presence of Calcium Ion." *Journal of Crystal Growth* 208 (1-4): 579-591.

Bae, S., and K. Hanna. 2015. "Reactivity of Nanoscale Zero-Valent Iron in Unbuffered Systems: Effect of pH and Fe (II) Dissolution." *Environmental Science & Technology* 49 (17): 10536-10543.

Bai, X., Y. Li, X. Jing, X. Zhao, and P. Zhao. 2023. "Response Mechanisms of Bacterial Communities and Nitrogen Cycle Functional Genes in Millet Rhizosphere Soil to Chromium Stress." *Frontiers in Microbiology* 14..

Baysinger, G., L. I. Berger, R. Goldberg, H. Kehiaian, K. Kuchitsu, G. Rosenblatt, D. Roth, and D. Zwillinger. 2015. *CRC Handbook of Chemistry and Physics*. Washington, D.C. National Institute of Standards and Technology.

Beck, M. 1987. "Critical Survey of Stability Constants of Cyano Complexes." *Pure and Applied Chemistry* 59 (12): 1703-1720.

Beckett, P. 1989. "The Use of Extractants in Studies on Trace Metals in Soils, Sewage Sludges, and Sludge-Treated Soils." *Advances in Soil Science* 9: 144.

Berthouex, P. M., and L. C. Brown. 1994. "Assessing the Difference of Two Averages." In *Statistics for Environmental Engineers*, 111-114. Boca Raton, Florida: CRC Press.

Boglaienko, D., H. Emerson, Y. Katsenovich, and T. Levitskaia. 2019. "Comparative Analysis of ZVI Materials for Reductive Separation of ^{99}Tc (VII) from Aqueous Waste Streams." *Journal of Hazardous Materials* 380: 120836.

Boglaienko, D., J. A. Soltis, R. K. Kukkadapu, Y. Du, L. E. Sweet, V. E. Holfeltz, G. B. Hall, E. C. Buck, C. U. Segre, H. P. Emerson, et al. 2020. "Spontaneous Redox Continuum Reveals Sequestered Technetium Clusters and Retarded Mineral Transformation of Iron." *Communications Chemistry* 3 (1): 1-11.

Boglaienko, D., M. E. Bowden, N. M. Escobedo, Q. M. Collins, A. R. Lawter, T. G. Levitskaia, and C. I. Pearce. 2024. "Different Routes of Bismuth Mineral Transformation during Pertechnetate and Perrhenate Uptake for Subsurface Remediation." *Environmental Science: Water Research & Technology* 10 (11): 2646-2654.

Bolyen, E., J. R. Rideout, M. R. Dillon, N. A. Bokulich, C. C. Abnet, G. A. Al-Ghalith, H. Alexander, E. J. Alm, M. Arumugam, F. Asnicar, et al. 2019. "Author Correction: Reproducible, Interactive, Scalable and Extensible Microbiome Data Science Using Qiime 2." *Nature Biotechnology* 37 (9): 1091-1091.

Brina, R., and A. G. Miller. 1992. "Direct Detection of Trace Levels of Uranium by Laser-Induced Kinetic Phosphorimetry." *Analytical Chemistry* 64 (13): 1413-1418.

Brunauer, S., P. H. Emmett, and E. Teller. 1938. "Adsorption of Gases in Multimolecular Layers." *Journal of the American Chemical Society* 60 (2): 309-319.

Callahan, B. J., P. J. McMurdie, M. J. Rosen, A. W. Han, A. J. A. Johnson, and S. P. Holmes. 2016. "DADA2: High-Resolution Sample Inference from Illumina Amplicon Data." *Nature Methods* 13 (7): 581-583.

Cartledge, G. 1966. "The Passivation of Iron in the Presence of Pertechnetate and Chromate Ions." *Journal of the Electrochemical Society* 113 (4): 328-333.

Chao, T. T., and L. Zhou. 1983. "Extraction Techniques for Selective Dissolution of Amorphous Iron Oxides from Soils and Sediments." *Soil Science Society of America Journal* 47 (2): 225-232.

Chen, Z.-F., Y.-S. Zhao, J.-W. Zhang, and J. Bai. 2015. "Mechanism and Kinetics of Hexavalent Chromium Chemical Reduction with Sugarcane Molasses." *Water, Air, & Soil Pollution* 226 (11): 363.

Christensen, A. N., M.-A. Chevallier, J. Skibsted, and B. B. Iversen. 2000. "Synthesis and Characterization of Basic Bismuth(III) Nitrates." *Journal of the Chemical Society, Dalton Transactions* (3): 265-270.

Chrysochoou, M., D. R. Ferreira, and C. P. Johnston. 2010. "Calcium Polysulfide Treatment of Cr(VI)-Contaminated Soil." *Journal of Hazardous Material* 179 (1-3): 650-657.

Coker, V. S., N. D. Telling, G. Van Der Laan, R. A. Pattrick, C. I. Pearce, E. Arenholz, F. Tuna, R. E. Winpenny, and J. R. Lloyd. 2009. "Harnessing the Extracellular Bacterial Production of Nanoscale Cobalt Ferrite with Exploitable Magnetic Properties." *ACS Nano* 3 (7): 1922-1928.

Dahl, S., P. Allain, P. Marie, Y. Mauras, G. Boivin, P. Ammann, Y. Tsouderos, P. Delmas, and C. Christiansen. 2001. "Incorporation and Distribution of Strontium in Bone." *Bone* 28 (4): 446-453.

de Lima Perini, J. A., and R. F. P. Nogueira. 2017. "Effect of Particle Size, Iron Ligands and Anions on Ciprofloxacin Degradation in Zero-Valent Iron Process: Application to Sewage Treatment Plant Effluent." *Journal of Chemical Technology and Biotechnology* 92 (9): 2300-2308.

DOE/RL-2011-102, Rev. 0. 2011. *Remedial Investigation/Feasibility Study and RCRA Facility Investigation/Corrective Measures Study Work Plan for the 200-DV-1 Operable Unit.* U.S. Department of Energy, Richland Operations Office, Richland, WA.

DOE/RL-2017-58.. 2017. *Technology Evaluation and Treatability Studies Assessment for the Hanford Central Plateau Deep Vadose Zone.* U.S. Department of Energy, Richland Operations Office, Richland, WA.

DOE/RL-2019-28, Rev. 0.. 2019. *200-DV-1 Operable Unit Laboratory Treatability Study Test Plan.* U.S. Department of Energy, Richland Operations Office, Richland, WA.

DOE/RL-2022-40, Rev. 0.. 2022. *Hanford Site Groundwater Monitoring Report for 2022.* U.S. Department of Energy, Richland Operations Office, Richland, WA.

DOE/RL-88-09. 1988. *183-H Solar Evaporation Basins Closure/Post-Closure Plan.* U.S. Department of Energy, Richland Operations Office, Richland, WA.

DOE/RL-92-24, Rev. 1.0. 1993. *Hanford Site Background: Part 1, Soil Background for Nonradioactive Analytes.* U.S. U.S. Department of Energy, Richland Operations Office, Richland, WA.

Dong, W., and S. C. Brooks. 2006. "Determination of the Formation Constants of Ternary Complexes of Uranyl and Carbonate with Alkaline Earth Metals (Mg^{2+}, Ca^{2+}, Sr^{2+}, and Ba^{2+}) Using Anion Exchange Method." *Environmental Science & Technology* 40 (15): 4689-4695.

Dong, W., W. P. Ball, C. Liu, Z. Wang, A. T. Stone, J. Bai, and J. M. Zachara. 2005. "Influence of Calcite and Dissolved Calcium on Uranium (VI) Sorption to a Hanford Subsurface Sediment." *Environmental Science & Technology* 39 (20): 7949-7955.

Dorozhkin, S. V. 1997. "Surface Reactions of Apatite Dissolution." *Journal of Colloid and Interface Science* 191 (2): 489-497.

Emenike, C. U., P. Agamuthu, S. H. Fauziah, P. N. Omo-Okoro, and B. Jayanthi. 2023. "Enhanced Bioremediation of Metal-Contaminated Soil by Consortia of Proteobacteria." *Water, Air, & Soil Pollution* 234 (12): 731.

Emerson, H. P., A. Gebru, D. Boglaienko, Y. P. Katsenovich, S. Kandel, and T. G. Levitskaia. 2020. "Impact of Zero Valent Iron Aging on Reductive Removal of Technetium-99." *Journal of Environmental Chemical Engineering* 8 (3): 103767.

Emerson, H. P., N. P. Qafoku, C. D. Johnson, J. E. Szecsody, M. S. Doughman, R. D. Mackley, and D. I. Kaplan. 2025a. "A Paradigm Shift for Evaluating Natural Attenuation of Radioactive Iodine in Soils and Sediments: Species-Specific Mechanisms and Pathways." *Journal of Environmental Management* 374: 124101.

EPA 815-B-16-012. 2020. *Cyanide Clarification of Free and Total Cyanide Analysis for Safe Drinking Water Act (SDWA) Compliance, Revision 1.0.* U.S. Environmental Protection Agency. Washington, DC.

Escobedo, N. M., S. A. Saslow, E. A. Cordova, A. R. Lawter, M. E. Bowden, O. Qafoku, C. T. Resch, N. Lahiri, N. D'Annunzio, D. Boglaienko, T. Levitskaia, C. I. Pearce, V. L. Freedman, and R. D. Mackley. 2025. "Part I: Structural Transformation of Bismuth-based Materials in Dynamic Aqueous Environments and Implications for Subsurface Contaminant Remediation." *ACS Earth and Space Chemistry* 9 (11): 2490-2508.

Evans, P. J., and M. M. Trute. 2006. "In Situ Bioremediation of Nitrate and Perchlorate in Vadose Zone Soil for Groundwater Protection Using Gaseous Electron Donor Injection Technology." *Water Environment Research* 78 (13): 2436-2446.

Evans, P. J., R. A. Fricke, K. Hopfensperger, and T. Titus. 2011. "In Situ Destruction of Perchlorate and Nitrate Using Gaseous Electron Donor Injection Technology." *Groundwater Monitoring & Remediation* 31 (4): 103-112.

Field, E. K., R. Gerlach, S. Viamajala, L. K. Jennings, B. M. Peyton, and W. A. Apel. 2013. "Hexavalent Chromium Reduction by Cellulomonas Sp. Strain Es6: The Influence of Carbon Source, Iron Minerals, and Electron Shuttling Compounds." *Biodegradation* 24 (3): 437-450.

Fuller, C., J. Bargar, and J. Davis. 2003. "Molecular-Scale Characterization of Uranium Sorption by Bone Apatite Materials for a Permeable Reactive Barrier Demonstration." *Environmental Science & Technology* 37 (20): 4642-4649.

Gerlach, R., E. K. Field, S. Viamajala, B. M. Peyton, W. A. Apel, and A. B. Cunningham. 2011. "Influence of Carbon Sources and Electron Shuttles on Ferric Iron Reduction by Cellulomonas Sp. Strain Es6." *Biodegradation* 22 (5): 983-995.

Gleyzes, C., S. Tellier, and M. Astruc. 2002. "Fractionation Studies of Trace Elements in Contaminated Soils and Sediments: A Review of Sequential Extraction Procedures." *Trends in Analytical Chemistry* 21 (6-7): 451-467.

Guan, X., Y. Sun, H. Qin, J. Li, I. M. Lo, D. He, and H. Dong. 2015. "The Limitations of Applying Zero-Valent Iron Technology in Contaminants Sequestration and the Corresponding Countermeasures: The Development in Zero-Valent Iron Technology in the Last Two Decades (1994–2014)." *Water Research* 75: 224-248.

Hall, G., J. Vaive, R. Beer, and N. Hoashi. 1996. "Selective Leaches Revisited, with Emphasis on the Amorphous E Oxyhydroxide Phase Extraction." *Journal of Geochemical Exploration* 56: 59-78.

Heslop, D., Y. Bi, A. Baig, M. Otsuka, and W. Higuchi. 2005. "A Comparative Study of the Metastable Equilibrium Solubility Behavior of High-Crystallinity and Low-Crystallinity Carbonated Apatites Using pH and Solution Strontium as Independent Variables." *Journal of Colloid and Interface Science* 289 (1): 14-25.

Hu, Q., P. Zhao, J. E. Moran, and J. C. Seaman. 2005. "Sorption and Transport of Iodine Species in Sediments from the Savannah River and Hanford Sites." *Journal of Contaminant Hydrology* 78 (3): 185-205.

Hughes, J. M., and J. F. Rakovan. 2015. "Structurally Robust, Chemically Diverse: Apatite and Apatite Supergroup Minerals." *Elements* 11 (3): 165-170.

Istok, J., J. Senko, L. R. Krumholz, D. Watson, M. A. Bogle, A. Peacock, Y.-J. Chang, and D. C. White. 2004. "In Situ Bioreduction of Technetium and Uranium in a Nitrate-Contaminated Aquifer." *Environmental Science & Technology* 38 (2): 468-475.

ITRC. 2017. *Remediation Management of Complex Sites.* Interstate Technology and Regulatory Council Washington, D.C. https://rmcs-1.itrcweb.org/.

Janusz, W., and E. Skwarek. 2016. "Study of Sorption Processes of Strontium on the Synthetic Hydroxyapatite." *Adsorption* 22 (4): 697-706.

Kaplan, D. I., M. E. Denham, S. Zhang, C. Yeager, C. Xu, K. A. Schwehr, H. P. Li, Y. F. Ho, D. Wellman, and P. H. Santschi. 2014. "Radioiodine Biogeochemistry and Prevalence in Groundwater." *Critical Reviews in Environmental Science and Technology* 44 (20): 2287-2335.

Kaplan, D. I., R. J. Serne, K. E. Parker, and I. V. Kutnyakov. 2000. "Iodide Sorption to Subsurface Sediments and Illitic Minerals." *Environmental Science & Technology* 34 (3): 399-405.

Katsenovich, Y. P., R. T. Gort, R. Gudavalli, J. Szecsody, V. L. Freedman, and N. P. Qafoku. 2021. "Silicon Concentration and pH Controls over Competitive or Simultaneous Incorporation of Iodate and Chromate into Calcium Carbonate Phases." *Applied Geochemistry* 128: 104941.

Kerisit, S. N., F. N. Smith, S. A. Saslow, M. E. Hoover, A. R. Lawter, and N. P. Qafoku. 2018. "Incorporation Modes of Iodate in Calcite." *Environmental Science and Technology* 52 (10): 5902-5910.

Kimmig, S., C. Thompson, S. Baum, and C. Brown. 2021. "Evaluation of Iodine Speciation and $^{129}I/^{127}I$ Ratios at Low Concentrations in Environmental Samples Using IC-ICP-MS." *Journal of Radioanalytical and Nuclear Chemistry* 327: 929-937.

Komlos, J., A. Peacock, R. K. Kukkadapu, and P. R. Jaffé. 2008. "Long-Term Dynamics of Uranium Reduction/Reoxidation under Low Sulfate Conditions." *Geochimica et Cosmochimica Acta* 72 (15): 3603-3615.

Konopka, A., A. E. Plymale, D. A. Carvajal, X. Lin, and J. P. McKinley. 2013. "Environmental Controls on the Activity of Aquifer Microbial Communities in the 300 Area of the Hanford Site." *Microbial Ecology* 66: 889-896.

Kourtev, P. S., C. H. Nakatsu, and A. Konopka. 2009. "Inhibition of Nitrate Reduction by Chromium(VI) in Anaerobic Soil Microcosms." *Applied and Environmental Microbiology* 75 (19): 6249-6257.

LAB-RPT-12-00001, Rev 0. 2012. *Laboratory Report on the Reduction and Stabilization (Immobilization) of Pertechnetate to Technetium Dioxide Using Tin (II) Apatite.* Washington River Protection Solutions, Richland, WA.

Lammers, L. N., H. Rasmussen, D. Adilman, J. L. deLemos, P. Zeeb, D. G. Larson, and A. N. Quicksall. 2017. "Groundwater Uranium Stabilization by a Metastable Hydroxyapatite." *Applied Geochemistry* 84: 105-113.

Larner, B. L., A. J. Seen, and A. T. Townsend. 2006. "Comparative Study of Optimised Bcr Sequential Extraction Scheme and Acid Leaching of Elements in the Certified Reference Material Nist 2711." *Analytica Chimica Acta* 556 (2): 444-449.

Lawter, A., T. Levitskaia, O. Qafoku, M. Bowden, F. Colon, and N. Qafoku. 2021. “Simultaneous Immobilization of Aqueous Co-Contaminants Using a Bismuth Layered Material.” *Journal of Environmental Radioactivity* 237: 106711.

Lee, J. H., J. K. Fredrickson, A. E. Plymale, A. C. Dohnalkova, C. T. Resch, J. P. McKinley, and L. Shi. 2015. “An Autotrophic H 2-Oxidizing, Nitrate-Respiring, T C (VII)-Reducing a Cidovorax Sp. Isolated from a Subsurface Oxic-Anoxic Transition Zone.” *Environmental Microbiology Reports* 7 (3): 395-403.

Levitskaia, T. G., N. P. Qafoku, M. E. Bowden, R. M. Asmussen, E. C. Buck, V. L. Freedman, and C. I. Pearce. 2022. “A Review of Bismuth (III)-Based Materials for Remediation of Contaminated Sites.” *ACS Earth and Space Chemistry* 6 (4): 883-908.

Liu, J., C. I. Pearce, O. Qafoku, E. Arenholz, S. M. Heald, and K. M. Rosso. 2012. “Tc (VII) Reduction Kinetics by Titanomagnetite (Fe3− xTixO4) Nanoparticles.” *Geochimica et Cosmochimica Acta* 92: 67-81.

Madejón, P., A. Pérez-de-Mora, P. Burgos, F. Cabrera, N. Lepp, and E. Madejón. 2010. “Do Amended, Polluted Soils Require Re-Treatment for Sustainable Risk Reduction?—Evidence from Field Experiments.” *Geoderma* 159 (1-2): 174-181.

McElroy, B., A. Keith, J. Glasgow, and S. Dasappa. 2003. “The Use of Zero-Valent Iron Injection to Remediate Groundwater: Results of a Pilot Test at the Marshall Space Flight Center.” *Remediation Journal* 13: 145-153.

McElroy, E., A. R. Lawter, D. Appriou, F. Smith, M. Bowden, O. Qafoku, L. Kovarik, J. E. Szecsody, M. J. Truex, and N. P. Qafoku. 2020. “Iodate Interactions with Calcite: Implications for Natural Attenuation.” *Environmental Earth Sciences* 79: 1-9.

McGrail, B. P., P. F. Martin, and C. W. Lindenmeier. 1996. “Accelerated Testing of Waste Forms Using a Novel Pressurized Unsaturated Flow (PUF) Method.” *MRS Online Proceedings Library* 465 (1): 253-260.

McNally, S. R. 2011. “The Status of Iodine and Selenium in Waikato Soils.” University of Waikato.

Meeussen, J. C. L., M. G. Keizer, and F. A. M. De Haan. 1992. “Chemical Stability and Decomposition Rate of Iron Cyanide Complexes in Soil Solutions.” *Environmental Science and Technology* 26 (3): 511-516

Miltzarek, G., C. Sampaio, and J. Cortina. 2002. “Cyanide Recovery in Hydrometallurgical Plants: Use of Synthetic Solutions Constituted by Metallic Cyanide Complexes.” *Minerals Engineering* 15 (1-2): 75-82.

Moore, R. C., C. I. Pearce, J. Morad, S. Chatterjee, T. Levitskaia, R. M. Asmussen, A. R. Lawter, J. J. Neeway, N. P. Qafoku, M. J. Rigali, et al. 2020. “Iodine Immobilization by Materials through Sorption and Redox-Driven Processes: A Literature Review.” *Science of the Total Environment* 716 (132920): 1-11.

Mossop, K. F., and C. M. Davidson. 2003. “Comparison of Original and Modified Bcr Sequential Extraction Procedures for the Fractionation of Copper, Iron, Lead, Manganese and Zinc in Soils and Sediments.” *Analytica Chimica Acta* 478 (1): 111-118.

Muller, K. A., C. D. Johnson, C. E. Bagwell, and M. J. Truex. 2021a. "Methods for Delivery and Distribution of Amendments for Subsurface Remediation: A Critical Review." *Groundwater Monitoring & Remediation* 41 (1): 46-75.

Muller, K. A., L. Zhong, and C. E. Bagwell. 2021b. "Characterizing the Influence of Organic Polymers on the Specific Reactivity of Particulate Remedial Amendments." *Frontiers in Environmental Science* 9: 703851.

NBL-345, Rev. 0. 1997. *Evaluation of Kinetic Phosphorescence Analysis for the Determination of Uranium.* New Brunswick Laboratory, Argonne, IL.

Nelson, N., Q. Hu, and M. Brusseau. 2003. "Characterizing the Contribution of Diffusive Mass Transfer to Solute Transport in Sedimentary Aquifer Systems at Laboratory and Field Scales." *Journal of Hydrology* 276 (1-4): 275-286.

Newsome, L., K. Morris, and J. R. Lloyd. 2014. "The Biogeochemistry and Bioremediation of Uranium and Other Priority Radionuclides." *Chemical Geology* 363: 164-184.

Newville, M. 2013. "Larch: An Analysis Package for XAFS and Related Spectroscopies." *Journal of Physics: Conference Series* 430 (1): 012007.

Nishiyama, Y., T. Hanafusa, J. Yamashita, Y. Yamamoto, and T. Ono. 2016. "Adsorption and Removal of Strontium in Aqueous Solution by Synthetic Hydroxyapatite." *Journal of Radioanalytical and Nuclear Chemistry* 307 (2): 1279-1285.

Nolan, J., and K. A. Weber. 2015. "Natural Uranium Contamination in Major US Aquifers Linked to Nitrate." *Environmental Science & Technology Letters* 2 (8): 215-220.

Oliveira, A. F., A. Kuc, T. Heine, U. Abram, and A. C. Scheinost. 2022. "Shedding Light on the Enigmatic TcO2· xH2O Structure with Density Functional Theory and EXAFS Spectroscopy." *Chemistry–A European Journal* 28 (59): e202202235.

Pan, Z., D. E. Giammar, V. Mehta, L. D. Troyer, J. G. Catalano, and Z. Wang. 2016. "Phosphate-Induced Immobilization of Uranium in Hanford Sediments." *Environmental Science & Technology* 50 (24): 13486-13494.

Paradis, C. J., S. Jagadamma, D. B. Watson, L. D. McKay, T. C. Hazen, M. Park, and J. D. Istok. 2016. "In Situ Mobility of Uranium in the Presence of Nitrate Following Sulfate-Reducing Conditions." *Journal of Contaminant Hydrology* 187: 55-64.

Pattrick, R. A., G. van Der Laan, C. M. B. Henderson, P. Kuiper, E. Dudzik, and D. J. Vaughan. 2002. "Cation Site Occupancy in Spinel Ferrites Studied by X-Ray Magnetic Circular Dichroism: Developing a Method for Mineralogists." *European Journal of Mineralogy* 14 (6): 1095-1102.

Pearce, C. I., C. M. B. Henderson, N. D. Telling, R. A. Pattrick, J. M. Charnock, V. S. Coker, E. Arenholz, F. Tuna, and G. van der Laan. 2010. "Fe Site Occupancy in Magnetite-Ulvospinel Solid Solutions: A New Approach Using X-Ray Magnetic Circular Dichroism." *American Mineralogist* 95 (4): 425-439.

Pearce, C. I., C. M. B. Henderson, R. A. Pattrick, G. van Der Laan, and D. J. Vaughan. 2006. "Direct Determination of Cation Site Occupancies in Natural Ferrite Spinels by $L_{2,3}$ X-Ray Absorption Spectroscopy and X-Ray Magnetic Circular Dichroism." *American Mineralogist* 91 (5-6): 880-893.

Pearce, C. I., D. Boglaienko, A. R. Lawter, E. A. Cordova, K. J. Cantrell, M. E. Bowden, N. Lahiri, O. Qafoku, S. T. Mergelsberg, and C. T. Resch. 2025. "Mechanisms of Interaction between Bismuth-Based Materials and Contaminants for Subsurface Remediation." *Journal of Materials Chemistry A* 13 (23): 17350-17375.

Pearce, C. I., J. P. Icenhower, R. M. Asmussen, P. G. Tratnyek, K. M. Rosso, W. W. Lukens, and N. P. Qafoku. 2018. "Technetium Stabilization in Low-Solubility Sulfide Phases: A Review." *ACS Earth and Space Chemistry* 2 (6): 532-547.

Pearce, C., R. C. Moore, J. W. Morad, R. M. Asmussen, S. Chatterjee, A. R. Lawter, T. G. Levitskaia, J. J. Neeway, N. P. Qafoku, and M. J. Rigali. 2020. "Technetium Immobilization by Materials through Sorption and Redox-Driven Processes: A Literature Review." *Science of the Total Environment* 716: 132849.

Peretyazhko, T., J. M. Zachara, S. M. Heald, B.-H. Jeon, R. K. Kukkadapu, C. Liu, D. Moore, and C. T. Resch. 2008. "Heterogeneous Reduction of Tc-99 (VII) by Fe (II) at the Solid–Water Interface." *Geochimica et Cosmochimica Acta* 72 (6): 1521-1539.

Perumal, S., W. Lee, and R. Atchudan. 2022. "A Review on Bismuth-Based Materials for the Removal of Organic and Inorganic Pollutants." *Chemosphere*: 135521.

Pierce, E. M., B. P. McGrail, P. F. Martin, J. Marra, B. W. Arey, and K. N. Geiszler. 2007. "Accelerated Weathering of High-Level and Plutonium-Bearing Lanthanide Borosilicate Waste Glasses under Hydraulically Unsaturated Conditions." *Applied Geochemistry* 22 (9): 1841-1859.

Pingitore Jr, N. E., F. W. Lytle, B. M. Davies, M. P. Eastman, P. G. Eller, and E. M. Larson. 1992. "Mode of Incorporation of Sr2+ in Calcite: Determination by X-Ray Absorption Spectroscopy." *Geochimica et Cosmochimica Acta* 56 (4): 1531-1538.

Piscopo, A. N., R. M. Neupauer, and D. C. Mays. 2013. "Engineered Injection and Extraction to Enhance Reaction for Improved in Situ Remediation." *Water Resources Research* 49 (6): 3618-3625.

Plymale, A. E., J. K. Fredrickson, J. M. Zachara, A. C. Dohnalkova, S. M. Heald, D. A. Moore, D. W. Kennedy, M. J. Marshall, C. Wang, and C. T. Resch. 2011. "Competitive Reduction of Pertechnetate ($^{99}TcO_4^-$) by Dissimilatory Metal Reducing Bacteria and Biogenic Fe (Ii)." *Environmental Science and Technology* 45 (3): 951-957.

PNL-21497. 1993. *Characterization of Hanford Tank Wastes Containing Ferrocyanides.* Pacific Northwest Laboratory, Richland, WA.

PNNL-14535, Rev. 0. 2004. *Integrated Field, Laboratory, and Modeling Studies to Determine the Effects of Linked Microbial and Physical Spatial Heterogeneity on Engineered Vadose Zone Bioremediation.* Pacific Northwest National Laboratory, Richland, WA.

PNNL-17031. 2007. *A Site-Wide Perspective on Uranium Geochemistry at the Hanford Site*. Pacific Northwest National Laboratory, Richland, WA.

PNNL-17674, Rev. 0. 2008. *Geochemical Characterization of Chromate Contamination in the 100 Area Vadose Zone at the Hanford Site.* Pacific Northwest National Laboratory, Richland, WA.

PNNL-18139. 2008. *The Geochemistry of Technetium: A Summary of the Behavior of an Artificial Element in the Natural Environment*. Pacific Northwest National Laboratory, Richland, WA.

PNNL-18303. 2009. *Sequestration of Sr-90 Subsurface Contamination in the Hanford 100-N Area by Surface Infiltration of a Ca-Citrate-Phosphate Solution.* Pacific Northwest National Laboratory, Richland, WA.

PNNL-18529. 2009. *300 Area Uranium Stabilization through Polyphosphate Injection: Final Report*. Pacific Northwest National Laboratory, Richland, WA.

PNNL-19277. 2010. *Conceptual Models for Migration of Key Groundwater Contaminants through the Vadose Zone and into the Upper Unconfined Aquifer Below the B-Complex.* Pacific Northwest National Laboratory, Richland, WA.

PNNL-19524, Rev. 0. 2010. *Hanford 100-N Area In Situ Apatite and Phosphate Emplacement by Groundwater and Jet Injection: Geochemical and Physical Core Analysis.* Pacific Northwest National Laboratory, Richland, WA.

PNNL-23367. 2014. *Hanford Apatite Treatability Test Report Errata: Apatite Mass Loading Calculation*. Pacific Northwest National Laboratory, Richland, WA.

PNNL-24297, Rev. 1.0. 2016. *Extended Leach Testing of Simulated Law Cast Stone Monoliths.* Pacific Northwest National Laboratory, Richland, WA.

PNNL-24709, Rev. 1.0. 2017. *Conceptual Model of Iodine Behavior in the Subsurface at the Hanford Site.* Pacific Northwest National Laboratory, Richland, WA.

PNNL-25303, Rev. 0. 2016. *Use of a Ca-Citrate-Phosphate Solution to Form Hydroxyapatite for Uranium Stabilization of Old Rifle Sediments: Laboratory Proof of Principle Studies.* Pacific Northwest National Laboratory, Richland, WA.

PNNL-26208. 2017. *Contaminant Attenuation and Transport Characterization of 200-DV-1 Operable Unit Sediment Samples.* Pacific Northwest National Laboratory, Richland, WA.

PNNL-26266, Rev. 1.0. 2018. *Geochemical, Microbial, and Physical Characterization of 200-DV-1 Operable Unit B-Complex Cores from Boreholes C9552, C9487, and C9488 on the Hanford Site Central Plateau.* Pacific Northwest National Laboratory, Richland, WA.

PNNL-26730. 2017. *The Evaluation of Novel Tin Materials for the Removal of Technetium from Groundwater.* Pacific Northwest National Laboratory, Richland, WA.

PNNL-27524, Rev. 0. 2018. *Contaminant Attenuation and Transport Characterization of 200-DV-1 Operable Unit Sediment Samples from Boreholes C9497, C9498, C9603, C9488, and C9513.* Pacific Northwest National Laboratory, Richland, WA.

PNNL-27846, Rev. 0. 2018. *Physical and Hydraulic Properties of Sediments from the 200-DV-1 Operable Unit.* Pacific Northwest National Laboratory, Richland, WA.

PNNL-28054. 2018. *Evaluation of Perched Water Post-Extraction Remedy Technologies: Interim Status Report.* Pacific Northwest National Laboratory, Richland, WA.

PNNL-28055, Rev. 0. 2018. *Evaluation of Central Plateau Remediation Alternatives: Interim Status Report.* Pacific Northwest National Laboratory, Richland, WA.

PNNL-28064, Rev. 1.0. 2019. *Evaluation of in Situ and Ex Situ Remediation Technologies for Iodine-129: Final Bench Scale Results.* Pacific Northwest National Laboratory, Richland, WA.

PNNL-29650, Rev. 0. 2020. *Evaluation of the Change in Uranium Mobility in Sediments from the Hanford 300-FF-5 Stage B Polyphosphate Field Injection.* Pacific Northwest National Laboratory, Richland, WA.

PNNL-31959, Rev. 0. 2021. *Combined Technologies for In Situ Remediation of Tc-99 and U in Subsurface Sediments.* Pacific Northwest National Laboratory, Richland, WA.

PNNL-35432, Rev. 0. 2025. *200-DV-1 Laboratory Treatability Testing: Proof-of-Principle Results.* Pacific Northwest National Laboratory, Richland, WA.

PNNL-35629, Rev. 0. 2024. *Nitrate and Nitrite at Hanford–from Tanks to Natural Attenuation.* Pacific Northwest National Laboratory, Richland, WA.

PNNL-65124. 2009. *Laboratory Development of Polyphosphate Remediation Technology for In Situ Treatment of Uranium Contamination in the Vadose Zone and Capillary Fringe.* Pacific Northwest National Laboratory, Richland, WA.

PNNL-34340, Rev. 0. 2023. *200-DV-1 Operable Unit Perched Water Zone Characterization: Borehole D0112.* Pacific Northwest National Laboratory, Richland, WA.

Qafoku, N. P., A. R. Lawter, E. C. Gillispie, E. McElroy, F. N. Smith, R. Sahajpal, K. Cantrell, and V. Freedman. 2022. "Calcium Carbonate Minerals as Scavengers of Metals and Radionuclides: Their Role in Natural Attenuation and Remediation." *Advances in Agronomy* 176: 115-152.

Qafoku, N. P., and J. P. Icenhower. 2008. "Interactions of Aqueous U (VI) with Soil Minerals in Slightly Alkaline Natural Systems." *Reviews in Environmental Science and Bio/Technology* 7 (4): 355-380.

Qafoku, O., C. I. Pearce, A. Neumann, L. Kovarik, M. Zhu, E. S. Ilton, M. E. Bowden, C. T. Resch, B. W. Arey, and E. Arenholz. 2017. "Tc (VII) and Cr (VI) Interaction with Naturally Reduced Ferruginous Smectite from a Redox Transition Zone." *Environmental Science & Technology* 51 (16): 9042-9052.

Rahman, Z., and L. Thomas. 2021. "Chemical-Assisted Microbially Mediated Chromium (Cr)(VI) Reduction under the Influence of Various Electron Donors, Redox Mediators, and Other Additives: An Outlook on Enhanced Cr (VI) Removal." *Frontiers in Microbiology* 11: 619766.

Rai, D., L. E. Eary, and J. M. Zachara. 1989. "Environmental Chemistry of Chromium." *Science of the Total Environment* 886: 15-23.

Rakovan, J. 2002. "Growth and Surface Properties of Apatite." *Reviews in Mineralogy and Geochemistry* 48 (1): 51-86.

Ravel, B., and M. Newville. 2005. "ATHENA, ARTEMIS, HEPHAESTUS: Data Analysis for X-Ray Absorption Spectroscopy Using IFEFFIT." *Journal of Synchrotron Radiation* 12 (Pt 4): 537-41.

Reeder, R. J., M. Nugent, G. M. Lamble, C. D. Tait, and D. E. Morris. 2000. "Uranyl Incorporation into Calcite and Aragonite: Xafs and Luminescence Studies." *Environmental Science & Technology* 34 (4): 638-644.

Regan, S., P. Hynds, and R. Flynn. 2017. "An Overview of Dissolved Organic Carbon in Groundwater and Implications for Drinking Water Safety." *Hydrogeology Journal* 25.

Reimus, P., J. Clay, and N. Jemison. 2022. "Restoration Insights Gained from a Field Deployment of Dithionite and Acetate at a Uranium in Situ Recovery Mine." *Minerals* 12 (6): 711.

Rennert, T., and T. Mansfeldt. 2002. "Sorption of Iron-Cyanide Complexes in Soils." *Soil Science Society of America Journal* 66 (2): 437-444.

Robinson, C., S. Shaw, J. R. Lloyd, J. Graham, and K. Morris. 2023. "Phosphate (Bio) Mineralization Remediation of 90sr-Contaminated Groundwaters." *ACS ES&T Water* 3 (10): 3223-3234.

Robinson, C., S. Shaw, J. R. Lloyd, J. Graham, and K. Morris. 2025. "Bioremediation of Uranium Contaminated Sites through the Formation of U (VI) Phosphate (Bio) Minerals." *Environmental Science: Water Research & Technology* 11 (3): 725-736.

Roehl, K. E., K. Czurda, T. Meggyes, F.-G. Simon, and D. Stewart. 2005. "Permeable Reactive Barriers." In *Trace Metals and Other Contaminants in the Environment*, 1-25. Elsevier.

RPP-53855. 2012. *Reduction and Stabilization (Immobilization) of Pertechnetate to an Immobile Reduced Technetium Species Using Tin (II) Apatite.* Washington River Protection Solutions, LLC, Richland, WA.

Saslow, S. A., S. Kerisit, T. Varga, K. C. Johnson, N. M. Avalos, A. R. Lawter, and N. P. Qafoku. 2019. "Chromate Effect on Iodate Incorporation into Calcite." *ACS Earth and Space Chemistry* 3: 1624-1630.

Schwehr, K., P. Santschi, D. Kaplan, C. Yeager, and R. Brinkmeyer. 2009. "Organo-Iodine Formation in Soils and Aquifer Sediments at Ambient Concentrations." *Environmental Science & Technology* 43 (19): 7258-7264.

SGW-47062, Rev. 0. 2010. *Treatability Test Report for Field-Scale Apatite Jet Injection Demonstration for the 100-NR-2 Operable Unit.* CH2M Hill Plateau Remediation Company, Richland, WA.

SGW-59614, Rev. 0. 2016. *300-FF-5 Operable Unit Enhanced Attenuation Stage A Delivery Performance Report.* CH2M Hill Plateau Remediation Company, Richland, WA.

SGW-63113, Rev. 0. 2020. *300-FF-5 Operable Unit Enhanced Attenuation Uranium Sequestration Completion Report.* CH2M Hill Plateau Remediation Company, Richland, WA.

SGW-67996, Rev. 0. 2022. *Field Summary Report for the 200-DV-1 Operable Unit Extractions Wells, FY2020-2022.* Central Plateau Cleanup Company, Richland, WA.

Shao, Q., C. Xu, Y. Wang, S. Huang, B. Zhang, L. Huang, D. Fan, and P. G. Tratnyek. 2018. "Dynamic Interactions between Sulfidated Zerovalent Iron and Dissolved Oxygen: Mechanistic Insights for Enhanced Chromate Removal." *Water Research* 135: 322-330.

Shi, J., B. Zhang, R. Qiu, C. Lai, Y. Jiang, C. He, and J. Guo. 2019. "Microbial Chromate Reduction Coupled to Anaerobic Oxidation of Elemental Sulfur or Zerovalent Iron." *Environmental Science \& Technology* 53 (6): 3198-3207.

Sposito, G. 1994. *Chemical Equilibria and Kinetics in Soils*. New York, NY: Oxford University Press.

SW-846 9010C/9012B. 2004. *SW-846 Hazardous Waste Test Methods.* U.S. Environmental Protection Agency, Washington, D.C.

Szecsody, J., D. P. Jansik, J. P. McKinley, and N. J. Hess. 2014. "Influence of Alkaline Co-Contaminants on Technetium Mobility in Vadose Zone Sediments." *Journal of Environmental Radioactivity* 135: 147-160.

Szecsody, J., H. P. Emerson, A. R. Lawter, C. T. Resch, M. L. Rockhold, R. D. Mackley, and N. P. Qafoku. 2023. "Vadose Zone Soil Flushing for Chromium Remediation: A Laboratory Investigation to Support Field-Scale Application." *Groundwater Monitoring & Remediation* 43 (2): 34-50.

Szecsody, J., M. J. Truex, M. J. Zhong, T. C. Johnson, N. P. Qafoku, M. D. Williams, W. J. Greenwood, E. L. Wallin, J. D. Bargar, and D. K. Faurie. 2012. "Geochemical and Geophysical Changes during Ammonia Gas Treatment of Vadose Zone Sediments for Uranium Remediation." *Vadose Zone Journal*: 1-13.

Szecsody, J., M. J. Truex, N. P. Qafoku, D. M. Wellman, T. Resch, and L. R. Zhong. 2013. "Influence of Acidic and Alkaline Waste Solution Properties on Uranium Migration in Subsurface Sediments." *Journal of Contaminant Hydrology* 151: 155-175.

Technical Report 96-03. 1996. *Reduction of Tc-99 (VII) and Np (V) in Solution by Ferrous Iron. A Laboratory Study of Homogeneous and Heterogeneous Redox Processes*. Royal Institute of Technology,. Stockholm, Sweden.

Toride, N., F. Leij, and M. T. Van Genuchten. 1995. *The Cxtfit Code for Estimating Transport Parameters from Laboratory or Field Tracer Experiments.* U.S. Salinity Laboratory Riverside, California: U.S. Department of Agriculture.

van den Berg, E. M., J. L. Rombouts, J. G. Kuenen, R. Kleerebezem, and M. C. van Loosdrecht. 2017. "Role of Nitrite in the Competition between Denitrification and DNRA in a Chemostat Enrichment Culture." *Amb Express* 7 (1): 91.

van der Laan, G., and B. Thole. 1991. "Strong Magnetic X-Ray Dichroism in 2p Absorption Spectra of 3d Transition-Metal Ions." *Physical Review B* 43 (16): 13401.

van der Laan, G., and I. Kirkman. 1992. "The 2p Absorption Spectra of 3d Transition Metal Compounds in Tetrahedral and Octahedral Symmetry." *Journal of Physics: Condensed Matter* 4 (16): 4189.

Vermeul, V. R., J. E. Szecsody, B. G. Fritz, M. D. Williams, R. C. Moore, and J. S. Fruchter. 2014. "An Injectable Apatite Permeable Reactive Barrier for In Situ ^{90}Sr Immobilization." *Groundwater Monitoring & Remediation* 34 (2): 28-41.

Watts, M., and C. Mitchell. 2009. "A Pilot Study on Iodine in Soils of Greater Kabul and Nangarhar Provinces of Afghanistan." *Environmental Geochemistry and Health* 31 (4): 503.

Webb, S. 2006. “Sixpack: A Graphical User Interface for Xas Analysis Using Ifeffit.” *Physica Scripta* 2005: 1011.

Webb, S. M. 2011. “The Microanalysis Toolkit: X-Ray Fluorescence Image Processing Software.” *AIP Conference Proceedings* 1365 (1): 196-199.

Wellman, D. M., J. G. Catalano, J. P. Icenhower, and A. P. Gamerdinger. 2005. “Synthesis and Characterization of Sodium Meta-Autunite, Na $[UO_2PO_4]\cdot 3H2_O$.” *Radiochimica Acta* 93 (7): 393.

Wellman, D. M., J. P. Icenhower, A. P. Gamerdinger, and S. W. Forrester. 2006. “Effects of pH, Temperature, and Aqueous Organic Material on the Dissolution Kinetics of Meta-Autunite Minerals,(Na, Ca) 2-1 $[(UO_2)(PO_4)]_2\cdot 3H_2O$.” *American Mineralogist* 91 (1): 143-158.

Wellman, D. M., J. S. Fruchter, V. R. Vermeul, E. Richards, D. P. Jansik, and E. Edge. 2011. “Evaluation of the Efficacy of Polyphosphate Remediation Technology: Direct and Indirect Remediation of Uranium under Alkaline Conditions.” *Technology & Innovation* 13 (2): 151-164.

Wellman, D. M., K. M. Gunderson, J. P. Icenhower, and S. W. Forrester. 2007. “Dissolution Kinetics of Synthetic and Natural Meta-Autunite Minerals, $X_{3\text{-}N}^{(n+)}[(UO_2)(PO_4)]_2\cdot xH_2O$, under Acidic Conditions.” *Geochemistry Geophysics Geosystems* 8.

Wentworth, C. K. 1922. “A Scale of Grade and Class Terms for Clastic Sediments.” *The journal of geology* 30 (5): 377-392.

WHC-2433-FP. 1994. *Determination of Total Cyanide in Hanford Site High-Level Wastes.* Westinghouse Hanford Company, Richland, WA.

Williams, A. G. B., and M. M. Scherer. 2001. “Kinetics of Cr(VI) Reduction by Carbonate Green Rust.” *Environmental Science and Technology* 35: 3488-3494.

Williams, J., A. A. Maria, Y. Katsenovich, S. Kandel, D. Boglaienko, H. P. Emerson, and T. G. Levitskaia. 2024. “Competitive Reduction of Pertechnetate and Chromate in Radioactive Waste Streams Via Zero-Valent Iron.” *ACS Earth and Space Chemistry* 8 (4): 712-722.

Williams, K. H., P. E. Long, J. A. Davis, M. J. Wilkins, A. L. N'Guessan, C. I. Steefel, L. Yang, D. Newcomer, F. A. Spane, and L. J. Kerkhof. 2011. “Acetate Availability and Its Influence on Sustainable Bioremediation of Uranium-Contaminated Groundwater.” *Geomicrobiology Journal* 28 (5-6): 519-539.

WSRC-MS-2005-00589.. 2005. *Gas: A Neglected Phase in Remediation of Metals and Radionuclides.* Savannah River National Laboratory, Aiken, SC.

WSRC-MS-94-0323. 1994. *Technology Summary of the In Situ Bioremediation Demonstration (Methane Biostimulation) Via Horizontal Wells at the Savannah River Site Integrated Demonstration Project.* Savannah River Site, Aiken, SC.

Wu, M., J. Li, C.-Y. Lai, A. O. Leu, S. Sun, R. Gu, D. V. Erler, L. Liu, L. Li, and G. W. Tyson. 2024. “Nitrate-Driven Anaerobic Oxidation of Ethane and Butane by Bacteria.” *The ISME Journal* 18 (1): wrad011.

Xin, J., S. Fan, M. Yuan, X. Wang, X. Zhang, and X. Zheng. 2020. "Effects of Co-Existing Nitrate on TCE Removal by mZVI under Different Pollution Load Scenarios: Kinetics, Electron Efficiency and Mechanisms." *Science of the Total Environment* 716.

Xu, Z., S. Wang, Y. Chen, H. Xu, Y. Wang, W. Huang, and X. Song. 2024. "Superior Nitrate and Chromium Reduction Synergistically Driven by Multiple Electron Donors: Performance and the Related Biochemical Mechanism." *Environmental Pollution* 358: 124507.

Yang, J. E., J. S. Kim, Y. S. Ok, and K. R. Yoo. 2007. "Mechanistic Evidence and Efficiency of Cr(VI) Reduction in Water by Different Sources of Zerovalent Irons." *Water Science and Technology* 55 (1-2): 197-202.

Yang, X., X. Qin, J. Xie, X. Li, H. Xu, and Y. Zhao. 2022. "Study on the Effect of Cr(VI) Removal by Stimulating Indigenous Microorganisms Using Molasses." *Chemosphere* 308: 136229.

Young, A. T., J. Feng, E. Arenholz, H. Padmore, T. Henderson, S. Marks, E. Hoyer, R. Schlueter, J. Kortright, and V. Martynov. 2001. "First Commissioning Results for the Elliptically Polarizing Undulator Beamline at the Advanced Light Source." *Nuclear Instruments and Methods in Physics Research Section A: Accelerators, Spectrometers, Detectors and Associated Equipment* 467: 549-552.

Zhang, S., C. Xu, D. Creeley, Y.-F. Ho, H.-P. Li, R. Grandbois, K. A. Schwehr, D. I. Kaplan, C. M. Yeager, and D. Wellman. 2013. "Iodine-129 and Iodine-127 Speciation in Groundwater at the Hanford Site, US: Iodate Incorporation into Calcite." *Environmental Science & Technology* 47 (17): 9635-9642.

Zhang, T., T. Wang, W. Wang, B. Liu, W. Li, and Y. Liu. 2020. "Reduction and Stabilization of Cr(VI) in Soil by Using Calcium Polysulfide: Catalysis of Natural Iron Oxides." *Environmental Research* 190: 109992.

Zhang, X., X. Gai, Z. Zhong, F. Bian, C. Yang, Y. Li, and X. Wen. 2021. "Understanding Variations in Soil Properties and Microbial Communities in Bamboo Plantation Soils Along a Chromium Pollution Gradient." *Ecotoxicology and Environmental Safety* 222: 112507.

Zhong, L., N. P. Qafoku, J. E. Szecsody, P. E. Dresel, and Z. F. Zhang. 2009. "Foam Delivery of Calcium Polysulfide to the Vadose Zone for Chromium (VI) Immobilization: A Laboratory Evaluation." *Vadose Zone Journal* 8 (4): 976-985.

Zhou, P., and B. H. Gu. 2005. "Extraction of Oxidized and Reduced Forms of Uranium from Contaminated Soils: Effects of Carbonate Concentration and pH." *Environmental Science & Technology* 39 (12): 4435-4440.

Zook, A., L. Collins, and C. Pietri. 1981. "Determination of Nanogram Quantities of Uranium by Pulsed-Laser Fluorometry." *Microchimica Acta* II: 457-468.

Appendix A – Cross-Technology Supplemental

A.1 Analytical Methods

A.1.1 Aqueous Phase Analytical Methods

A.1.1.1 Inductively Coupled Plasma Mass Spectrometry

Metals

Select samples were analyzed quantitatively for U, Tc, Ag, As, Ba, Cd, Cr, Cs, Cu, Hg, Mo, Pb, Re, Ru, Sb, and Se using a Thermo Scientific X-Series II quadrupole inductively coupled plasma mass spectrometer (ICP-MS) with an Elemental Scientific Incorporated (ESI) SC4 DX FAST auto-sampler interface. All samples and standards were diluted with 2% Fisher Scientific Optima trace metal grade nitric acid and twice deionized water with a resistivity no less than 18.0 MΩ·cm. A 20-µg/L internal standard (ISTD) solution was added in-line to all samples, standards, and blanks during the analysis to monitor and correct for instrument fluctuations. Instrument detection limits (IDLs) were established by running a low-level calibration standard seven consecutive times and multiplying the standard deviation of those seven replicates by 3.143 (Student's t-test value). This process was repeated three times on non-consecutive days, and the values were averaged to establish a working IDL in µg/L.

The instrument was calibrated using standards made by the High-Purity Standards Corporation to generate calibration curves. The calibration standards ranged from 0.05 to 5 µg/L, with a High Calibration Verification (HCV) standard of 10 µg/L used to verify the upper linear calibration range. The calibration was initially verified by analyzing an Initial Calibration Verification (ICV) standard and then during sample analysis by analyzing Continuing Calibration Verification (CCV) standards every 10 samples at a minimum. Calibration blanks were analyzed following each calibration verification solution to flush the instrument and to confirm that potential carryover effects were not a factor. To help provide an independent check on accuracy, the ICV and CCV standards were sourced from Inorganic Ventures, a different supplier than that of the calibration standards.

I-127 Analysis

Samples were analyzed quantitatively at mass 127 using either a Thermo Scientific X-Series II quadrupole ICP-MS with an ESI SC4 DX FAST auto-sampler interface or a Thermo Scientific iCAP-RQ quadrupole ICP-MS with a Teledyne CETAC Technologies ASX-560 auto-sampler interface. All samples and standards were diluted with a solution of 0.5% triethylene tetramine and twice deionized water with a resistivity no lower than 18.0 MΩ·cm. The triethylene tetramine solution is made by Inorganic Ventures (product # UNS-2B). IDLs were established as described for metals.

<u>X-Series II ICP-MS Calibration</u>

The instrument was calibrated using standards made by the High-Purity Standards Corporation to generate calibration curves. The calibration standards ranged from 0.05 to 5 µg/L, with an HCV standard of 10 µg/L used to verify the upper linear calibration range. The calibration was verified with an ICV and during sample analysis with a CCV run every 10 samples at a minimum. Calibration blanks were analyzed following each calibration verification solution to flush the instrument and to confirm that potential carryover effects were not a factor. The calibration was independently verified using standards made by Inorganic Ventures. A 20-µg/L ISTD solution was added in-line to all samples, standards, and blanks during the analysis to monitor and correct for instrument fluctuations.

iCAP-RQ ICP-MS Calibration

The instrument was calibrated using standards made by the High-Purity Standards Corporation. The calibration standards ranged from 0.02 to 3 µg/L, with an HCV standard of 5 µg/L used to verify the upper linear calibration range. The calibration was verified with an ICV and during sample analysis with a CCV run every 10 samples at a minimum. Calibration blanks were analyzed following each calibration verification solution to flush the instrument and to confirm that potential carryover effects were not a factor. The calibration was independently verified using standards made by Inorganic Ventures. A 200-ng/L ISTD solution was added in-line to all samples, standards, and blanks during the analysis to monitor and correct for instrument fluctuations.

A.1.1.2 Inductively Coupled Plasma Optical Emission Spectrometry

Select samples were analyzed quantitatively for Ag, Al, As, B, Ba, Be, Bi, Ca, Cd, Co, Cr, Cs, Cu, Fe, Gd, K, Li, Mg, Mn, Mo, Na, Ni, P, Pb, Re, S, Sb, Se, Si, Sn, Sr, Ti, Tl, V, Zn, and Zr using a PerkinElmer Optima 8300 dual view inductively coupled plasma optical emission spectrometer with a PerkinElmer S-10 auto-sampler interface or for Al, Ba, Ca, Cr, Fe, Mg, Mn, Na, P, Si, and Sr using a PerkinElmer model Optima 2100DV with PerkinElmer S-93-plus auto-sampler. All samples and standards were diluted with 2% Fisher Scientific Optima trace metal grade nitric acid and twice deionized water with resistivity no less than 18.0 MΩ·cm. Samples were run at several dilutions to bring their various elemental concentrations within the optimal analytical ranges of the instrument and to provide another level of result confirmation. An ISTD solution was added in-line to all samples, standards, and blanks to monitor and correct for instrument fluctuations.

IDLs were determined using the procedure described in Section A.1.1.1 (Metals).

The instruments were calibrated using standards made by the High-Purity Standards Corporation or Inorganic Ventures to generate calibration curves. The range of the calibration curves for the PerkinElmer Optima 8300 dual view was 50 ng/L to 50 µg/L. The range of the calibration curves for the PerkinElmer Optima 2100DV was 0.5 to 3,000 µg/L. This calibration was verified with an ICV and during sample analysis with a CCV run every 10 samples at a minimum. Calibration blanks were analyzed following each calibration verification solution to flush the instrument and to confirm that potential carryover effects were not a factor. The calibration was independently verified using standards made by Inorganic Ventures or High-Purity Standards, depending on which was used for the calibration as different sets of standards were used for calibration and verification.

A.1.1.3 Anion Chromatography

Samples were analyzed quantitatively using a Dionex Reagent-Free Ion Chromatography System (RFICS) 2000 with an AS-1 auto-sampler interface, a Dionex RFICS 5000 with an AS-AP auto-sampler interface, or a Dionex ICS-2000 anion chromatograph with AS40 auto-sampler. The anions analyzed were bromide (Br^-), chloride (Cl^-), fluoride (F^-), nitrite (NO_2^-), nitrate (NO_3^-), phosphate (PO_4^{3-}), and sulfate (SO_4^{2-}). All samples and standards were diluted with twice deionized water with a resistivity no less than 18.0 MΩ·cm. IDLs were determined using the procedure described in Section A.1.1.1 (Metals). This process was repeated three times on non-consecutive days and averaged to establish a working IDL in mg/L.

The instruments were calibrated using a multi-element anion standard purchased from Inorganic Ventures to generate calibration curves. The calibration standards ranged from 0.03 to 7.5 mg/L or 25 to 120 mg/L, with an HCV standard of 30 mg/L, used to verify the upper linear calibration range. The calibration was verified with an ICV and during sample analysis with a CCV run every 10 samples at a minimum.

Calibration blanks were analyzed following each calibration verification solution to flush the instrument and to confirm that potential carryover effects were not a factor. The calibration was independently verified using anion standards purchased from SPEX CertiPrep.

A.1.1.4 Liquid Scintillation Counting of Tc-99

Tc was measured for select samples (for gas-phase chemical sequestration and particulate-phase chemical reduction and sequestration) using a PerkinElmer 3100TR liquid scintillation counter. A series of seven quench standards were used for Tc-99 to accurately convert the energy-specific light emission spectra into Tc-99 concentrations. The detection limit was approximately 0.12 µg/L (2 pCi/mL) by liquid scintillation counting (LSC) for a 1.0-mL sample with 1-hour count times, although detection limits varied based on the total volume of sample analyzed for LSC. For sequential extraction samples, Extractions 1 and 4 used 1.0 mL of sample with 5.0 mL of Opti-Fluor cocktail (PerkinElmer). Extractions 2 and 3 used 1.0 mL of sample with 5.0 mL of Hionic-Fluor cocktail (PerkinElmer). Extraction 5 used 0.25 mL of sample with 5.0 mL of Ultima Gold AB cocktail (PerkinElmer). In all cases, 6.5-mL plastic LSC vials were used. Duplicate samples were prepared randomly from 10% of samples. Five extraction blanks were run for each set of samples along with three ISTDs.

A.1.1.5 Kinetic Phosphorescence Analysis of Uranium

U was analyzed for select samples (for gas-phase chemical sequestration and particulate-phase chemical reduction and sequestration) with a kinetic phosphorescence analyzer (KPA) as U(VI). The samples were reacted with Uraplex, and phosphorescence was induced by a pulsed nitrogen laser with an excitation wavelength of 425 nm. Measurement of the ultraviolet (UV) emission was at 515 nm (Brina and Miller 1992). The detection limit for U was 0.5 µg/L for KPA. U detection limits for KPA were higher in specific matrices, though all samples were acidified with 2% HNO_3 prior to analysis. For example, some pH 2.3 acetic acid extractions of zero valent iron/sulfur modified iron (SMI) experiments were orange colored and had U detection limits of 50 to 200 µg/L. Daily 7-point calibration standards were used (0.25 to 30 µg/L, SPEX CertiPrep) and 30 µg/L verification standards (High-Purity Standards) in water and extraction solutions.

Uraplex from Chemchek, Inc. (Richland, WA) was used for all samples prior to July 15, 2023, after which Chemchek no longer supplied Uraplex. Based on a 1978 patent (4198568, J. Robbins and J. Kinrade), Uraplex was synthesized at Pacific Northwest National Laboratory (PNNL) (formula in Table A.1) and used for all samples after July 15, 2023. This PNNL Uraplex was 150 mM total phosphate that was 90% orthophosphate and 10% straight chain (pyro- and tripoly-) and cyclic (trimeta- and hexameta-) polyphosphates. In terms of performance, fresh Chemchek Uraplex with a new laser cartridge in the KPA showed the greatest sensitivity at all uranium concentrations (Figure A.1, 5/11/11 calibration). This performance is consistent with independent analysis of others (Zook et al. 1981; NBL-345). The Chemchek fresh and old Uraplex calibrations in 2022 and 2023 showed slightly lower sensitivity, likely due to the decreased output of the laser after 10 years. The PNNL Uraplex (Figure A.1, black dots) showed the same to slightly better sensitivity at all uranium concentrations compared to the 2022 and 2023 Chemchek Uraplex. The PNNL Uraplex was mixed and used within a week because over time polyphosphates depolymerize, which decreases the U concentration sensitivity.

Table A.1. Composition of Uraplex synthesized at PNNL.

Compound	Formula	CAS Number	Solubility (g/100 mL)	Formula Wt (g/mol)	Mass Added (g/L)
Na_2HPO_4	Na_2HPO_4	7558-79-4	7.7	142	12.71
NaH_2PO_4	NaH_2PO_4	7558-80-7	50.9	120	1.895
Na Pyro-PO_4	$Na_4(PO_4)_2 \cdot 10H_2O$	7722-88-5	6.7	466	1.514
Na Tripoly-PO_4	$Na_4P_3O_{10}$	7758-29-4	14.5	368	1.196
Na Trimeta-PO_4	$Na_3P_3O_9$	7785-84-4	22	305.9	0.994
Na Hexameta-PO_4	$(NaPO_4)_6$	68915-31-1	0.2	611.8	0.7158

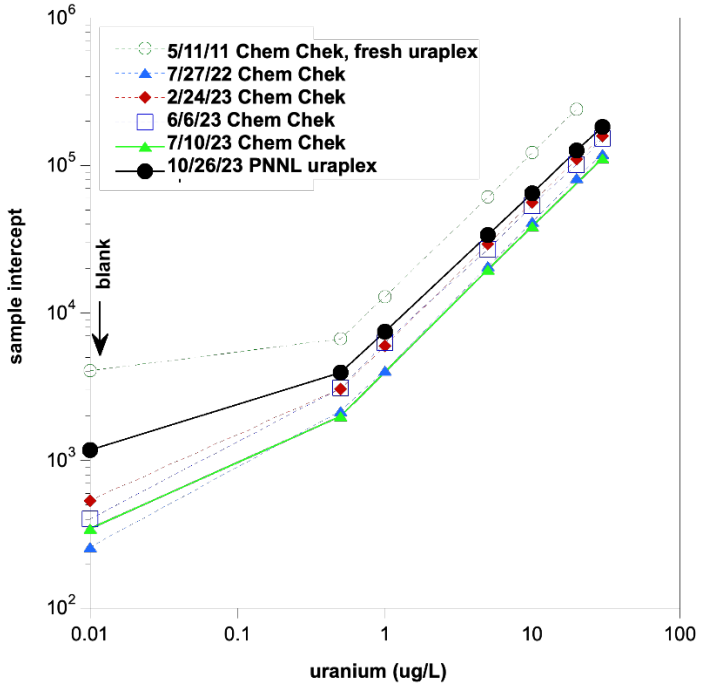

Figure A.1. Comparison of Chemchek and PNNL Uraplex.

A.1.1.6 Hexavalent Chromium by UV-Vis

The 0.2-µm filtered aqueous Cr(VI) was analyzed via reaction with 1,5-diphenylcarbazide, following a modified Hach Method 8023 (based on EPA Method 7196A) with adjusted liquid volumes. All standards and samples were measured at room temperature. For each sample, 20 µL of 10% nitric acid and 50 µL of 1,5-diphenylcarbazide solution were added to 2 mL of filtered supernatant or deionized water. The cuvette was capped, inverted to ensure mixing, and left to react for 10 minutes. Absorbance was then measured at 540 nm using a Hach DR/4000 spectrophotometer. All results for aqueous Cr(VI) by UV-Vis are presented as For Information Only (FIO).

A.1.1.7 Ammonia

Ammonia samples were extracted differently depending on timepoints for the gas-phase biotechnology. For the initial time, ammonia was measured using the filtered supernatant obtained from a 2:1 water-to-sediment ratio extraction. For all subsequent timepoints, the extraction was performed within the same tube containing the sediment and residual water from the initial 2:1 water-to-sediment ratio extraction.

The sediment-to-solution ratio was adjusted to 1:1 by adding 1 M calcium chloride. The mixtures were briefly vortexed, and the resulting slurry was placed on a slow shaker (30–60 rpm) for approximately 1 hour. Samples were then centrifuged at 5,000 to 10,000 *g* for 10 minutes, the aqueous phase was then filtered through a 0.2-µm filter and stored at 4 °C until analysis (within 24 hours) using the HACH Method #10023 (colorimetric analysis following the reaction of ammonia with chlorine and salicylate). All results for aqueous ammonia are presented as FIO.

A.1.1.8 Cyanide

Samples were preserved by adjusting the sample pH to 12 using 6 N NaOH and stored at 4 °C in the dark until the samples were shipped to GEL Laboratories, LLC (Charleston, SC) for analysis for free and total cyanide. Total cyanide analysis followed SW-846 Test Method 9010C, *Total and Amenable Cyanide: Distillation*, SW-846 Test Method 9012B, *Total and Amenable Cyanide (Automated Colorimetric, With Off-Line Distillation*), and SW-846 9010C/9012B. Free cyanide analysis followed ASTM D4282(2022), *Standard Test Method for Determination of Free Cyanide in Water and Wastewater by Microdiffusion*.

A.1.1.9 PFBA

Pentafluorobenzoic acid (PFBA) was used as an alternative non-reactive tracer (to bromide) in bismuth columns at a concentration of 200 mg/L (Nelson et al. 2003). Effluent samples were analyzed via a Thermo Scientific Evolution 220 UV-Visible Spectrophotometer at a wavelength of 262 nm (PNNL-17031). Concentrations of PFBA in samples were determined using a 6-point calibration curve [1, 10, 50, 100, 200, 1,000 mg/L; approximate limit of detection was 0.5 mg/L (Nelson et al. 2003)].

A.1.2 Additional Analyses

A.1.2.1 Water Content

Sample water content was determined using ASTM D2216-19. Subsamples of sediment were dried at 110 °C for several days until less than a 0.1% change was observed between two consecutive dry weight measurements.

A.1.2.2 pH

Effluent pH was measured using a standard electrode (e.g., Thermo Scientific Orion Ross 8102 BNUWP) with a three-point calibration. The sediment pH was measured following a protocol based on EPA Method 0945D (soil and waste pH) (SW-846 9010C/9012B). A 1:1 sediment-to-water ratio was used. Samples were vortexed at the highest setting for 90 seconds, then centrifuged at 1,000 g for 15 minutes at room temperature (~21 °C). Following centrifugation, the supernatant was immediately filtered through a 0.2-µm syringe filter using a 1-mL syringe into a clean glass vial. The pH of the filtrate was measured using a calibrated Horiba pH-22 handheld pH electrode. pH measurements were conducted either the same day or within 24 hours to minimize changes in CO_2 equilibration. If pH was not measured immediately, samples were stored at room temperature.

A.1.3 *In Situ* Dissolved Oxygen Monitoring

Select column experiments [Sn(II)-PO_4, Appendix F; calcium polysulfide (CPS), Poly-PO_4, or CPS+PolyCPS+Poly-PO_4, Appendix J] included oxygen monitoring via oxygen sensors (PSt3 Oxygen Sensor Spots, PreSens, Germany) attached inside the column, with one sensor placed near the inlet end and one placed near the outlet end. Oxygen measurements were recorded by a fiber optic oxygen meter, using a polymer optical fiber probe to read the sensor spot through the clear PVC column. PreSens

Measurement Studio 2 software was used to collect and process the data. Due to light sensitivity, oxygen sensor spots were kept covered between measurements. All results are FIO.

A.2 Supplemental Experimental Methods

A.2.1 Long-Term Batch Experiments

Sacrificial batch experiments were conducted to understand the impact of contact time of contaminants of interest with amendments on long-term sequestration with sampling up to approximately 1 year. Sediments were prepared as described in Section 2.4.1 with sequential addition of PCOIs (with and without CoCOIs) and then amendments. The total volume added during contamination and treatment was equivalent to approximately 1 pore volume (PV) at 100% saturation with a porosity of 0.3 to replicate as closely as possible the solid-to-liquid ratios under field conditions. For amendments targeting reduction, samples were initially prepared in the absence of oxygen (N_2 atmosphere) and exposed to air at 28 days to mimic re-introduction of air over time. At each sampling point, the sediment sample was sacrificed with initial centrifugation to recover pore water followed by sequential extractions as described in Section A.2.3.

A.2.2 Water Extractions

To quantify PCOI or CoCOI concentrations in pore water for vadose zone technologies, a 2:1 sediment-to-ultrapure-water extraction was conducted. The mixture was agitated at 60 rpm for 1 hour. Then, solutions were centrifuged at 3,000 rpm for 10 minutes and filtered with a 0.2-µm polytetrafluoroethylene (PTFE) syringe filter. Finally, supernatant was analyzed for relevant constituents, depending on the PCOI or CoCOI.

A.2.3 Alkaline Extractions

A tetramethylammonium hydroxide (TMAH) extraction was used to dissolve precipitates associated with iodine. Previous research has demonstrated nearly quantitative removal of iodine from certified standard sediments with TMAH (McNally 2011; Watts and Mitchell 2009). For the extraction, approximately 1 g of sediment was reacted with 20 mL of 5% TMAH (50 g/L solution) at 70 °C for 3 hours.

A.2.4 Sequential Extractions

Sequential liquid extractions have been used to characterize a wide variety of metals present in sediments in multiple surface phases (Beckett 1989; Mossop and Davidson 2003; Chao and Zhou 1983; Gleyzes et al. 2002; Hall et al. 1996; Larner et al. 2006). A series of extractions are used to evaluate the different forms of PCOIs or CoCOIs in the sediment, including *Extraction 1:* aqueous, *Extraction 2:* adsorbed, *Extraction 3:* reduced and readily oxidized, *Extraction 4:* precipitated in calcite, and *Extraction 5:* precipitated into hard-to-extract phases (i.e., oxides, silicates, aluminosilicates). Note that although targeted fractions are identified for each extraction step, each of these phases is operationally defined and may not be representative of the actual phases released. However, each step of the extractions represents a relative decrease in mobilization potential of the phases with which the PCOIs or CoCOIs are associated, providing a qualitative understanding of the potential for re-mobilization.

Technologies that involve a reduction process use all five sequential extractions at selected time intervals. Technologies that do not involve a reduction process generally use four sequential extractions, omitting the third (i.e., reducible, oxidizable). Further, the assumption for Extraction 3 is that the mass of dissolved oxygen in the liquid (and O_2 diffusing into liquid from the air headspace) is greater than the mass of reduced contaminants (and other phases such as ferrous iron precipitates) on the sediment surface. In

addition, the first extraction step could be omitted in saturated batch experiments if the supernatant was analyzed prior to extractions, although in some cases the first extraction was still conducted in saturated experiments.

Extractions were conducted in PTFE or polycarbonate centrifuge tubes or other compatible containers at a 1:3 or 1:2 sediment-to-solution ratio. Volumes indicated for each extraction assume 5 g of sediment with a liquid volume of 15 mL (for a 1:3 ratio), but this was adjusted depending on the actual sediment mass and ratio as stated for each technology. For these extractions, the first step was to remove an aliquot of the sediment from the batch or column and weigh the sediment that was placed in the centrifuge tube in an anaerobic chamber, as some PCOI or CoCOI phases may be reduced (and could be readily oxidized). The exact weight of sediment added was recorded (to at least 10 mg accuracy). Upon sampling, the tube was centrifuged at 3,000 rpm for 10 minutes, then liquid was drawn off the top of the sediment and filtered with a syringe filter prior to analysis.

For technologies not involving microbes, 0.22- or 0.45-µm polyvinylidene fluoride or polyethersulfone or PTFE filters were used, while equivalent 0.2-µm pore size syringe filters were used for any technologies involving microbes. Nylon filters were used for Extractions 1 through 4 (PTFE filters for Extraction 5) for the gas-phase bioreduction and sequestration technology (Appendix K). Extractions 1 through 4 were conducted at room temperature (20 to 25 °C), and Extractions 1 and 2 were conducted in the glovebox under anaerobic conditions. A preparation blank and blank spike were also prepared to check background contaminant concentrations (blanks) and confirm that contaminants were soluble in extractions and results were reproducible and without interferences (blank spikes) for each extraction. The blanks consisted of the extraction solutions (i.e., reagents 1 through 5) without contaminants added to solution.

Each extraction is described in greater detail below based on a 1:3 sediment-to-solution ratio.

Extraction 1. “Aqueous”: 15 mL of *anaerobic* synthetic groundwater (SGW) or synthetic perched water (SPW) prepared in degassed ultrapure water (≥ 18 MΩ·cm) was mixed with 5 (± 0.5) g of sediment (or smaller mass at the same sediment-to-solution ratio) in an anaerobic chamber. The tube was placed in a compatible container for 50 minutes and mixed by placing the tube on a slow (< 30-rpm) mixer.

Extraction 2. “Adsorbed/Exchangeable”: 15 mL of the *anaerobic* ion exchange solution [0.5 M magnesium nitrate ($Mg[NO_3]_2$) prepared in degassed ultrapure water (≥ 18 MΩ·cm); dissolved oxygen removed from solution by vigorous N_2 bubbling for 15 minutes followed by opening inside an N_2 vacuum chamber for 15 minutes, and then solution was stored in an anaerobic chamber until use] was added to the tube containing sediment after the previous extraction solution was removed in an anaerobic chamber, and mixed for 50 minutes.

Extraction 3. “Reduced, Readily Oxidized”: 15 mL of ion exchange solution [0.5 M $Mg(NO_3)_2$ prepared in ultrapure water, ≥ 18 MΩ·cm] was added to the tube containing sediment after the previous extraction solution was removed *outside* the anaerobic chamber with air headspace and mixed for 50 minutes.

Extraction 4. “Carbonates”: 15 mL of the pH 2.3 acetic acid solution [0.66 mL glacial acetic acid (CH_3COOH,17.4 mol/L) plus 47.2 g $Ca(NO_3)_2{\cdot}4H_2O$, pH 2.3, balance deionized H_2O to 2.0 liters] was added to the tube containing sediment after the previous extraction solution was removed and mixed for 5 days (±3 hours).

Extraction 5. “Residual/Other”: 15 mL of 8 mol/L nitric acid was added to the tube containing sediment after the previous extraction solution was removed and mixed intermittently for 2 to 3 hours at 95 °C or heated in a mod block without mixing (2 hours at 95 °C).

Sequential extraction results presented in this report are shown as a fraction of PCOI or CoCOI in each extraction. These results were normalized based on the total mass initially added to the system. Depending on the PCOI or CoCOI and its behavior and natural abundance in the sediments, recoveries may fluctuate. For example, the total recovery as summed across all extractions is frequently < 100% because the final extraction does not completely dissolve all solids. In addition, the sequential extraction results are discussed based on the summation of Extractions 4 and 5 for immobile and Extraction 3 for temporarily immobile when referring to the 50% minimum threshold for all PCOIs except nitrate, which is quantified based on the transformation of aqueous NO_3^- to gaseous nitrogen species. In addition, PCOIs and CoCOIs may not be distributed homogenously in sediments (i.e., a sediment aliquot may not be representative), and some solids may be lost during the extraction process. If PCOIs or CoCOIs remain in the solid phase after the fifth extraction, the resulting immobilized fraction estimated will be conservatively low. However, for naturally occurring PCOIs or CoCOIs, the recovery is often > 100% due to background concentrations found in the sediments used in these tests, though it can also be due to their distribution in sediments. For U, recoveries may be greater than 1.0 due to the presence of naturally occurring U and heterogeneity in composite sediments.

A.3 Supplemental Water-Saturated Column Results

A.3.1 Control Column Comparisons

Each set of column experiments that were conducted for the various water-saturated technologies included control columns that did not receive treatments. Control experiments were designed to estimate the mobility of PCOIs (with and without CoCOIs) under relevant site conditions without treatment (i.e., natural conditions). These data are important to compare the technologies to a no-treatment option. In addition, it is beneficial to compare the control column results with each other to confirm that experiments were conducted consistently across technology testing. Although experimental protocols were standardized, there is potential for small deviations in testing approaches and conditions among the various groups of experiments.

Figure A.2 and Figure A.4 compare the breakthrough curves and release profiles for control columns for Tc-99 for Cold Creek Unit gravel (CCug) and perching zone sand (PZsd) sediments, respectively. Breakthrough is observed consistently near 1 PV, as shown in the breakthrough curve figures and in apparent R_f values summarized in Table A.2. These results demonstrate that experiments were conducted with relatively consistent conditions (e.g., flow rate and configuration) with relatively consistent estimates of physical properties (porosity, particle density, etc.). Tc-99 is present as the pertechnetate anion (TcO_4^-) under the conditions in SGW and SPW solutions. Tc, therefore, is expected to show little reactivity with sediments in the absence of a reductant with relatively little adsorption based on its previously summarized behavior (PNNL-18139).

Figure A.3 and Figure A.5 compare the breakthrough curves and release profiles for control columns for U CCug and PZsd sediments, respectively. It is important to note that the effluent U breakthrough curves are more variable, likely due to the complex speciation in solution and potential for precipitation and dissolution of carbonates as the pH fluctuates, as depicted in Figure A.6, from the Appendix H of the Phase 1 report (PNNL-35432).

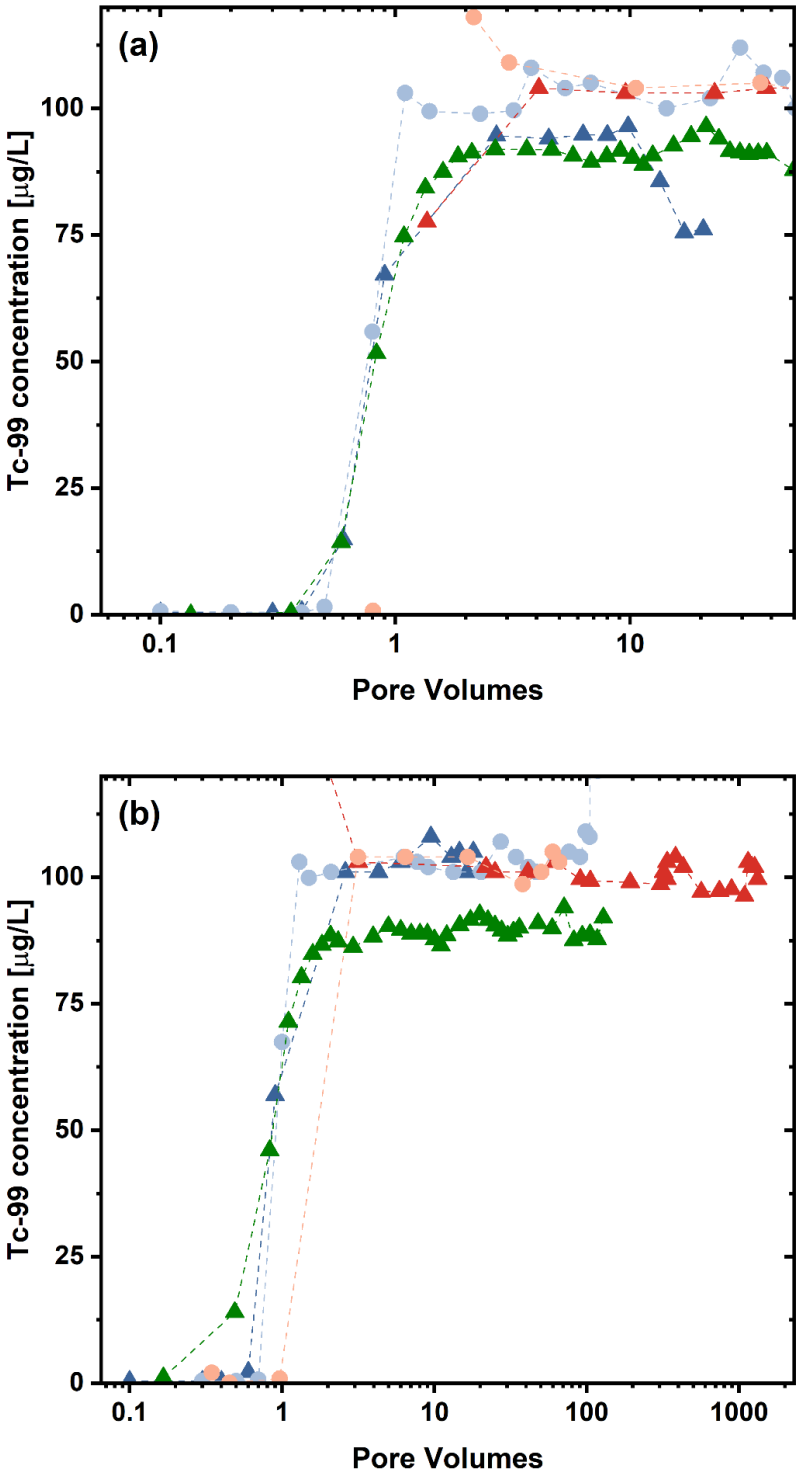

Figure A.2. Breakthrough of Tc-99 in µg/L as compared across all control columns for CCug sediments during loading with (a) only PCOIs and (b) PCOIs and co-contaminants of interest (CoCOIs).

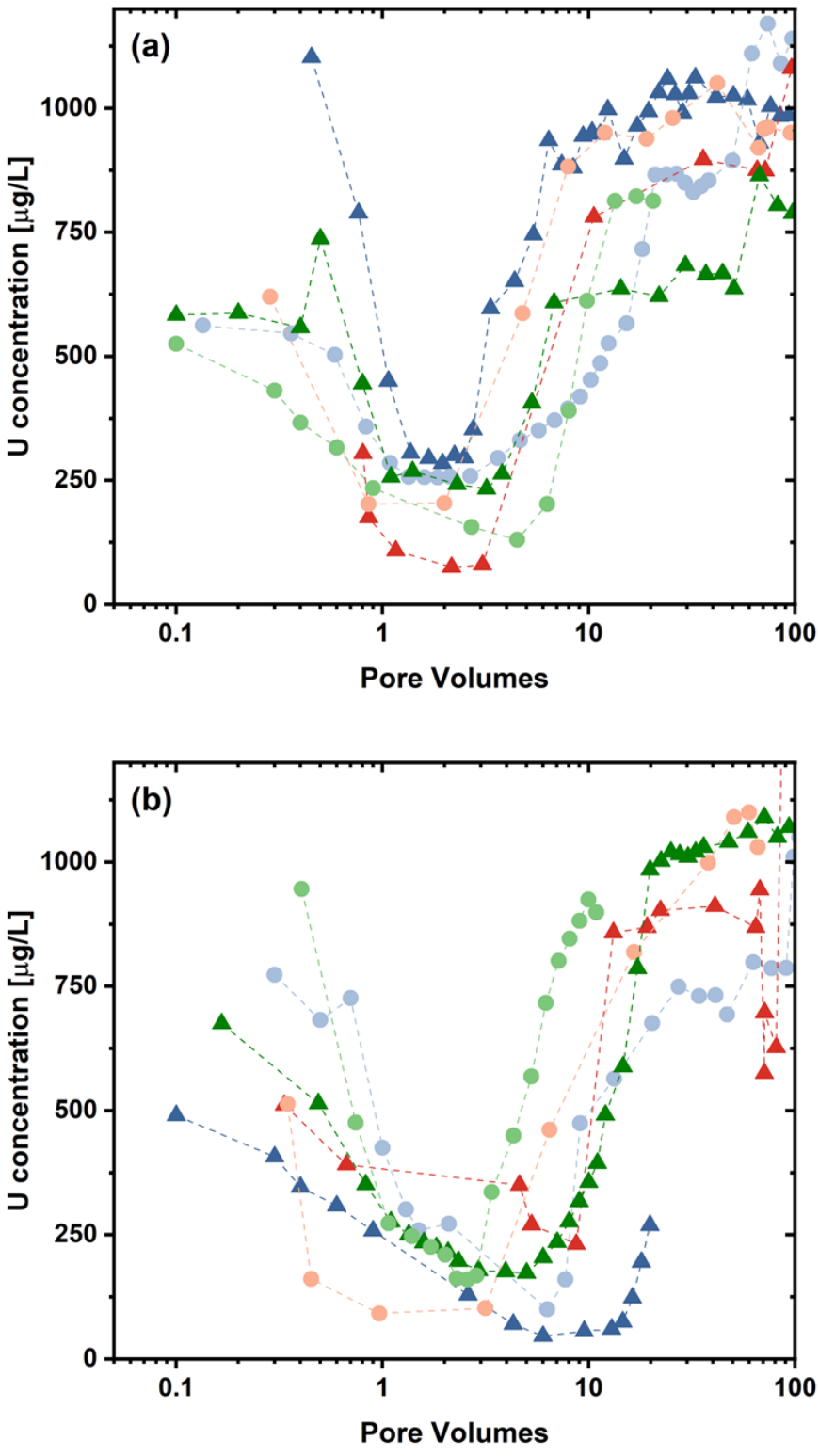

Figure A.3. Breakthrough of U in µg/L as compared across all control columns for CCug sediments during loading with (a) only PCOIs and (b) PCOIs and CoCOIs.

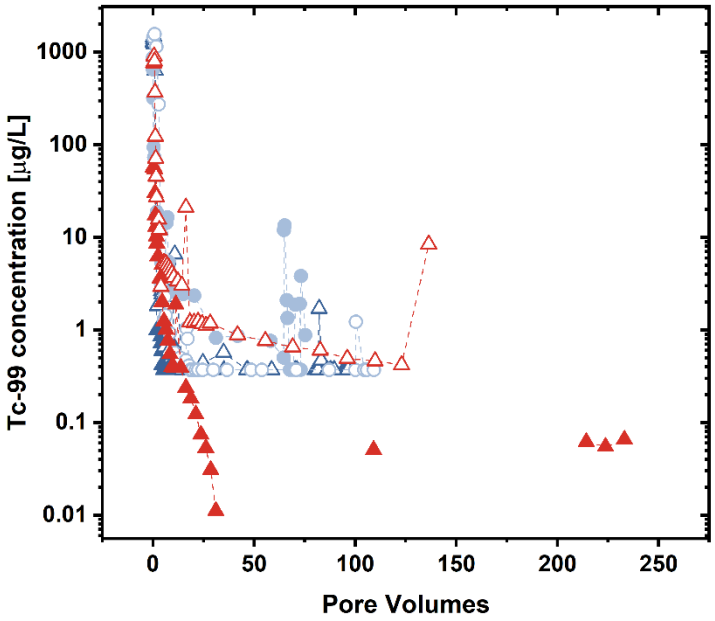

Figure A.4. Release of Tc-99 in µg/L as compared across all control columns for PZsd sediments and injection of SPW for leaching.

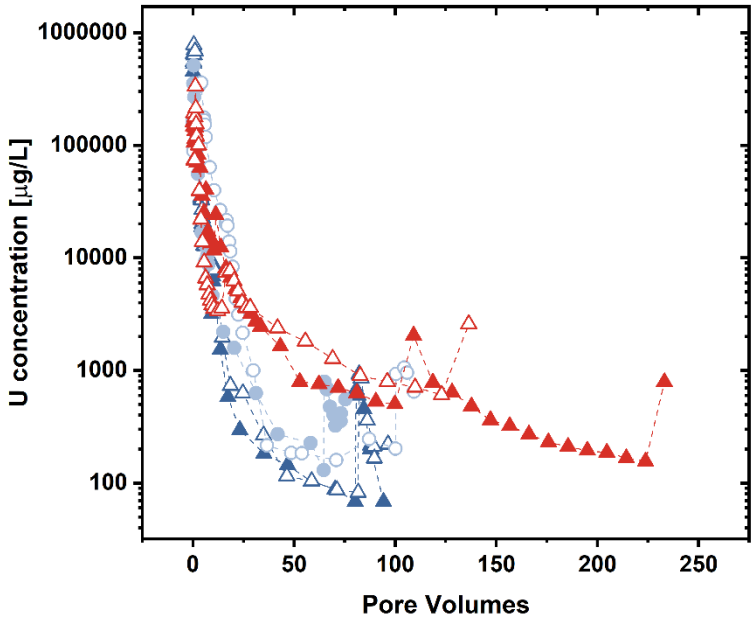

Figure A.5. Release of U in µg/L as compared across all control columns for PZsd sediments and injection of SPW for leaching.

Table A.2. Summary of breakthrough PV for Tc-99 and U for control columns for CCug sediment columns conducted for the BY Cribs groundwater conditions.

Tc		U	
PCOIs	PCOIs+CoCOIs	PCOIs	PCOIs+CoCOIs
0.7	0.6	5.8	7.5
0.7	0.8	4.1	19.8
0.2	0.9	4.1	6.5
0.0	0.0	1.1	4.5
0.7	0.4	1.4	0.7
1.1	0.7	12.4	7.7

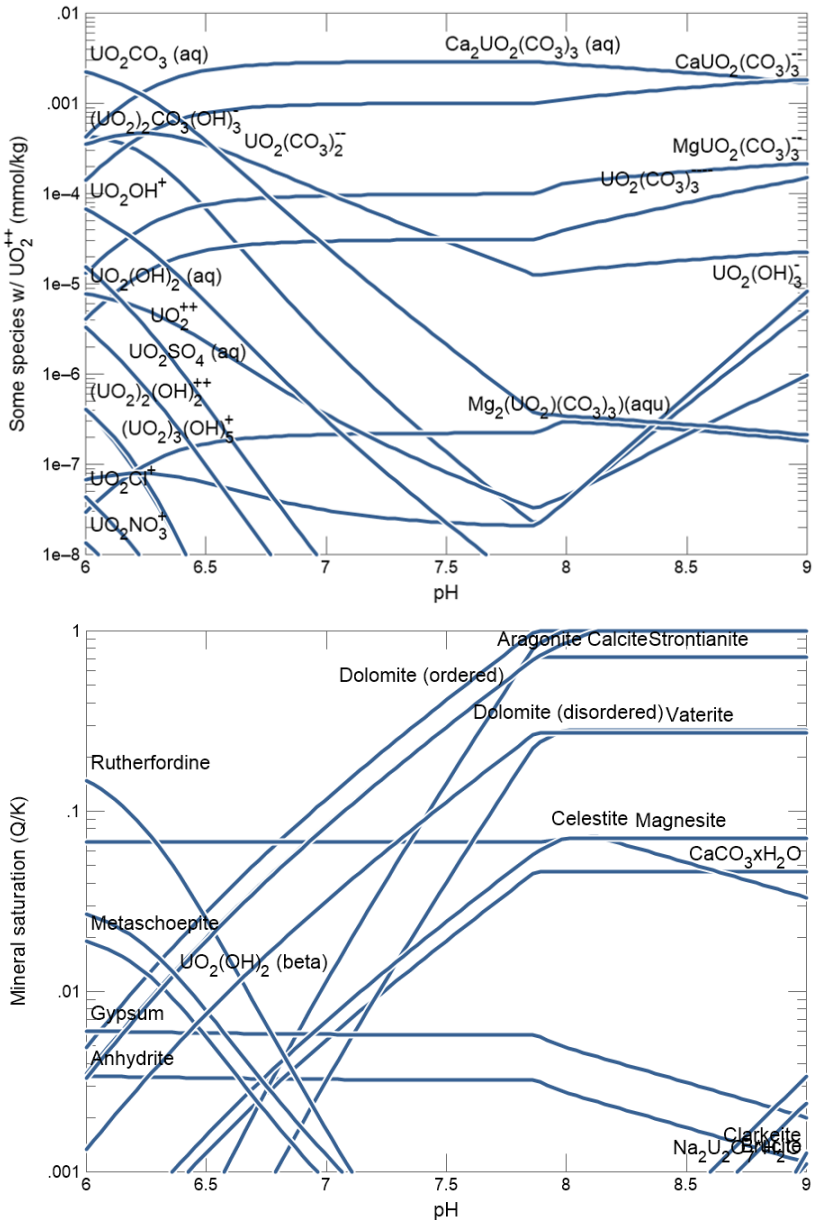

Figure A.6. Uranium speciation predicted in the aqueous phase (*top*) and mineral saturation for all species (*bottom*) in SGW as predicted by Geochemist Workbench.

A.3.2 Bromide Tracer Comparison

CXTFit (version 2.0, U.S. Department of Agriculture, Washington, D.C.) (Toride et al. 1995) was used to fit bromide tracer data collected in the columns to calculate dispersion coefficients for the two primary sediments used in the water-saturated experimental conditions (Sections 3.2.1 and 3.2.2 for PZsd and CCug sediments, respectively). This analysis assumes steady-state conditions with respect to flow. Here, an inverse, deterministic, equilibrium, convection-dispersion equation was solved based on input of bromide effluent concentrations over time. The models were constrained based on a pulse input of bromide, and it was assumed that the initial concentration was zero and mass and application masses were known and accurate. All results and fits summarized here are FIO.

Table A.3 summarizes the dispersion coefficient estimates. For the PZsd and CCug sediments, averages are shown with standard deviations based on at least eight columns with R^2 values > 0.8 for the analyses. For the Hanford formation (Hf) sediments, fits are shown based on the three types of experiments conducted for the gas-phase sequestration technology (Section 3.1.1), including saturated leaching experiments similar to those conducted for the technologies for the water-saturated conditions, infiltration experiments, and pressurized unsaturated flow experiments described in Section 2.3.1.

Significant changes in dispersion were not observed with different amendments except for SMI. When SMI was present, the dispersion coefficients were much higher due to SMI's relatively large particle size. The control columns without SMI had an average value of 9.6 ± 7.2 cm^2/h (N=2) as compared to the SMI-amended columns with an average value of 78 ± 29 cm^2/h (N=5).

Table A.3. Summary of dispersion coefficient estimates for sediments based on CXTFit calculations. Note: All results are FIO. Averages with standard deviation represent > 8 fits.

Sediment	Degree of Saturation (%)	Dispersion Coefficient (cm^2/h)
CCug	100	2.6±1.9
PZsd	100	6.6±12.3
Hf	100	11.7
	84 (infiltration)	66
	47 (pressurized unsaturated flow)	0.18

A.3.3 Breakthrough Curve Fitting

The objective of this curve analysis was to model and interpret breakthrough curves obtained from column transport experiments. These curves represent the evolution of contaminant concentrations (e.g., uranium or Tc) over time or pore volumes during reactive transport through porous media. By fitting these curves using mechanistic or empirical models, the project team aimed to extract meaningful transport parameters, detect breakthrough events, and support mechanistic interpretation or predictive modeling.

To capture the diverse transport behaviors observed in experimental data, the following mathematical models were used:

- **Logistic Function**

$$y(x) = \frac{a}{(1 + e^{-c(x-d)})} + b$$

a: amplitude (difference between upper and lower asymptotes)
b: baseline offset
c: growth rate
d: inflection point (center of the transition)

- **Exponential Growth Function**

$y(x) = a \times e^{bx} + c$
a: initial scale
b: exponential rate (controls steepness)
c: offset
Initial guesses for a and b are derived from log-transformed data using the first and last observed concentrations.

- **Hill Function**

$$y(x) = a \times \frac{x^b}{c^b + x^b}$$
a: maximum asymptote
b: slope control (steepness)
c: concentration at half-saturation

- **Cubic Polynomial**

$y(x) = ax^3 + bx^3 + cx + d$
Polynomial coefficients are determined by standard least-squares regression.

Each model was fit to the experimental data. Models that failed to converge or produced implausible values (e.g., negative concentrations) were excluded. The models were evaluated using the root mean square error (RMSE):

$$RMSE = \sqrt{\frac{\sum_{i=1}^{n}(y_i - \hat{y}_i)^2}{n}}$$

Among all valid models, the one with the lowest RMSE was selected as the best fit. This best-fit curve was then used for further analysis and visualization. After identifying the best-fit model, the breakthrough point was estimated from the fitted curve using a derivative analysis. The first derivative, dy/dx, indicates the rate of change of concentration, while the second derivative, d^2y/dx^2, indicates inflection or curvature change. A plateau or breakthrough was identified when the slope dy/dx dropped below a threshold (e.g.,

0.0001 × data range) and the second derivative became negative. Alternatively, if the fitted curve reached within 1% of the influent concentration and continued rising, it was considered a breakthrough: $|y(x)/C_0 - 1| < 0.01$. If no plateau was detected from derivatives, a local maximum in the observed data (after the initial rise) was used as an estimate. The corresponding x (e.g., time or PV) at which this point occurred was reported as the breakthrough time (in units of PV).

This curve-fitting framework provided a rigorous and automated way to extract meaningful transport behavior from columns; examples are shown in Figure A.7. The Hill function was the best fit, most often followed by the logistic function, although some cases were most consistent with the exponential or cubic polynomial. In general, the logistic function was the most appropriate for conditions where background U was mobilized from sediments during the first few PVs of injection, while the Hill function was a better fit for traditional breakthrough curve features. These empirical fits and corresponding estimates of breakthrough PV provide a basis for quantifying reactive transport in porous media. While the current curve fitting approach provides a useful empirical means to characterize breakthrough behavior and estimate retardation, it does not account for the underlying physical and chemical processes governing reactive transport. These models are purely empirical and do not incorporate mechanistic representations of flow, sorption kinetics, or geochemical interactions. As a result, they have limited predictive capability outside the conditions of the original experiments and cannot simulate system responses to changing boundary conditions, flow regimes, or reactive parameters.

Future work in reactive transport modeling can build on the current curve fitting analysis by incorporating non-linear or time-dependent adsorption and a network of chemical reactions using models that more explicitly describe sorption and species and phase transformation processes. For example, equilibrium sorption models based on a K_d can be used for initial assessments of contaminant retardation. More advanced approaches such as the kinetic Langmuir model can capture nonlinear sorption with finite site capacity and time-dependent uptake, making it more suitable for systems where sorption does not reach equilibrium rapidly. Additionally, distributed rate models can be employed to represent sorption behaviors occurring over a spectrum of kinetic rates, which is particularly relevant for systems with a high degree of spatial and temporal heterogeneities. These geochemical models can be integrated into numerical simulators like PFLOTRAN or eSTOMP to simulate coupled flow and transport processes. Future efforts could also include model calibration using inverse methods and PEST or data assimilation techniques, incorporation of multicomponent geochemical reactions (e.g., redox, precipitation/dissolution, adsorption/desorption), and evaluation of system responses under transient flow or perturbation scenarios, such as stop-flow events. Such enhancements would improve the model’s predictive capabilities for complex subsurface environments and support the design of long-term remediation and monitoring strategies.

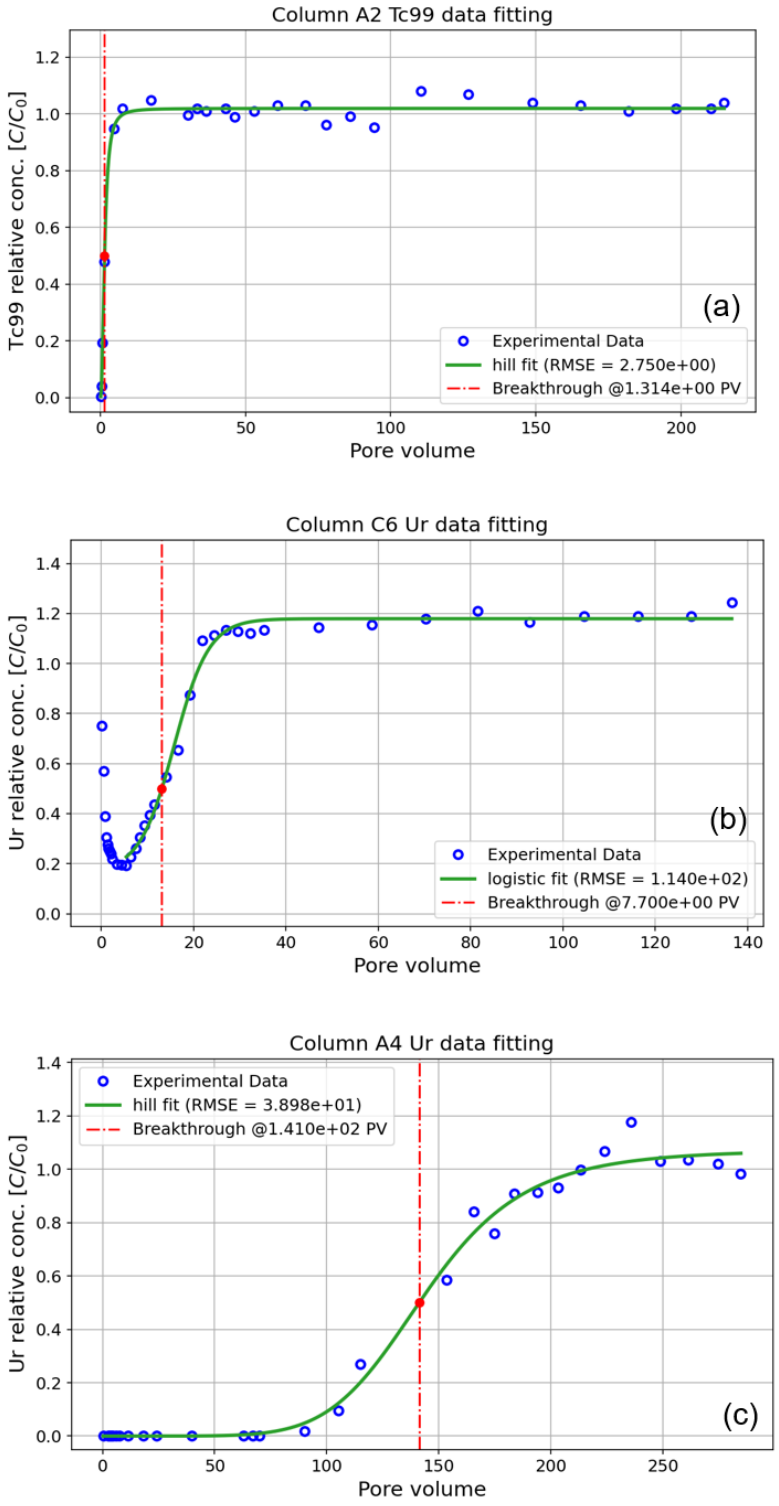

Figure A.7. Example breakthrough curve fits for (a) early breakthrough of Tc, (b) significant initial release of background U, and (c) U with significant retardation due to amendment.

Appendix B Solid Phase Characterization Methods

B.1 Sample Preparation for Analysis at Stanford Synchrotron Radiation Lightsource (SSRL)

Samples were prepared from sediments remaining from column leach testing (as described in Section 2.4), or from batch tests with higher concentrations of contaminants (as described in the following paragraph). Concentrations of contaminants of interest remaining in the solution phase were measured (as described in Appendix A, Section A.1.1), then select samples were dried under an N_2 atmosphere and prepared as bulk samples or as thin sections for mapping.

Sediments [Cold Creek Unit gravel (CCug) and perching zone sand (PZsd), 2 g] and respective treatments all at 10 wt% [bismuth subnitrate (BSN), sulfur modified iron (SMI), Sn(II)-PO_4, calcium polysulfide (CPS), Poly-PO_4, and Ca-Cit-PO_4 (Table B.1)] were placed in 50-mL centrifuge tubes on the benchtop. Sediment and treatment were then exposed to contaminants (Tc and U, both at 100 mg/L) in 10 mL of synthetic perched water (SPW) or synthetic groundwater (SGW) under oxic conditions. Two sets of controls were set up, containing (1) treatment and contaminants without sediment and (2) sediment and contaminants without treatment. The tubes were shaken at < 30 rpm for 5 days and then centrifuged at 3,000 rpm for 10 minutes. The supernatant was filtered through a 0.2-µm polytetrafluoroethylene filter and submitted for analysis. The remaining solid samples were rinsed with anoxic SGW (3 mL) and allowed to dry in an anoxic chamber (100% N_2) for a minimum of 72 hours.

Table B.1. Conditions for solid phase batch experiments.

Batch ID	Targeted [Tc-99] (mg/L)	Targeted [U] (mg/L)	Amendment	Amendment Mass (g)	Sediment (2 g)	Solution	Solution Volume (mL)
Sn(II)-PO_4-PZsd	100	100	Sn(II)-PO_4	0.12	PZsd	SPW	8.9
Sn(II)-PO_4-CCug	100	100	Sn(II)-PO_4	0.12	CCug	SGW	8.9
BSN-PZsd	100	100	BSN	0.2	PZsd	SPW	8.9
BSN-CCug	100	100	BSN	0.2	CCug	SGW	8.9
SMI-PZsd	100	100	SMI	0.12	PZsd	SPW	8.9
SMI-CCug	100	100	SMI	0.12	CCug	SGW	8.9
SMI+Poly-PO_4-PZsd	100	100	SMI + Poly-PO_4	0.05 g SMI + 1.67 mL PolyP + 2 mL $CaCl_2$	PZsd	SPW	5.23
SMI+ Poly-PO_4-CCug	100	100	SMI + Poly-PO_4	0.05 g SMI + 1.67 mL PolyP + 2 mL $CaCl_2$	CCug	SGW	5.23
CPS-PZsd	100	100	CPS	0.86 mL CPS	PZsd	SPW	8.04
CPS-CCug	100	100	CPS	0.86 mL CPS	CCug	SGW	8.04
CPS+ Poly-PO_4-PZsd	100	100	CPS+ Poly-PO_4	0.86 mL CPS + 1.67 mL PolyP	PZsd	SPW	6.37
CPS+ Poly-PO_4-CCug	100	100	CPS+ Poly-PO_4	0.86 mL CPS + 1.67 mL PolyP	CCug	SGW	6.37
Ca-Cit-PO_4-PZsd-SPW	100	100	Ca-Cit-PO_4	5 mL	PZsd	SPW	0
Ca-Cit-PO_4-CCug	100	100	Ca-Cit-PO_4	5 mL	CCug	SGW	0
Sn(II)-PO_4	100	100	Sn(II)-PO_4	2	-	SGW	0
BSN	100	100	BSN	2	-	SGW	8.9
SMI	100	100	SMI	2	-	SGW	8.9
PZsd	100	100	-	-	PZsd	SPW	8.9
CCug	100	100	-	-	CCug	SGW	8.9

Phosphate solutions

- **Calcium-citrate-phosphate (Ca-Cit-PO_4):** For 1 liter, dissolve calcium citrate components (36.15 mM $CaCl_2$ [5.314 g] + 90.38 mM $Na_3C_6H_5O_7 \times 2H_2O$ [26.581 g]) in 500 mL volume and phosphate components (19.4 mM Na_2HPO_4 [2.754 g] + 3.4 mM NaH_2PO_4 [0.408 g] + 1.2 mM $(NH_4)_2HPO_4$ [0.158 g]) in a separate 500-mL volume. Note: The original synthesis requires 1.67× Ca as there is PO_4 and 2.5× more citrate than Ca. However, total Ca and citrate are decreased based on the 2:1 liquid-to-solid ratio in batch experiments and approximately 2 meq of Ca/100 g in sediments (dissolve each solution slowly).
- **Polyphosphate (Poly-PO_4):** For 200 mL, dissolve 3.02 g Na_2HPO_4 + 0.48 g NaH_2PO_4 + 0.40 g $Na_5P_3O_{10}$ to prepare a 144 mM total PO_4 solution. Solution diluted for batch experiments (1.67 mL into 10 mL total volume in batch experiment to reach 24 mM total PO_4). Solutions prepared in aerobic groundwater or perched water simulants as specified.
- **Calcium chloride (Ca):** For 1 liter, dissolve 21.26 g of $CaCl_2$ to prepare 144.6 mM solution. Solution diluted to 1/4 for calcium polyphosphate solutions in batch experiments (2.5 mL into 10 mL total volume in batch experiment to reach 36.2 mM total Ca).

B.1.1 Thin Section Preparation

Thin sections were prepared on a benchtop with slow drying epoxy (two parts by volume of EpoThin 2 epoxy, catalog #20-3440-032, with one part by volume of EpoThin 2 hardener, catalog #20-3442-016, Buehler Inc., Lake Bluff, IL) inside aluminum tubing [1.7-cm (0.7-in.) ID and 2.5-cm (1-in.) length]. Approximately 0.4 to 0.8 grams of sediment was added to 3 mL of epoxy, mixed for 2 minutes with a wooden stir stick, then degassed in a vacuum desiccator (using 10 cycles from ambient pressure to 1 atmosphere). After samples were dried overnight, the bottom was cut flush with ultrapure water as the cutting fluid [Isomet 1000 diamond blade thin sectioning saw, catalog #11-128, with a 12.7-cm (5-in.) diameter diamond sectioning blade, catalog #812-321, Buehler, Inc., Lake Bluff, IL]. Samples were then sanded using silicon carbide sandpaper and ultrapure water, followed by 600 grit sand paper (catalog #817-106, Ted Pella, Inc., Redding, CA) and a rinse with acetone, 15 minutes of polishing with nylon polishing cloth (catalog #816-63, Ted Pella, Inc., Redding, CA) or Rayon velvet polishing cloth (catalog #816-109, Ted Pella Inc.), and 1 μm diamond polish (catalog #40-6244, Metadi II, Buehler Incl, Lake Bluff, IL) or 0.3 μm aluminum oxide powder (catalog #4507, International Crystalline Laboratories, Garfield, NJ), and ending with a methanol rinse.

B.1.2 Bulk Sample Preparation

Dry sediments collected from batch tests were ground into a powder using a mortar and pestle before being packed (~50 mg) into stainless steel washers and covered with Kapton tape (inside the anaerobic chamber). These washers were nested into 3-D printed holders containing two columns of four samples each for a total of eight samples per holder. Holders were covered in Kapton tape for secondary containment.

B.1.3 X-ray Fluoresce (XRF)

Preliminary XRF analysis was performed using a Bruker M4 Plus Tornado instrument. Data were collected using a Rhodium (50kV and 300μA) or Tungsten (50kV and 700μA) X-ray source at a chamber pressure of 10 mbar. The instrument is equipped with dual 60-mm^2 silicon drift detectors, dual charge-coupled device cameras, and a sample stage with automated XYZ positioner. Elemental maps were acquired using a time/pixel of 25 ms or greater while point scans were collected using a live time of 120 s. All data were processed using the Bruker Espirit M4 software.

B.1.4 Microprobe X-ray Fluorescence (μXRF)

μXRF element maps were collected at the SSRL beamline 2-3 to resolve potential correlation between U, Tc, P, Ca, Fe, Si, Al, S, Sn, and Bi.

At SSRL beamline 2-3, an Si(111) φ = 90° double-crystal monochromator was used to select the incident energy, with N_2-filled ion chambers to monitor the flux. Fluorescence was collected using a one-element Si-drift Vortex detector. The monochromator was calibrated to the Zr absorption K-edge (17998 eV) using Zr foil. Preliminary, coarse scale, μXRF maps were collected at 17200 eV with a 25-μm beam size, 25-μm step size, and a dwell time of 25 msec to identify locations rich in U, and other elements of interest. From this map, several areas rich in U and other elements were selected for mapping at a finer scale using a step size of 5 μm. U "hot spots" were identified in fine maps for U L_3-edge (17166 eV) X-ray absorption near edge structure (XANES) spectroscopy measurements.

All μXRF element maps were analyzed and compiled using the MicroAnalysis Toolkit (Webb 2011).

B.1.5 X-ray Absorption Spectroscopy (XAS)

X-ray absorption spectroscopy (XAS) bulk measurements. Tc-99 K-edge and U L_3-edge XANES and extended X-ray absorption fine structure (EXAFS) data were collected at the SSRL beamline 11-2. The fluorescence signal was collected using a 100-channel Ge detector (Canberra EGPX Planar Segmented Germanium Detector). An Si(220) monochromator was set to an orientation of 90° for Tc-99 K-edge measurements and to 0° for U L_3-edge measurements. Ion chambers were filled with N_2 to monitor the flux and detuned by 25%. Initial energy calibration was performed using an Mo foil (K-edge 20000 eV) for Tc-99 measurements and Y foil (K-edge 17038 eV) for U measurements. Tc-99 K-edge (21044 eV) XANES pre-edge region was collected from 20815 to 21015 eV with a step size of 10 eV and collection time of 1 second; and the edge region was collected up to 21095 eV with a step size of 0.35 eV and 1-second collection time. Tc-99 K-edge EXAFS data were collected to 15.2 $Å^{-1}$ with a 0.05 $Å^{-1}$ step size and collection time of 1 second. U L_3-edge (17166 eV) XANES pre-edge region was collected from 16808 to 17008 eV with a step size of 10 eV and collection time of 1 second, calibration region from 17018 to 17068 eV for Y K-edge with a step size of 0.35 eV and collection time of 1 second, followed by another pre-edge region from 17068 to 17147 eV with a step size of 5 eV and collection time of 1 second. The edge region was collected from 17147 to 17197 eV with a step size of 0.35 eV and 1-second collection time. U L_3-edge EXAFS data were collected to 15.2 $Å^{-1}$ with a 0.05 $Å^{-1}$ step size and collection time of 1 second.

Data pre-processing was performed using SixPack (Webb 2006) and Athena software (Demeter package version 0.9.26). Linear combination analysis for Tc-99 K-edge and U L_3-edge XANES and U L_3-edge EXAFS was performed in Larch (version 0.9.81) (Newville 2013). Tc-99 K-edge EXAFS analysis was done in Artemis (Demeter package version 0.9.26) (Ravel and Newville 2005).

Figure B.1 shows the U L-edge XANES spectra for the CCug and PZsd sediments compared to reference spectra for U-bearing mineral phases, confirming that U is predominantly present in the sediments as a uranyl [U(VI)] phase in both sediments. The slight shift of the edge to lower energy for the PZsd suggests some of the U may be slightly reduced.

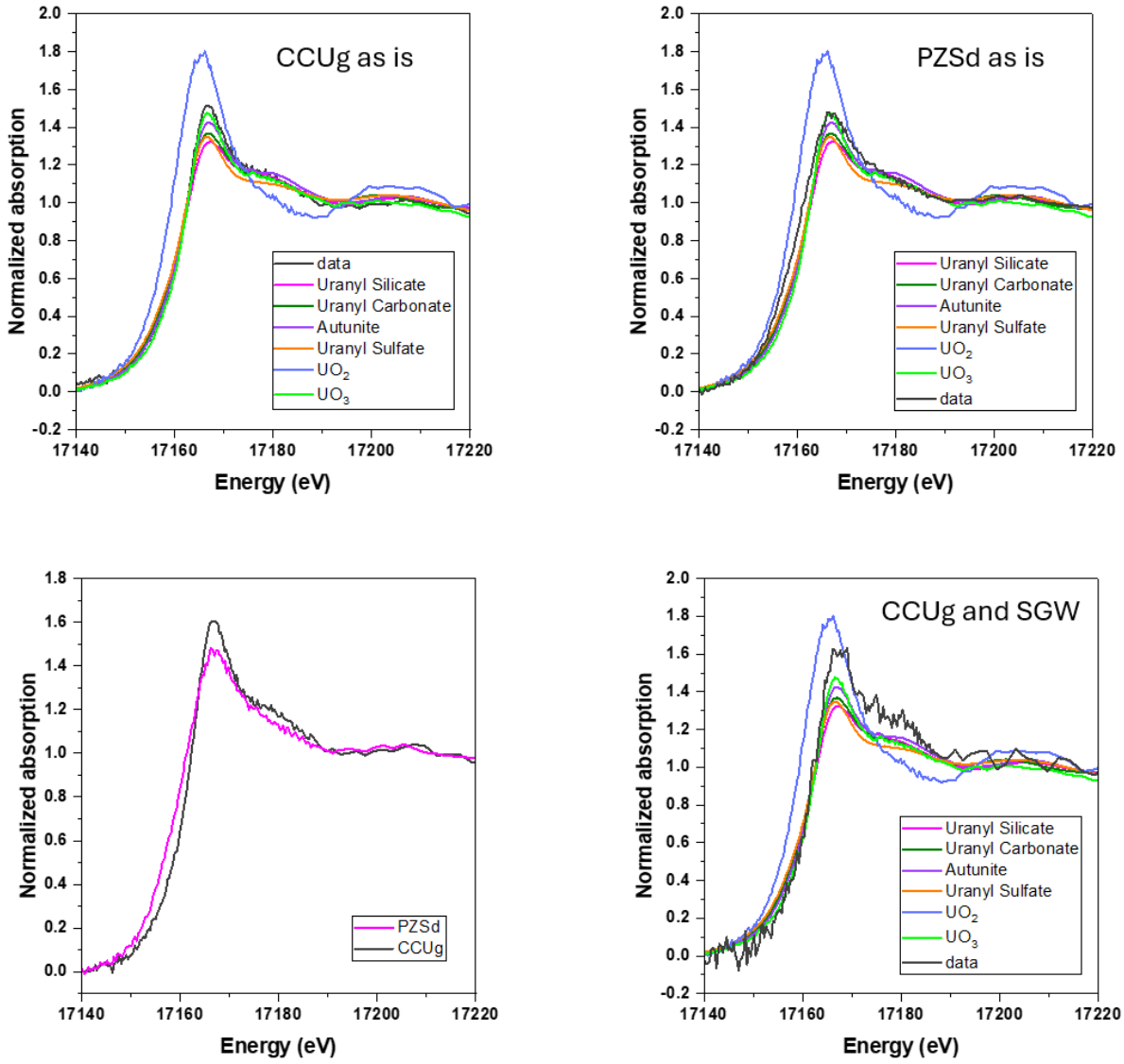

Figure B.1. U L-edge XANES spectra for CCug and PZsd sediments and in CCug sediment after exposure to SGW, along with spectra for reference U-bearing minerals. PNNL610, 611, 612.

B.2 X-ray Magnetic Circular Dichroism at Advanced Light Source (ALS)

X-ray absorption spectra at the Fe $L_{2,3}$ -edges were collected at room temperature on beamline 4.0.2 at the Advanced Light Source in Berkeley, CA, using an eight-pole resistive magnet end-station (Arenholz and Prestemon 2005). Beamline 4.0.2 is equipped with an elliptically polarizing undulator source and a variable-included-angle monochromator, providing soft X-rays with a resolving power near 6,000 at the Fe $L_{2,3}$ edges (Young et al. 2001).

The SMI powders were ground and mounted on a carbon table attached to the sample manipulator in an N_2-filled glove box. The sample manipulator was loaded into the end station under anaerobic conditions. The sample was positioned with the X-ray beam entering parallel to the magnetic field and perpendicular to the sample surface.

The XAS was monitored in total-electron yield mode. At each energy point, the XAS was measured for two opposite magnetization directions by reversing the applied field of 0.4 T. After normalization to the incident beam intensity, the X-ray magnetic circular dichroism (XMCD) spectrum was obtained as the difference between the two XA spectra (Pattrick et al. 2002). Following the collection of Fe $L_{2,3}$ XMCD data, a nonlinear least-squares analysis of the XMCD spectra was conducted to quantify the Fe(II)/Fe(III) ratios of the samples (van der Laan and Kirkman 1992; Liu et al. 2012). To obtain the relative amounts of Fe on the three sites, the experimental spectra were fitted by means of a nonlinear least-squares analysis, using calculated spectra for each of the Fe sites (Pearce et al. 2010). Calculations were done as described by van der Laan and Thole (1991). The experimental spectra were fitted over the L_3 main peaks only, which has been previously shown to give meaningful results (Pattrick et al. 2002; Pearce et al. 2006). The estimated random error per cation site occupancy value is ±0.02 (Coker et al. 2009).

Figure B.2 shows the Fe L-edge XAS and XMCD spectrum for the Hanford formation (Hf). The spectrum is characteristic of Fe present in Fe-bearing clay minerals, and the lack of an XMCD spectrum suggests that no magnetic redox active minerals, e.g., magnetite, are present in this sediment.

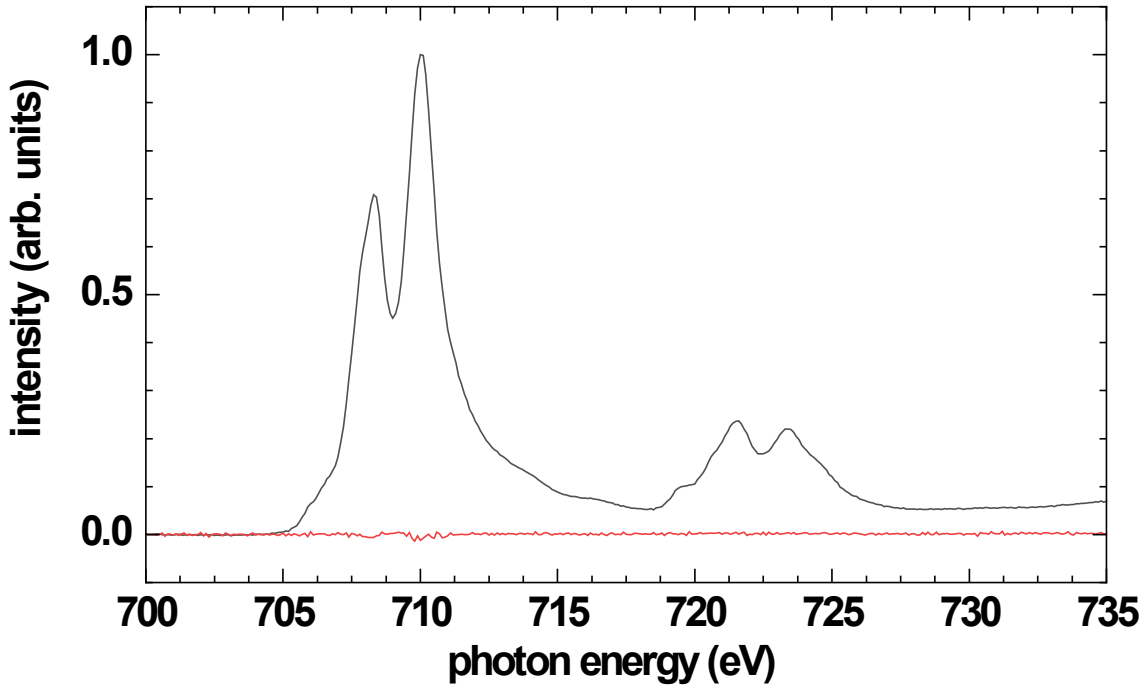

Figure B.2. Fe L edge XAS (black) and XMCD (red) for Hf (as is), suggesting that the Fe is predominantly present in Fe-bearing clay minerals (Qafoku et al. 2017).

B.3 X-ray Diffraction (XRD)

The < 2-mm size fractions for the CCug, Hf, PZsd sediments, and vadose zone sediments from BY and 216-S-9 Crib were dried at ambient conditions and then powdered using a mortar and pestle. Zinc oxide powder (Standard Reference Material 1979, National Institute of Standards and Technology) was added at 10 wt% to the pulverized sediments and homogenized a second time using a mortar and pestle. XRD patterns were collected with Cu Kα radiation (λ=1.5418 Å) using a Rigaku Miniflex II unit. The Miniflex was operated at 30 kV and 15 mA and patterns were collected between 3 and 90 °2θ, using a scan width of 0.04° and a 5-second count time. Identification of material phases was carried out using JADE XRD pattern processing software and reference patterns from the International Centre for Diffraction Data powder diffraction database. Quantitation of material phases was done using TOPAS software.

B.4 Brunauer-Emmett-Teller (BET) Surface Area Analysis

Sediments [Hf, CCug, PZsd, and vadose zone sediments from BY Cribs and S9 (S9-B and S9-C) Cribs] were analyzed in triplicate by the BET method for specific surface area using an accelerated surface area and porosity system (ASAP 2020) from Micromeritics. Nitrogen gas adsorption and desorption isotherms were recorded at 77K by volumetric adsorption in a relative pressure range, P/P_o, of 0.05 to 0.30. Specific surface area was calculated from these pressure ranges using the BET equation. Samples were prepared prior to analysis by degassing 1.0 g of material in vacuum (100 mm Hg) at 25 °C overnight to remove humidity and possible contaminants. Degas parameters were chosen based on previous experience with similar materials and to avoid material decomposition. An alumina standard (Micromeritics) with a known surface area of 26.6 ± 2.0 m^2/g was analyzed before and after analysis of samples. The average measured surface area of all standard measurements was 25.02 m^2/g (three replicates). These values are within 6% of the certified value.

Amendments (SMI, SnAp-A, and SnAp-B) were analyzed in triplicate by the BET method for specific surface area using a TriStar II Plus Surface Area and Porosity Analyzer from Micromeritics. Nitrogen gas adsorption and desorption isotherms were recorded at 77K by volumetric adsorption in a relative pressure range, P/P_o, of 0.05 to 0.30. Specific surface area was calculated from these pressure ranges using the BET equation. Samples were prepared prior to analysis by degassing 1.0 g of material in vacuum (100 mm Hg) at 25 °C overnight to remove humidity and possible contaminants. Degas parameters were chosen based on previous experience with similar materials and to avoid material decomposition. An alumina standard (Micromeritics) with a known surface area of 26.6 ± 2.0 m^2/g was analyzed before and after analysis of samples. The average measured surface area of all standard measurements was 26.22 m^2/g (five replicates). These values are within 2% of the certified value.

B.5 Particle Size Analysis

Sieve and laser particle size analysis were conducted previously and are described in Appendix A, Section A.2, of the Phase 1 report (PNNL-35432). Figure B.1 compares the laser particle size analysis for the < 2-mm size fraction for each of the sediments used in testing. Based on the Wentworth classification scale (Wentworth 1922), the CCug, BY, and Hf sediments were all classified as sands; however, the PZsd and 216-u sediments were sandy silts (Figure B.3).

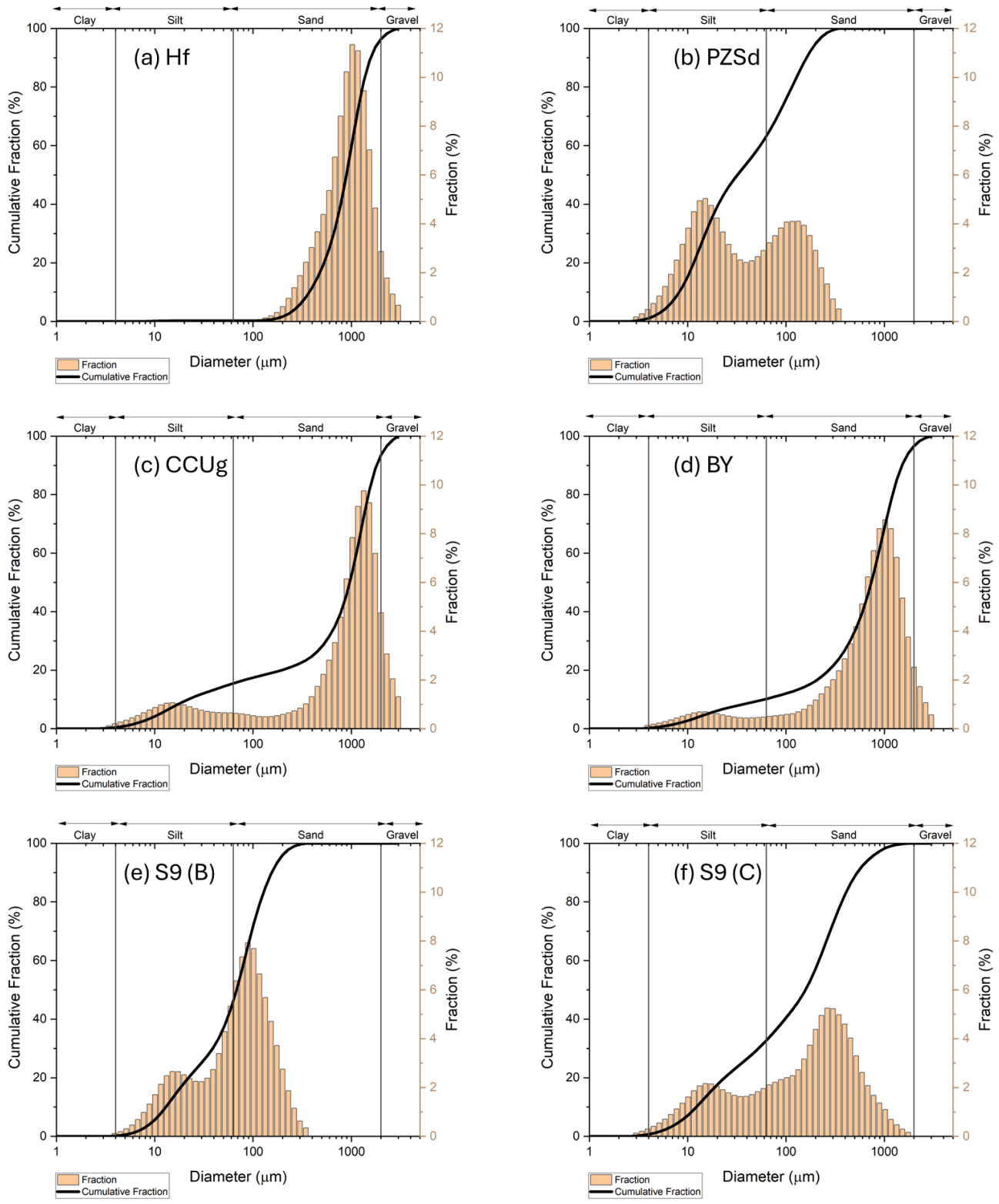

Figure B.3. Laser particle size analysis for the < 2-mm size fraction of the composite sediments: (a) Hf, (b) PZsd, (c) CCug, (d) BY, (e) 216-S-9 (B – batch), and (f) 216-S-9 (C – column).

Appendix C – Microbial Characterization

C.1 Microbial Characterization Methods

Microbial characterization and analyses were conducted to investigate the microbial communities that drive bioremediation processes, such as nitrate and metal reduction, before and after reaction with amendments. By comparing pre- and post-treatment microbial communities, the project team aimed to identify changes in native soil microbes that may correlate with contaminant reduction. Understanding these shifts helps identify which microbial taxa are key players in the system under various conditions. To achieve this, DNA was extracted from samples and sequenced to analyze microbial community composition. Quantitative polymerase chain reaction (qPCR) was used for select samples to help further understand the microbial processes potentially transforming contaminants of interest, like nitrate. These data are presented For Information Only (FIO).

C.1.1 DNA Extraction

Microbial DNA was extracted from 0.25 g of sediment using the DNeasy PowerSoil Pro Kit (Qiagen) following the manufacturer's instructions. Extractions blanks using the kit reagents were included with each batch for quality control. DNA quality and quantity were quantified using a NanoDrop 8000 UV-Vis Spectrophotometer (Thermo Scientific, Wilmington, DE). To enhance efficiency in testing nitrate reduction targets, select samples of DNA were purified and concentrated through ethanol precipitation using 3 M sodium acetate in 100% ethanol (on ice prior to extraction) at pH 5.2, followed by centrifugation and resuspension in 1 M Tris-EDTA buffer pH 8.

C.1.2 Quantitative Polymerase Chain Reaction (qPCR)

Microbial biomass was determined using qPCR with both universal 16S rRNA gene primers and universal archaeal primers. Additionally, functional genes associated with nitrate reduction, including *nirS, nirK, narG*, and *napA,* were evaluated. All primers were obtained from Integrated DNA Technologies (IDT, Coralville, IA). The qPCR assays were performed using a Bio-Rad CFX Opus 96 Real-Time PCR System (Bio-Rad Laboratories, Hercules, CA). Amplification and real-time fluorescence measurements were conducted using an Advanced SYBR Green supermix kit (Bio-Rad Laboratories, Hercules, CA). Each qPCR reaction had a final volume of 20 µL and contained 1X hot-start Sso7d-fusion polymerase, SYBR Green dye, dNTPs, $MgCl_2$, stabilizers, and 1-5 µL of DNA.

Amplification conditions included an initial denaturation step of 2 to 10 minutes at 98 °C, followed by 40 cycles of denaturation at 98 °C for 30 seconds, annealing at specific primer temperatures (Table C.1) for 30 seconds and extension at 72 °C for 30 seconds. Fluorescence was measured at the end of each extension step. Standard curves were established using genomic DNA from *Escherichia coli* K-12 for bacteria, *Methanosarcina acetivorans* for archaea, and *Pseudomonas stutzeri* for nitrate reduction genes, including *nirS*, n*irK*, n*arG*, and n*apA*.

Table C.1. NO_3 reduction qPCR primers for select samples for gas-phase bioreduction. (These data are FIO.)

Target	Functional Gene	Primer Name	Primer Sequence	Annealing Temp (°C)
Bacteria	16S rRNA	518F	CCAGCAGCCGCGGTAATACG	48
		805R	GACTACCAGGGTATCTAATCC	
Archaea	16S rRNA	A8F	TCC GGT TGA TCC TGC C	55
		A344R	TCG CGC CTG CTC CIC CCC GT	
Nitrite	*nirS*	nirS1F	CCTAYTGGCCGCCRCART	63
		nirS6R	CGTTGAACTTRCCGGT	
Nitrite	*nirK*	nirK1F	GGMATGGTKCCSTGGCA	63-58
		nirK5R	GCCTCGATCAGRTTRTGG~~TT~~	
Nitrate reductase	*narG*	narG 1960F	TAYGTSGGCCARGARAA	55
		narG 2659R	TTYTCRTACCABGTBGC	
Periplasmic nitrate reductase	*napA*	napA V17F	TGGACVATGGGYTTYAAYC	61
		napA 4R	ACYTCRCGHGCVGTRCCRCA	
Sequencing	16S rRNA	515F	GTGYCAGCMGCCGCGGTAA	50
		806R	GGACTACNVGGGTWTCTAAT	

C.1.3 Amplicon Sequencing Generation and Processing

Sequencing was conducted on an Illumina MiSeq System (Illumina; San Diego, CA), using a MiSeq Reagent Kit v2 (Illumina) for 2×300 base pairs paired-end sequencing. The targeted region for amplification was the V4 region of the 16S rRNA gene. Polymerase chain reaction (PCR) was performed using Invitrogen Platinum II 2X Master Mix (Thermo Fisher Scientific). PCR reactions were prepared with universal bacteria primers at a final concentration of 0.2 µM, 1× of hot-start polymerase, and 5 µL of DNA for a final volume of 50 µL. Amplification included an initial denaturation step for 3 minutes at 94 °C, followed by 30 cycles of denaturation at 94 °C for 45 seconds, annealing at 50 °C for 60 seconds, and extension at 72 °C for 90 seconds, followed by a final extension for 10 minutes. Amplicons were purified using a 1.8× ratio of AMPure XP Beads (Beckman Coulter Life Sciences), following the manufacturer's instructions, and eluted to a final volume of 40 µL with nuclease-free water.

Multiplex barcodes were added using the Platinum II 2X Master Mix (Thermo Fisher Scientific) at a final concentration of 1×. Barcode i7 and i5 were each included at a concentration of 0.25 µM. The reaction contained 5 µL of cleaned DNA and nuclease-free water diluted to a final volume of 25 µL. The reaction began with an initial denaturation step of 3 minutes at 95 °C, followed by eight cycles of denaturation at 95 °C for 30 seconds, annealing at 55 °C for 30 seconds, and extension at 72 °C for 30 seconds, followed by a final extension for 5 minutes. Amplicons were purified as previously described and eluted to a final volume of 50 µL with nuclease-free water. Cleaned and barcoded amplicons were quantified with Picogreen dsDNA (Thermo Fisher Scientific) high-sensitivity assay in triplicate. Samples were pooled into a single tube containing 40 ng of DNA from each sample, using 40 µL for samples with low concentrations, and cleaned and concentrated with the Zymo Clean and Concentrator kit following the manufacturer's instructions (Zymo Research). The final sample was diluted to a concentration of 2 nM. Following the standard Illumina library preparation protocol, the samples were loaded onto the MiSeq system for v2 sequencing. This process used a 500-cycle nano flow cell with a 15% PhiX spike-in to ensure sequencing accuracy.

16S rRNA amplicon sequencing samples were processed using QIIME2 version 2021.4 (Bolyen et al. 2019). Samples were denoised and quality filtered with DADA2 (Callahan et al. 2016). Taxonomy was classified using the SILVA 138 database (https://resources.qiime2.org/).

Appendix D – Gas-Phase Sequestration: Carbon Dioxide

Gas-phase chemical sequestration of I-129 [primary contaminant of interest (PCOI), present as iodate, IO_3^-] is summarized here with treatment via CO_2 gas with U, Sr, Tc, and Cr as potential co-contaminants of interest (CoCOIs). The goal of the technology is to inject CO_2 gas, which subsequently partitions into vadose zone pore water, dissolving carbonate minerals and eventually precipitating calcite. Note that although CO_2 gas supplies aqueous carbonate, calcium needs to come from pore water or ion exchange sites on sediments. Waste sites that released highly acidic wastes such as at the 216-U-8 Crib and 300 Area may be too significantly depleted in calcium as well as carbonate, especially near the surface, where acids have dissolved carbonate minerals and flushed ions to greater depths. Although the PCOI is I-129 (as iodate), given the significantly higher concentrations of natural I-127 in Hanford formation (Hf) sediments and lack of isotopic specificity in this technology, experiments were conducted with I-127 (naturally occurring isotope), as a field CO_2 treatment would need to sequester all I-127 and I-129 (i.e., iodate incorporation into calcite is not isotope specific). The specific objectives for this technology areas follows:

1. Quantify the decrease in I-129 (or I-127 as iodate) mass and removal rate in A and S sediments with no co-contaminants [described in the Phase 1 report (PNNL-35432)].
2. Quantify the decrease in I-129 (or I-127 as iodate) mass and removal rate in A and S sediments with co-contaminants [described in the Phase 1 report (PNNL-35432)].
3. Quantify I-129 (or I-127) sequestration at different water content (WC; most experiments are described in the Phase 1 report, but additional results are described in Section D.2).
4. Quantify the stability of immobilized I-129 (I-127) and co-contaminant species as well as potential remobilization rates (described in Section D.3).
5. Quantify CO_2 transport at 2 to 8 wt% WC (described in Section D.4).

D.1 Supplemental Methods

D.1.1 CO_2 Gas Treatment Methods

For CO_2 gas, sediments at 4 wt% (vadose zone average) or 8 wt% WC (higher WC characteristic of finer grain zones) were packed into columns [1.3- to 2.6-cm (0.5- to 1-in.) diameter by 16-cm (6.3-in.) length] and 10 to 30 pore volumes (PVs) of 100% CO_2 gas were injected through the column over the course of 5 minutes. Using Henry's law (based on the partition coefficient, K_H, for CO_2), the retardation of CO_2 gas was 1.26 at 4 wt% WC and 1.74 at 8 wt% WC. The volume of gas injected (10 PVs for 4 wt% WC, 30 PVs for 8 wt% WC sediments) was to ensure gas-pore water equilibrium was achieved in all sediments. Column ends were then sealed and had no flow for 60 days to allow calcite to precipitate. At 60 days, 10 to 30 PVs of air was injected into columns to simulate return to natural pore water pH conditions. Columns were sealed again and had no flow for an additional 60 days. In a previous study of a different vadose zone technology [organic gas followed by CO_2 gas (PNNL-35432)], the treatment time was evaluated for CO_2 gas. For this comparison, some sediment columns were injected with 100% CO_2 over 5 minutes (as was done in this study) and other sediment columns were injected with 100% CO_2 over 5 minutes and hooked up to a large (1-liter) metallized bag containing 100% CO_2 for 1,500 hours. There was no difference in treatment performance for Tc, Sr, Cr, I-127, and nitrate, so injections for 5 minutes were used here.

D.1.2 Leach Experiments

After CO_2 and subsequent air treatment, three different types of columns were conducted to evaluate the change in contaminant mobility: (1) water-saturated leach experiments, (2) infiltration experiments, and (3) pressurized unsaturated flow (PUF) infiltration experiments (McGrail et al. 1996). Note that water and contaminant advection in water-saturated experiments is largely controlled by the pressure gradient, whereas in infiltration experiments, advection is dominated by gravity and capillary suction. This results in greater breakthrough curve tailing for infiltration experiments (Szecsody et al. 2023), likely from pore water advecting at different rates (i.e., gravity-driven advection in larger pores and slower capillary-driven advection in smaller pores).

Water-saturated leach experiments were the same as described for other water-saturated technologies (Section 2.4.1), in which approximately 100 PVs of synthetic groundwater was injected through the column with a residence time of 6 hours, and effluent samples were used to quantify the PCOI (I-127 present as iodate) and CoCOIs (U, Tc, chromate, Sr, nitrate).

Infiltration experiments consisted of dripping water on the top of an open-ended column [2.6-cm (1-in.) diameter by 16-cm (6.3-in.) length] at a specified rate to achieve a 6-hour residence time. The bottom of the column contained a thin (3-mm) layer of sand (#20 sieve size or 841 μm), then a thin (3-mm) layer of sand (#12 sieve size or 1.68 mm), then a coarse plastic screen to allow water to drip out the bottom of the column into a fraction collector. At the end of the infiltration columns, seven sediment samples were collected at different vertical depths. The average water saturation was 84% for the untreated column and 79% for the CO_2/air-treated column.

PUF experiments were conducted to understand contaminant of interest leaching under unsaturated conditions. These systems have been described previously for waste form dissolution (Pierce et al. 2007). Briefly, PUF infiltration testing here used 1.91-cm (0.75-in.) diameter by 7.72-cm (3-in.) length polyetheretherketone columns packed with untreated or CO_2/air treated sediments. The inlet (upper) end of the column had two fittings for water injection and air pressure injection. The bottom of the column had a 0.5-μm porous titanium frit to maintain a ~0.3 bar water saturation (i.e., desaturated at greater than 0.3 bar) and thus allow water to pass through it but not air. The air pressure at the top of the column was maintained at 1 to 1.5 psi and was data logged hourly throughout the 1,900-hour experiment. The initial WC in sediment was 4.0 wt%.

Water was injected at a rate of 2 mL/day using a Kloehn syringe pump in each column. The effluent end of the column was attached to a Kloehn syringe pump with eight-way head so that a total of eight effluent samples could be collected in sealed 20-mL glass vials with septa tops to eliminate evaporation loss. Effluent samples were collected for 48 hours each. Each column was hung on a strain gauge so that the column weight (i.e., WC in the sediment) could be data logged hourly throughout the experiment. During the experiment, water was injected at the top of the column and flowed through the outlet frit at the bottom of the column, while it also accumulated within the unsaturated sediment. For the untreated sediment column initially at 4 wt% WC (~25% saturation), the average WC was 14 wt% (72.0% saturation), so there was a 50.6-hour residence time in the column. The CO_2/air treated sediment column initially at 4 wt% WC (25% saturation) had an average WC of 9.1 wt% (45.5% saturation) and a 33.0-hour residence time.

Differences in average WC between the two columns may have been caused by the differences in permeability of the outlet frits, as the sediment was the same in both columns. Note that during each PUF infiltration experiment, the WC in the column fluctuated. For each effluent sample collected over a 48-hour period, the average WC was calculated (based on hourly weight measurements), so a PV for each sample was calculated. The average PV was 5.3 ± 2.0 mL for the untreated sediment column and 2.6 ±

1.0 mL for the treated sediment column. The PV of each sample was used to calculate the cumulative PVs injected. After 1,800 hours of water injection into the PUF columns, 80 mg/L bromide in synthetic groundwater was then injected at the same rate into the columns. In this case, the sample frequency was every 8 hours over 2.3 to 4.6 PVs.

D.2 Unsaturated Batch Results

Unsaturated batch experiments were conducted to evaluate sequestration of iodate and CoCOIs in Hf sediments at 8 wt% WC and 216-S-9 sediments at 2 and 8 wt% WC. With a 60-day treatment of 100% CO_2 gas followed by 90 days of air treatment to neutralize the pH and increase calcite precipitation, both Hf and 216-S-9 sediments at 8 wt% WC showed a 13% to 15% decrease in iodate mobility compared to triplicate no-treatment experiments (Figure D.1a and b). In addition, at 2 wt% WC in the 216-S-9 sediment, there was no change in iodate mobility (Figure D.1c). The performance of the CO_2 treatments in these batch experiments is significantly less than the performance threshold, although some previous experiments did show a much greater decrease in iodate mobility in Hf and 216-S-9 sediments at 4 wt% WC. Experimental details are described in Appendix A, Section A.2.1.

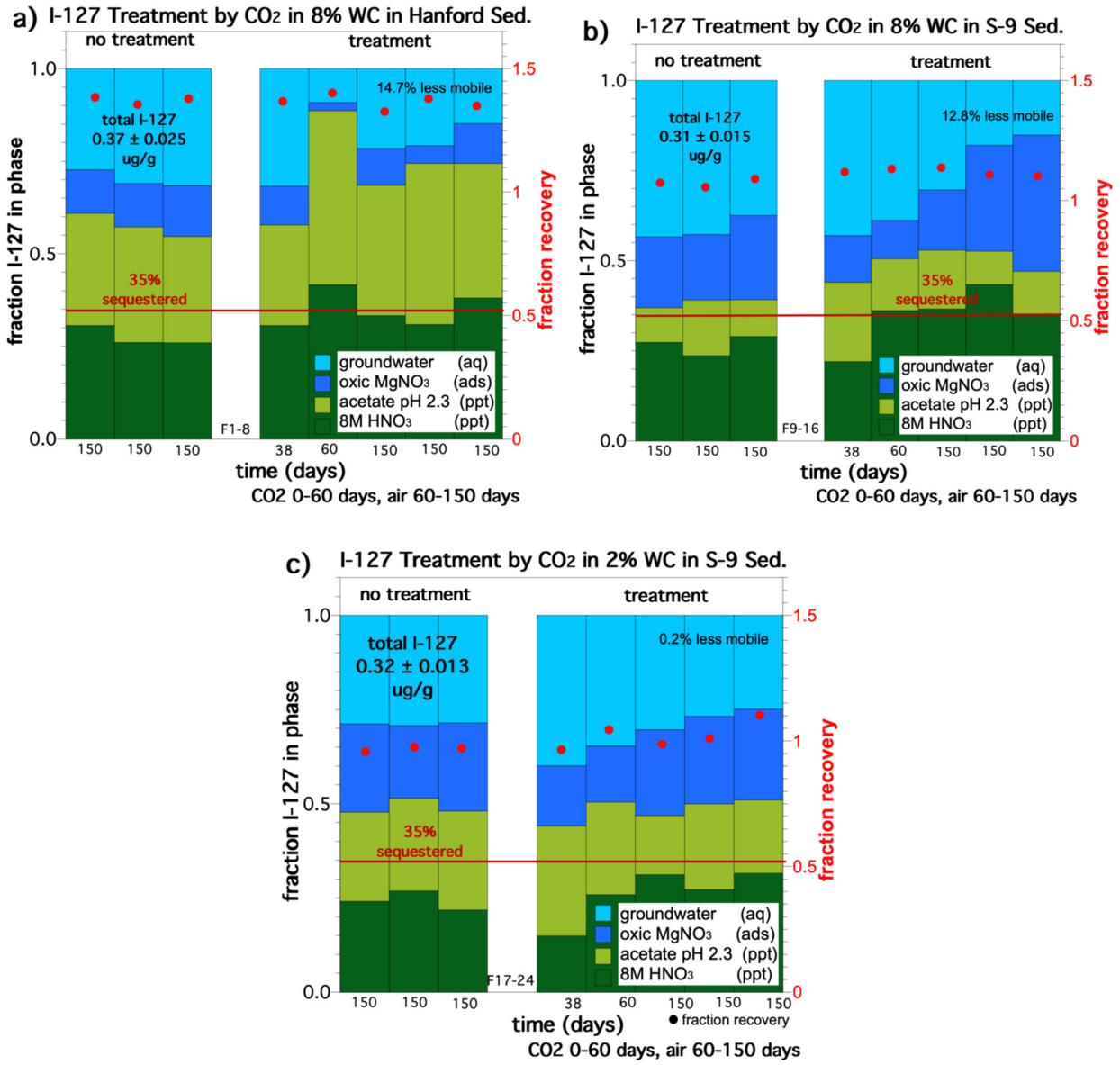

Figure D.1. I-127 (as iodate) sequestration using CO_2 gas in (a) Hf sediment at 8 wt% WC, (b) 216-S-9 sediment at 8 wt% WC, and (c) 216-S-9 sediment at 2 wt% WC.

Although CO_2 gas did not sequester significant iodate, it performed for some CoCOIs under specific conditions. For Tc-99 (as pertechnetate, TcO_4^-), mobility increased by 2.3% in the Hf sediment at 8 wt% WC but was 35% less mobile in the 216-S-9 sediment at 8 wt% WC and 7.2% less mobile in the 216-S-9 sediment at 2 wt% WC (Figure D.2a-c). In contrast, U mobility was unchanged by CO_2/air in the Hf or 216-S-9 sediment at different WC (Figure D.2d-f). Similarly, Sr mobility was also unchanged by CO_2/air in the Hf and 216-S-9 sediments (Figure D.2g-i). These results were unexpected, as carbonates can incorporate both uranium and Sr^{2+} into the structure (Pingitore Jr et al. 1992; Reeder et al. 2000). This may indicate that minimal calcite precipitation occurred under these conditions. Finally, there was a minimal decrease in Cr (present as chromate, CrO_4^{-2}) mobility from CO_2/air with 8.4% less mobile Cr for the Hf sediment at 8 wt% WC, 0.7% less mobile for the 216-S-9 sediment at 8 wt% WC, and 2.1% less mobile for the 216-S-9 sediment at 2 wt% WC (Figure D.2j-l).

Previous characterization of solid phase inorganic carbon following batch experiments did not, unfortunately, show a consistent increase as a result of CO_2 gas treatment (Table 4.5 in PNNL-35432). For the Hf sediment, the fraction of inorganic carbon increased from 0.00% to 0.06 ± 0.04% after CO_2 treatment, whereas for the 216-S-9 sediment, the fraction of inorganic carbon decreased from 0.28 ± 0.04 to 0.00%. These results indicate that the amount of calcite that precipitates from CO_2 treatment may be small (or none) and may be dependent on sediment and condition. Calcium (or Mg or Sr) in the sediment is also needed for calcite to precipitate with CO_2 gas treatment. Ca^{2+} measurements in sequential batch extractions (described within, Figure D.3a-c) indicate that (a) there is sufficient aqueous and adsorbed Ca^{2+} in both sediments for calcite precipitation (i.e., ~100 ug/g aqueous Ca^{2+}, ~250 ug/g adsorbed Ca^{2+}) and (b) the Ca^{2+} in the aqueous, adsorbed, acetic acid, and nitric acid extractable fractions did not change as a result the CO_2 treatment. Therefore, there is little evidence of calcite precipitation.

Additional metals were also measured in sequential extractions, as these provide information about the calcite precipitation process. For example, aqueous or adsorbed Ca^{2+} is needed for calcite precipitation. Hf sediment had greater aqueous (0.1 mg/g) and adsorbed Ca^{2+} (0.4 mg/g) than 216-S-9 sediment (aqueous 0.07 mg/g, adsorbed 0.25 mg/g; Figure D.3a-c), possibly due to impacts from acidic CoCOIs in the 216-S-9 sediment. However, Ca^{2+} was sufficient for both sediments to precipitate calcite. Unfortunately, Ca data show that there is no difference in the aqueous, adsorbed, acetic acid extractable, and nitric acid extractable fractions from CO_2 treatment. It was expected that aqueous and adsorbed Ca^{2+} would decrease and the acetic acid extractable fraction (dissolving primarily calcite) would increase CO_2-treated sediments. High silica in aqueous solution can slow calcite precipitation and increase metals incorporation. Both the Hf and 216-S-9 sediment had approximately 10 µg/g aqueous silica (Figure D.3d-f). Injection of 100% CO_2 gas (first 60 days) decreased the pH to some extent and may create anaerobic conditions. This may lead to some ferrous or Mn-containing surface phases reducing contaminants, as shown in some previous studies [Tc, (Szecsody et al. 2014)] If reducing conditions were present, iodate would be transformed to iodide and would not incorporate into precipitating calcite. However, total iron and manganese in extractions showed nearly no aqueous or adsorbed mass (Figure D.3g-l), including with CO_2 gas treatment, indicating no readily available abiotic electron donors.

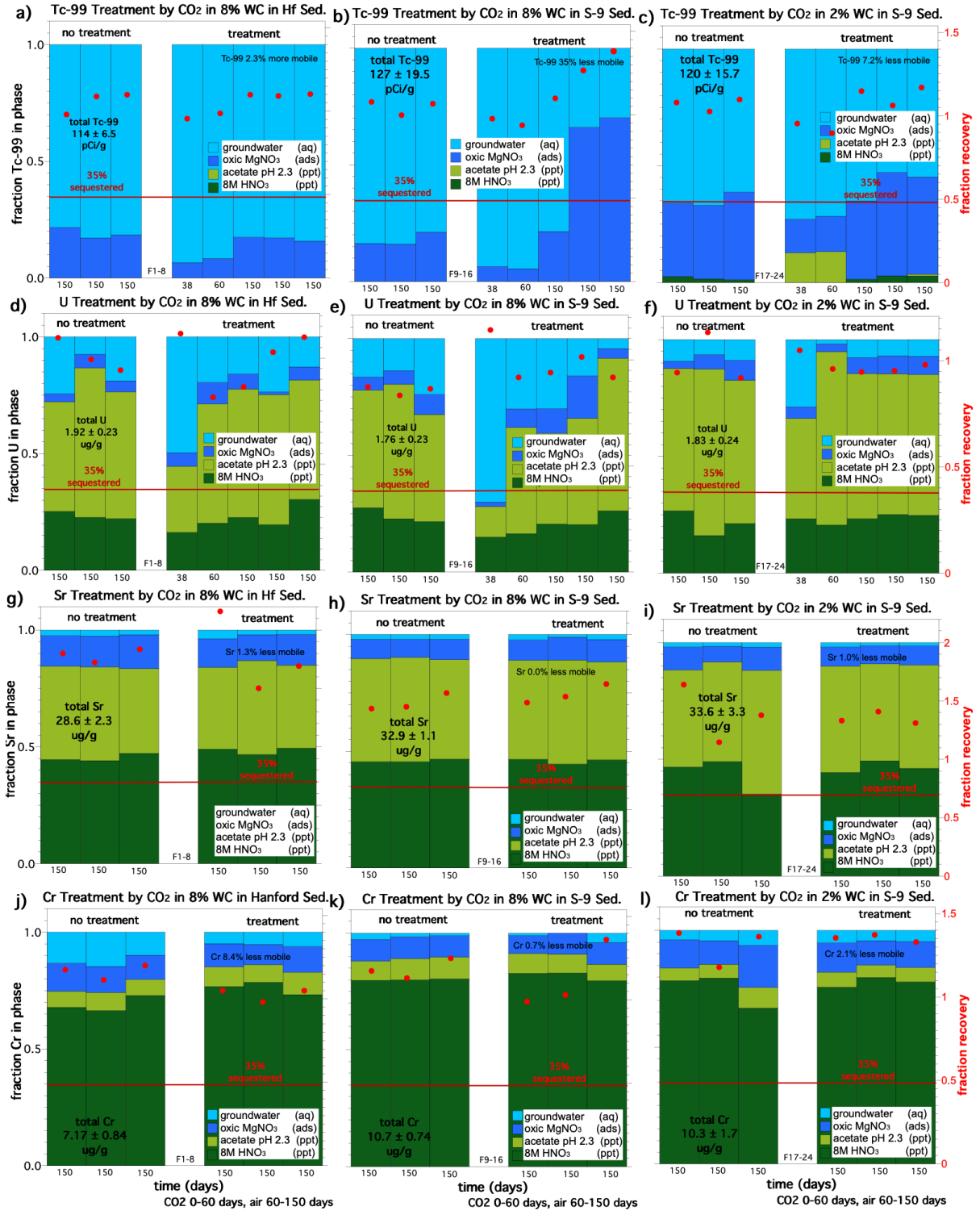

Figure D.2. Sequestration using CO_2 gas for (a) Tc-99 in Hf sediment at 8 wt% WC, (b) Tc-99 in 216-S-9 sediment at 8 wt% WC, (c) Tc-99 in 216-S-9 sediment at 2 wt% WC, (d) U in Hf sediment at 8 wt% WC, (e) U in 216-S-9 sediment at 8 wt% WC, (f) U in 216-S-9 sediment at 2 wt% WC, (g) Sr in Hf sediment at 8 wt% WC, (h) Sr in 216-S-9 sediment at 8 wt% WC, (i) Sr in 216-S-9 sediment at 2 wt% WC, (j) Cr in Hf sediment at 8 wt% WC, (k) Cr in 216-S-9 sediment at 8 wt% WC, and (l) Sr in 216-S-9 sediment at 2 wt% WC.

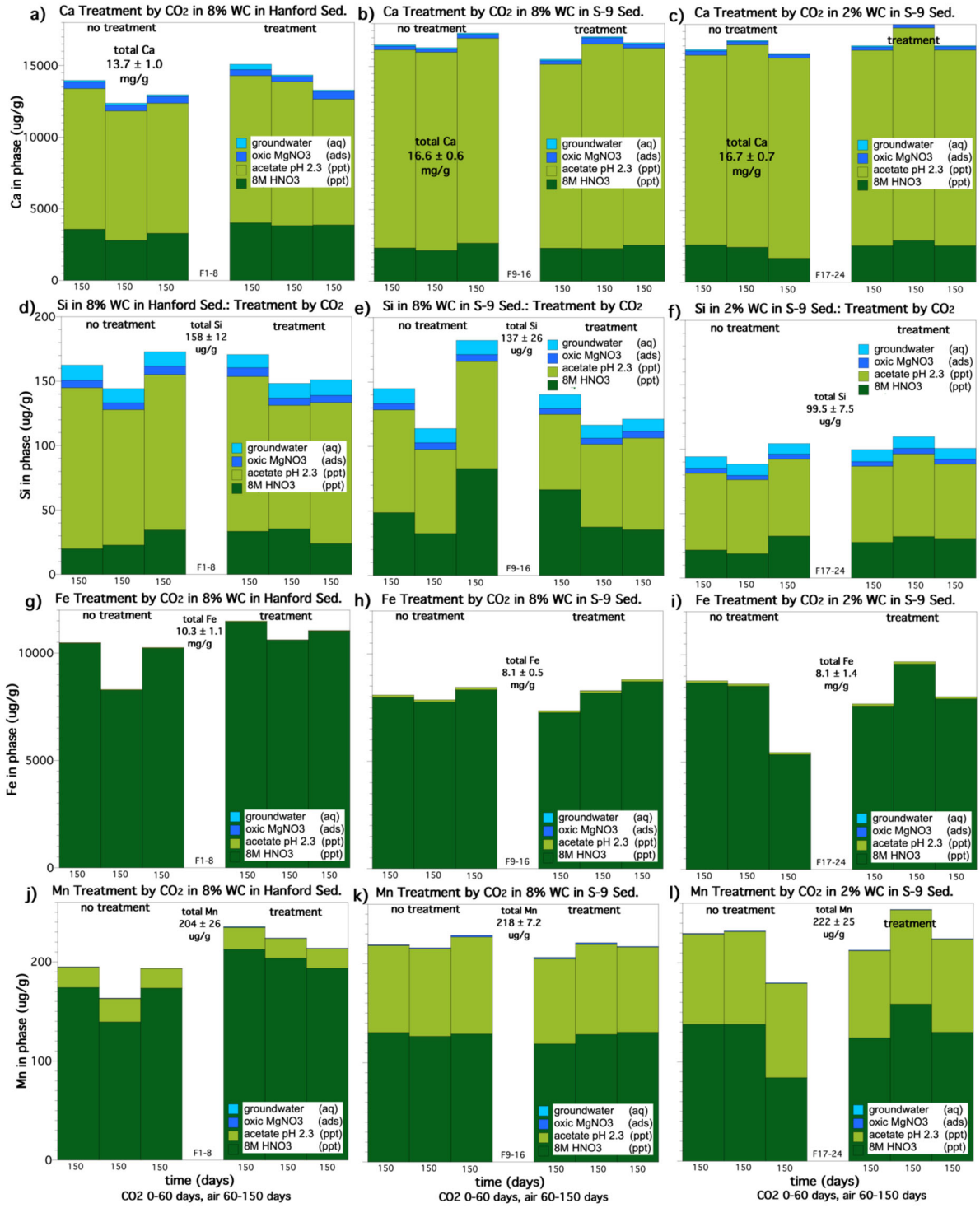

Figure D.3. Changes in metals distribution from CO_2/air treatment for (a) Ca Hf sediment at 8 wt% WC, (b) Ca in 216-S-9 sediment at 8 wt% WC, (c) Ca in 216-S-9 sediment at 2 wt% WC, (d) Si in Hf sediment at 8 wt% WC, (e) Si in 216-S-9 sediment at 8 wt% WC, (f) Si in 216-S-9 sediment at 2 wt% WC, (g) Fe in Hf sediment at 8 wt% WC, (h) Fe in 216-S-9 sediment at 8 wt% WC, (i) Fe in 216-S-9 sediment at 2 wt% WC, (j) Mn in Hf sediment at 8 wt% WC, (k) Mn in 216-S-9 sediment at 8 wt% WC, and (l) Mn in 216-S-9 sediment at 2 wt% WC.

D.3 Variably Saturated Column Results

D.3.1 I-129/I-127 Sequestration

For this objective, variably-saturated leach experiments were conducted on gas-treated sediment columns (Section 2.2). Gas treatment of unsaturated sediment columns was conducted as described in Section D.1 for batch studies with 60 days of reaction with 100% CO_2 followed by 90 days of air. Leach experiments were used to quantify the change in contaminant mobility and consisted of (1) water-saturated leach experiments for the Hf sediment, (2) water-saturated leach experiments for the 216-S-9 sediment, (3) infiltration leach experiments (82% water saturation) for the 216-S-9 sediment, and (4) PUF infiltration leach experiments (40% to 54% water saturation) for the 216-S-9 sediment. For the Hf sediment, water-saturated leach columns showed 12% less I-127 leached from the CO_2-treated column compared to the untreated column (Figure D.4). Stop flow events at 3 and 10 PVs showed a slight increase in I-127, indicating slow release from the sediment.

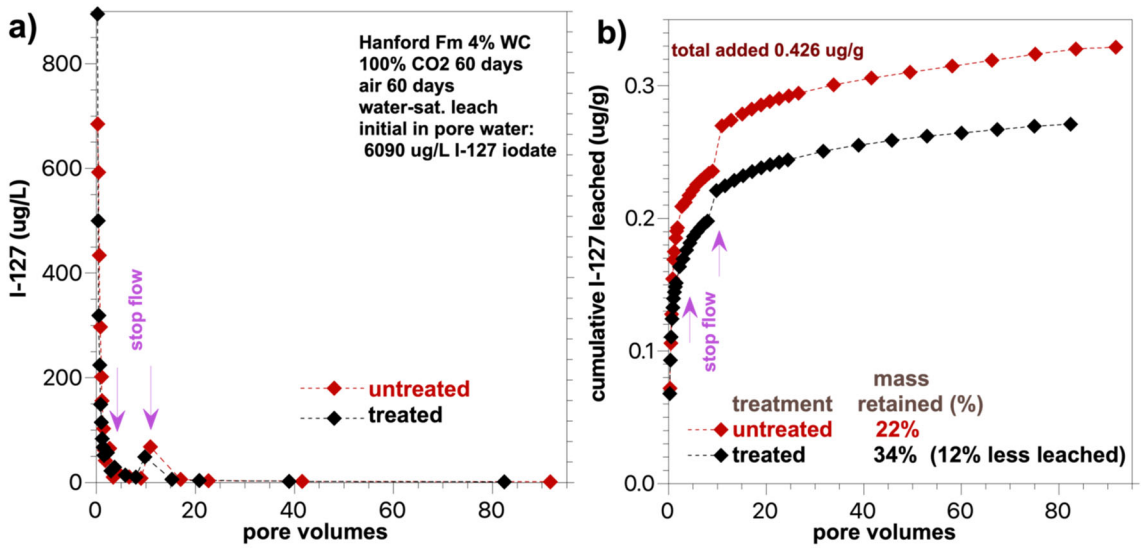

Figure D.4. Water-saturated leaching of I-127 (as iodate) in Hf sediment after sequestration using CO_2 gas as shown by (a) aqueous I-127 effluent concentrations and (b) cumulative aqueous I-127 mass leached.

For the 216-S-9 sediment, water-saturated experiments with CO_2 treatment resulted in 5.9% or 13.6% less (duplicate experiments) I-127 leached compared to the untreated leach experiment (Figure D.5a and b). For the infiltration experiments (80% saturation), 13% greater I-127 leached from the CO_2-treated column compared to the untreated sediment (Figure D.5c and d).

Sequential extractions were conducted in the post-leach sediments with analysis of Tc-99 and U CoCOIs. I-127 was not analyzed in these acidic extractions due to iodine mass loss that occurs in acidic samples. For PUF infiltration experiments (40% to 54% saturation), which have a 33- to 51-hour residence time per PV, 5.0% greater I-127 was leached in the CO_2-treated column compared to the untreated column (Figure D.5e and f). Tetramethylammonium hydroxide extractions (alkaline pH; Appendix A, Section A.2.3) were conducted on the post-leach PUF sediments. These extractions showed the same result as the leach data: The CO_2 treatment had no significant effect on the I-127 retained by the sediment (inset plot in Figure D.5f).

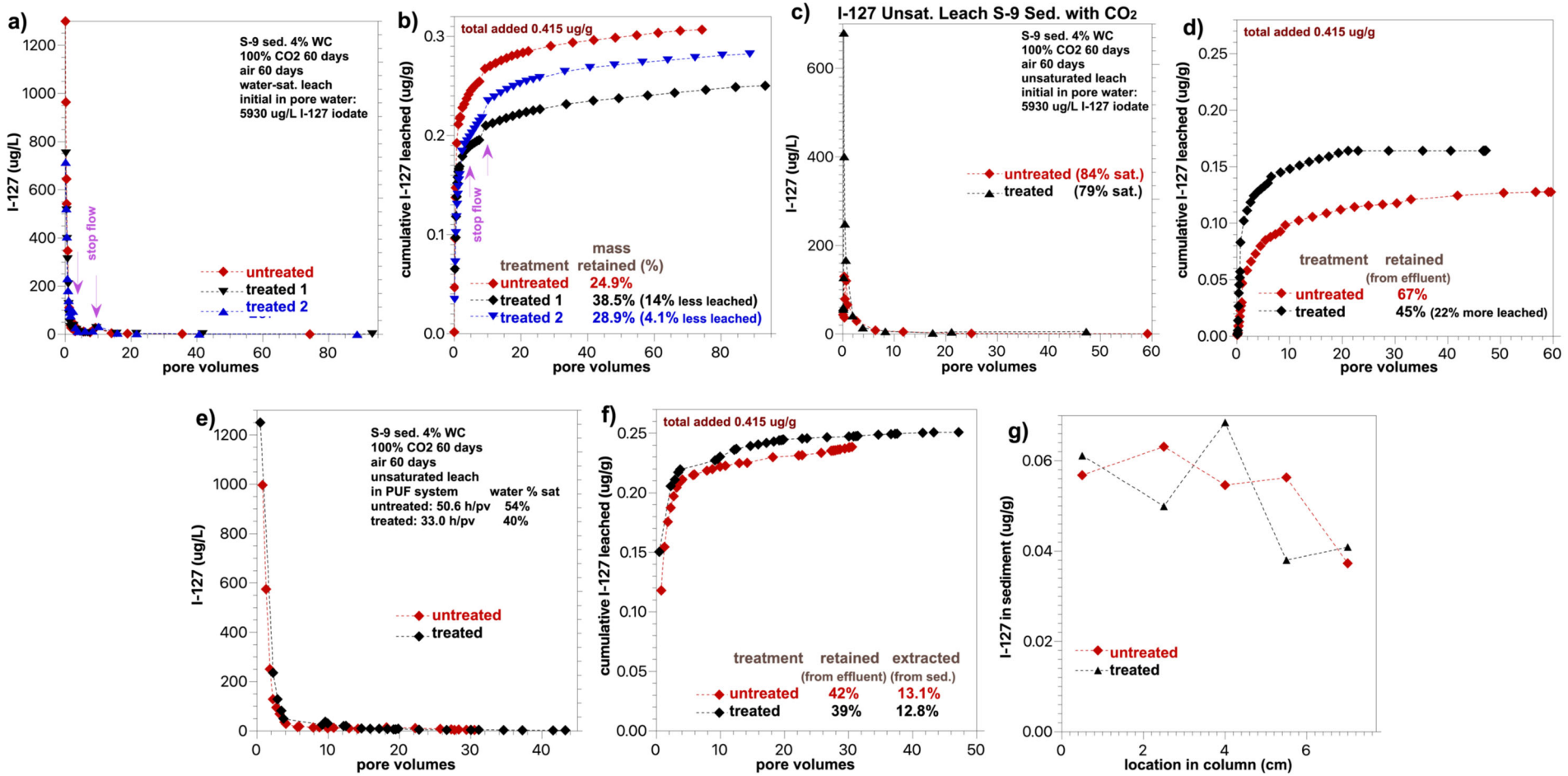

Figure D.5. Leaching of I-127 (as iodate) in 216-S-9 sediment after sequestration using CO_2 gas as shown by (a) water-saturated I-127 effluent concentrations (18% WC), (b) water-saturated cumulative I-127 effluent mass, (c) infiltration (79-84% saturation) I-127 effluent concentrations, (d) infiltration cumulative I-127 effluent mass, (e) PUF infiltration (40% to 54% saturation) I-127 effluent concentrations, (f) PUF infiltration cumulative I-127 effluent mass, and (g) I-127 extracted mass from the sediment after the PUF infiltration leach.

Stop flow events during water-saturated column experiments were used to calculate the release rate of I-127 from surface phases. I-127 release rates were also calculated during flow before stop flow events. Stop flow events were not conducted during infiltration experiments, as water flow would not stop (i.e., continued drainage out of the column during stops). A working sequestration technology would remove contaminant mass from solution (compared to untreated sediment) and additionally release the contaminant from the surface at a slower rate (compared to untreated sediment). For the Hf and 216-S-9 sediments, there was no systematic difference between I-127 release rates in untreated and CO_2/air-treated sediments (Table D.1), which is not surprising considering that none to minimal I-127 mass was removed from solution from the CO_2/air treatment.

Table D.1. I-127 release rates calculated from column data during flow and during stop events.

Sediment	Treatment	Stop Flow (PV)	Release Rate during Stop (µg/kg/day)	Release Rate during Stop (1/day)	Release Rate during Flow (µg/lg/day)	Release Rate during Flow (1/day)
Hf	none	2.58	10.1	0.053	80.3	0.416
		10.9	3.60	0.015	15.4	0.064
Hf	CO_2/air	2.24	2.18	0.014	80.6	0.533
		9.78	2.30	0.011	16.2	0.081
216-S-9	none	2.43	8.52	0.039	50.8	0.232
		9.18	1.14	0.004	15.3	0.060
216-S-9	CO_2/air	2.47	1.68	0.010	50.0	0.296
		9.49	1.29	0.007	8.71	0.044
216-S-9	CO_2/air	2.36	8.18	0.051	126	0.784
		10.1	1.09	0.005	23.3	0.106

D.3.2 Tc Sequestration

For Tc-99 in the Hf sediment, water-saturated columns showed that CO_2 treatment resulted in 28% less Tc-99 mass leached (Figure D.6). Post-experiment extractions, however, did not show a difference between Tc-99 retained in untreated and CO_2-treated sediments (inset graph in Figure D.6a), although there is generally more error in extractions than aqueous effluent measurements, so the effluent mass data is considered more accurate.

For Tc-99 in 216-S-9 sediment, water-saturated leach experiments showed that CO_2 treatment resulted in 15% to 18% less leaching (Figure D.7a and b) compared to untreated sediment. Post-experiment extractions showed similar results, with 17% to 25% greater Tc-99 mass retained in the sediment (inset graph, Figure D.7d). In contrast, for the infiltration experiments at 80% water saturation, CO_2 gas resulted in 7% greater Tc-99 leaching (Figure D.7c and d), but extractions showed 38% greater retention in the CO_2-treated sediment (inset graph in Figure D.7c). It is possible that extractions are less representative due to incomplete mixing during sub-sampling. The greater retained mass in sediment extractions is based on two nonzero points (out of seven) and thus is likely less accurate than the cumulative effluent mass (Figure D.7d). For the PUF infiltration experiments at 40 to 54 wt% WC with much longer residence times (33 to 51 hours), leach experiments showed that CO_2 gas had 7.4% less leaching (Figure D.7e and f). Post-leach extractions, however, showed no difference in Tc-99 retained between untreated and CO_2-treated sediments.

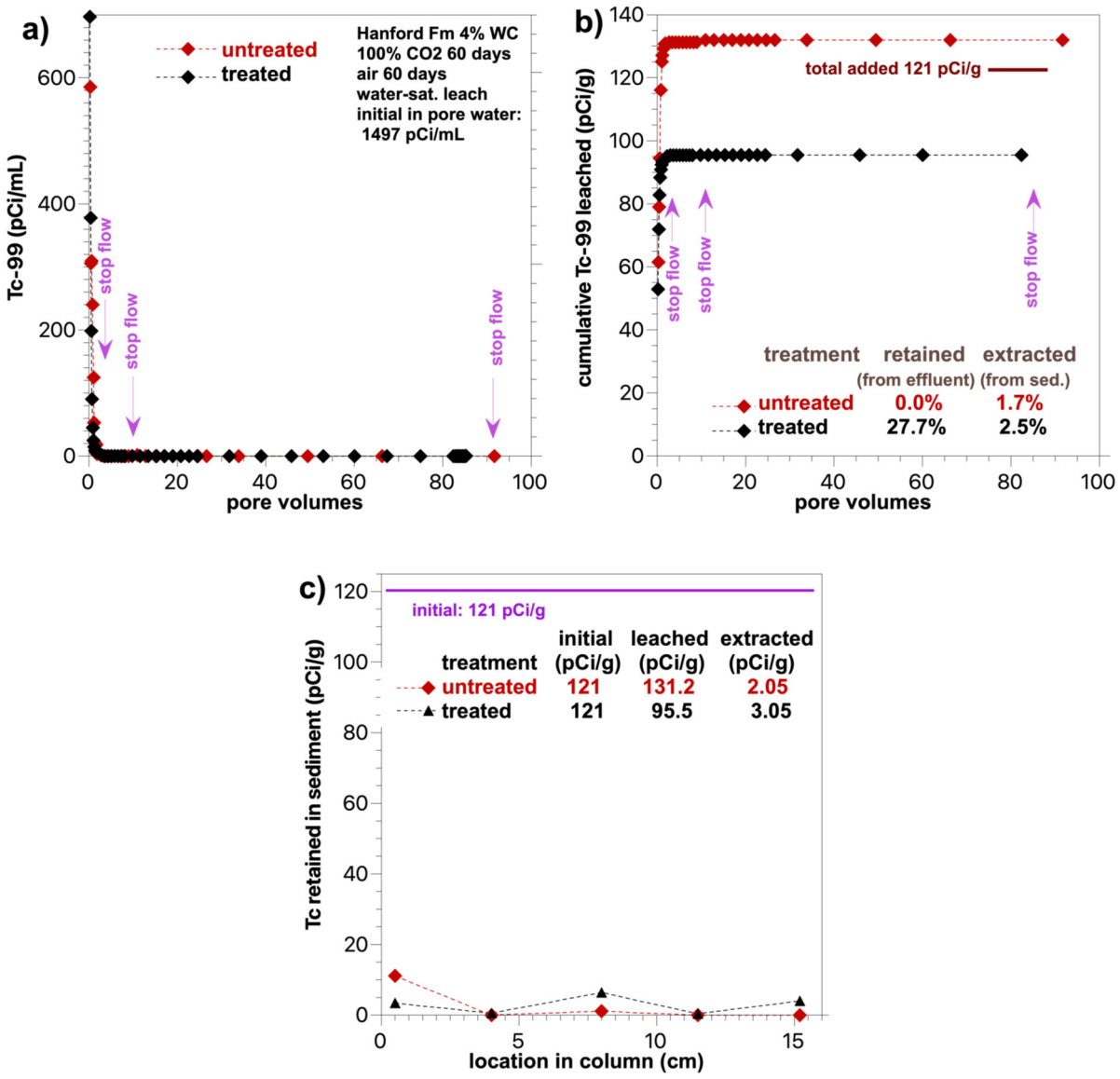

Figure D.6. Water-saturated leaching of Tc-99 in Hf sediment after sequestration using CO_2 gas as shown by (a) Tc-99 effluent concentration, (b) cumulative Tc-99 effluent mass, and (c) extracted Tc-99 mass.

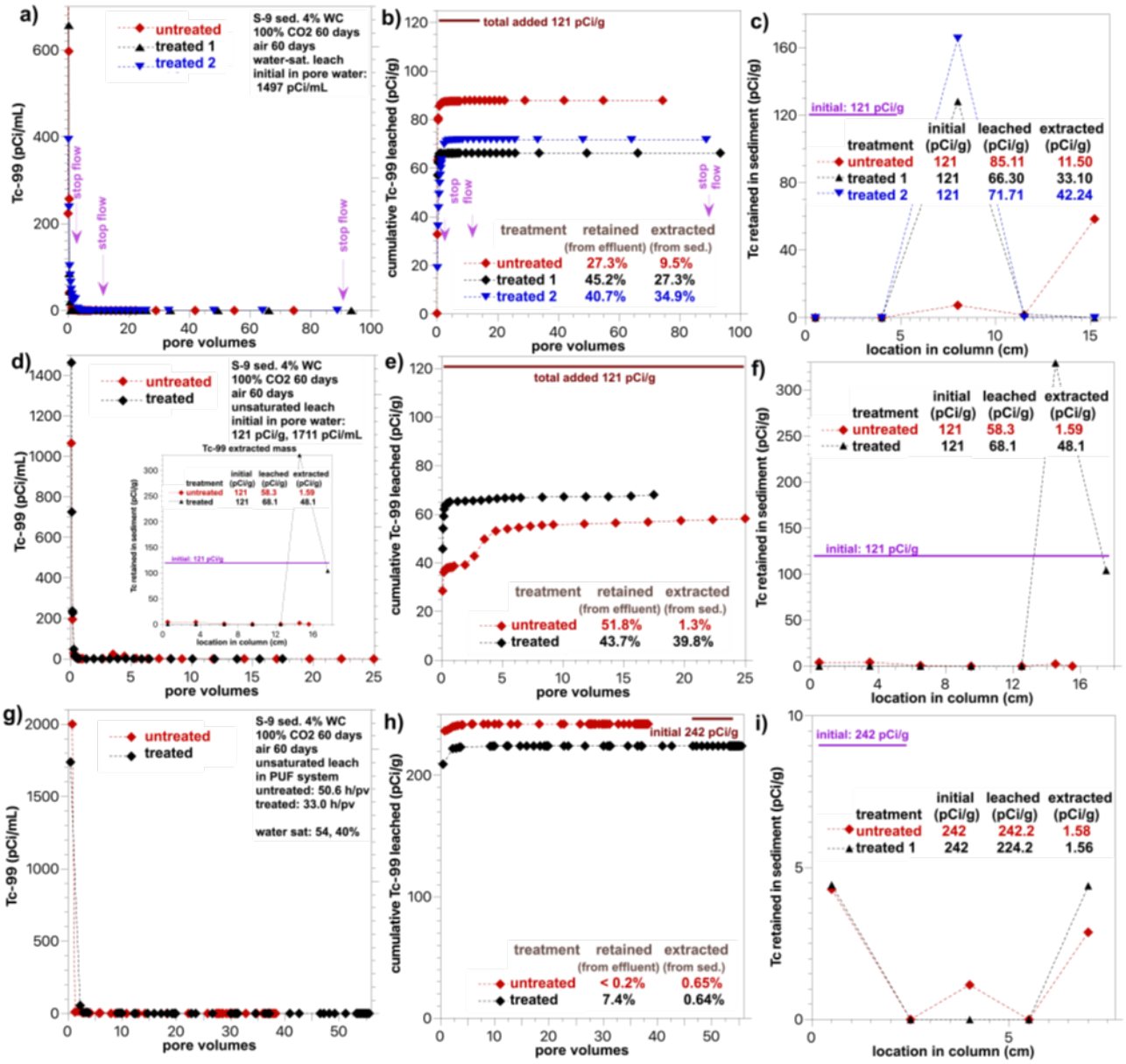

Figure D.7. Leaching of Tc-99 (as iodate) in 216-S-9 sediment after sequestration using CO_2 gas as shown by (a) water-saturated Tc-99 effluent concentrations, (b) water-saturated cumulative Tc-99 effluent mass, (c) extracted Tc-99 mass, (d) infiltration (79 to 84 wt% WC) Tc-99 effluent concentrations, (e) infiltration cumulative Tc-99 effluent mass, (f) extracted Tc-99 mass, (g) PUF infiltration (40 to 54 wt% WC) Tc-99 effluent concentrations, (h) PUF infiltration cumulative Tc-99 effluent mass, and (i) extracted Tc-99 mass.

Stop flow events during water-saturated column experiments were used to calculate the release rate of Tc-99 from surface phases. Tc-99 release rates were also calculated during flow before stop flow events. Although there were three stop flow events in each column, Tc-99 concentrations were below detection limits by 10 PVs, so there was no change in concentration for the third stop flow event at 90 PVs. For the Hf sediment, Tc-99 release rates were the same in untreated and CO_2/air-treated experiments at ~2.5 PVs

but slower for the CO_2/air-treated experiment at 10 PVs (fifth column, Table D.2). In contrast, the Tc-99 release rate was faster in the CO_2/air-treated sediment than in the untreated sediment.

Table D.2. Tc release rates calculated from column data during flow and during stop events.

Sediment	Treatment	Stop Flow (PV)	Release Rate during Stop (pCi/kg/day)	Release Rate during Stop (1/day)	Release Rate during Flow (pCi/kg/day)	Release Rate during Flow (1/day)
Hf	None	2.58	-0.807	-6.15E-06	5.85	4.46E-05
		10.9	1.00E-01	7.59E-07	0.00E+00	0.000
Hf	CO_2/air	2.24	-0.822	-8.64E-06	10.5	1.11E-04
		9.78	1.79E-02	1.87E-07	0.00E+00	0.000
216-S-9	None	2.43	-0.004	-5.04E-08	3.22	3.69E-05
		9.18	4.50E-02	5.29E-07	0.00E+00	0.000
216-S-9	CO_2/air	2.47	0.122	1.85E-06	0.00	0.00E+00
		9.49				
216-S-9	CO_2/air	2.36	2.36	3.38E-05	34.7	4.97E-04
		10.1				

Blank cells denote Tc-99 concentration(s) were below detection limit, so a rate could not be calculated.

D.3.3 U Sequestration

For U in Hf sediment, water-saturated leach experiments showed that CO_2 treatment resulted in 1% less U mass leached compared to untreated sediment by 80 PVs, although through most of the leach experiments a greater mass of U was leaching from the CO_2-treated sediment (Figure D.8). Post-experiment extractions also showed 14% less U retained in the CO_2-treated sediments (inset graph in Figure D.8a).

For U in the 216-S-9 sediment, water-saturated leach experiments showed that CO_2 treatment resulted in 3% greater or 18% less leaching in duplicate experiments (Figure D.9a and b) compared to leaching in the untreated sediment. Post-experiment extractions showed different results, with 7% to 8% greater U mass retained in the CO_2-treated sediment (inset graph, Figure D.9a). Similarly, for the infiltration experiments at 80% water saturation, the CO_2 treatment resulted in 4% less leaching (Figure D.9c and d), but extractions showed only 2% greater retention in the CO_2-treated sediment (inset graph in Figure D.9c). For the PUF infiltration experiments at 40 to 54 wt% WC and much longer residence times (33 to 51 hours), leach experiments showed that CO_2-treated sediment had 14% less U leaching (Figure D.9e and f), which was consistent with the post-leach extractions showing 2% greater U retention in the CO_2-treated sediments.

Stop flow events during water-saturated column experiments were used to calculate the release rate of U from surface phases. U release rates were also calculated during flow before stop flow events for comparison. All untreated and treated columns showed a net U uptake at the first stop flow event (i.e., negative release rate, column 5, Table D.3), likely from slow adsorption of aqueous Ca-uranyl-carbonate species to the sediment. The second stop flow event at ~10 PVs did show that CO_2/air-treated sediments had a 20% to 30% slower U release rate compared to untreated Hf and 216-S-9 sediments. The third stop flow event at ~80 PVs showed a 60% decrease in U release rate for the Hf sediment compared to the untreated sediment (i.e., F26 vs. F25). For the 216-S-9 sediment, CO_2/air treatment resulted in a 49% to 73% decrease in the U release rate compared to untreated sediment (i.e., F28 and F29 compared to F27).

Although there appeared to be consistency in the effect of the CO_2/air treatment for U sequestration, the U mass sequestered was inconsistent.

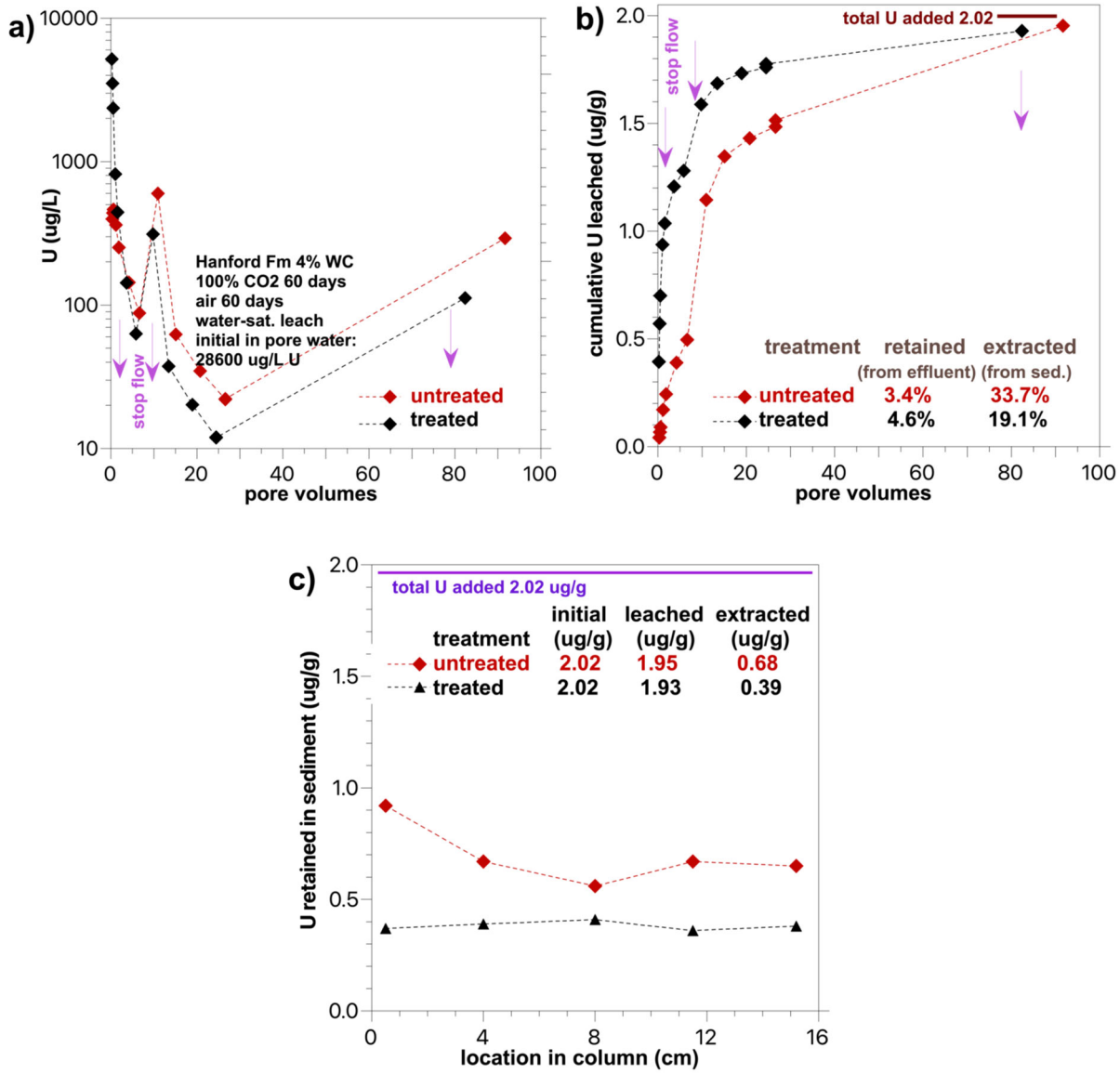

Figure D.8. Water-saturated leaching of U in Hf sediment after sequestration using CO_2 gas as shown by (a) U effluent concentration, (b) cumulative U effluent mass, and (c) post-leach extractable U mass.

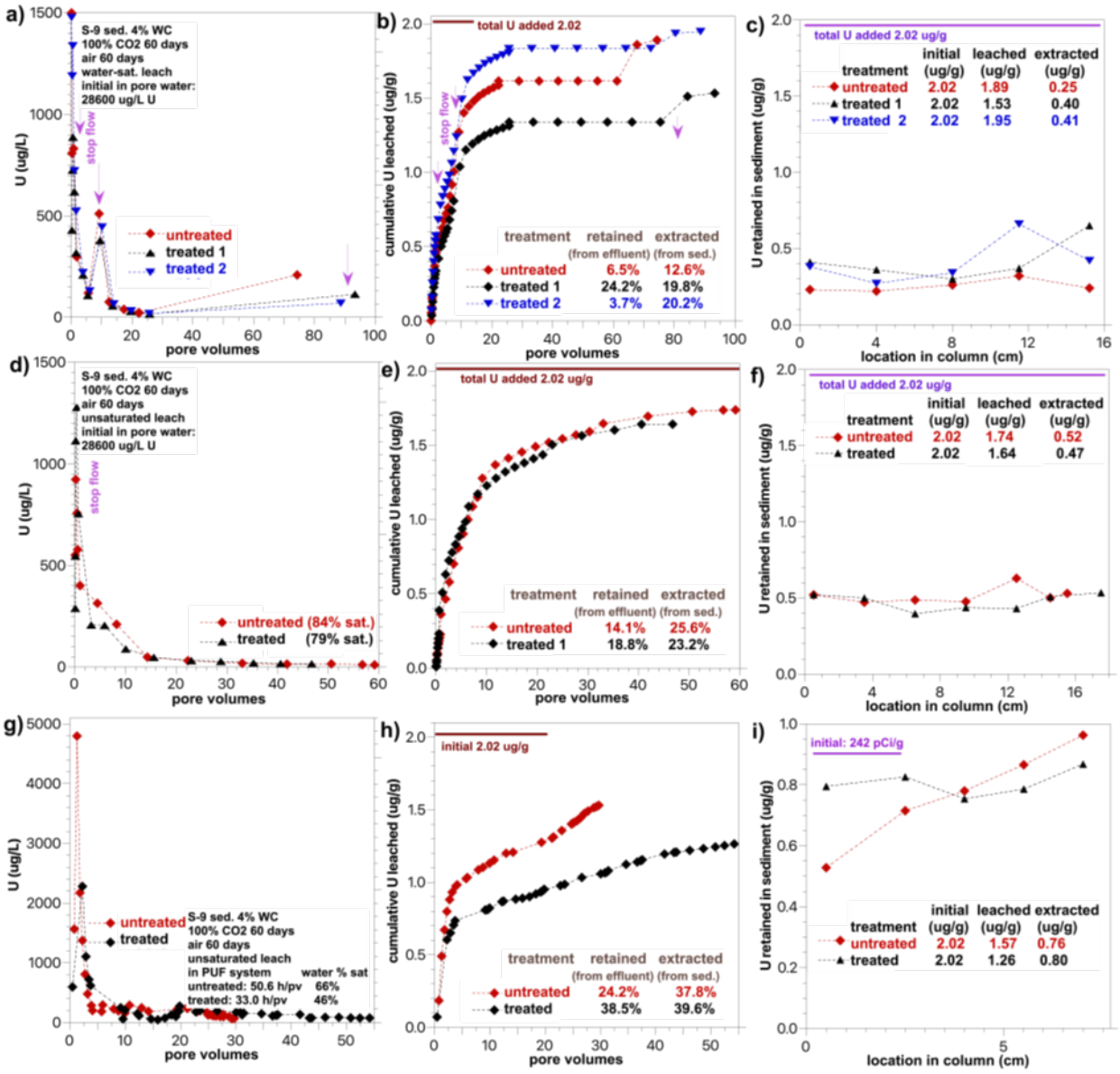

Figure D.9. Leaching of U in 216-S-9 sediment after sequestration using CO_2 gas as shown by (a) water-saturated U effluent concentrations, (b) water-saturated cumulative U effluent mass, (c) extracted U mass, (d) infiltration (79% to 84% saturation) U effluent concentrations, (e) infiltration cumulative U effluent mass, (f) extracted U mass, (g) PUF infiltration (40% to 54% saturation) U effluent concentrations, (h) PUF infiltration cumulative U effluent mass, and (i) extracted U mass.

Table D.3. U release rates calculated from column data during flow and during stop events.

Sediment	Treatment	Stop Flow (PV)	Release Rate during Stop (pCi/kg/day)	Release Rate during Stop (1/day)	Release Rate during Flow (pCi/kg/day)	Release Rate during Flow (1/day)
Hf	None	2.58	-23.8	-0.079	482	1.60
		10.9	9.36	0.008	657	0.575
		92.0	4.54	0.003	42.4	0.028
Hf	CO_2/air	2.24	-62.9	-0.061	694	0.669
		9.78	7.39	0.005	294	0.207
		82.8	1.68	0.001	18.6	0.011
216-S-9	None	2.43	-39.1	-0.082	561	1.18
		9.18	11.7	0.009	595	0.468
		74.6	3.16	0.002	39.9	0.025
216-S-9	CO_2/air	2.47	-22.7	-0.054	502	1.19
		9.49	8.05	0.008	385	0.371
		93.8	1.63	0.001	27.1	0.020
216-S-9	CO_2/air	2.36	-64.0	-0.112	853	1.49
		10.1	9.37	0.006	469	0.315
		89.1	0.85	0.001	30.5	0.017

D.3.4 Bromide Tracer Breakthrough

Approximately 80 mg/L of bromide was injected into columns to evaluate transport of water through the sediment. Water-saturated transport through Hf and 216-S-9 sediments generally showed little tailing, indicating injected water was moving through most of the sediment pores (Figure D.10a and b). In contrast, during infiltration experiments in 216-S-9 sediments at 80% water saturation, some tailing was observed, with earlier (i.e., closer to 0.5 PVs) but incomplete breakthrough at 3 PVs (i.e., Br concentration did not reach injected concentration by 3 PVs, Figure D.10c). This may indicate that infiltrating water was moving through some of the pores, but a fraction of the pore water was not mobile or was moving more slowly. Finally, during PUF infiltration experiments, bromide breakthrough was retarded and exhibited greater tailing to 4.6 PVs (Figure D.10d), also indicating a fraction of immobile pore water. Dispersion coefficients for variably saturated experiments (PUF and leach) are summarized in Appendix A, Section A.3.

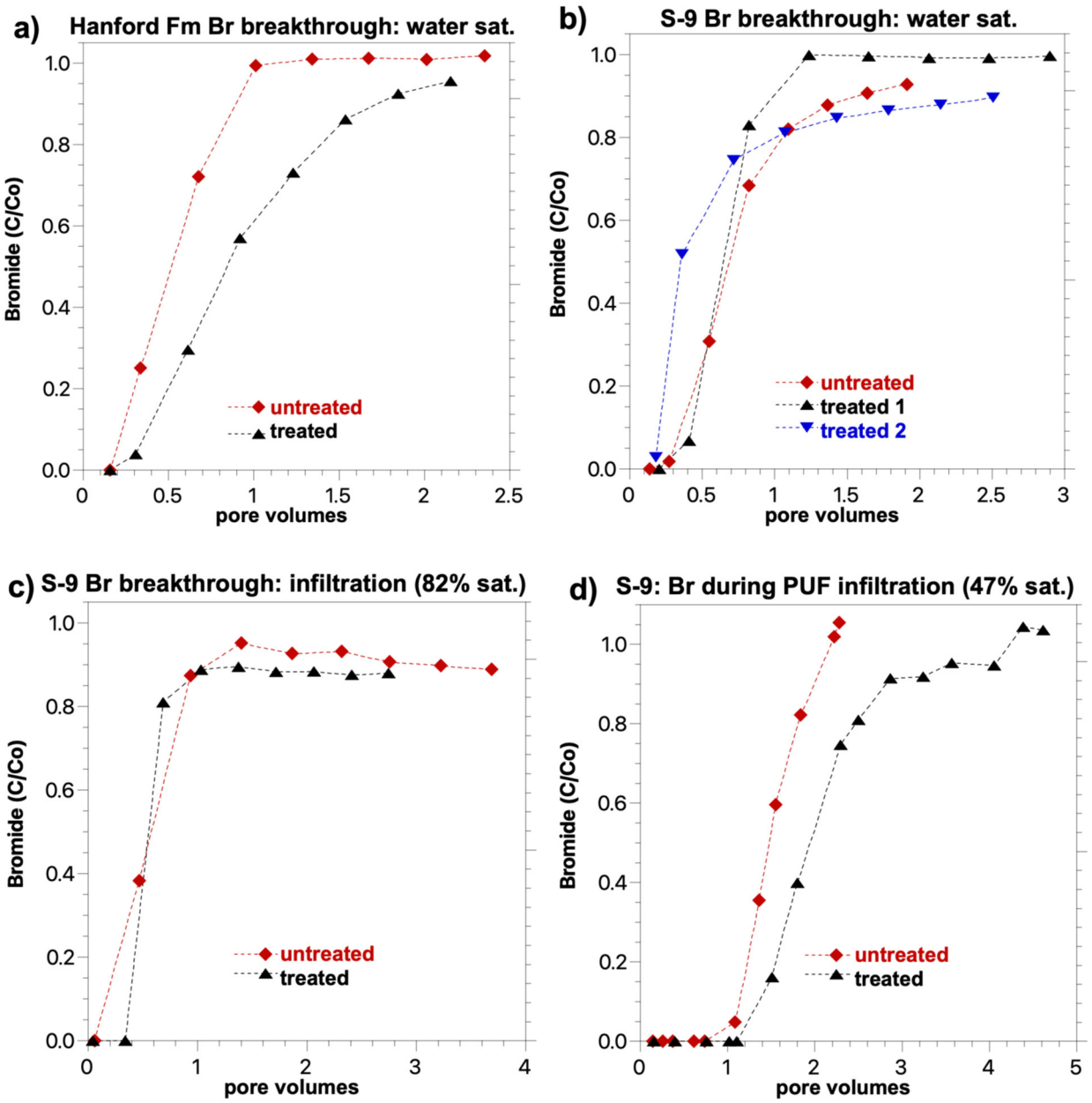

Figure D.10. Bromide breakthrough in columns containing (a) water-saturated Hf sediment, (b) water-saturated 216-S-9 sediment, (c) 216-S-9 sediment during infiltration (80% water saturation), and (d) 216-S-9 sediment during PUF infiltration (50% water saturation).

D.4 Gas Transport Results in Variably Saturated Sediments

The objective here was to characterize two processes that influence CO_2 gas transport in unsaturated sediments: (1) retardation from gas-to-liquid partitioning and (2) CO_2 gas density. Based on Henry's law liquid/gas equilibrium partition coefficient (K_h = 1.137, dimensionless), CO_2 gas should have a retardation factor of 1.26 at 4 wt% WC and 1.74 at 8 wt% WC. Therefore, there should be slight retardation of the injection of CO_2 gas relative to a tracer that increases at higher WC. CO_2 also has a higher gas density (1.839 kg/m^3) than air (1.205 kg/m^3), so it should sink in the vadose zone. Density

sinking is more apparent at slower gas velocity, so it would be more apparent at greater distance from injection wells (during gas injection) or at all locations once injections end due to decreasing flow rates.

At 4 wt% WC, five experiments were conducted with CO_2 gas injection into the column mounted horizontally (i.e., no gravity effects). These had an average retardation of 0.72 ± 0.03 compared to the retardation of 1.26 calculated from Henry's law (Figure D.11a). The lower experimental value may be caused by the relatively rapid CO_2 injection (~4 minutes residence time), so there may be some kinetic effects of the CO_2 not partitioning to all the pore water within the short residence time. The kinetic effect appears to be more pronounced at 8 wt% WC (Figure D.11b), with greater breakthrough curve tailing. A larger kinetic effect at 8 wt% WC may be caused by slower CO_2 gas partitioning into pore water present in a thicker film on grains compared to 4 wt% WC. With the column mounted vertically, at 4 wt% WC, the four injection experiments injecting at the top of the column (i.e., the dense CO_2 will sink due to gravity along with advection) had an average retardation of 0.581 ± 0.133 (i.e., faster than horizontally mounted due to the addition of CO_2 gas gravity sinking). Five injection experiments injecting at the bottom of the column (i.e., flow upward) resulted in an average CO_2 retardation of 0.785 ± 0.039, slower than horizontal injections as the dense CO_2 gas was diffusing upward more slowly than in horizontal injections.

At 8 wt% WC, horizontally injected CO_2 had an average retardation of 1.45 ± 0.019 compared to the Henry's law calculated retardation of 1.74. Downward vertical CO_2 injections had an average retardation of 1.24 ± 0.050 and upward vertical CO_2 injections had an average retardation of 1.54 ± 0.075. Therefore, CO_2 gas can be easily injected at field scale with a small impact from the retardation but with a significant density sinking effect. The density sinking effect could be controlled by CO_2 gas injections above a confining layer or using recirculation.

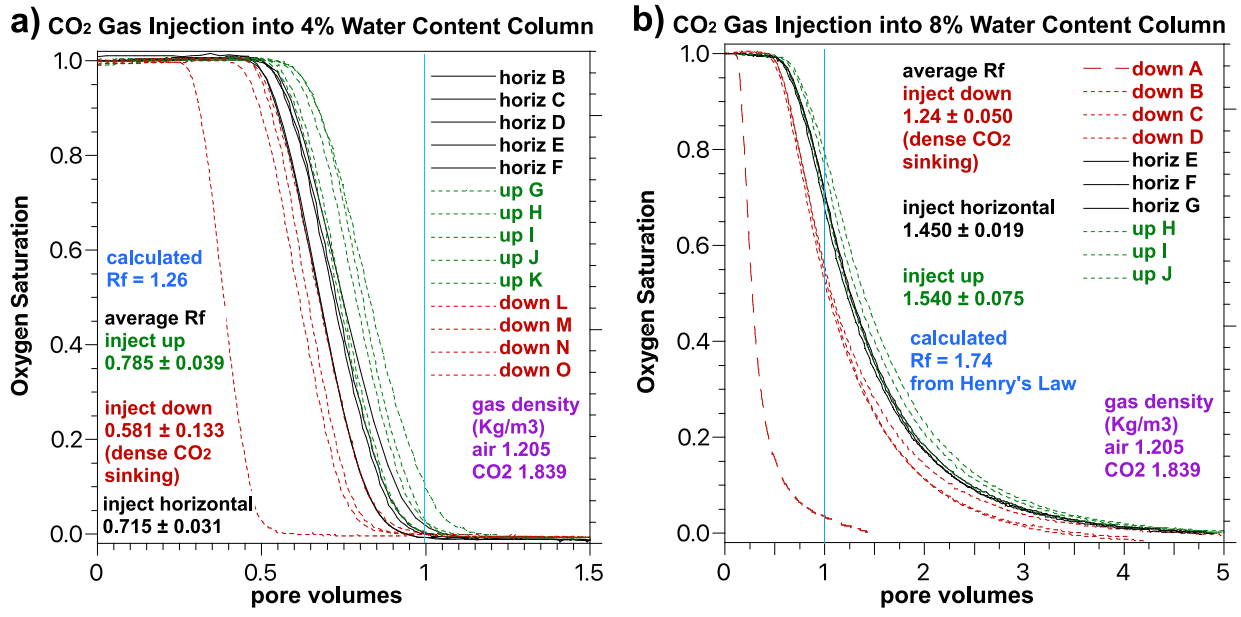

Figure D.11. CO_2 gas injection experiments in a 5-cm (2-in.) diameter by 79-cm (31.1-in.) length column packed with Hf sediment at (a) 4 wt% WC and (b) 8 wt% WC.

D.5 Summary of Performance of CO_2 Gas for Vadose Zone

This technology uses CO_2 gas injection into vadose zone sediments to increase pore water carbonate concentration and cause calcite to precipitate, which may incorporate I-129 (as iodate) and other CoCOIs. There is evidence that the CO_2 gas partitions into pore water from the decreasing pH measurements after CO_2 gas injections (PNNL-35432). However, there is no direct evidence that calcite precipitates. Inorganic carbon concentrations in sediments were measured before and after CO_2 gas treatment for the two sediments (Hf and 216-S-9). Results were inclusive as to whether the total inorganic carbon concentrations changed with treatment, likely due to the presence of high calcite in the sediment initially and the likelihood that only a small mass of calcite may have precipitated. C-14-labeled CO_2 gas could be used in future experiments under conditions that promote better calcite precipitation to confirm the mass of calcite that precipitates from this treatment. Slow calcite precipitation should also promote greater incorporation of contaminants. Earlier batch studies included a limited number of experiments with the addition of nitrate, silica, citrate, and Mg-sulfate, all of which should slow calcite precipitation (PNNL-35432, Section 4.3.3.3). Unfortunately, sequential extractions in untreated and treated samples showed no consistent change in the I-127 fractions in different phases.

Another effect of the CO_2 gas injection that can affect contaminant mobility is the advection of soil zone air that includes oxygen away from the injected area. In a previous study, an oxic Hf sediment (Environmental Restoration Disposal Facility pit, 40-ft depth) that was placed under anoxic conditions with N_2 gas slowly reduced and precipitated pertechnetate (Szecsody et al. 2014). Similarly, CO_2 gas treatment results in anaerobic sediment, and there may be slow abiotic/biotic reduction of contaminants such as pertechnetate, chromate, and uranium, so the change in pertechnetate mobility observed (described below) may not be influenced by precipitating calcite. Of these three CoCOIs, chromate should be most readily reduced. Batch experimental data, however, does not show any difference in chromate mobility with CO_2 treatment (Figure D.2j-l), so it appears unlikely that 60 days of CO_2 followed by 90 days of air treatment reduced any contaminants.

The purpose of experiments for this technology in this Phase 2/3 study was to quantify (1) the stability of the immobilized I-129 (or I-127 as iodate) and CoCOIs with > 50% mobility change threshold, (2) remobilization rates, and (3) mechanisms that control CO_2 gas advection in vadose zone sediments. Based on the 24 batch experiments and 9 columns conducted in Phase 2 (and batch experiments in Phase 1), I-127 mobility change with CO_2 gas treatment was inconsistent and at best was well below a 50% threshold to recommend further study. All batch and column sediments were at vadose zone WCs (4% to 8% g/g) for the 60 days of 100% CO_2 treatment, which was followed by 90 days of air treatment to neutralize pH and accelerate calcite precipitation.

Contaminant mobility change was measured by sequential extractions in batch experiments and by water-saturated or low water saturation leaching in columns. Batch experiments in two sediments at different WC showed 0% to 15% less I-127 mobility after CO_2 treatment. The Hf sediment in a water-saturated leach with a 6-hour residence time (after CO_2 gas treatment of 4 wt% WC sediment for 60 days) showed 12% less I-127 leached. For the 216-S-9 sediment under the same water-saturated leach conditions, experiments showed 6% to 14% less I-127 leached. Infiltration experiments with the 216-S-9 sediment at 82 wt% WC (and 6-hour residence time) showed 13% greater I-127 leaching compared to untreated sediment. Finally, in conditions most representative of leaching in the vadose zone, PUF infiltration experiments at 56 wt% WC and 41-hour residence time showed no difference in I-127 leaching with CO_2 treatment. Differences between batch and 1-D leach results of mobility change for I-127 and CoCOIs (Tc and U) highlight that while 1-D leach experiments take considerable additional effort, results are likely more accurate and reflect field conditions (and effect) due to similarities in (1) advection of water and contaminants through sediment and (2) high sediment-to-solution ratio.

Use of CO_2 gas for immobilization of CoCOI Tc-99 was more promising, as batch experiments showed a 3% to 35% decrease in mobility. In nine columns, CO_2 treatment of Hf and 216-S-9 sediments resulted in a weak to moderate (7% to 28%) decrease or an 8% increase in pertechnetate mobility in one case. For the Hf sediment water-saturated leach (6-hour residence time), 28% less Tc-99 leached compared to leaching in untreated sediment. For the 216-S-9 sediment water-saturated leach, 10% to 15% less Tc-99 leached from the CO_2 treatment. For the 216-S-9 sediment with an infiltration leach (82 wt% WC), 8% greater Tc-99 leached because of the CO_2 treatment. For the PUF infiltration experiments at 56 wt% WC and 41-hour residence time, 7% less Tc-99 leached because of the CO_2 treatment. As described earlier, because the CO_2/air did not treat chromate, it is unlikely that changes in Tc-99 mobility were caused by reduction because Tc-99 (as pertechnetate) required greater reducing conditions compared to chromate.

CO_2 gas did not sequester CoCOI U, even though U incorporates into calcite. Batch experiments with two sediments showed no change. In column leach studies, CO_2 treatment of Hf and 216-S-9 sediments resulted in an inconsistent 13% increase to 20% decrease in U mobility. For the Hf sediment water-saturated leach (6-hour residence time), 13% more U leached compared to leaching in untreated sediment. For the 216-S-9 sediment water-saturated leach, 6% to 8% less U leached because of the CO_2 treatment. For the 216-S-9 sediment with an infiltration leach (82 wt% WC), there was no difference in leaching because of the CO_2 treatment compared to untreated leaching. For the PUF infiltration experiments at 56 wt% WC and 41-hour residence time, 20% less U leached because of the CO_2 treatment. The lack of a decrease in U mobility (and likely no U incorporation into precipitating calcite) is consistent with the hypothesis that calcite precipitation likely was minimal under the CO_2 treatment conditions in this study.

CO_2 gas also did not sequester CoCOI Sr, although precipitation as Sr-carbonate can occur. Batch experiments with two sediments at two WCs showed 0% to 1.3% less Sr mobility with CO_2 treatment, which was significantly less than previous batch experiments in Phase 1 (PNNL-35432). Finally, the use of CO_2 gas for CoCOI Cr was weakly effective as batch experiments showed a 0.7% to 8.4% decrease in mobility.

In terms of mechanisms controlling CO_2 gas transport in vadose zone sediments, the gas/pore water partitioning is small (retardation of 1.26 at 4 wt% WC, 1.74 at 8 wt% WC), but the high density of the CO_2 gas relative to air causes significant density sinking. The density sinking effect could be controlled by CO_2 gas injections above a confining layer or using recirculation.

Appendix E – Gas-Phase Bioreduction: Ethane

E.1 Supplemental Methods

All experiments were conducted in duplicate using vadose zone sediments from 216-S-9 Crib (C9512, 120-ft depth). 216-S-9 Crib sediments have been characterized geochemically and microbially previously at depths of 19 to 20 m (62 to 65 ft) and 37 to 38 m (122 to 125 ft) (PNNL-26208), although core depths used in this study are also characterized herein (Section 2.1). The 216-S-9 background concentrations of NO_3^- and Cr were measured in both aqueous and solid phases. In batch experiments [core from 38.1 to 38.4 m (125.0 to 126.0 ft) below ground surface, bgs], the aqueous phase concentration of NO_3^- was determined to be 7.8 µg/g. For static columns [core from 38.4 to 38.7 m (126.0 to127.0 ft) bgs], the aqueous phase NO_3^- concentration was slightly lower, measuring 7.5 µg/g, likely due to small differences in Cr concentrations with depth. Pore water chromium was below the detection limit of 0.02 µg/g, while solid-phase chromium was measured at approximately 13.7 µg/g.

216-S-9 sediment was subsampled directly from bulk core material without sieving to maintain representative native microbiological populations. This technology is designed to use microbial processes with subsequent transformation of contaminants. To ensure the accuracy of results, all experiments were conducted using aseptic techniques and proper biological handling protocols to minimize external contamination and to preserve the integrity of the native microbial community. Additionally, a biological safety cabinet was used for all sample preparation for molecular analyses [quantitative polymerase chain reaction (qPCR) and sequencing] to ensure a controlled and contamination-free environment.

To quantify concentrations of aqueous (or pore water) NO_3^-, NO_2^-, and Cr (only in static column samples), a 2:1 sediment-to-water extraction was conducted (additional details in Appendix A, Section A.2.2). The filtered supernatant was analyzed for nitrate and nitrite using ion chromatography (details in Section A.1.1.3), whereas Cr was analyzed using an inductively coupled plasma optical emission spectrometer (ICP-OES) (Section A.1.1.2). To quantify solid phase Cr concentrations (static column samples), an acid extraction was performed using 8 M HNO_3 at a 1:3 sediment-to-liquid ratio (additional details in Appendix A, Extraction 5 in Section A.2.3) and samples were analyzed via ICP-OES (additional details in Appendix A, Section A.1.1.2).

Ammonium (NH_4^+) concentrations were quantified via UV-vis methods (Section A.1.1.7) following either the ultrapure water extraction (at timepoint 0) or a similar extraction (1:1 water-to-sediment extraction with 1 M $CaCl_2$ for all other timepoints). Water content (WC) and pH were measured on sub-samples (details in Sections A.1.2.1 and A.1.2.2, respectively). Microbial DNA was extracted from sediment (details in Appendix C, Section C.1.1) at each timepoint. Results are presented in Section E.3.

The WCs for the batch and static columns were planned to be at 4 wt% and 8 wt%. However, WC was measured on subsamples (Section A.1.2.1), and initial concentrations were found to be lower than expected. To address concerns regarding microbial survival in drier conditions over extended periods, water levels were increased by adding anoxic water to each vial to increase WC to desired levels. The sterile anoxic water was prepared by boiling approximately 30 mL of filtered (0.2-µm-diameter pore) ultrapure water for 10 minutes with subsequent cooling while purging and sparging with N_2 gas until the water cooled to room temperature. Samples were then placed inside a Coy anaerobic chamber (approximately 2% H_2, 98% N_2, O_2 < 20 mg/L), where sparged water was added using a hypodermic needle through a rubber septum. WCs were re-measured at final timepoints to ensure that water was not evaporating from the sealed system. While the addition of water during the experiment to correct WC prevents direct comparison to initial measurements, the final timepoints indicate WC is consistent with targeted levels.

Statistical analysis was conducted to compare the effects of N_2 gas with and without ethane for nitrate reduction. This analysis was performed to determine if the observed differences between treatments were significant or due to random variability. A one-way analysis of variance (ANOVA) was performed on the percent nitrate (mMol/L) in each experimental sample and grouped based on time point, starting NO_3^- concentration, and the presence or absence of Cr. A Tukey's honest significant difference (HSD) *post hoc* test was then applied to identify pairwise differences between the treatment conditions. All analyses were conducted in RStudio using the dplyr, broom, and base stats packages. Results are presented in Section E.5.

E.1.1 Objective 1: Quantify NO_3^- Transformation via Treatment with Ethane Gas without Cr

216-S-9 sediment was spiked with water with or without NO_3^- at concentrations of 100, 1,000, or 10,000 µg/g (NO_3^- added as sodium nitrate) in individual sterile bottles. The spiked sediment was thoroughly mixed and then allowed to dry until reaching a final WC of either 4 or 8 wt%. Subsequently, 10 g of sediment from each condition (or specific nitrate concentration at the various WC levels) was transferred into sterile 10-mL serum vials and sealed using butyl rubber septa and aluminum crimp top seals. Vials were purged with N_2 gas for 3 to 5 minutes to generate anaerobic conditions. Supplemental gas was added with sterile 3-mL syringes equipped with 23-gauge, 2.54-cm (1-in.) length needles that had been degassed with N_2. Three milliliters of headspace gas was removed from each vial, then either 3 mL of 100% ethane gas (Sigma) was withdrawn from the septum of an airtight foil gas bag (Supelco) or 3 mL of N_2 gas was immediately injected into the vial headspace, resulting in a gas composition of > 24% ethane and < 76% N_2 at atmospheric pressure.

Vials were stored at room temperature in the dark until sampling, which occurred at 0, 55, 97, 147, and 195 days. Each vial received a spike of either 3 mL of ethane or 3 mL of N_2 gas after 3 mL of headspace was removed (to maintain atmospheric pressure) during every sampling event.

E.1.2 Objective 2: Quantify NO_3^- Transformation via Treatment with Ethane Gas with Cr

216-S-9 sediment [38.4 to 38.7 m (126 to 127 ft) bgs] was spiked with 100 µg/g NO_3^- (added as sodium nitrate) and 1.6 µg/g Cr (added as hexavalent chromium, CrO_4^-) in individual sterile bottles. The spiked sediment was thoroughly mixed and then allowed to dry until reaching a final WC of either 4 or 8 wt%. Subsequently, 10 g of sediment from each condition was transferred into sterile 11-mL serum vials and sealed. Vials were purged with N_2 gas for 3 to 5 minutes to create anaerobic conditions. Supplemental gas was added with sterile 3-mL syringe equipped with a 23-gauge, 5.1-cm (2-in.) needle that had been degassed with N_2. A total of 1.5 mL of headspace gas was removed from each vial, then either 1.5 mL of 100% ethane gas (Sigma) was withdrawn from the septum of an airtight foil gas bag (Supelco) or 1.5 mL of N_2 gas was immediately injected into the vial headspace, resulting in a gas composition of > 41% ethane and < 59% N_2 at atmospheric pressure. After the gas injection, vials were gently tapped on the bench to compress the sediment, simulating the natural packing process in the subsurface.

Vials were stored at room temperature in the dark with sampling occurring at 0, 59, and 129 days. Each vial received a spike of either 3 mL of ethane or 3 mL of N_2 gas after 3 mL of headspace was removed (to maintain atmospheric pressure) following every sampling event. The treatment increased gas composition to > 82% ethane and < 18% N_2 at atmospheric pressure, though actual concentrations depended on consumption of ethane over time.

E.2 Variably Saturated Static Column Results for Chromium

Results show reduction of chromium as a co-contaminant with N_2 gas or ethane gas, presenting data on total aqueous chromium, aqueous chromate (provided For Information Only, FIO), and solid-phase chromium reduction rates. All errors are reported as one standard deviation.

The reduction of aqueous total chromium and chromate concentrations exhibited similar trends over time for both ethane gas and nitrogen gas treatments (Figure E.1). At 4 wt% WC, chromium concentrations decreased from approximately 1.8 to 0.5 µg/g in both treatments. At 8 wt% WC, aqueous chromium concentrations decreased from approximately 1.7 to 0.7 µg/g with ethane gas and to 0.5 µg/g with N_2 gas, demonstrating insignificant performance between the two gases across water conditions.

Total solid-phase chromium was measured over 129 days for all treatments. Minor fluctuations were observed between ethane gas and N_2 gas, with variations of approximately ±1.5 µg/g over time. This could be due to natural heterogeneity in sediments, variability during sampling, and/or geochemical changes over time, such as pH. Note that the acid extraction is not a total dissolution of sediments; therefore, some Cr may not have been recovered.

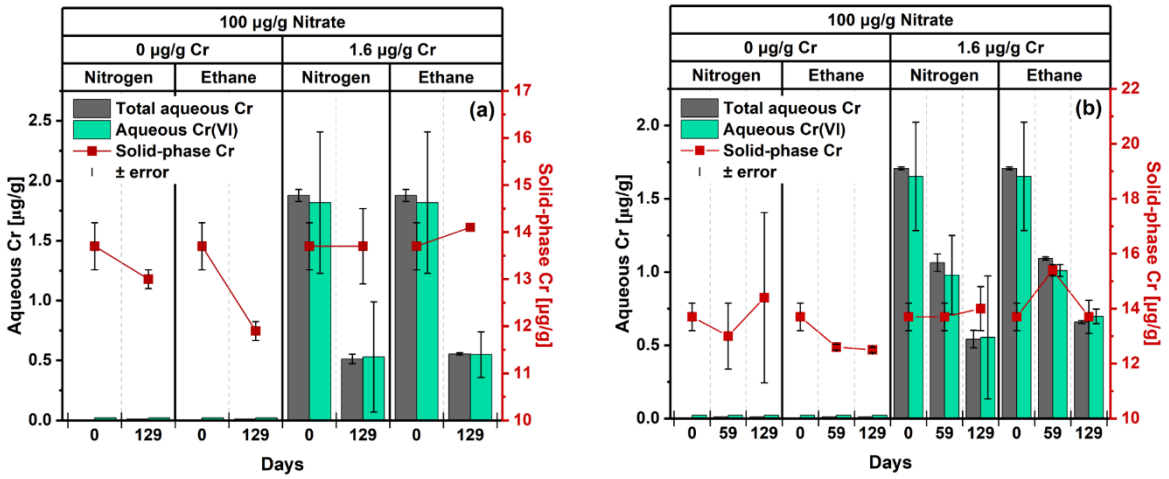

Figure E.1. Total aqueous chromium and chromate (FIO) (primary y-axis indicates concentration in µg/g) and solid phase chromium (secondary y-axis indicates concentration in µg/g) at various timepoints in (a) 4 wt% and (b) 8 wt% WC in 216-S-9 sediments with N_2 gas with and without ethane gas. The 0 µg/g (added Cr) samples are used as a control and show background Cr in solid phase. All errors are reported as one standard deviation.

First-order kinetic rates were calculated using total aqueous chromium concentration changes over time (Table E.1). Columns conducted under 4% WC only had two timepoint samples, and therefore there is no error between the regression line and the actual values. Results show that chromium reduction rates (per day) are slightly higher at 4 wt% compared to 8 wt% WC. However, reduction rates are similar between the two gas treatments, with N_2 gas yielding slightly higher rates. These data show the addition of ethane gas does not enhance chromium reduction in the absence of oxygen (N_2 gas atmosphere). Instead, reduction will continue under anoxic conditions, with the potential for reduction slightly decreasing at lower WC conditions – though the small number of data points makes statistical comparison challenging. Depending on the extent of microbially generated reducing conditions, this reduction may not occur when oxygen (from air) is present.

Table E.1. First-order chromium removal rate constant in the 216-S-9 sediment in static columns with N_2 gas with or without ethane gas.

Water Content (wt%)	Added Nitrate Concentration (µg/g)	Added Cr Concentration (µg/g)	Gas Treatment	Rate Constant (k) (day^{-1})	R^2
4	100	1.6	Nitrogen	0.0101	-
4	100	1.6	Ethane	0.0095	-
8	100	1.6	Nitrogen	0.0090	0.995
8	100	1.6	Ethane	0.0074	0.999

E.3 Quantitative Polymerase Chain Reaction (qPCR) Results

216-S-9 sediment cores exhibited low biomass in the initial material, which was further reduced under experimental conditions and upon the addition of NO_3^-. Biomass calculations based on qPCR results indicate low bacterial biomass across all WCs and treatments of 216-S-9 sediment for both the batch and column experiments. Although the presence of bacterial DNA was confirmed in each sample (Figure E.2), many values fell below the detection limit (48.3 gene copies per sample) for the universal bacteria primers (Appendix C, Table C.1) and amplification conditions used. Archaeal DNA may be present in some samples; however, limited replication and low copy numbers led to inconclusive results that require further investigation.

Despite the successful development of standard curves, targets for *nirS*, *nirK*, and n*arG* were not detected. In contrast, analysis for *napA* suggests that low biomass may be present in some of the initial core materials and possibly within the experimental samples. The lack of replication highlights the need for further investigation to determine the potential presence of *napA*, a gene crucial for converting nitrate to nitrite under anaerobic conditions. Sequencing attempts support the qPCR data, revealing insufficient DNA for sequencing despite multiple efforts at polymerase chain reaction amplification.

It seems likely that the low starting biomass combined with the extreme conditions, specifically low water availability and high levels of NO_3^-, created an environment too challenging for microorganisms to proliferate. Sequencing results from the liquid-phase bioreduction experiments (Appendix K, Section K.4.6) demonstrated that the addition of simulated groundwater, even without a carbon source, significantly impacted microbial communities and increased biodiversity.

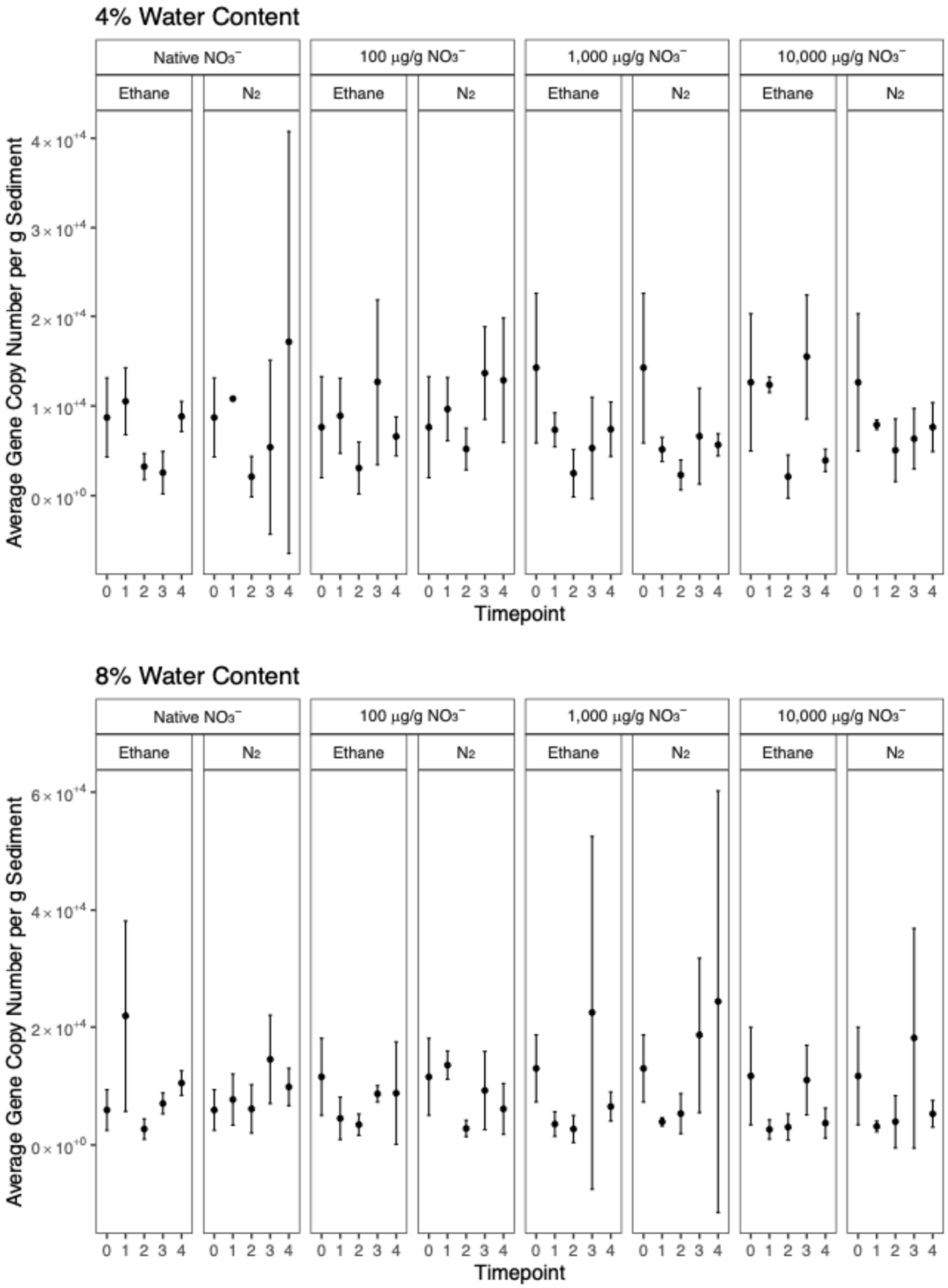

Figure E.2. Average gene copy per gram for total bacteria across treatments and timepoints for 4 wt% (top) and 8 wt% (bottom) WC for batch experiments. Column experiments (not pictured) showed similar results with low biomass across samples and treatments. These data are FIO.

E.4 pH Monitoring Results

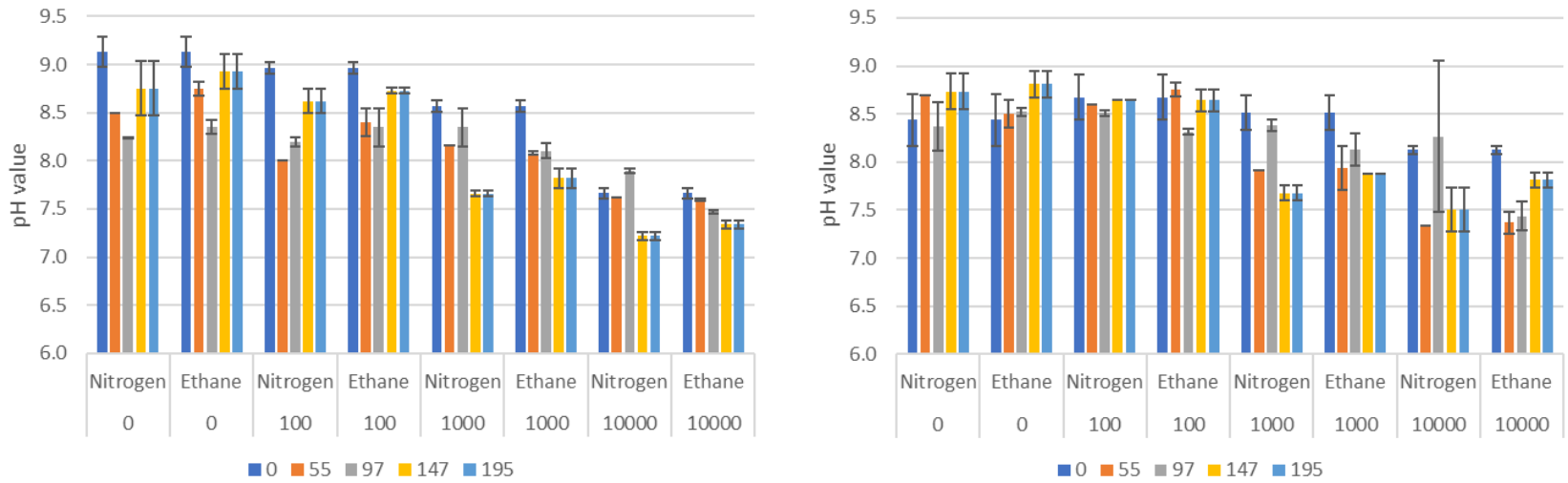

Figure E.3. pH in water extracts from batch experiments without Cr over 195 days at 4 wt% WC (*left*) and 8 wt% WC (*right*). Starting concentrations of nitrate ranged from background (7.8 µg/g) to 10,000 µg/g nitrate.

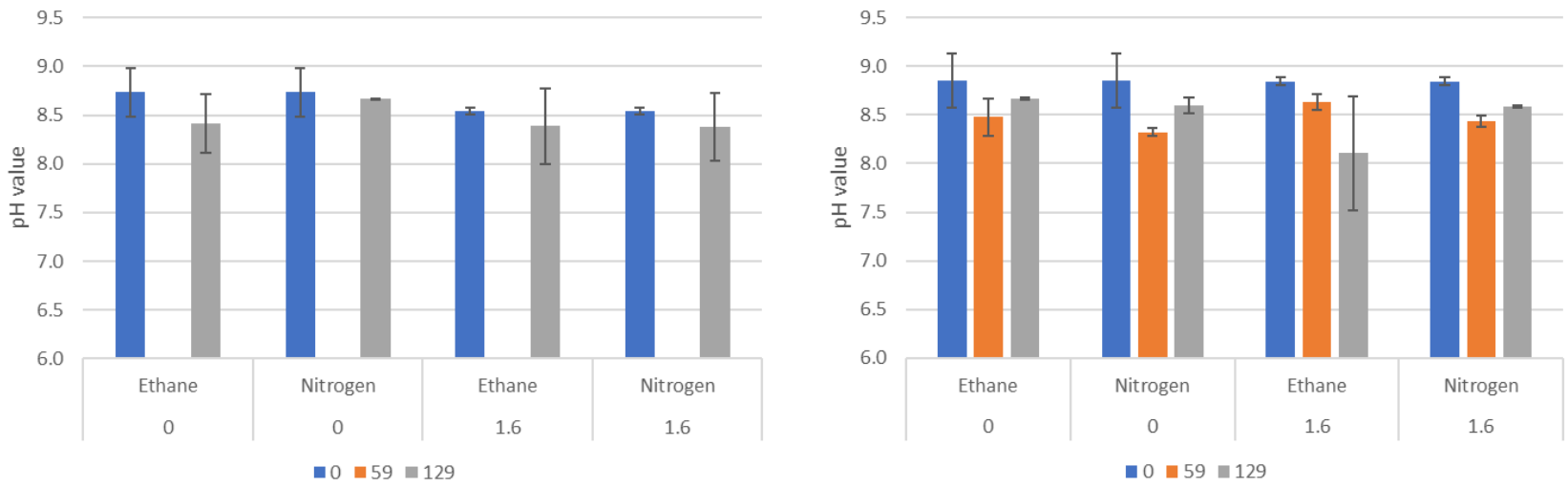

Figure E.4.pH in water extracts from static columns (100 µg/g nitrate) with Cr (0-1.6 µg/g) over 129 days at 4 wt% WC (left) and 8 wt% WC (right).

E.5 pH Monitoring Results

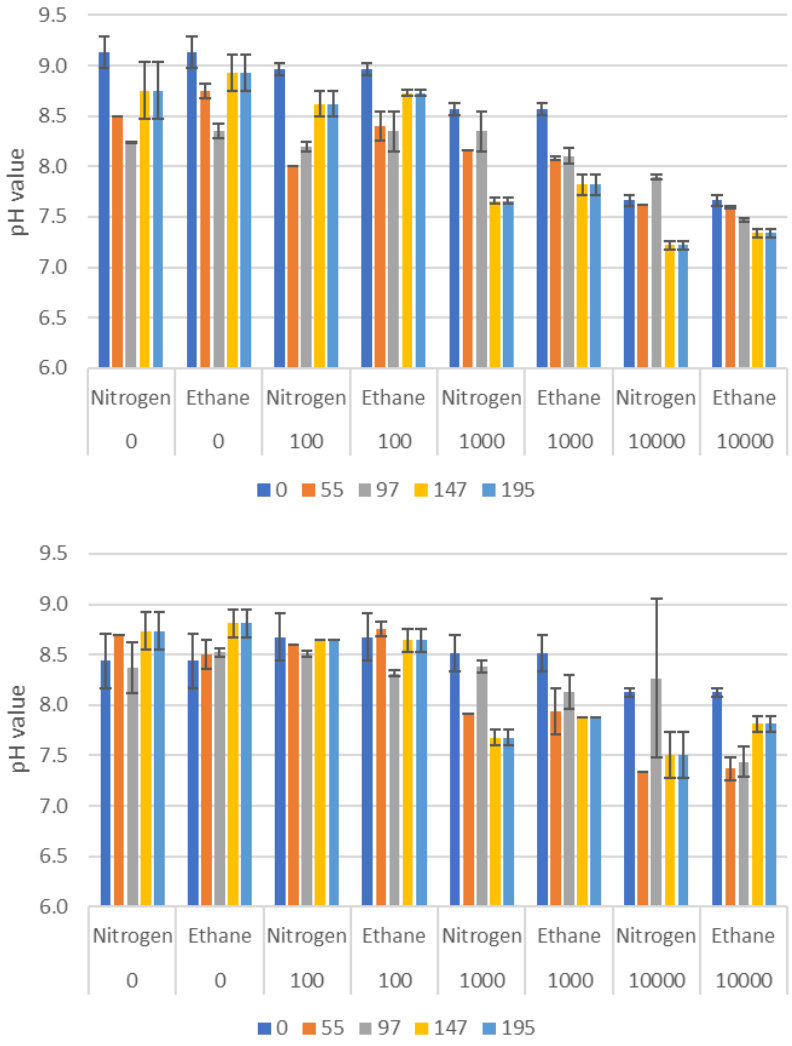

Figure E.3. pH in water extracts from batch experiments without Cr over 195 days at 4 wt% WC (*left*) and 8 wt% WC (*right*). Starting concentrations of nitrate ranged from background (7.8 µg/g) to 10,000 µg/g nitrate.

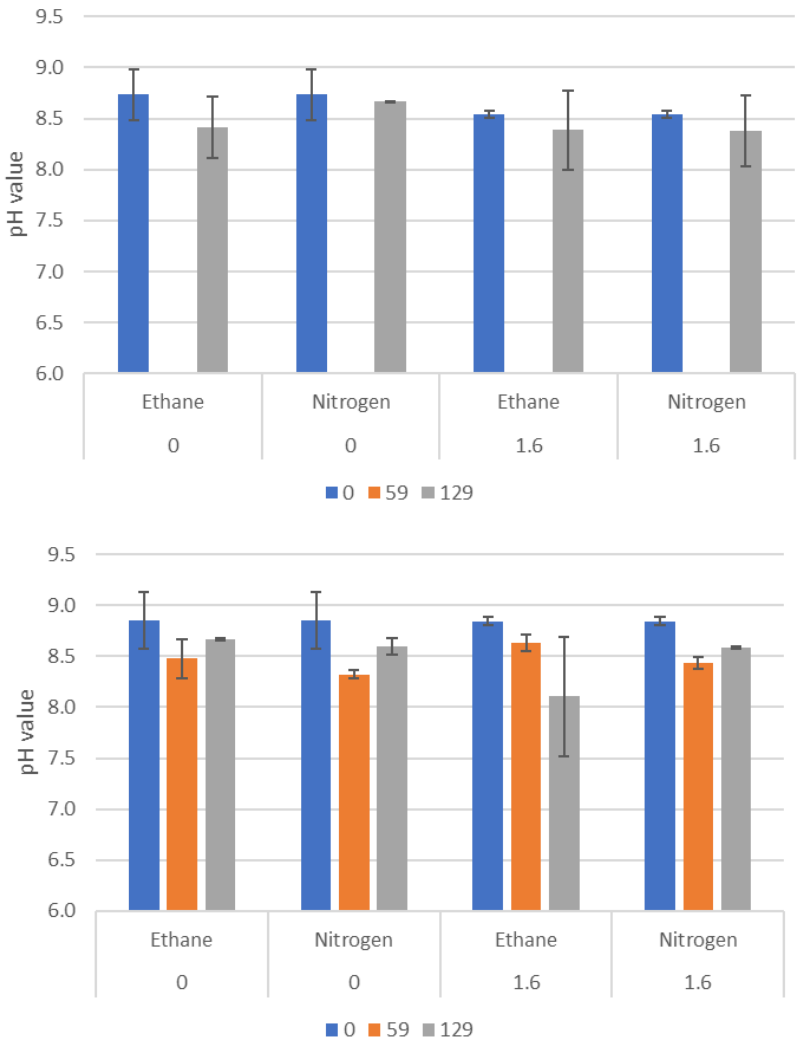

Figure E.4. pH in water extracts from static columns (100 µg/g nitrate) with Cr (0-1.6 µg/g) over 129 days at 4 wt% WC (left) and 8 wt% WC (right).

Appendix F – Particulate-Phase Sequestration: Tin Apatite

The purpose of this task is the sequestration of U and Tc-99 (primary contaminants of interest, PCOIs) in the presence of I-129 as iodate, nitrate, Cr, and Sr (co-contaminants of interest, CoCOIs) in water-saturated zones using particulate Sn(II) apatite [Sn(II)-PO_4]. This amendment functions as a strong reductant to reduce then precipitate Tc, U, and other contaminants. Additionally, the Sn(II)-PO_4 may be able to coat precipitated contaminants, creating a barrier to slow or prevent reoxidation over time.

This task is targeting direct treatment of contamination in perched water beneath the B Complex and/or via formation of a permeable reactive barrier in groundwater under BY Cribs as the primary treatment zones. Potential secondary treatment zones include 216-U-1 and -2, S-SX tanks, S and T Cribs, C tanks, and BC Cribs. The specific objectives of this technology are as follows:

1. Quantify Tc-99 and U immobilization and order of magnitude removal rate in various combinations: (1) with/without sediment, (2) with/without delivery fluid and (3) with/without co-contaminants [described in the Phase 1 report (PNNL-35432)].
2. Determine the immobilization rates for U and Tc-99 with/without co-contaminants for (1) B Complex perched water and (2) BY Crib application (in groundwater).
3. Quantify the longevity of U and Tc-99 with/without co-contaminants for (1) B Complex perched water and (2) BY Crib application.

Objectives 2 and 3 were tested in 1-D leach columns as described in Sections F.3.2 and F.3.1 for B Complex perched water conditions and BY Cribs groundwater conditions, respectively.

F.1 Supplemental Methods

Sn(II)-PO_4 particles were synthesized following the procedure described previously (LAB-RPT-12-00001), including alternative steps as outlined in PNNL-26730; this process is fully described in Appendix E, Section E.1, of the Phase 1 report (PNNL-35432). The Sn(II)-PO_4 was stored in an anaerobic chamber and was ground to a powder prior to use.

F.1.1 Saturated Column Testing for BY Cribs Groundwater Conditions

Experiments targeted the BY Cribs groundwater table within the Central Plateau. Columns were conducted as described in Section 2.4.2 with the exception of mixing the particulate amendment into the sediment prior to packing the columns, targeting 0.5 wt% Sn(II)-PO_4. The column study was conducted in two replicate treatments (Treatment-A and Treatment-B) and included a control column containing sediment but no Sn(II)-PO_4 (Control-C). A second set of column experiments were conducted following the same protocol, but this time the influent solution included co-contaminants (iodine, Cr, Sr, and NO_3). Treatment-D and Treatment-E contained Sn(II)-PO_4 while Control-F did not.

F.1.2 Saturated Column Testing for Perched Water Conditions

Columns used to represent a perched water scenario were prepared with contaminants mixed directly into the sediment prior to packing the columns as described in Section 2.4.1. Treatment-G and Treatment-H included 0.5 wt% Sn(II)-PO_4, while Control-I contained the contaminated sediment without Sn(II)-PO_4. These columns did not include a loading phase but were run similarly to the BY Cribs columns beginning at the leaching phase. The control for these columns was shared by the liquid phase chemical sequestration technology and is presented in Appendix I.

An additional set of perched water columns was prepared using 2-cm (0.8-in.) diameter by 60-cm (23.6-in.) length PVC columns, packed with perching zone sand (PZsd) sediment containing 0.5 wt% Sn(II)-PO_4. The columns were saturated with synthetic perched water (SPW), then plugged to prevent flow. At predetermined sampling times, fractions of the fluid were collected by injecting a known amount of solution equivalent to a fraction of a pore volume (PV) into one end of the horizontal column and collecting effluent from the other end. The intent was to collect a single PV from the column over time with each fraction of a PV representing a different fluid residence time up to hundreds of hours as each fraction of volume moves across the column in a plug-flow-type pattern. Then, the release of contaminants from sediments over time was measured and kinetic release rates were calculated. After the last sample was collected, the column was split into five sections, with each section being 10 to 14 cm (4 to 5.5 in.) long, in an anaerobic chamber, and sequential extractions (as described in Appendix A, Section A.2.4) were conducted on three of the five sections, representing the influent end, effluent end, and middle of the column.

To compare this method with static columns (or high solid:solution batch studies), a similar experiment was set up in batch conditions using 15 g of perched water sediment mixed with 0.5 wt% Sn(II)-PO_4 and 3 mL of SPW. Duplicate samples were sacrificed for sequential extractions at 5, 28, and 300 days.

F.2 Long-Term Experiments

F.2.1 Plug Flow Columns for Perched Water Conditions

Within the 1 to 1.5 PV test, the control column reached complete breakthrough for Tc-99 while the treated columns retained all of the Tc-99 (Figure F.1). In post-experiment sequential extractions, treated columns (“K” and “L”) showed a significantly higher fraction of Tc-99 in the harder-to-extract phases than the control (“J”) (0.9 in treated columns vs. 0.4 in the control column, Figure F.1).

Approximately 30% of the U was released during the leaching of treated columns, while 60% to 70% of the U was leached out from the control column (Figure F.1). In post-experiment sequential extractions, U retention in hard-to-extract phases was fairly similar between the treated columns and the control (fractions of 0.7 to 0.9), but more of the U from the treated columns was found in the 8M HNO_3 extraction than in the control columns, where more of the U was recovered from the slightly more mobile carbonate phase (Figure F.3). Due to difficulties with flushing the outlet after each sampling and carefully controlling flow to minimize mixing within the column between sample collections, the total recovery for Tc-99 and U was variable, ranging from 0.2 to 0.7 (Figure F.2 and Figure F.3). To improve the data obtained from these long columns, static column (or high solid-to-solution ratio batch experiments) were conducted.

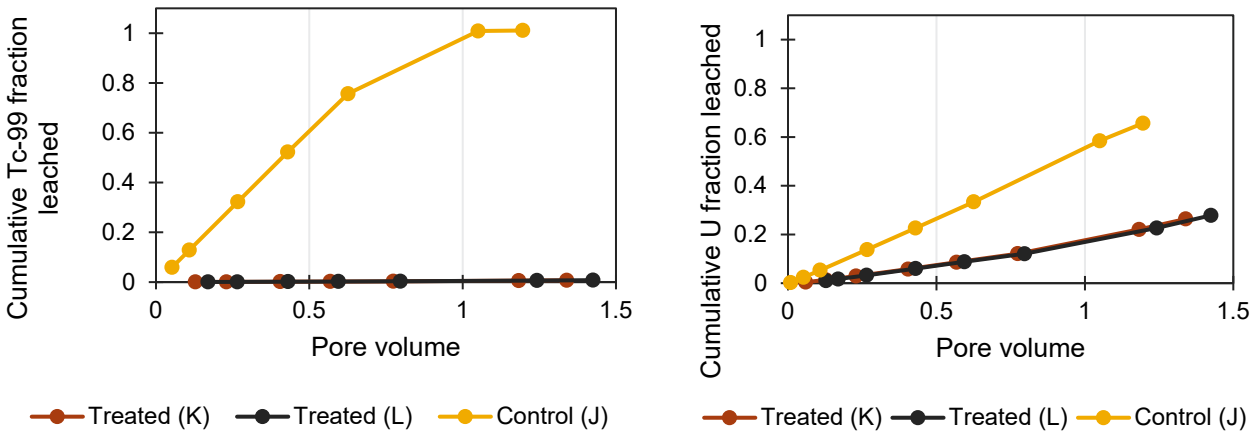

Figure F.1. Cumulative fraction leached for Tc-99 (*left*) and U (*right*) for long columns treated with Sn(II)-PO_4 ("K" and "L" and control column "J").

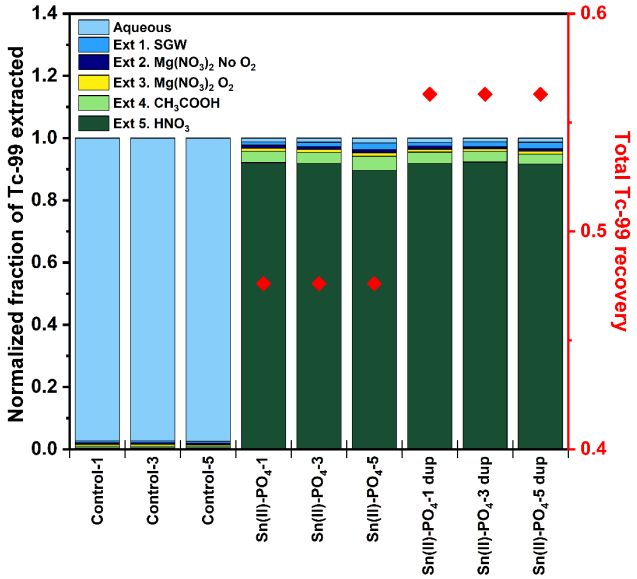

Figure F.2. Change in Tc-99 sequestration from Sn(II)-PO_4 treatment of contaminant-spiked PZsd sediment in synthetic groundwater (SGW) reacted with Sn(II)-PO_4 via sequential extractions after 672 hours compared to controls without treatment. Note: The figure shows the normalized recovery across each extraction in stacked bars and total fraction recovered in each sample in red diamonds. PW-J was the control; PW-K and PW-L were treated with Sn(II)-PO_4. The number in each sample name indicates the section, with 1 being the inlet, 3 being the middle, and 5 being the outlet.

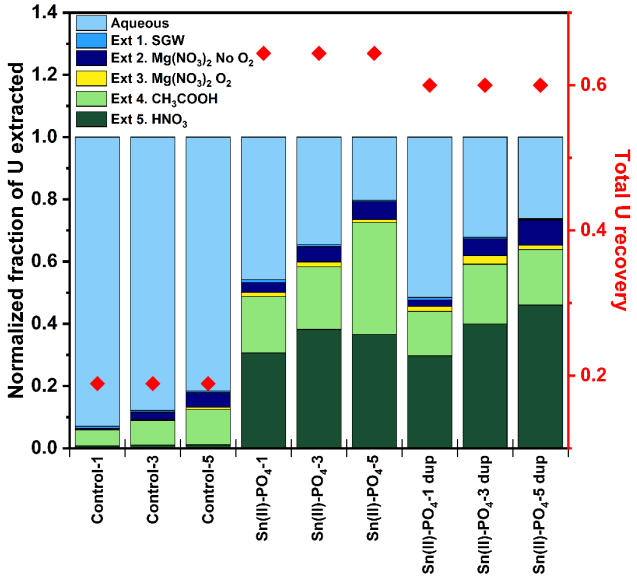

Figure F.3. Change in U sequestration from Sn(II)-PO_4 treatment of contaminant-spiked PZsd sediment in SGW reacted with Sn(II)-PO_4 via sequential extractions after 672 hours compared to controls without treatment. Note: The figure shows the normalized recovery across each extraction in stacked bars and total fraction recovered in each sample in red diamonds. PW-J was the control; PW-K and PW-L were treated with Sn(II)-PO_4. The number in each sample name indicates the section, with 1 being the inlet, 3 being the middle, and 5 being the outlet.

F.2.2 Long-Term Batch Experiments

Results of the long-term batch tests demonstrated immobilization of nearly all Tc-99 in the presence of Sn(II)-PO_4, with > 90% Tc-99 retained in hard-to-extract phases by 5 days. Tests were exposed to air after 28 days, and by 300 days still retained most or all of the Tc-99 (Figure F.4). Controls showed significantly lower (< 30%) immobilization of Tc. Similar to long-term columns, U mobility was similar with and without treatment based on pore water analysis. However, some differences were observed with sequential extractions. More U was extracted in the hardest-to-mobilize fraction (8 M HNO_3) with Sn(II)-PO_4, while most of the U immobilized in the control tests was extracted during the acetic acid extraction (targeting carbonate phases) (Figure F.5).

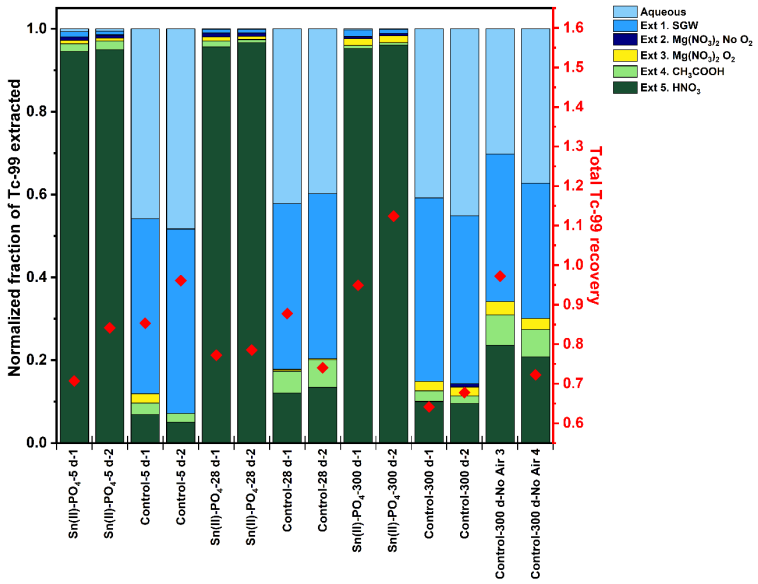

Figure F.4. Change in Tc-99 sequestration from Sn(II)-PO_4 treatment of contaminant-spiked PZsd sediment in SGW reacted with Sn(II)-PO_4 via sequential extractions after 300 days compared to controls without treatment. Note: The figure shows the normalized recovery across each extraction in stacked bars and total fraction recovered in each sample in red diamonds.

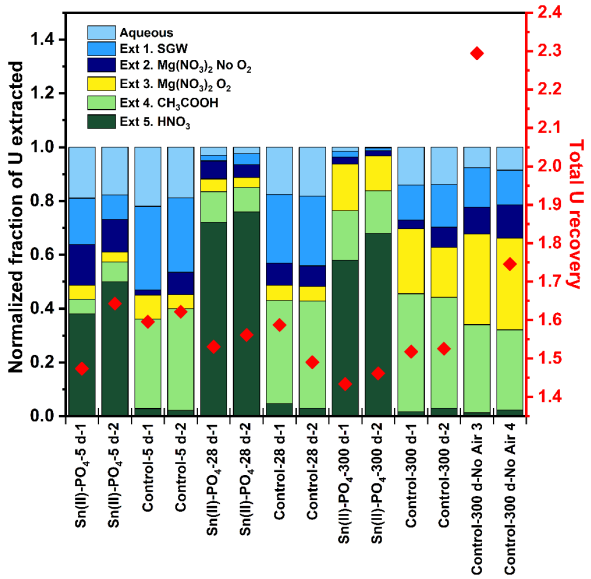

Figure F.5. Change in U sequestration from Sn(II)-PO_4 treatment of contaminant-spiked PZsd sediment in SGW reacted with Sn(II)-PO_4 via sequential extractions after 300 days compared to controls without treatment. Note: The figure shows the normalized recovery across each extraction in stacked bars and total fraction recovered in each sample in red diamonds.

F.3 Saturated Column Results for Tc-99 and U

F.3.1 BY Cribs Groundwater Conditions

For Cold Creek Unit gravel (CCug) columns containing Sn(II)-PO_4 (Treated – A and Treated – B), Tc-99 loading in the columns increased steadily over the first 200 PVs. At 200 PVs, the influent solution was switched to SGW (i.e., leaching phase), during which little or no Tc-99 was released from the Sn(II)-PO_4-treated sediments (Figure F.6). In the associated control, however, Tc-99 uptake was minimal, and Tc-99 was released relatively quickly after switching to the leaching phase. Based on these results, Sn(II)-PO_4 was able to immobilize (i.e., accumulate) almost 3.5 µg of Tc-99 per g of solid [sediment + Sn(II)-PO_4] (Table F.1). However, more could likely be immobilized under these conditions, as the limit of Tc-99 removal was not reached in these experiments, and the subsequent oxidized leach step was not sufficient to re-mobilize the Tc-99 (Figure F.6). Stop flow events had little effect on the rate of uptake or removal for treated columns (Figure F.10), indicating that reactions between the Sn(II)-PO_4 are kinetically fast and stable.

When CoCOIs were added to the system, little to no Tc-99 was immobilized by the Sn(II)-PO_4 (Figure F.6 and Table F.1) and any remaining Tc-99 was released during the leaching step. The high concentration of Cr (a CoCOI) may have led to a large decrease in the Sn(II)-PO_4 reductive capacity, which would decrease Tc-99 (as pertechnetate) reduction and immobilization. The release rate of Tc-99 during flow (i.e., before each stop flow event) increased over time in all columns that contained CoCOIs, but the release rate was stable during each of the stop flows (Figure F.10).

The post-experiment 8 M HNO_3 extractions showed higher Tc-99 concentrations in the influent end of the Sn(II)-PO_4-treated columns, with little Tc-99 present at the effluent end (Figure F.8). These results complement the effluent data that demonstrated that the Sn(II)-PO_4 was not fully depleted; as the Tc-99 was pulled out of solution early in the column, there was less Tc-99 present toward the effluent end. This spatial distribution also suggests that Tc-99 was quickly removed from solution by the Sn(II)-PO_4, as it was precipitated mainly near the column inlet.

For U, the treated columns immobilized roughly 14 µg of U per g of solid [sediment + Sn(II)-PO_4] (Table F.2). In the leaching step, some of that U was remobilized (~42%), indicating a different retention mechanism for U as compared to Tc-99 (Figure F.7). During the first stop flow event, uptake for PCOI-only treated columns increased while release rate increased in the control columns (Figure F.11). In subsequent stop flow events (Stop Flows 2 and 3), the release rate of U decreased in all columns compared to the previous stop flow, with the highest rate observed in the control columns, followed by the treated PCOI + CoCOI columns and then the treated PCOI-only columns (Figure F.11).

U immobilization was significantly reduced in the presence of CoCOIs (Figure F.7 and Table F.2). During the leaching step, U was released; performance of the treated columns and control columns was nearly identical (Figure F.7 and Table F.2). U reduction by the Sn(II)-PO_4 would have been reduced, but U was also held by Sn(II)-PO_4 by strong sorption to the apatite surface. In the high ionic strength solution with CoCOIs, this U adsorption likely decreased.

In the post-column extractions, U distribution was uniform across the sections of the treated columns, suggesting the U uptake rate was uniform (Figure F.9).

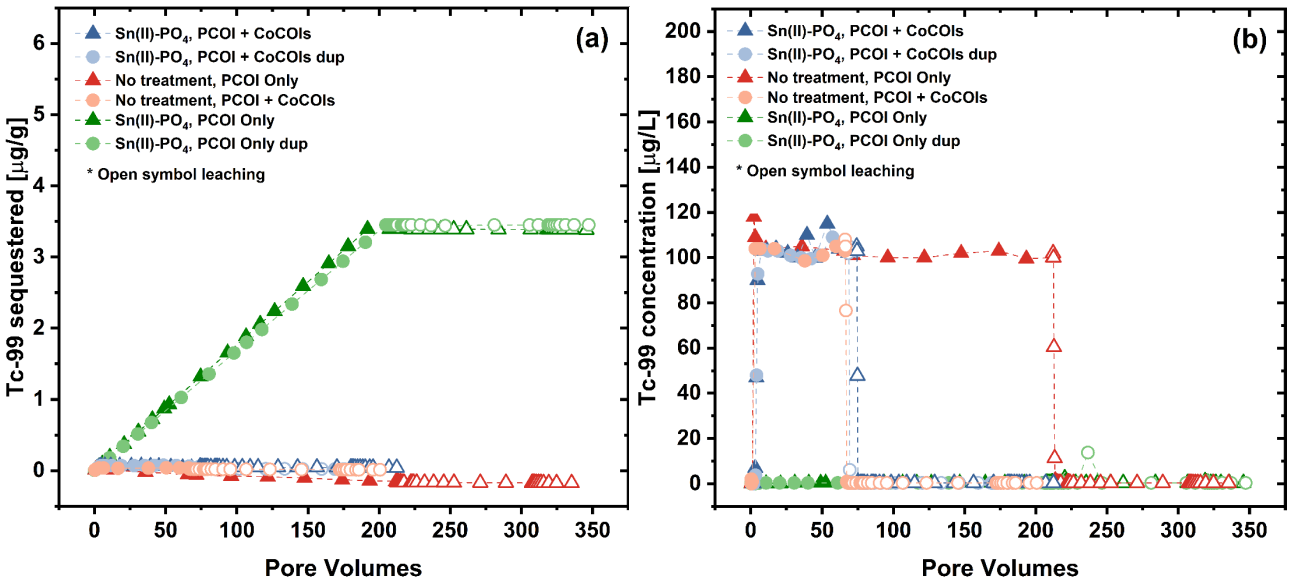

Figure F.6. Tc during loading and leaching with CCug sediment with and without Sn(II)-PO_4 treatment: (a) accumulation of Tc-99 (in µg/g) and (b) aqueous concentrations of Tc-99 (in µg/L). Note: "Dup" stands for duplicate. Filled symbols indicate loading phase while open symbols represent the leaching phase with SGW.

Table F.1. Tc estimated retention after loading and leaching in CCug sediments without and with treatment [Sn(II)-PO_4] after equilibrium of amendments for approximately 6 weeks in the absence of oxygen.

Conditions	Loading (µg/g)	Leaching (µg/g)
No treatment, PCOIs	0[(a)]	0[(a)]
No treatment, PCOIs + CoCOIs	0.04	0.01
Sn(II)-PO_4, PCOIs	3.39	3.38
Sn(II)-PO_4, PCOIs, dup	3.45	3.45
Sn(II)-PO_4, PCOIs + CoCOIs	0.04	0.02
Sn(II)-PO_4, PCOIs + CoCOIs, dup	0.06	0.04

(a) Negative values are reported as "0."

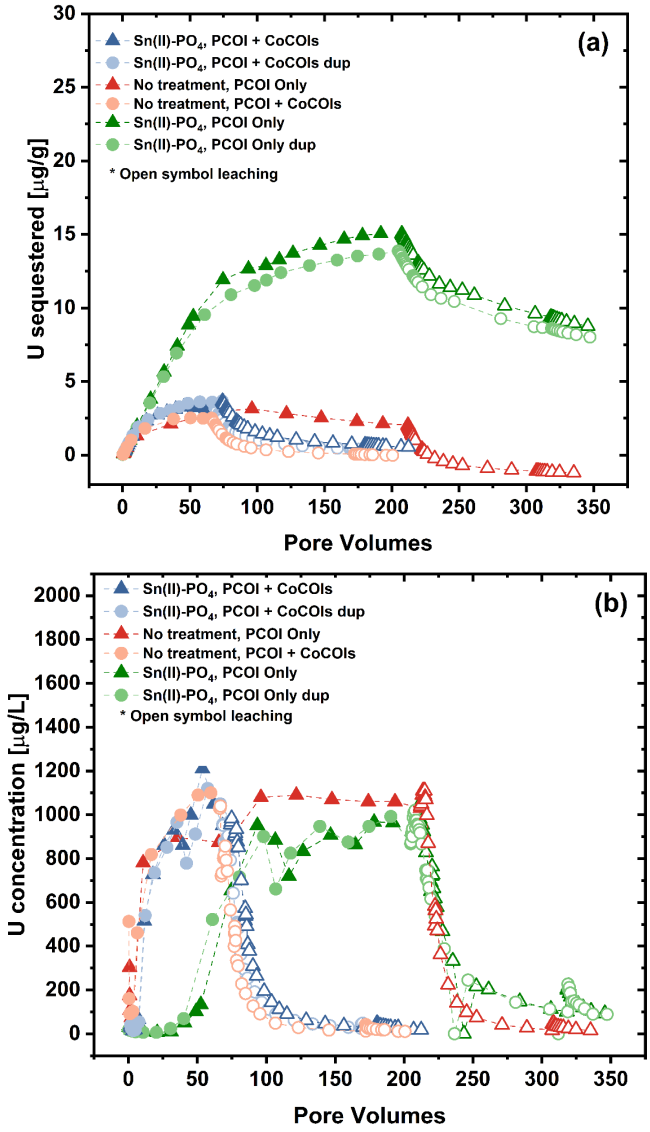

Figure F.7. U during loading and leaching with CCug sediment with and without Sn(II)-PO_4 treatment: (a) accumulation of U (in µg/g) and (b) aqueous concentrations of U (in µg/L). Note: "Dup" stands for duplicate. Filled symbols indicate loading phase while open symbols represent the leaching phase with SGW.

Table F.2. U estimated retention after loading and leaching in CCug sediments without and with Sn(II)-PO_4.

Conditions	Loading (µg/g)	Leaching (µg/g)
No treatment, PCOIs	4.92	1.68
No treatment, PCOIs + CoCOIs	5.39	2.86
Sn(II)-PO_4, PCOIs	17.9	11.6
Sn(II)-PO_4, PCOIs, dup	16.8	10.9
Sn(II)-PO_4, PCOIs + CoCOIs	6.12	3.25
Sn(II)-PO_4, PCOIs + CoCOIs, dup	6.57	3.43

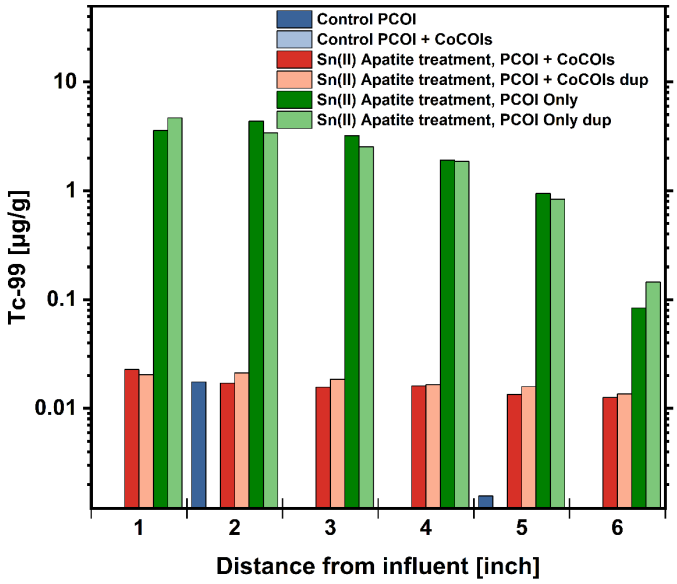

Figure F.8. Tc distribution (in µg/g) across columns with CCug sediment with and without Sn(II)-PO_4 based on 8 M HNO_3 extractions. Note: "Dup" stands for duplicate.

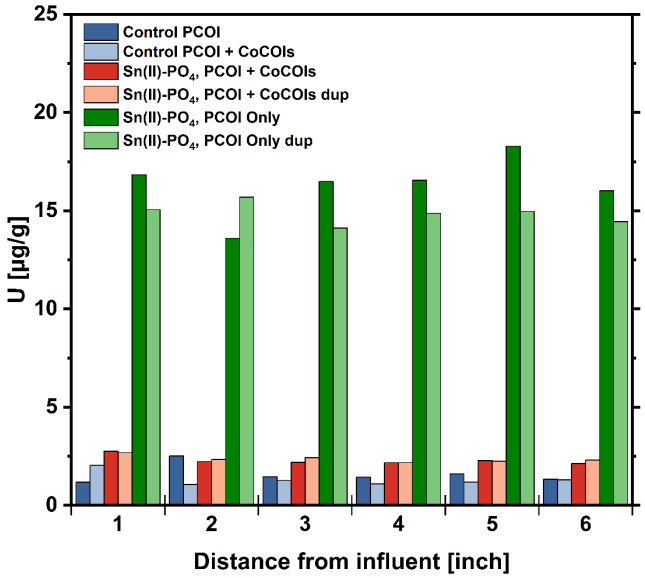

Figure F.9. U distribution (in µg/g) across columns with CCug sediment with and without Sn(II)-PO_4 based on 8 M HNO_3 extractions. Note: "Dup" stands for duplicate.

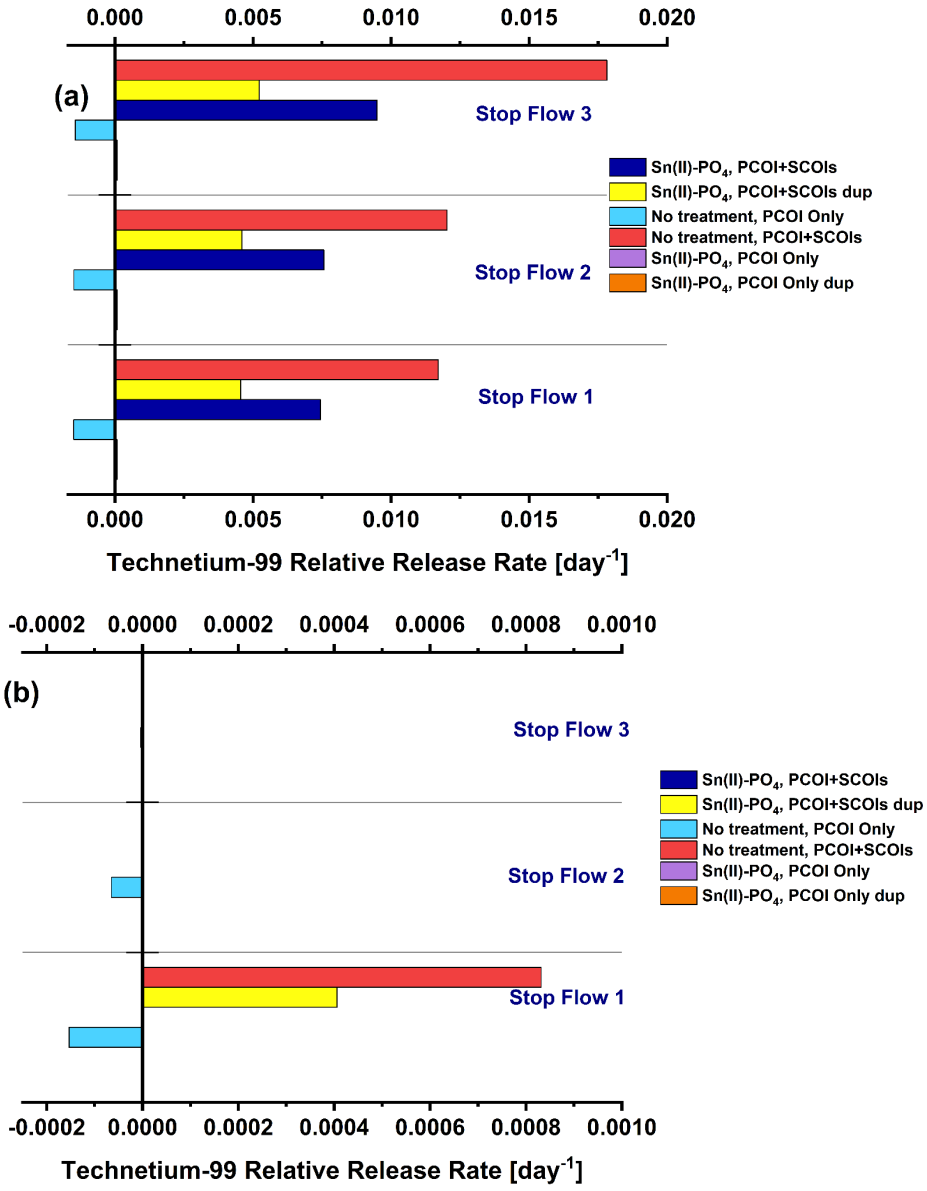

Figure F.10. Tc normalized release rates (a) before and (b) during leaching from columns with CCug sediment with and without Sn(II)-PO_4 treatment, estimated leaching rate (day^{-1}) during each stop flow. Note: "Dup" stands for duplicate.

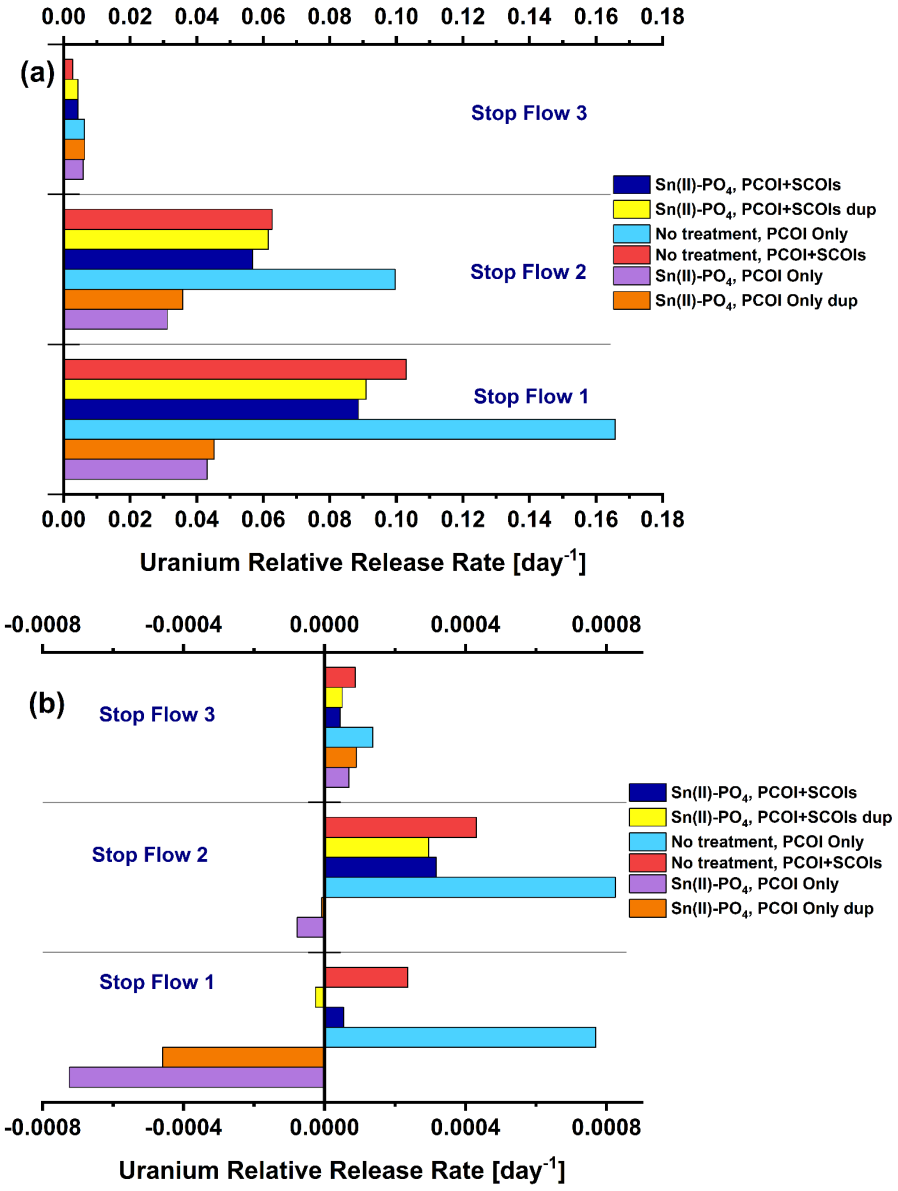

Figure F.11. U normalized release rates (a) before and (b) during leaching from columns with CCug sediment with and without Sn(II)-PO_4 treatment, estimated leaching rate (day^{-1}) during each stop flow. Note: "Dup" stands for duplicate.

F.3.2 Perched Water Conditions

In the PZsd columns, contaminants were mixed into the sediment and reacted for 48 to 72 hours. Then, Sn(II)-PO_4 was mixed into the contaminated sediments, saturated with SPW, and plugged to react in the absence of flow for 28 days before leaching. Less than 10% of Tc-99 was released during the leaching phase in treated columns (Figure F.12a), while the control column released nearly all Tc. The relative release rates show Tc-99 release decreased over time in all columns (treated and control) (Figure F.16).

Tc concentrations in post-leach treated PZsd sediments were low (0.19 µg/g) compared to treated CCug sediments (~3.5 µg/g) and were uniform across the sections of each Sn(II)-PO_4 column (Figure F.9, Figure F.14, Table F.1, and Table F.3).

In perched water conditions, the treated columns released around 80% of the total U over 140 PVs (Figure F.13a), compared to nearly all of the U for the control column in less than 30 PVs. During stop flow events, the relative release rate of U did not change for treated columns but the control column showed some variability (Figure F.17). After leaching, 35 to 38 µg/g U remained in the sediment (Table F.3).

In post-leach treated PZsd sediment extractions, U was lower at the influent end than the effluent end of the columns (15 to 40 µg/g), showing movement of the U in the direction of the effluent, and higher than post-leach treated CCug columns (13 to 16 µg/g, Figure F.15).

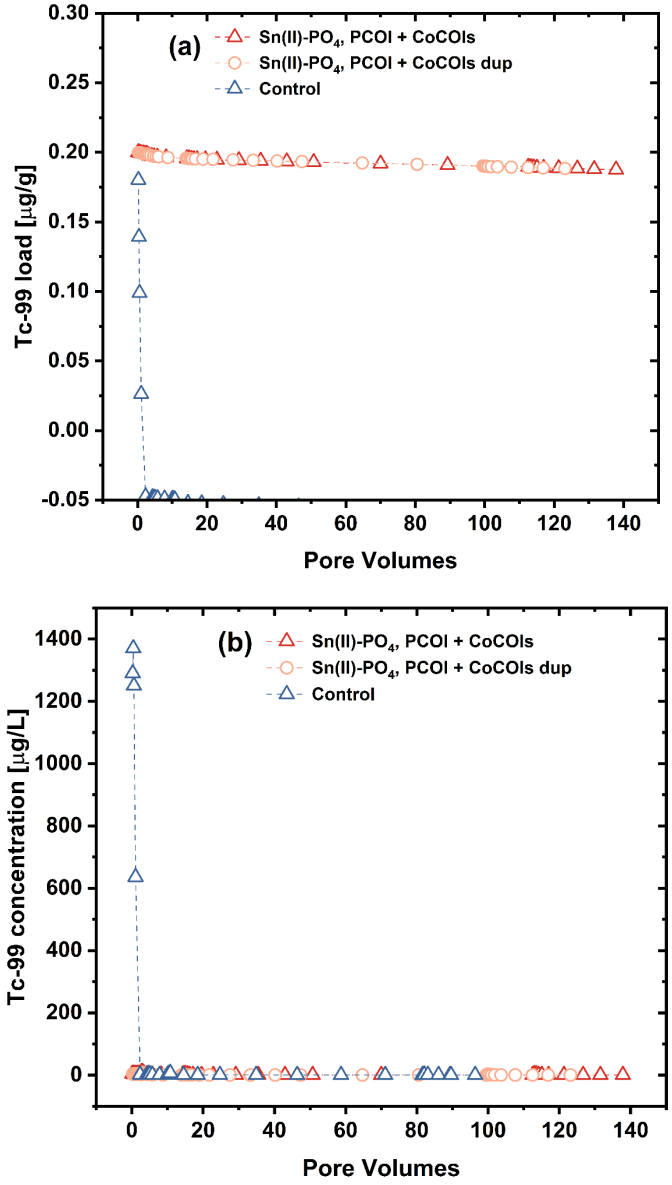

Figure F.12. Tc remaining during leaching with PZsd sediment with and without Sn(II)-PO_4 after equilibration of amendments for approximately 6 weeks: (a) accumulation of Tc-99 (in µg/g) and (b) aqueous concentrations of Tc-99 (in µg/L). Note: "Dup" stands for duplicate.

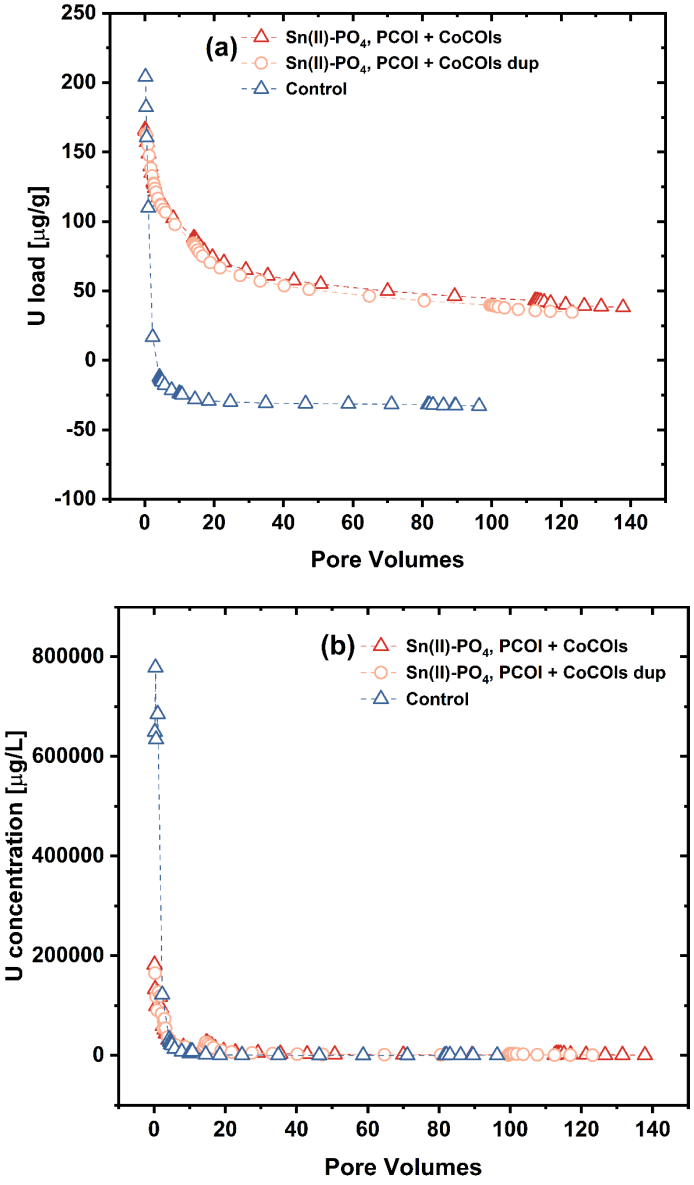

Figure F.13. U remaining during leaching with PZsd sediment with and without Sn(II)-PO_4 after equilibration of amendments for approximately 6 weeks: (a) accumulation of U (in µg/g) and (b) aqueous concentrations of U (in µg/L). Note: "Dup" stands for duplicate.

Table F.3. Tc and U estimated retention after leaching in PZsd sediments without and with Sn(II)-PO_4.

Conditions	U (µg/g)	Tc (µg/g)
No treatment	0[(a)]	0[(a)]
Sn(II)-PO_4	38.1	0.19
Sn(II)-PO_4, dup	34.7	0.19

(a) Negative values are reported as "0."

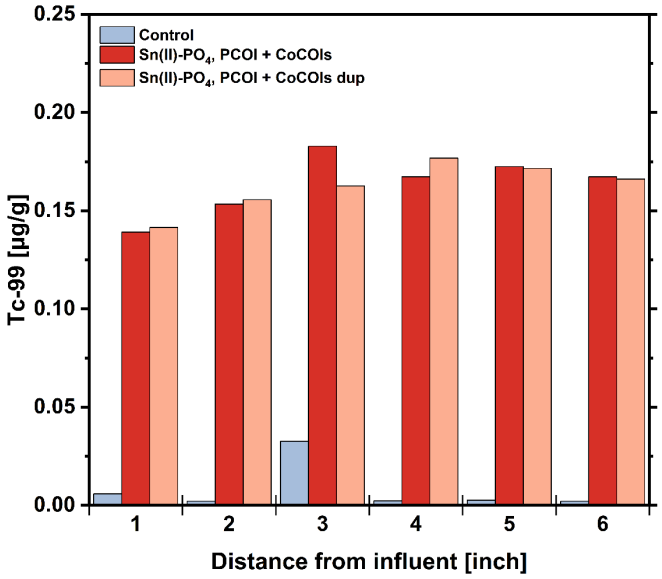

Figure F.14 Tc distribution (in µg/g) across columns with PZsd sediment with and without Sn(II)-PO_4 based on 8 M HNO_3 extractions. Note: "Dup" stands for duplicate.

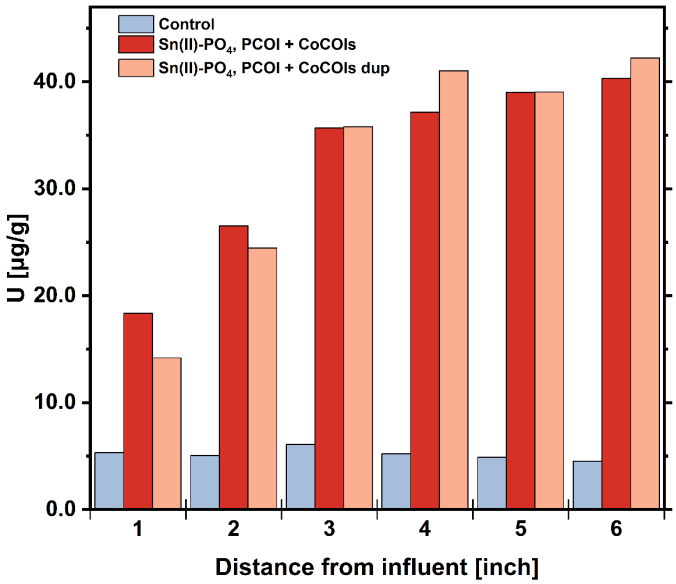

Figure F.15. U distribution (in µg/g) across columns with PZsd sediment with and without Sn(II)-PO_4 based on 8 M HNO_3 extractions. Note: "Dup" stands for duplicate.

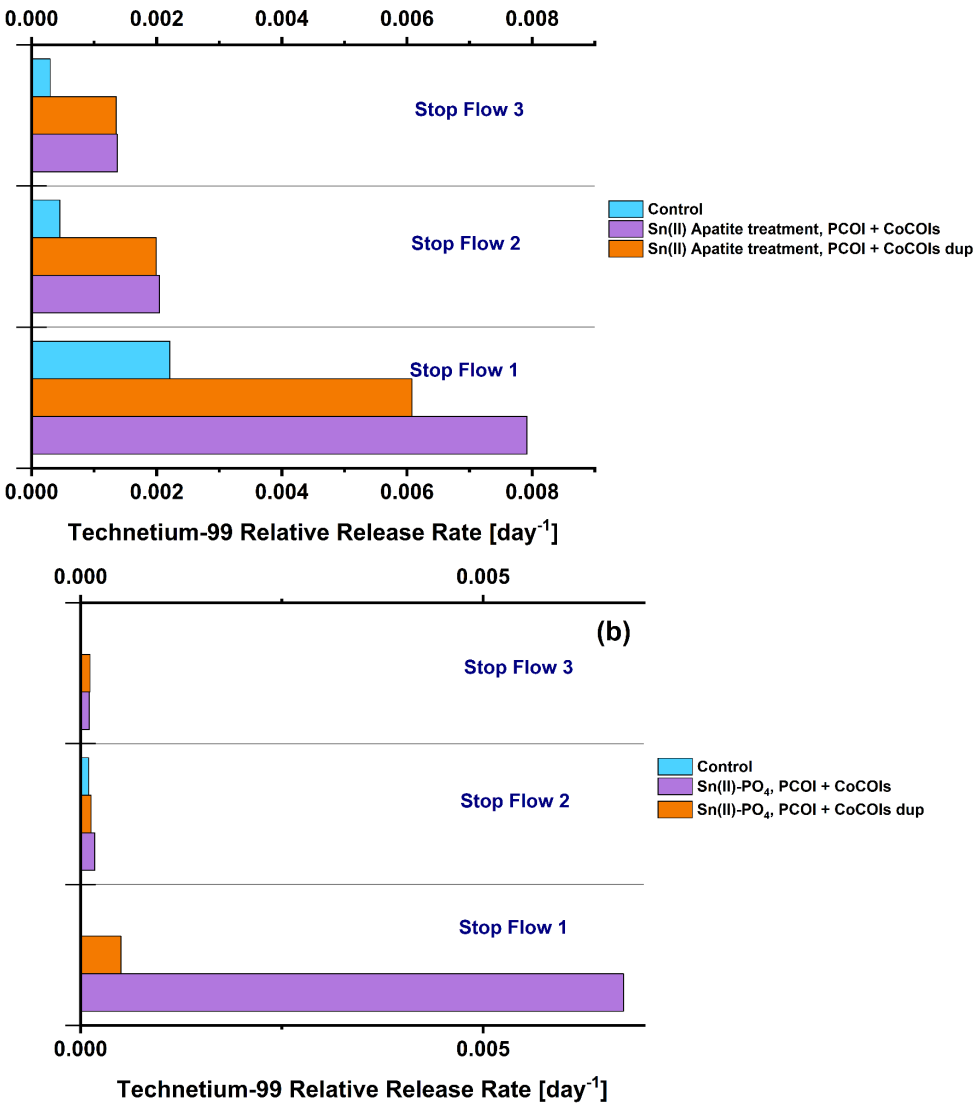

Figure F.16. Tc normalized release rates during leaching from columns with PZsd sediment with and without Sn(II)-PO_4, estimated leaching rate (day^{-1}) (a) before and (b) during each stop flow. Note: "Dup" stands for duplicate.

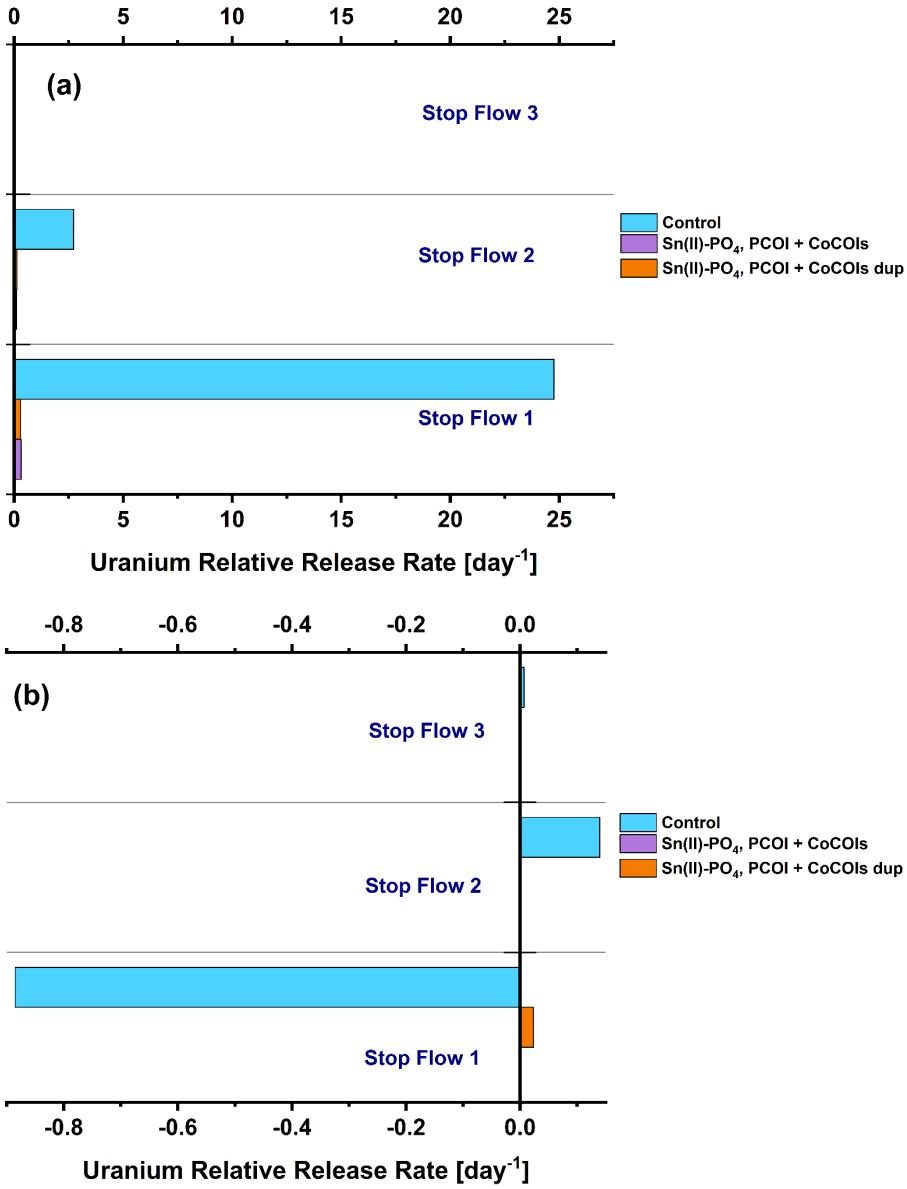

Figure F.17. U normalized release rates during leaching from columns with PZsd sediment with and without Sn(II)-PO_4, estimated leaching rate (day^{-1}) (a) before and (b) during each stop flow. Note: "Dup" stands for duplicate.

F.3.3 Long-term Tc-99 and U Stability

For pre-leach sediment combined with Sn(II)-PO_4, X-ray microprobe and fine maps showed potential association of U with Fe (Figure F.18). A select spot was further characterized using X-ray absorption near edge structure (XANES) and showed U was present predominantly as U(VI) (Figure F.19). Characterization of a post-leach CCug Sn(II)-PO_4 column sample showed U was present, most likely as U(IV) or a mixture of oxidation states, in all analyzed locations (Figure F.20 and Figure F.21). Due to low signal-to-noise ratio of the spectra and a very small energy shift between U(IV) and U(VI) L3 edges, it is not clear if there was a mixture of U oxidation states or one U oxidation state, but it is possible U was reduced after reaction to Sn(II)-PO_4. Comparison of derivatives of normalized absorption plots was inconclusive because of high noise of the collected U L3 edge XANES data.

Tc in the pre-leach sediment combined with Sn(II)-PO_4 and in post-leach treated CCug sediment was present as TcO_2, a reduced form of Tc-99 (Figure F.22 and Figure F.23). Linear combination analysis of the corresponding Tc-99 K-edge XANES spectra resulted in 98 ± 1% TcO_2 and 2 ± 1% TcO_4- in the pre-leach sample (Figure F.22) and 100% TcO_2 in the post-leach treated CCug sample (Figure F.23). Additional characterization indicated the Tc-99 may be associated with Sn, but Tc-99 K-edge extended X-ray absorption fine structure (EXAFS) data fit suggests possibility of Tc-P path around 3.7 Å (Table F.4 and Figure F.22). Here, Tc-99 association with Sn is not excluded at longer interatomic distances.

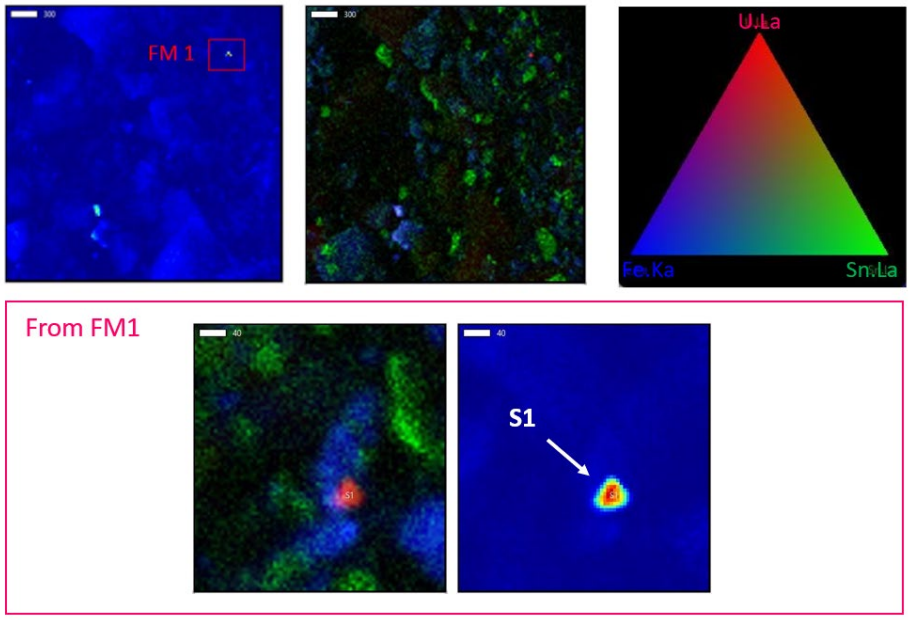

Figure F.18. X-ray microprobe coarse (*top row*) and fine maps (*bottom row*) showing areas of interest for U from batch experiment solids prepared under BY Cribs conditions with Sn(II)-PO_4. The tricolor maps in the top and bottom rows show the correlation of U (*red*), Fe (*blue*), and Sn (*green*) in the thin section, as shown in the triangular legend. In the bottom row, the right map shows a U element map and the white arrow points to spots selected for U L3-edge XANES, S1 (Figure F.19). Scale is 300 µm in the top row and 40 µm in the bottom row.

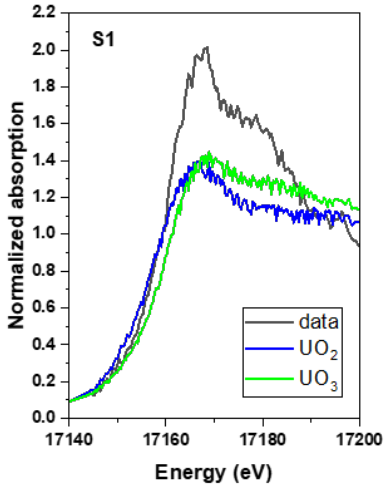

Figure F.19. U L3-edge XANES on spot S1 chosen on fine map [on Figure F.18; sample was prepared during batch experiments under BY Cribs conditions containing Sn(II)-PO_4].

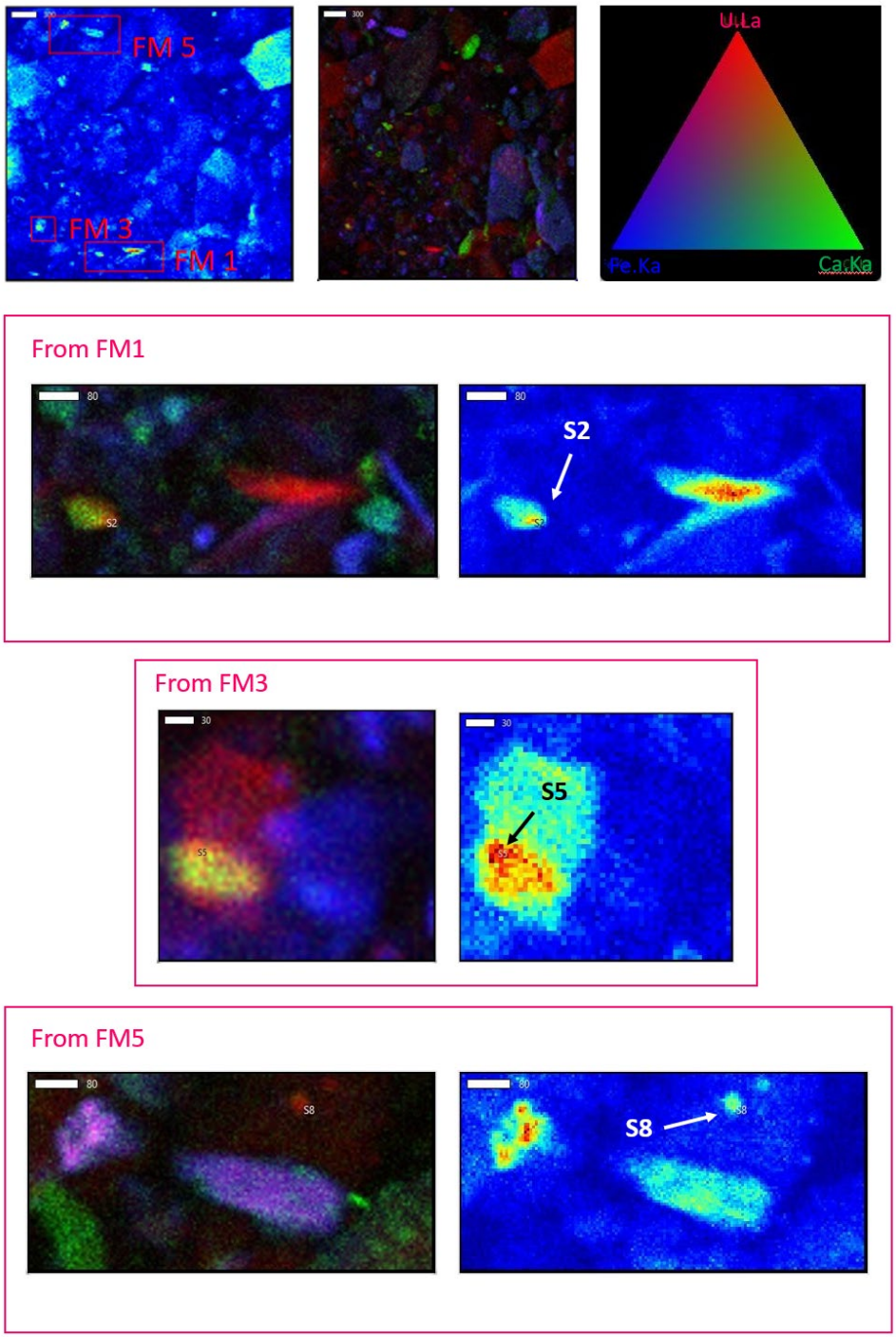

Figure F.20. X-ray microprobe coarse (*top row*) and fine maps (*subsequent rows*) showing areas of interest for U for post-leach solids from the CCug Sn(II)-PO_4 PCOI-only duplicate column. The tricolor maps in the middle of the top rows and the left side of the additional rows show correlation of U (*red*), Fe (*blue*), and Sn (*green*) in the thin section, as shown in the triangular legend (*top right*). The top left and right sides of the additional rows show U elemental maps. The white and black arrows point to the spots selected for U L3-edge XANES: S2, S5, and S8 (see Figure F.21). The scale is 300 µm in the top row and 30 or 80 µm in the additional rows.

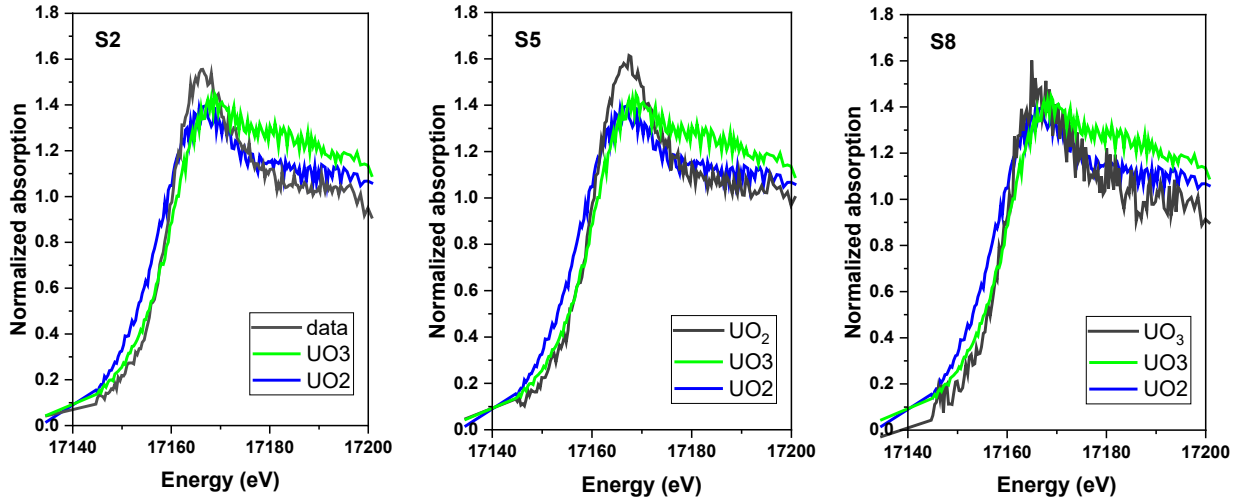

Figure F.21. U L3-edge XANES on spots S2, S5, S8 chosen on fine maps (on Figure F.11) of the post-leach solids from the CCug Sn(II)-PO_4 PCOI-only duplicate column.

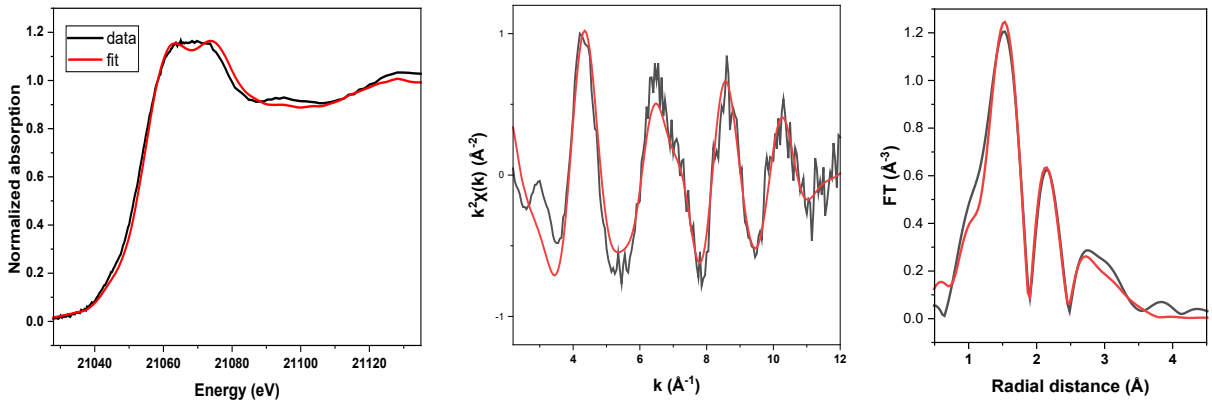

Figure F.22. Pre-leach CCUg batch sediment with Sn(II)-PO_4 Tc-99 K-edge XANES, and EXAFS data with corresponding linear combination and shell by shell fit. Data – *black* and fit – *red* lines. The linear combination fit (LCF) range is from -35 to 75 eV below and above the edge. EXAFS fit parameters and fit results are listed in Table F.4.

Table F.4. Tc K-edge EXAFS fit results from EXAFS shown in Figure F.22. Fitting ranges are $3 < k < 11$ $Å^{-1}$; $1.2 < R < 4.0$ Å. The amplitude reduction factor is set to a literature value of $S_0^2 = 0.8$ (Oliveira et al. 2022).

Path	CN	R (Å)	σ^2 ($Å^2$)	ΔE_0 (eV)	*R*-factor
Tc-O	4.6 ± 0.7	2.03 (1)[a]	0.002 (1)		
Tc-Tc	1.6 ± 0.8	2.57 (1)	0.006 (3)	-5.2 ± 1.6	0.017
Tc-P	6[b]	3.72 (3)	0.011 (3)		

(a) Numbers in parentheses are uncertainties in the last digit.
(b) Fixed value due to high error on CN.
CN = coordination number; R = interatomic distance (Å); σ2 = EXAFS Debye-Waller factor (Å2); ΔE0 = shift in energy (eV); R-factor = closeness of fit.

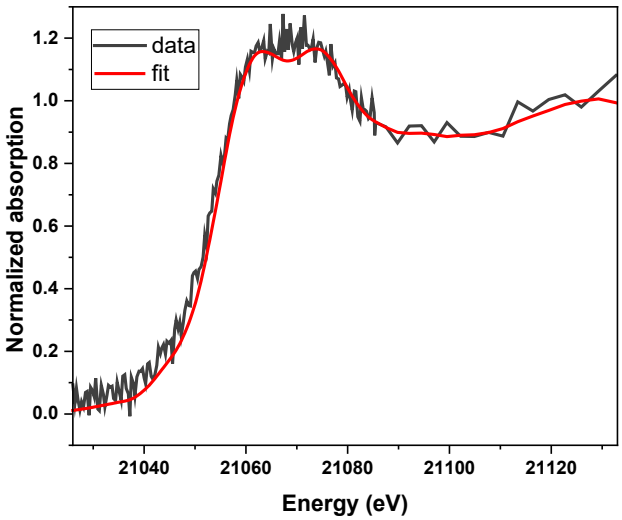

Figure F.23. Post-leach solids from the CCUg Sn(II)-PO_4 PCOI-only duplicate column1 Tc-99 K-edge XANES data with LCF. Data – *black* and fit – *red* lines. The LCF range is from -35 to 75 eV below and above the edge.

F.4 Saturated Column Results for Co-contaminants for BY Cribs Groundwater

F.4.1 Co-contaminant Effluent Monitoring

When CoCOIs were present in CCug sediments (Treated – D, Treated – E, and Control – F), both nitrate and Cr concentrations initially increased during the loading phase but decreased to less than the initial µg/g concentration during the leaching phase (Table F.5). Nitrate concentrations were similar in treated and untreated columns (Figure F.24). Cr was lower in effluent, leading to a higher solid phase loading estimate in treated columns during the initial loading phase, indicating some reduction and precipitation of Cr (Figure F.25). During the leaching phase (beginning between 66 and 74 PVs), the Cr concentration was returned to similar concentrations in the treated and untreated columns (Table F.5). The similar uptake of Sr in the treated and untreated columns shows the sediment has a high affinity for Sr, with a steady increase in µg/g concentrations during the loading phase (up to 300 µg/g); during the leaching phase, however, the Sr was released back into solution, with the final concentration being < 50 µg/g (Figure F.26, Table F.5).

Table F.5. Cr, Sr, and nitrate estimated retention after loading and leaching in CCug sediments without and with treatment [Sn(II)-PO_4]. Negative values indicate more leaching of contaminants from the sediment than were added, suggesting leaching of background CoCOIs also occurred.

	Chromium		Strontium		Nitrate	
Conditions	Loading (µg/g)	Leaching (µg/g)	Loading (µg/g)	Leaching (µg/g)	Loading (µg/g)	Leaching (µg/g)
No treatment, PCOIs + CoCOIs	-5.84	-20.1	285	12.7	-0.01	-0.02
Sn(II)-PO_4, PCOIs + CoCOIs	-9.28	-18.0	284	42.3	-0.04	-0.04
Sn(II)-PO_4, PCOIs + CoCOIs, dup	- 4.25	- 13.9	297	32.3	-0.05	-0.06

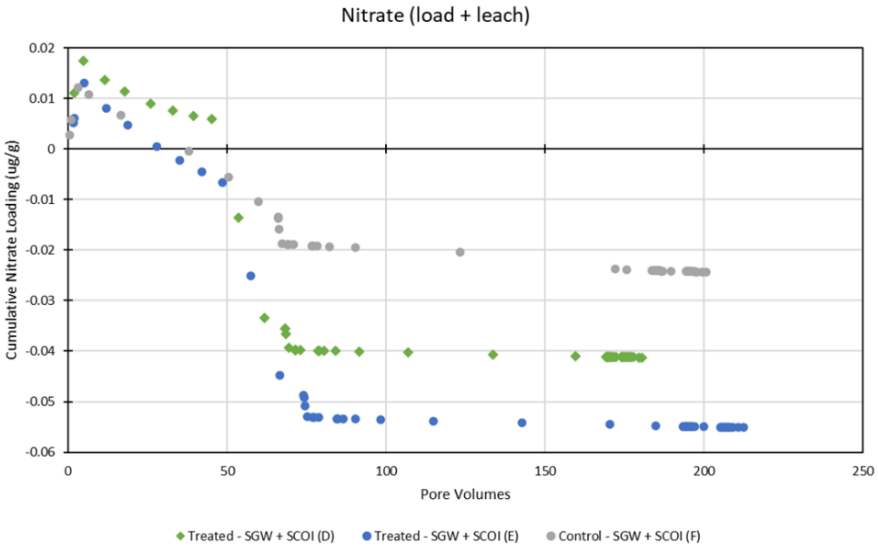

Figure F.24. Nitrate during loading and leaching with CCug sediment with and without Sn(II)-PO_4 treatment, accumulation of nitrate (in µg/g).

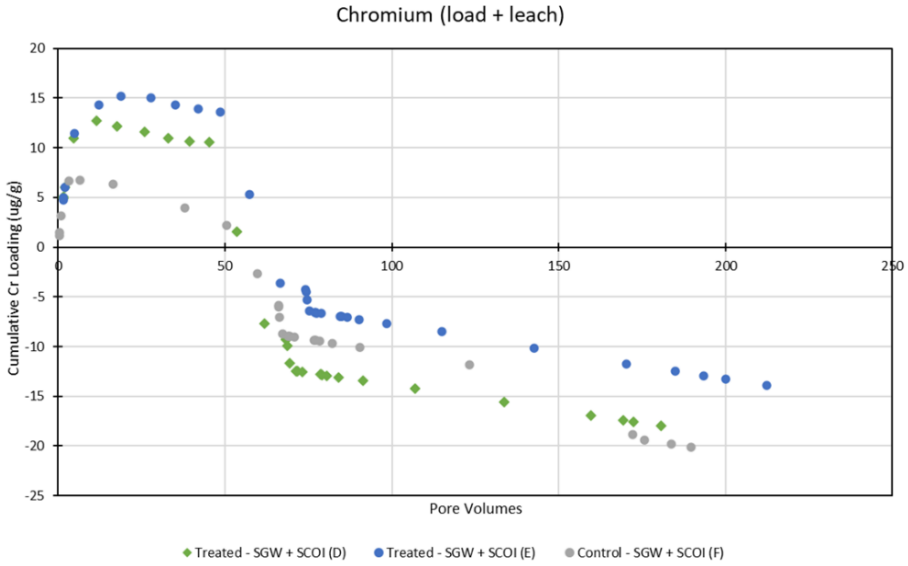

Figure F.25. Cr during loading and leaching with CCug sediment with and without Sn(II)-PO_4 treatment, accumulation of Cr (in µg/g).

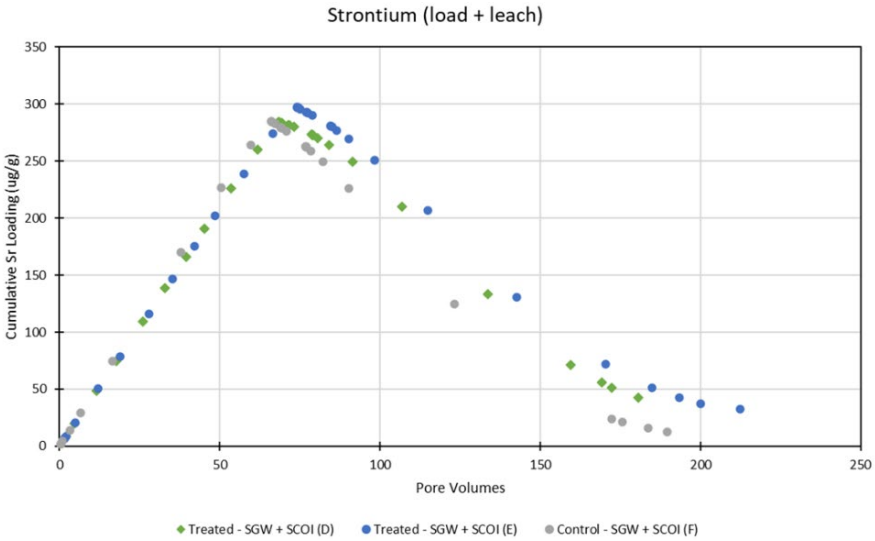

Figure F.26. Sr during loading and leaching with CCug sediment with and without Sn(II)-PO_4 treatment, accumulation of Sr (in µg/g).

F.5 Supplemental Saturated Column Geochemical Monitoring

F.5.1 Oxygen Monitoring

Oxygen was monitoring using oxygen sensor spots (PreSens, Germany) on the inlet and outlet ends of select CCug columns with and without treatment. Oxygen increased at the start of the tests in both the treated and control columns. After stop flows, the oxygen level decreased temporarily, with a larger decrease observed in the treated column at the inlet end (Figure F.27).

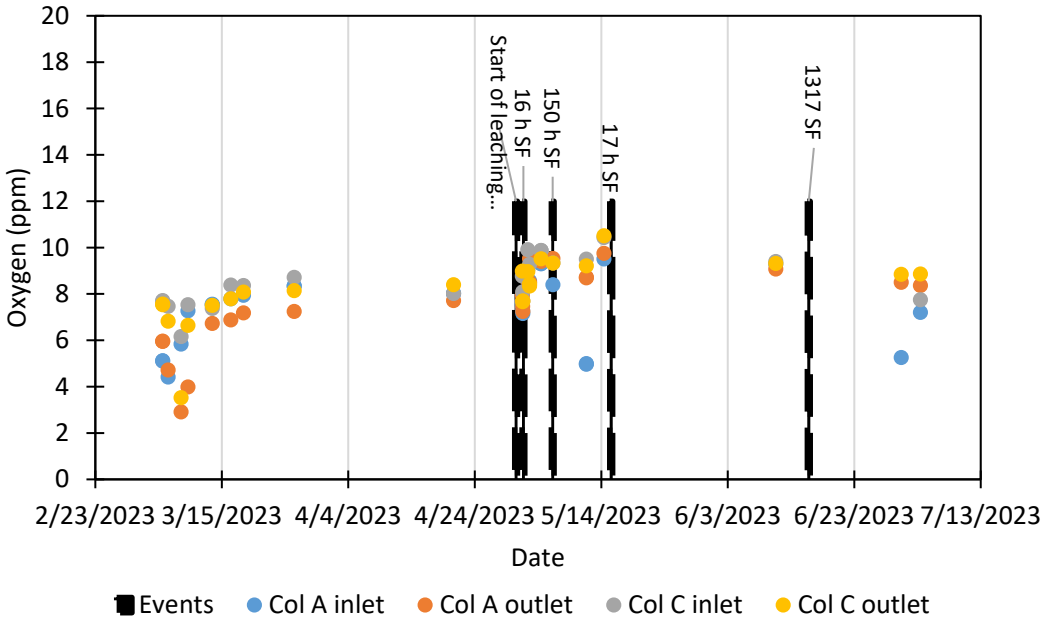

Figure F.27. Oxygen monitoring on the inlet and outlet ends of CCug columns A (Treated) and C (Control). Black vertical lines represent stop flow events. Results are For Information Only.

F.5.2 pH Monitoring

In the first 25 PVs, the treated CCug columns had a slight decrease in pH from 8.5 to 7.5. After this initial decrease, the pH returned to approximately 8, similar to the control column, and remained there throughout the rest of the loading and the leaching phase (Figure F.28). In the columns with added CoCOIs, the pH did not dip in the beginning of the loading phase; pH in these columns was likely influenced and stabilized by the addition of CoCOIs (Figure F.29). For columns treated with perched water, the pH fluctuated between 8.3 and 9.3 (Figure F.30).

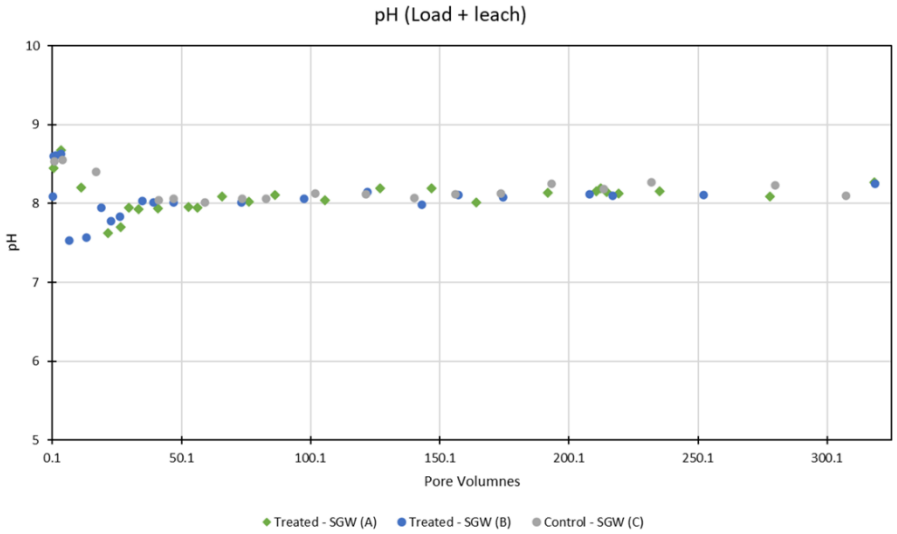

Figure F.28. pH during loading and leaching with CCug sediment with and without Sn(II)-PO_4 treatment.

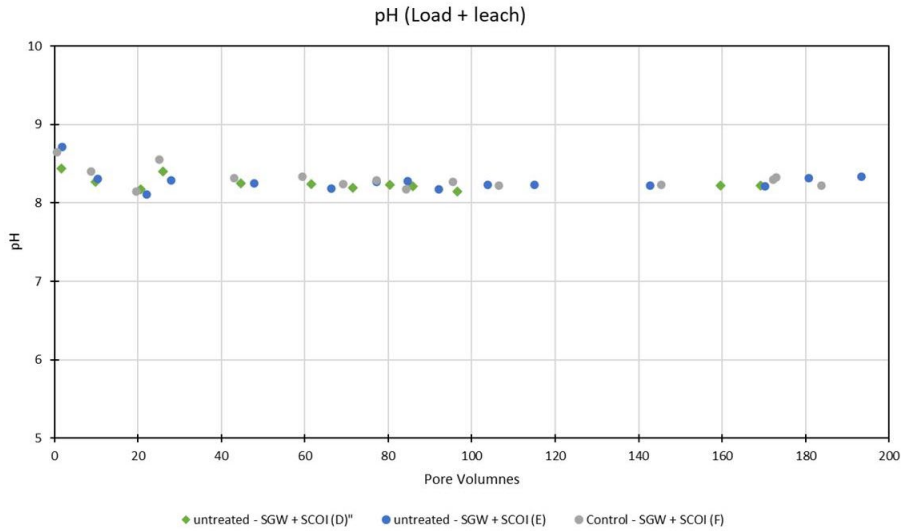

Figure F.29. pH during loading and leaching with CCug sediment and CoCOIs with and without Sn(II)-PO_4 treatment.

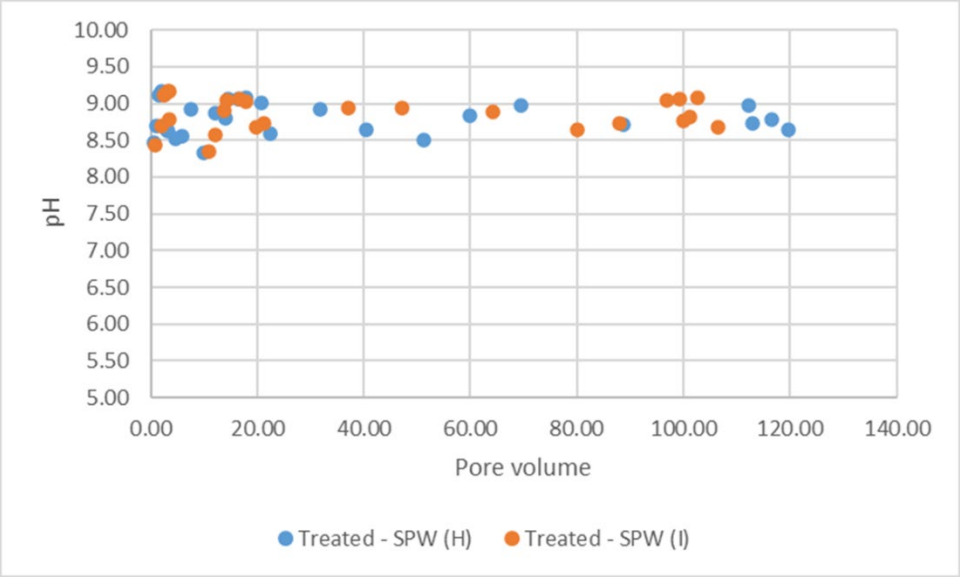

Figure F.30. pH during loading and leaching with PZsd sediment and CoCOIs with Sn(II)-PO_4 treatment.

F.5.3 Amendment Monitoring

With the exception of the Sn(II)-PO_4-treated, PCOI-only duplicate column, Sn concentration increased across the column, with the highest concentration found in the effluent end (Figure F.31). This may indicate movement of the particulates during the column tests.

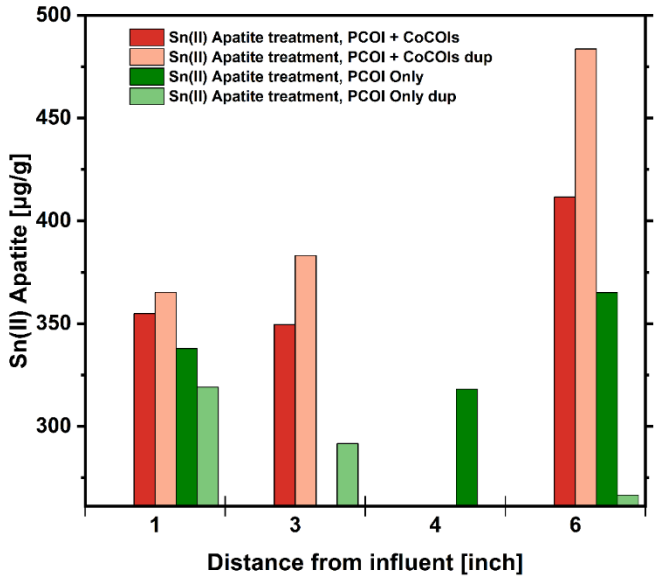

Figure F.31. Sn(II)-PO_4 distribution (in µg/g) across columns with CCug sediment with and without Sn(II)-PO_4 treatment based on 8 M HNO_3 extractions. Note: "Dup" stands for duplicate. Extractions 1, 3, and 6 were extracted with the exception that section 4 was used instead of section 3 for the Sn(II)-PO_4-treated, PCOI-only column.

F.5.4 Bromide Tracer Breakthrough

Bromide tracer tests for treated and control columns show a typical breakthrough behavior with full breakthrough of the Br tracer occurring at 2 PVs in both CCug and PZsd column tests (Figure F.32 and Figure F.33, respectively). These breakthrough curves indicate that the Sn(II)-PO_4 treatment did not cause any changes (e.g., precipitation) that affected porosity.

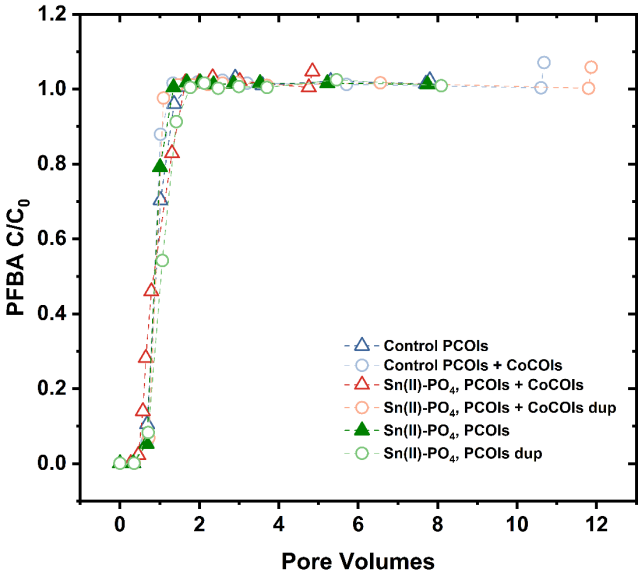

Figure F.32. Effluent Br (in mg/L) during and after tracer injection at 80 mg/L Br into columns with CCug sediment with and without treatment [Sn(II)-PO_4].

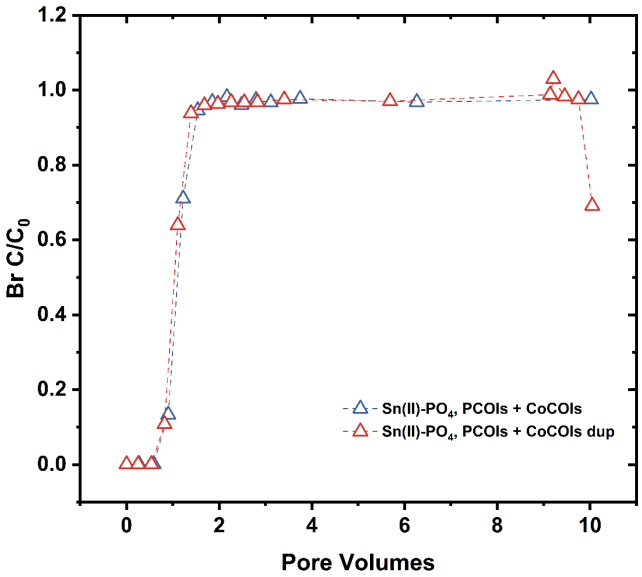

Figure F.33. Effluent Br (in mg/L) during and after tracer injection at 80 mg/L Br into columns with PZsd sediment with and without treatment [Sn(II)-PO_4].

F.6 Summary of Performance of Tin Apatite for Groundwater

For the BY Cribs groundwater conditions, Sn(II)-PO_4 performed well and is recommended for Tc-99 and, while less effective, may be appropriate for U as well. However, when CoCOIs are present, Sn(II)-PO_4 performance is greatly diminished. In perched water conditions, Sn(II)-PO_4 is recommended for Tc-99 and U.

For Tc-99 in BY Cribs groundwater conditions, Sn(II)-PO_4 showed significant immobilization and retention of Tc. With CoCOIs present, however, removal of Tc-99 decreased to almost nothing. Further investigation would be necessary to determine the cause, as the presence of high concentrations of nitrate as a CoCOI did not affect performance of Sn(II)-PO_4 under the perched water scenario, indicating the issue was not related to depletion of available reduction capacity by nitrate, but may be greatly affected by reduction of chromate that was present in the CoCOI water.

U sequestration was significant without CoCOIs, but some U was remobilized during the leaching phase. This indicates a different mechanism than Tc-99 for removal by Sn(II)-PO_4 as Tc-99 was well retained in hard-to-extract phases. With CoCOIs present, little difference was observed between treated and control columns for U immobilization.

Compared to the control column, Cr and nitrate were reduced and Sr release was slowed. However, additional characterization to better calculate mass balance of these CoCOIs is necessary before making a recommendation for use of Sn(II)-PO_4 as treatment for CoCOIs.

Under perched water conditions, sequestration of Tc-99 was significant, with nearly all or all Tc-99 immobilized and retained in hard-to-extract phases. This was confirmed with the long column experiments used to obtain rate information as well as the long-term batch experiments. A significant concentration of U was also retained at the termination of the leach columns; the long columns and the long-term batch data both show 50% to 75% of the U was in hard-to-extract phases.

Appendix G – Particulate-Phase Reduction & Sequestration: Sulfur Modified Iron & Polyphosphate

The purpose of this task is the sequestration of U and Tc-99 (primary contaminants of interest, PCOIs) in the presence of I-129 as iodate, nitrate, Cr, and Sr (co-contaminants on interest, CoCOIs) in water-saturated zones using a solid phase reductant (sulfur modified iron, SMI) followed by a polyphosphate (Poly-PO_4) solution to precipitate apatite. This technology functions via injection of the high-density reductant SMI with a delivery fluid (xanthan gum or other) to reductively precipitate contaminants, followed by injection of Poly-PO_4 to precipitate apatite that may either incorporate contaminants (i.e., U) or coat reduced/precipitated contaminants (i.e., Tc).

This combined treatment is targeting contamination in perched water and BY Cribs as the primary treatment zones, with treatment via formation of a permeable reactive barrier in groundwater under BY Cribs. Potential secondary treatment zones include 216-U-1 and -2, S-SX tanks, S and T Cribs, C tanks, and BC Cribs. Note that the SMI mass fraction in previous batch experiments was 0.7 wt% [Phase 1 report (PNNL-35432)], which was higher than the 0.1% SMI (g/g) used in batch and 1-D column studies reported within. The specific objectives of this technology are as follows:

1. Quantify the decrease in Tc-99 and U mass and order of magnitude removal rate in various combinations: (1) with/without sediment, (2) with/without delivery fluid, (3) with/without co-contaminants, and (4) with zero valent iron (ZVI) or SMI [described in the Phase 1 report (PNNL-35432)].
2. Determine the immobilization rates for U and Tc-99 with/without co-contaminants for (1) perched water and (2) BY Crib application (in groundwater).
3. Quantify the longevity of U and Tc-99 with/without co-contaminants for (1) perched water and (2) BY Crib application.

Objectives 2 and 3 were tested in 1-D leach columns as described in Sections G.3 and G.2 for perched water conditions and BY Cribs groundwater conditions, respectively, based on the batch experiments described in Section G.4.

G.1 Supplemental Methods

Additional column tests were conducted with and without Poly-PO_4 to quantify the performance of treatment with SMI only as compared to the two-step approach with SMI+Poly-PO_4. These experiments were conducted as described in Section 2.4. However, testing was only conducted for conditions with CoCOIs. Additional batch experiments were also conducted with Tc-99 and U in the perching zone sand (PZsd) sediment with SMI, which were analyzed by X-ray absorption near edge structure (XANES) and extended X-ray absorption fine structure (EXAFS) to quantify Tc-99 and U surface phases. In these experiments, 100 ppm Tc-99 and 100 ppm U in 10 mL of solution were reacted with 0.5 g SMI and 2 g of the PZsd sediment to reach contaminant concentrations that were high enough for analysis. These data are summarized in this appendix.

G.2 Long-Term Batch Results

For this subtask, water-saturated, static batch experiments were conducted in packed porous media (i.e., sediment-to-water ratio of ~5g:1mL) to evaluate PCOI (Tc, U) change in sequestration rate (i.e., removal rate of Tc-99 and U sequestered by SMI/PO_4), and subsequent reoxidation rate at longer periods after the sediment/water/SMI/PO_4 system becomes oxidized. Generic experimental details for long-term batch experiments are provided in Section 2.4, with sequential extractions in Appendix A, Section A.2.3. Note that the ZVI or SMI fraction mass in previous batch experiments was 0.7 wt% [Phase 1 report (PNNL-35432)], which was higher than the 0.1% SMI (g/g) used in batch and 1-D column studies reported here. The reduction rate with just SMI was evaluated at 0.2 and 7 days, Poly-PO_4 was added at 7 days, then the additional sequestration that occurred as the result of phosphate precipitation was evaluated at 8, 14, and 50 days. At 50 days, these systems were exposed to an oxic atmosphere, and the subsequent reoxidation rate was evaluated at 100 and 300 days.

For Tc-99 in the PZsd sediment, the addition of 0.1% SMI did decrease the mobile Tc-99 fraction from 66% (aqueous and adsorbed) to 9% by 7 days, but then some Tc-99 was remobilized with the addition of the Poly-PO_4 solution, as by 50 days the fraction of mobile Tc-99 increased to 16% (Figure G.1a). The subsequent oxidation of the sediment from 50 to 299 days resulted in additional Tc-99 remobilization, and by 299 days the mobile fraction was 35%. Therefore, the SMI+Poly-PO_4 treatment under perched water conditions (high nitrate) did decrease Tc-99 mobility by 57% initially (when the system was still reduced), but long-term (250 days) oxidation caused some Tc-99 remobilization, so by 299 days the decrease in Tc-99 mobility had dropped from 66% to 35% (i.e., 31%).

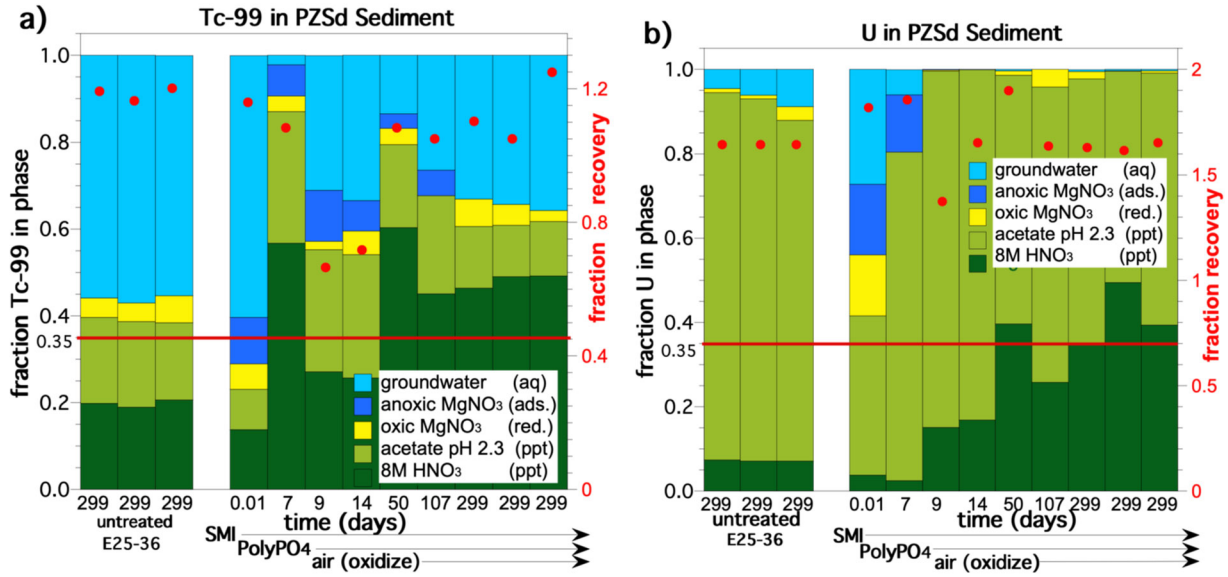

Figure G.1. Change in sequestration of Tc-99 (a) and U (b) in PZsd sediment following treatment with SMI as a reductant followed by Poly-PO_4 to precipitate apatite in batch experiments up to 299 days, with Poly-PO_4 added at 7 days and air exposure at 50 days.

Additional batch experiments were conducted with 100 ppm Tc-99 and 100 ppm U in the PZsd sediment with SMI, which were analyzed by XANES and EXAFS to quantify Tc-99 and U surface phases. Linear combination analysis of bulk Tc-99 K-edge XANES showed that the majority (92% to 95%) of Tc-99 was reduced to Tc(IV) that was present as a mixture of phases, including Tc(IV) oxide (TcO_2), Tc(IV) oxide associated with magnetite (up to 24%), and Tc(IV) sulfide (Tc_2S_7), with the remaining fraction present as Tc(VII) in pertechnetate (Figure G.2). EXAFS fitting showed four O atoms at 2.03 ± 0.01 Å,

which is characteristic of the first shell Tc-O path in TcO_2 (Oliveira et al. 2022), intrachain Tc-99 in the second shell (Tc-Tc path at 2.55 ± 0.03 Å), and disordered Fe in the third shell, suggesting that short dimeric TcO_2 chains coordinated to an Fe oxide, likely magnetite (Fe_3O_4) on the oxidized surface of the SMI particles (Figure G.3 and Table G.1). X-ray magnetic circular dichroism (XMCD) confirmed that the surface of the as-received SMI particles was oxidized from iron metal to oxidized magnetite, and that grinding in a glovebox exposed fresh surfaces with a higher Fe(II) content, closer to stoichiometric magnetite (Figure G.2).

For U in the PZsd sediment, the addition of 0.1% SMI significantly decreased the mobile U fraction from 8% to < 0.3% by 9 days (Figure G.1b). The addition of Poly-PO_4 solution at 8 days additionally decreased U mobility. The oxidation of the system at 50 days to 200 days did not remobilize the uranium. This is likely because aqueous U species react with phosphate to form autunite and U(VI)-substituted apatite in an oxidizing environment. Bulk U XANES on 100-ppm U batch samples showed that after SMI and Poly-PO_4 addition, the U was not reduced and remained as U(VI) (Figure G.4).

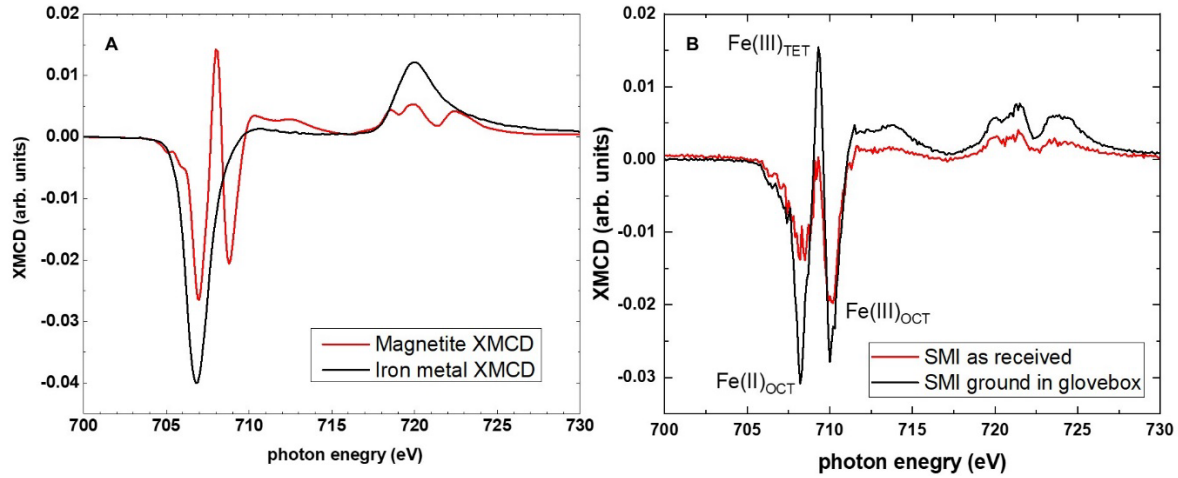

Figure G.2. XMCD spectra for (A) magnetite and iron metal standards and (B) SMI as received and after grinding in a glovebox.

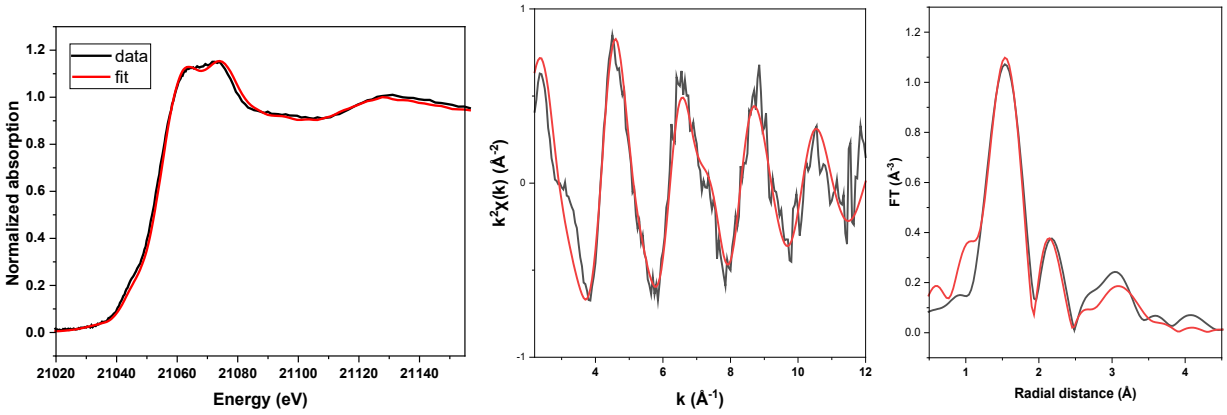

Figure G.3. Tc K-edge XANES and EXAFS data with corresponding linear combination and shell by shell fit for pre-leached PZsd sediments treated with SMI+Poly-PO_4 in a batch. Data – *black* and fit – *red* lines. The linear combination fit (LCF) range is from -35 to 75 eV below and above the edge. EXAFS fit parameters and fit results are listed in Table G.1 (sample PNNL620).

Table G.1. Tc K-edge EXAFS fit results for pre-leached PZsd sediments treated with SMI+Poly-PO_4 in a batch. Fitting ranges are $3 < k < 11$ Å^{-1}; $1.2 < R < 4.0$ Å. The amplitude reduction factor was set to a literature value, $S_0^2 = 0.8$ (Oliveira et al. 2022).

Path	CN	R (Å)	σ^2 (Å^2)	ΔE_0 (eV)	*R*-factor
Tc-O	3.6 ± 0.6	2.03 (1)[(a)]	0.002 (1)	3.7 ± 0.7	0.023
Tc-Tc	2.3 ± 0.5	2.55 (3)	0.015 (4)		
Tc-Fe	6[(b)]	3.56 (2)	0.018 (3)		

(a) Numbers in parentheses are uncertainties in the last digit.
(b) Fixed value due to high error on CN.
CN = coordination number; R = interatomic distance (Å); σ^2 = EXAFS Debye-Waller factor (Å^2); ΔE_0 = shift in energy (eV); *R*-factor = closeness of fit

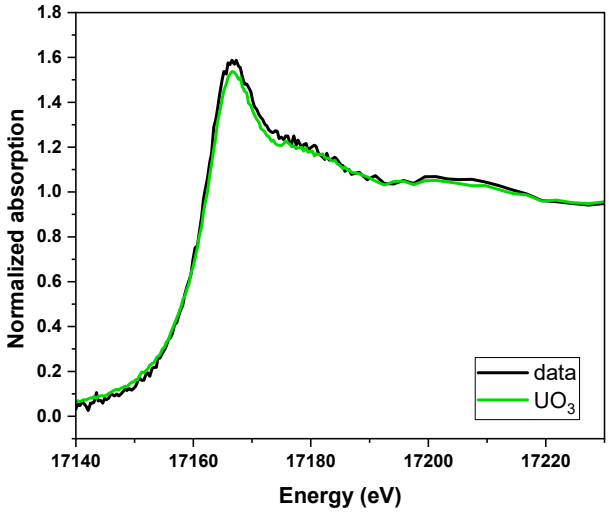

Figure G.4. U L3-edge XANES of the PZsd sediment treated with SMI+Poly-PO_4 in a batch as compared with a UO_3 standard showing primarily U(VI) (sample PNNL620).

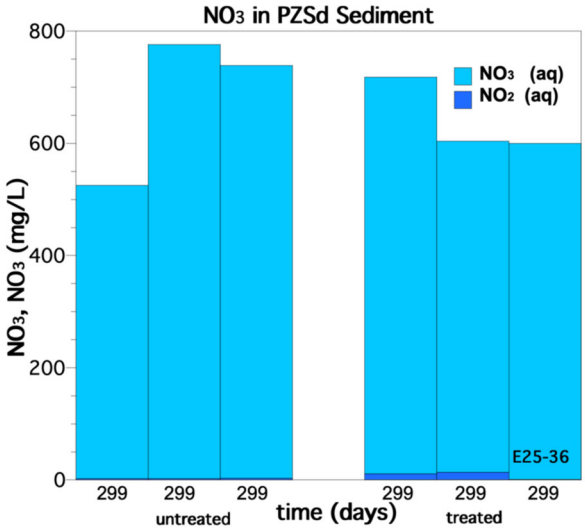

Figure G.5. Change in transformation of nitrate in PZsd sediment following treatment with SMI as a reductant followed by Poly-PO_4 to precipitate apatite in batch experiments up to 299 days with Poly-PO_4 added at 7 days and air exposure at 50 days. Results show no significant transformation over 299 days.

For Tc-99 in the Cold Creek Unit gravel (CCug) sediment with no CoCOIs added, the addition of 0.1% SMI resulted in a large decrease in mobile Tc-99 fraction from 65% (untreated, Figure G.6a) to 11% at 7 days in batch experiments. By 50 days, the mobile Tc-99 fraction was 4%, indicating Tc-99 (as aqueous and adsorbed pertechnetate) was slowly being reduced. During the time that the sediment was oxidized between 50 and 299 days, Tc-99 mobility increased to 43% – only 23% less mobile than untreated sediment. This mobility increase for Tc-99 is indicative of slow oxidation of the reduced Tc-99 surface phases and implies that these precipitates were not well (or were only partially) coated by the apatite precipitate. For Tc-99 in the CCug sediment with contaminants present, the addition of 0.1% SMI resulted in a more substantial decrease in Tc-99 mobility than without CoCOIs. The Tc-99 mobile fraction in untreated sediment (Figure G.6c) of 84% decreased to 9% by 7 days and to 4% by 50 days. Sediment oxidation from 50 to 299 days did result in a small increase in Tc-99 mobility to 8%. These results suggest an interaction between CoCOIs and Tc, such as aqueous Sr^{2+} and carbonate precipitation coating some reduced/precipitated Tc.

Parallel batch experiments conducted with the CCug sediment, SMI, and 100 ppm U and Tc-99 were used to evaluate contaminant sequestration mechanisms. Bulk Tc-99 K-edge XANES showed that the Tc(VII) was predominantly reduced to Tc(IV), up to 100%, as a mixture of TcO_2 (72% to 92%) and Tc(IV) associated with magnetite (up to 23%), linear combination analysis returned combinatorics of very similar statistics. The remaining fraction could be represented as Tc(VII) and Tc_2S_7 (4% to 9%), Figure G.7 and Table G.2. EXAFS fitting showed that Tc-99 first shell had four O atoms at 2.03 ± 0.01 Å, which is characteristic of TcO_2 (Oliveira et al. 2022), two Tc-99 atoms at 2.56 ± 0.02 Å from intrachain Tc-99 in the second shell, and possibly disordered Fe in the third shell (relatively large Debye-Waller factor, 0.021 $Å^2$, indicates dynamic and structural disorder), suggesting that short dimeric TcO_2 chains coordinated to an Fe oxide, likely magnetite (Fe_3O_4) on the oxidized surface of the SMI particles (Figure G.2). In this case, the addition of the Poly-PO_4 solution at 8 days did not increase Tc-99 mobility, and the X-ray absorption spectroscopy (XAS) data indicated that Tc-99 oxidation state and speciation was not changed by Poly-PO_4 addition.

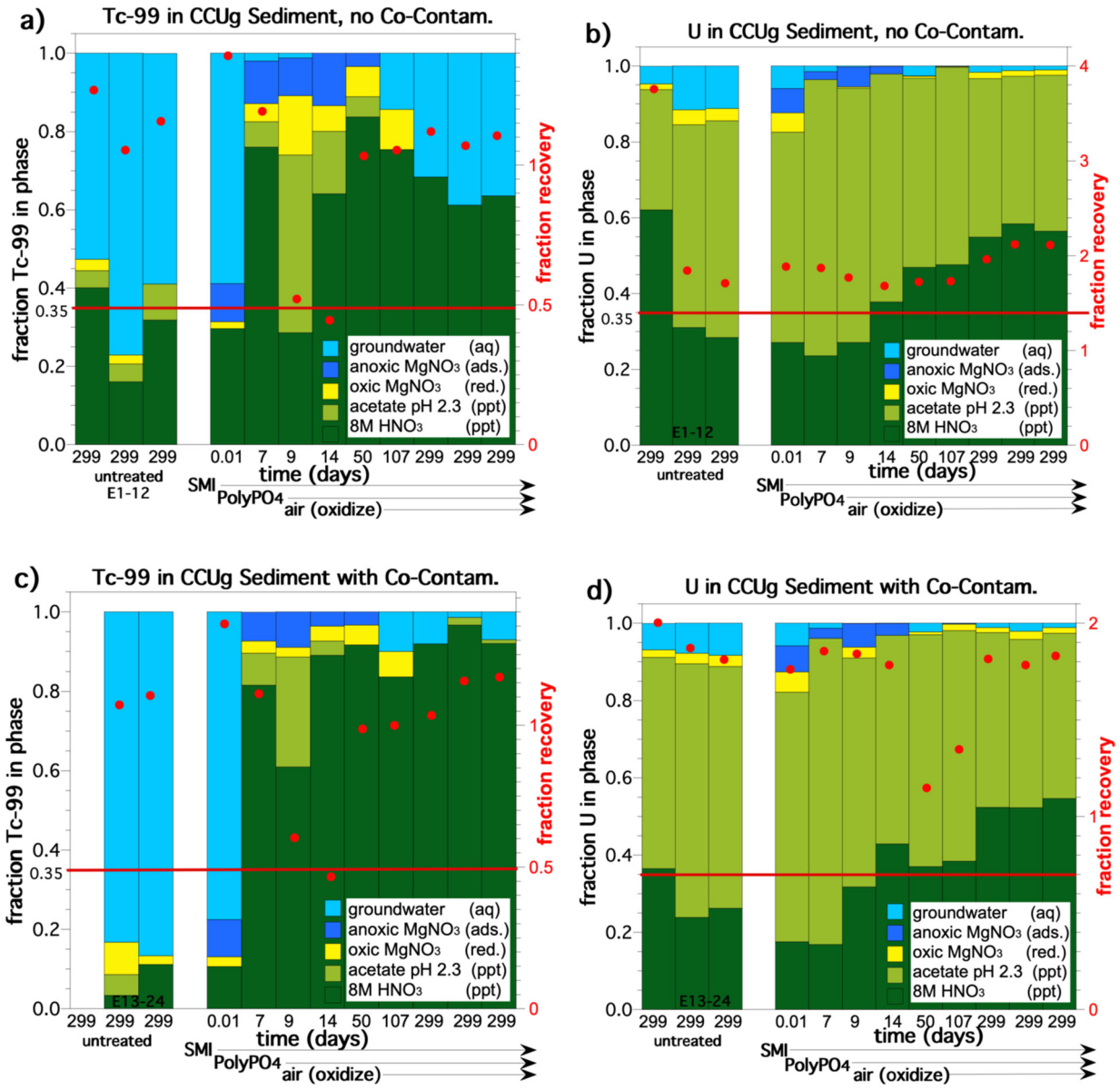

Figure G.6. Batch experiment sequestration using SMI as a reductant followed by Poly-PO_4 to precipitate apatite in CCug sediment with (a) Tc-99 without co-contaminants, (b) U without co-contaminants, (c) Tc-99 with co-contaminants, and (d) U with co-contaminants.

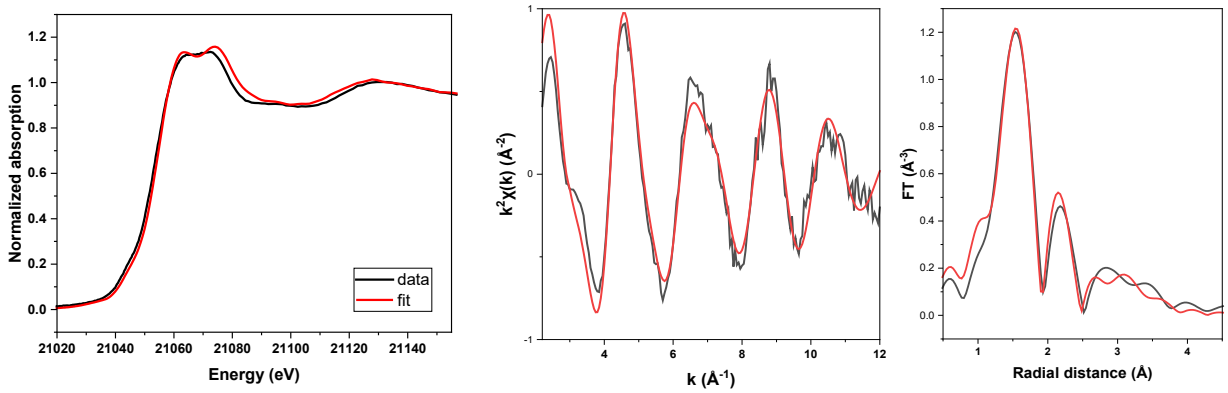

Figure G.7. Tc K-edge XANES and EXAFS data with corresponding LCF and shell by shell fit. Data – *black* and fit – *red* lines. The LCF range is from -35 to 75 eV below and above the edge. EXAFS fit parameters and fit results are listed in Table G.2 (sample PNNL619).

Table G.2. Tc K-edge EXAFS fit results. Fitting ranges are $3 < k < 11$ Å^{-1}; $1.2 < R < 4.0$ Å. The amplitude reduction factor is set to a literature value of $S_0^2 = 0.8$ (Oliveira et al. 2022).

Path	CN	R (Å)	σ^2 (Å^2)	ΔE_0 (eV)	*R*-factor
Tc-O	4.0 ± 0.2	2.03 (1)[(a)]	0.002[(f)]	4.0 ± 1.4	0.027
Tc-Tc	2.2 ± 0.4	2.56 (2)	0.012 (2)		
Tc-Fe	6[(b)]	3.56 (3)	0.021 (5)		

(a) Numbers in parentheses are uncertainties in the last digit.
(b) Fixed value due to high error on CN.
CN = coordination number; R = interatomic distance (Å); σ^2 = EXAFS Debye-Waller factor (Å^2); ΔE_0 = shift in energy (eV); *R*-factor = closeness of fit

For U in the CCug sediment with no CoCOIs added, the addition of 0.1% SMI resulted in a large decrease in U mobility from 13% (untreated sediment, Figure G.6b) to 4% by 7 days (i.e., SMI treatment only). The addition of the Poly-PO_4 solution at 8 days increased U mobility slightly at 9 days, then decreased the mobile U fraction to 3% by 50 days. Oxidation of the sediment between 50 and 299 days resulted in a further decrease in U mobility to 1%. A further change in the U surface phases is indicated by the slow increase in the 8 M HNO_3-extractable U from 25% at 7 days to 52% at 299 days, possibly from the crystallization of U-bearing apatite. For U in the CCug sediment with CoCOIs, the addition of 0.1% SMI decreased U mobility significantly, similar to without CoCOIs. U mobility decreased from 10% (untreated, Figure G.6d) to 4% (SMI only, 7 days), then to 3% (50 days, SMI + Poly-PO_4), then to 1.5% after the subsequent 250 days of oxidation. So, in contrast to Tc, the presence of CoCOIs had little effect on U mobility with SMI and Poly-PO_4 addition, likely due to the formation of autunite and U-bearing apatite.

For the parallel batch experiments conducted with high concentrations of U and Tc-99 to evaluate contaminant sequestration mechanisms, X-ray microprobe mapping showed that U in the CCug sediment after SMI addition was correlated with Fe (Figure G.8). XANES analysis of U hotspots revealed that U associated with Fe particles had been reduced to U(IV), whereas U-rich particles not associated with Fe were a mixture of U(VI) and U(VI) dominated by U(VI) (Figure G.9).

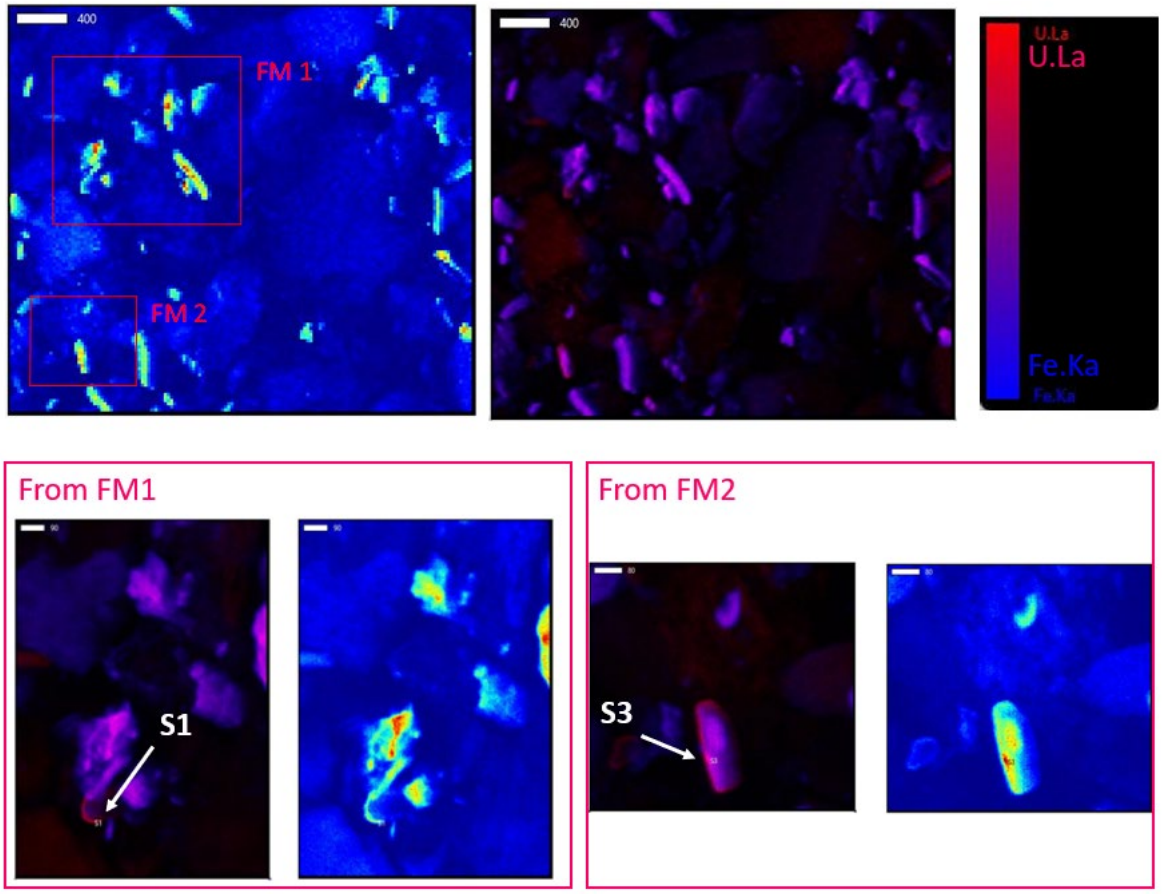

Figure G.8. X-ray microprobe coarse (*top row*) and fine (*bottom row*) maps showing areas of interest for U. The white arrows point to two spots selected for U L3-edge XANES, S1 and S3 (sample PNNL588).

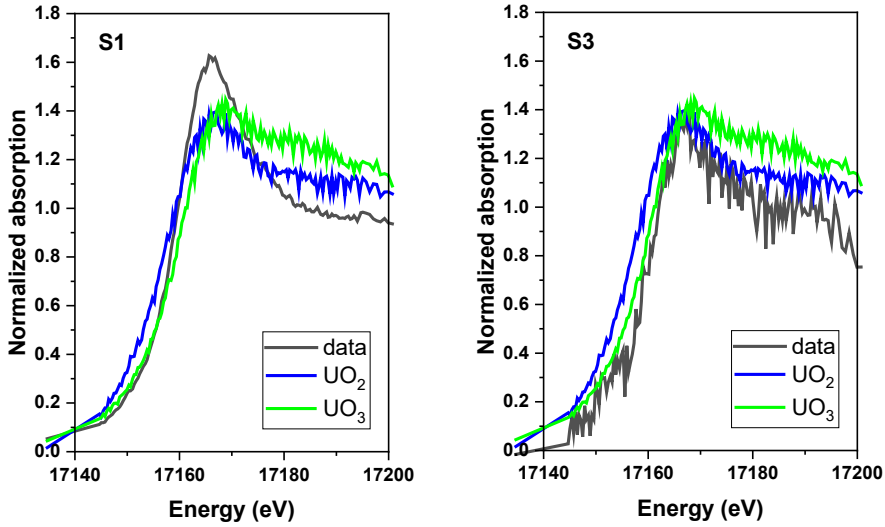

Figure G.9. U L3-edge XANES on spots S1 and S3 chosen on fine maps (on Figure G.8) (sample PNNL588).

For some of the batch experiments with CCug sediment, CoCOIs Cr (chromate), Sr, I-127 (iodate), and nitrate were present. Although chromate is easily reduced and is difficult to oxidize, the presence of 0.1% SMI (and subsequent Poly-PO_4) had no effect on the mobile chromate concentration (Figure G.10a), possibly due to the SMI reductive capacity (i.e., electron donor) being smaller than the sum of the redox reactive contaminants (i.e., electron acceptors). CoCOI Sr was not expected to be affected by the presence of SMI or Poly-PO_4, and results at 299 days confirmed that there was no effect (Figure G.10b). Iodine present as I-127 iodate is readily reduced to iodide, but both exhibit only a small amount of adsorption and no known precipitates. Measurements of the total I-127 (i.e., not iodate or iodide species) showed that the presence of SMI and Poly-PO_4 resulted in a 65% loss in mobile iodine. The small fraction of adsorbed I-127 in the untreated sediment (dark blue, Figure G.10c) decreased to zero for the SMI/PO_4-treated sediment. This may indirectly indicate that the I-127 initially added as iodate (which exhibits little sorption) was reduced to iodide (which exhibits almost no sorption). Finally, nitrate present as a CoCOI was not reduced in the presence of SMI and Poly-PO_4 (Figure G.10d).

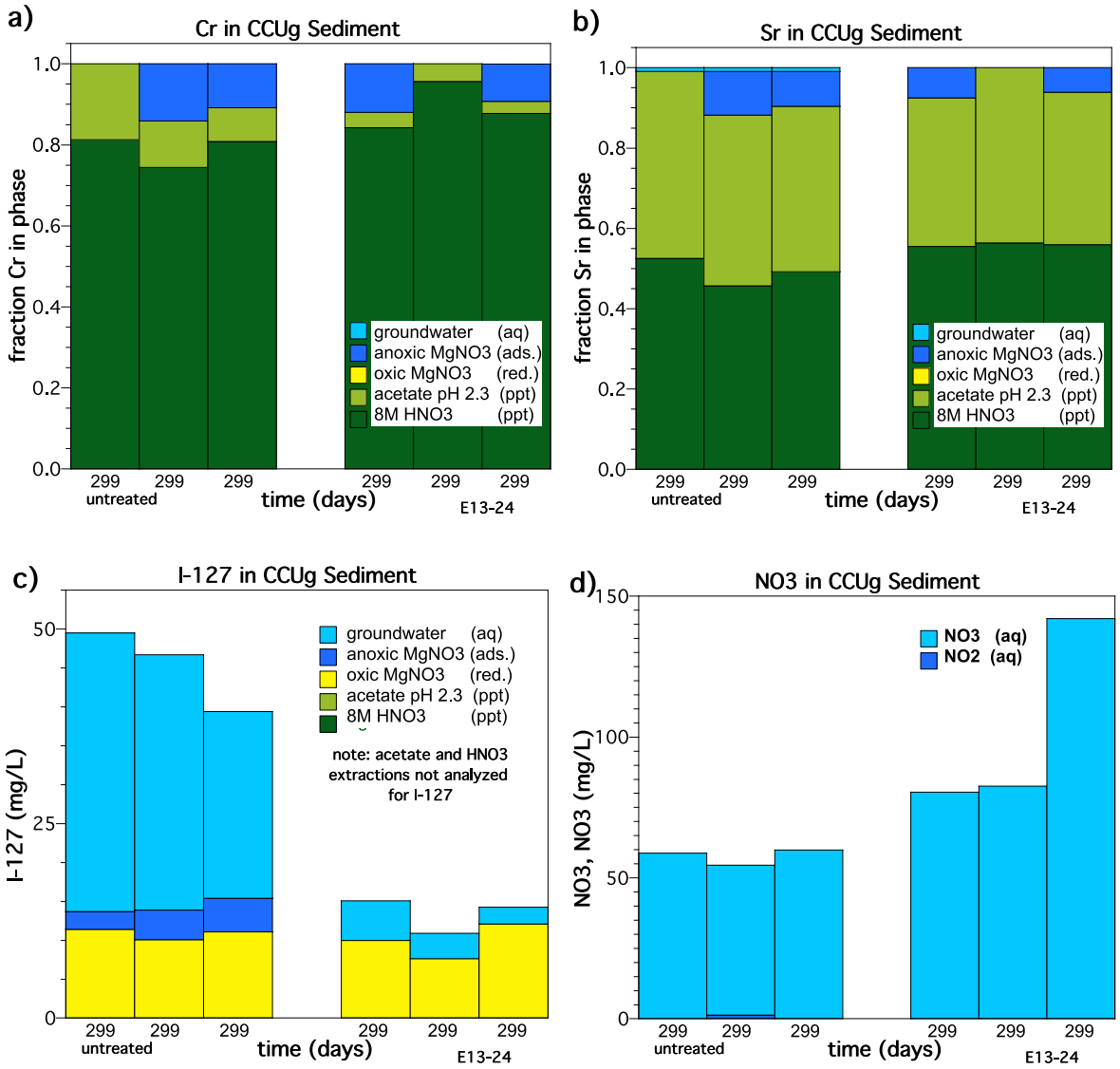

Figure G.10. Batch experiment with CCug sediment with SMI as a reductant followed by Poly-PO_4 to precipitate apatite, showing effects on the concentration of co-contaminants: (a) Cr, (b) Sr, (c) I-127 (as iodate), and (d) nitrate.

G.3 Saturated Column Results for Perched Water conditions

G.3.1 Tc and U Sequestration with SMI+Poly-PO_4

Water-saturated 1-D column leach experiments were conducted with approximately 220 pore volumes (PVs) of synthetic perched water (SPW) injected into each column. Sediments were initially treated for 7 days with just 0.1% SMI, followed by 30 days of Poly-PO_4 treatment. During injection of SPW, only 20% to 23% of the Tc-99 leached from the SMI/PO_4-treated sediment compared to nearly all for the untreated sediment (Figure G.11a and b). Post-leach extractions indicated that a higher fraction of Tc-99 (90% to 95%) was retained in the SMI-laden sediment compared with 8.3% for the untreated sediment (inset graph, Figure G.11a). A higher fraction of uranium was retained in the same sediment columns with SMI/PO_4 treatment (Figure G.11c and d), with leaching data indicating 83% to 92% U retained (i.e., only 7% to 17% leached by 220 PVs) and post-leach extractions indicating 90% to 100% of the U retained (inset graph, Figure G.11c).

Although U [as U(VI) aqueous species] is more difficult to reduce compared with Tc-99 [as pertechnetate, $Tc(VII)O_4^-$], U(VI) aqueous species also directly react with phosphate, forming precipitates of autunite and U-laden apatite. Uranium, although sequestered initially at a high fraction, was slowly leaching out, possibly indicating that the U-phosphate precipitates formed had moderate solubility. Over the time scale of months to years, freshly precipitated Ca-phosphate (amorphous) slowly crystallizes into apatite. Clearly, with long amendment (i.e., SMI and phosphates) and contaminant contact times (37 days in this case), good performance of a small amount of SMI (0.1 wt%) is observed. In contrast, groundwater applications with much shorter residence times do not show as good a performance (described in the following section), indicating the importance of long contact times for formation of low-solubility phosphate precipitates.

Changes in contaminant concentrations during stop flow events were used to calculate sediment/amendment uptake or release rates to further quantify the longevity of contaminant sequestration. For Tc, although significant mass was retained in the SMI/PO_4-treated sediment, the calculated release rates during stop flows were similar to untreated sediments (Table G.3, fifth column). Tc-99 release rates calculated during flow (prior to stop flow events) were six times smaller for treated vs. untreated sediments at 2 PVs (Table G.3, 7th column). In contrast, stop flow data for U did show a one to three order of magnitude slower release rate for SMI/PO_4-treated sediments compared to untreated sediments (Table G.4, fifth column). Negative release rates (i.e., net U uptake) also occurred in experiment E41 for 2 and 10 PV stop flows.

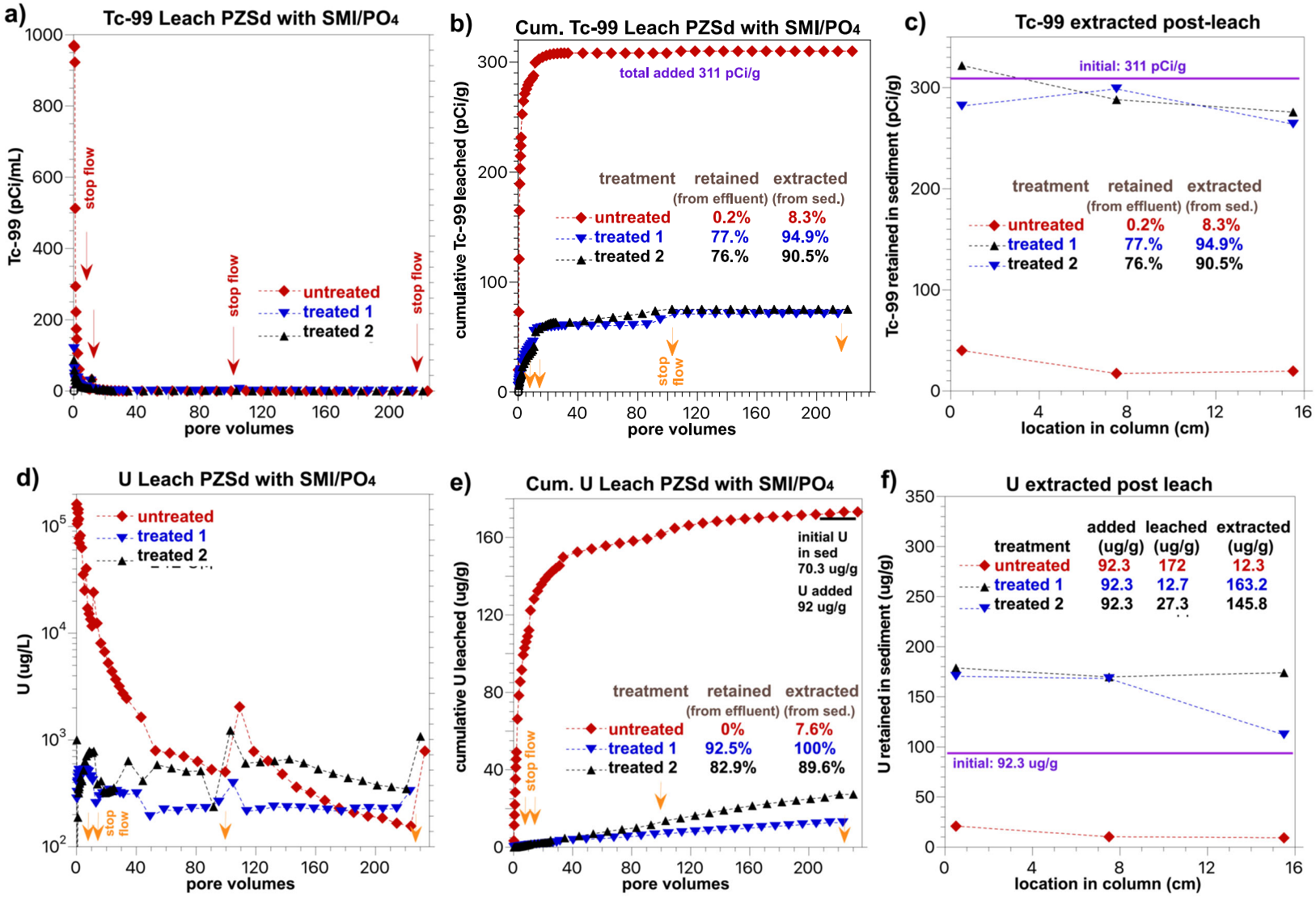

Figure G.11. PZsd sediment treatment with SMI and Poly-PO_4 showing changes in (a) Tc-99 leach concentration, (b) cumulative Tc-99 leached, (c) Tc-99 extracted, (d) U leach concentration, (e) cumulative U leached, and (f) U extracted.

Table G.3. Tc release rates calculated from column data in PZsd sediment during flow and during stop events.

#	Treatment	Stop Flow (h)	Stop Flow (PV)	Release Rate during Stop (µg/kg/day)	Release Rate during Stop (1/day)	Release Rate during Flow (µg/kg/day)	Release Rate during Flow (1/day)
E40	Untreated	14.5	1.94	-10.2	-4.42E-05	181	7.79E-04
	Untreated	161	10.4	0.814	2.83E-06	8.39	2.91E-05
	Untreated	396	99.8	0.0113	3.65E-08	0.00	0.00E+00
	Untreated	482	224	0.0019	6.29E-09	1.18	3.81E-06
E41	SMI/PO_4	14.5	2.05	3.03	1.49E-04	32.3	1.58E-03
	SMI/PO_4	161	9.77	0.667	1.46E-05	8.70	1.91E-04
	SMI/PO_4	396	95.6	0.064	9.73E-07	0.00	0.00E+00
	SMI/PO_4	482	214	-0.011	-1.48E-07	1.54	2.17E-05
E42	SMI/PO_4	14.5	2.12	3.663	2.19E-04	25.0	1.50E-03
	SMI/PO_4	161	10.6	0.962	2.32E-05	8.78	2.12E-04
	SMI/PO_4	396	93.0	0.010	1.32E-07	0.944	1.28E-05
	SMI/PO_4	482	221	-0.010	-1.36E-07	1.53	2.03E-05

Table G.4. U release rates calculated from column data in PZsd sediment during flow and during stop events.

#	Treatment	Stop Flow (h)	Stop Flow (PV)	Release Rate during Stop (µg/kg/day)	Release Rate during Stop (1/day)	Release Rate during Flow (µg/kg/day)	Release Rate during Flow (1/day)
E40	Untreated	14.5	1.94	3,513	7.15E-02	88,637	1.80E+00
	Untreated	161	10.4	399	3.56E-03	14,798	1.32E-01
	Untreated	396	99.8	20.3	1.17E-04	637	3.68E-03
	Untreated	482	224	6.84	3.95E-05	198	1.14E-03
E41	SMI/PO_4	14.5	2.05	-43.8	-2.26E-01	648	3.34E+00
	SMI/PO_4	161	9.77	-1.18	-1.13E-03	563	5.39E-01
	SMI/PO_4	396	95.6	1.71	2.62E-04	325	4.97E-02
	SMI/PO_4	482	214	1.10	8.69E-05	283	2.23E-02
E42	SMI/PO_4	14.5	2.12	15.6	1.00E-01	0.798	5.61E-04
	SMI/PO_4	161	10.6	0.798	5.61E-04	996	7.01E-01
	SMI/PO_4	396	93.0	13.1	1.13E-03	311	2.68E-02
	SMI/PO_4	482	221	7.94	2.91E-04	455	1.67E-02

G.3.2 Electron Mass Balance and Co-contaminant Sequestration

For the PZsd sediment, the high concentration of nitrate present was not reduced to nitrite, as nitrate concentrations were the same in SMI/PO_4-treated and untreated sediments (Figure G.12a). The PZsd columns were designed to approximate source area treatment for perched water conditions. As such, there was no flow for 37 days of SMI/PO_4 treatment, which was followed by injection of air-saturated pore water (with no contaminants) to evaluate treatment performance. The calculated electron balance indicates that (1) about 10% of the SMI reductive capacity (i.e., electron donor, assumed all Fe^o) was used to reduce U and Tc-99 (blue line near the top of Figure G.12b), and (2) 90 PVs of oxygen-saturated water was sufficient to oxidize the remaining SMI electron donating capacity (red line, Figure G.12b). Therefore, leaching (Figure G.11) should result in oxidizing conditions for Tc-99 and U from 90 to

220 PVs. Despite the oxidizing conditions, very little Tc-99 was released from the sediment, confirming that the reduced Tc, present as short dimeric TcO_2 chains coordinated to Fe oxide, was resistant to oxidation; this would not have been the case if it was present as a pure TcO_2 phase, which would be readily oxidized unless coated by apatite.

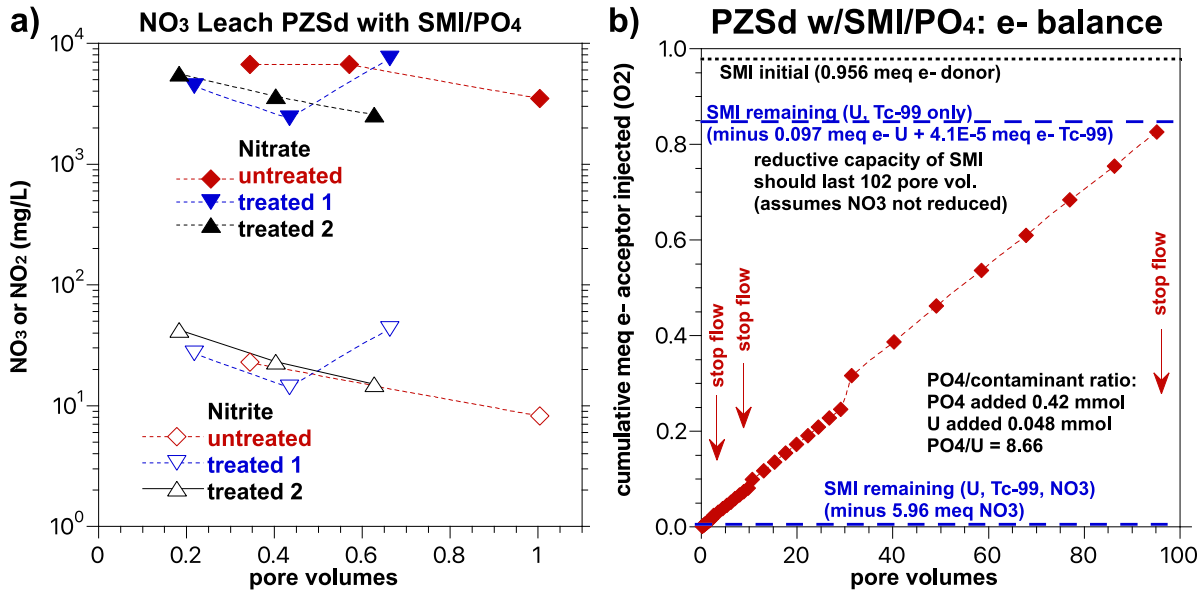

Figure G.12. PZsd sediment treatment with SMI and Poly-PO_4 showing changes in (a) nitrate and nitrite and (b) electron donor (SMI) compared with electron acceptors (U, Tc, with and without NO_3) added to sediments by e^- balance in *blue* with increasing e^- consumption by O_2 during injection in *red*.

G.3.3 Supplemental Saturated Column Geochemical Monitoring

The pH and dissolved oxygen measurements in effluent samples provide an indirect indication of the effect of the SMI/PO_4 treatment. There was little difference in the pH between untreated and SMI/PO_4-treated sediments (Figure G.13a), indicating that the buffering capacity of the sediment carbonates was sufficient for the 0.1% SMI present. In previous batch studies with 0.7% SMI, the pH increased up to 9.5 (PNNL-35432). The oxygen saturation (measured in effluent samples), in contrast, showed no or low oxygen in the SMI/PO_4-treated effluent samples initially (Figure G.13b), indicating the treatment did result in reducing (or at least O_2-free) conditions. Oxygen saturation increased over 100 PVs, as the SMI was oxidized by the influent oxygen. This was consistent with the calculated reduction capacity (Figure G.12b) of about 100 PVs.

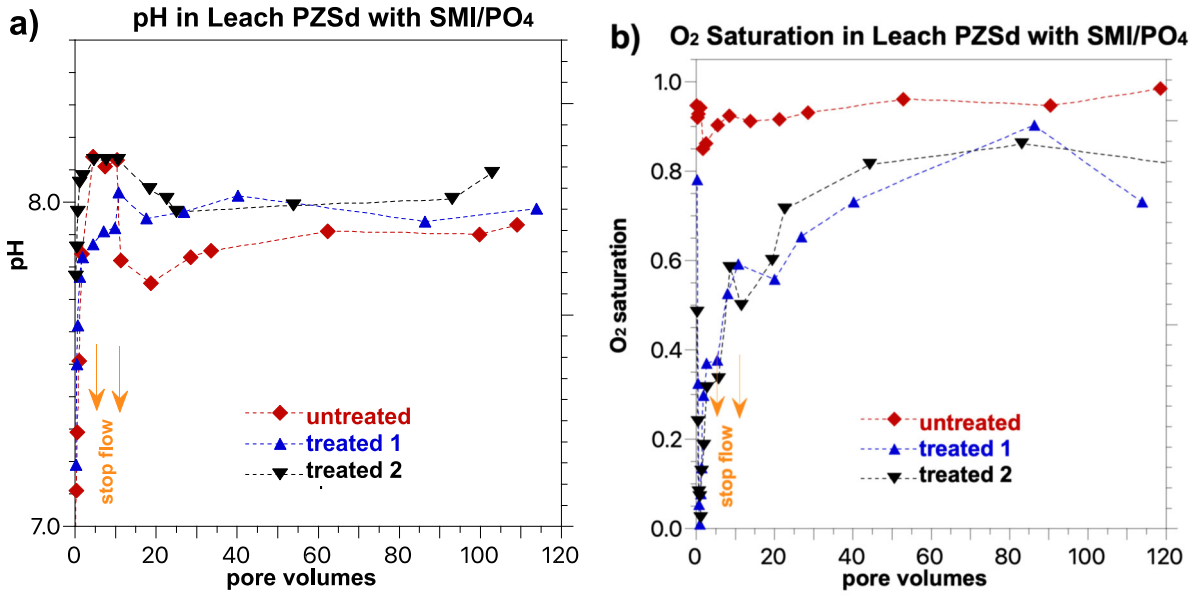

Figure G.13. PZsd sediment treatment with SMI and Poly-PO_4 showing changes in (a) pH and (b) O_2 saturation.

G.4 Saturated Column Results for BY Cribs Groundwater conditions

G.4.1 Tc Sequestration

PCOIs (Tc and U) were injected into CCug sediment without and with co-contaminants (nitrate, chromate, Sr^{2+}, I-127 as iodate) to evaluate the effect of SMI+Poly-PO_4 treatment on the primary contaminant removal mass, rate, and longevity when the system was oxidized. As shown with the PZsd sediment, with long (37-day) contact time, Tc-99 [added as pertechnetate, $Tc(VII)O_4^-$] was reduced to dimeric $Tc(IV)O_2$ chains coordinated to Fe oxide and remained immobilized after oxidation. For groundwater application, SMI and Poly-PO_4 were added to the CCug sediment, then contaminants were injected with a residence time in the column of 6 hours [approximating a groundwater flow rate of 0.6 m (2 ft) per day]. With the CCug sediment, 40% to 45% of the Tc-99 was removed from solution (Figure G.14a, first 100 PVs) during contaminant injection, with solid phase characterization showing that the mechanism of removal was the same as in the PZsd sediment, i.e., reduction of soluble pertechnetate ($Tc(VII)O_4^-$) to insoluble dimeric $Tc(IV)O_2$ chains coordinated to Fe oxide.

After a subsequent injection of 120 PVs of oxic water, very little of the reduced Tc-99 was remobilized, leaving 33% to 45% of the Tc-99 retained in the sediment (Figure G.14b). Post-leach extractions indicated that 32% to 35% of the Tc-99 was retained (inset graph, Figure G.14a). Calculation of the total electron acceptors injected into the column (i.e., Tc-99 and U) indicated that the reduction capacity of the 0.1% SMI should be consumed by 200 PVs (Figure G.19e, green line). Another calculation conducted with likely field conditions, with Tc, U, and assumed 100% saturation of dissolved oxygen, showed that the SMI in the sediment would be oxidized by 90 PVs (Figure G.19e, purple line). Therefore, although this SMI/PO_4 technology works well for Tc-99 as pertechnetate, site-specific conditions of all electron acceptors (including dissolved oxygen and nitrate) are needed to adjust the fraction of SMI to achieve greater longevity.

Groundwater application of SMI and Poly-PO_4 in CCug sediment to remove Tc-99 and U in the presence of co-contaminants (some of which are redox reactive) resulted in dramatically different behavior (Figure G.13c and d) than in the absence of co-contaminants (Figure G.13a and b). With co-contaminants, there was no difference in Tc-99 breakthrough between SMI/PO_4-treated and untreated sediments, and less than 1.5% of the Tc-99 was retained in the column (based on post-leach extractions, inset in Figure G.13c). The reason for this lack of SMI reactivity with the Tc-99 [pertechnetate, $Tc(VII)O_4^-$] is the high chromate (CrO_4^2) concentration. Cr(VI) is readily reducible to Cr(III), which causes nearly all the oxidation of the 0.1% SMI by 35 PVs (Figure G.19f, green line). Nitrate is also present at a high concentration, but very little of it is reduced (Figure G.19d). I-127 as iodate is also present but is calculated to oxidize only about 0.2% of the SMI.

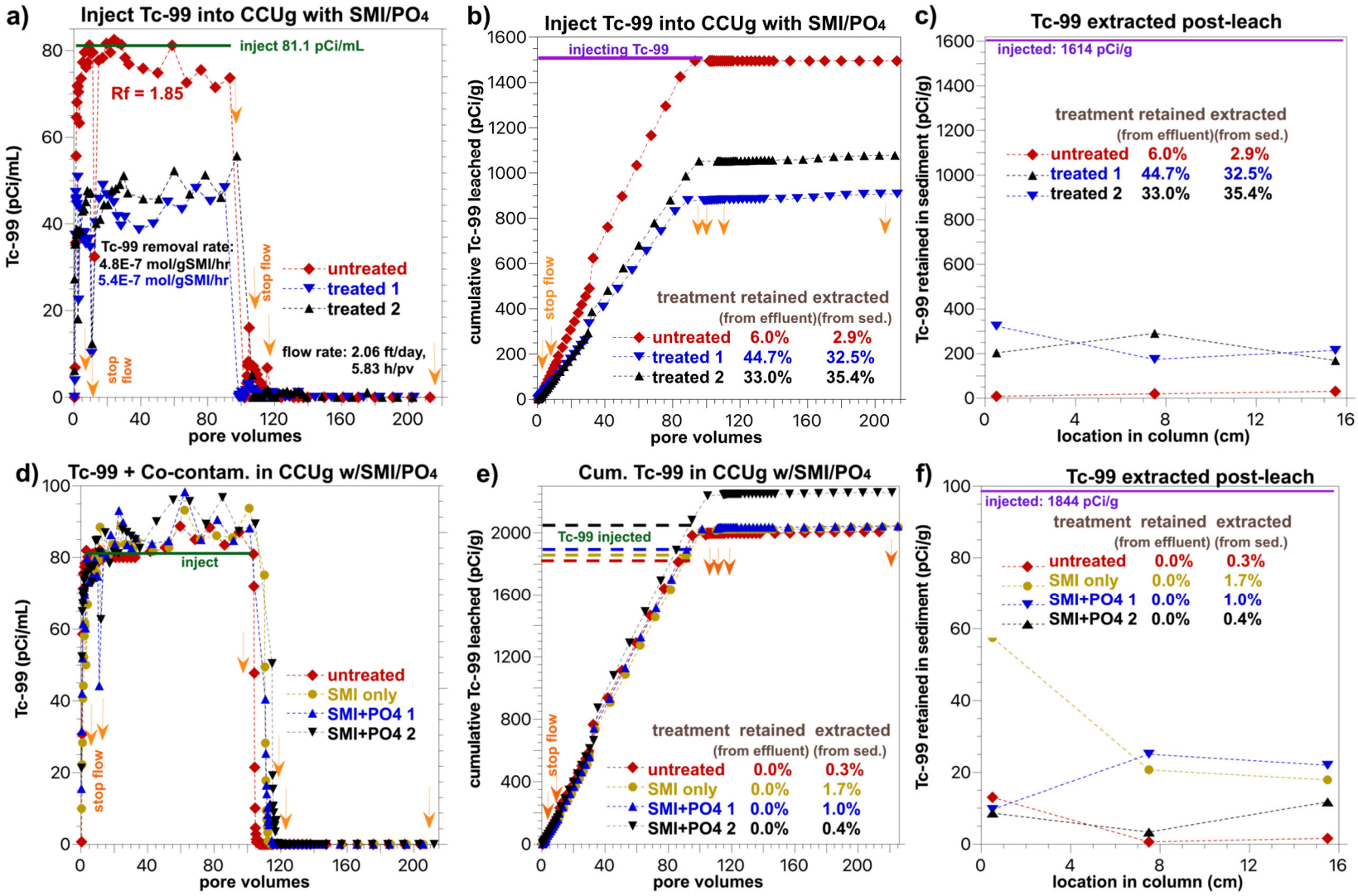

Figure G.14. CCug sediment treatment with SMI and Poly-PO_4 showing changes in (a) Tc-99 leach concentration (no co-contaminants), (b) cumulative Tc-99 leached (no co-contaminants), (c) Tc-99 extracted, (d) Tc-99 leach concentration with co-contaminants, (e) cumulative Tc-99 leached with co-contaminants, and (f) Tc-99 extracted with co-contaminants.

Changes in contaminant concentrations during stop flow events were used to calculate sediment/amendment uptake or release rates to further quantify the longevity of contaminant sequestration. For Tc-99 in experiments without co-contaminants, although leach experiments showed ~40% of Tc-99 was retained, calculated Tc-99 release rates were the same in untreated and SMI/PO_4-treated sediments (Table G.5, sixth column). However, Tc-99 release rates calculated from concentrations during flow (before stop flow events) did show ~20% lower release rates for SMI/PO_4-treated vs. untreated sediment at 2.5 PVs (Table G.5, eighth column). For Tc-99 experiments with co-contaminants, although leach experiments showed little difference in retention between untreated and treated sediments, Tc-99 release rates were systematically lower or negative (i.e., net uptake) for SMI/PO_4-treated sediments (Table G.3, fifth column). This is consistent with the PZsd results (previous section) where long contact time resulted in good sequestration of Tc. In these CCUg experiments, stop flows ranged from 15 hours (at 2.5 PVs) to 450 hours (at 100 PVs), and the lowest Tc-99 release rates occurred with longer stop flows. Tc-99 release rates showed that the SMI treatment only (experiment E54, Table G.6, sixth column) did not sequester Tc-99 as well as the SMI/PO_4 treatment at 100 PVs (i.e., experiments E55 and E56), indicating the phosphate treatment may have coated some of the reduced Tc-99 phases.

Table G.5. Tc release rates calculated from columns without co-contaminants in CCUg sediment during flow and during stop events.

#	Treatment	Stage	Stop Flow (h)	Stop Flow (PV)	Release Rate during Stop (µg/kg/day)	Release Rate during Stop (1/day)	Release Rate during Flow (µg/kg/day)	Release Rate during Flow (1/day)
E50	Untreated	Load	14.5	2.75	-1.87	-7.22E-05	76.8	2.97E-03
	Untreated	Load	161	11.4	-1.41	-8.45E-06	86.7	5.21E-04
	Untreated	Load	396	93.3	-0.908	-6.07E-07	80.3	5.37E-05
	Untreated	Leach	13.7	104	2.12	1.42E-06	8.92	5.96E-06
	Untreated	Leach	162	114	0.161	1.08E-07	1.44	9.62E-07
	Untreated	Leach	315	213	-0.020	-1.32E-08	1.40	9.33E-07
E51	SMI/PO_4	Load	14.5	2.38	-7.82	-4.55E-04	58.2	3.39E-03
	SMI/PO_4	Load	161	9.83	-0.778	-1.00E-05	39.6	5.09E-04
	SMI/PO_4	Load	396	90.1	-0.636	-7.24E-07	55.5	6.32E-05
	SMI/PO_4	Leach	13.7	100	-0.329	-3.74E-07	1.31	1.49E-06
	SMI/PO_4	Leach	162	110	-0.022	-2.44E-08	0.780	8.85E-07
	SMI/PO_4	Leach	315	203	-0.021	-2.29E-08	1.53	1.68E-06
E52	SMI/PO_4	Load	14.5	1.96	-5.67	-4.17E-04	47.9	3.53E-03
	SMI/PO_4	Load	161	10.0	-1.111	-1.24E-05	59.2	6.61E-04
	SMI/PO_4	Load	396	97.4	-0.665	-6.32E-07	69.8	6.64E-05
	SMI/PO_4	Leach	13.7	108	0.000	0.00E+00	0.00	0.00E+00
	SMI/PO_4	Leach	162	117	-0.039	-3.70E-08	1.54	1.46E-06
	SMI/PO_4	Leach	315	202	0.000	0.00E+00	0.00	0.00E+00

Table G.6. Tc release rates calculated from columns with co-contaminants in CCug sediment during flow and during stop events.

#	Treatment	Stage	Stop Flow (h)	Stop Flow (PV)	Release Rate during Stop (µg/kg/day)	Release Rate during Stop (1/day)	Release Rate during Flow (µg/kg/day)	Release Rate during Flow (1/day)
E53	Untreated	Load	14.5	2.85	0.977	2.67E-05	98.3	2.68E-03
	Untreated	Load	161	10.9	0.310	1.66E-06	98.7	5.29E-04
	Untreated	Load	396	98.2	-0.081	-4.08E-08	109	5.49E-05
	Untreated	Leach	13.7	109	0.227	1.13E-07	0.738	3.70E-07
	Untreated	Leach	162	118	0.000	0.00E+00	0.000	0.00E+00
	Untreated	Leach	315	211	-0.011	-5.23E-09	0.951	4.74E-07
E54	SMI	Load	14.5	2.55	-3.09	-1.38E-04	78.9	3.52E-03
	SMI	Load	161	10.5	-1.12	-7.13E-06	103	6.54E-04
	SMI	Load	396	101	-0.24	-1.21E-07	1,182	7.24E-02
	SMI	Leach	13.7	112	-0.060	-2.93E-08	1.19	5.87E-07
	SMI	Leach	162	121	0.000	0.00E+00	0.000	0.00E+00
	SMI	Leach	315	216	-0.003	-1.53E-09	0.246	1.20E-07
E55	SMI/PO_4	Load	14.5	2.27	-2.67	-9.80E-05	91.6	3.36E-03
	SMI/PO_4	Load	161	10.1	-0.39	-2.41E-06	98.2	6.14E-04
	SMI/PO_4	Load	396	101	-0.6	-3.07E-07	116	5.66E-05
	SMI/PO_4	Leach	13.7	113	1.76	8.56E-07	7.11	3.45E-06
	SMI/PO_4	Leach	162	122	0.005	2.47E-09	0.000	0.00E+00
	SMI/PO_4	Leach	315	215	-0.012	-5.99E-09	0.985	4.76E-07
E56	SMI/PO_4	Load	14.5	2.24	-0.97	-3.19E-05	99.8	3.27E-03
	SMI/PO_4	Load	161	11.0	0.33	1.77E-06	109	5.76E-04
	SMI/PO_4	Load	396	105	-0.5	-2.30E-07	119	5.34E-05
	SMI/PO_4	Leach	13.7	117	0.97	4.32E-07	4.61	2.06E-06
	SMI/PO_4	Leach	162	125	0.000	0.00E+00	0.000	0.00E+00
	SMI/PO_4	Leach	315	212	-0.005	-2.13E-09	0.866	3.85E-07

G.4.2 U Sequestration

Injection of Tc-99 and U (no co-contaminants) into SMI/PO_4-treated sediments resulted in the retention of 19% of the U (Figure G.15a and b), which was consistent with post-leach extractions showing 16% to 20% greater U retention for the treated compared to untreated sediment. Injection of Tc-99 and U with CoCOIs into SMI/PO_4-treated sediments was similar, with 15% to 30% greater U retention compared to untreated sediment based on leach experiments (Figure G.15c and d). Post-leach extractions showed similar results, with 19% to 23% retention in SMI/PO_4-treated sediments and 5% in SMI-only treated sediment (inset in Figure G.15c). These results show much better performance for U than for Tc-99 (Figure G.14), even though Tc-99 (as pertechnetate) is easier to reduce than U (as uranyl carbonate), likely due to U sequestration by the phosphate (i.e., precipitation of autunite and U-laden apatite), as evidenced by solid phase characterization results showing that the majority of the U is not reduced and remains U(VI) upon removal from solution. The greater U retention in extractions for the SMI/PO_4-treated sediments compared to the SMI-only treated sediments is consistent with this hypothesis (Figure G.15a and c, inset graphs).

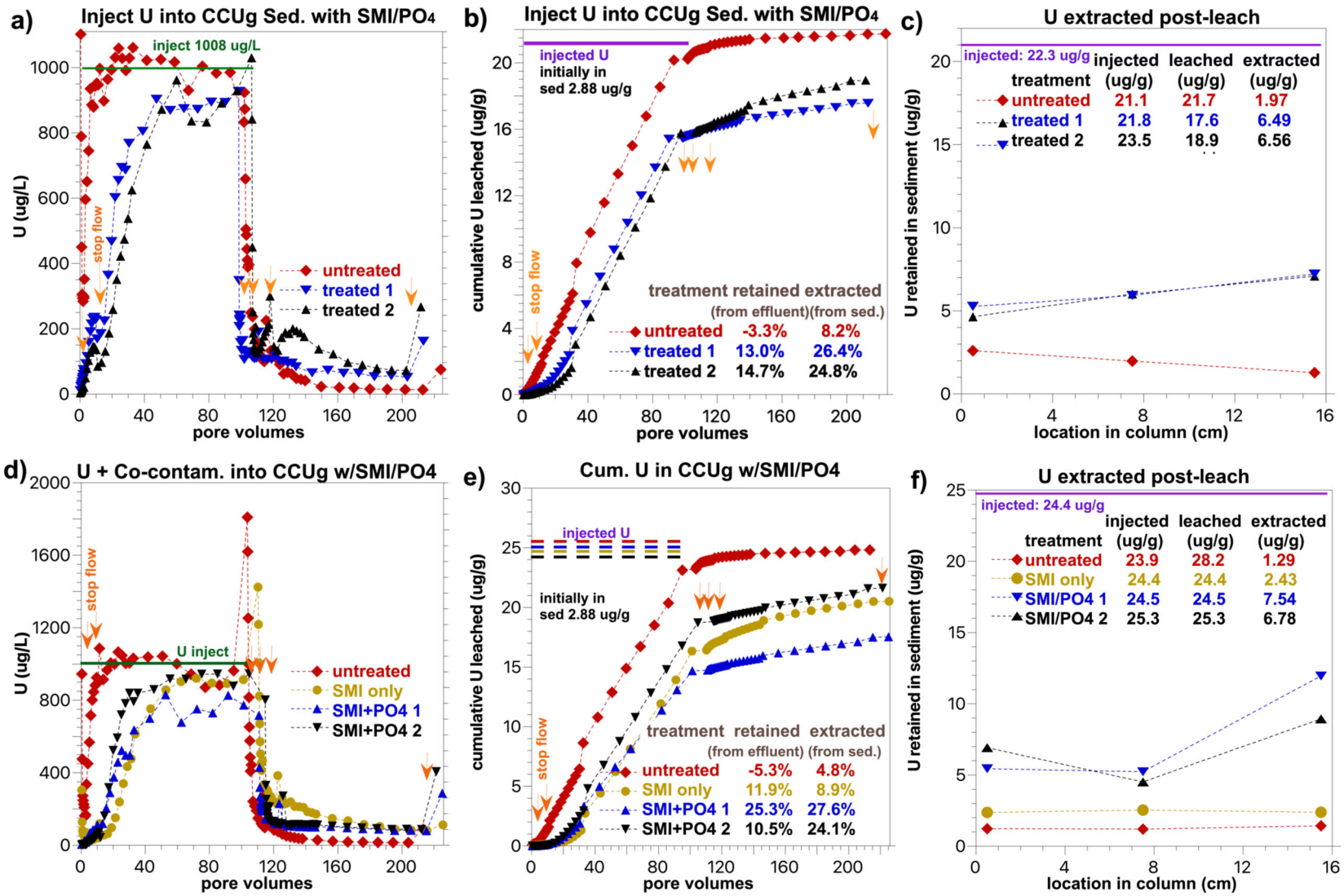

Figure G.15. CCug sediment treatment with SMI and Poly-PO_4 showing changes in (a) U leach concentration (no co-contaminants), (b) cumulative U leached (no co-contaminants), (c) U leach concentration with co-contaminants, and (d) cumulative U leached with co-contaminants.

For U in experiments without co-contaminants, leach experiments showed ~20% retention of U, and calculated U release rates were initially lower for SMI/PO_4-treated sediments (Table G.7, sixth column) at 2 and 11 PVs, but they then increased and were similar to release rates for untreated sediments by 100 PVs. Electron mass balance during flow indicated that the SMI should be oxidized by 200 PVs (Figure G.19e). For U experiments with CoCOIs, leach experiments showed ~20% U retention in treated sediments and stop flow data showed net U uptake rates at 2, 10, and 100 PVs for SMI/PO_4-treated sediments (Table G.8, sixth column, experiments E55, E56), in contrast to high rates of U release from untreated (E53) and SMI-only treated (E54) sediments. These results, in combination with solid phase characterization, show that the mechanisms of U and Tc-99 removal from solution were different for the SMI/PO_4-treatment. Tc-99 was removed from solution by the addition of SMI, resulting in reduction of soluble pertechnetate [$Tc(VII)O_4^-$] to insoluble dimeric $Tc(IV)O_2$ chains coordinated to Fe oxide; further addition of phosphate had no impact on Tc-99 removal or retention. Soluble uranyl species [$U(VI)O_2^{2+}$] were not readily reduced by SMI but were mostly removed from solution by the phosphate portion of the SMI/PO_4 treatment, resulting in the incorporation of U [as $U(VI)O_2^{2+}$] into low-solubility phosphate precipitates, such as autunite and U-laden apatite.

Table G.7. U release rates calculated from columns without co-contaminants in CCug sediment during flow and during stop events.

#	Treatment	Stage	Stop Flow (h)	Stop Flow (PV)	Release Rate during Stop (µg/kg/day)	Release Rate during Stop (1/day)	Release Rate during Flow (µg/kg/day)	Release Rate during Flow (1/day)
E50	Untreated	Load	14.5	2.75	63.3	2.21E-01	384	1.34E+00
	Untreated	Load	161	11.4	1.49	8.03E-04	1,033	5.56E-01
	Untreated	Load	396	93.3	-1.87	-9.29E-05	1,074	5.32E-02
	Untreated	Leach	13.7	104	1.89	9.39E-05	424	2.10E-02
	Untreated	Leach	162	114	3.71	1.77E-04	109	5.21E-03
	Untreated	Leach	315	213	-0.05	-2.49E-06	49.1	2.26E-03
E51	SMI/PO_4	Load	14.5	2.38	-2.46	-1.27E-01	86.0	4.43E+00
	SMI/PO_4	Load	161	9.83	-1.9	-5.98E-03	261	8.33E-01
	SMI/PO_4	Load	396	90.1	0.45	2.90E-05	1,024	6.65E-02
	SMI/PO_4	Leach	13.7	100	8.63	5.56E-04	154	9.90E-03
	SMI/PO_4	Leach	162	110	2.53	1.63E-04	126	8.13E-03
	SMI/PO_4	Leach	315	203	1.82	1.04E-04	58.9	3.36E-03
E52	SMI/PO_4	Load	14.5	1.96	-1.72	-2.89E-01	33.2	5.59E+00
	SMI/PO_4	Load	161	10.0	-1.63	-7.96E-03	171	8.33E-01
	SMI/PO_4	Load	396	97.4	1.33	8.44E-05	1,165	7.39E-02
	SMI/PO_4	Leach	13.7	109	21.2	1.33E-03	168	1.05E-02
	SMI/PO_4	Leach	162	117	2.76	1.69E-04	267	1.64E-02
	SMI/PO_4	Leach	315	202	3.21	1.70E-04	90.9	4.81E-03

Table G.8. U release rates calculated from columns with co-contaminants in CCug sediment during flow and during stop events.

#	Treatment	Stage	Stop Flow (h)	Stop Flow (PV)	Release Rate during Stop (µg/kg/day)	Release Rate during Stop (1/day)	Release Rate during Flow (µg/kg/day)	Release Rate during Flow (1/day)
E53	Untreated	Load	14.5	2.85	47.7	2.18E-01	210	9.61E-01
	Untreated	Load	161	10.9	6.03	3.80E-03	1,125	7.09E-01
	Untreated	Load	396	98.2	11.26	4.87E-04	1,205	5.21E-02
	Untreated	Leach	13.7	109	10.1	4.29E-04	512	2.17E-02
	Untreated	Leach	162	118	6.05	2.52E-04	122	5.07E-03
	Untreated	Leach	315	211	1.22	4.94E-05	17.6	7.11E-04
E54	SMI	Load	14.5	2.55	6.87	1.19E-01	58.8	1.02E+00
	SMI	Load	161	10.5	2.50	1.88E-02	52.8	3.99E-01
	SMI	Load	396	101	6.72	4.12E-04	1,182	7.24E-02
	SMI	Leach	13.7	112	15.8	9.42E-04	535	3.19E-02
	SMI	Leach	162	121	4.79	2.76E-04	302	1.74E-02
	SMI	Leach	315	216	0.51	2.50E-05	105	1.74E-02
E55	SMI/PO_4	Load	14.5	2.27	-2.53	-3.80E-01	33.4	5.01E+00
	SMI/PO_4	Load	161	10.1	-0.49	-3.88E-03	146	1.14E+00
	SMI/PO_4	Load	396	101	-4.53	-3.08E-04	1,015	6.91E-02
	SMI/PO_4	Leach	13.7	113	12.0	8.04E-04	247	1.66E-02
	SMI/PO_4	Leach	162	122	3.5	2.28E-04	159	1.05E-02
	SMI/PO_4	Leach	315	215	3.4	1.95E-04	105	6.00E-03
E56	SMI/PO_4	Load	14.5	2.24	-1.02	-4.86E-01	8.40	3.99E+00
	SMI/PO_4	Load	161	11.0	-0.93	-1.36E-02	95.7	1.39E+00
	SMI/PO_4	Load	396	105	-1.89	-1.01E-04	1,261	6.74E-02
	SMI/PO_4	Leach	13.7	117	21.6	1.14E-03	185	9.80E-03
	SMI/PO_4	Leach	162	125	4.89	2.55E-04	159	8.28E-03
	SMI/PO_4	Leach	315	212	5.27	2.44E-04	116	5.37E-03

G.4.3 Co-contaminant Sequestration

Co-contaminants were present in some CCug sediments with SMI only or SMI/PO_4 treatments (Figure G.16). As described in the two previous sections, the presence of Cr as chromate (CrO_4^{2-}) highly impacted Tc-99 and U treatment by 20 PVs (Figure G.19f) compared to treated sediments with no co-contaminants, which oxidize by 200 PVs (Figure G.19e). Cr has been shown previously to passivate ZVI surfaces, reducing corrosion, which can inhibit reduction of Tc-99 (Cartledge 1966; Guan et al. 2015; de Lima Perini and Nogueira 2017; Williams et al. 2024). Notably, recent research has shown that when the Fe^0:(Tc+Cr) molar ratio decreases to less than 100, ZVI may no longer reduce Tc-99 and Cr (Williams et al. 2024).

Injected chromate was initially reduced (Figure G.17) in SMI and SMI/PO_4-treated sediments (first few PVs, Figure G.16a) compared to untreated sediment, but was not reduced at 25 and 100 PVs, implying the reductive capacity of the SMI was depleted. Injected Sr^{2+}, which is not redox reactive, also showed low initial concentrations (Figure G.16b), but this was likely caused by the high adsorption of Sr^{2+} to mineral phases in the sediment, similar to Ca^{2+} (i.e., estimated breakthrough PV of 100 to 125). The injected Sr^{2+}

might initially be oversaturated and precipitate as $SrCO_3$. By 100 PVs, the Sr^{2+} effluent concentration was the same as the influent concentration. The total I-127 effluent concentration was the same as the influent concentration for SMI, SMI/PO_4, and untreated sediments (Figure G.16c). The I-127, initially present as iodate ($I(V)O_3^-$), may have been reduced to iodide (I^-) but exhibited only a small amount of adsorption (i.e., both are mobile). The nitrate concentration was measured only after stop flow events and showed no difference in effluent concentration for SMI, SMI/PO_4, and untreated sediments. The nitrite concentration was slightly above detection limits for some samples, indicating < 2% nitrate reduction in all sediments (likely microbial since both treated and untreated sediments were the same).

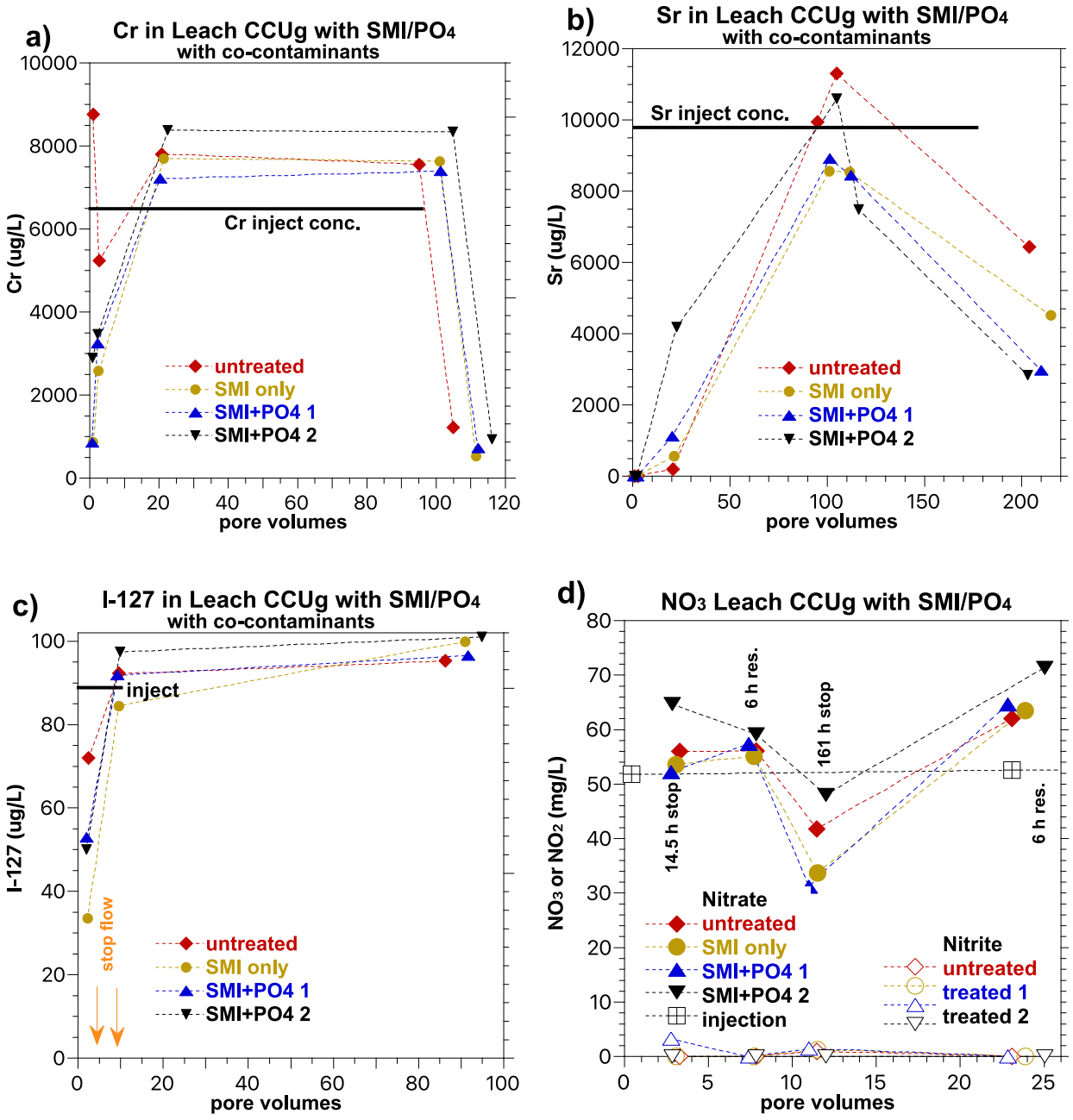

Figure G.16. CCug sediment treatment with SMI and Poly-PO_4 showing changes in co-contaminant concentrations (a) Cr, (b) Sr, (c) I-127, and (d) nitrate and nitrite.

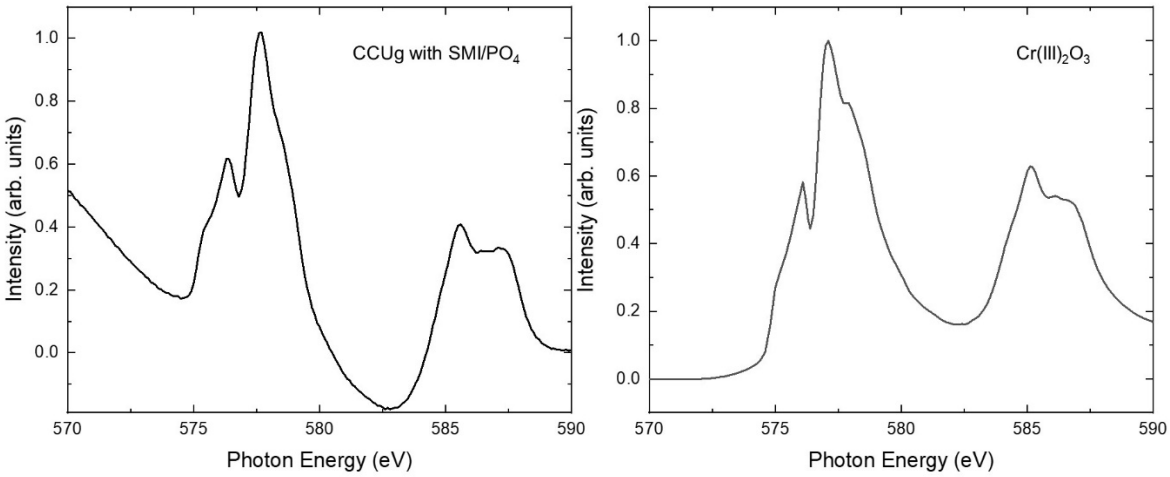

Figure G.17. Cr L-edge XAS for CCug sediment treatment with SMI and Poly-PO_4 and a $Cr(III)_2O_3$ standard showing that Cr has been reduced from Cr(VI) to Cr(III).

The initial SMI and 35-mM Poly-PO_4 treatment in the CCug sediments mainly resulted in some reductive capacity (as previously described) and phosphate precipitation. Measurement of aqueous PO_4 in effluent samples showed none for untreated and SMI-only treated sediments and a maximum of 1.2 mmol/L (in the first sample at 0.2 PVs) for the SMI/PO_4-treated sediments. By 20 PVs, aqueous phosphate was less than 0.1 mmol/L (Figure G.18).

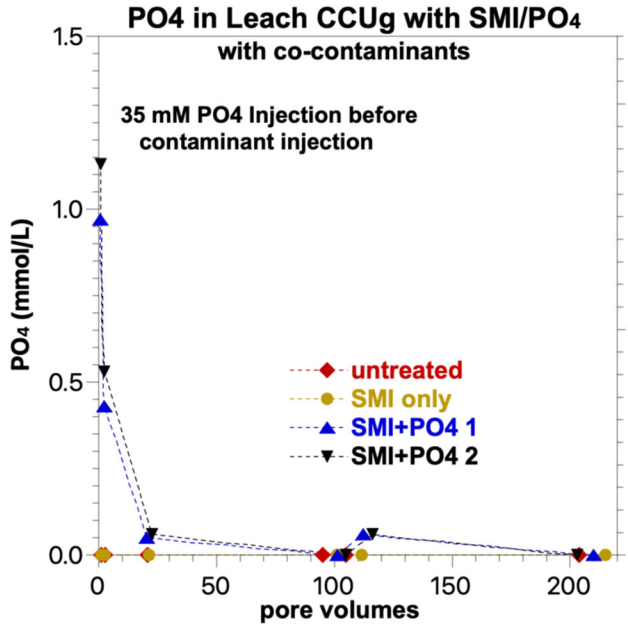

Figure G.18. Phosphate leaching in CCug sediment during injection of Tc, U, and co-contaminants.

G.4.4 Geochemical Monitoring

The pH and dissolved oxygen measurements in effluent samples provide an indirect indication of the effect of the SMI/PO_4 treatment. The initial pH of the SMI/PO_4-treated sediment experiments (i.e., first 10 PVs) was slightly elevated (i.e., pH peak at 8.8) compared to untreated sediments (peak at 8.5) for CCug sediments without and with contaminants (Figure G.19a and c). The oxygen saturation, however, was not initially different between untreated and treated sediments (Figure G.19b and d) in the first 10 PVs, indicating that the contaminants (and co-contaminants) injected may have consumed much of the SMI reductive capacity during flow. These results differ from initial dissolved oxygen measurements in the PZsd sediment (Figure G.13b), where the 37-day treatment before flow started removed dissolved oxygen in the water. There was still some reductive capacity in the CCug sediments, as evidenced by the low dissolved oxygen measurements after the 450-hour stop flow at 100 PVs without co-contaminants (Figure G.19b), but not with co-contaminants (Figure G.19d), consistent with the hypothesis that reduction of chromate consumed nearly all of the reductive capacity of the SMI.

The calculated electron balance during flow with contaminant injection (no co-contaminants) indicated that the SMI reductive capacity should be depleted by 200 PVs (Figure G.19e, green diamonds). In these laboratory experiments, Tc-99 and U were injected in an anaerobic solution. In a hypothetical field case, where the upgradient water would be oxic (assuming air-saturation), the combination of dissolved oxygen, Tc, and U would deplete the SMI reductive capacity by 80 PVs (Figure G.19e, purple triangles). Note that Hanford Site groundwater dissolved oxygen varies spatially, so site specific geochemical conditions are needed to simulate the longevity of a reduced barrier.

The calculated electron balance during flow with contaminant injection that included co-contaminants indicated that the SMI reductive capacity should be depleted by 35 PVs (Figure G.19f, green diamonds). If dissolved oxygen were present, the SMI reductive capacity would be depleted by 31 PVs (Figure G.19f, purple triangles). The reason for this rapid reductive capacity loss is the reduction of co-contaminants. The milliequivalence fraction of electron acceptors injected that oxidizes the SMI is (1) nitrate at 61%, (2) Cr at 38%, (3) U at 0.3%, (4) I-127 at 0.2%, and (5) Tc-99 at 0.005%. Because either nitrate is not reduced or only a small fraction is reduced (Figure G.16d), the SMI reductive capacity is mainly being oxidized by chromate reduction (76x higher electron consumption than U, I-127, and Tc-77 combined). If a field site contained this combination of contaminants, greater reductive capacity would be suggested (i.e., more than the 0.1% SMI used in these experiments) to increase barrier longevity.

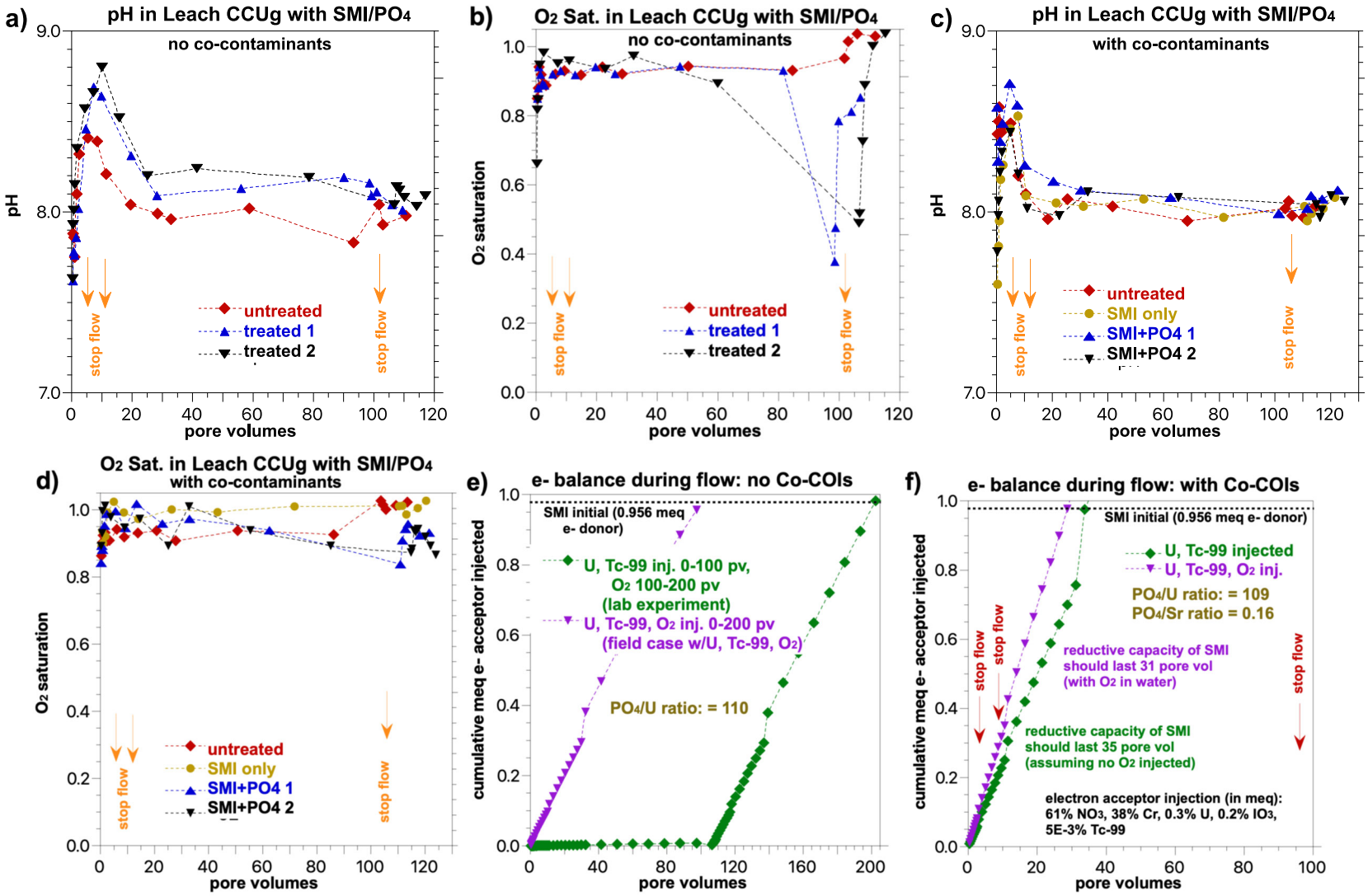

Figure G.19. CCug sediment treatment with SMI and Poly-PO_4 showing changes in (a) pH (no CoCOIs), (b) oxygen saturation (no CoCOIs), (c) pH (with CoCOIs), (d) oxygen saturation (with CoCOIs), (e) electron donor/acceptor balance (no CoCOIs), and (f) electron donor/acceptor balance (with CoCOIs).

G.4.5 Bromide Tracer Breakthrough

Injection of 80 mg/L bromide was used in columns to evaluate physical transport through the sediment. Bromide in the PZsd sediment showed similar breakthrough for untreated and SMI/PO_4-treated sediments (Figure G.20a). In contrast, in the CCug sediments with no co-contaminants present, bromide breakthrough happened sooner in SMI/PO_4-treated sediments compared to untreated sediment (Figure G.20b). Finally, bromide injection in CCug sediment in experiments with co-contaminants present showed the slowest breakthrough for the untreated sediment compared to SMI or SMI/PO_4-treated sediments, but the differences were small (Figure G.20c).

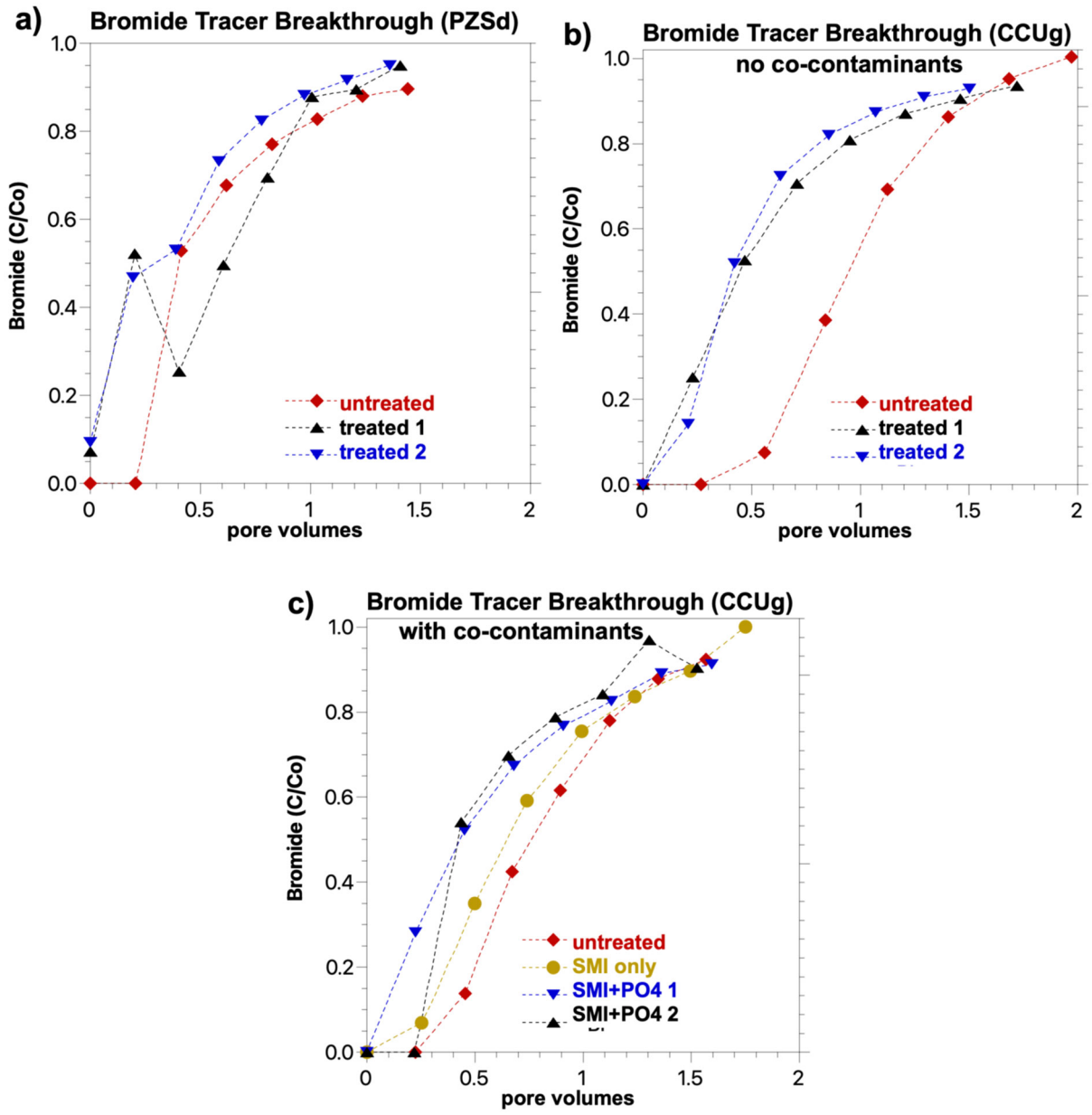

Figure G.20. Bromide breakthrough in columns: (a) PZsd sediment, (b) CCug sediment, no CoCOIs, and (c) CCug sediment with CoCOIs.

G.5 Summary of Performance of Sulfur Modified Iron and Polyphosphate for Groundwater

G.5.1 Perched Water Application

Batch experiments in PZsd (perched) sediments showed that 0.1% SMI+Poly-PO_4 treatment resulted in fair performance for Tc-99 and very good performance for U. These batch experiments covered a range of conditions: (1) initial SMI-only treatment for 7 days, (2) subsequent Poly-PO_4 treatment from 7 to 50 days, and (3) oxidation of the system from 50 to 300 days. Tc-99 mobility decreased from 66% to 9% during SMI-only treatment, then slowly remobilized during PO_4 and oxidation periods to 35%. These results indicate that reduced/precipitated Tc-99 phases (under these perched water conditions) were not well coated by phosphate precipitates. In contrast, U with an initial mobile fraction of 8% was decreased to less than 0.3% by the SMI treatment, then decreased further with phosphate treatment and oxidation (based on increasing hard-to-extract surface phases). This is likely because aqueous U species react with phosphate to form autunite and U-substituted apatite in reducing or oxidizing environments.

During flow in 1-D columns, the 0.1% SMI+Poly-PO_4 treatment also resulted in fair performance for Tc-99 and very good performance for U, although there were differences between column and batch results. Injection of contaminant-free water resulted in leaching of only 23% of the Tc-99 (i.e., 77% retained). After the initial breakthrough of Tc-99 at 0 to 10 PVs, only a small amount of Tc-99 was slowly remobilized between 10 and 90 PVs (4%), then no additional Tc-99 was remobilized between 90 and 220 PVs (82 days). Although the SMI-laden sediment in the columns should have been oxidized by 100 PVs (40 days), these results contrast with batch experiments in which a large fraction of Tc-99 was remobilized during oxidation from 50 to 300 days. For U in PZsd sediment leach experiments, the 0.1% SMI+Poly-PO_4 treatment resulted in 10% to 20% U breakthrough (i.e., 80% to 90% U retained) compared to untreated sediment leaching. However, during the 220 PVs (42 days) of water injection, a small fraction of U was slowly leaching out (i.e., 5% to 10% from 20 to 220 PVs). These results are also in contrast to 300-day batch experiments, which did not show U remobilization behavior. Clearly, differences between batch and 1-D columns with the same sediment, water, sediment-to-water ratio, and contaminants reflect the influence of flow advecting mobile (aqueous) species away from surface species (precipitated, reduced, incorporated, coated). Results in columns likely better approximate field conditions with water advection.

The 0.1% SMI+Poly-PO_4 treatment performed well for Tc-99 and U, likely because the reductive capacity of the barrier was not consumed by the high nitrate also present in the PZsd sediment. Nitrate and nitrite measurements in columns indicated that nitrate was not being degraded to nitrite even after the initial 37 days of 0.1% SMI+Poly-PO_4 treatment before flow.

Although the 0.1% SMI had approximately the same reductive capacity as other liquid and solid reductant technologies, it is hypothesized that the slow reduction of Tc-99 and U observed may be related to the reductive capacity being concentrated at small SMI particle surfaces with low surface area in contrast to liquid reductant technologies (Ca polysulfide, for example), which result in the reductive capacity being distributed over a larger surface area in small FeS (and other metal sulfide) precipitates. While batch experiments (50 days of reduction) and perched water experiments (37 days of reduction) worked well, short SMI-contaminant contact time experiments (i.e., groundwater, 6-hour contact time) performed poorly. Surface phase analysis of the surface precipitates showed that Tc-99 was primarily present as Tc(IV), even in oxidized sediment. Tc-99 was not just reduced by the SMI but likely coated by phosphate or other precipitates that prevented the surface Tc(IV) precipitate from oxidizing and remobilizing. Field-scale ZVI and SMI permeable reactive barrier performance over years has shown large increases in pH, which not only reduces contaminants but results in precipitation of calcite, Fe-hydroxide carbonates,

and lower concentrations of ferrihydrite, goethite, green rust, amakinite, and magnetite (Roehl et al. 2005). It is hypothesized that the carbonate precipitates may contribute to the coating of Tc(IV) precipitates, slowing reoxidation.

G.5.2 BY Cribs Groundwater Application

Batch experiments in CCug sediments showed that 0.1% SMI+Poly-PO_4 treatment resulted in only fair performance for Tc-99 (without co-contaminants), good performance for Tc-99 with co-contaminants present, and very good performance for U without and with co-contaminants. For Tc-99 without co-contaminants, mobility decreased from 65% to 11% during SMI treatment (0 to 7 days), decreased slightly (mobile fraction 4%) during subsequent Poly-PO_4 treatment (7 to 50 days), but then slowly remobilized to 43% during oxidation (50 to 300 days). This mobility increase for Tc-99 is indicative of slow oxidation of the reduced Tc-99 surface phases and implies that these were not well (or only partially) coated by the apatite precipitate. For Tc-99 in the presence of co-contaminants, the mobile fraction decreased from 84% (untreated) to 9% during SMI treatment (0 to 7 days), decreased slightly to 4% during Poly-PO_4 treatment (7 to 50 days), then only remobilized slightly to 8% during oxidation (50 to 300 days). These results suggest an interaction between co-contaminants and Tc, such as aqueous Sr^{2+} and carbonate precipitation coating some reduced/precipitated Tc.

For U, batch experiments in CCug sediment decreased mobility (without or with co-contaminants) from 13% to 4% during SMI treatment (0 to 7 days), then Poly-PO_4 treatment decreased mobility to 3% (7 to 50 days). During oxidation (50 to 300 days), U mobility decreased to < 1%, indicating that incorporation of U(VI) species in autunite or apatite in oxic sediment is a better treatment than reduction of U(VI) species by SMI. A further change in the U surface phases is noted by the slow increase in the 8M HNO_3-extractable U from 25% at 7 days to 52% at 299 days, possibly from the crystallization of U-bearing apatite.

During flow in 1-D columns, the 0.1% SMI+Poly-PO_4 treatment resulted in moderate performance for Tc-99 removal (i.e., 33% to 45% Tc-99 immobilized) without CoCOIs, but performance for Tc-99 removal in the presence of co-contaminants was poor (i.e., 0.4% to 1.7% of Tc-99 was immobilized). In contrast to perched water experiments with PZsd sediment with 37 days of SMI+Poly-PO_4 treatment before leaching, in these CCug columns, Tc-99 and U (without or with co-contaminants) were injected with a 6-hour residence time, so there was much less contaminant-amendment contact time. Tc-99 breakthrough curves (without co-contaminants) showed a relatively constant 45% Tc-99 uptake (rate 5x 10-7 mol Tc-/g SMI/h) during Tc-99 injection (0 to 100 PVs), then very little Tc-99 remobilization during the subsequent 120 PVs of oxic water injection (to 220 PVs or 42 days). The calculated longevity of the reduced SMI was about 200 PVs. A field-scale barrier [i.e., 9-m (30-ft) diameter] with the same 0.1% SMI and Poly-PO_4 treatment is equivalent to 60 of these 15-cm (6-in.) long laboratory columns end to end. Upgradient flow into the barrier with no CoCOIs would result in complete Tc-99 sequestration within a few feet. In contrast, the calculated longevity of the reduced SMI in the presence of CoCOIs was 35 PVs. As a result, Tc-99 breakthrough curves (with CoCOIs) showed nearly no Tc-99 uptake during Tc-99 injection (0 to 100 PVs) and no release during the subsequent oxic water injection (100 to 220 PVs).

In contrast to Tc, U can be reduced/precipitated by SMI and precipitated as autunite or apatite by Poly-PO_4; therefore, oxidation of the SMI did not affect U sequestration to the same extent as Tc-99 sequestration. During flow in 1-D columns, the 0.1% SMI+Poly-PO_4 treatment resulted in fair performance for U removal (i.e., 19% to 30% of U was retained) without co-contaminants and about the same performance with co-contaminants (i.e., 14% to 28% of U was retained). During oxic water leaching (i.e., from 90 to 220 PVs or 42 days), slow U release from the sediment was observed. Short U-phosphate contact times result in precipitation of amorphous or semi-crystalline phosphate phases with

higher solubility, but longer U-phosphate contact times (i.e., oxic experiment times from 50 to 300 days) allow for recrystallization of apatite and autunite, likely resulting in greater sequestration of U. A field-scale barrier [i.e., 9-m (30-ft) diameter] with the same 0.1% SMI and Poly-PO_4 treatment would have greater U-amendment contact times, so long-term batch experiments likely better reflect what would occur.

Changes in co-contaminant concentrations measured during flow are consistent with co-contaminant impact on Tc-99 and U sequestration. Chromate is easily reduced, and the high Cr injection concentration consumes most of the SMI reductive capacity. Consequently, initial Cr breakthrough concentrations are low (i.e., 10% to 60% of injection Cr concentration), likely due to reduction, then increase by 30 PVs, which is similar to the calculated SMI reductive capacity in the presence of co-contaminants (35 PVs). Nitrate was not or only slightly reduced, as effluent concentrations were the same as injection concentration, and nitrite concentrations were zero or only slightly above detection limits. I-127 and Sr were not affected by the treatment, and breakthrough was the same in untreated and SMI/PO_4-treated sediments.

Appendix H – Particulate-Phase Sequestration: Bismuth

The purpose of this task is the sequestration of U and Tc-99 (primary contaminants of interest, PCOIs) in the presence of I-129 as iodate, nitrate, Cr, and Sr (co-contaminants of interest, CoCOIs) in water-saturated zones using particulate bismuth subnitrate (BSN). This amendment functions through different mechanisms for different contaminants, including anion exchange or outer-sphere complexation for pertechnetate, inner layer intercalation for uranyl carbonate, and inner-sphere complexation for iodate and chromate anions. This technology is unique within the DV-1 study in that is does not rely on reduction, and therefore there is less likelihood of remobilization due to oxidation.

This treatment targets contamination in perched water and BY Cribs as the primary treatment zones, via formation of a permeable reactive barrier in groundwater under BY Cribs. Potential secondary treatment zones include 216-U-1 and -2, S-SX tanks, S and T Cribs, C tanks, and BC Cribs.

The specific objectives of this technology are as follows:

1. Quantify Tc-99 and U immobilization and order of magnitude removal rate in various combinations: (1) with/without sediment, (2) with/without delivery fluid, and (3) with/without co-contaminants [described in the Phase 1 report (PNNL-35432)].
2. Determine the immobilization rates for U and Tc-99 with/without co-contaminants for (1) perched water and (2) BY Crib application (in groundwater).
3. Quantify the longevity of U and Tc-99 with/without co-contaminants for (1) perched water and (2) BY Crib application.

Objectives 2 and 3 were tested in 1-D leach columns as described in Sections H.3.1 and H.3.2 for BY Cribs groundwater conditions and perched water conditions, respectively.

H.1 Supplemental Methods

BSN particles were purchased from Sigma Aldrich (Merck, Germany). BSN was used as received.

H.1.1 Methods for BY Cribs Groundwater Conditions

Experiments targeted the BY Cribs groundwater table within the Central Plateau. Columns were conducted as described in Section 2.4.2 with mixing of the particulate amendment into sediment prior to packing the columns, targeting 1.5 wt% BSN in sediment. The column study was conducted in two replicates (Treatment-A and Treatment-B) and included a control column containing sediment but no BSN (Control-C). A second set of column experiments was conducted following the same protocol, but the influent solution included CoCOIs (iodine, Cr, Sr, and NO_3). Treatment-D and Treatment-E contained BSN while Control-F did not.

H.1.2 Methods for Perched Water Conditions

Columns used to represent a perched water scenario were prepared with contaminants mixed directly into the sediment prior to packing the columns, as described in Section 2.4.1. Treatment-G and Treatment-H included 1.5 wt% BSN, while Control-I contained the contaminated sediment without BSN. These columns did not include a loading phase, but were conducted similarly to the BY Cribs column leaching phase. To approximate the water-saturated field conditions in the perched water system, static columns (before high solid:solution batch) were set up using 15 g of perched water sediment with 1.5 wt% BSN mixed in and 3 mL of synthetic perched water. Sacrificial experiments were set up in duplicate for

termination at 1 and 4 hours, and 1, 5, 28, 90, 180, and 300 days. After collecting liquid samples, solid samples from the 5-, 28-, and 300-day experiments were homogenized and used for sequential extractions.

H.2 Long-Term Batch Results

U immobilization in long-term batch experiments showed an increase between 5 and 28 days, with BSN immobilizing approximately twice as much as the controls (0.7-0.9 fraction in BSN vs. 0.4-0.5 in the controls) (Figure H.1). After 28 days, one set of tests remained under anaerobic conditions ("no air"), while another set was exposed to air. At 300 days, air exposure made little difference in the immobilization of U, as expected because contaminant immobilization by BSN does not involve a redox reaction. At this sampling point, nearly all U in the BSN tests was found in the carbonate or hard-to-extract phases (Ext. 4 and 5, Figure H.1). Additional U was immobilized by the controls at 300 days, but was mostly found in the easily remobilized phases (Ext. 1-3).

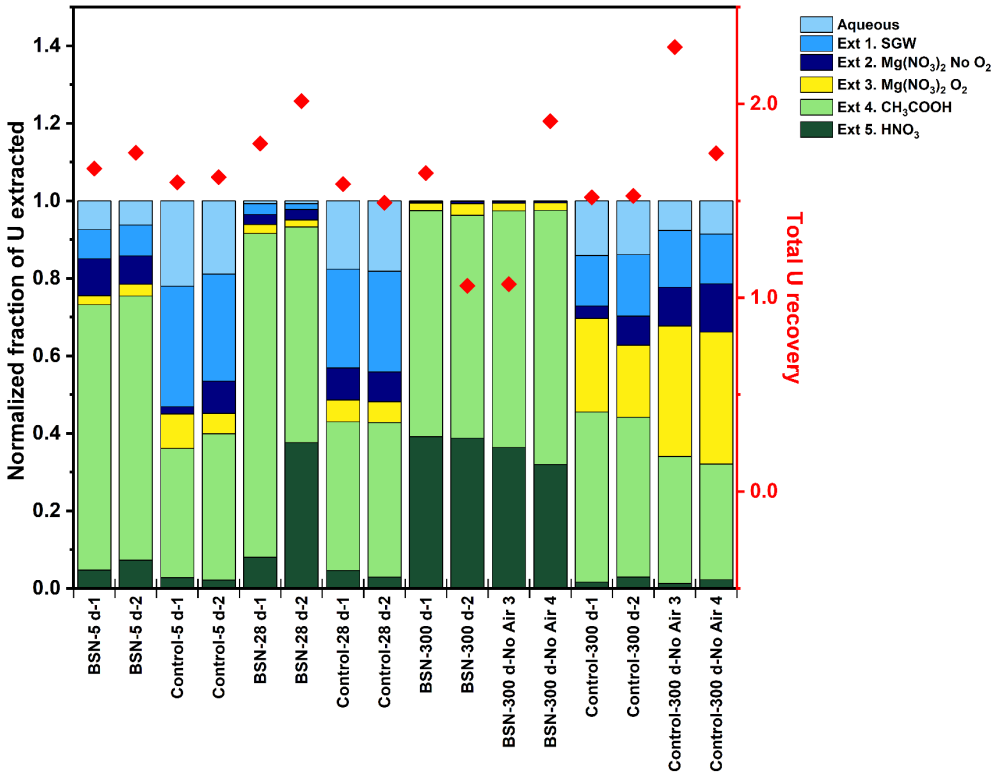

Figure H.1. Change in U sequestration via sequential extractions at different time points showing effect of treatment of contaminant-spiked perching zone sand (PZsd) sediment in synthetic ground water (SGW) with BSN compared to controls without treatment. Note: The left side of the figure shows the solid phase U concentration (in µg/g) recovered in each sequential extraction while the right side of the figure shows the total U recovered by each sequential extraction.

Tc immobilization increased in BSN batch tests between 5 and 28 days (Figure H.2). At 28 days, the BSN batch tests reached 80% immobilized Tc, compared to 20% in the control tests. After 28 days, the remaining tests were split, with one set remaining under anaerobic conditions ("no air") and another set exposed to air. By 300 days, the extent of Tc-99 immobilization had decreased in all tests, with a higher decrease in those exposed to air. Tc-99 K-edge X-ray absorption spectroscopy (XAS) (Figure H.15) shows Tc-99 immobilized by BSN remained in the initial $Tc(VII)O_4^-$ form. This suggests that Tc-99 is

removed by anion exchange or outer-sphere complexation, not by a redox reaction, so the decrease in Tc-99 immobilization is not due to reoxidation. BSN transitions to bismutite when exposed to groundwater (Pearce et al. 2025), which does not immobilize Tc-99 as well as the starting BSN material. This transition may be the cause of the reduction in Tc-99 immobilization between 28 days and 300 days. It is possible that exposure to air accelerated the transition of BSN to bismutite, resulting in less Tc-99 immobilized in the tests exposed to air. In the immobilized phases (Ext. 4 and 5), the treated and control tests performed roughly in the same way. However, the treated tests showed higher temporarily immobilized Tc-99 in Ext. 3 compared to the controls (Figure H.2).

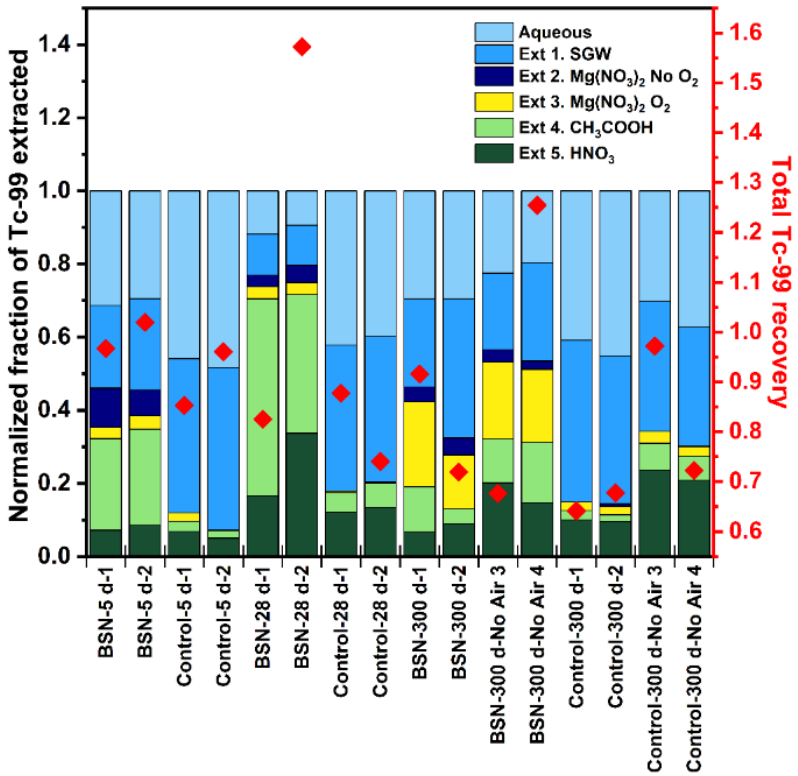

Figure H.2. Change in Tc-99 sequestration via sequential extractions at different time points with BSN treatment of contaminant-spiked PZsd sediment in SGW compared to controls without treatment. Note: The left side of the figure shows the solid phase Tc-99 concentration (in µg/g) recovered in each sequential extraction while the right side of the figure shows the total Tc-99 recovered by each sequential extraction.

H.3 Saturated Column Results for Tc-99 and U

H.3.1 BY Cribs Groundwater Conditions

For Cold Creek Unit gravel (CCug) columns containing BSN (Treated – A and Treated – B), all U was removed from the aqueous phase for the first ~100 pore volumes (PVs) (Figure H.3b). After 100 PVs, not all of the U was removed, but U loading continued to increase until the experiment switched to the leaching phase at ~300 PVs. In the associated control, U uptake was minimal and was released after switching to the leaching phase. U loading for the BSN columns reached 42 to 43 µg U per g of solid (BSN + sediment), although some U was released during the leaching phase, with a final concentration of 25 to 26 µg/g (Figure H.3a; Table H.1).

With CoCOIs (Sr, I-129, Cr, and nitrate) present, the breakthrough of U was significantly delayed (300 PV for PCOI+CoCOIs vs. 100 PVs for PCOI only) (Figure H.3b). This is reflected in U uptake and release behavior, which followed the same general pattern as the PCOI-only columns, but reached a higher maximum U uptake of 68 to 71 µg/g (Figure H.3a; Table H.1). This could be due to the additional nitrate competing with carbonate and slowing mineral transformation to bismutite, allowing more U to be incorporated. It could also indicate secondary interactions with CoCOIs (e.g., Sr and carbonate). During the leaching phase, some U was remobilized, with a final concentration of ~50 µg/g.

Release rates were significantly increased for control (no treatment) columns during all three stop flows (Figure H.4). For treated columns, there was a slight decrease in release rate for some columns, but overall, the immobilization of U does not appear to be kinetically controlled.

In the BY Cribs treatment scenario, U was evenly distributed across all columns, with one outlier at the influent end of the CoCOI duplicate column with high U concentration and in the CoCOI column at the effluent end with a lower concentration of U (Figure H.5).

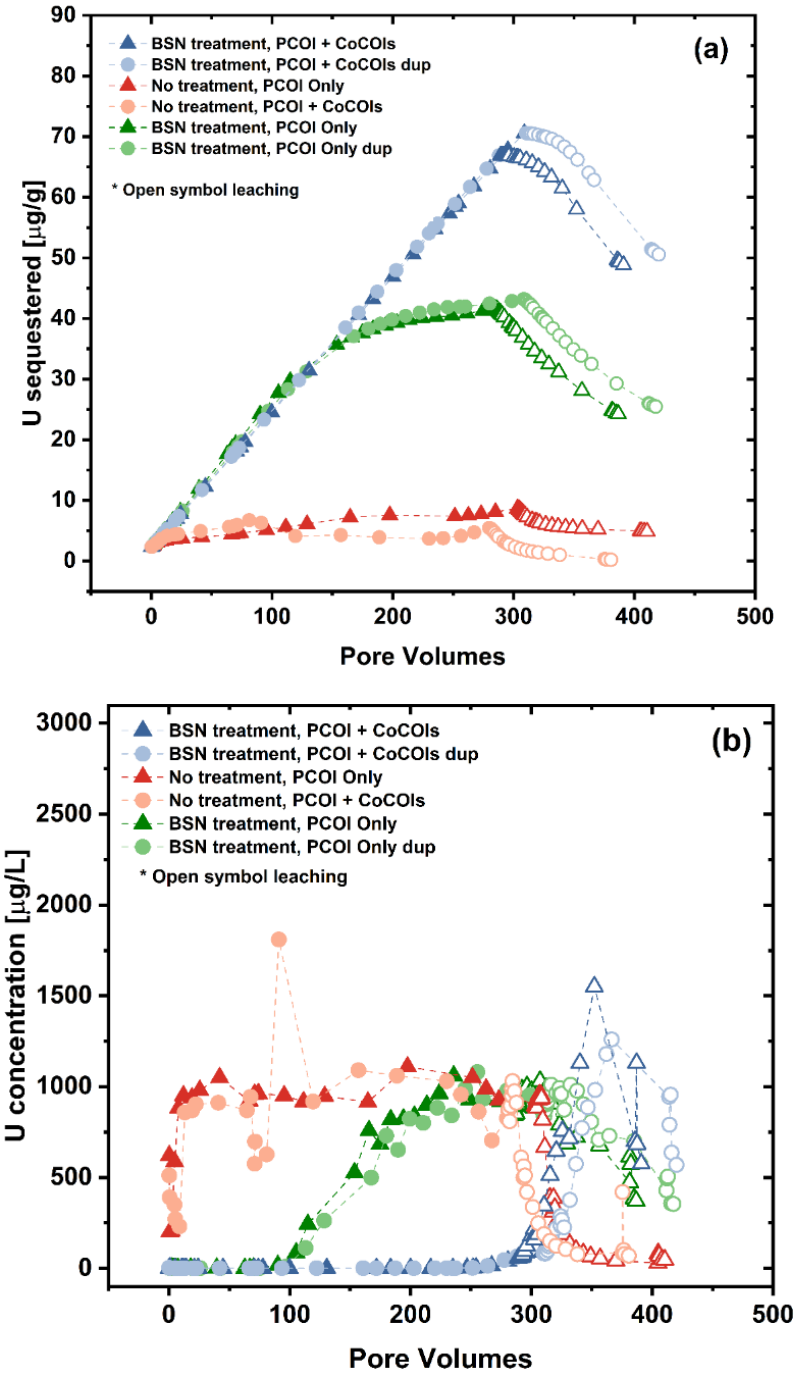

Figure H.3. U during loading and leaching of PCOIs with CCug sediment with and without BSN treatment and with or without CoCOIs: (a) accumulation of U (in µg/g) and (b) aqueous concentrations of U (in µg/L). Note: "Dup" stands for duplicate. Filled symbols indicate contaminant of interest loading phase while open symbols represent the leaching phase with SGW.

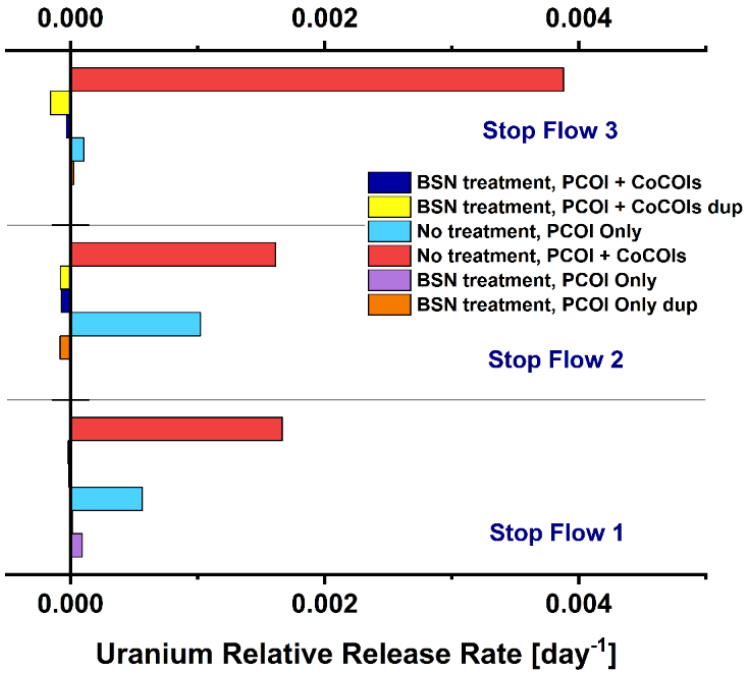

Figure H.4. U normalized release rates during leaching from columns with CCug sediment with and without BSN treatment, estimated leaching rate (day^{-1}) during each stop flow. Note: "Dup" stands for duplicate.

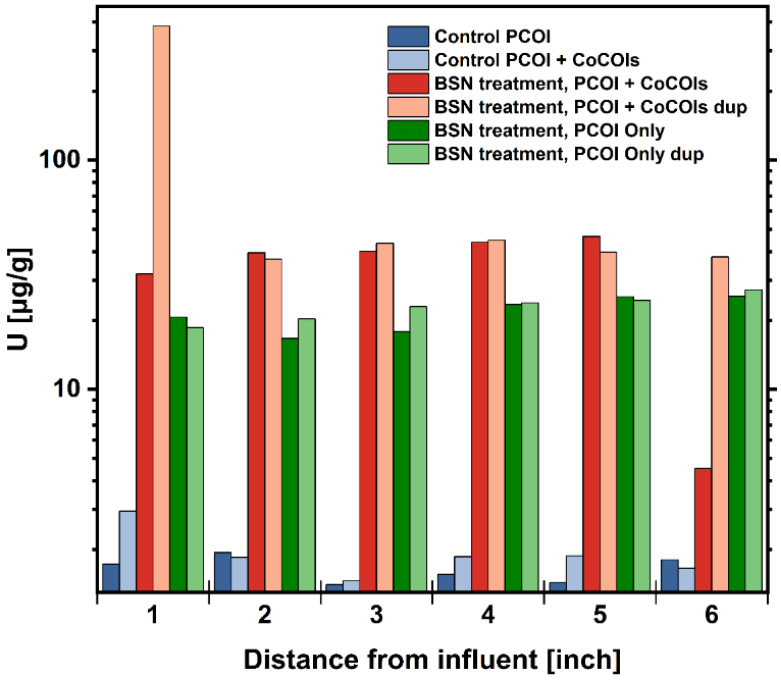

Figure H.5. U distribution (in µg/g) across columns with CCug sediment with and without BSN treatment based on 8 M HNO_3 extractions. Note: "Dup" stands for duplicate.

Table H.1. U estimated retention after loading and leaching in CCug sediments without and with treatment (BSN).

Conditions	Loading (µg/g)	Leaching (µg/g)
No treatment, PCOIs	9.31	5.49
No treatment, PCOIs + CoCOIs	6.09	0.82
BSN, PCOIs	42.3	24.89
BSN, PCOIs, dup	43.8	26.1
BSN, PCOIs + CoCOIs	71.2	51.2
BSN, PCOIs + CoCOIs, dup	67.5	49.5

For Tc, complete breakthrough was slightly delayed in the treated columns compared to the control column. Breakthrough in the treated columns and control columns, with or without CoCOIs, was nearly identical and almost no Tc-99 was immobilized (< 3 µg/g) (Figure H.6, Table H.2). Previous batch studies have shown that the BSN undergoes hydrolysis and incorporation of hydroxide into the structure upon exposure to groundwater, which lowers the solution pH. If the pH drops below 5.4, there is insufficient carbonate in solution to induce the transformation to bismutite, which does not immobilize Tc, and a specific "unknown" Bi phase form, likely a clustered structure of bismuth basic nitrate, that does immobilize Tc-99 (Boglaienko et al. 2024; Escobedo et al. 2025). In these columns, release of carbonate from the sediment and the presence of carbonate in synthetic groundwater likely resulted in the transformation of BSN into bismutite; therefore, Tc-99 was not immobilized. In addition, sediment constituents can compete for exchange sites and can physically restrict access to these sites, further preventing Tc-99 immobilization.

The release rate of Tc-99 was slightly decreased during stop flow events for treated columns, particularly for the treated columns with CoCOIs. Release rate increased during the first stop flow for one treated column, but the increase was small (0.017 day^{-1}) (Figure H.7). Tc concentration was variable across the columns, but the concentration in all columns was low, so even small changes in concentration look like large differences (Figure H.8).

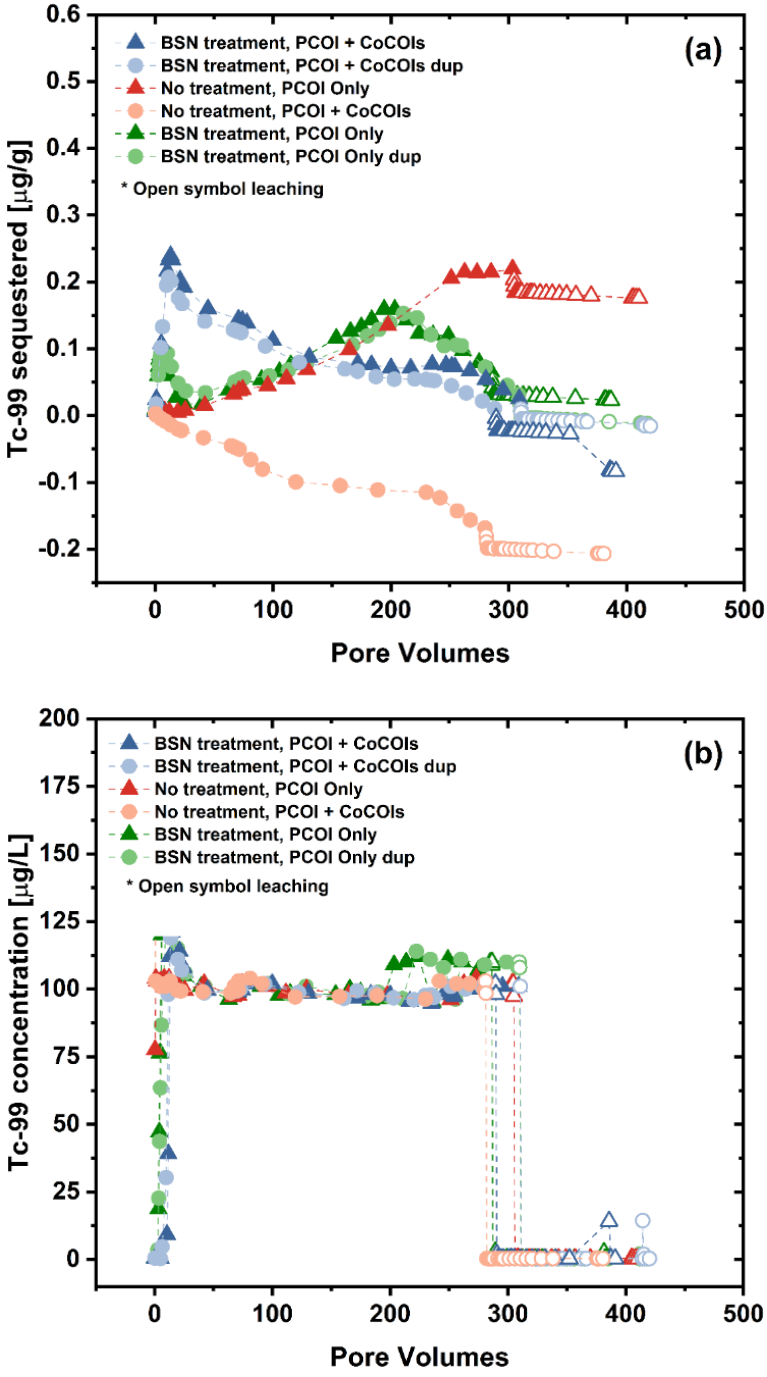

Figure H.6. Tc during loading and leaching of PCOIs with CCug sediment with and without BSN treatment and with or without CoCOIs: (a) accumulation of Tc-99 (in µg/g) and (b) aqueous concentrations of Tc-99 (in µg/L). Note: "Dup" stands for duplicate. Filled symbols indicate PCOI loading phase while open symbols represent the PCOI leaching phase with SGW.

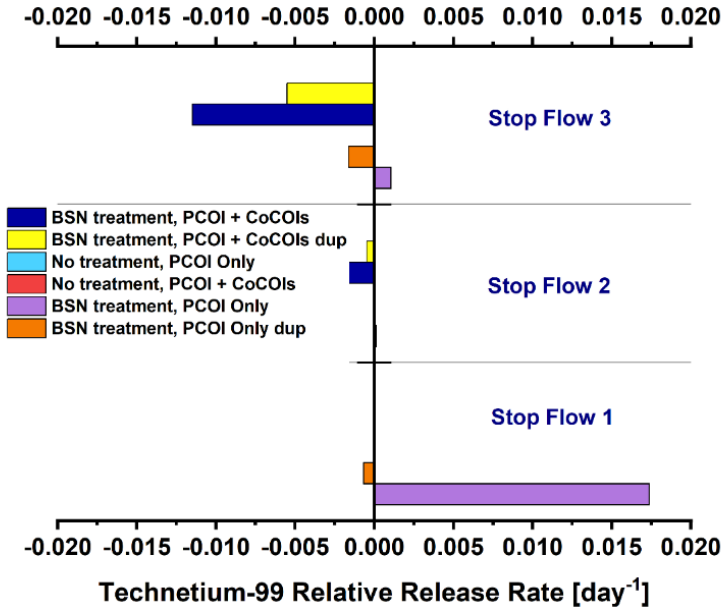

Figure H.7. Tc normalized release rates during leaching from columns with CCug sediment with and without BSN treatment, estimated leaching rate (day^{-1}) during each stop flow. Note: "Dup" stands for duplicate.

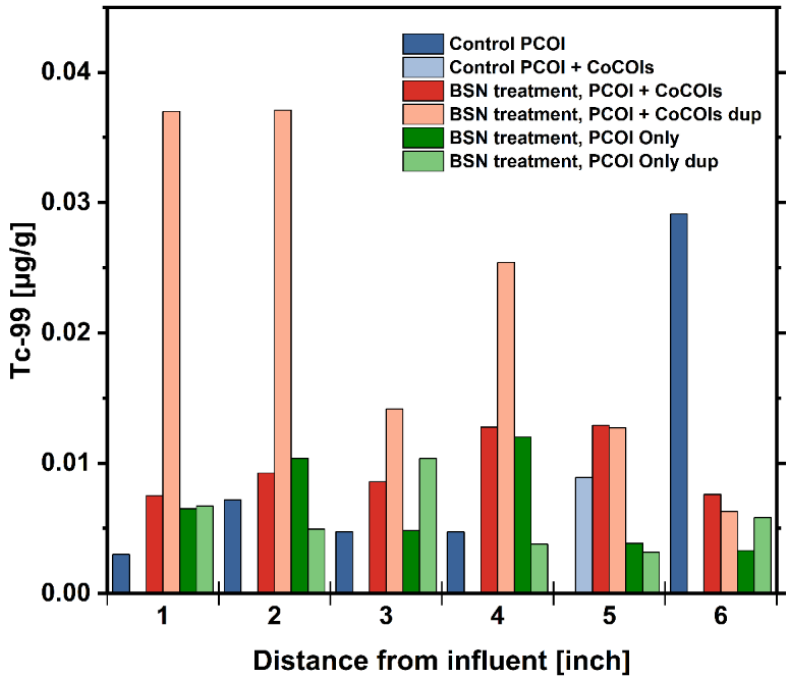

Figure H.8. Tc distribution (in µg/g) across columns with CCug sediment with and without BSN treatment based on 8 M HNO3 extractions. Note: "Dup" stands for duplicate.

Table H.2. Tc estimated retention after loading and leaching in CCug sediments without and with treatment (BSN).

Conditions	Loading (µg/g)	Leaching (µg/g)
No treatment, PCOIs	0.22	0.18
No treatment, PCOIs + CoCOIs	0[(a)]	0[(a)]
BSN, PCOIs	0.07	0.02
BSN, PCOIs, dup	0.03	0[(a)]
BSN, PCOIs + CoCOIs	0.03	0[(a)]
BSN, PCOIs + CoCOIs, dup	0.01	0[(a)]

(a) Negative values are reported as "0."

H.3.2 Perched Water Conditions

For perched water conditions, BSN retained more U than the control column, but it was challenging to determine the amount of U retained due to heterogeneity in U concentrations in the initial sediment. Based on the results shown in Figure H.9a, the treated columns and the control column ended with -21 to -148 and -289 µg/g U, respectively (Table H.3). The starting concentration of U in the columns was calculated from the concentration of U that was added to the columns and the average measured concentration of U that was initially present in the sediment. However, the U distribution within the sediment can be highly variable, and the negative values for U retention are likely a result of this heterogeneity, suggesting that the sediment used in these columns had a higher initial U concentration than the average measured value. Despite this heterogeneity, the results show that the two treated columns performed significantly better than the control (Figure H.9, Table H.3).

The U release rate remained stable during stop flows two and three, but there was a significant increase in release of U for one of the treated columns during the first stop flow (+0.5 day^{-1}) (Figure H.10). In the perched water scenario columns, U was evenly distributed across the column in post-testing characterization (Figure H.11).

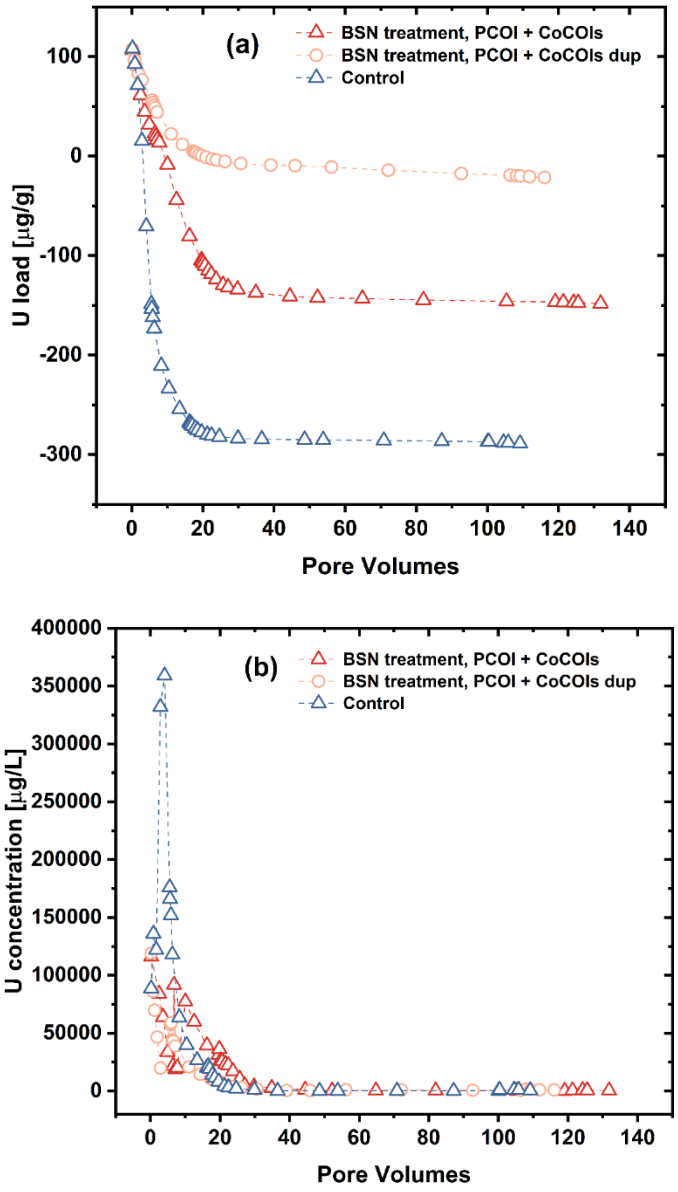

Figure H.9. U remaining during leaching of PCOIs and CoCOIs from PZsd sediment with BSN (Bi treatment) and without BSN (control) after equilibration for approximately 6 weeks: (a) accumulation of U (in µg/g) and (b) aqueous concentrations of U (in µg/L). Note: "Dup" stands for duplicate.

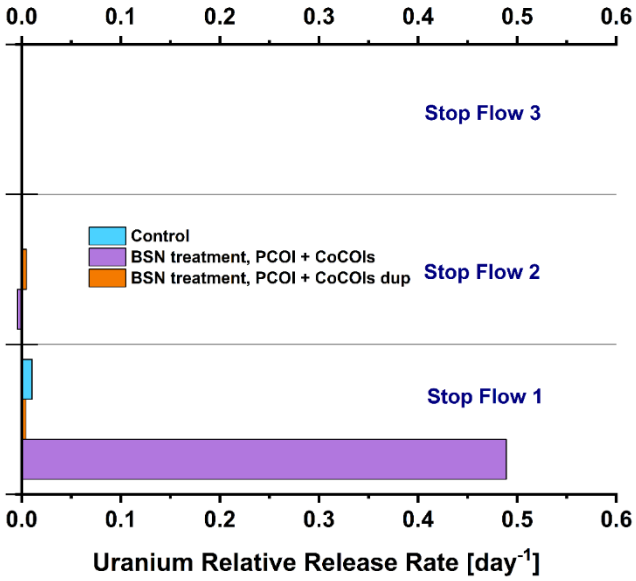

Figure H.10. U normalized release rates during leaching from columns with PZsd sediment with and without BSN treatment estimated leaching rate (day^{-1}) during each stop flow. Note: "Dup" stands for duplicate.

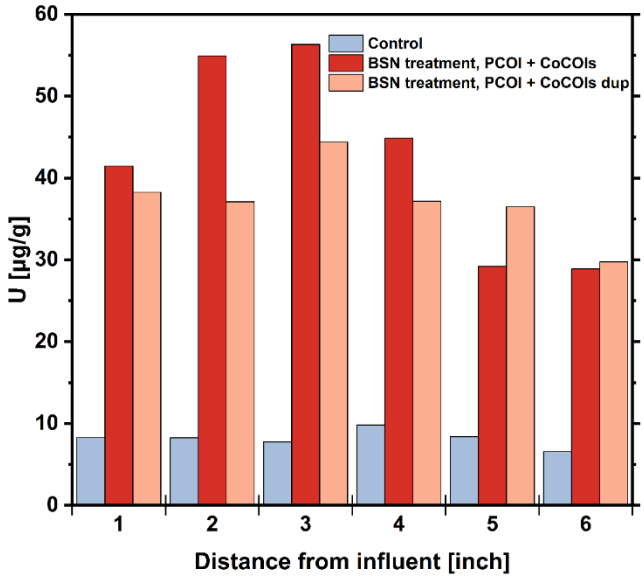

Figure H.11. U distribution (in µg/g) across columns with PZsd sediment with and without BSN treatment based on 8 M HNO_3 extractions. Note: "Dup" stands for duplicate.

Tc loading in the columns with BSN was low (> 0.05 to 0.05 µg/g Tc) but still greater than in the control columns without BSN (> 0.05 µg/g Tc) (Figure H.12, Table H.3). Tc-99 release rates from all columns were similar, except for a decrease in release rate for one column with BSN during the first stop flow (Figure H.13). The Tc-99 concentration in the solid phase was too low to provide significant insight into the distribution of Tc-99 across the columns (Figure H.14).

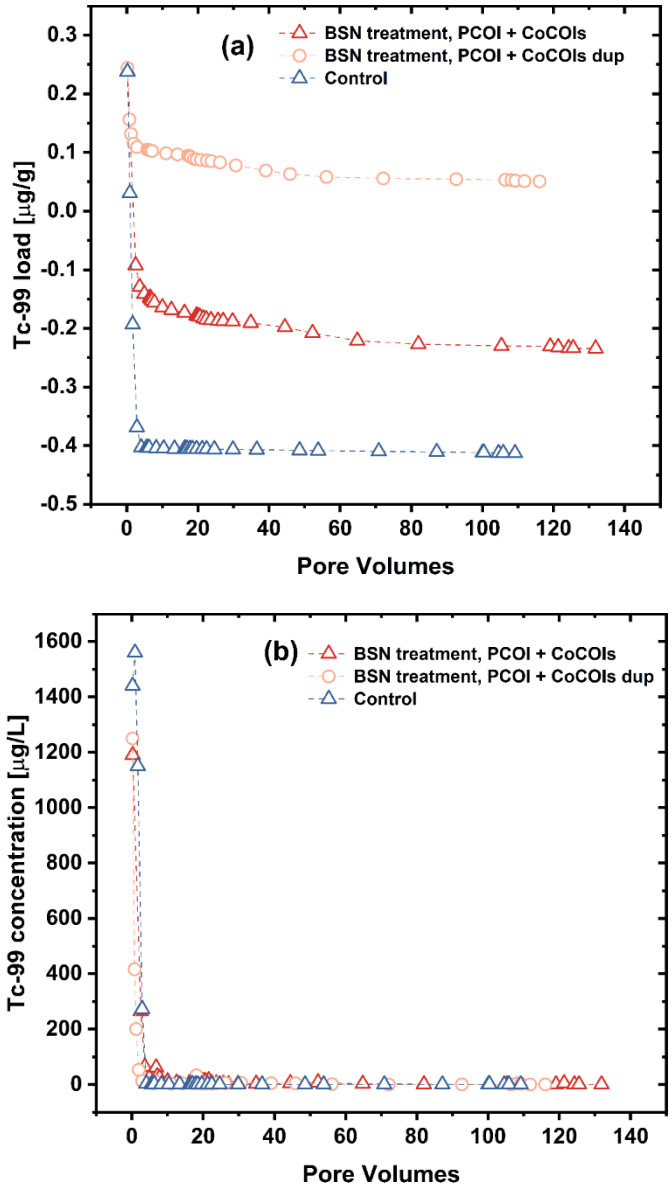

Figure H.12. Tc remaining during leaching with PZsd sediment with and without BSN treatment after equilibration of amendments for approximately 6 weeks: (a) accumulation of Tc-99 (in µg/g) and (b) aqueous concentrations of Tc-99 (in µg/L). Note: "Dup" stands for duplicate.

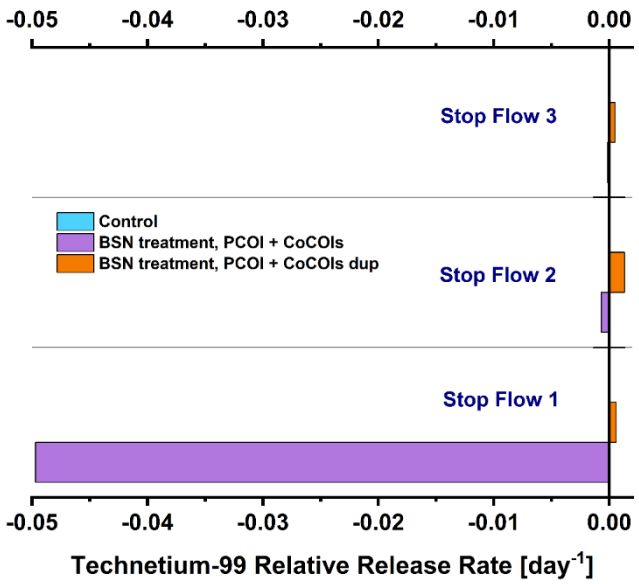

Figure H.13. Tc normalized release rates during leaching from columns with PZsd sediment with and without treatment (with BSN) estimated leaching rate (day^{-1}) during each stop flow. Note: "Dup" stands for duplicate.

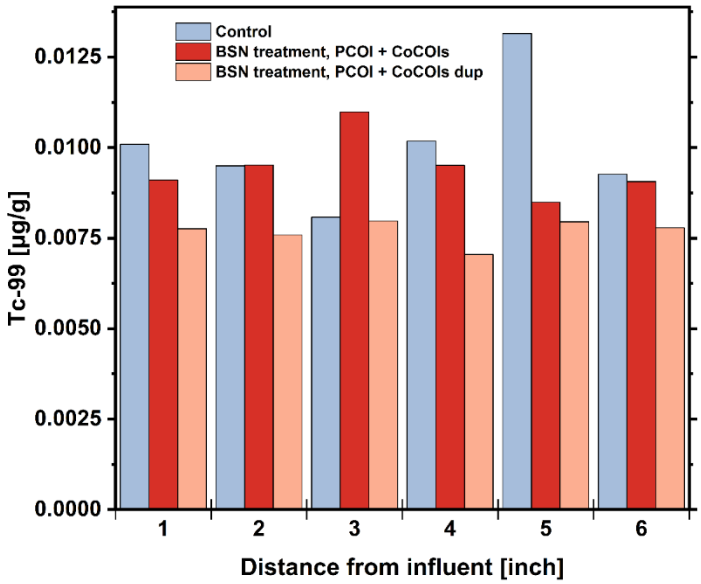

Figure H.14. Tc distribution (in µg/g) across columns with PZsd sediment with and without BSN treatment based on 8 M HNO_3 extractions. Note: "Dup" stands for duplicate.

Table H.3. U and Tc-99 estimated retention after leaching in long-term batch experiments using PZsd sediments without and with treatment (BSN). Note: Initial U and Tc-99 were estimated to be 111 and 0.25 µg/g, respectively. Actual initial U concentration was likely higher, possibly due to heterogeneous U distribution in the sediment, demonstrated by the negative U concentration values at the end of the test.

Conditions	U (µg/g)	Tc (µg/g)
No treatment	-289[(a)]	0[(b)]
BSN	-148[(a)]	0[(b)]
BSN, dup	-21.4	0.05

(a) Negative values due to heterogenous concentrations of U in PZsd.
(b) Negative values due to analytical error are reported as 0.

H.3.3 Long-Term Tc-99 and U Stability

With BSN, with or without PZsd sediment, Tc-99 was present in oxidized form as TcO_4^- [Tc(VII)] (Figure H.15 and Figure H.16), which is to be expected as BSN is not a reductive technology. Comparison of the Tc-99 K-edge X-ray absorption near edge structure (XANES) spectra for BSN with and without sediment did not reveal differences in its electronic structure and coordination (Figure H.17). Previous work has shown that Tc-99 is likely to be associated with Bi on the surface, while U is likely to be associated with Bi in the mineral structure (Pearce et al. 2025); however, due to low concentrations, this could not be confirmed via solid phase characterization.

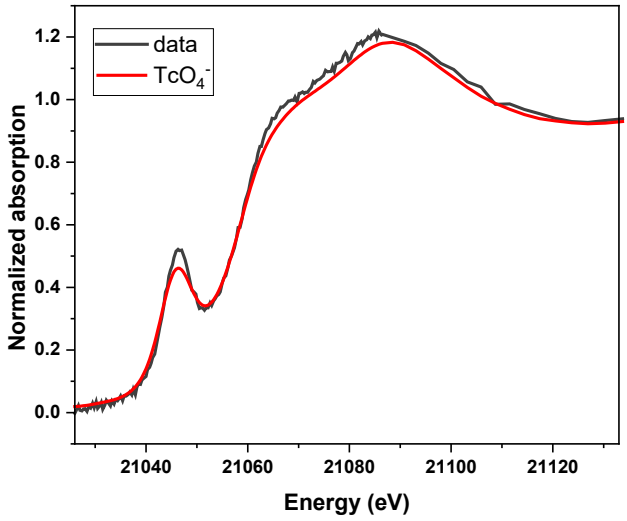

Figure H.15. Tc K-edge XANES spectra for BSN without sediments (black) and a TcO_4^- standard (red). PNNL629

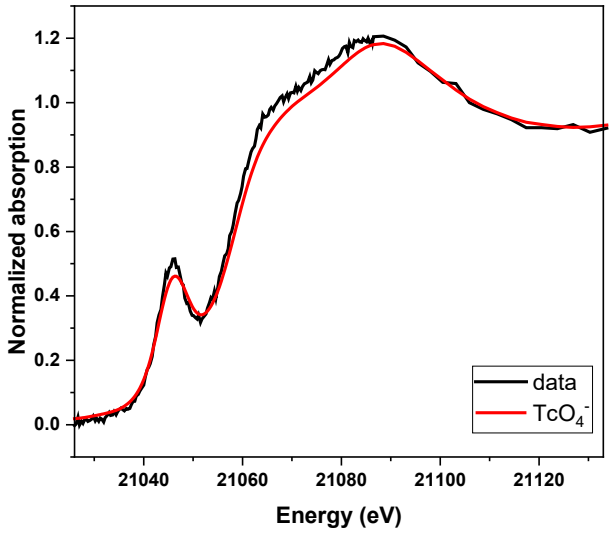

Figure H.16. Tc K-edge XANES spectra for BSN with PZsd sediment (black) and a TcO_4^- standard (red). PNNL616

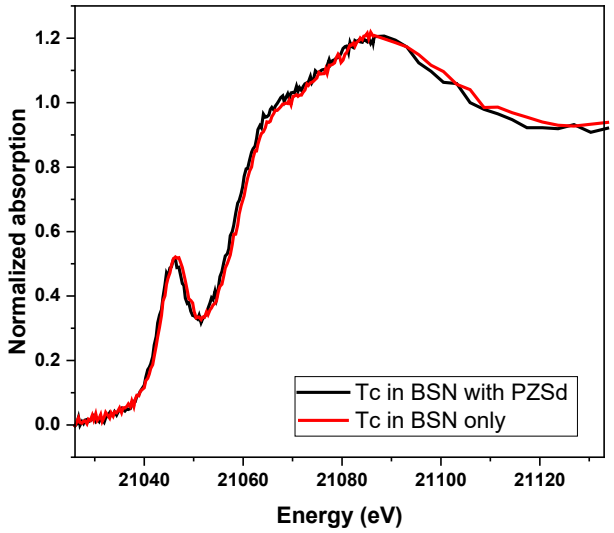

Figure H.17. Comparison of Tc-99 K-edge XANES spectra for Tc-99 in BSN with PZsd sediment (black) and for BSN without sediment (red). PNNL616 and 629

H.4 Saturated Column Results for Co-contaminants for BY Cribs Groundwater

H.4.1 Co-contaminant Effluent Monitoring

Effluent was periodically analyzed for CoCOIs during the loading and leaching phases of the CCug column testing. Infrequent sample analysis does not permit precise calculations, so a general summary is presented here.

As BSN uptakes carbonate and transforms from BSN to bismutite, nitrate is released from the BSN (Lawter et al. 2021). As expected, nitrate was elevated to 11,000 to 13,000 mg/L in the treated columns. After the first 5 to 10 PVs, the effluent nitrate concentration decreased to 50 mg/L, matching the concentration in the control column and the influent concentration.

In the control column, Sr was removed from the aqueous phase from the start of the test. However, in the BSN columns, Sr concentration initially ranged from 11.4 to 15 mg/L for the first 10 to 20 PVs before dropping below detection limit, matching the control column. All three columns increased similarly to a max of ~30 mg/L at around 100 to 150 PVs, then steadily decreased throughout the remainder of the test.

Complete breakthrough of iodine occurred in the control column within the first 20 PVs but was retarded in the BSN columns, with breakthrough occurring around 65 to 70 PVs, indicating initial uptake of iodine, as iodate, by BSN.

Cr breakthrough occurred within the first few PVs in the control column but was delayed in the BSN columns for the first 40 PVs. After switching to the leaching phase, the control column quickly decreased to below detection limits but the BSN columns slowly leached Cr.

H.5 Saturated Column Geochemical Monitoring

H.5.1 Amendment Monitoring

In the CCug columns, the pH for all columns started around 8.5, then initially decreased in the BSN columns to a minimum of 7.5 to 7.8. By 30 to 40 PVs, the pH increased to ~8, similar to the control column Bi concentration that was measured in the influent (1), middle (3), and effluent (6) sections of the treated CCug columns. Concentration was similar across the columns, ranging from 8.5 to 11 mg/g, indicating homogenous distribution of the particulates throughout the columns (Figure H.18).

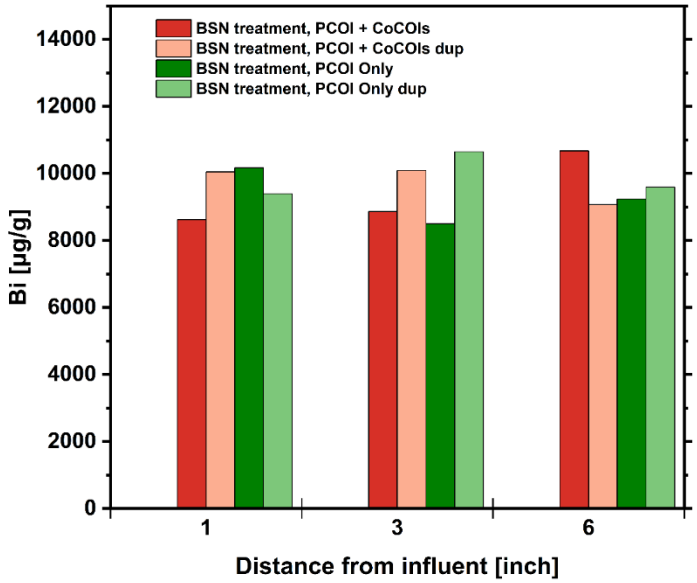

Figure H.18. Bi distribution (in µg/g) across columns with CCug sediment with and without BSN treatment based on 8 M HNO_3 extractions. Note: “Dup” stands for duplicate.

H.5.2 pH Data

In the CCug columns, the pH for all columns started around 8.5, then initially decreased in the BSN columns to a minimum of 7.5 to 7.8. By 30 to 40 PVs, the pH increased to ~8, similar to the control column. In all other columns (CCug with CoCOIs and PZsd columns), the pH for all columns with and without BSN was ~8.2 to 9.2.

H.5.3 PFBA Tracer Breakthrough

Approximately 200 mg/L of pentafluorobenzoic acid (PFBA) was injected into CCug and PZsd columns to monitor transport of water through the sediment. This nonreactive tracer was chosen in place of bromide due to observations of interaction with BSN in previous experiments. A lower limit of detection was a limitation of this tracer. However, breakthrough curves were established. There was generally little tailing in the CCug untreated and BSN treated columns, indicating transport of water through most of the sediment pores and that the BSN did not alter the porosity (Figure H.19). In contrast, the PZsd columns showed atypical breakthrough behavior. This could be due to the tight packing of the clay dominant sediment (Figure H.20). Cracking was observed throughout the column experiments, potentially introducing favorable transport paths for the PFBA to travel.

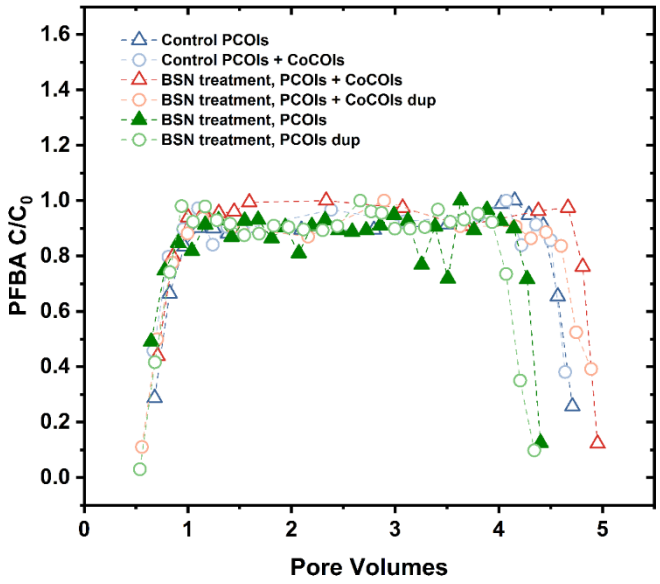

Figure H.19. Effluent PFBA (in mg/L) during and after tracer injection at 200 mg/L PFBA into columns with CCug sediment with and without treatment (BSN).

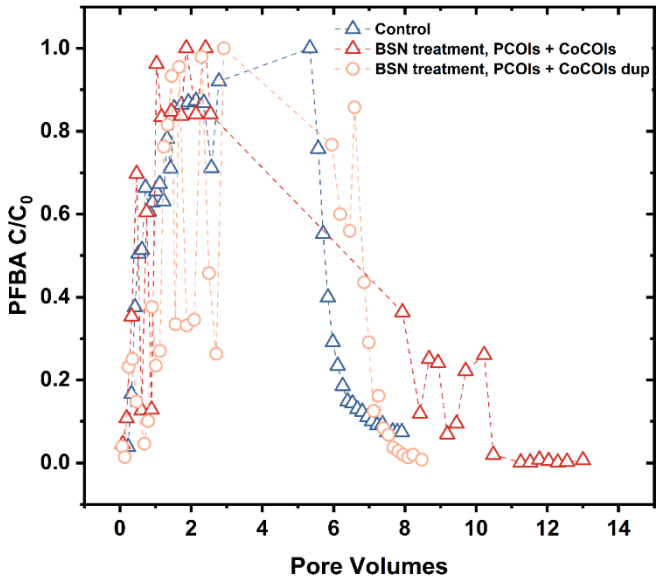

Figure H.20. Effluent PFBA (in mg/L) during and after tracer injection at 200 mg/L PFBA into columns with PZsd sediment with and without treatment (BSN).

H.6 Summary of Performance for Bismuth in Groundwater

For the BY Cribs groundwater conditions, BSN is recommended for immobilization of U, and BSN also has the potential to immobilize Cr (as chromate) and I (as iodate). BSN is not recommended for immobilization of Tc, Sr, or nitrate.

Immobilization of U by BSN was significant without CoCOIs and PCOIs and increased in the presence of CoCOIs. This is consistent with Phase 1 results and other studies of U removal by bismuth-based materials (Lawter et al. 2021; Pearce et al. 2025). Under BY Cribs conditions, there is sufficient carbonate in solution such that U is present as uranyl carbonate, and the nitrate in BSN is exchanged with carbonate/uranyl carbonate, resulting in the formation of a layered bismutite structure with uranyl carbonate in the interlayer. Negatively charged uranyl carbonate can also be sorbed to the positively charged $[Bi_2O_2]^{2+}$ layers on the surface of the particles. This uranyl carbonate in the interlayer is immobilized, but the U adsorbed to the surface of the particles is likely released during the leaching phase. Even with remobilization of the surface sorbed U, the final loading on the bismuth-based material is significant (25 µg/g without CoCOIs and 50 µg/g with CoCOIs).

Under BY Cribs groundwater conditions, more Tc-99 was immobilized in columns containing BSN than in the control columns without BSN. However, the high carbonate concentrations (both released from the sediments and present in the groundwater), resulting in transformation into bismutite, along with competition for U for available sorption sites, resulted in less Tc-99 immobilization than has been demonstrated in other studies where BSN was transformed into an unidentified $Bi(NO_3)_x(OH)_yO_z$ phase and Tc-99 was retained (Boglaienko et al. 2024; Pearce et al. 2025). The transformation of BSN into the layered bismutite structure under BY Cribs groundwater conditions is advantageous for immobilization and retention of U but inhibits immobilization of Tc; therefore, it is unlikely that both U and Tc-99 can be simultaneously immobilized by BSN.

For CoCOIs, breakthrough of Cr (as chromate) and I (as iodate) was delayed in columns with BSN compared to the control columns without BSN. Immobilization of anionic chromate and iodate by BSN has been attributed to inner-sphere adsorption (Pearce et al. 2025). BSN was not able to immobilize

positively charged Sr^{2+}, with higher concentrations present in the effluent from columns containing BSN compared to the control columns in the initial PVs. Within the first 20 to 30 PVs, the Sr concentration in the effluent from the column containing BSN decreased to below detection limits, matching the control column and indicating that the negative effect of BSN on Sr immobilization was short lived. Nitrate concentrations in the effluent from the columns containing BSN were also higher than the control columns. This is because carbonate (e.g., uranyl carbonate) in solution is exchanged for the charge-balancing nitrate in the BSN structure. While the increase in effluent nitrate concentration was temporary and short in duration (5 to 10 PVs), overall the concentration of nitrate in the effluent from the column with BSN was similar to that for the control column.

For perched water conditions, both U and Tc-99 were immobilized to a greater extent in the column with BSN than in the control column, but the amount of U and Tc-99 immobilization was not significant. This contrasts with the results from the long-term batch experiments conducted under perched water conditions, where both U and Tc-99 were retained in immobile or mostly immobile phases within 5 days and immobilization continued to increase over 28 days. These results highlight the importance of conducting treatability studies under flow conditions where continuous influx of solution species, e.g., carbonate and nitrate, to the system changes the performance of the treatment.

Air exposure did not affect immobilization of U or Tc-99 by BSN because the mechanism involves intercalation and inner- or outer-sphere adsorption, not a redox reaction. Transformation of BSN to carbonate-rich bismutite between 28 and 300 days may have allowed some remobilization of PCOIs but still retained 30% to 50% of the Tc-99 and 80% to 90% of the U. Results of the long-term batch tests show significantly higher immobilization and uptake of Tc-99 than the leach columns, indicating that the lack of flow and increased reaction times under batch conditions were more favorable for Tc-99 immobilization.

Appendix I – Liquid-Phase Chemical Sequestration: Calcium Citrate Phosphate

The purpose of this task is the sequestration of U and Tc-99 (primary contaminants of interest, PCOIs) in the presence of I-129 as iodate, nitrate, Cr, and Sr (co-contaminants of interest, CoCOIs) in water-saturated zones using a liquid calcium citrate phosphate (Ca-Cit-PO_4) solution to precipitate apatite. This technology functions via injection of Ca-Cit-PO_4 to precipitate apatite that may either incorporate or coat contaminants removed from the liquid phase via different mechanisms. Depending on microbiological activity, there is potential for generation of reducing conditions, which could reductively precipitate redox-sensitive contaminants (e.g., Tc).

This treatment is targeting contamination in perched water and BY Cribs as the primary treatment zones, via formation of a permeable reactive barrier in groundwater under BY Cribs. Potential secondary treatment zones include 216-U-1 and -2, S-SX tanks, S and T Cribs, C tanks, and BC Cribs.

The specific objectives of this technology are as follows:

1. Quantify Tc-99 and U immobilization and order of magnitude removal rate in various combinations: (1) with/without sediment and (2) with/without co-contaminants [described in the Phase 1 report (PNNL-35432)].
2. Determine the immobilization rates for U and Tc-99 with/without co-contaminants for (1) perched water and (2) BY Crib application (in groundwater).
3. Quantify the longevity of U and Tc-99 with/without co-contaminants for (1) perched water and (2) BY Crib application.

Objectives 2 and 3 were tested in 1-D leach columns as described in Sections I.2.2 and I.2.1 for perched water conditions and BY Cribs groundwater conditions, respectively.

I.1 Supplemental Methods

Additional column testing was conducted to understand the impact of:

1. Aging on mobility of contaminants of interest in untreated (control columns)
2. Amendment delivery via a static batch system or flowing conditions

The columns were conducted under the perched water conditions with perching zone sand (PZsd) sediments (described in Section 2.4). The additional control column included reaction of PCOIs (with and without CoCOIs) with sediments for 1 week with subsequent leaching (labeled *control*) to allow for comparison with aging for approximately 6 weeks (labeled *aged control*). Both of these control columns fall within the range of all control columns, as compared in Appendix A, Section A.3.1.

An additional Ca-Cit-PO_4 column was also conducted for the perched water conditions with PZsd sediments to understand the impact of delivery of the amendment in a batch system (labeled *S* for static) or with flow in 1-D columns (labeled *F* for flow). Initially, there were concerns that the initial mobilization during injection was not relevant to field conditions due to the relatively larger volume of the subsurface expected to be treated. However, treatment was relatively unsuccessful with and without flow.

These data are summarized in this appendix.

I.2 Saturated Column Results for Tc-99 and U

This section presents results from monitoring the PCOIs (Tc and U) during loading (for the BY Cribs groundwater condition only) and leaching (for both BY Cribs groundwater and perched water conditions). For the BY Cribs groundwater experiments, the flow of contaminants into a potential permeable reactive barrier was simulated in 1-D columns. Because PCOIs and CoCOIs were added directly to sediments, a loading phase was not conducted for the perched water conditions. However, amendments were delivered either by (1) addition to a batch (or bottle) of sediments as delineated by an *S* for static or (2) injection into columns as delineated by an *F* for flow.

Data are summarized, including all column results based on the total accumulation within the column (the amount sequestered in μg/g), the effluent concentration (in μg/L), the rate of release from sediments as normalized to the solid phase concentration both prior to stop flow events and during stop flow events (in day^{-1}), and distribution across the column as determined by extraction with 8 M HNO_3. These different results highlight the potential for amendments to sequester PCOIs and CoCOIs based on the total quantity taken up into columns and rates of release at different points in experiments.

I.2.1 BY Cribs Groundwater Conditions

For the BY Cribs groundwater conditions, U uptake is significant in the absence and presence of CoCOIs, as shown in Figure I.1. For the no-treatment scenario, the contaminant effluent concentrations did not quite reach the influent concentrations (breakthrough), although injection only occurred for approximately 25 pore volumes (PVs). For comparison, breakthrough was reached within 100 PVs with or without CoCOIs in all control columns (Appendix A, Section A.3.1). During the first two stop flow events, which occurred shortly after switching to leaching with synthetic groundwater (SGW), significant adsorption and desorption were likely occurring simultaneously (a lack of equilibrium) as the normalized release rates are highly variable before and during stop flows (Figure I.2). Release rates show a significant increase (positive value) in release prior to stop flow and a decrease in release (negative value) during stop flow event 1, especially for the control column with CoCOIs. Moreover, there was greater release of U during stop flows when CoCOIs were present. By the third stop flow event, at around 100 PVs of leaching, leaching rates before and during the stop flow had decreased significantly.

For treatment with Ca-Cit-PO_4, there was a significant delay in breakthrough of U, which did not reach influent concentrations until > 150 PVs without CoCOIs and > 200 PVs with CoCOIs. This result is consistent with the likely uptake of U in apatite as shown in previous research with apatite-forming solutions (Fuller et al. 2003; SGW-47062; Lammers et al. 2017; PNNL-25303; PNNL-19524). Overall, loading of U reached a maximum of > 25 and 12 μg/g with and without CoCOIs, respectively, as shown in Table I.1. Uptake was greater in the presence of CoCOIs, including Sr. Breakthrough results (Figure I.2) were also consistent with sectioning and acid leaching (Figure I.3), with a relatively consistent U distribution across the column with treatment, indicating that the maximum loading capacity was achieved under these conditions (as confirmed by reaching effluent breakthrough).

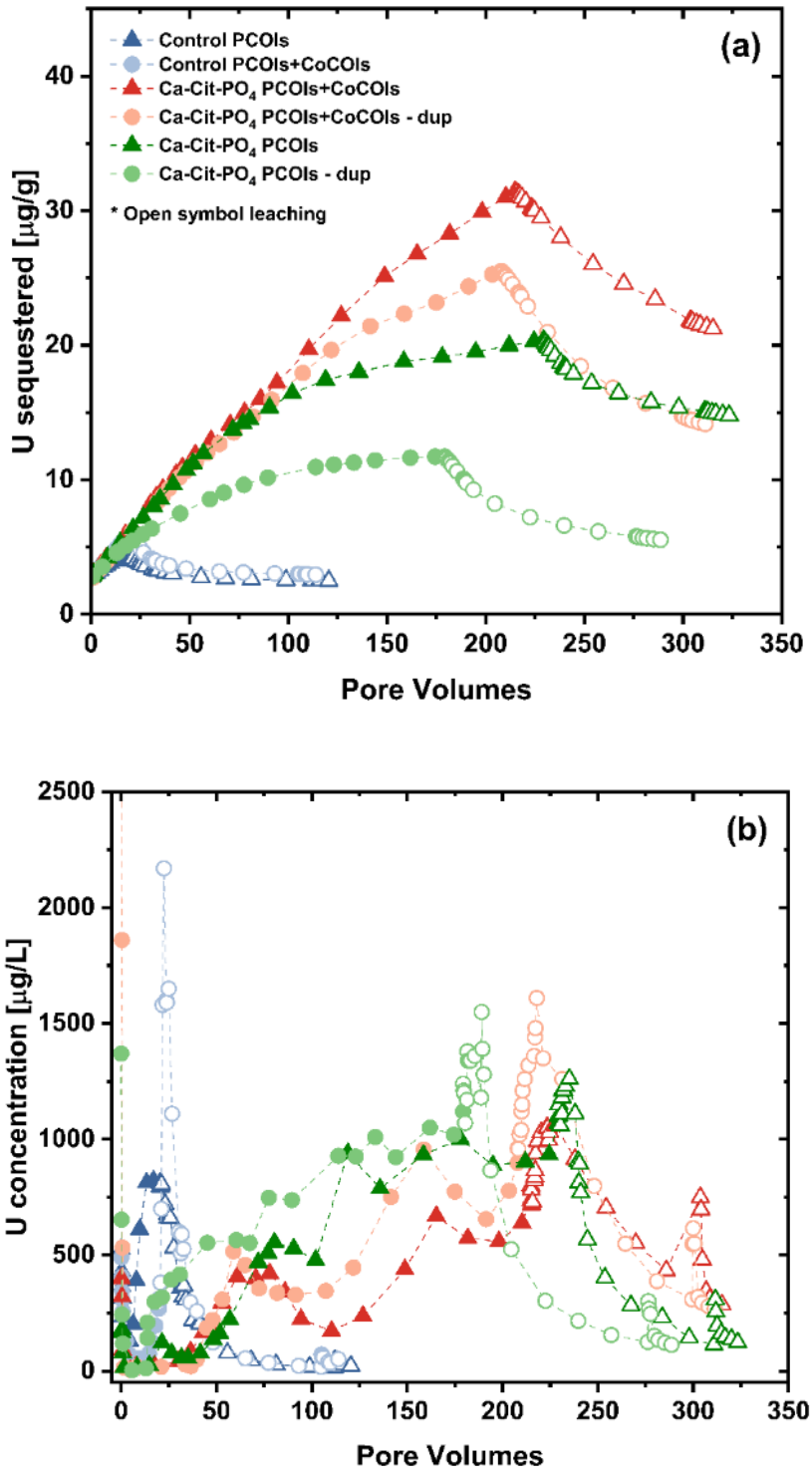

Figure I.1. U during loading and leaching with Cold Creek Unit gravel (CCug) sediment without and with treatment with Ca-Cit-PO_4 after equilibration of amendments for approximately 6 weeks in the absence of oxygen: (a) accumulation of U (in µg/g) and (b) aqueous concentrations of U (in µg/L). Note: "Dup" stands for duplicate. Filled symbols indicate loading phase while open symbols represent the leaching phase with SGW.

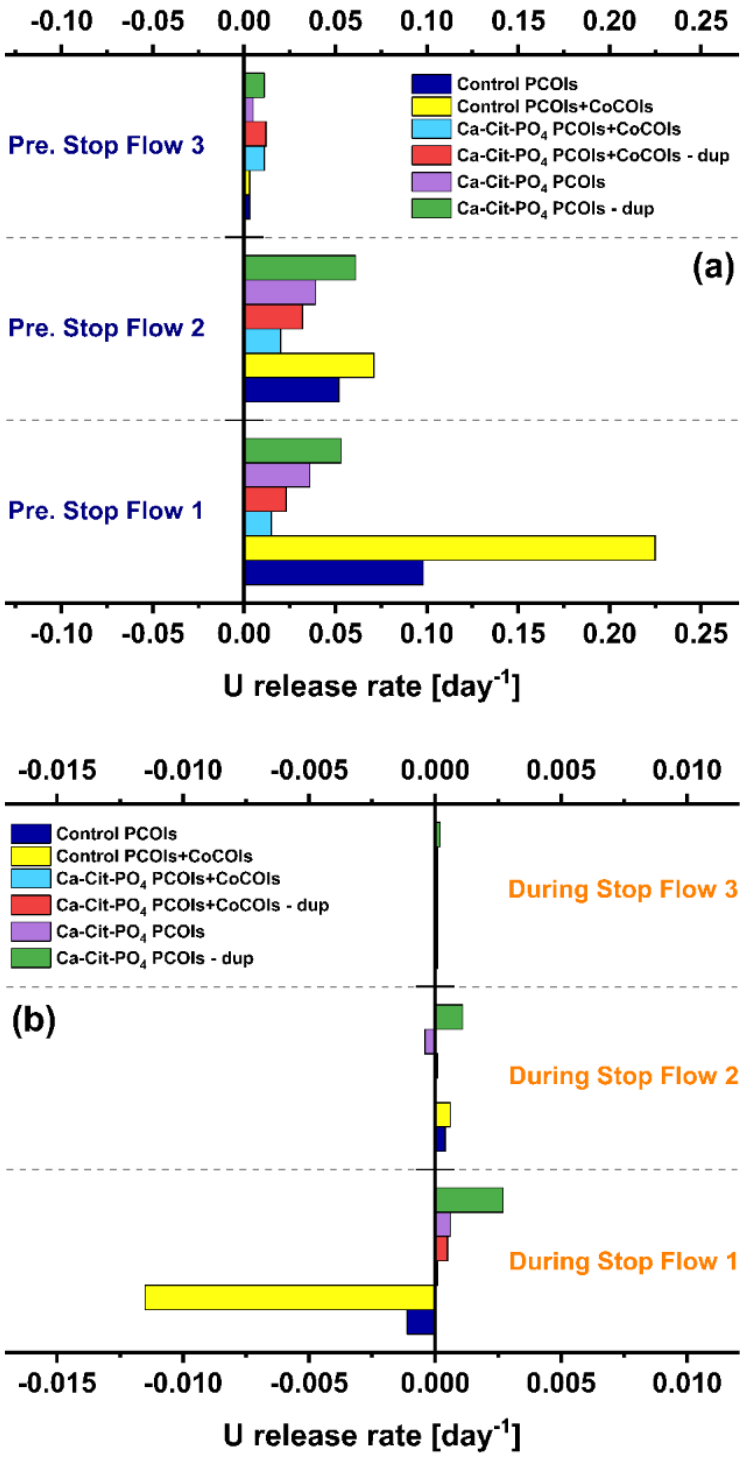

Figure I.2. U normalized release rates during leaching from columns with CCug sediment without and with treatment (with Ca-Cit-PO_4) based on 8 M HNO_3 extractions: (a) estimated leaching rate (day^{-1}) prior to each stop flow and (b) estimated leaching rate (day^{-1}) during each stop flow. Note: "Dup" stands for duplicate.

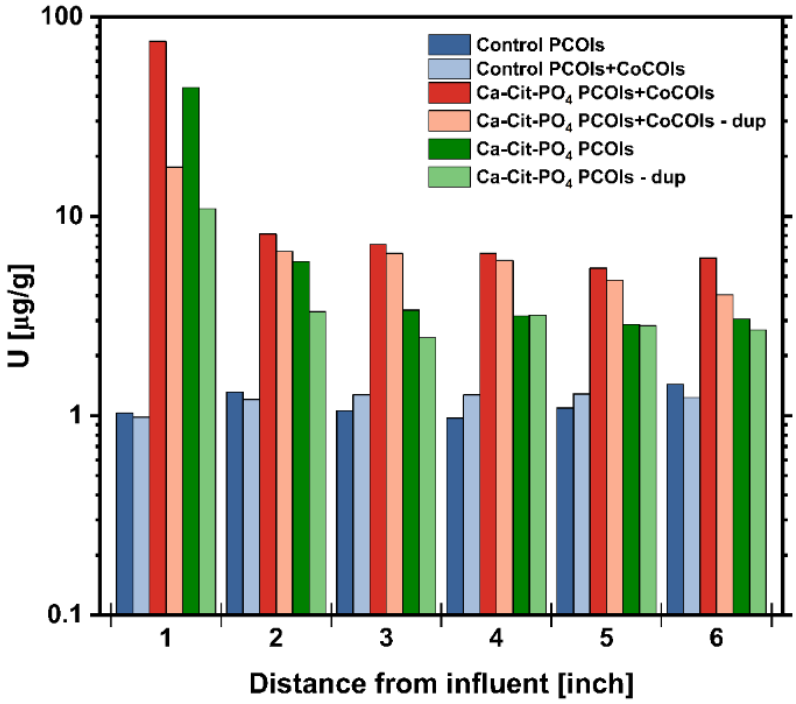

Figure I.3. U distribution (in µg/g) across columns with CCug sediment without and with treatment (with Ca-Cit-PO_4) based on 8 M HNO_3 extractions. Note: "Dup" stands for duplicate.

Table I.1. U estimated recovery after loading and leaching in CCug sediments without and with treatment (Ca-Cit-PO_4) after equilibrium of amendments for approximately 6 weeks in the absence of oxygen.

Conditions	Loading (µg/g)	Leaching (µg/g)
No treatment, PCOIs	4.32	1.09
No treatment, PCOIs + CoCOIs	6.04	1.19
Ca-Cit-PO_4, PCOIs	20.4	10.6
Ca-Cit-PO_4, PCOIs, dup	11.8	4.3
Ca-Cit-PO_4, PCOIs + CoCOIs	31.5	15.9
Ca-Cit-PO_4, PCOIs + CoCOIs, dup	25.6	7.9

For the BY Cribs groundwater conditions, Tc-99 uptake is insignificant in the absence and presence of CoCOIs without treatment, as shown in Figures I.4 through I.6. For the Ca-Cit-PO_4 treatment with CoCOIs, contaminant effluent concentrations reached the influent concentrations (breakthrough) within a few PVs – similar to control columns, likely due to relatively fast consumption of reduction capacity by dissolved O_2, Tc, Cr, and NO_3^-. This resulted in < 0.06 µg/g of Tc-99 initially sequestered after loading as shown in Table I.2. However, the maximum loading of Tc-99 with treatment when CoCOIs were not present was significantly higher than in the presence of CoCOIs (as shown in Figure I.4 and Table I.2, with > 3.2 µg/g of Tc-99 sequestered in the absence of CoCOIs). Therefore, competing CoCOIs likely consumed the majority of the reduction capacity rather than the low dissolved O_2 during solution injection (as loading solutions with contaminants were de-gassed to remove air and O_2). The trends observed here are consistent with previous batch testing in Phase 1 at 1:2 solid-to-liquid ratios (PNNL-35432); however,

reduction capacity was likely consumed more quickly in the column system due to the continuous flow and introduction of more reducible contaminants.

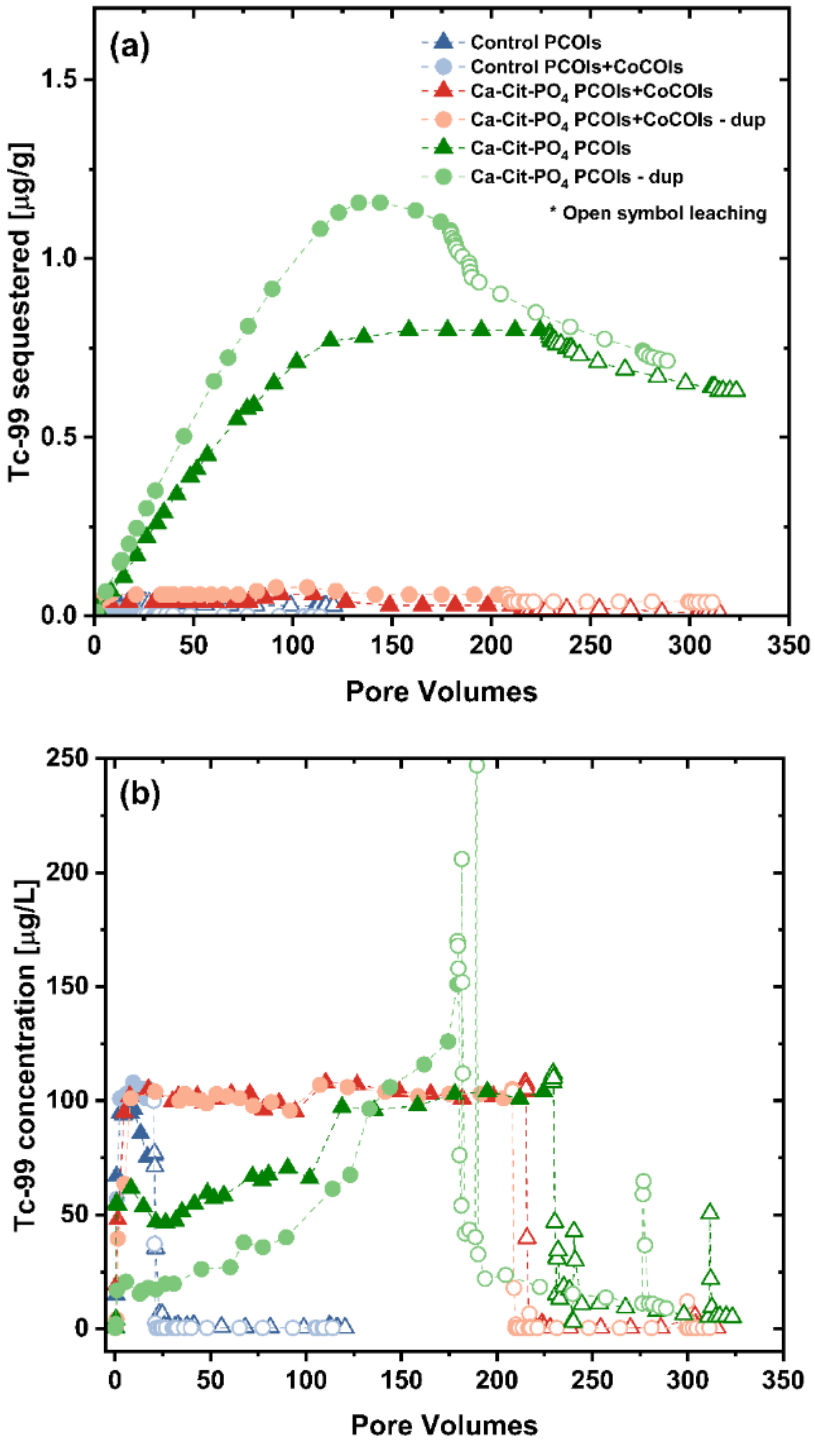

Figure I.4. Tc accumulation in CCug sediment without and with treatment (with Ca-Cit-PO_4) after equilibration of amendments for approximately 6 weeks in the absence of oxygen: (a) accumulation of Tc-99 (in µg/g) and (b) aqueous concentrations of Tc-99 (in µg/L). Note: "Dup" stands for duplicate. Filled symbols indicate loading phase while open symbols represent the leaching phase with SGW.

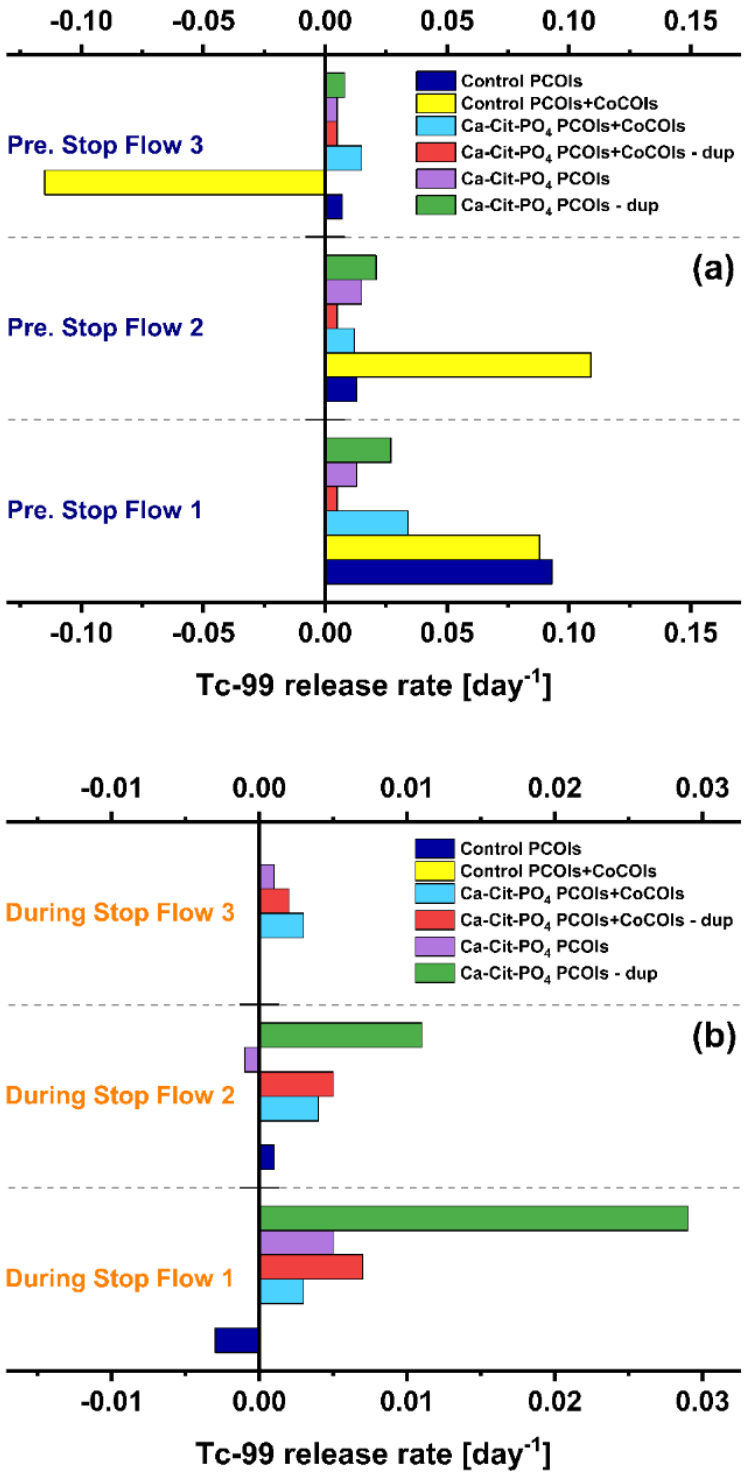

Figure I.5. Tc normalized release rates during leaching from columns with CCug sediment without and with treatment (with Ca-Cit-PO_4) based on 8 M HNO_3 extractions: (a) estimated leaching rate (day^{-1}) prior to each stop flow and (b) estimated leaching rate (day^{-1}) during each stop flow. Note: "Dup" stands for duplicate.

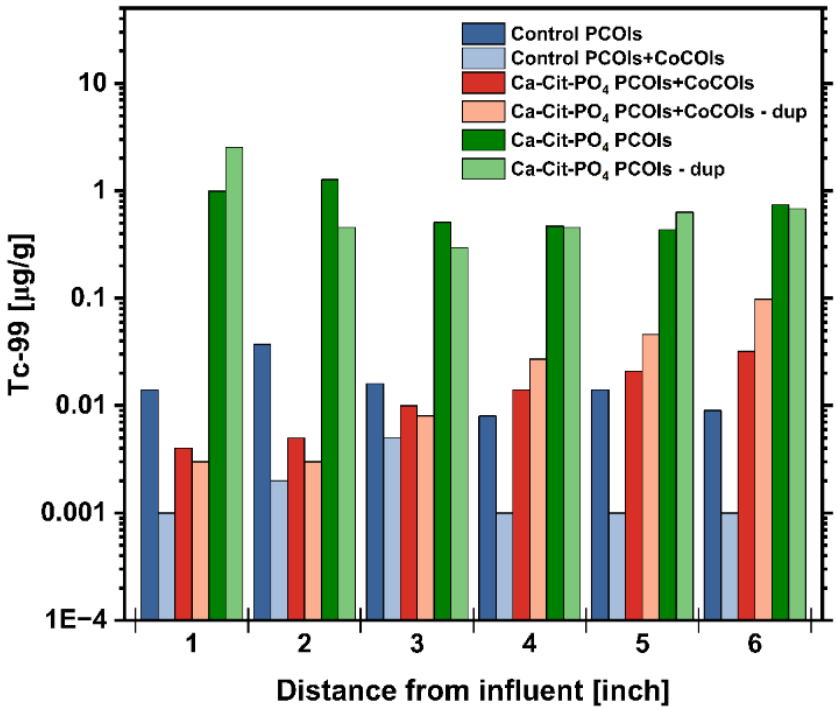

Figure I.6. Tc distribution (in µg/g) across columns with CCug sediment without and with treatment (with Ca-Cit-PO_4) based on 8 M HNO_3 extractions. Note: "Dup" stands for duplicate.

Table I.2. Tc estimated recovery after loading and leaching in CCug sediments without and with treatment (Ca-Cit-PO_4) after equilibrium of amendments for approximately 6 weeks in the absence of oxygen.

Conditions	Loading (µg/g)	Leaching (µg/g)
No treatment, PCOIs	0.05	0.02
No treatment, PCOIs + CoCOIs	0.02	0.00
Ca-Cit-PO_4, PCOIs	0.79	0.72
Ca-Cit-PO_4, PCOIs, dup	1.08	0.86
Ca-Cit-PO_4, PCOIs + CoCOIs	0.03	0.01
Ca-Cit-PO_4, PCOIs + CoCOIs, dup	0.06	0.03

I.2.2 Perched Water Conditions

For the perched water conditions, U initial leaching in the effluent of the untreated columns was significant (Figure I.7b), and this was consistent for a control column prepared at the time of leaching (control) and 6 weeks prior when other columns were treated (aged control). Moreover, the amount of U sequestered in the sediments decreased significantly during leaching (Figure I.7a), ending with only < 5.3 µg/g of U sequestered based on 8 M HNO_3 extractions after sectioning the columns (Table I.3). During estimation of sequestered U in µg/g, there were negative values reported, likely due to heterogeneity of background U in the composite sediments and fluctuation in effluent U during experiments. (Not every sample can be analyzed in the breakthrough curves.)

While the background U was accounted for in estimates based on an average of U recovered in digestions, there was variability, which is difficult to account for during leaching. Hence, the U remaining after leaching was estimated from 8 M HNO_3 extractions of sediments after sectioning instead of effluent monitoring.

For treatment with Ca-Cit-PO_4, there was no significant delay in release as compared to without treatment (Figure I.7). This was observed in both treatment methods, with flow conditions ("F" labeled results) and under static conditions ("S" labeled results). Most of the U was leached relatively quickly, with the majority mobilized in the first 20 PVs (Table I.3). However, there were no clear trends in leaching rates before and during stop flows (Figure I.8) outside of the general decrease with time of leaching. After sectioning, there was no clear trend across the column, though there may have been slightly more U remaining near the effluent end (Figure I.9). Release of Tc-99 under perched water conditions was significant with and without treatment (Figure I.10), and negligible Tc-99 was sequestered with treatment (Figure I.11, Figure I.12, and Table I.3).

This result suggests that release of Tc-99 and U was not significantly delayed with Ca-Cit-PO_4 treatment. It is possible that these high ionic strength conditions did not favor formation of low-solubility apatite and/or complexation with U. In addition, the high nitrate concentrations may have consumed reduction capacity generated from microbial consumption of citrate. Therefore, this technology is not recommended for conditions where there are high ionic strength plumes with NO_3^- as the amount of reductant needed would have to be scaled to reduce the NO_3^- prior to reduction of Tc.

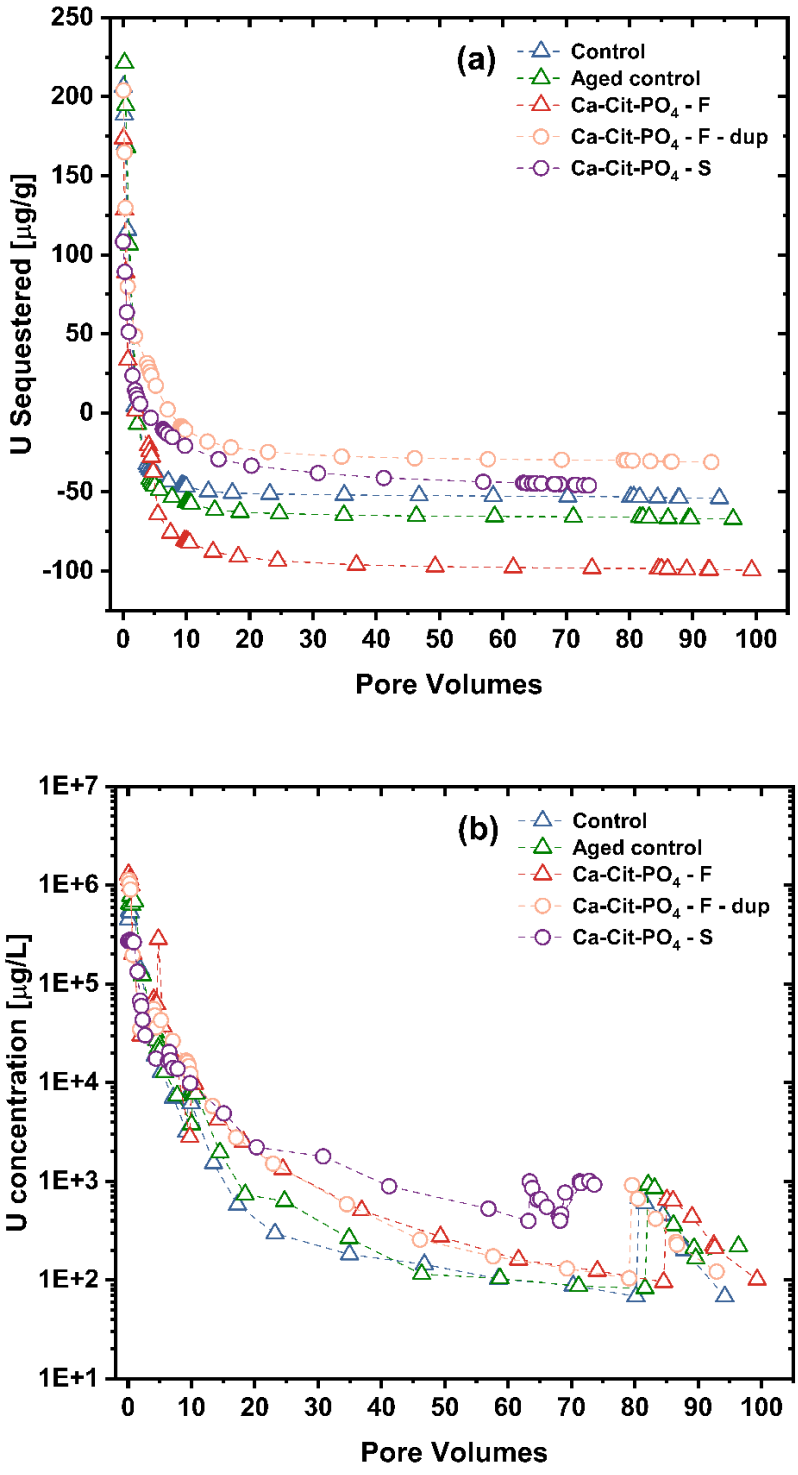

Figure I.7. U remaining during leaching with PZsd sediment without and with treatment (with Ca-Cit-PO_4) after equilibration of amendments for approximately 6 weeks in the absence of oxygen: (a) accumulation of U in sediments (in µg/g) and (b) aqueous concentrations of U (in µg/L). Note: "Dup" stands for duplicate.

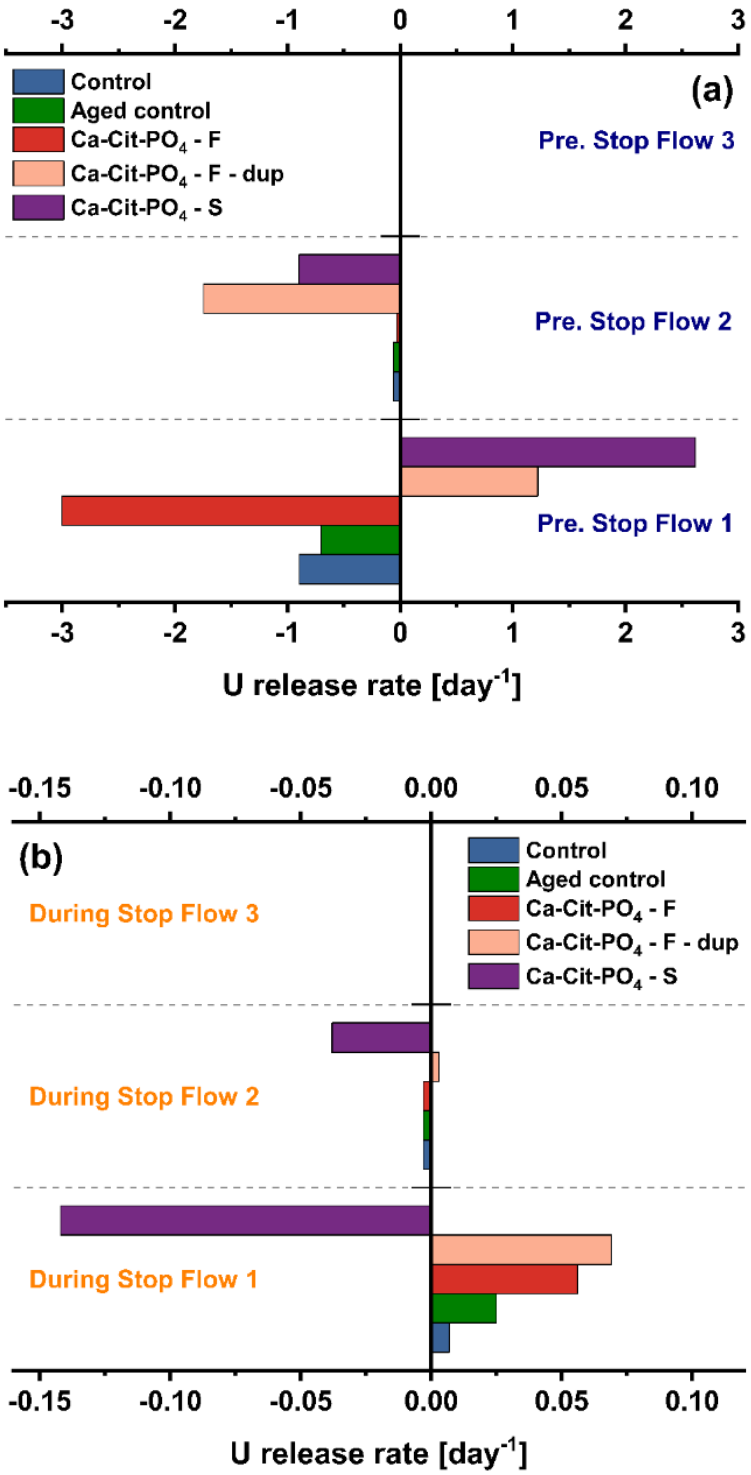

Figure I.8. U normalized release rates during leaching from columns with PZsd sediment without and with treatment (with Ca-Cit-PO_4) based on 8 M HNO_3 extractions, *top* – estimated leaching rate (day^{-1}) prior to each stop flow and *bottom* – estimated leaching rate (day^{-1}) during each stop flow. Note: "Dup" stands for duplicate.

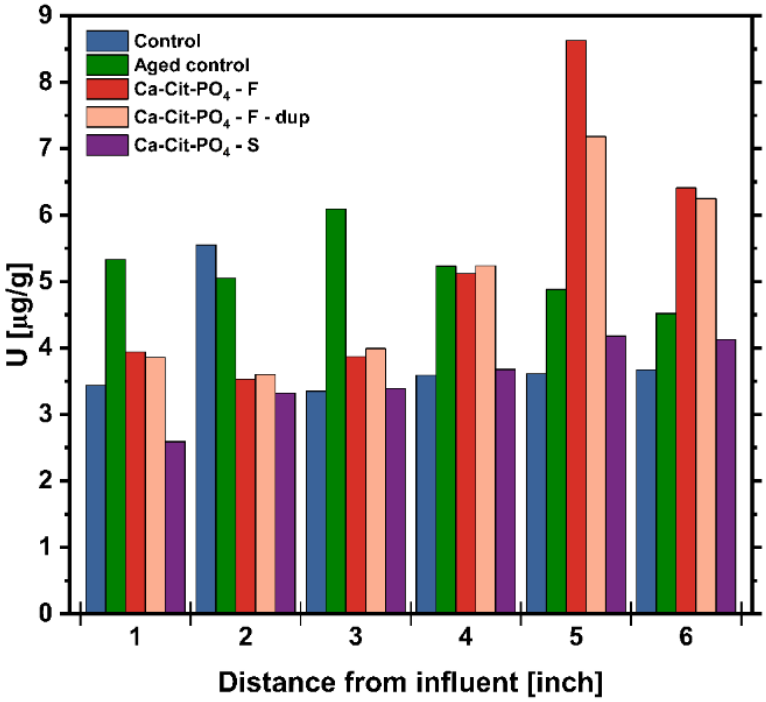

Figure I.9. U distribution (in µg/g) across columns with PZsd sediment without and with treatment (with Ca-Cit-PO_4) based on 8 M HNO_3 extractions. Note: "Dup" stands for duplicate; "F" delineates treatment occurred after column packing via injection; "S" delineates treatment occurred prior to column packing in a batch setup.

Table I.3. U and Tc-99 estimated recovery after leaching in PZsd sediments without and with treatment (Ca-Cit-PO_4) after equilibrium of amendments for approximately 6 weeks in the absence of oxygen. Note: Initial U and Tc-99 were estimated to be 109 and 0.27 µg/g, respectively. Two control columns are included with (aged) and without treatment for 6 weeks prior to leaching. F stands for amendment treatment with flow and S stands for amendment treatment in static batch conditions.

Conditions	U (µg/g)	Tc (µg/g)
No treatment	3.87	0.00
No treatment (aged)	5.25	0.01
F-Ca-Cit-PO_4	5.26	0.00
F-Ca-Cit-PO_4, dup	4.98	0.00
S-Ca-Cit-PO_4	3.36	0.02

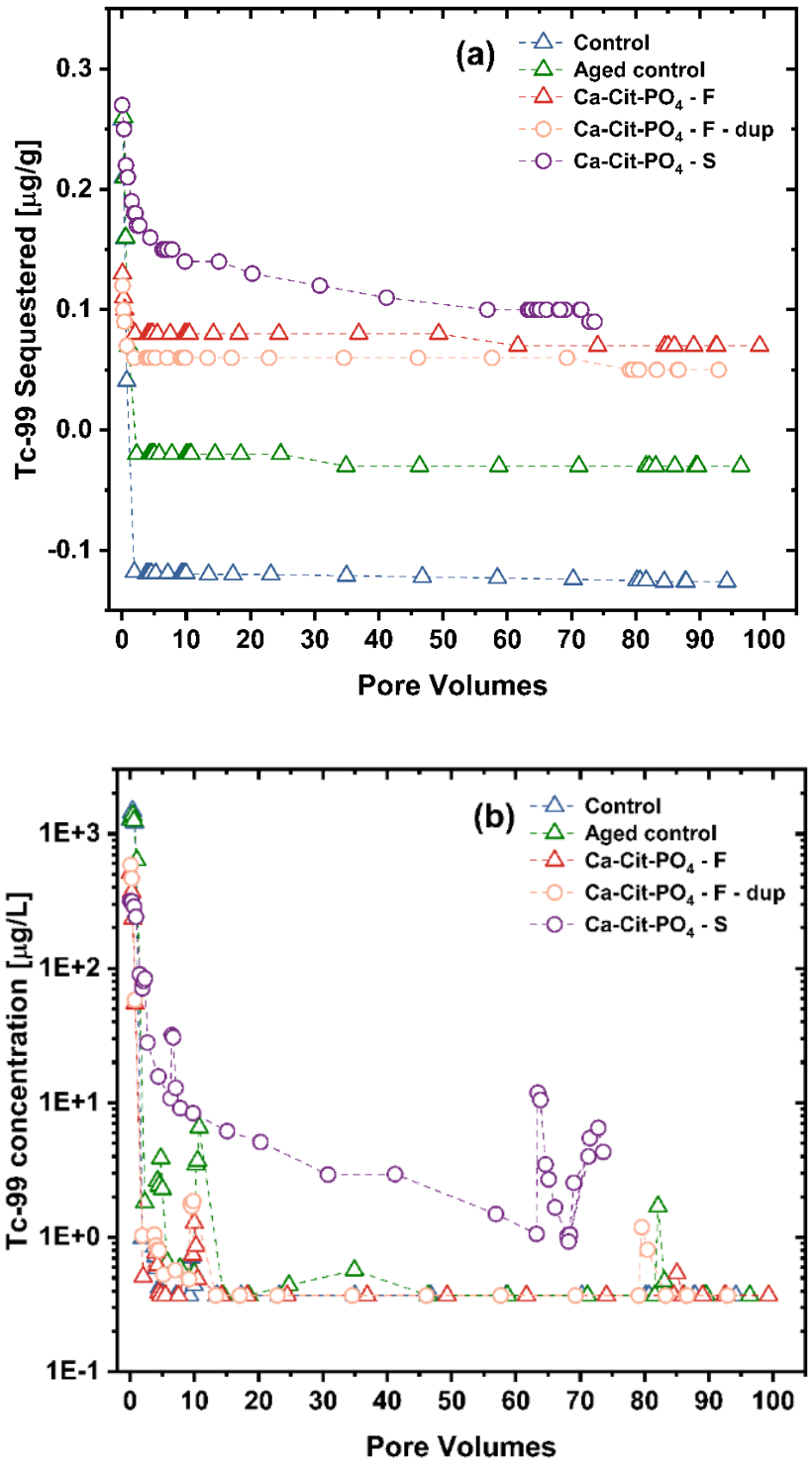

Figure I.10. Tc remaining during leaching with PZsd sediment without and with treatment (with Ca-Cit-PO_4) after equilibration of amendments for approximately 6 weeks in the absence of oxygen: (a) accumulation of Tc-99 in sediments (in µg/g) and (b) aqueous concentrations of Tc-99 (in µg/L). Note: "Dup" stands for duplicate; "F" delineates treatment occurred after column packing via injection; "S" delineates treatment occurred prior to column packing in a batch setup.

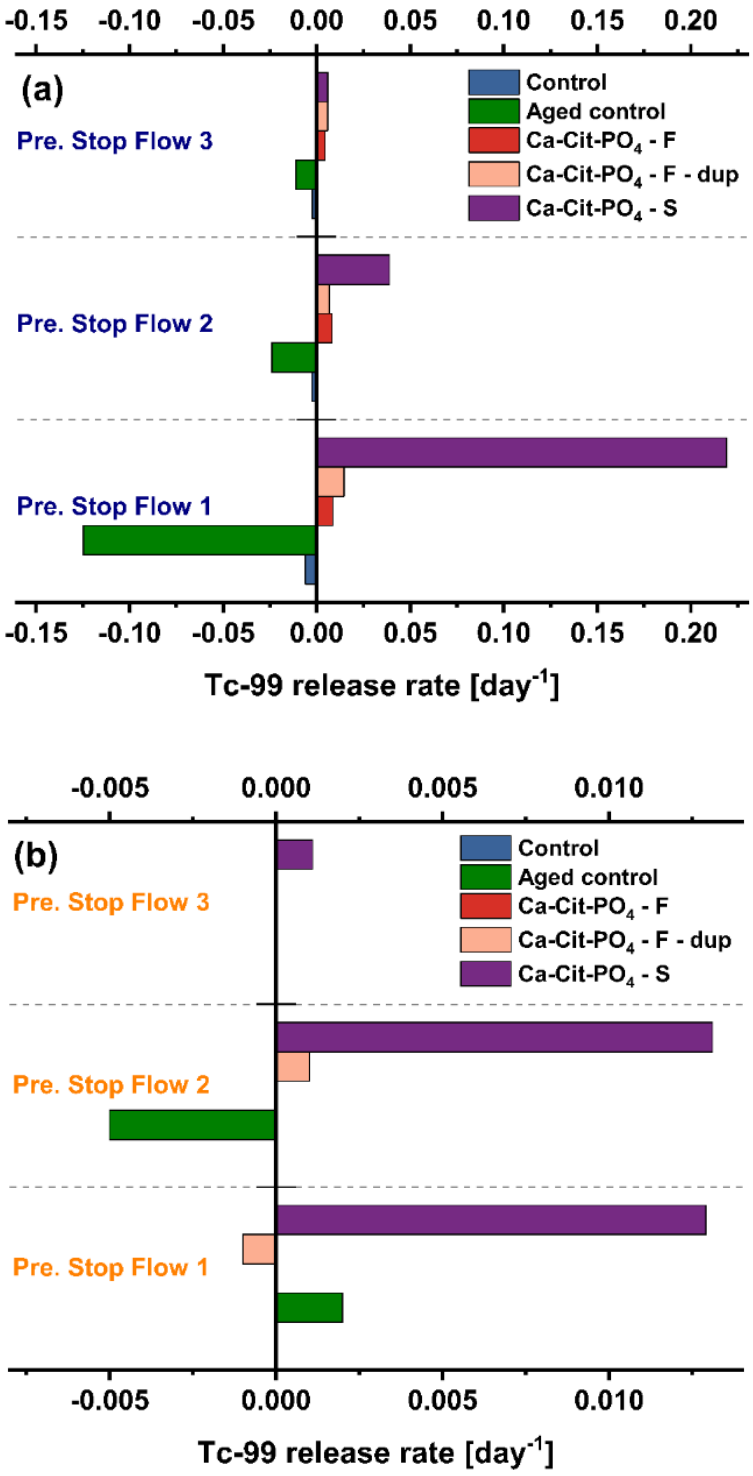

Figure I.11. Tc normalized release rates during leaching from columns with PZsd sediment without and with treatment (with Ca-Cit-PO_4) based on 8 M HNO_3 extractions, (a) estimated leaching rate (day^{-1}) prior to each stop flow and (b) estimated leaching rate (day^{-1}) during each stop flow. Note: "Dup" stands for duplicate; "F" delineates treatment occurred after column packing via injection; "S" delineates treatment occurred prior to column packing in a batch setup.

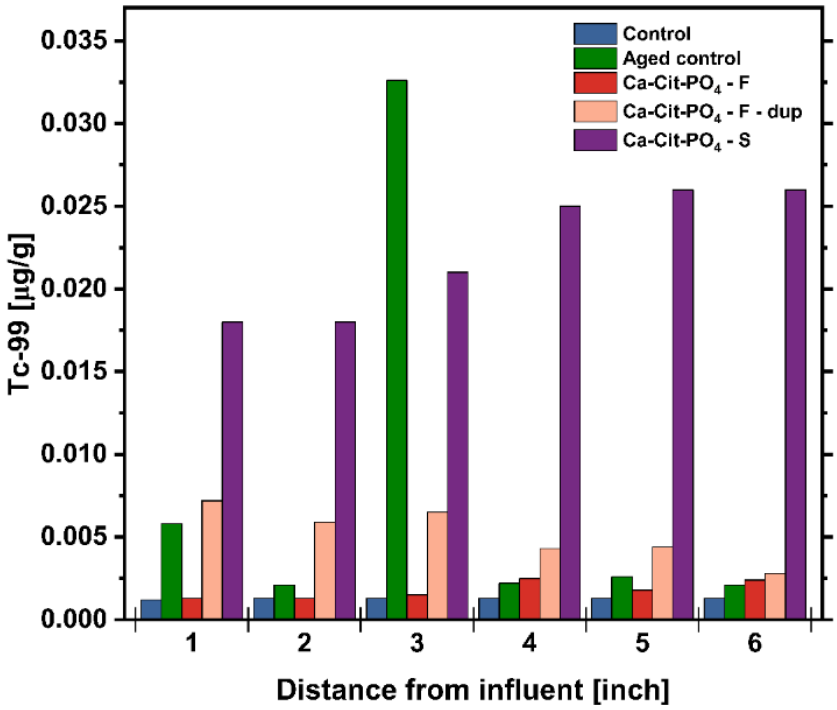

Figure I.12. Tc distribution (in µg/g) across columns with PZsd sediment without and with treatment (with Ca-Cit-PO_4) based on 8 M HNO_3 extractions. Note: "Dup" stands for duplicate; "F" delineates treatment occurred after column packing via injection; "S" delineates treatment occurred prior to column packing in a batch setup.

I.2.3 Long-Term Tc-99 and U Stability

X-ray absorption spectroscopy (XAS) and X-ray fluorescence (XRF) measurements were collected on select samples to better understand elemental distribution, oxidation states, and coordination. Data for U are shown for BY Cribs groundwater conditions based on column samples prepared after reaction with Ca-Cit-PO_4. In post-leached sediments, U was associated with both Fe and Ca (Figure I.13), though it suggests only a correlation. U may have precipitated on or near Fe- and Ca-containing minerals. X-ray absorption near edge structure (XANES) results show that U was mostly likely U(VI) in all three locations analyzed (Figure I.14), highlighting that conditions were likely not reached for reduction of U. This result is consistent with Tc-99 as only partial reduction of Tc-99 was observed, indicating it was unlikely for U to be reduced based on its reduction potential being lower than Tc. Data for Tc-99 are shown for perched water conditions based on batch samples (pre-leach) prepared after reaction with Ca-Cit-PO_4. Linear combination fitting estimated a mixed Tc-99 oxidation state with 0.66±0.01 as Tc(IV) and 0.34±0.01 as Tc(VII) as shown in Figure I.15.

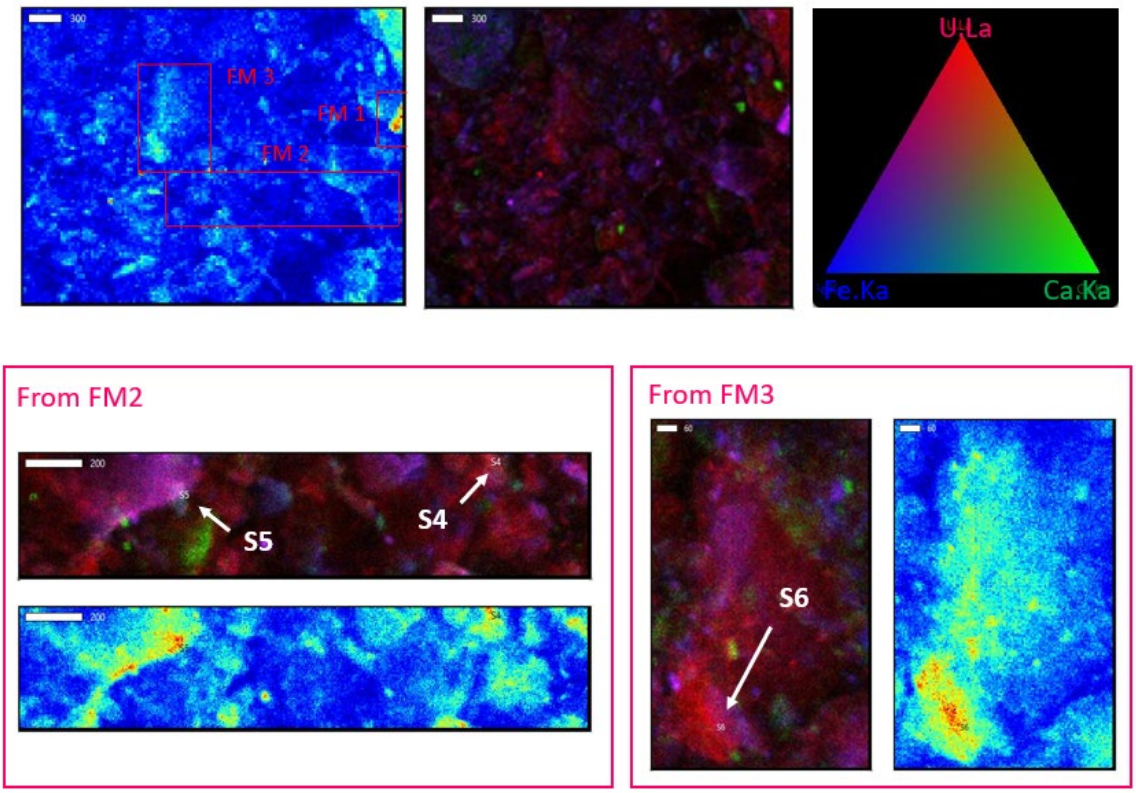

Figure I.13. XRF mapping results for post-leach CCug sediments treated with Ca-Cit-PO_4 in columns with coarse (*top row*) and fine maps (*bottom row*) showing areas of interest for U alongside Fe and Ca. Note: The white arrows point to the spots selected for U L3-edge XANES, S4, S5, and S6. PNNL605.

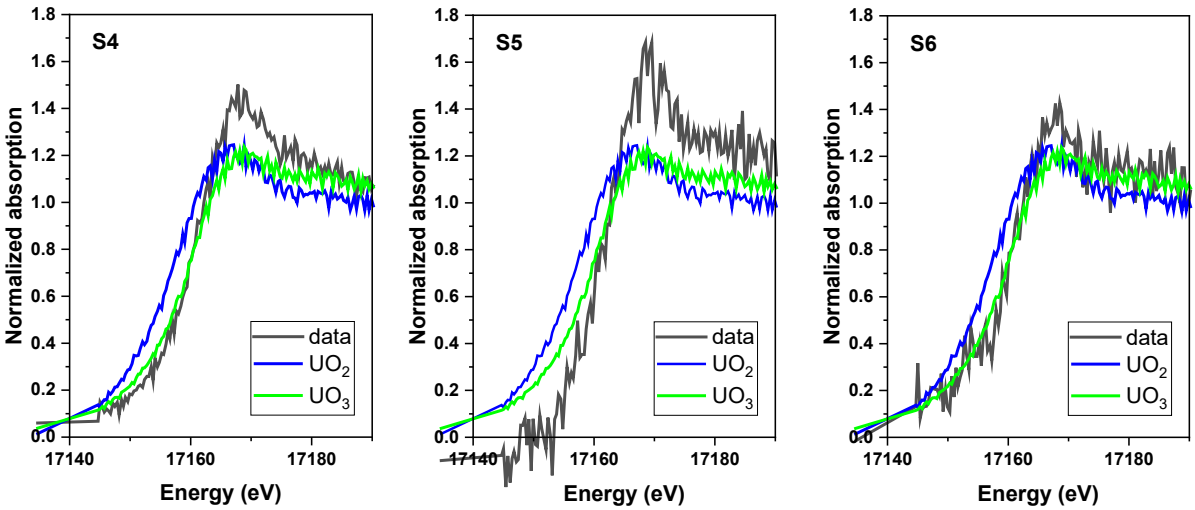

Figure I.14. U L3-edge XANES on the three different locations (S4, S5, and S6) on post-leaching sediments treated in columns with Ca-Cit-PO_4. Note: Locations were chosen based on variable U concentrations observed during XRF mapping (on Figure I.13) of the column sediment. PNNL605. U is most likely U(VI) in all spots.

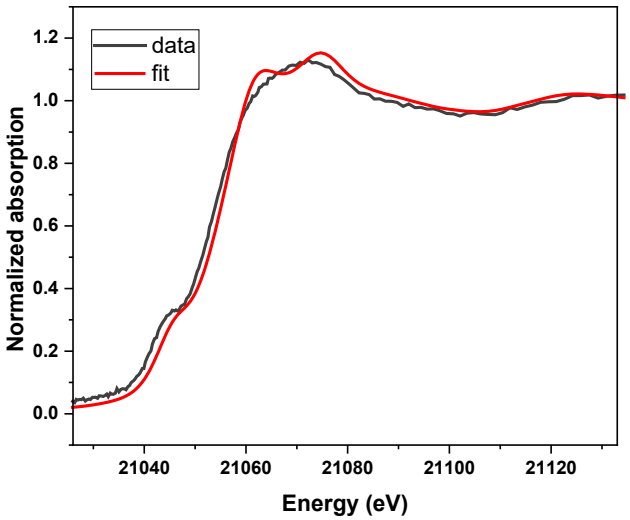

Figure I.15. XANES results for Tc-99 K-edge on pre-leach PZsd sediments from batch treatment with Ca-Cit-PO_4 with corresponding linear combination fit. Data – *black* and fit – *red* lines. The linear combination fit range is from -43 to 97 eV below and above the edge. Tc-99 PNNL626.

I.3 Saturated Column Results for Co-contaminants

I.3.1 BY Cribs Groundwater Conditions

For CoCOIs, including I, Cr, and Sr, data were collected from monitoring effluent concentrations and distribution in sediments post-leaching (only for Cr and Sr). These results show that the mobility of I is not significantly decreased with Ca-Cit-PO_4 treatment (Figure I.16). However, loadings into sediments cannot be confirmed based on post-leaching column sectioning, as acidic conditions were used for leaching to target PCOIs but likely volatilize iodine. Regardless, the potential for uptake of I in apatite was not promising with this technology.

During loading of Cr, there was a delay for Cr in effluent as compared to the control. Moreover, during leaching, a small amount of Cr was released during early stop flow events within the first 10 PVs, though significant leaching was not observed after that point. There was an increase in loading of Cr in sediments (Figure I.17) based on post-leach sectioning and extraction in 8 M HNO_3. Although there was fluctuation across the column, there was a ~10-fold increase in solid phase Cr, based on extractions conducted after the leaching phase.

In the first 100 PVs of loading into these columns, there was a clear delay in effluent Sr (Figure I.18) for columns treated with Ca-Cit-PO_4. Sr also showed an increasing amount with distance from the injection end of the column. This may indicate slow Sr precipitation (as Sr-carbonate, for example). In addition, significant Sr was mobilized in the first few PVs, similar to observations for U, consistent with release of natural Sr from sediments during initial injection of solutions. It is likely that the reaction times did not allow for incorporation of Sr into apatite over time, based on the high concentrations of Sr being released during leaching (open symbols). Solid phase Sr concentrations also slowly increased with distance from the influent injection side of the column post-leaching, based on sectioning results, potentially showing that significant release of Sr could still occur over time. There was little nitrate reduction observed under groundwater conditions (Figure I.19). Under perched water conditions of high nitrate concentration and 6

weeks of reaction time before leaching, significant nitrate reduction was observed for the column in which nitrate was added to the sediment prior to packing into the column (Figure I.20).

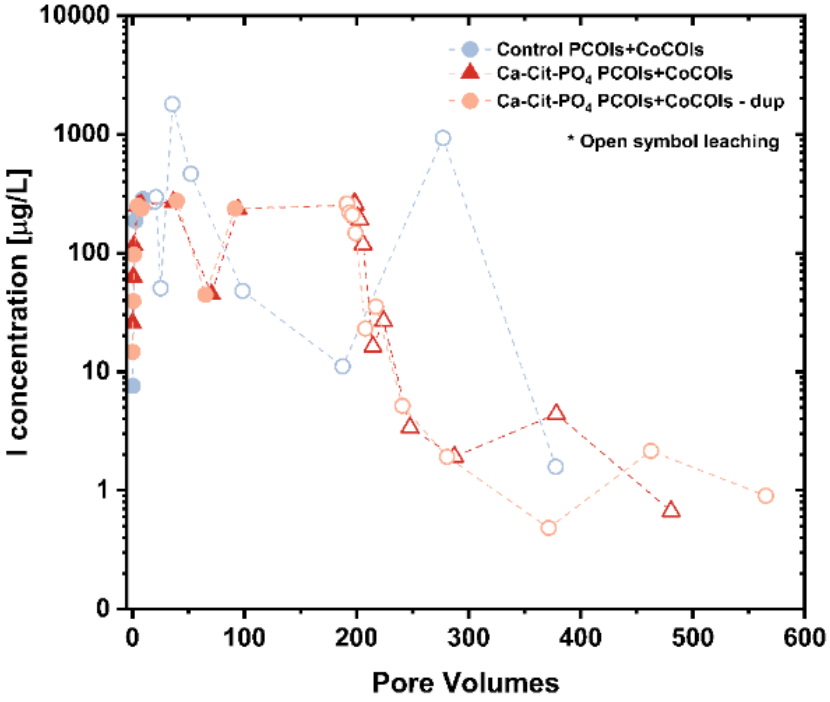

Figure I.16. Effluent I (in µg/L) during loading and leaching of CCug sediment without and with treatment after equilibration of amendments for approximately 6 weeks in the absence of oxygen. Note: “Dup” stands for duplicate.

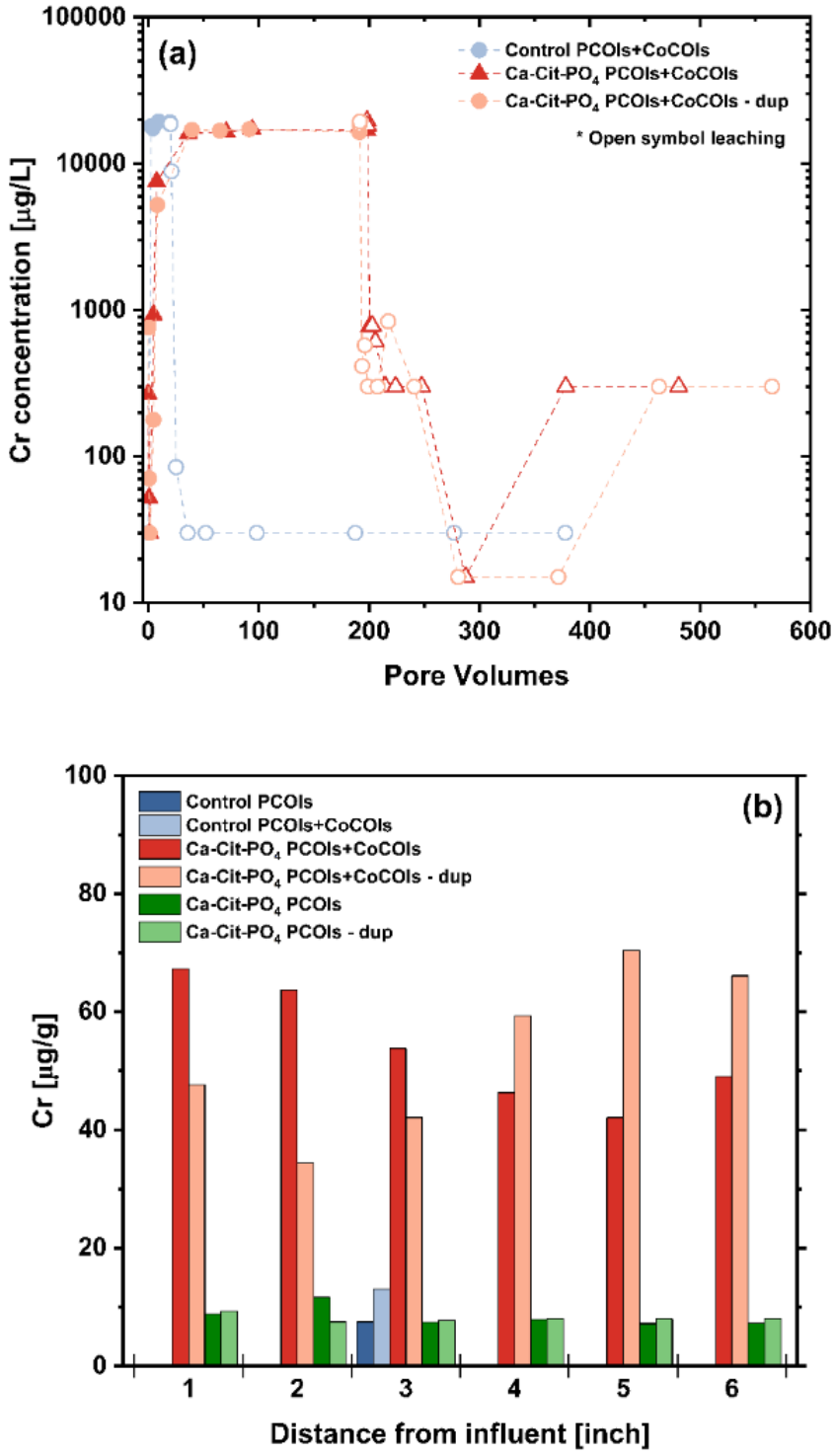

Figure I.17. (a) Effluent Cr (in µg/L) during loading and leaching and (b) Cr distribution (in µg/g) across columns based on 8 M HNO_3 extractions with CCug sediment without and with treatment (with Ca-Cit-PO_4) after equilibration of amendments for approximately 6 weeks in the absence of oxygen. Note: "Dup" stands for duplicate.

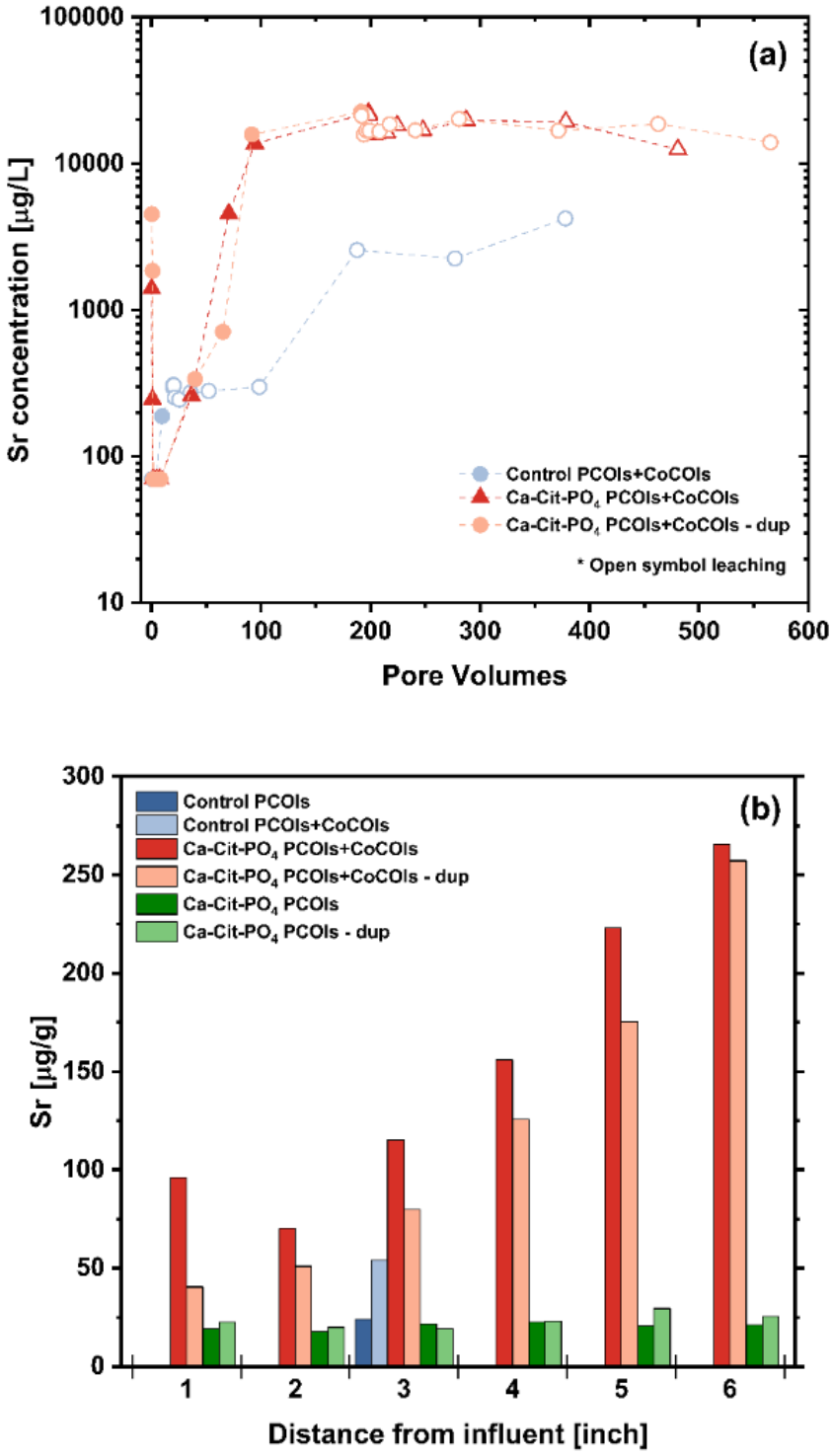

Figure I.18. (a) Aqueous Sr (in µg/L) during loading and leaching and (b) Sr distribution (in µg/g) across columns based on 8 M HNO_3 extractions with CCug sediment without and with treatment (with Ca-Cit-PO_4) after equilibration of amendments for approximately 6 weeks in the absence of oxygen. Note: "Dup" stands for duplicate.

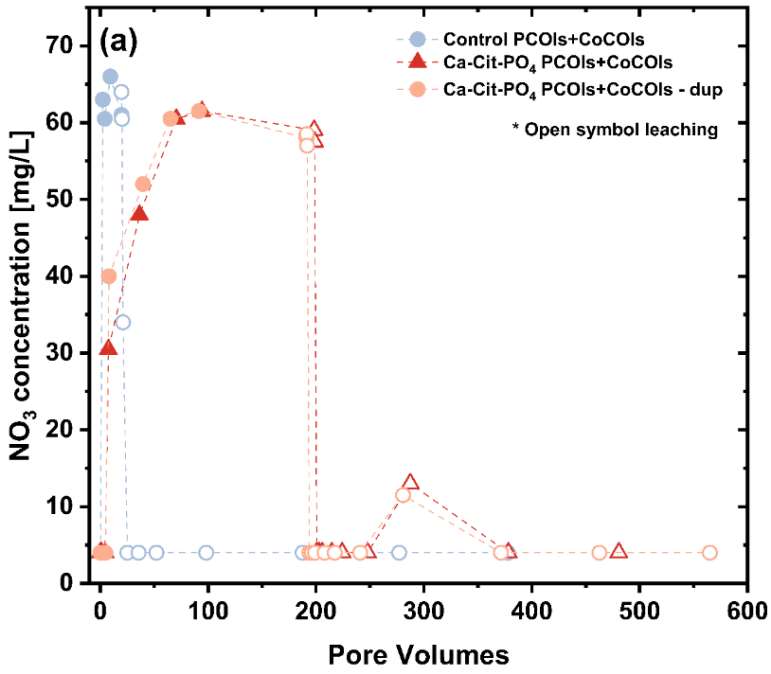

Figure I.19. Aqueous nitrate (in mg/L) during loading and leaching with CCug sediment without and with treatment (with Ca-Cit-PO_4) after equilibration of amendments for approximately 6 weeks in the absence of oxygen. Note: "Dup" stands for duplicate.

I.3.2 Perched Water Table Conditions

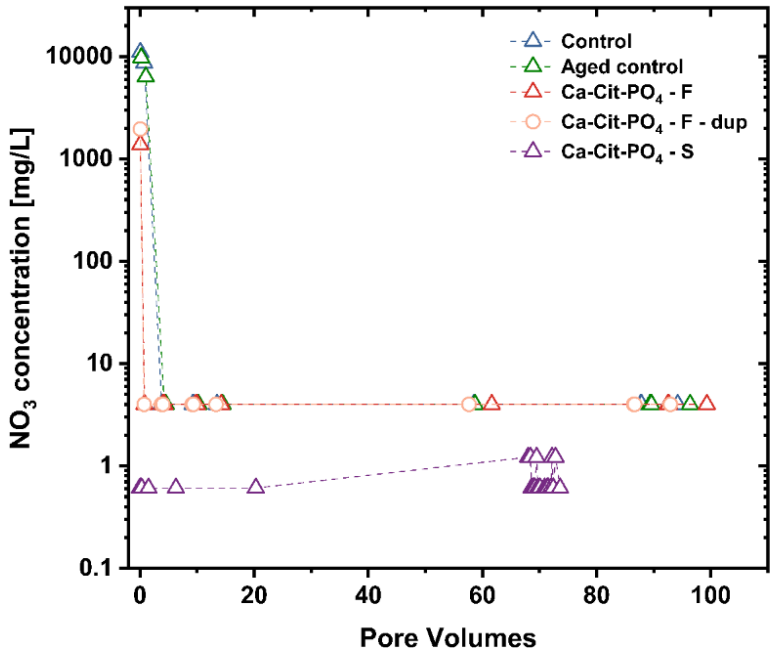

Figure I.20. Aqueous nitrate (in mg/L) during leaching with PZsd sediment without and with treatment (with Ca-Cit-PO_4) after equilibration of amendments for approximately 6 weeks in the absence of oxygen. Note: "Dup" stands for duplicate; "F" delineates treatment occurred after column packing via injection; "S" delineates treatment occurred prior to column packing in a batch setup.

I.4 Saturated Column Geochemical Monitoring

I.4.1 pH Monitoring

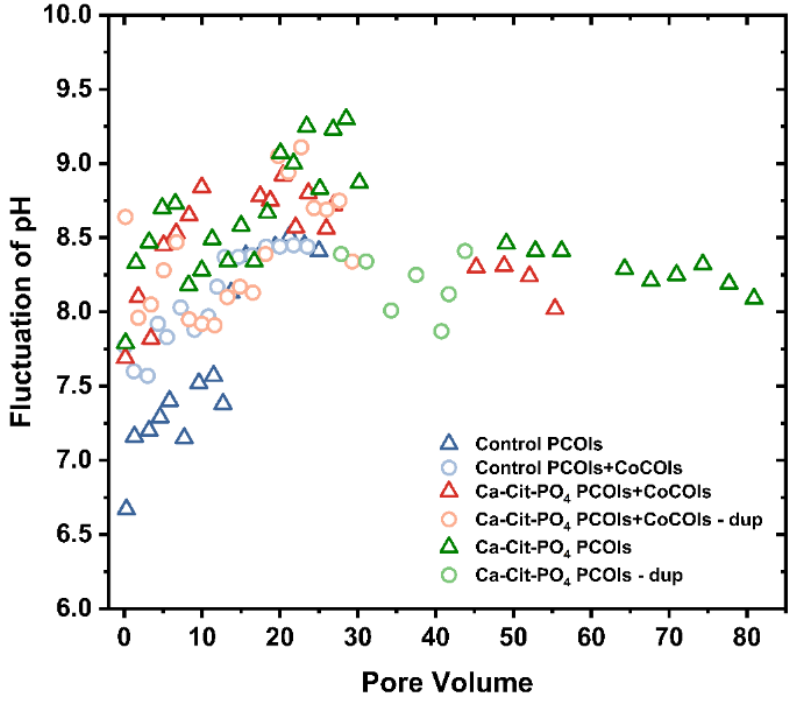

Figure I.21. Fluctuation of pH over time during leaching with CCug sediment without and with treatment (with Ca-Cit-PO_4) after equilibration of amendments for approximately 6 weeks in the absence of oxygen. Note: "Dup" stands for duplicate. Ca-Cit-PO_4 treatment was conducted via injection of amendments into columns under flowing conditions.

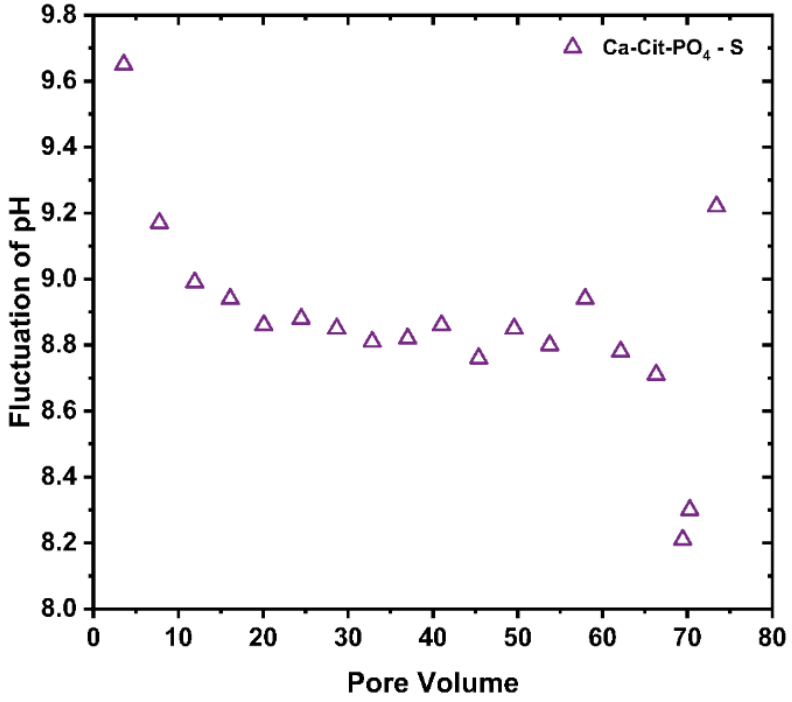

Figure I.22. Fluctuation of pH over time during leaching with PZsd sediment without and with treatment (with Ca-Cit-PO_4) after equilibration of amendments for approximately 6 weeks in the absence of oxygen. Note: "S" delineates treatment occurred prior to column packing in a batch setup.

I.4.2 Amendment Monitoring Data

For both BY Cribs groundwater and perched water conditions, there was less P measured in the sediments in the BY Cribs groundwater condition and significant P was leached for treated columns (Figure I.23). It is likely that much of the calcium phosphate minerals precipitated initially from Ca-Cit-PO_4 was leached during the loading of contaminants and subsequent leach, which occurred over hundreds of PVs. Similar results were observed under perched water conditions (Figure I.24). These results confirm that calcium phosphate precipitates will leach over time, though predictions could be projected based on solubility and groundwater chemistry and flow rates, if specific phases are identified. It is possible that carbonated apatites or other substitutions occurred during precipitation, leading to more soluble phases. The presence of high ionic strength (especially under perched water conditions), high metals (especially with CoCOIs in BY Cribs groundwater conditions), and alkalinity may have led to formation of lower solubility calcium phosphate phases (e.g., orthophosphates) as opposed to apatite (Rakovan 2002). If formed, many heavy metal phosphates have a higher solubility than apatite, though their solubility tends to decrease with increasing calcium substitution (Ayati and Madsen 2000). In addition, carbonated apatites have been shown to form previously in the presence of elevated carbonate concentrations, exhibiting lower crystallinity and higher solubility (Hughes and Rakovan 2015; Heslop et al. 2005).

I.4.2.1 BY Cribs Groundwater Conditions

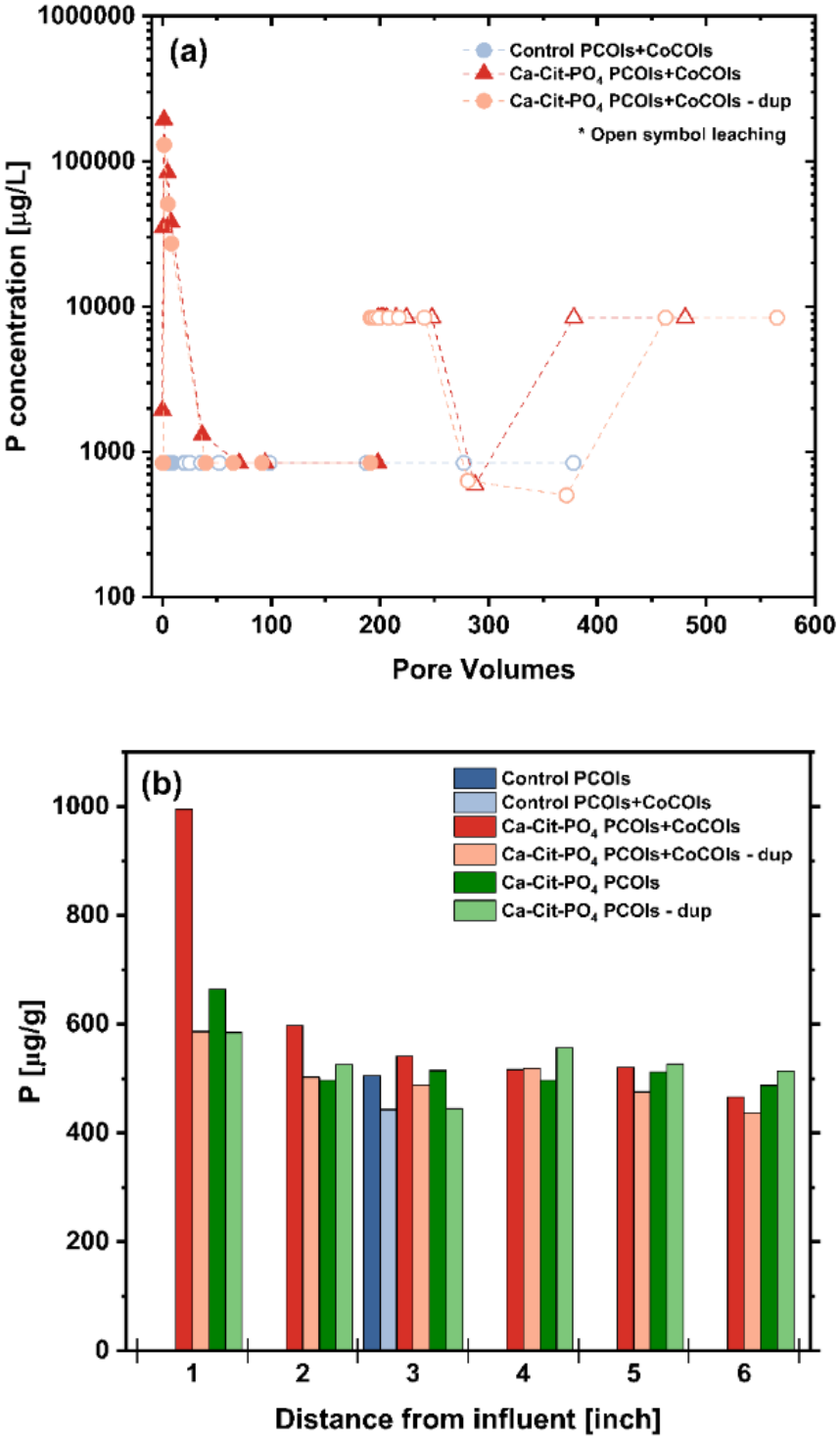

Figure I.23. (a) Effluent P (in µg/L) during loading and leaching and (b) P distribution (in µg/g) across columns based on 8 M HNO_3 extractions with CCug sediment without and with treatment (with Ca-Cit-PO_4) after equilibration of amendments for approximately 6 weeks in the absence of oxygen. Note: "Dup" stands for duplicate.

I.4.2.2 Perched Water Conditions

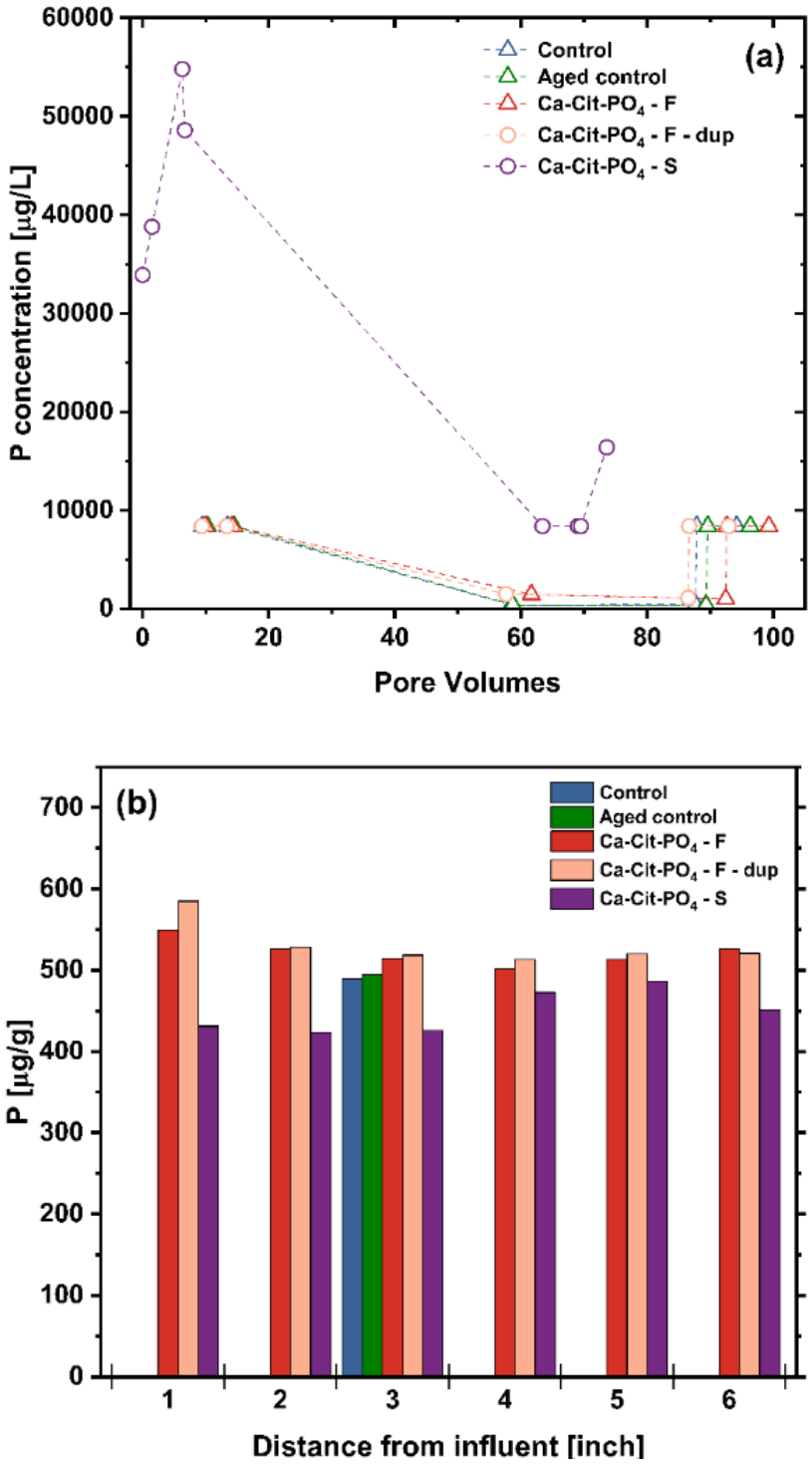

Figure I.24. (a) Effluent P (in µg/L) during leaching and (b) P distribution (in µg/g) across columns based on 8 M HNO_3 extractions with PZsd sediment without and with treatment (with Ca-Cit-PO_4) after equilibration of amendments for approximately 6 weeks in the absence of oxygen. Note: "F" delineates treatment occurred after column packing via injection; "S" delineates treatment occurred prior to column packing in a batch setup.

I.4.3 Bromide Tracer Breakthrough

Results are summarized here for bromide breakthrough curves collected at the end of experiments, after the approximately 100-PV leaching step. Bromide curves are similar and repeatable, suggesting that the amendments (Ca-Cit-PO_4) did not have a significant impact on the flow of water through the CCug columns (Figure I.25). There was a small difference between the two no-treatment columns with and without aging for PZsd sediments as shown in Figure I.26. However, this was more likely a fluctuation in flow rates from syringe pumps as each column received solution via its own syringe pump. Occasional fluctuations in flow rates occurred, especially for PZsd sediments due to its finer size fractions as compared to CCug (Appendix B, Section B.5), which led to slightly elevated back pressure during injection. Moreover, differences were not observed in the PZsd sediments between the treated and untreated columns (Appendix J, Figure J.45). Bromide breakthrough curves are fit for dispersion and compared across all technologies in Appendix A, Section A.3.2.

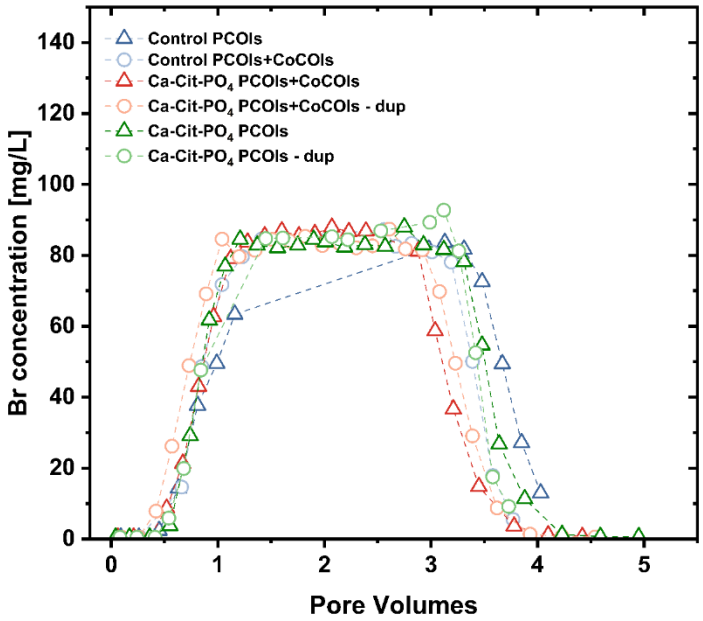

Figure I.25. Effluent Br (in mg/L) during and after tracer injection at 80 mg/L Br into columns with CCug sediment without and with treatment (with Ca-Cit-PO_4). Note: "Dup" stands for duplicate.

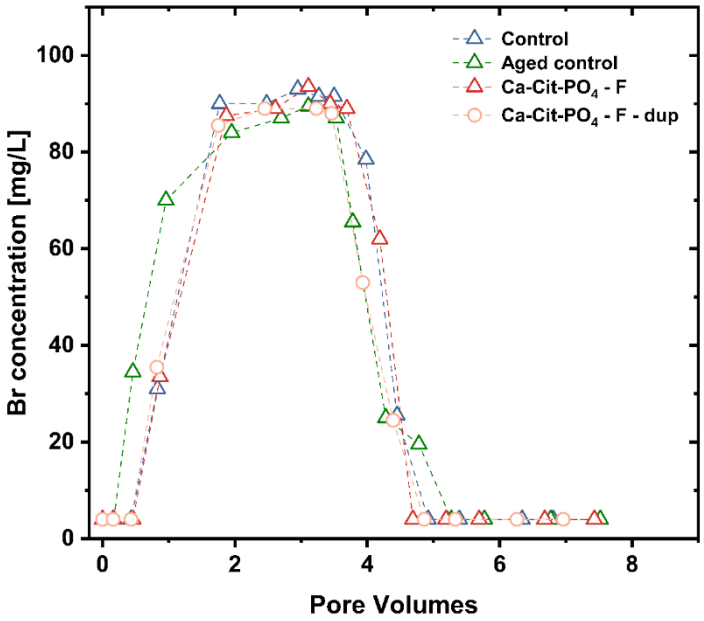

Figure I.26. Effluent Br (in mg/L) during and after tracer injection at 80 mg/L Br into columns with PZsd sediment without and with treatment (with Ca-Cit-PO_4). Note: "Dup" stands for duplicate; "F" delineates treatment occurred after column packing via injection.

I.5 Summary of Performance of Calcium Citrate Phosphate for Groundwater

For the BY Cribs groundwater conditions, Ca-Cit-PO_4 is recommended for U as well as Cr and nitrate, but it is not recommended for Tc. For the perched water conditions, Ca-Cit-PO_4 is not recommended for Tc-99 or U but may perform well for nitrate or other readily reducible PCOIs and CoCOIs.

U sequestration was significant with Ca-Cit-PO_4 treatment in the presence and absence of CoCOIs, although uptake was greater with CoCOIs present. Results for U were consistent with previous testing in Phase 1 (PNNL-35432) and at the Old Rifle Processing Site in Rifle, CO (PNNL-25303), suggesting adsorption, incorporation, and/or coating with calcium phosphate. Notably, some U in the solid phase may have been present as U(IV), suggesting partial reduction prior to sequestration with calcium phosphate, though XAS results were inconclusive.

For Tc-99 in BY Cribs groundwater, conditions were likely not reducing enough with Ca-Cit-PO_4 as minimal uptake was observed in both conditions (with and without CoCOIs) for BY Cribs groundwater. Partial (incomplete) Tc-99 reduction was observed in XAS results for Tc-99 in batch experiments, although conditions in columns could not be confirmed as XAS results are not available. Some sequestration was also observed in previous batch testing for Phase 1. Overall, results were consistent with a small fraction of Tc-99 being reductively precipitated.

For CoCOIs, increased loading was observed for Cr and Sr, but not I, with some transformation of nitrate based on effluent monitoring. For reducible CoCOIs, their reduction potentials may be compared to further elucidate redox conditions within columns (reduction order expected to be nitrate > Cr > Tc-99 > U). For example, the delay in nitrate breakthrough suggests transformation of nitrate to nitrite and potentially further. In addition, the significant increase in loading of Cr highlights that it was likely

reduced to Cr(III). Therefore, conditions were relatively reducing but not sufficient for complete reduction of Tc-99 and U.

Significant loading of Sr was also observed. However, significant release of Sr also occurred during the leaching phase. It is possible that Sr was desorbed due to insufficient time for slower incorporation mechanisms to occur (Szecsody et al. 2014; Janusz and Skwarek 2016; Nishiyama et al. 2016) or apatite was dissolving and concurrently releasing Sr. Because there was a concurrent increase in aqueous P in effluent during leaching, it is likely dissolution of apatite with concurrent release of adsorbed or incorporated Sr. Exchange of adsorbed Sr would also be encouraged due to the elevated Ca and Mg concentrations in synthetic perched water during leaching (0.56 and 2.7 mM, respectively, Table 2.6).

For the perched water conditions, sequestration of U and Tc-99 was not significant as compared to without treatment, likely due to the impact of high ionic strength and nitrate competing for reduction capacity and potentially leading to precipitation of more soluble calcium phosphate phases. Therefore, this technology is not recommended for Tc-99 and U for conditions where there are high ionic strength plumes with NO_3^- as the amount of reductant needed would have to be scaled to reduce the NO_3^- prior to reduction of Tc. However, it may treat PCOIs and CoCOIs that are more readily reduced (e.g., nitrate and Cr).

Appendix J – Liquid-Phase Chemical Reduction & Sequestration: Calcium Polysulfide & Polyphosphate

The purpose of this task is the sequestration of U and Tc-99 (primary contaminants of interest, PCOIs) in the presence of I-129 as iodate, nitrate, Cr, and Sr (co-contaminants of interest, CoCOIs) in water-saturated zones using a liquid phase reductant (calcium polysulfide, CPS) followed by a polyphosphate (Poly-PO_4) solution to precipitate apatite. This technology functions via injection of CPS to reductively precipitate contaminants, followed by injection of Poly-PO_4 to precipitate apatite that may either incorporate contaminants (i.e., U) or coat reduced/precipitated contaminants (i.e., Tc).

This combined treatment is targeting contamination in perched water and BY Cribs as the primary treatment zones, with treatment via formation of a permeable reactive barrier in groundwater under BY Cribs. Potential secondary treatment zones include 216-U-1 and -2, S-SX tanks, S and T Cribs, C tanks, and BC Cribs.

The specific objectives of this technology are as follows:

1. Quantify the decrease in Tc-99 and U mass and order of magnitude removal rate in various combinations: (1) with/without sediment, (2) with/without delivery fluid, (3) with/without co-contaminants, and (4) with zero valent iron or sulfur modified iron [described in the Phase 1 report (PNNL-35432)].
2. Determine the immobilization rates for U and Tc-99 with/without co-contaminants for (1) perched water and (2) BY Crib application (in groundwater).
3. Quantify the longevity of U and Tc-99 with/without co-contaminants for (1) perched water and (2) BY Crib application.

Objectives 2 and 3 were tested in 1-D leach columns as described in Sections J.3.2 and J.3.1 for perched water conditions and BY Cribs groundwater conditions, respectively, based on the batch experiments described in Section J.2.

J.1 Supplemental Methods

For the BY Cribs groundwater conditions, amendments were delivered in a stepwise fashion with injection of approximately 1 pore volume (PV) of each amendment sequentially (CPS and then Poly-PO_4) followed by one repeat injection of both amendments. These conditions are similar to previous testing on delivery of calcium and phosphate solutions (Wellman et al. 2011). However, amendment delivery will likely need further testing and optimization due to the expected challenges of scaling to a large-scale field scenario.

Additional column tests were conducted with and without Poly-PO_4 to quantify the performance of treatment with CPS only as compared to the two-step approach with CPS+Poly-PO_4. These experiments were conducted as described in Section 2.4. However, testing was only conducted for conditions with CoCOIs.

These data are summarized within this appendix.

J.2 Long-Term Batch Results

J.2.1 Tc and U Sequestration with CPS+Poly-PO_4

Tc sequestration for the BY Cribs groundwater conditions was similar for no treatment [i.e., addition of only synthetic groundwater (SGW)] and only Poly-PO_4 treatment (~10%), highlighting the importance of reduction of TcO_4^- to Tc^{+4} for immobilization. When CPS is added to the system, sequestration increases significantly, from 10% to > 50% in the immobile fractions (Extractions 4 and 5). Moreover, the addition of Poly-PO_4 further increases sequestration based on results at 230 and 270 days (as shown in Figure J.1 and Figure J.2).

For the perched water conditions, Tc-99 sequestration was similarly increased with CPS treatment; however, the increase in sequestration with the sequential treatment with Poly-PO_4 was not observed (as shown in Figure J.5 to Figure J.8). Although there was more variability in results and recoveries, these data suggest that the relatively high ionic strength conditions of the perched water may impact precipitation of apatite from Poly-PO_4 solutions and/or consume reduction capacity.

U sequestration was significantly increased with Poly-PO_4 treatment with and without CPS for the BY Cribs groundwater conditions at 230 and 270 days, respectively (Figure J.3 and Figure J.4). However, results for the CPS treatment alone were similar, suggesting that redox conditions were not adequate for U reduction and subsequent precipitation in this batch system. Results for the perched water conditions show similar trends from 5 to 270 days, albeit with an overall decrease in sequestration for all conditions, although results and recoveries exhibited high variability (Figure J.9 and Figure J.10).

These results extend those reported in Sections 4.7 and 4.8 of the Phase 1 report (PNNL-35432), as the experiments were conducted over longer periods (i.e., 42 vs. 270 days) and under more realistic sediment-to-water ratios (i.e., 1:2 vs. 5:1). Overall, the observed trends were similar. However, contaminant sequestration was increased under the more field-relevant sediment-to-water ratio in the BY Cribs groundwater and the perched water conditions.

J.2.1.1 BY Cribs Groundwater Conditions

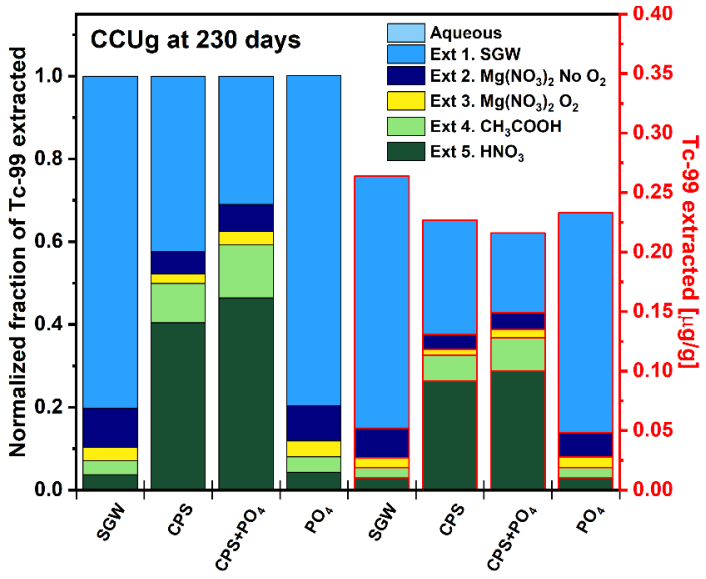

Figure J.1. Changes in Tc-99 sequestration from liquid-phase treatment of contaminant-spiked Cold Creek Unit gravel (CCug) sediment in SGW reacted with CPS, Poly-PO_4, or CPS+Poly-PO_4 via sequential extractions after 230 days compared to controls without treatment. Note: The left side of the figure shows the normalized fraction recovered in each sequential extraction while the right side of the figure shows the solid phase concentration (in µg/g) recovered in each sequential extraction.

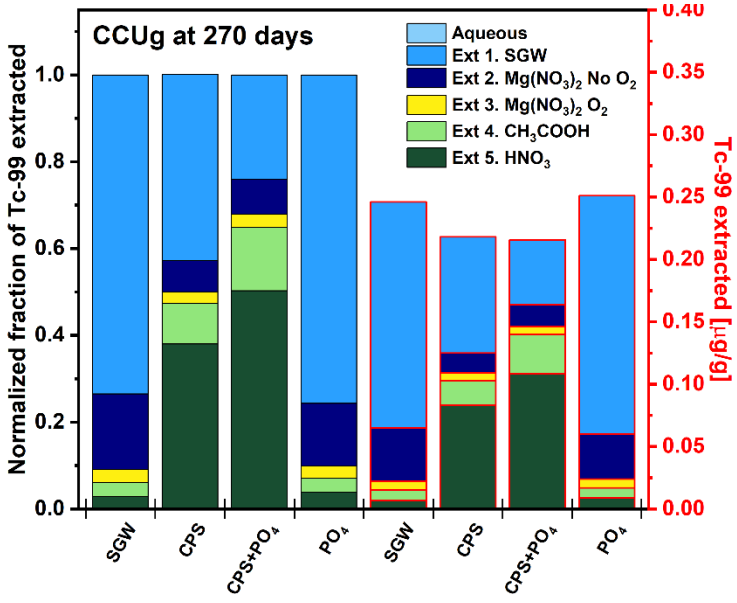

Figure J.2. Changes in Tc-99 sequestration from liquid-phase treatment of contaminant-spiked CCug sediment in SGW reacted with CPS, Poly-PO_4, or CPS+Poly-PO_4 via sequential extractions after 270 days compared to controls without treatment. Note: The left side of the figure shows the normalized fraction recovered in each sequential extraction while the right side of the figure shows the solid phase concentration (in µg/g) recovered in each sequential extraction.

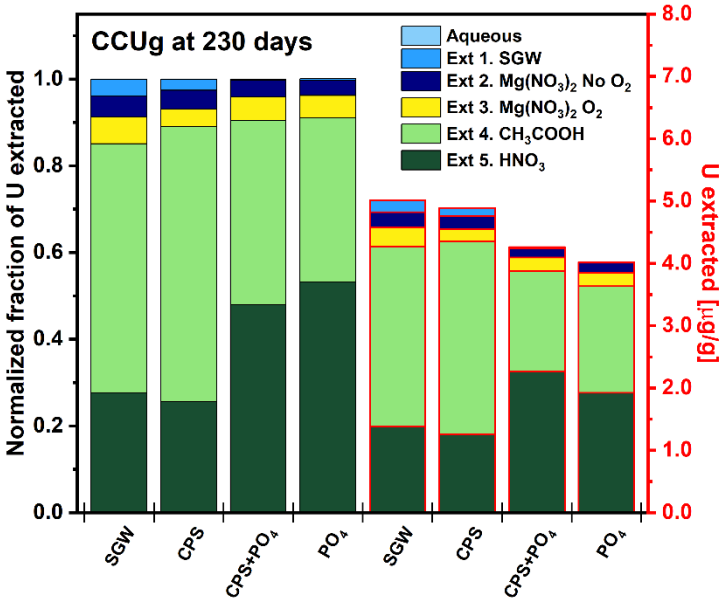

Figure J.3. Changes in U sequestration from liquid-phase treatment of contaminant-spiked CCug sediment (with CoCOIs) in SGW reacted with CPS, Poly-PO_4, or CPS+Poly-PO_4 via sequential extractions after 230 days compared to controls without treatment. Note: The left side of the figure shows the normalized fraction recovered in each sequential extraction while the right side of the figure shows the solid phase concentration (in µg/g) recovered in each sequential extraction.

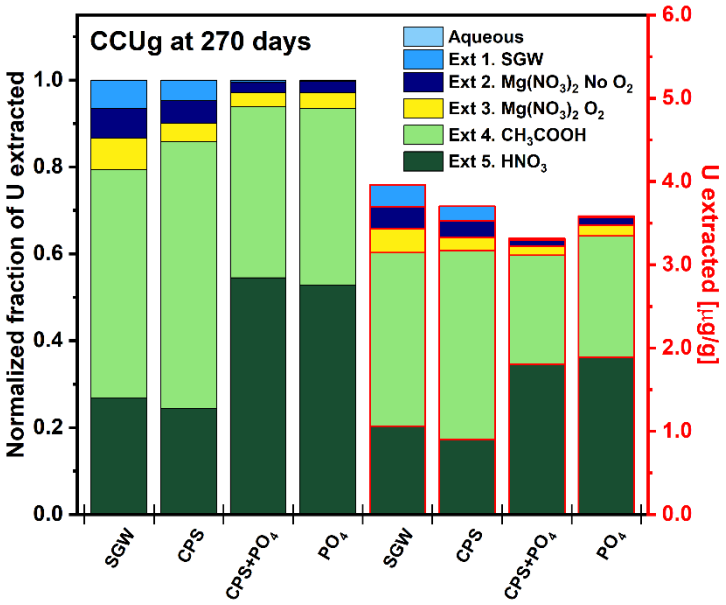

Figure J.4. Changes in U sequestration from liquid-phase treatment of contaminant-spiked CCug sediment (with CoCOIs) in SGW reacted with CPS, Poly-PO_4, or CPS+Poly-PO_4 via sequential extractions after 270 days compared to controls without treatment. Note: The left side of the figure shows the normalized fraction recovered in each sequential extraction while the right side of the figure shows the solid phase concentration (in µg/g) recovered in each sequential extraction.

J.2.1.2 Perched Water Conditions

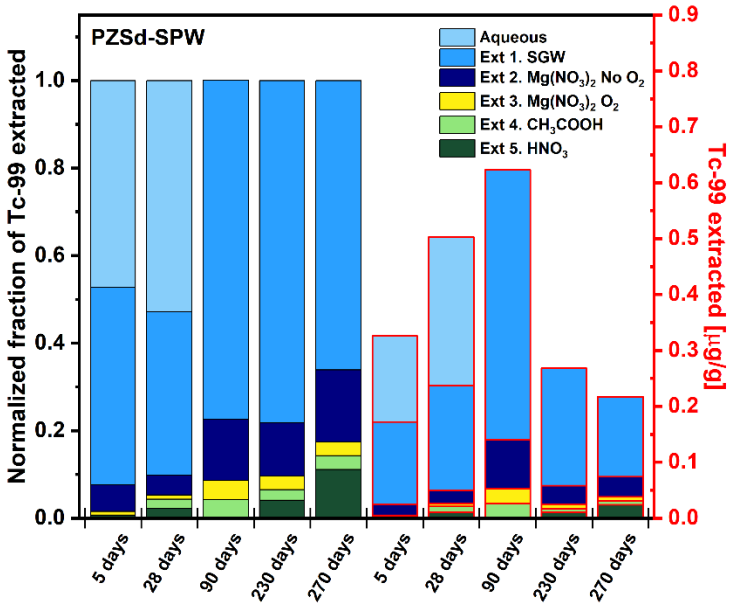

Figure J.5. Changes in Tc-99 sequestration from liquid-phase treatment of contaminant-spiked perching zone sand (PZsd) sediment in synthetic perched water (SPW) via sequential extractions up to 270 days. Note: The left side of the figure shows the normalized fraction recovered in each sequential extraction while the right side of the figure shows the solid phase concentration (in µg/g) recovered in each sequential extraction. For 90-day results, Extraction 5 could not be analyzed.

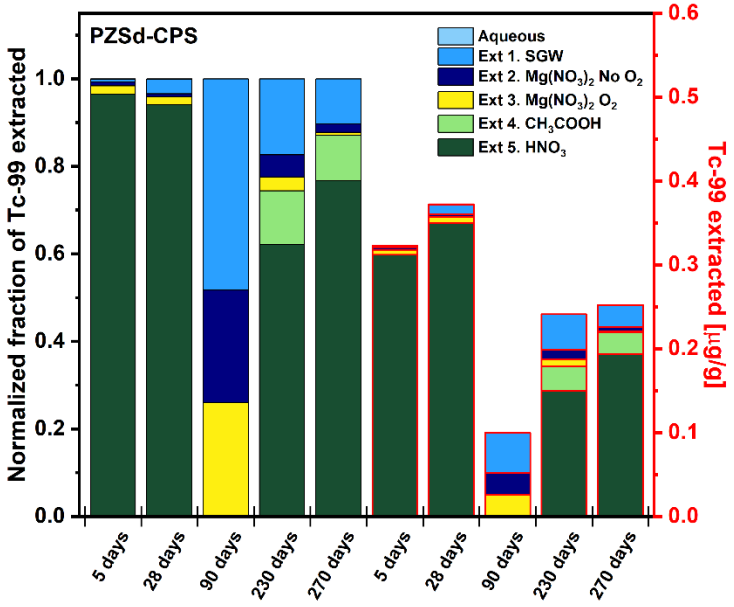

Figure J.6. Changes in Tc-99 sequestration from liquid-phase treatment of contaminant-spiked PZsd sediment in SPW with CPS via sequential extractions up to 270 days. Note: The left side of the figure shows the normalized fraction recovered in each sequential extraction while the right side of the figure shows the solid phase concentration (in µg/g) recovered in each sequential extraction. For 90-day results, Extraction 5 could not be analyzed.

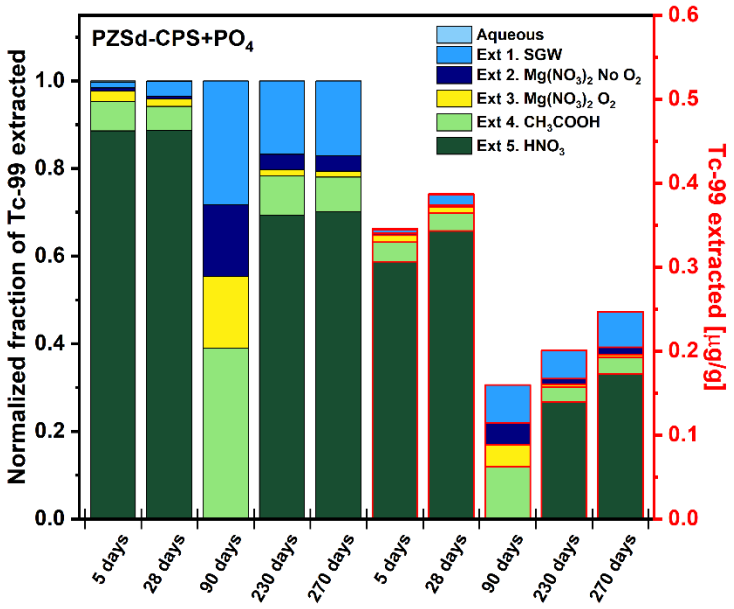

Figure J.7. Changes in Tc-99 sequestration from liquid-phase treatment of contaminant-spiked PZsd sediment in SPW with CPS+Poly-PO_4 via sequential extractions up to 270 days. Note: The left side of the figure shows the normalized fraction recovered in each sequential extraction while the right side of the figure shows the solid phase concentration (in µg/g) recovered in each sequential extraction. For 90-day results, Extraction 5 could not be analyzed.

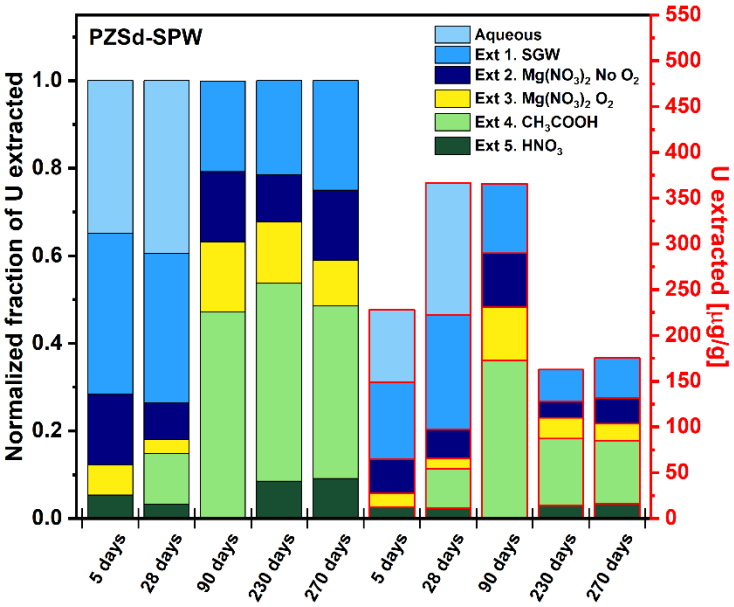

Figure J.8. Changes in U sequestration from liquid-phase treatment of contaminant-spiked PZsd sediment in SPW via sequential extractions up to 270 days. Note: The left side of the figure shows the normalized fraction recovered in each sequential extraction while the right side of the figure shows the solid phase concentration (in µg/g) recovered in each sequential extraction. For 90-day results, Extraction 5 was unable to be analyzed.

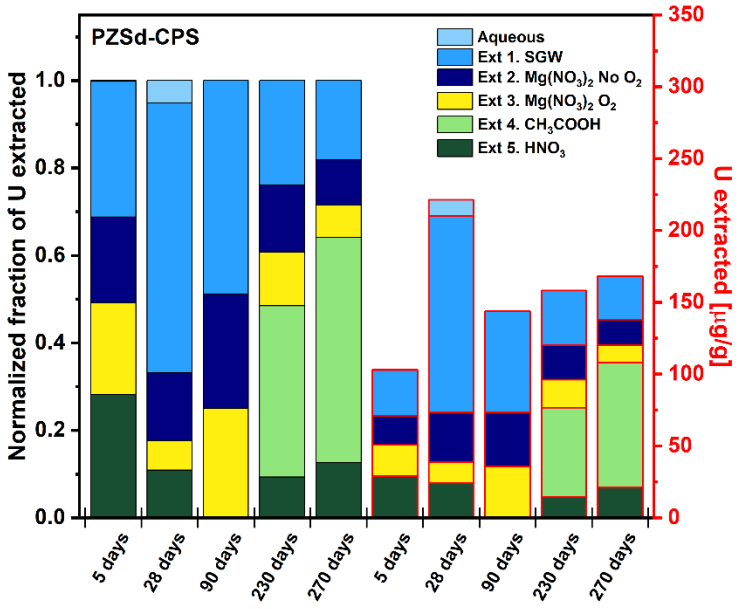

Figure J.9. Changes in U sequestration from liquid-phase treatment of contaminant-spiked PZsd sediment in SPW with CPS via sequential extractions up to 270 days. Note: The left side of the figure shows the normalized fraction recovered in each sequential extraction while the right side of the figure shows the solid phase concentration (in µg/g) recovered in each sequential extraction. For 90-day results, Extractions 4 and 5 could not be analyzed.

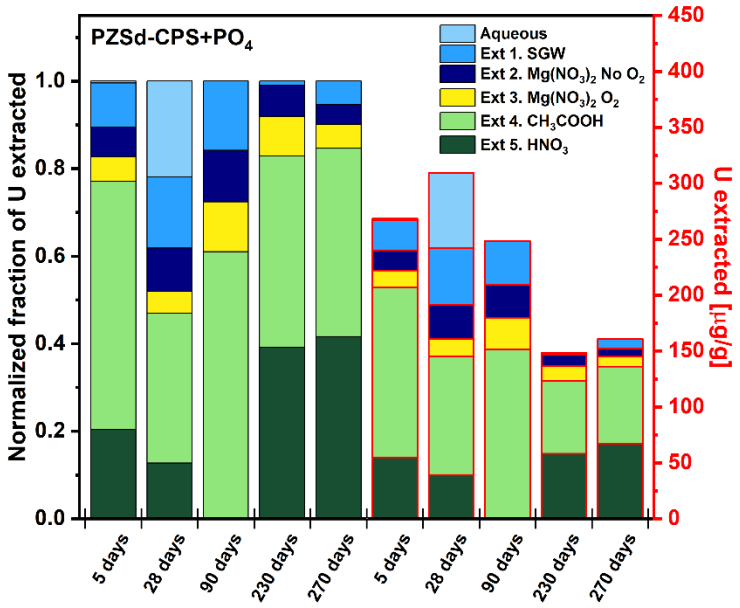

Figure J.10. Changes in U sequestration from liquid-phase treatment of contaminant-spiked PZsd sediment in SPW with CPS+Poly-PO_4 via sequential extractions up to 270 days. Note: The left side of the figure shows the normalized fraction recovered in each sequential extraction while the right side of the figure shows the solid phase concentration (in µg/g) recovered in each sequential extraction. For 90-day results, Extraction 5 could not be analyzed.

J.2.2 Supplemental Results for BY Cribs Groundwater Conditions

J.2.2.1 CoCOI Results

The sequestration of CoCOIs was also monitored via sequential extractions, including Cr and Sr. However, nitrate and I were not routinely monitored in sequential extractions due to instabilities in acidic solutions. For Cr, similar behavior to Tc was observed, likely because Cr and Tc are impacted by similar reductive precipitation processes (Figure J.11). Cr behavior was similar for the control and Poly-PO_4-treated sediments (~60% present in the immobile Extractions 4 and 5), while sequestration was significantly increased when the CPS reductant was present (> 95% in Extractions 4 and 5). These results are consistent with previous research using reductants for immobilization of Cr, including CPS (Chrysochoou et al. 2010; Williams and Scherer 2001; Alowitz and Scherer 2002; Yang et al. 2007; Zhong et al. 2009). For Sr, a small decrease in sequestration was observed with CPS treatment as compared to the control (Figure J.12), while a small increase in sequestration was observed when Poly-PO_4 was present (with or without CPS, results were similar). Previous work showed significant sequestration of Sr with Ca-Cit-PO_4 (PNNL-18303).

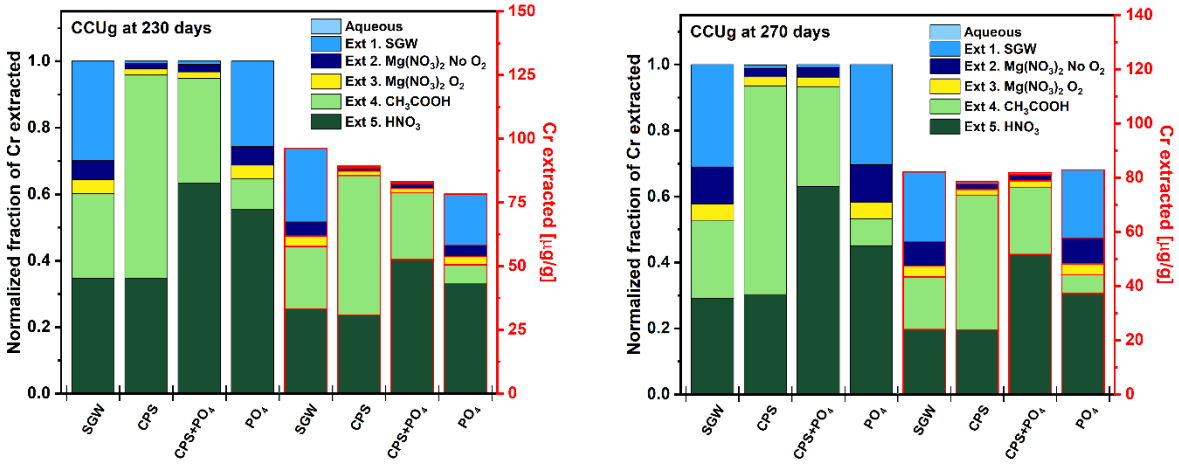

Figure J.11. Change in Cr sequestration from liquid-phase treatment of contaminant-spiked CCug sediment in SGW reacted with CPS, Poly-PO_4, or CPS+Poly-PO_4 via sequential extractions after (*left*) 230 days and (*right*) 270 days compared to controls without treatment. Note: The left side of the figure shows the normalized fraction recovered in each sequential extraction while the right side of the figure shows the solid phase concentration (in µg/g) recovered in each sequential extraction.

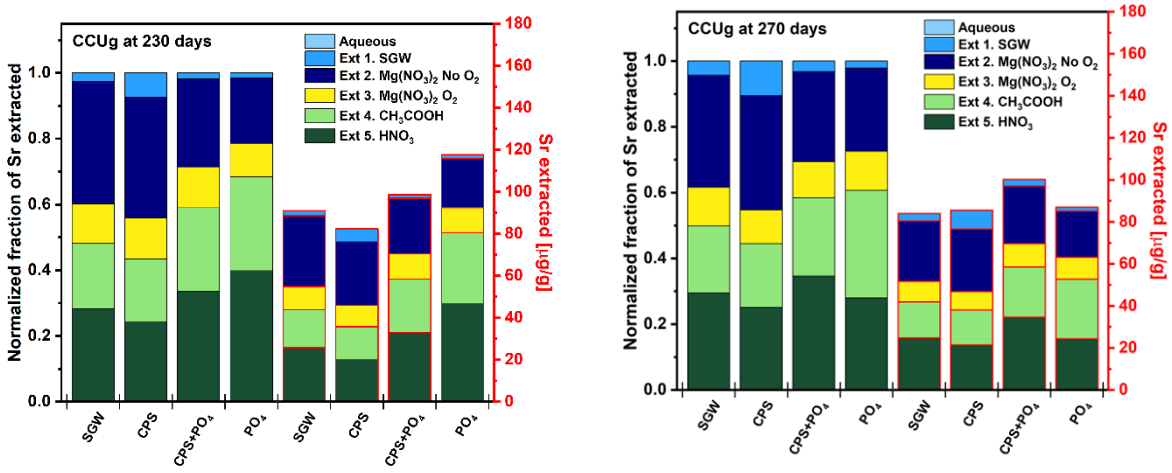

Figure J.12. Change in Sr sequestration from liquid-phase treatment of contaminant-spiked CCug sediment in SGW reacted with CPS, Poly-PO_4, or CPS+Poly-PO_4 via sequential extractions after (*left*) 230 days and (*right*) 270 days compared to controls without treatment. Note: The left side of the figure shows the normalized fraction recovered in each sequential extraction while the right side of the figure shows the solid phase concentration (in µg/g) recovered in each sequential extraction.

J.2.2.2 Amendment Monitoring Data

Phosphorus (P) and sulfur (S) were also monitored in sequential extractions to understand the changes in total and sequestered P and S. Because the extractions included strong acids, species were not measured, just total P and S using an inductively coupled plasma optical emission spectrometer. Results showed that P was relatively immobile under natural conditions (SGW, or without treatment), with similar results for CPS treatment. However, there was a significant increase in total P in the Poly-PO_4 treatments, as expected, with a small shift in mobility with time (as compared at 230 and 270 days) (Figure J.13). For S, the distribution under natural conditions was relatively similar across each of the extraction solutions, suggesting a wide variability in S-containing phases. Moreover, the mobility of natural S was not significantly impacted by the Poly-PO_4 treatments. However, the CPS amendments added nearly all mobile S phases that were readily dissolved in the first extraction. These results are consistent with expectations as most of the S was added as sulfide, S^{2-}, though it is notable that the S remained relatively mobile over longer periods based on these extraction results at 230 and 270 days (Figure J.14). These results may have implications for future treatment at the field scale as the S would be significantly more mobile than P in the subsurface in the long-term.

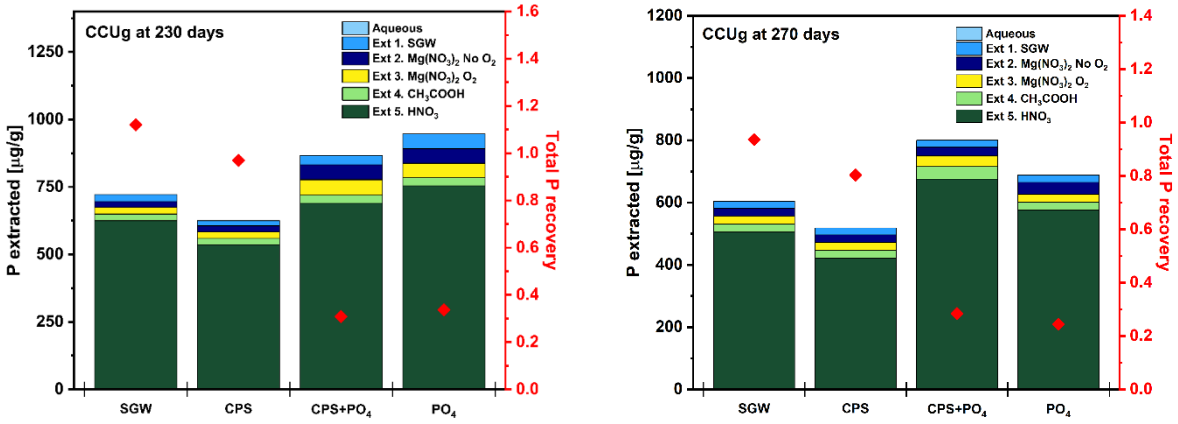

Figure J.13. Change in P sequestration from liquid-phase treatment of contaminant-spiked CCug sediment in SGW reacted with CPS, Poly-PO_4, or CPS+Poly-PO_4 via sequential extractions after (*left*) 230 days and (*right*) 270 days compared to controls without treatment. Note: The left side of the figure shows the solid phase concentration (in µg/g) recovered in each sequential extraction while the right side of the figure shows the total recovery in each sequential extraction.

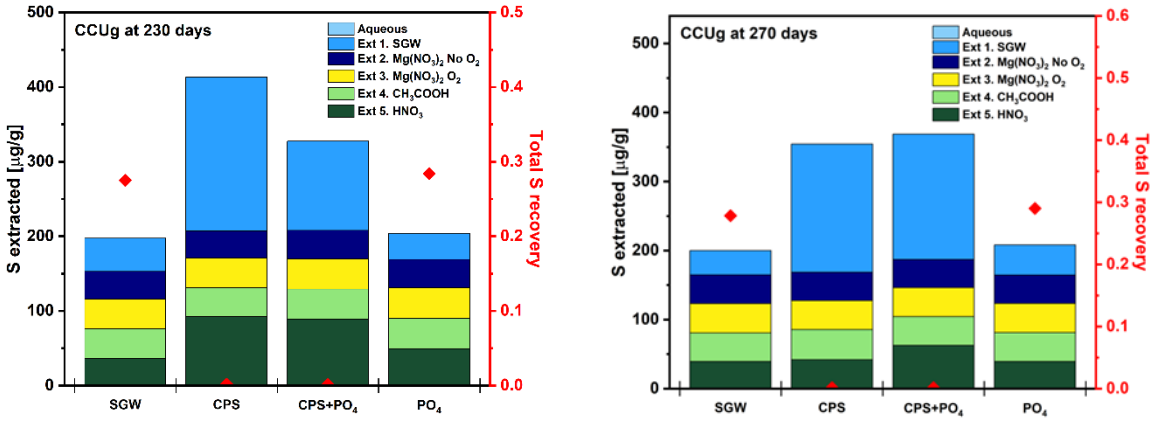

Figure J.14. Change in S sequestration from liquid-phase treatment of contaminant-spiked CCug sediment in SGW reacted with CPS, Poly-PO_4, or CPS+Poly-PO_4 via sequential extractions after (*left*) 230 days and (*right*) 270 days compared to controls without treatment. Note: The left side of the figure shows the normalized fraction recovered in each sequential extraction while the right side of the figure shows the solid phase concentration (in µg/g) recovered in each sequential extraction.

J.2.2.3 Perched Water Conditions

For the perched water conditions, P is naturally relatively immobile as shown in Figure J.15 and remained immobile with addition of Poly-PO_4 (with or without CPS), likely due to apatite precipitation. This result was similar to observations in the BY Cribs groundwater conditions (Figure J.13). In addition, S mobility was similar in both perched water conditions (Figure J.16) and BY Cribs groundwater conditions (Figure J.14), with a significant fraction of S measured in each extraction under natural conditions and a significant increase in mobile S in the first extraction with addition of CPS. Significant changes with time up to 270 days were not observed, although there was some variability in the results.

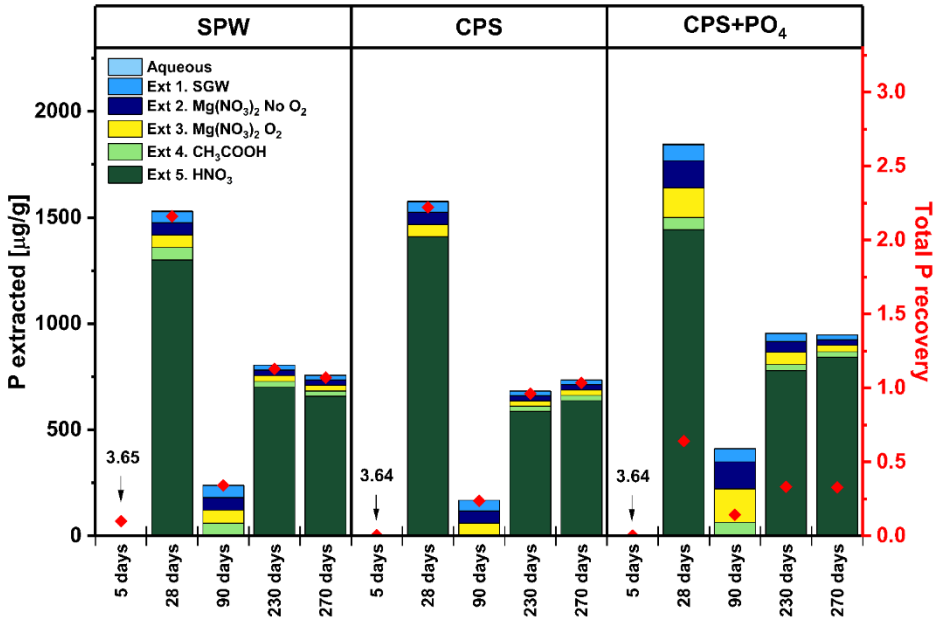

Figure J.15. Change in P sequestration from liquid-phase treatment of contaminant-spiked PZsd sediment in (*left*) SPW, (*middle*) CPS, and (*right*) CPS+Poly-PO_4 via sequential extractions up to 270 days. Note: The left side of the figure shows the solid phase concentration (in µg/g) recovered in each sequential extraction while the right side of the figure shows the total recovery in each sequential extraction. At 5 days, only "Aqueous" fractions were analyzed, and at 90 days, Extraction 5 could not be analyzed.

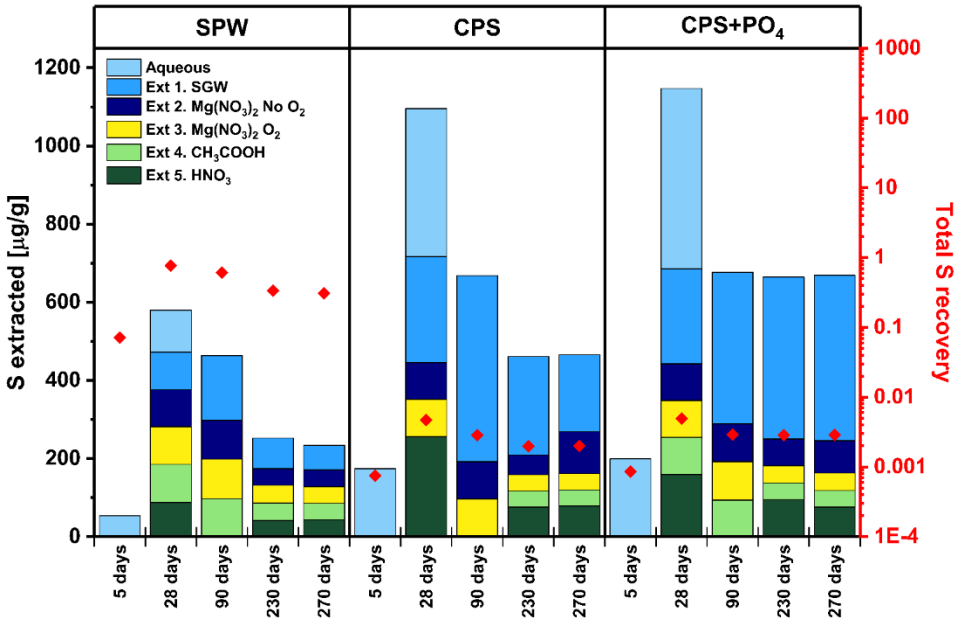

Figure J.16. Change in S sequestration from liquid-phase treatment of contaminant-spiked PZsd sediment in SPW via sequential extractions up to 270 days. Note: The left side of the figure shows the solid phase concentration (in µg/g) recovered in each sequential extraction while the right side of the figure shows the total recovery in each sequential extraction. At 5 days, only "Aqueous" fractions were analyzed, and at 90 days, Extraction 5 could not be analyzed.

J.3 Saturated Column Results for Tc-99 and U

This section presents results for monitoring the PCOIs (Tc and U) during loading (for the BY Cribs groundwater condition only) and leaching (for both BY Cribs groundwater and perched water conditions). Because contaminants of interest were added directly to sediments, a loading phase was not conducted for the perched water conditions, while the BY Cribs groundwater experiments simulated the flow of contaminants into a potential permeable reactive barrier. Data are summarized, including all column results based on the total accumulation within the column (the amount sequestered in μg/g), the effluent concentration (in μg/L), the rate of release from sediments as normalized to the solid phase concentration both prior to stop flow events and during stop flow events (in day^{-1}), and distribution across the column as determined by extraction with 8 M HNO_3. These different results highlight the potential for amendments to sequester PCOIs and CoCOIs based on the total quantity taken up into columns and rates of release at different points in experiments.

J.3.1 BY Cribs Groundwater Conditions

For the BY Cribs groundwater conditions, U uptake was significant in the absence and presence of CoCOIs, as shown in Figure J.17. For the no-treatment scenario or with CPS treatment, the contaminant effluent concentrations reached the influent concentrations (breakthrough) by 100 PVs. Moreover, the maximum loading of U without treatment was higher in the presence of CoCOIs (as shown in Figure J.17), although a similar amount remained with or without CoCOIs after the leaching phase of the experiments, suggesting greater mobility of U initially retained in the presence of CoCOIs. During the first two stop flow events, which occurred shortly after switching to leaching in SGW, significant adsorption and desorption were likely occurring simultaneously (a lack of equilibrium) as the normalized release rates were highly variable before and during stop flows (Figure J.18). However, there was greater release of U during stop flows when CoCOIs were present. By the third stop flow, at around 100 PVs of leaching, leaching rates before and during the stop flow had decreased significantly.

When treated with CPS, there was a small increase in removal of U as compared to the control (> 11 vs. 4 μg/g after the loading phase, as shown in Figure J.17 and Table J.1), indicating potential for some enhanced removal of U due to either reductive precipitation or shifts in the pH caused by CPS reacting in the system. However, more than 70% of the U was mobilized out of the column during the leaching phase, suggesting that U did not remain reduced. While dissolved oxygen remained below detection limits during the initial treatment phase of experiments, oxygen increased during contaminant loading and leaching, indicating that some oxygen was present during loading even after degassing solutions and attaching N_2 gas bag onto bottles as well as during the leaching phase with SGW equilibrated with air. During stop flow events, however, dissolved oxygen decreased over time (Figure J.38). Therefore, while there was likely some initial reduction of U, it would be expected to re-oxidize. Moreover, the pH did not fluctuate significantly and remained near 8.5 (Figure J.37) except during the first 50 PVs of injection and after the last stop flow near 300 PVs. In the first 50 PVs, there were likely significant reactions taking place as the system re-equilibrated with fresh SGW, PCOIs, and CoCOIs. However, the pH increase near 300 PVs for CPS+Poly-PO_4 treatment may indicate significant dissolution of apatite with the longer stop flow (~500 hours) (Dorozhkin 1997).

For treatment with both CPS+Poly-PO_4, there was a significant delay in breakthrough of U, which never reached more than 50% of the influent concentrations. This result was consistent with the significant potential for uptake of U in apatite as shown in Figure J.17 and previous research with apatite-forming solutions (Fuller et al. 2003; SGW-47062; Lammers et al. 2017; PNNL-25303; PNNL-29650). Overall, loading of U reached a maximum of approximately 40 μg/g, as shown in Table J.1; however, more U likely could have been loaded since complete breakthrough was not reached after more than 200 PVs of injection. Moreover, uptake was significant with and without CoCOIs, including Sr. Breakthrough results

(Figure J.17) were also consistent with sectioning and acid leaching (Table J.1) with a relatively consistent U distribution across the column for the untreated and CPS-treated columns as the maximum loading capacity was achieved under these conditions (i.e., complete breakthrough). However, for the CPS+Poly-PO_4-treated columns where breakthrough was incomplete, the concentration was highest near the inlet and then decreased across the column where maximum uptake had not yet been reached.

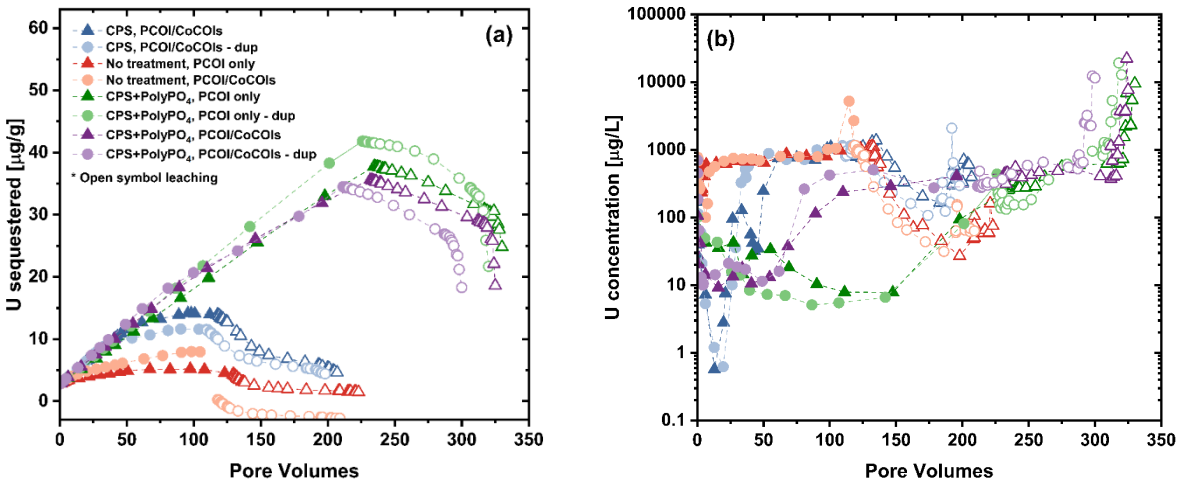

Figure J.17. U during loading and leaching with CCug sediment without and with treatment (with CPS or CPS+Poly-PO_4) after equilibration of amendments for approximately 6 weeks in the absence of oxygen: (a) accumulation of U (in µg/g) in the solid phase and (b) aqueous effluent concentrations of U (in µg/L). Note: "Dup" stands for duplicate. Filled symbols indicate loading phase while open symbols represent the leaching phase with SGW.

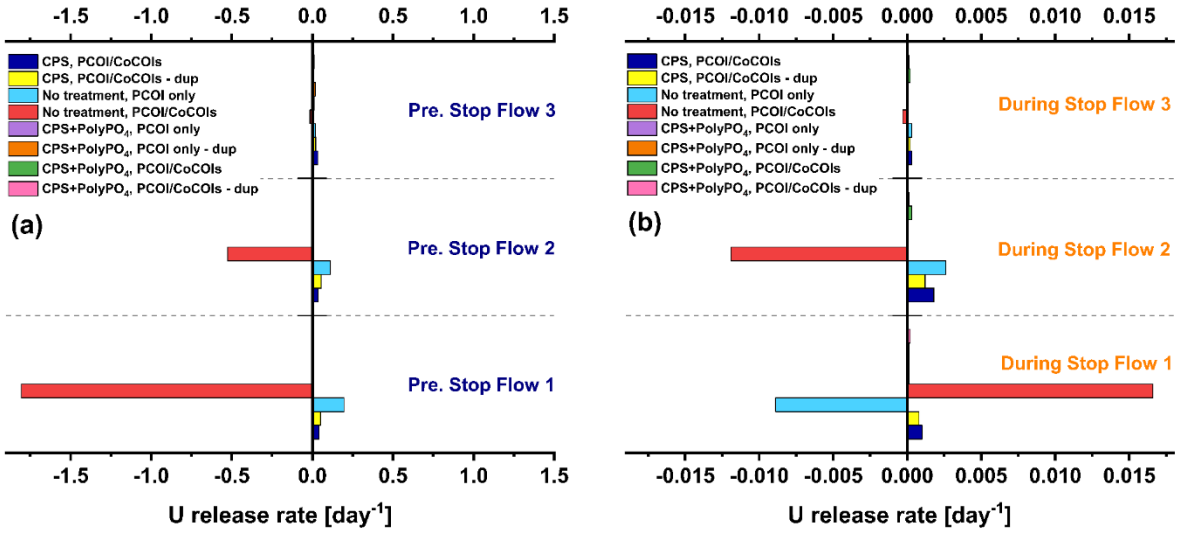

Figure J.18. U normalized release rates during leaching from columns with CCug sediment without and with treatment (with CPS or CPS+Poly-PO_4) based on 8 M HNO_3 extractions: (a) estimated leaching rate (day^{-1}) prior to each stop flow and (b) estimated leaching rate (day^{-1}) during each stop flow. Note: "Dup" stands for duplicate.

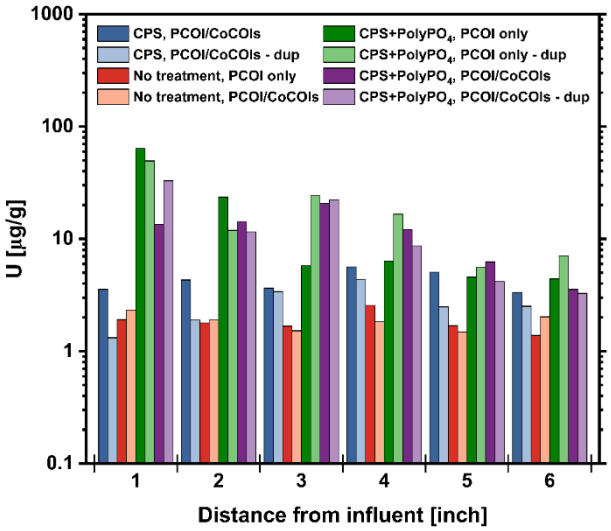

Figure J.19. U distribution (in µg/g) across columns with CCug sediment without and with treatment (with CPS or CPS+Poly-PO_4) based on 8 M HNO_3 extractions. Note: "Dup" stands for duplicate.

Table J.1. U estimated recovery after loading and leaching in CCug sediments without and with treatment (CPS or CPS+Poly-PO_4) after equilibrium of amendments for approximately 6 weeks in the absence of oxygen.

Conditions	Loading (µg/g)	Leaching (µg/g)
No treatment, PCOIs	4.4	1.7
No treatment, PCOIs + CoCOIs	0.4	1.7
CPS, PCOIs + CoCOIs	14.0	4.3
CPS, PCOIs + CoCOIs, dup	11.7	2.8
CPS+Poly-PO_4, PCOIs	37.8	16.9
CPS+Poly-PO_4, PCOIs, dup	41.9	17.5
CPS+Poly-PO_4, PCOIs + CoCOIs	35.7	11.7
CPS+Poly-PO_4, PCOIs + CoCOIs, dup	34.6	12.7

For the BY Cribs groundwater conditions, Tc-99 uptake was insignificant in the absence and presence of CoCOIs without treatment, as shown in Figure J.20. Moreover, the highest relative release rate, as measured just before stop flow events, was measured for the no-treatment column with CoCOIs, as shown in Figure J.21. For the CPS treatment with CoCOIs, contaminant effluent concentrations reached the influent concentrations (breakthrough) within a few PVs, likely due to relatively fast consumption of reduction capacity by dissolved O_2, Tc, Cr, and NO_3^-. This resulted in < 0.7 µg/g of Tc-99 initially sequestered after loading, as shown in Table J.2.

Similar results were observed with CPS+Poly-PO_4 with CoCOIs present. This result was expected as the Poly-PO_4 treatment should not significantly consume reduction capacity. However, the maximum loading of Tc-99 with treatment when CoCOIs were not present was significantly higher than in the presence of CoCOIs (as shown in Figure J.21 and Table J.2 with > 3.2 µg/g of Tc-99 sequestered in the absence of CoCOIs). Therefore, competing CoCOIs likely consumed the majority of the reduction capacity rather than the low dissolved O_2 during solution injection (as loading solutions with contaminants were de-

gassed to remove air and O_2). The trends observed here are consistent with batch testing (Section J.2) at field-relevant solid to liquid ratios and previous batch testing Phase 1 at 1:2 solid to liquid ratios (PNNL-35432); however, reduction capacity was consumed more quickly in the column system due to the continuous flow and introduction of more reducible contaminants.

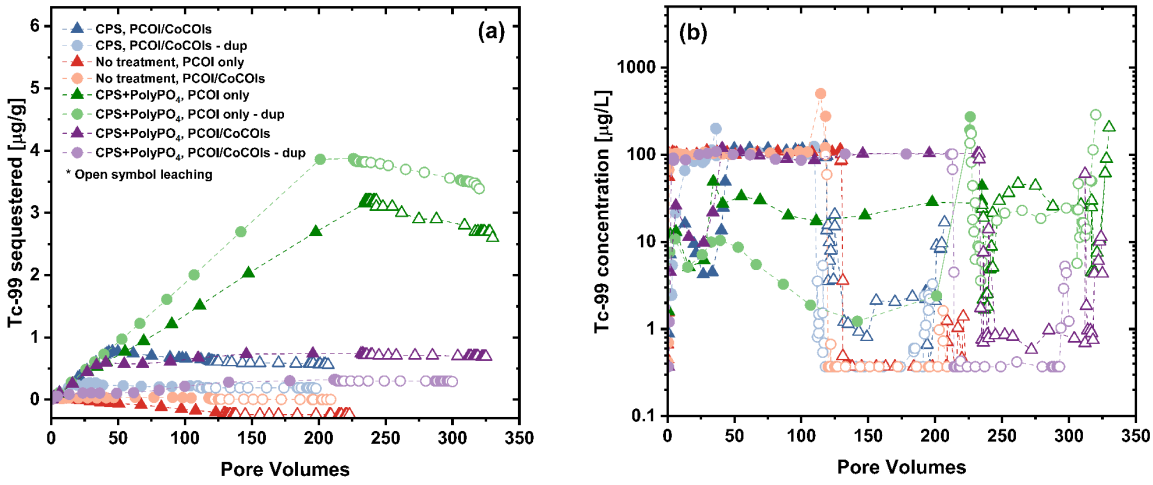

Figure J.20. Tc-99 accumulation in CCug sediment without and with treatment (with CPS or CPS+Poly-PO_4) after equilibration of amendments for approximately 6 weeks in the absence of oxygen: (a) accumulation of Tc-99 (in µg/g) in the solid phase and (b) aqueous concentrations of Tc-99 (in µg/L) in effluent. Note: "Dup" stands for duplicate. Filled symbols indicate loading phase while open symbols represent the leaching phase with SGW.

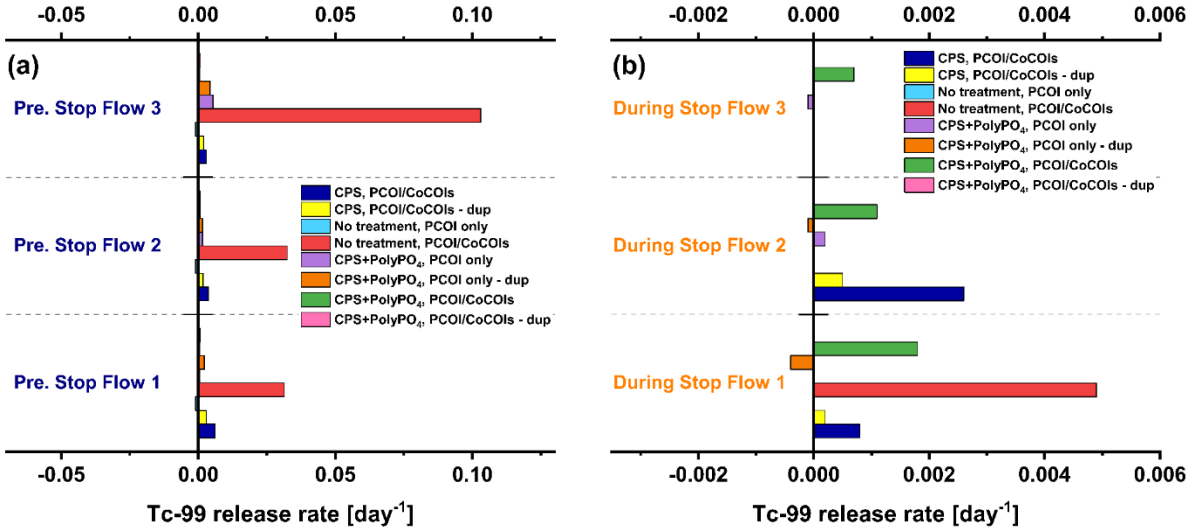

Figure J.21. Tc-99 normalized release rates during leaching from columns with CCug sediment without and with treatment (with CPS or CPS+Poly-PO_4) based on 8 M HNO_3 extractions: (a) estimated leaching rate (day^{-1}) prior to each stop flow and (b) estimated leaching rate (day^{-1}) during each stop flow. Note: "Dup" stands for duplicate.

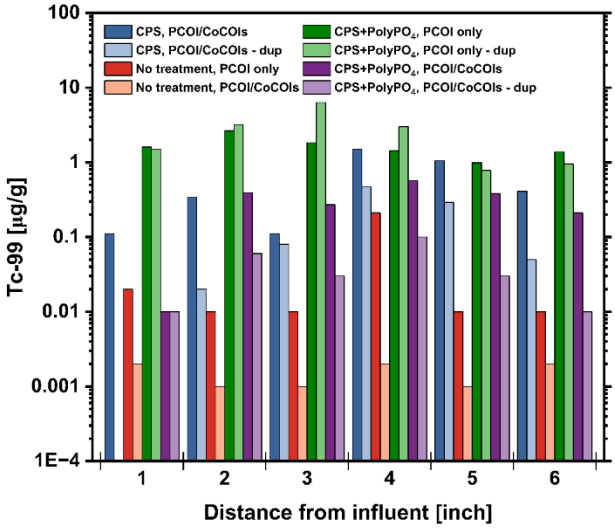

Figure J.22. Tc-99 distribution (in µg/g) across columns with CCug sediment without and with treatment (with CPS or CPS+Poly-PO_4) based on 8 M HNO_3 extractions. Note: "Dup" stands for duplicate.

Table J.2. Tc-99 estimated recovery after loading and leaching in CCug sediments without and with treatment (CPS or CPS+Poly-PO_4) after equilibrium of amendments for approximately 6 weeks in the absence of oxygen.

Conditions	Loading (µg/g)	Leaching (µg/g)
No treatment, PCOIs	0	0
No treatment, PCOIs + CoCOIs	0.03	0
CPS, PCOIs + CoCOIs	0.6	0.7
CPS, PCOIs + CoCOIs, dup	0.2	0.2
CPS+Poly-PO_4, PCOIs	3.2	1.6
CPS Poly-PO_4, PCOIs, dup	3.9	2.4
CPS+Poly-PO_4, PCOIs + CoCOIs	0.7	0.3
CPS+Poly-PO_4, PCOIs + CoCOIs, dup	0.3	0.0

J.3.2 Perched Water Conditions

For the perched water conditions, initial concentrations of U in the effluent of the untreated columns and release rates were significant (Figure J.23b), based on the relative release rate both prior to and during the first stop flow event during the first few PVs of leaching (Figure J.24). Moreover, the amount of U sequestered in the sediments decreased significantly during leaching (Figure J.23a), ending with only about 4 µg/g of U sequestered based on 8 M HNO_3 extractions after sectioning the columns (Figure J.25 and Table J.3). During estimation of sequestered U in µg/g shown in Figure J.23a, there were negative values reported, likely due to heterogeneity of U in the composite sediments and fluctuation in effluent U during experiments. (Not every sample could be analyzed in the breakthrough curves.) While the background U was accounted for in estimates based on an average of U recovered in digestions, there was variability, which is difficult to account for during leaching. Hence, the U remaining after leaching was estimated from 8 M HNO_3 extractions of sediments after sectioning instead of effluent monitoring.

For treatment with both CPS+Poly-PO_4, there was a significant delay in release as compared to without treatment (Figure J.23); however, more than 85% of U was leached over 80 to 90 PVs (Figure J.24). After sectioning, there was a clear trend of increasing concentration of U remaining in sediments with distance from the inlet (Figure J.25). This result suggests that release of U under the conditions in these columns may be solubility controlled (Wellman et al. 2006, 2007). Once aqueous concentrations and solid phase species of U are better understood in the perched water, additional experiments may be necessary to understand the potential use of this technology. However, results showed a significant delay in release of U with treatment.

Release of Tc-99 under the perched water conditions was significant with and without treatment. The treatment with CPS+Poly-PO_4 only marginally reduced the release of Tc-99 in this system (Table J.3, Figure J.25 through Figure J.28), likely due to the significant NO_3^- present, which consumed the reduction capacity. Therefore, this technology is not recommended for conditions where there are high ionic strength plumes with NO_3^- as the amount of reductant needed would have to be scaled to reduce the NO_3^- prior to reduction of Tc.

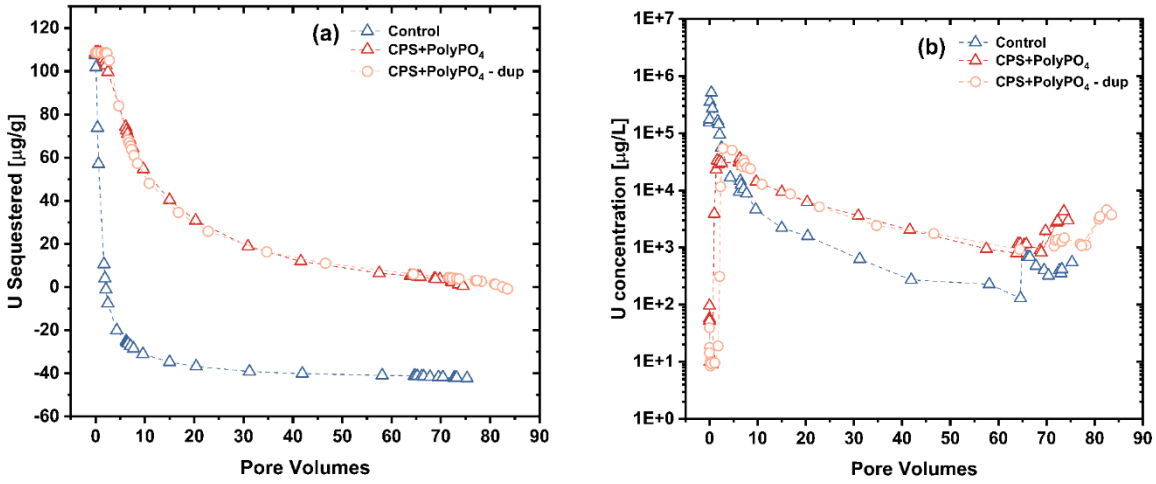

Figure J.23. U remaining during leaching with PZsd sediment without and with treatment (with CPS or CPS+Poly-PO_4) after equilibration of amendments for approximately six weeks in the absence of oxygen, (a) accumulation of U in sediments (in µg/g) in sediments and (b) aqueous concentrations of U (in µg/L) in effluent. Note: "Dup" stands for duplicate. Filled samples indicate loading phase while open symbols represent the leaching phase with SPW. Negative values for U loaded in "a" are likely due to fluctuation in background U in sediments.

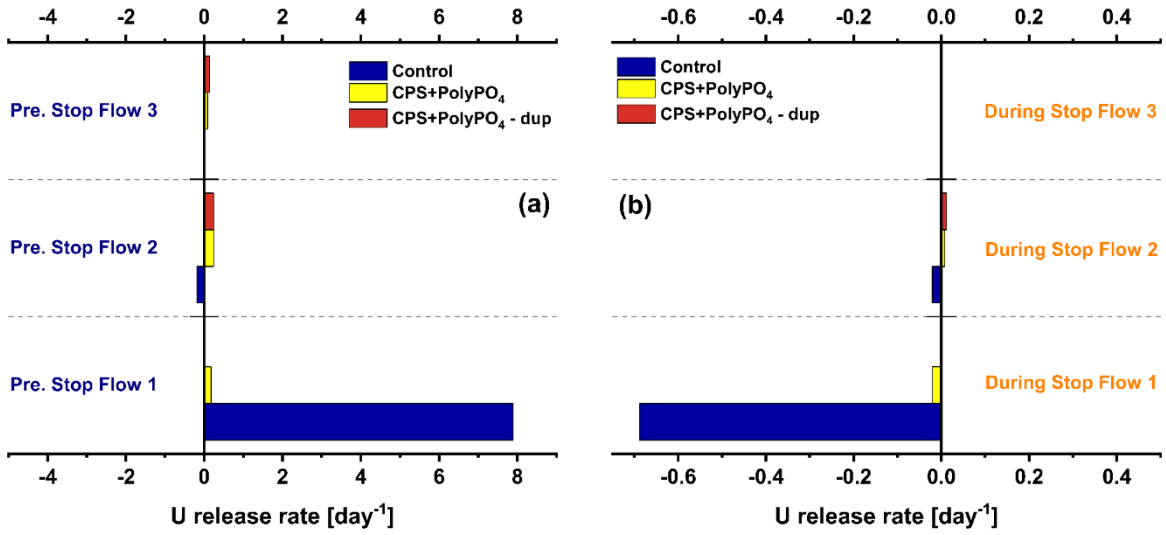

Figure J.24. U normalized release rates during leaching from columns with PZsd sediment without and with treatment (with CPS or CPS+Poly-PO_4) based on 8 M HNO_3 extractions: (a) estimated leaching rate (day^{-1}) prior to each stop flow and (b) estimated leaching rate (day^{-1}) during each stop flow. Note: "Dup" stands for duplicate.

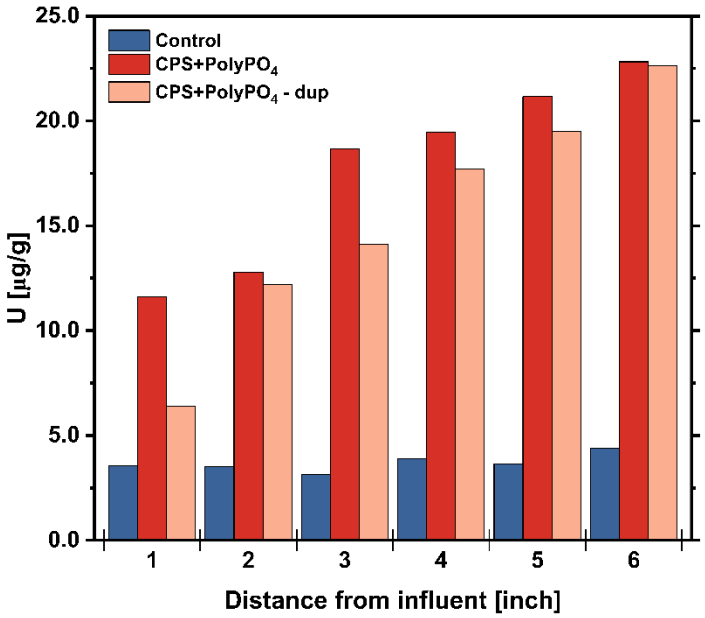

Figure J.25. U distribution (in µg/g) across columns with PZsd sediment without and with treatment (with CPS or CPS+Poly-PO_4) based on 8 M HNO_3 extractions. Note: "Dup" stands for duplicate.

Table J.3. U and Tc-99 estimated recovery after leaching in PZsd sediments without and with treatment (CPS or CPS+Poly-PO_4) after equilibrium of amendments for approximately 6 weeks in the absence of oxygen. Note: Initial U and Tc-99 were estimated to be 109 and 0.27 µg/g, respectively.

Conditions	U (µg/g)	Tc (µg/g)
No treatment	4.1	0.02
CPS+Poly-PO_4	16.2	0.09
CPS+Poly-PO_4, dup	14.5	0.09

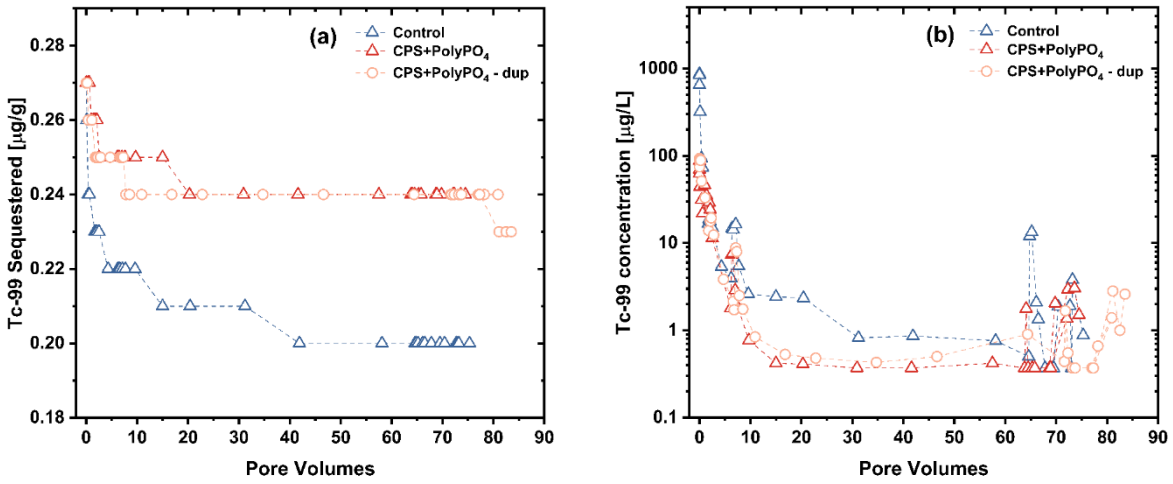

Figure J.26. Tc remaining during leaching with PZsd sediment without and with treatment (with CPS or CPS+Poly-PO_4) after equilibration of amendments for approximately 6 weeks in the absence of oxygen: (a) accumulation of Tc-99 in sediments (in µg/g) in solid phase and (b) aqueous concentrations of Tc-99 (in µg/L) in effluent. Note: "Dup" stands for duplicate. Filled samples indicate loading phase while open symbols represent the leaching phase with SPW.

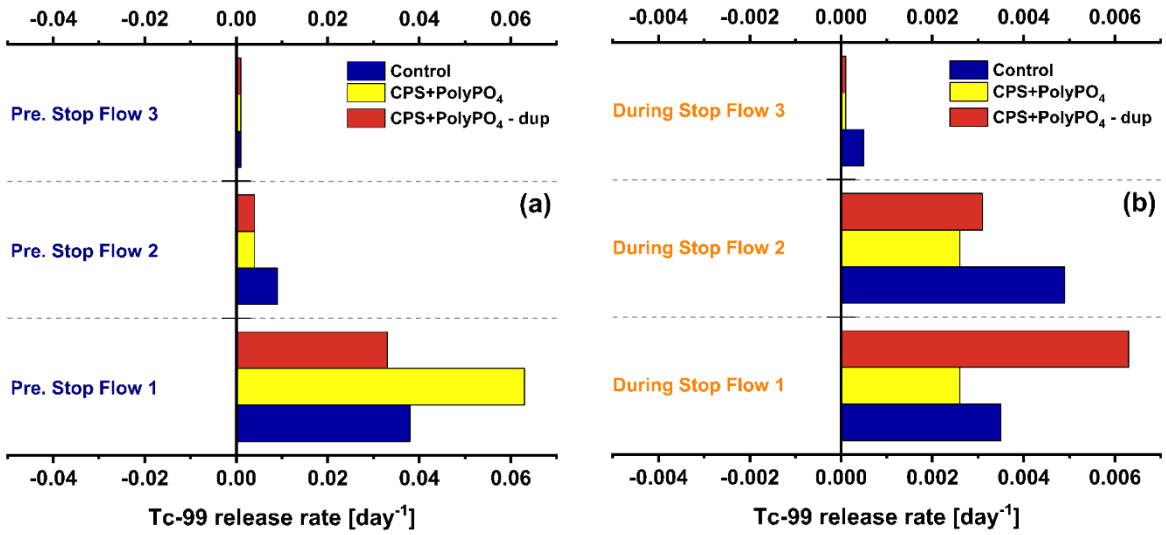

Figure J.27. Tc normalized release rates during leaching from columns with PZsd sediment without and with treatment (with CPS or CPS+Poly-PO_4) based on 8 M HNO_3 extractions: (a) estimated leaching rate (day^{-1}) prior to each stop flow and (b) estimated leaching rate (day^{-1}) during each stop flow. Note: "Dup" stands for duplicate.

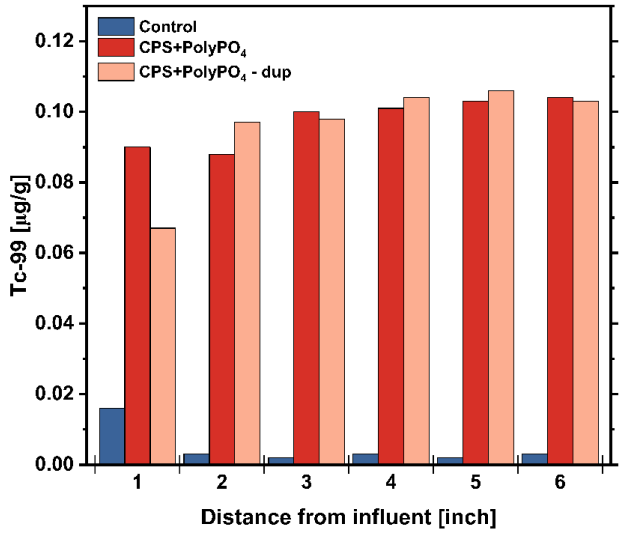

Figure J.28. Tc-99 distribution (in µg/g) across columns with PZsd sediment without and with treatment (with CPS or CPS+Poly-PO_4) based on 8 M HNO_3 extractions. Note: "Dup" stands for duplicate.

J.3.3 Long-Term Tc-99 and U Stability

X-ray absorption spectroscopy (XAS) and X-ray fluorescence (XRF) measurements were collected on select samples to better understand elemental distribution, oxidation states, and coordination. Data are shown for BY Cribs groundwater conditions based on batch and column samples prepared after reaction with amendments. Data could not be collected for U due to detection limitations, interferences, and configuration challenges. However, data were collected for select samples with Tc, including batch

samples treated with CPS or CPS+Poly-PO_4 and column sediments with CPS+Poly-PO_4 after loading and leaching.

First, with reaction with only CPS in batch experiments, Tc-99 was present as 100% Tc_2S_7 with Tc-99 present as the +4 oxidation state (reduced) based on bulk extended X-ray absorption spectroscopy (EXAFS) results, as shown in Figure J.29. Then, after subsequent treatment with Poly-PO_4 in batch experiments, XRF mapping showed clear correlations between Tc, Ca, S, and P (Figure J.30), potentially due to precipitation of sulfides and subsequent formation and coating with apatite. However, it is unclear if the P was associated with apatite mineral phases and whether apatite (if present) was coating the sulfides. Finally, post-leaching XAS [including both X-ray absorption near edge structure (XANES) and EXAFS, Figure J.31] characterization of sediments from columns with CCug sediments treated with CPS+Poly-PO_4 showed that the majority of Tc-99 in the solid phase was still Tc(IV). Linear combination fitting of results showed 0.92 ± 0.02 Tc(IV) and 0.08 ± 0.02 Tc(VII).

For U, there was a correlation between Fe and U (Figure J.32), potentially indicating reductive precipitation by or with iron, following batch treatment of CCug sediments with CPS+Poly-PO_4. Moreover, there was a relatively homogenous distribution of Ca, suggesting precipitation of calcium phosphate phases. In addition, XANES results (Figure J.33) were inconclusive from the microprobe but suggested a mixture of U(IV) and U(VI), which indicates that some U reduction occurred. Similar results were observed post-leaching in sediments from columns, confirming that there was likely a mixture of U oxidation states in precipitates (Figure J.34 and Figure J.35).

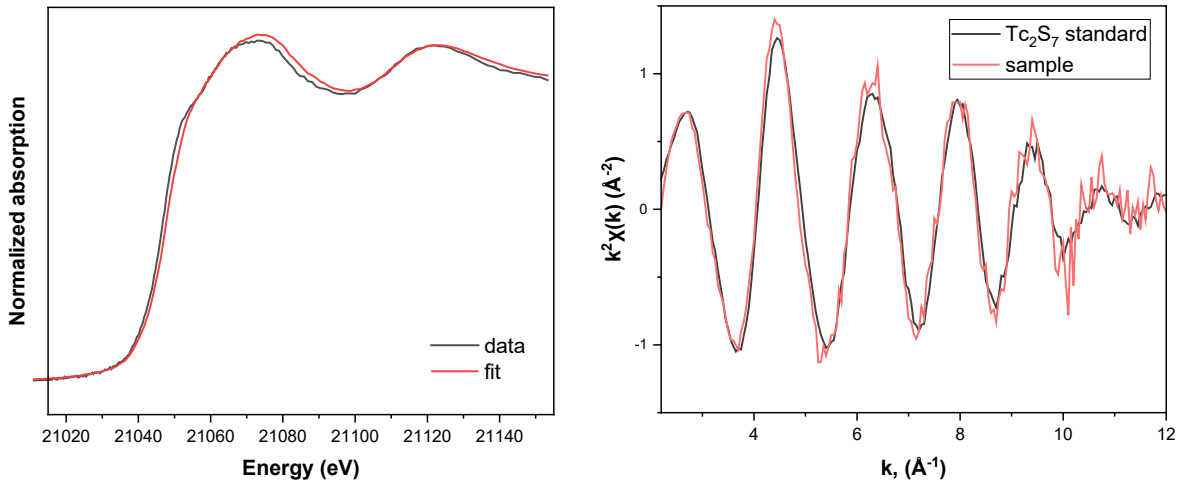

Figure J.29. EXAFS results for Tc-99 for batch samples where CCug sediments were reacted with CPS for approximately 1 week prior to washing and preparation for analysis. Linear combination fitting with Tc_2S_7 standard (*left*) and comparison of Tc-99 K-edge EXAFS oscillations of the sample with the Tc_2S_7 standard (*right*), highlighting the sample and standard agreement.

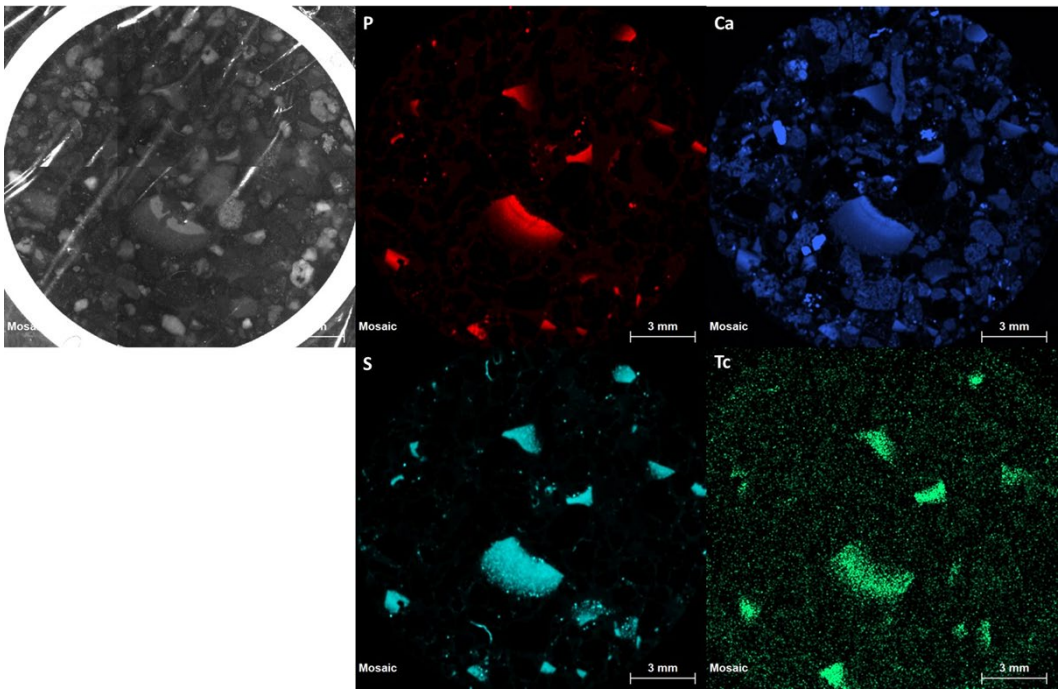

Figure J.30. XRF mapping results for pre-leach CCug sediments treated with CPS+Poly-PO_4 in a batch highlighting strong correlations of Tc, Ca, S, and P potentially correlation of sulfide phases with apatite.

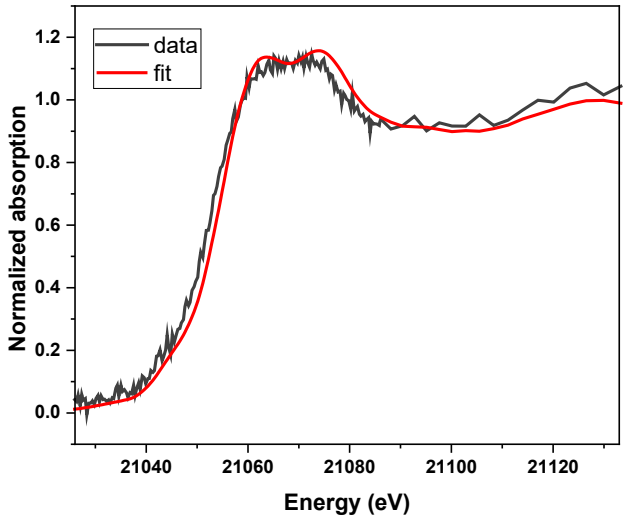

Figure J.31. Tc-99 K-edge XANES data with corresponding linear combination fit (LCF) for post-leach for CCug sediments from columns treated with CPS+Poly-PO_4. Note: Data – *black* and fit – *red* lines. The LCF range is from -43 to 97 eV below and above the edge.

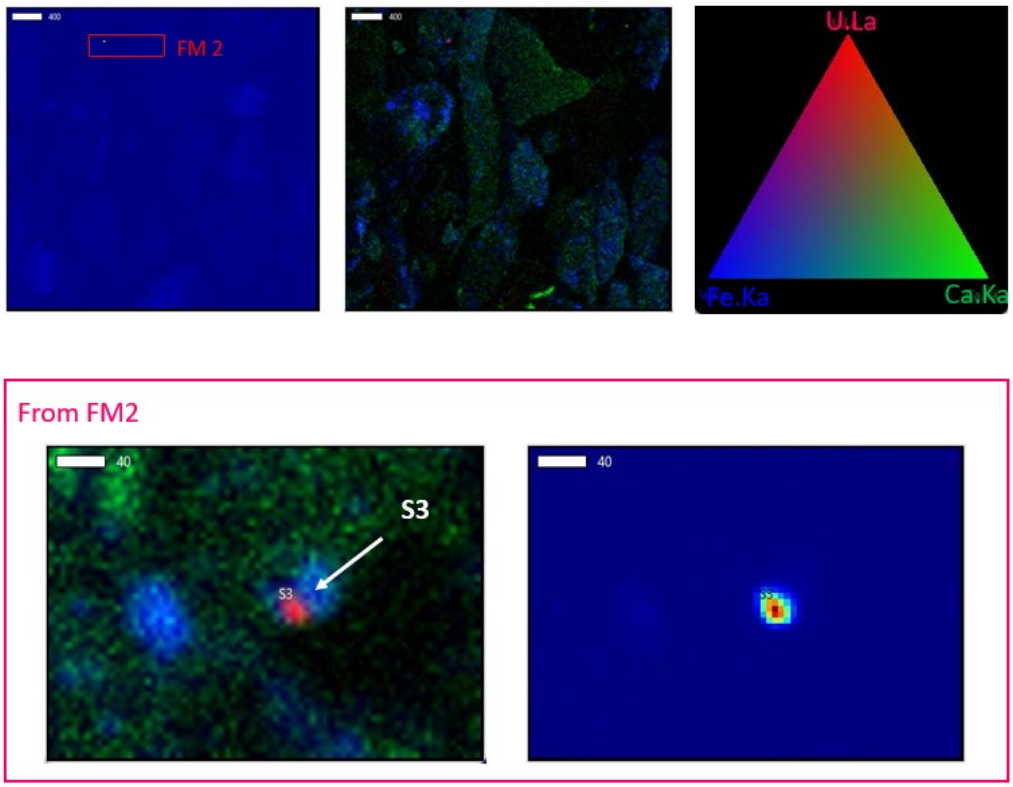

Figure J.32. XRF for Fe, Ca, and U collected on the microprobe with coarse (*top*) and fine (*bottom*) maps showing areas of interest for U for pre-leach CCug sediments treated in a batch with CPS+Poly-PO_4. Note: The white arrow points to the spot selected for U L3-edge XANES, S3.

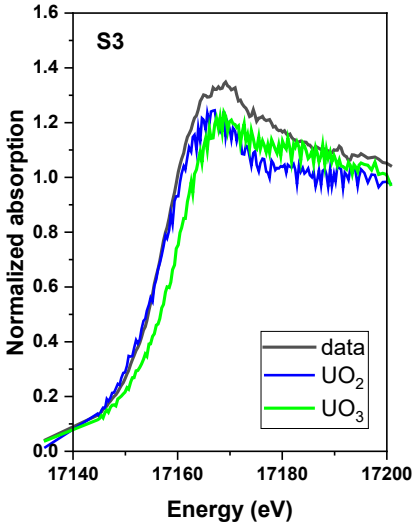

Figure J.33. XANES results for U L3-edge on pre-leach CCug sediments treated in a batch with CPS+Poly-PO_4 showing a mixture of U(IV) and U(VI). Note: Spot (S3) chosen on the fine map (on Figure J.31).

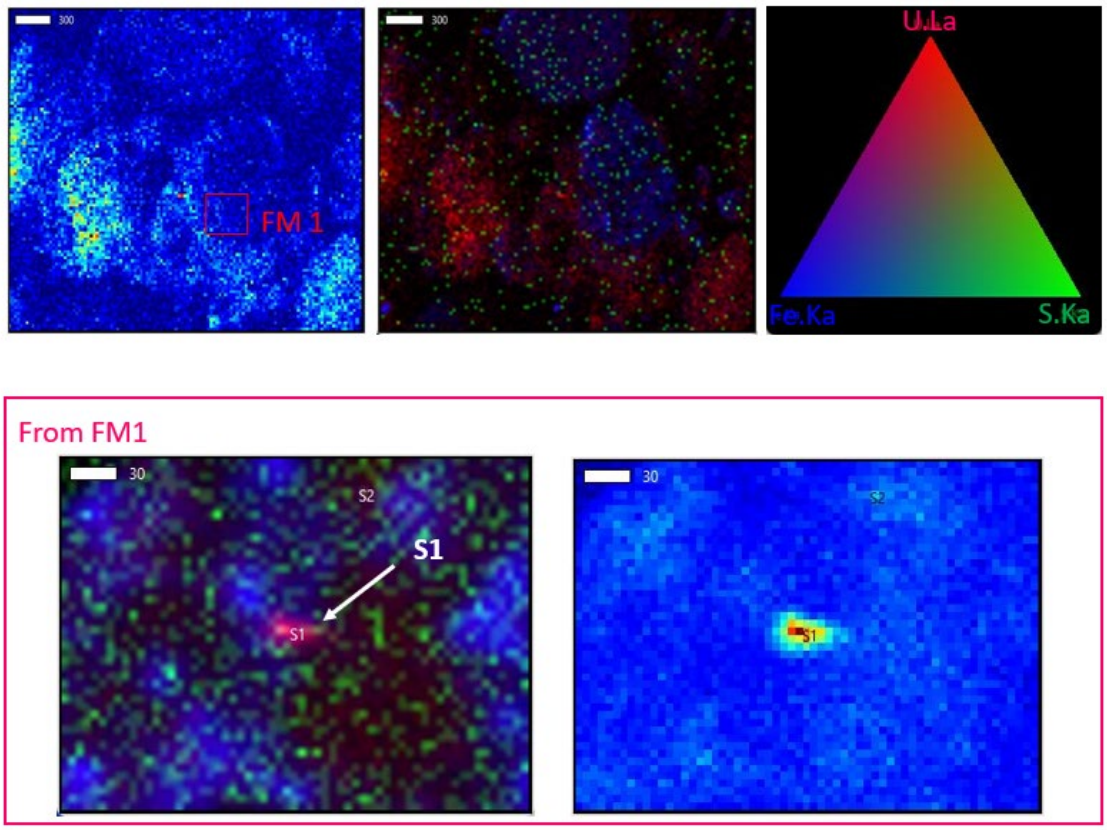

Figure J.34. XRF for Fe, S, and U collected on the microprobe with coarse (*top*) and fine (*bottom*) maps showing areas of interest for U for post-leach of CCug sediments treated with CPS+Poly-PO_4 in columns. Note: The white arrow points to the spots selected for U L3-edge XANES, S1.

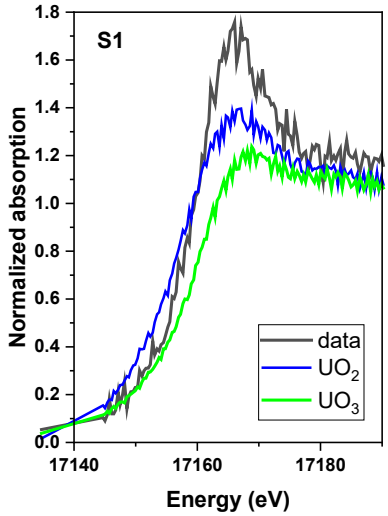

Figure J.35. XANES results for U L3-edge on post-leach CCug sediments from columns treated with CPS+Poly-PO_4 that are inconclusive but likely predominantly U(IV). Note: Spot (S3) chosen on the fine map (on Figure J.33). U L3-edge XANES on the spot S1 chosen on fine map (on Figure J.33) of the column sediment.

J.4 Saturated Column Results for Co-contaminants for BY Cribs Groundwater

For CoCOIs, including I, Cr, and Sr, data were collected for monitoring effluent concentrations and distribution in sediments post-leaching (only for Cr and Sr). These results showed that the mobility of I was significantly decreased with Poly-PO_4 treatment (Figure J.36). However, loadings into sediments cannot be confirmed based on post-leaching column sectioning, as acidic conditions were used for leaching to target PCOIs but likely volatilized iodine. Regardless, the potential for uptake of I in apatite is promising, though there was measurable release during stop flows based on I spikes during leaching.

For Cr, there was a significant increase in loading of Cr in sediments (Figure J.30) based on post-leach sectioning and extraction in 8 M HNO_3. Though there was fluctuation across the column and with CPS vs. CPS+Poly-PO_4, this was likely due to heterogeneity of the CPS reductant across the column. In addition, significant leaching of Cr after the loading phase was not observed, consistent with Cr remaining reduced even after the reduction capacity was consumed (Rai et al. 1989; Chrysochoou et al. 2010; Zhang et al. 2020).

In the first 50 PVs of loading into these columns, there was a clear decrease in effluent Sr for columns with and without CPS+Poly-PO_4. It is likely that the reaction times did not allow for incorporation of Sr into apatite over time. Therefore, the points where effluent Sr increased during leaching in columns treated with CPS+Poly-PO_4 may indicate the point where adsorption sites are saturated with respect to Sr, potentially due to the slower incorporation mechanisms (PNNL-23367; Janusz and Skwarek 2016; Nishiyama et al. 2016), though researchers have also reported significant release depending on the conditions of adsorption (Dahl et al. 2001). Moreover, there was a significant release of Sr at the last stop flow around 300 PVs for columns with and without treatment, suggesting dissolution of a precipitate. For CPS+Poly-PO_4, significantly greater release of Sr was observed. It may be that the apatite was beginning to release surface Sr or another precipitate (e.g., $SrCO_3$ as was thermodynamically favorable in speciation modeling, Appendix A, Section A.3.1). There was also a concurrent increase in pH near this point, which could be indicative of apatite and/or hydroxyapatite dissolution (Dorozhkin 1997), and an increase in aqueous P in effluent was also observed (Figure J.43). Because the loading phase continued for longer for treated columns, it is unlikely that the differences in Sr leaching were due to the amendment and more likely that they represent precipitation of Sr under conditions with and without treatment.

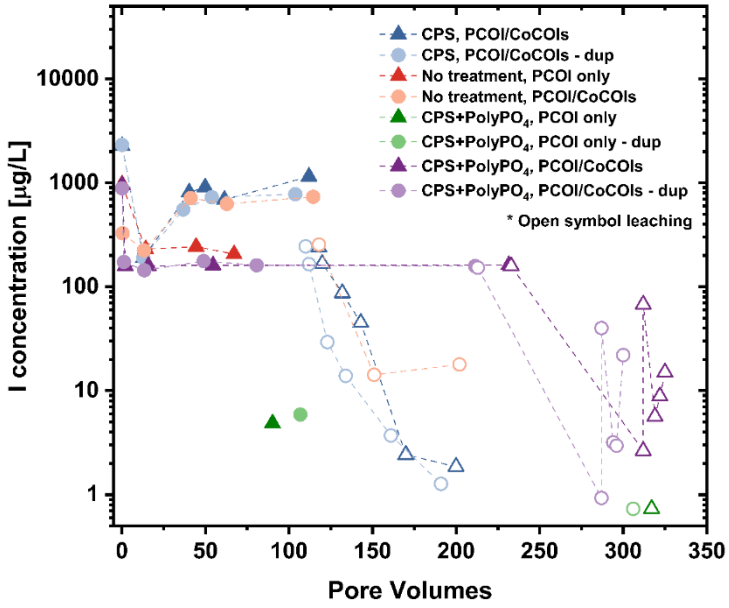

Figure J.36. Aqueous I (in µg/L) during loading and leaching with CCug sediment without and with treatment (with CPS or CPS+Poly-PO_4) after equilibration of amendments for approximately 6 weeks in the absence of oxygen. Note: "Dup" stands for duplicate. Filled samples indicate loading phase while open symbols represent the leaching phase with SGW.

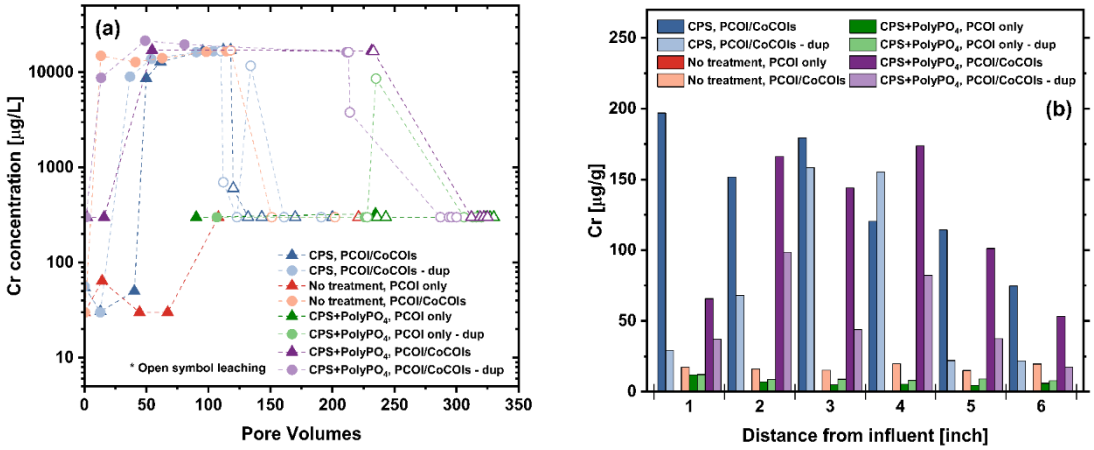

Figure J.37. (a) Aqueous Cr (in µg/L) during loading and leaching and (b) Cr distribution (in µg/g) across columns based on 8 M HNO_3 extractions with CCug sediment without and with treatment (with CPS or CPS+Poly-PO_4) after equilibration of amendments for approximately 6 weeks in the absence of oxygen. Note: "Dup" stands for duplicate. Filled samples indicate loading phase while open symbols represent the leaching phase with SGW.

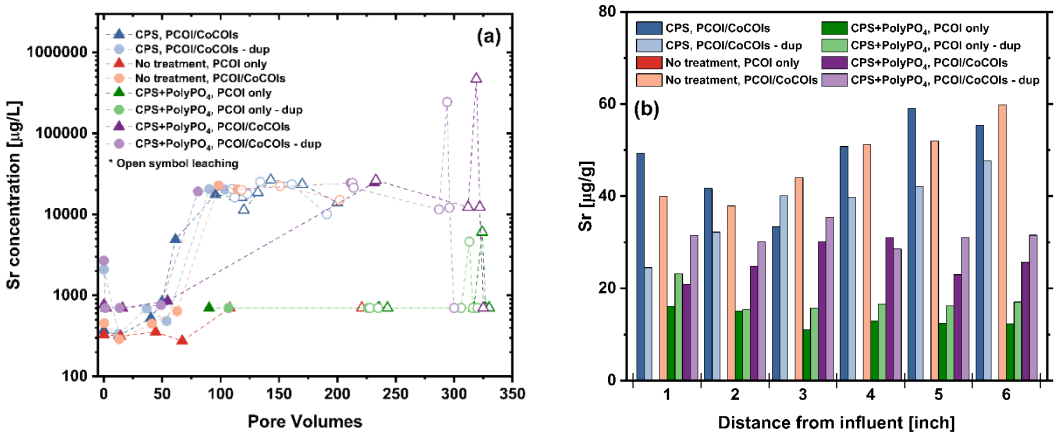

Figure J.38. (a) Aqueous Sr (in µg/L) during loading and leaching and (b) Sr distribution (in µg/g) across columns based on 8 M HNO_3 extractions with CCug sediment without and with treatment (with CPS or CPS+Poly-PO_4) after equilibration of amendments for approximately 6 weeks in the absence of oxygen. Note: "Dup" stands for duplicate. Filled samples indicate loading phase while open symbols represent the leaching phase with SGW.

J.5 Saturated Column Geochemical Monitoring

J.5.1 pH and Dissolved Oxygen Data

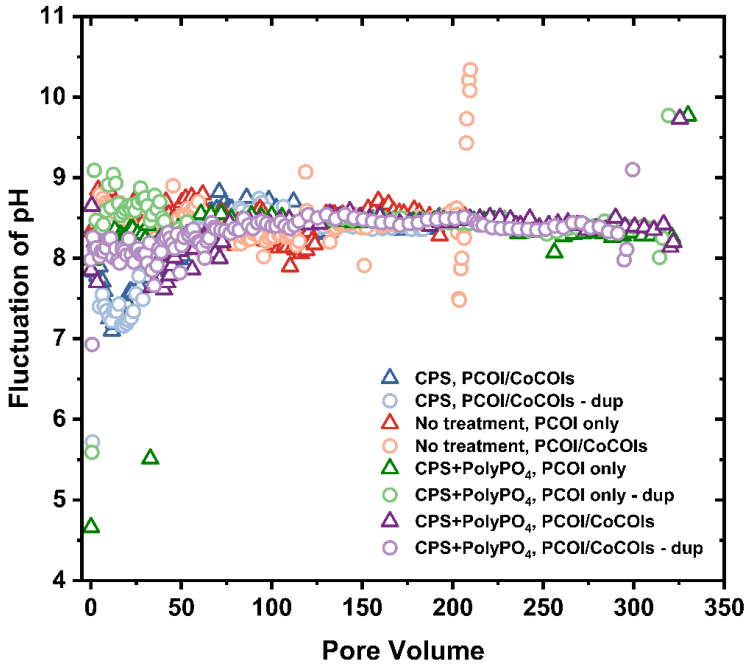

Figure J.39. Fluctuation of pH over time during loading and leaching with CCug sediment without and with treatment (with CPS or CPS+Poly-PO_4) after equilibration of amendments for approximately 6 weeks in the absence of oxygen. Note: "Dup" stands for duplicate.

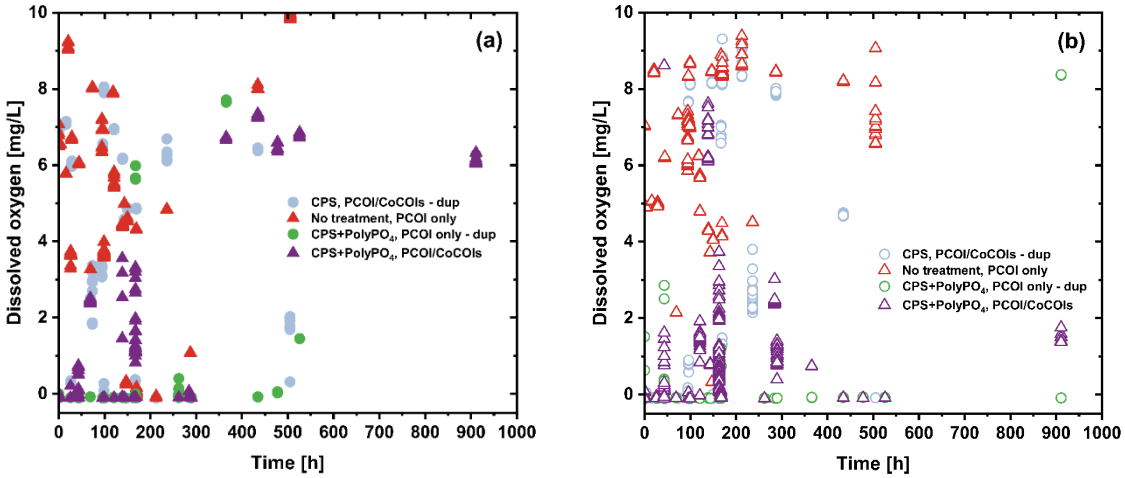

Figure J.40. Fluctuation of dissolved oxygen over time during (a) loading and (b) leaching with CCug sediment without and with treatment (with CPS or CPS+Poly-PO_4)w after equilibration of amendments for approximately 6 weeks in the absence of oxygen. Note: "Dup" stands for duplicate. Results are For Information Only.

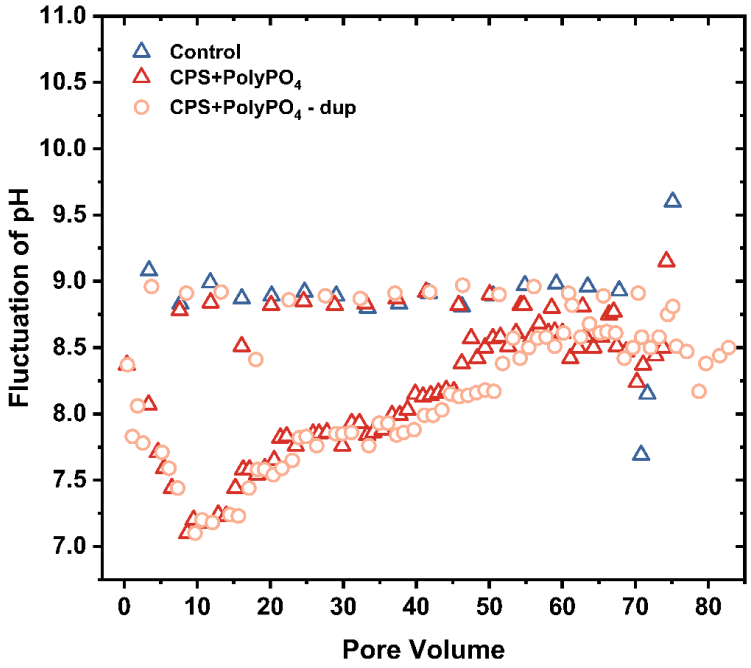

Figure J.41. Fluctuation of pH over time during leaching with PZsd sediment without and with treatment (with CPS or CPS+Poly-PO_4) after equilibration of amendments for approximately 6 weeks in the absence of oxygen. Note: "Dup" stands for duplicate.

J.5.2 Amendment Monitoring Data

For both BY Cribs water table and perched water conditions, there was a significant loading of S observed, even after 100 PVs of leaching, as shown in Figure J.42 and Figure J.44. There was a greater loading of S into the sediments for the perched water conditions, likely due to its addition in a batch configuration as opposed to direct injection into the columns and less injection of water over the course of the experiments. This suggests that a significant amount of the S could advect out of treatment zones in the field, depending on groundwater flow rates and targeted zone of treatment. There was also less P measured in the sediments in the BY Cribs groundwater condition, which was not readily discernible as increased when compared to the untreated columns (Figure J.43). Therefore, it is likely that much of the apatite precipitated initially from Poly-PO_4 was leached during the loading of contaminants and subsequent leach, which occurred over hundreds of PVs. It is possible that Ca:P ratios were not sufficient for formation of apatite. Future work could consider using a combination of sodium polysulfide and CPS to generate the best conditions for apatite formation in the presence of sulfide. For the perched water conditions, similar to observations for S, there was more P measured post-leaching with column sectioning as compared to BY Cribs groundwater conditions. These results confirm that apatite will also leach over time, though predictions could be projected based on solubility and groundwater chemistry and flow rates.

J.5.2.1 BY Cribs Groundwater Conditions

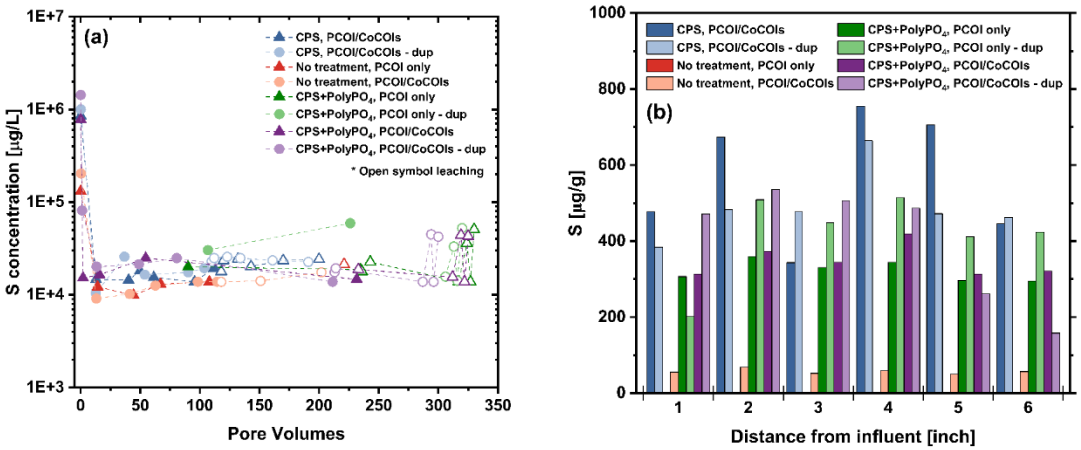

Figure J.42. (a) Effluent S (in µg/L) during loading and leaching and (b) S distribution (in µg/g) across columns based pm 8 M HNO_3 extractions with CCug sediment without and with treatment (with CPS or CPS+Poly-PO_4) after equilibration of amendments for approximately 6 weeks in the absence of oxygen. Note: "Dup" stands for duplicate. Filled samples indicate loading phase while open symbols represent the leaching phase with SGW.

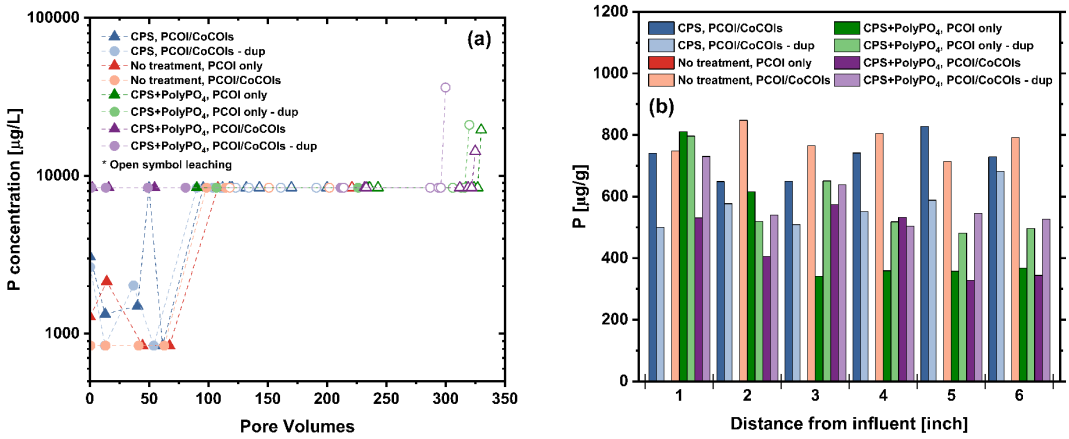

Figure J.43. (a) Effluent P (in µg/L) during loading and leaching and (b) P distribution (in µg/g) across columns based on 8 M HNO_3 extractions with CCug sediment without and with treatment (with CPS or CPS+Poly-PO_4) after equilibration of amendments for approximately 6 weeks in the absence of oxygen. Note: "Dup" stands for duplicate. Filled samples indicate loading phase while open symbols represent the leaching phase with SGW.

J.5.2.2 Perched Water Conditions

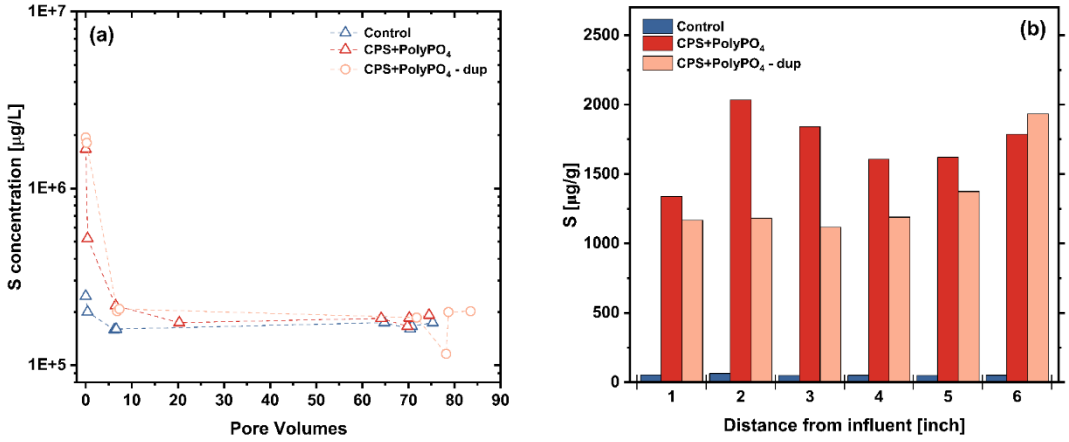

Figure J.44. (a) Aqueous S (in µg/L) during leaching and (b) S distribution (in µg/g) across columns post-leaching based on 8 M HNO_3 extractions with PZsd sediment without and with treatment (with CPS or CPS+Poly-PO_4) after equilibration of amendments for approximately 6 weeks in the absence of oxygen. Note: "Dup" stands for duplicate. Filled samples indicate loading phase while open symbols represent the leaching phase with SGW.

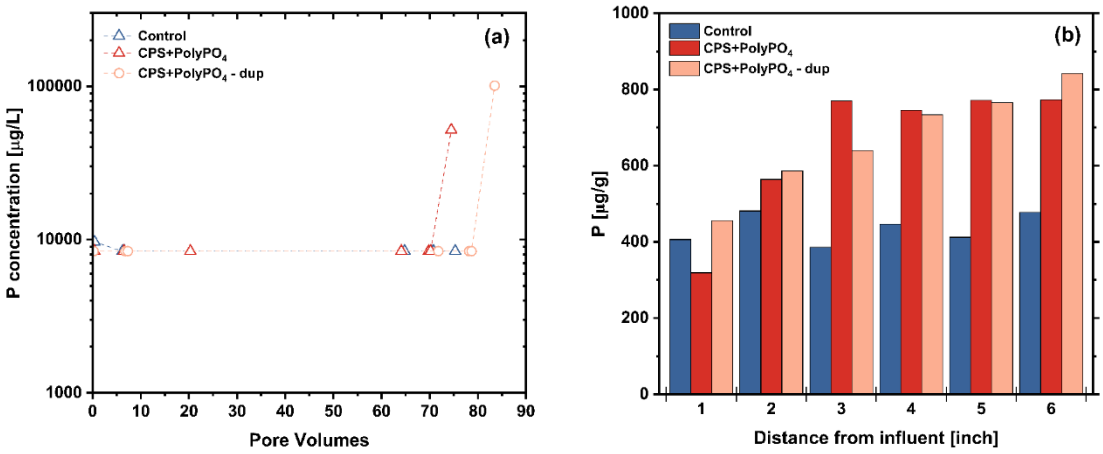

Figure J.45. (a) Aqueous P (in µg/L) during leaching and (b) P distribution (in µg/g) across columns post-leaching based on 8 M HNO_3 extractions with PZsd sediment without and with treatment (with CPS or CPS+Poly-PO_4) after equilibration of amendments for approximately 6 weeks in the absence of oxygen. Note: "Dup" stands for duplicate. Filled samples indicate loading phase while open symbols represent the leaching phase with SGW.

J.5.3 Bromide Tracer Breakthrough

Results are summarized here for bromide breakthrough curves collected at the end of experiments, after the approximately 100-PV leaching step. Bromide curves were similar and repeatable, suggesting that the amendments (CPS or CPS+Poly-PO_4) did not have a significant impact on the flow of water through the columns. There was a small difference between the no treatment and CPS treatment vs. the CPS+Poly-PO_4 breakthrough curves for the CCug sediments, as shown in Figure J.44; however, this was more likely a fluctuation in bromide injection concentrations as the tracer injections were conducted in two groups of four columns (all no treatment and CPS for one group and CPS+Poly-PO_4 conditions for the second group). Moreover, differences were not observed in the PZsd sediments between the treated and untreated columns (Figure J.45). Bromide breakthrough curves are fit for dispersion and compared across all technologies in Appendix A, Section A.3.2.

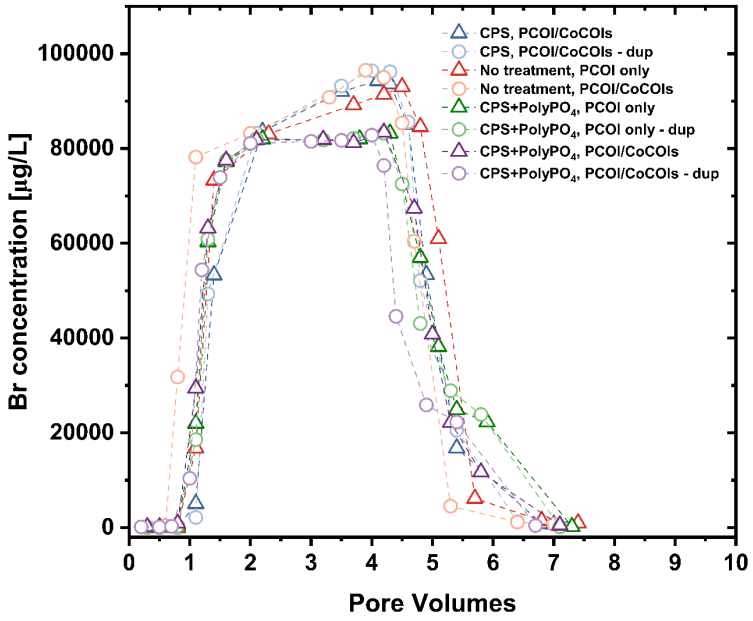

Figure J.46. Effluent Br (in µg/L) during and after tracer injection at 80 mg/L Br into columns with CCug sediment without and with treatment (with CPS or CPS+Poly-PO_4). Note: "Dup" stands for duplicate. Br tracer injections conducted after leaching step in columns.

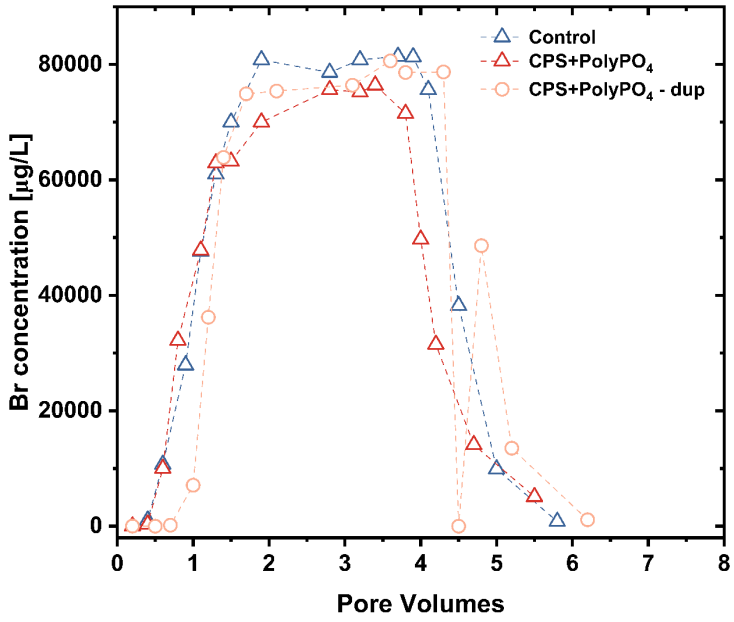

Figure J.47. Effluent Br (in µg/L) during and after tracer injection at 80 mg/L Br into columns with PZsd sediment without and with treatment (with CPS or CPS+Poly-PO_4). Note: "Dup" stands for duplicate. Br tracer injections conducted after leaching step in columns.

J.6 Summary of Performance of Calcium Polysulfide and Polyphosphate for Groundwater

For the BY Cribs groundwater conditions, U and Tc-99 sequestration was significant with CPS+Poly-PO_4 treatment, with CPS facilitating the reduction of Tc-99 and Poly-PO_4 sequestering U based on both batch experiments up to 270 days and column leaching experiments over 300 PVs. Poly-PO_4 treatment alone did not sequester Tc. However, it performs well for U based on previous injections at the Hanford Site and batch experiments presented here and previously (PNNL-35432). In addition, some sequestration of potential CoCOIs was observed, including I and Sr via Poly-PO_4 and Cr via CPS.

For the perched water conditions, sequestration of Tc-99 was not significantly greater with treatment as compared to without treatment, likely due to the impact of high ionic strength and nitrate competing for reduction capacity. Leaching of U was significant both with and without treatment. However, with CPS+Poly-PO_4 treatment, U release was significantly delayed, likely due to solubility controls. These results highlight the challenges of treatment within the perched water zone. Depending on the amount of nitrate that may be present, this technology may not be appropriate for Tc-99 treatment. However, Poly-PO_4 may still perform well for U under these conditions, depending on flow rates and reaction times.

Appendix K – Liquid-Phase Bioreduction & Sequestration: Molasses & Polyphosphate

The purpose of this task is sequestration of U and Tc-99 (primary contaminants of interest, PCOIs) in the presence of I-129 as iodate (IO_3^-), nitrate (NO_3^-), Cr, and Sr (co-contaminants of interest, CoCOIs) in water-saturated zones using food-grade black strap unsulfured molasses and a polyphosphate (Poly-PO_4) solution. Molasses is an organic amendment used to stimulate the native microbial community in sediments to bioreduce contaminants to less mobile forms such as for Tc, U, and Cr. It is also used for wastewater treatment and groundwater remediation of nitrate via reduction to nitrite (NO_2^-) and then to nitrogen gas (N_2) to decrease nitrate concentration in water. Poly-PO_4 is added to precipitate apatite that may either incorporate contaminants like U or coat reduced/precipitated contaminants such as Tc.

This combined treatment is targeting contamination in perched water and BY Cribs as the primary treatment zones, with treatment via formation of a permeable reactive barrier in groundwater under BY Cribs. Potential secondary treatment zones include 216-U-1 and -2, S-SX tanks, S and T Cribs, C tanks, and BC Cribs. Note that the amount of molasses added is different from previous batch experiments in the Phase 1 report (PNNL-35432). Molasses was added to Phase 1 batch experiments at 0.39 g/L total organic carbon (TOC). For perched water-saturated batch and 1-D column experiments, molasses was added at 1.09 g/L TOC for both. For BY Cribs water-saturated 1-D column studies, molasses was added at TOC of 26 g/L.

The specific objectives of this technology are as follows:

1. Quantify the decrease in Tc-99 and U mass and order of magnitude removal rate in various combinations: (1) with/without sediment, (2) with/without co-contaminants, and (3) with/without treatment [described in the Phase 1 report (PNNL-35432)].
2. Determine the immobilization rates for U and Tc-99 with/without co-contaminants for (1) perched water and (2) BY Crib application (in groundwater).
3. Quantify the longevity of U and Tc-99 with/without co-contaminants for (1) perched water and (2) BY Crib application.

Objectives 2 and 3 were tested in 1-D leach columns as described in Section K.3 for perched water conditions, based on the batch experiments described in Section K.2. Objectives 2 and 3 were also tested in 1-D load/leach columns as described in Section K.4 for BY Cribs groundwater conditions.

K.1 Supplemental Methods

K.1.1 Long-Term Static Batch Studies

Water-saturated batch experiments with treatment using molasses+Poly-PO_4 were performed following experimental procedures described in Appendix A, Section A.2.1 and in Section A.2.3. (for sequential extractions). Batch experiments were conducted in packed porous media using a sediment-to-water ratio of 5g:1 mL and kept in an MBraun anoxic chamber (100% N_2, O_2 < 0.1 ppm) to evaluate changes in sequestration rate for PCOIs (nitrate, Tc, and U). Perching zone sand (PZsd) sediments were first artificially contaminated with PCOIs, then amended with molasses (indicating the start of the experiment at time zero) and subsampled at time points 0, 6, 38, and 75 days. Then, a 35-mM Poly-PO_4 solution was added to the remaining sediment and subsampled at time points 83, 104, and 138 days. The addition of molasses+Poly-PO_4 was spaced out by 75 days to allow the microbes to generate reducing conditions

needed to sequester the PCOIs. Sequential extractions to evaluate the mobility of Tc-99 and U with treatment were performed on sediments from time points 83, 104, and 138 days.

K.1.2 Perched Water Column Conditions

PZsd sediments used in perched water columns (Table K.1) were artificially contaminated with PCOIs (nitrate, Tc, and U), amended with molasses and then with a 35-mM Poly-PO_4 solution. Sediments were kept in an MBraun anoxic chamber, where they equilibrated for 75 days with molasses and then 30 days with Poly-PO_4 (for a total of 105 days) prior to the start of column leaching studies with oxic synthetic perched water (SPW).

Table K.1. Perched water columns and conditions tested.

Column Test Name	PCOIs	Molasses	Poly-PO_4
Mol+Poly-PO_4 treatment, PCOIs[(a)]	Tc, U, and NO_3^-	Y	Y
No treatment, PCOIs[(b)]		N	N

(a) Performed in duplicate.
(b) Performed as a single column.

K.1.3 BY Cribs Groundwater Column Conditions

Cold Creek Unit gravel (CCug) sediments used in BY Cribs groundwater columns (Table K.2) were amended with molasses first and then with a 35-mM Poly-PO_4 solution. The addition of molasses and then Poly-PO_4 was spaced 21 days to allow the microbes to generate reducing conditions needed to sequester PCOIs (Tc and U). After Poly-PO_4 was added, sediments were equilibrated inside the MBraun anoxic chamber for an additional 30 days before packing into columns and injecting them synthetic groundwater (SGW) with PCOIs or PCOIs+CoCOIs (Sr, Cr, IO_3^-, NO_3^-) for up to 100 pore volumes (PVs).

Table K.2. BY Cribs groundwater columns and conditions tested.

Column Test Name	Contaminants of Interest	Molasses	Poly-PO_4
Mol+Poly-PO_4 treatment, PCOIs[(b)]	Tc and U	Y	Y
No treatment, PCOIs[(b)]		N	N
Mol+Poly-PO_4 treatment, PCOIs+CoCOIs[(a)]	Tc, U, NO_3^-, Cr, Sr, and I	Y	Y
No treatment, PCOIs+CoCOIs[(b)]		N	N

(a) Performed in duplicate.
(b) Performed as a single column.

K.2 Long-Term Batch Results

Static long-term batch experiments were conducted at a solid-to-solution ratio of 5 g:1 mL to evaluate changes in sequestration rates for nitrate, Tc, and U as PCOIs with treatment. Aqueous subsamples collected from time points 0, 6, 38, and 75 days were used to evaluate sequestration rates with molasses, while subsamples collected at time points 83, 104, and 138 days were used to evaluate sequestration rates and contaminant mobility with Poly-PO_4 (75 days after molasses treatment).

Results for batch studies showed that the amount of molasses added to PZsd sediments significantly reduced the starting nitrate concentration (Figure K.1). Nitrate reduction in PZsd sediments without the addition of molasses was observed to be minimal. For instance, the aqueous concentration of nitrate was decreased from ≈10,000 mg/L at 0 days to ≈4,000 mg/L at 6 days post molasses treatment and was consistent with Phase 1 batch testing results (PNNL-35432). After 6 days, the aqueous nitrate concentration increased to ≈7,700 mg/L but remained lower compared to the no-treatment control, which had nitrate concentrations > 8,000 mg/L for the entire testing. The addition of Poly-PO_4 at 75 days post molasses treatment significantly decreased the concentration of nitrate to ≈2,600 mg/L and increased the concentration of nitrite to 235 mg/L at 83 days. The concentration of aqueous nitrate and nitrite continued to fluctuate through 138 days of testing. Unlike the results from Phase 1 batch studies, which showed no nitrate remaining in the aqueous phase beyond 7 days, nitrate was still present at 138 days. In theory, adding more molasses would yield to more nitrate reduction, as nitrate reduction is limited based on carbon availability as an electron source. The remaining nitrate, which serves as a competing and more favorable electron donor (Istok et al. 2004), has important implications for Tc-99 and U sequestration rates as explained below.

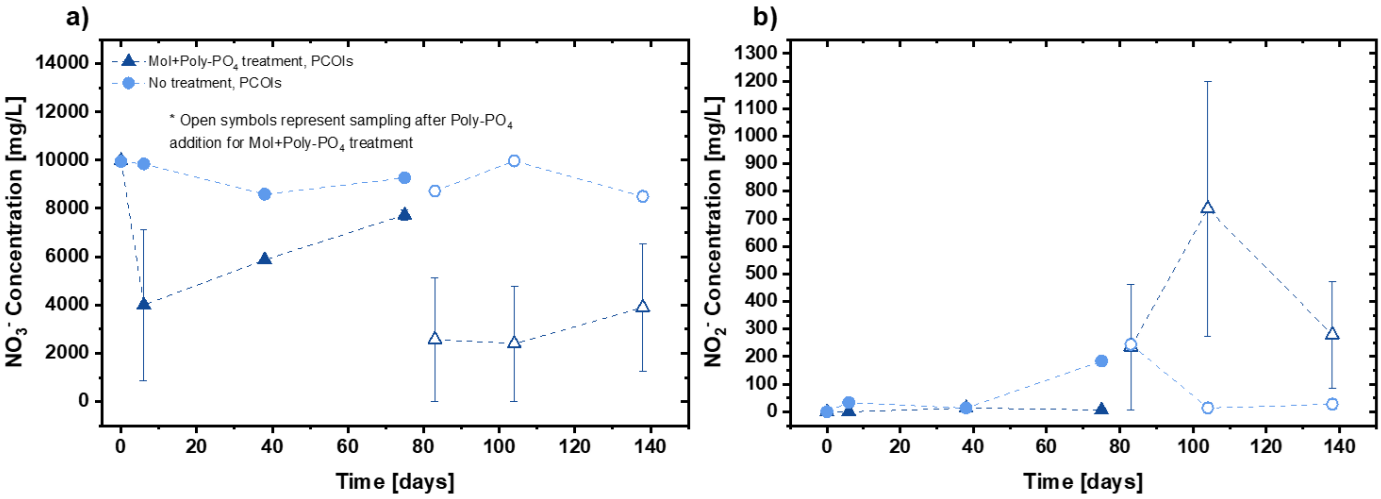

Figure K.1. Effluent concentration of nitrate, NO_3^- (a) and nitrite, NO_2^- (b) in long-term static batch studies treated with (*triangles*) or without (*circles*) molasses from 0 to 75 days (*solid-filled symbols*) followed by Poly-PO_4 (*open symbols*, 83 to 138 days). Note: Errors bars represent one standard deviation of duplicate samples. The "No treatment" control did not receive amendment at any time; pore water was balanced with SPW.

For Tc, the addition of molasses slightly increased the rate of Tc-99 sequestration between 38 to 75 days (Figure K.2). The addition of Poly-PO_4 at 75 days further increased the rate of Tc-99 sequestration compared with molasses alone. Sequential extraction results for Tc-99 are shown in Figure K.3 for time points 83 to 138 days. The results show Tc-99 to be more mobile with treatment, possibly due to the high ionic strength of the Poly-PO_4 solution added after 75 days.

The rate of U sequestration was not improved with the addition of molasses and Poly-PO_4 relative to the no-treatment control (Figure K.4). In addition, the mobility of U appeared to increase slightly with treatment, possibly due to the high ionic strength of the Poly-PO_4 (Figure K.5).

In the Phase 1 batch studies with molasses treatment, nitrate was mostly reduced by 7 days of testing, Tc-99 was mostly reduced by 14 days, and U was mostly reduced by 91 days. Given that nitrate is a preferred electron donor over Tc-99 and U by most bacteria (Istock et al. 2004) and that the reduction of nitrate, Tc, and U happened in a stepwise order in the Phase 1 batch studies, the current studies could

have added more molasses than was added in Phase 1 to completely reduce all of the nitrate and increase the reduction rate of Tc-99 and U.

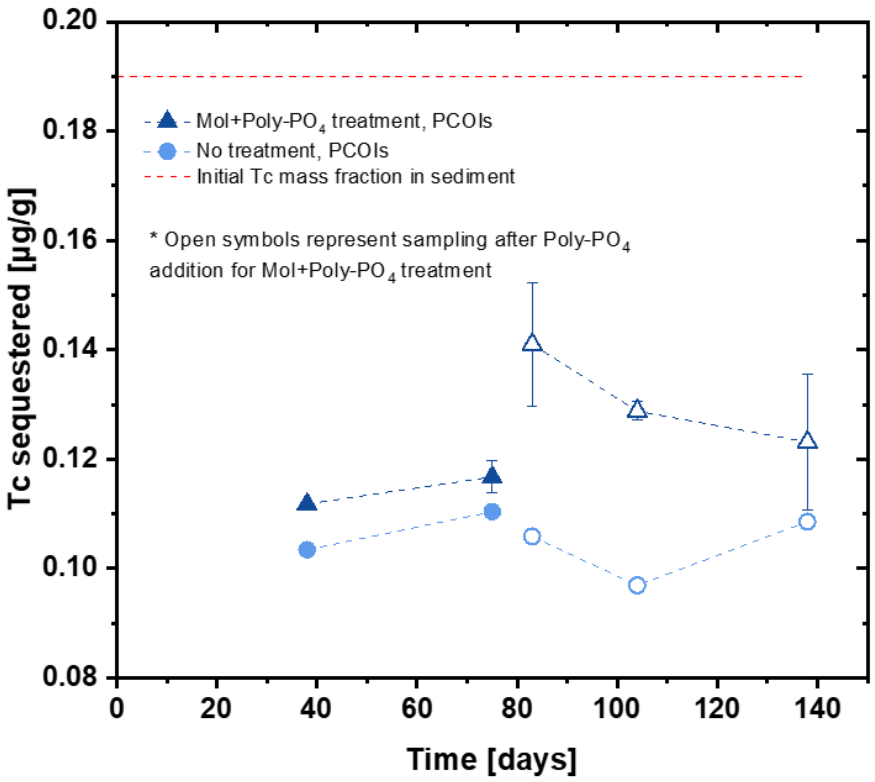

Figure K.2. Mass fraction of Tc-99 (in µg/g) sequestered in long-term static batch studies treated with (*triangles*) or without (*circles*) molasses from 0 to 75 days (*solid-filled symbols*) followed by Poly-PO_4 (*open symbols*, 83 to 138 days). Note: Errors bars represent one standard deviation of duplicate samples. The "No treatment" control did not receive amendment at any time; pore water was balanced with SPW. The dotted red line indicates the measured Tc-99 mass fraction in sediment prior to treatment.

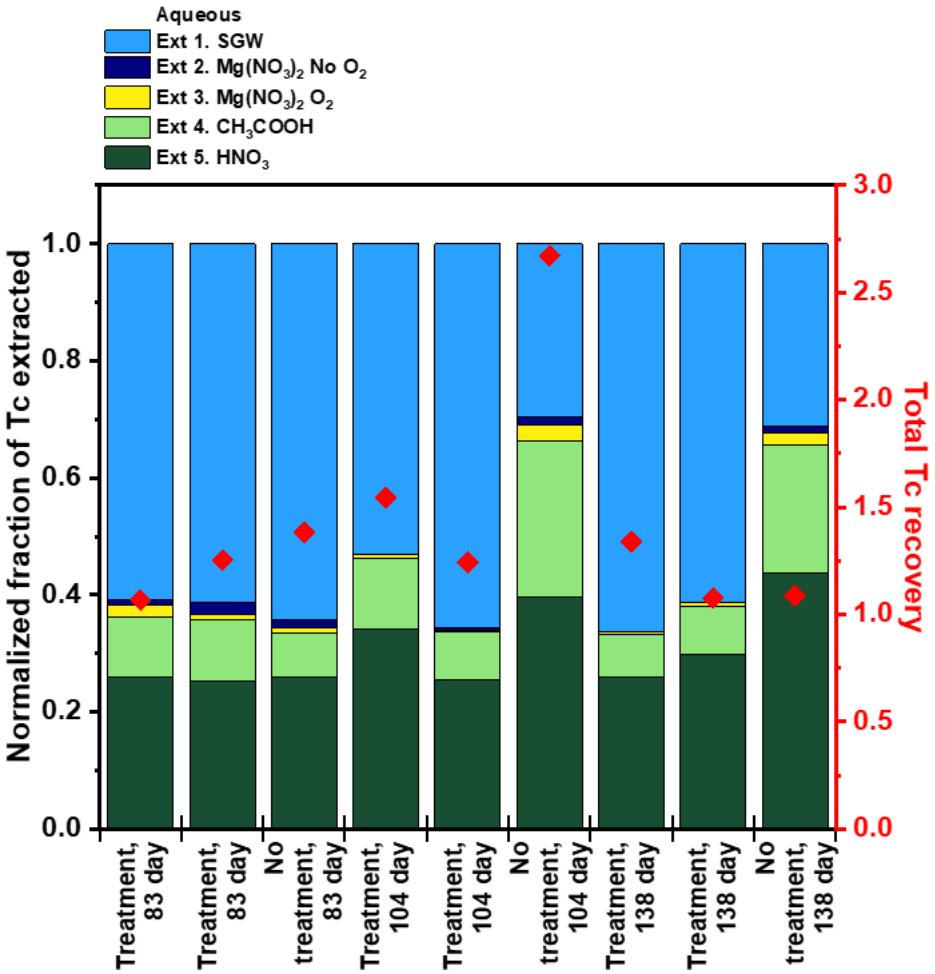

Figure K.3. Changes in Tc-99 sequestration from liquid-phase treatment of contaminant-spiked PZsd sediment reacted with molasses+Poly-PO_4 for time points 83, 104, and 138 days (for "treatment" sample names). Note: Treatment with Poly-PO_4 occurred after 75 days in "treatment" sample names only. The left side of the figure shows the normalized fraction recovered in each sequential extraction while the right side of the figure shows the solid phase concentration (in µg/g) recovered in each sequential extraction.

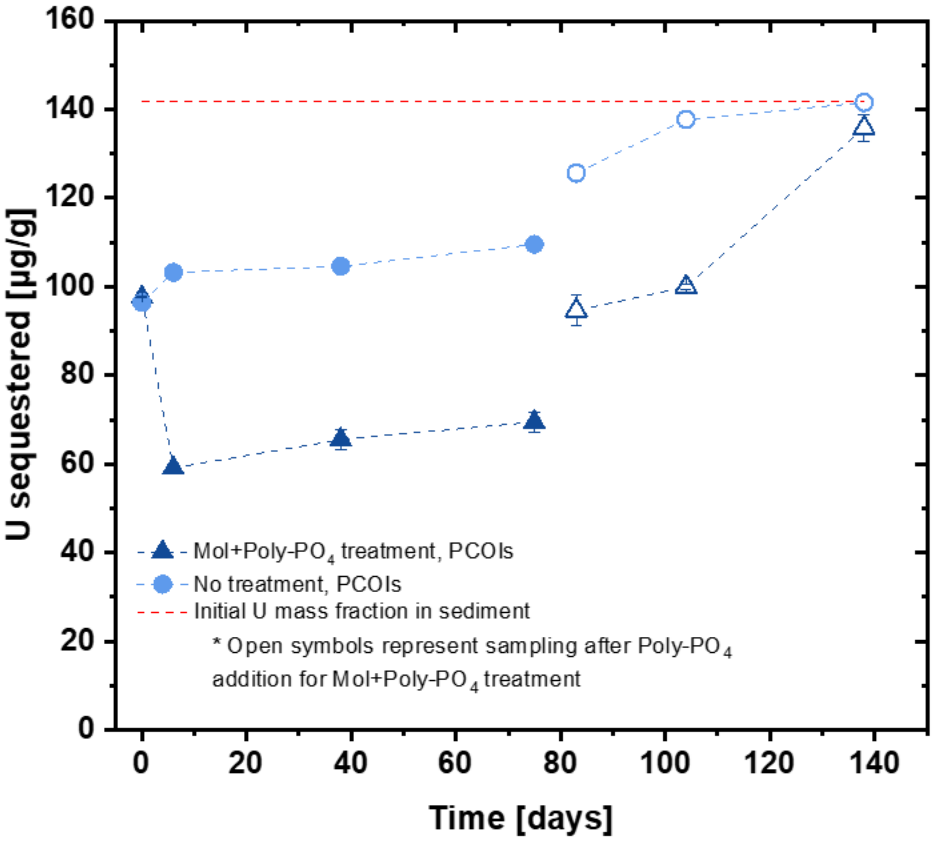

Figure K.4. Changes in U sequestration from liquid-phase treatment of contaminant-spiked PZsd sediment reacted with molasses+Poly-PO_4 for time points 83, 104, and 138 days (for "treatment" sample names). Note: Treatment with Poly-PO_4 occurred after 75 days in "treatment" sample names only. The left side of the figure shows the normalized fraction recovered in each sequential extraction while the right side of the figure shows the solid phase concentration (in µg/g) recovered in each sequential extraction.

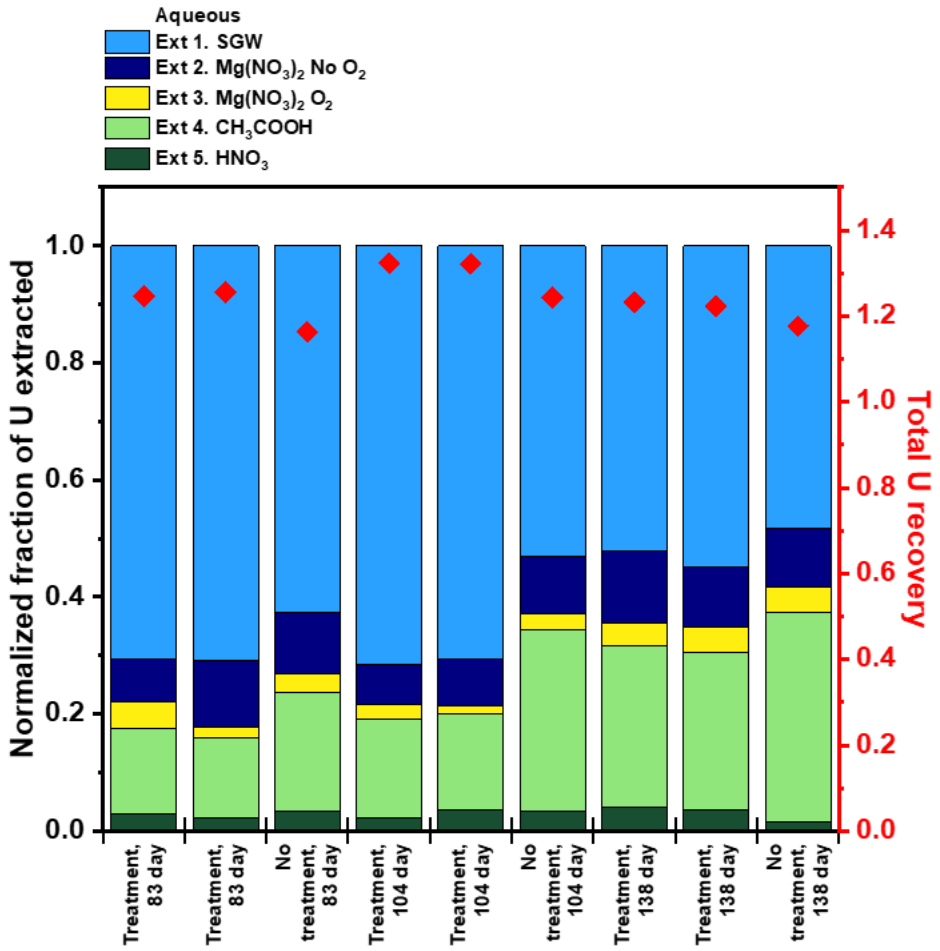

Figure K.5. Changes in U sequestration from liquid-phase treatment of contaminant-spiked PZsd sediment reacted with molasses+Poly-PO_4 for time points 83, 104, and 138 days. Note: Treatment with Poly-PO_4 occurred after 75 days in "treatment" sample names only. The left side of the figure shows the normalized fraction recovered in each sequential extraction while the right side of the figure shows the solid phase concentration (in µg/g) recovered in each sequential extraction.

K.3 Saturated Column Results for Perched Water Conditions

Saturated columns for perched water conditions were prepared by artificially contaminating PZsd sediments with PCOIs (Tc, U, and nitrate), followed by treatment with molasses (added to a TOC of 1.09 g/L) and then Poly-PO_4. After a 105-day equilibration period with treatment, sediments were packed into columns and then injected with aerated SPW for up to ≈130 PVs with stop flows at 2, 10, and 100 PVs.

K.3.1 Tc and U Sequestration

Treatment with molasses+Poly-PO_4 resulted in significantly greater nitrate reduction when compared to the untreated sediment column, and as a result less nitrate was leached after treatment. The concentration of nitrate measured in the column effluent during leaching (Figure K.6a) was used as an indication of nitrate reduction, where a lower nitrate concentration in the aqueous phase means more nitrate was

reduced during the 105-day equilibration period. As noted in Figure K.6, a higher concentration of nitrate was leached from the no-treatment sediment column compared to treatment with molasses+Poly-PO_4. This means that 88% of the nitrate was leachable without treatment in comparison to 52% to 56% with molasses+Poly-PO_4 treatment. For treated sediment columns, this is likely the portion of nitrate that was not microbially reduced during the equilibration period and indicates that the microbial community had not shifted from nitrate reduction yet. For all testing conditions, a majority of the nitrate was leached within 5 PVs of testing (Figure K.6a inset). Detectable nitrite concentrations measured in the no-treatment sediment column indicate that the PZsd sediment has some reduction capacity (Figure K.6b inset).

The amount of molasses used in sediment columns did not result in significant differences in Tc-99 and U sequestration, since the amount added did not result in the complete reduction of nitrate during the equilibration period. Both Tc-99 and U were leached within 5 PVs of injecting oxic SPW regardless of treatment and could indicate that these were not reduced during the equilibration period and remained soluble (Figure K.7c and a, respectively). U and Tc-99 sequestration rates (irrespective of the treatment) were both < 0 µg/g by then end of leaching (Figure K.7d and b, respectively).

The calculated normalized relative release rates for Tc-99 and U before stop flow (pre stop flow) and during stop flow events were used to quantify the longevity of contaminant sequestration with molasses+Poly-PO_4 treatment. As shown in Figure K.8a, the Tc-99 release rates calculated with Tc-99 concentrations before stop flow 1 were < 0 µg/kg/day and indicated Tc-99 uptake. Also, the pre-stop flow 1 release rates were more negative with treatment using molasses+Poly-PO_4 and indicated a greater extent of Tc-99 uptake with treatment as well. The same observation with respect to Tc-99 uptake was also noted during stop flow 1 (Figure K.8b). For U, treatment with molasses+Poly-PO_4 increased the relative release rate as seen in Figure K.9a (calculated using U concentrations before the stop flow) and Figure K.9b (during stop flow).

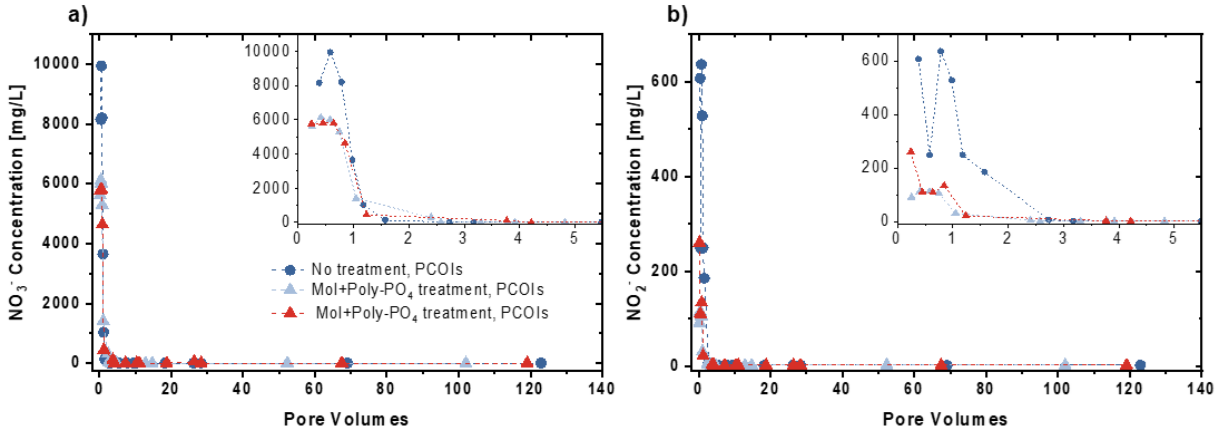

Figure K.6. Effluent concentration of nitrate, NO_3^- (a) and nitrite, NO_2^- (b) in saturated columns for perched water conditions with (*triangles*) and without (*circles*) molasses+Poly-PO_4 treatment. The inset in the upper right corner shows a snapshot of first 5 PVs of leach testing.

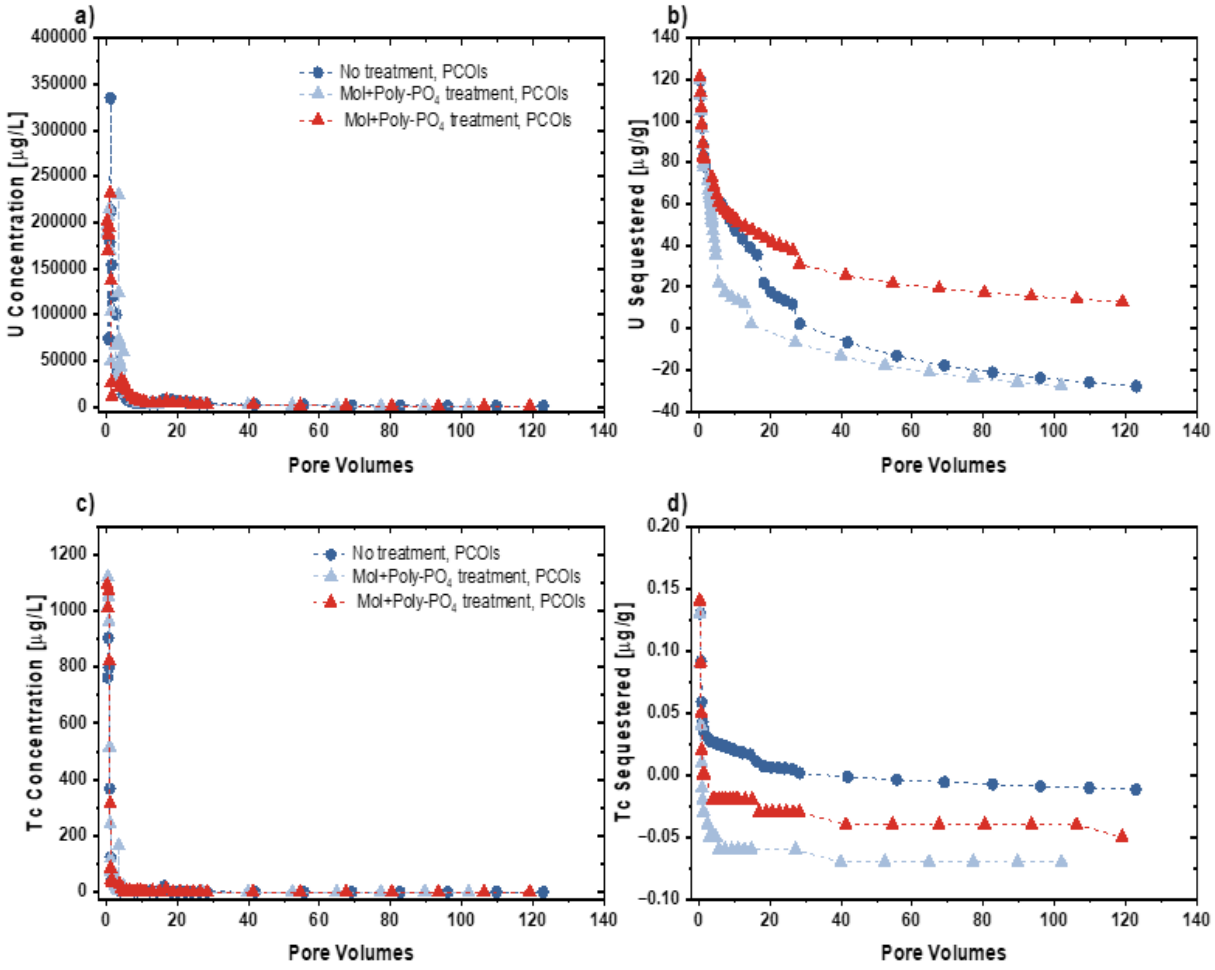

Figure K.7. Effluent concentration (*left*) and mass fraction sequestered in sediment (*right*) of uranium, U (a and b) and technetium-99, Tc-99 (c and d) in saturated columns for perched water conditions with (*triangles)* and without (*circles)* molasses+Poly-PO_4 treatment.

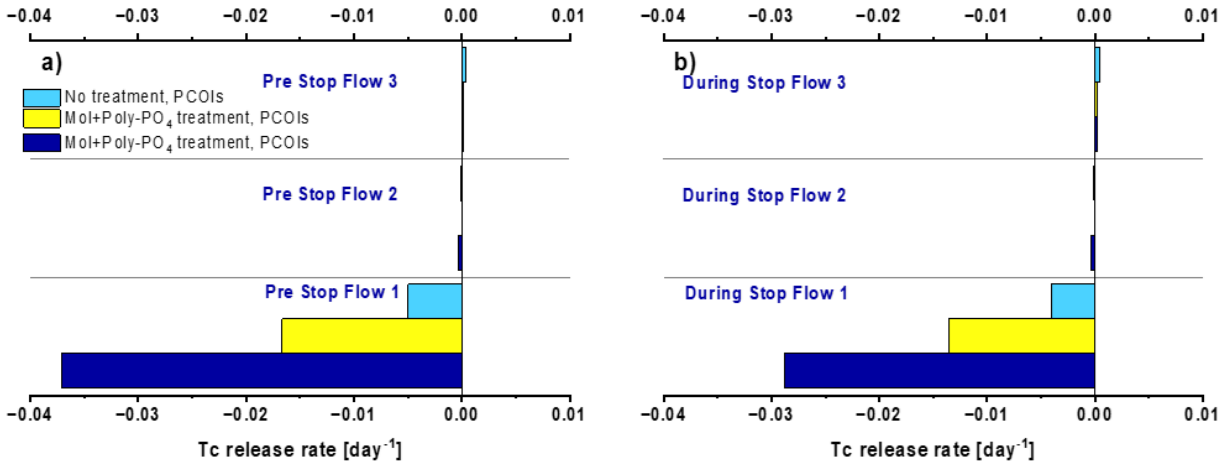

Figure K.8. Tc normalized release rates in saturated columns for perched water conditions with and without molasses+Poly-PO_4 treatment: (a) estimated leaching rate (day^{-1}) prior to each stop flow and (b) estimated leaching rate (day^{-1}) during each stop flow.

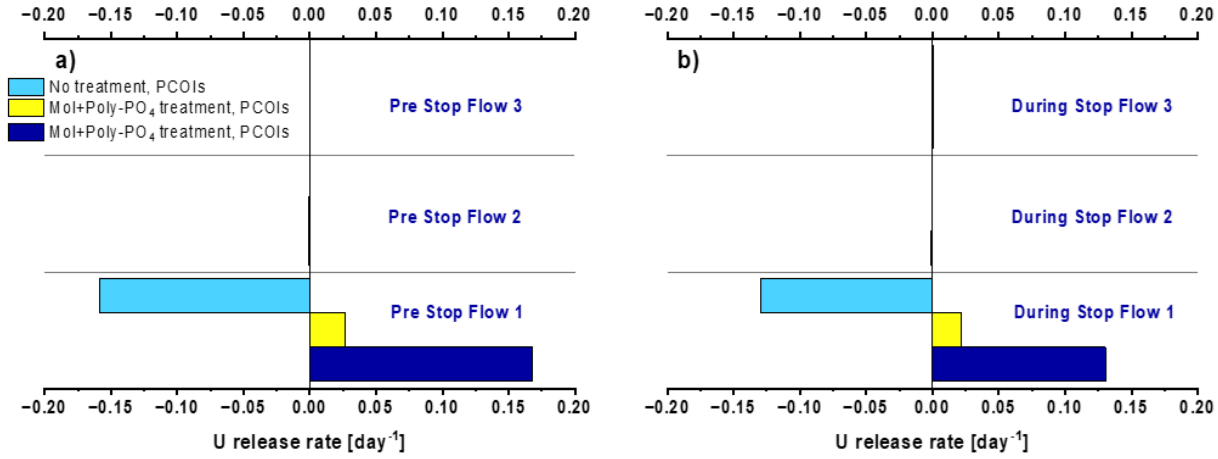

Figure K.9. U normalized release rates in saturated columns for perched water conditions with and without molasses+Poly-PO_4 treatment: (a) estimated leaching rate (day^{-1}) prior to each stop flow and (b) estimated leaching rate (day^{-1}) during each stop flow.

K.3.2 Geochemical Monitoring

Measurements were also taken on effluent samples collected from water-saturated column studies for perched water conditions throughout the leaching phase to monitor pH (Figure K.10). Treatment with molasses+Poly-PO_4 did not appear to drastically change the pH in PZsd sediments, even though the addition of molasses was expected to indirectly decrease the pH due to its impact on the microbial community (i.e., the production of organic acids from metabolic processes). It could be that the high bicarbonate (HCO_3^-) in SPW was buffering the pH.

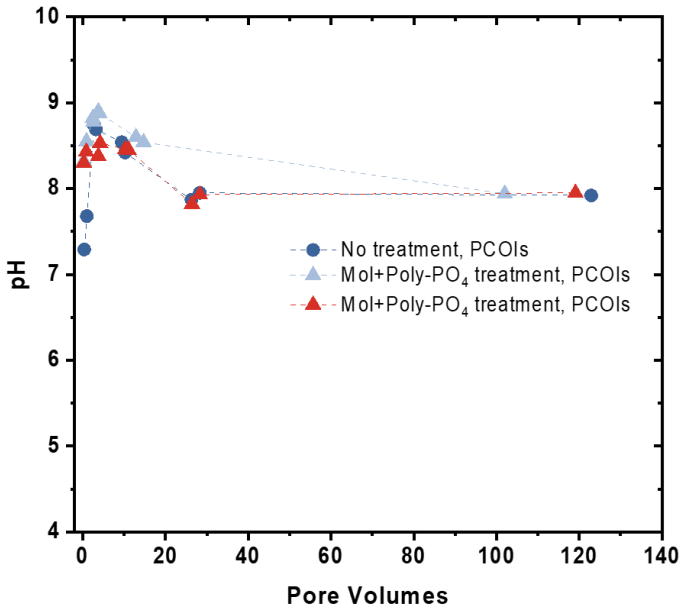

Figure K.10. Effluent pH in saturated columns for perched water conditions with (*triangles*) and without (*circles*) molasses+Poly-PO_4 treatment.

K.3.3 Bromide Tracer Breakthrough

A 65-mg/L bromide solution was injected at the end of the leaching phase in each column to evaluate physical transport through sediments. Overall, the bromide breakthrough curves were similar in all conditions tested (Figure K.11).

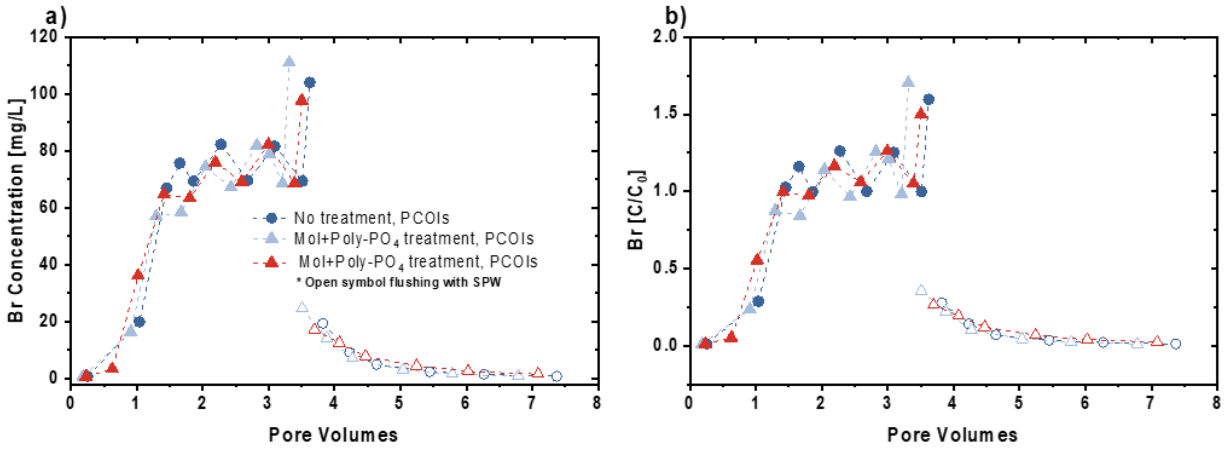

Figure K.11. Effluent concentration (a) and fraction of the concentration in effluent over the concentration of the influent solution (C/C_0) (b) of bromide (Br^-) in saturated columns for perched water conditions with (*triangles)* and without (*circles)* molasses+Poly-PO_4 treatment. The Br^- tracer test was performed at the end of the leaching phase for all sediment columns. Open symbol indicates flushing using SPW with no Br^- tracer.

K.4 Saturated Column Results for BY Cribs Groundwater Conditions

The experiments discussed in the following subsections attempted to simulate the reaction of PCOIs (Tc and U) with a permeable reactive barrier emplaced in a sediment column. Molasses was added to CCug sediments to stimulate the bioreduction of redox-sensitive metals and nitrate, and Poly-PO_4 was added to precipitate phosphate minerals (like apatite) that either incorporate or coat reduced metals to keep them from becoming oxidized and mobile again. In summary, SGW spiked with PCOIs or with PCOIs+CoCOIs (NO_3^-, Cr, Sr and IO_3^-) was injected into sediment columns for approximately 100 PVs. Then, the sediment columns were leached with oxic SGW for approximately 100 PVs and with stop flow events at 2, 10, and 100 PVs.

K.4.1 Tc Sequestration

A considerable improvement in performance was noted with treatment using molasses+Poly-PO_4 (Figure K.12). In the presence of PCOIs only, most of the Tc-99 injected (at an average influent concentration of 86 µg/L) was entirely removed from solution through 100 PVs. Without treatment and with PCOIs only, Tc-99 breakthrough occurred considerably sooner. In addition, more Tc-99 was sequestered in the sediment columns with molasses+Poly-PO_4 during loading (injection with SGW+PCOIs) and leaching (Figure K.13). For reference, 1.66 µg/g Tc-99 was sequestered by treated sediments compared to only 0.01 µg/g without treatment at the end of the loading phase. Also, 1.18 µg/g Tc-99 was retained by the sediment column with molasses+Poly-PO_4, whereas no Tc-99 was retained in the untreated sediment column.

In the presence of CoCOIs, Tc-99 breakthrough in sediment columns with molasses+Poly-PO_4 was achieved sooner, at ≈40 PVs (Figure K.12). The amount of Tc-99 sequestered by treated sediments was about half the amount sequestered with PCOIs only. For instance, between 0.76 and 0.81 µg/g, Tc-99 was sequestered at the end of the loading phase and between 0.62 and 0.72 µg/g was retained at the end of the leaching phase when CoCOIs were present (Figure K.13).

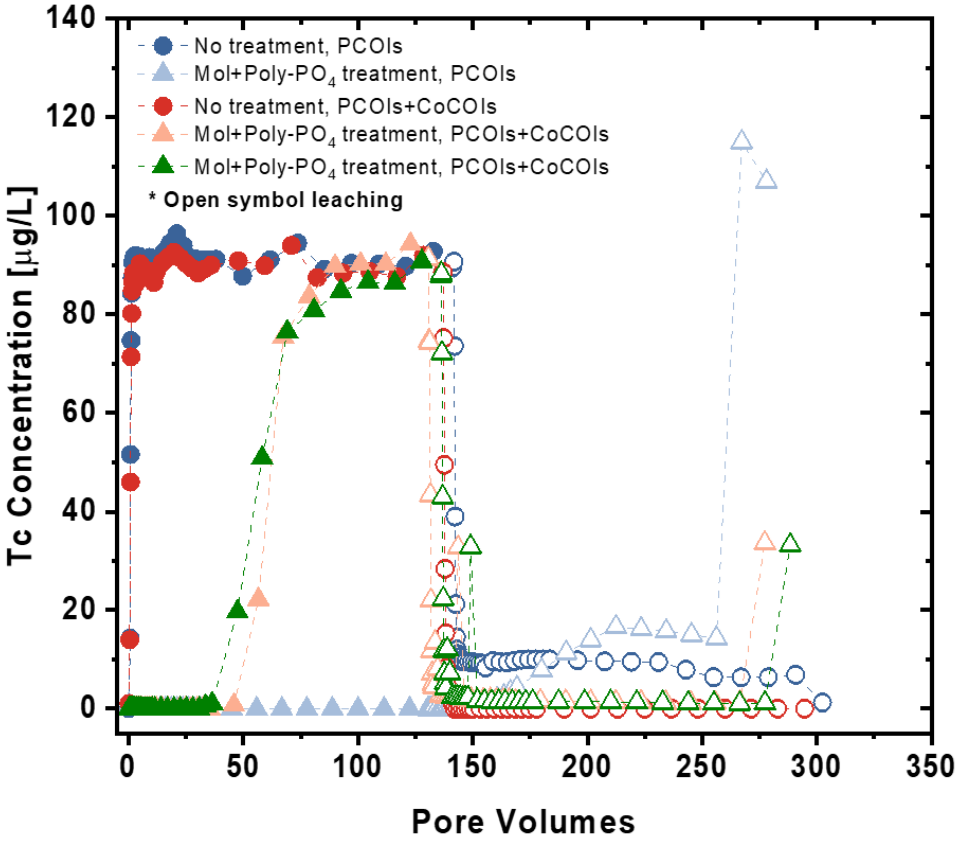

Figure K.12. Effluent concentration of technetium-99 (Tc) in saturated columns for BY Cribs groundwater conditions with (*triangle)* or without (*circle)* molasses+Poly-PO_4 treatment. Experiments were performed with either PCOIs (Tc and U) or PCOIs and CoCOIs (NO_3^-, Cr, Sr, and IO_3^-). Solid filled symbols indicate effluent concentrations measured in the loading phase and open symbols indicate effluent concentrations measured in the leaching phase.

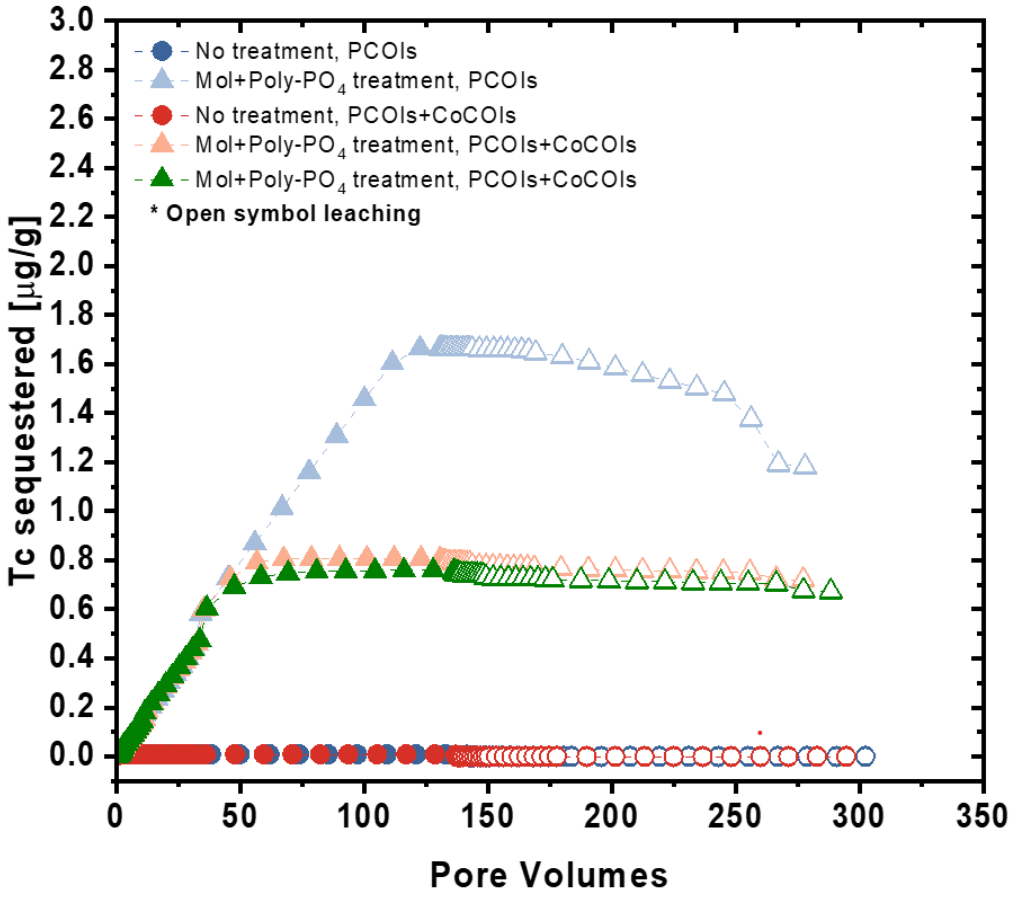

Figure K.13. Cumulative technetium-99 (Tc) mass fraction sequestered in saturated columns for BY Cribs groundwater conditions with (*triangle)* or without (*circle)* molasses+Poly-PO_4 treatment. Experiments were performed with either PCOIs (Tc and U) or PCOIs and CoCOIs (NO_3^-, Cr, Sr, and IO_3^-). Solid filled symbols indicate fractions calculated in the loading phase and open symbols indicate fractions calculated in the leaching phase.

Tc measurements collected during the leaching phase were used to calculate normalized relative release rates to quantify the longevity of contaminant sequestration with molasses+Poly-PO_4. In the presence of PCOIs, significantly more Tc-99 was sequestered by the treated sediment column during the leaching phase, but release rates calculated using Tc-99 concentrations before stop flows (pre stop flows 2 and 3) were higher compared to the untreated sediment column (Figure K.14a). The Tc-99 release rates during stop flows 1 and 2 (with stop flow durations of 15 and 161 hours, respectively) were also higher with treatment (Figure K.14b). During the third stop flow (692 hours in duration), the Tc-99 release rate was < 0 day^{-1} in sediment columns with and without molasses+Poly-PO_4 treatment, indicating uptake of Tc. However, the rate was more negative (indicating more Tc-99 uptake) in treated sediments (-8.48×10^{-5} day^{-1}) compared to no treatment (-1.40×10^{-5} day^{-1}). In the presence of CoCOIs and treatment with molasses+Poly-PO_4, the Tc-99 release rates (before and after stop flows) were lower compared to Tc-99 release rates calculated for tests with PCOIs (Figure K.14a and b). These results indicate that the presence of CoCOIs did not appear to negatively impact the longevity of Tc-99 sequestration using molasses+Poly-PO_4 as treatment.

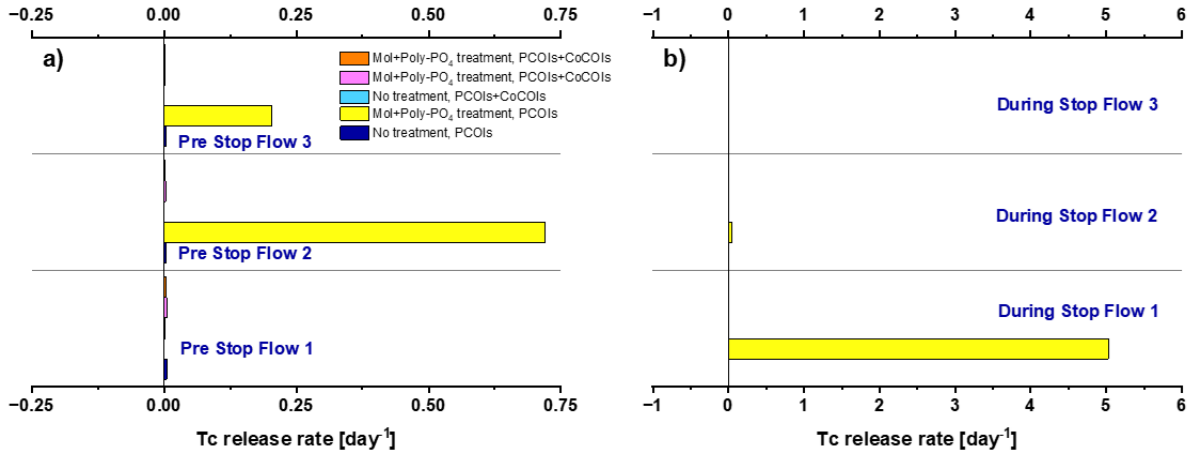

Figure K.14. Tc normalized release rates in saturated columns for BY Cribs groundwater conditions with and without molasses+Poly-PO_4: (a) estimated leaching rate (day^{-1}) prior to each stop flow and (b) estimated leaching rate (day^{-1}) during each stop flow. Experiments were performed with either PCOIs (Tc and U) or PCOIs and CoCOIs (NO_3^-, Cr, Sr, and IO_3^-).

K.4.2 U Sequestration

Treatment with molasses+Poly-PO_4 removed most of the U from influent solution through 100 PVs (injected at an average concentration of 812 µg/L, Figure K.15). The cumulative mass fraction U sequestered due to treatment was 19 µg/g vs. 4 µg/g in untreated sediments at the end of the loading phase (Figure K.16), but more than half of the sequestered U by molasses+Poly-PO_4 treatment was leached, resulting in only 7 µg/g U retained. However, the amount retained by the end of the leaching phase was still higher compared to no treatment (2 µg/g, Figure K.16).

In the presence of CoCOIs, U breakthrough was achieved sooner, at approximately 50 PVs, with molasses+Poly-PO_4 treatment (Figure K.15). However, the mass fraction of U sequestered with CoCOIs by the end of the loading phase was between 16 and 19 µg/g and was similar to the results with PCOIs only. Lastly, slightly more U was retained by sediments treated with molasses+Poly-PO_4 with CoCOIs (ranging from 10 and 11 µg/g) compared to PCOIs only (7 µg/g, Figure K.16).

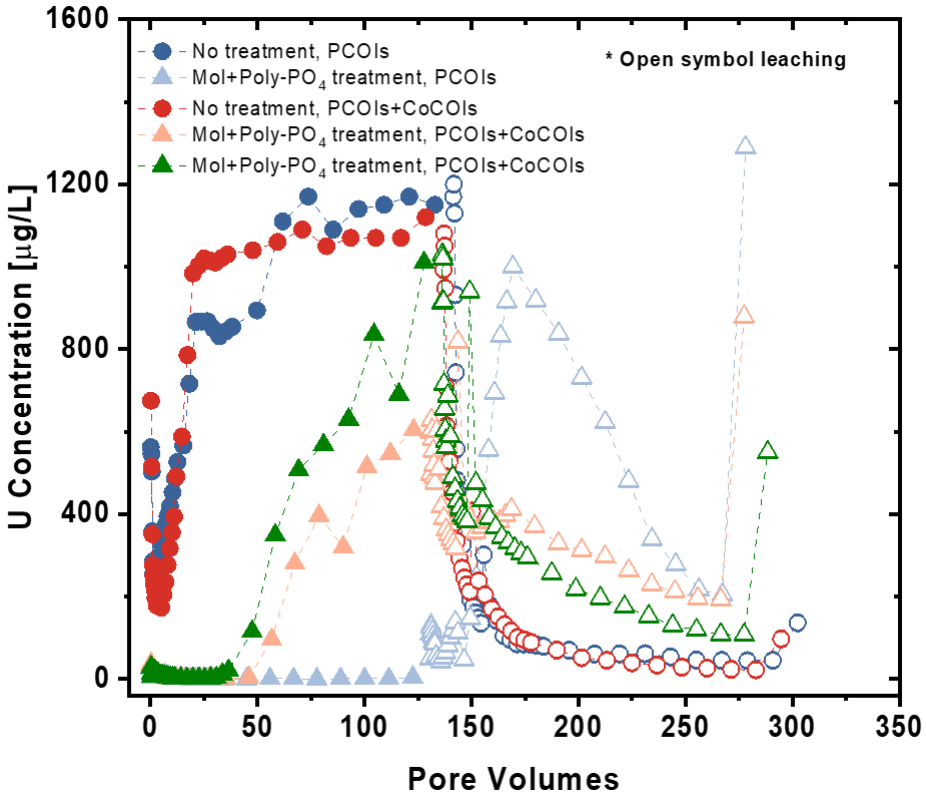

Figure K.15. Aqueous U concentrations measured in effluent samples collected from water-saturated columns for BY Cribs groundwater conditions with or without molasses+Poly-PO_4 treatment. Experiments were performed in the presence of PCOIs (Tc and U) and with or without CoCOIs (NO_3^-, Cr, Sr, and IO_3^-). Solid filled symbols indicate measurements collected during the loading phase and open symbols indicate those collected during the leaching phase of testing.

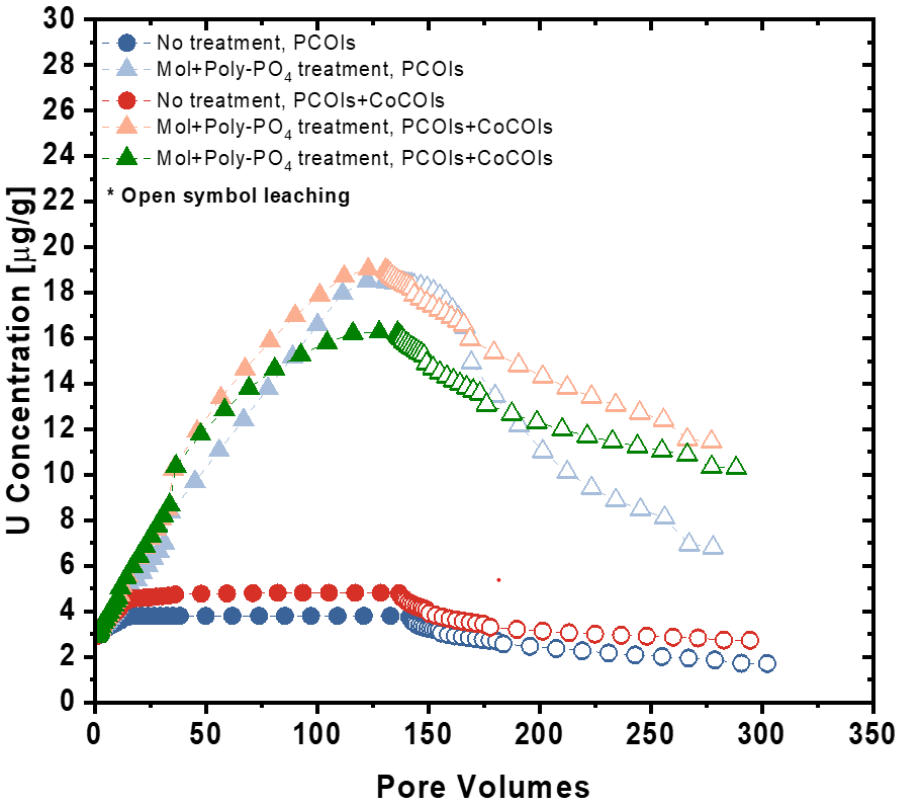

Figure K.16. Cumulative U sequestration calculated in effluent samples collected from water-saturated columns for BY Cribs groundwater conditions with or without molasses+Poly-PO_4 treatment. Experiments were performed in the presence of PCOIs (Tc and U) and with or without CoCOIs (NO_3^-, Cr, Sr, and IO_3^-). Solid filled symbols indicate measurements collected during the loading phase and open symbols indicate those collected during the leaching phase of testing.

The normalized release rates for U calculated from concentrations measured in the leaching phase are provided in Figure K.17. As previously stated, these rates were used to quantify the longevity of U sequestration with molasses+Poly-PO_4 treatment. Relative release rates for U calculated using concentrations measured before the stop flow indicated U release rates were higher with treatment compared to no treatment (Figure K.17a). However, during stop flows 1 and 2, the release rate was < 0 day^{-1} and indicated U uptake by sediments treated with molasses+Poly-PO_4 (Figure K.17b). With CoCOIs present and treatment with molasses+Poly-PO_4, U release rates before stop flows 1 to 3 were lower in comparison to testing performed with PCOIs only. During stop flows, the U release rates were higher when CoCOIs were present vs. PCOIs only.

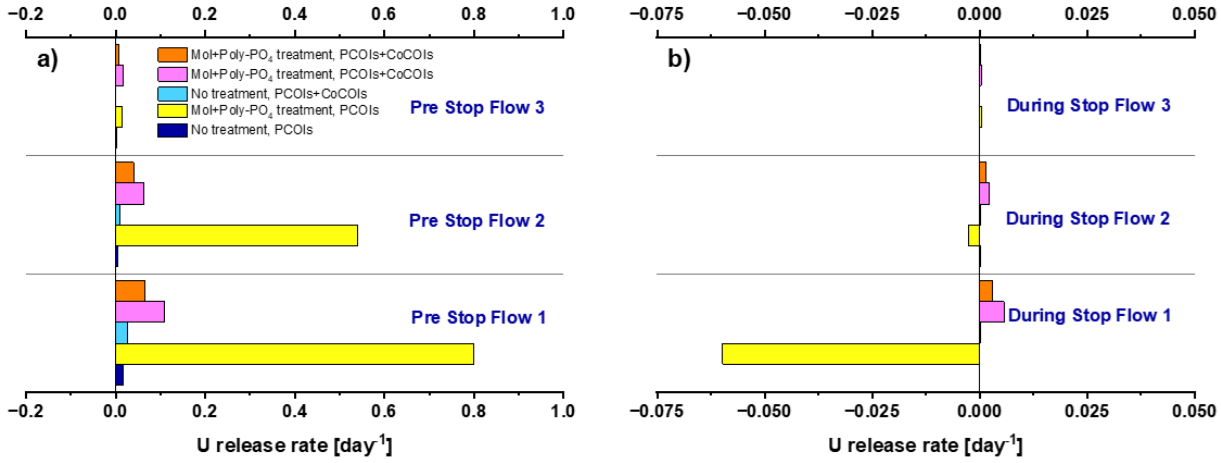

Figure K.17. U normalized release rates in saturated columns for BY Cribs groundwater conditions with and without molasses+Poly-PO_4: (a) estimated leaching rate (day^{-1}) prior to each stop flow and (b) estimated leaching rate (day^{-1}) during each stop flow. Experiments were performed with either PCOIs (Tc and U) or PCOIs and CoCOIs (NO_3^-, Cr, Sr, and IO_3^-).

K.4.3 Co-contaminant Sequestration

CoCOIs nitrate (NO_3^-), strontium (Sr), chromium (Cr), and iodate (IO_3^-) were added to influent solutions in addition to PCOIs (Tc and U) to evaluate the impacts on Tc-99 and U sequestration by molasses+Poly-PO_4 during the loading phase. Measured concentrations for nitrate and nitrite (NO_2^-, a product of nitrate reduction) are presented in Figure K.18, and measured concentrations for Sr and Cr are presented in Figure K.19 for the loading phase only. IO_3^- concentrations were not measured.

Nitrate was injected at an average concentration of 43 mg/L, and only minimal nitrate reduction occurred with treatment using molasses+Poly-PO_4 (Figure K.18). This could be due to the short residence time (~4 hours) in the columns. For reference, complete nitrate reduction was achieved after 7 days of treatment with molasses in Phase 1 experiments (PNNL-35432). Therefore, a longer residence time would allow for more nitrate reduction to occur. Figure K.18b confirms that some nitrate reduction occurred up to 40 PVs. Nitrate reduction is known to re-oxidize Tc, but that does not appear to be the case based on Tc-99 concentration results in Figure K.12 for CoCOIs. Nitrate reduction (and reduction to nitrite) appeared to cease after 40 PVs, possibly due to the exhaustion of electrons in the sediment.

Cr was injected into water-saturated columns at an average concentration of approximately 13 mg/L, and treatment with molasses+Poly-PO_4 resulted in complete removal until 40 PVs. Treatment did not appear did not appear to impact Sr when injected at an average concentration of 20 mg/L.

Prior to testing as columns, sediments were equilibrated for a total of 51 days with molasses+Poly-PO_4 treatment. During this time, treated sediments turned dark grey in color. No additional solid phase characterization was performed on these sediments to evaluate the change in minerology due to treatment, but it is suspected that the color change to dark grey could be due to the reduction of Fe(III) to soluble Fe(II). The only confirmation of this reaction were measurable Fe concentrations in effluent from columns treated with molasses+Poly-PO_4 at the start of the loading phase that was not noted with the untreated sediment column (Figure K.20). This change in sediment color and detectable Fe concentrations in effluent indicated redox conditions in the columns.

For treatments with molasses+Poly-PO_4, detectable concentrations of phosphate (PO_4^{-3}) were measured at the start of the loading phase, indicating that some of the Poly-PO_4 may have leached out during testing.

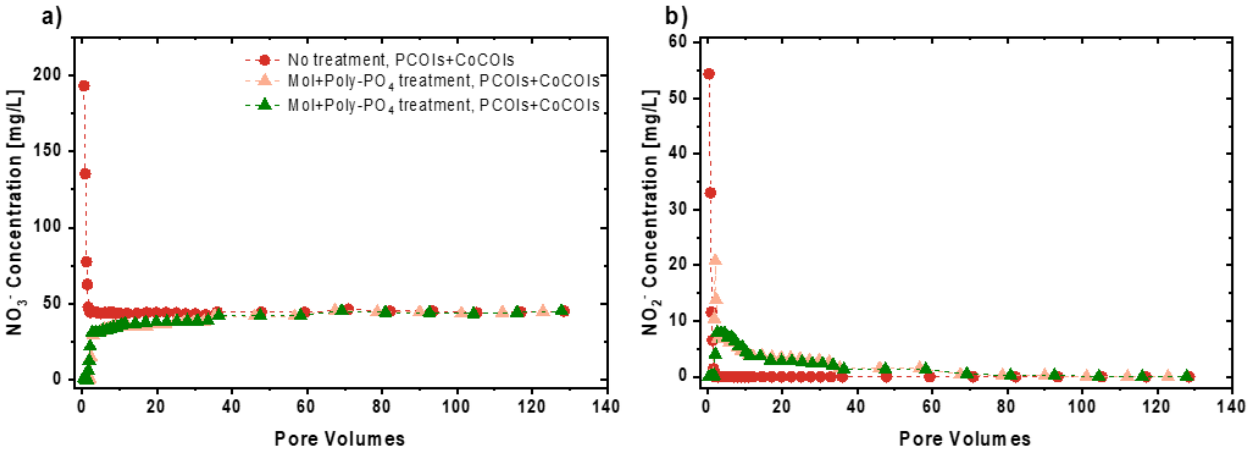

Figure K.18. Effluent concentration of nitrate (NO_3^-) (a) and nitrite (NO_2^-) (b) in water-saturated columns for BY Cribs groundwater conditions with (*triangle)* or without *(circle)* molasses+Poly-PO_4 treatment. Experiments were performed with PCOIs (Tc and U) and CoCOIs (NO_3^-, Cr, Sr, and IO_3^-).

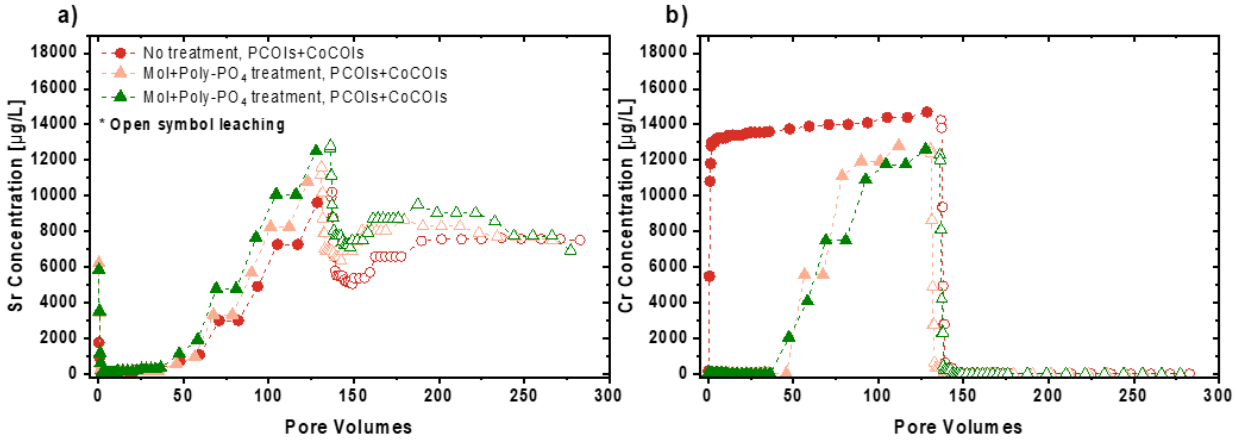

Figure K.19. Effluent concentration of strontium (Sr) (a) and chromium (Cr) (b) in water-saturated columns for BY Cribs groundwater conditions with (*triangle)* or without *(circle)* molasses+Poly-PO_4 treatment. Experiments were performed with PCOIs (Tc and U) and CoCOIs (NO_3^-, Cr, Sr, and IO_3^-).

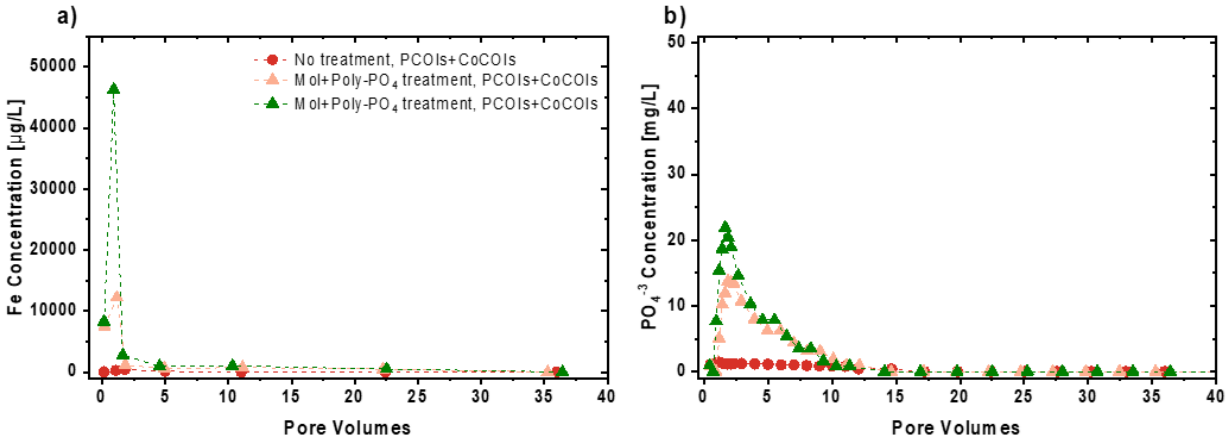

Figure K.20. Effluent concentration of iron (Fe) (a) and phosphate (PO_4^{-3}) (b) in water-saturated columns for BY Cribs groundwater conditions with (*triangle)* or without *(circle)* molasses+Poly-PO_4 treatment. Experiments were performed with PCOIs (Tc and U) and CoCOIs (NO_3^-, Cr, Sr, and IO_3^-).

K.4.4 Geochemical Monitoring

Effluent samples collected from water-saturated columns for BY Cribs groundwater conditions were measured for pH during the first 20 PVs of the loading phase (Figure K.21). The results indicated that the pH was considerably lower in sediments treated with molasses+Poly-PO_4 compared to untreated sediments and could confirm microbial activity. The addition of black strap unsulfured molasses could have directly (since this form of molasses is acidic itself) or indirectly decreased the pH through its impact on the existing microbial community. Treated sediments incubated for a total of 51 days and initially had an effluent pH < 6 at the start of the loading phase (Figure K.21) and as injection continued beyond 2 PVs, the pH increased to 7.5. These changes in the effluent pH during the first 20 PVs did not appear to impact the sequestration of Tc-99 and U (Figure K.12 and Figure K.15, respectively).

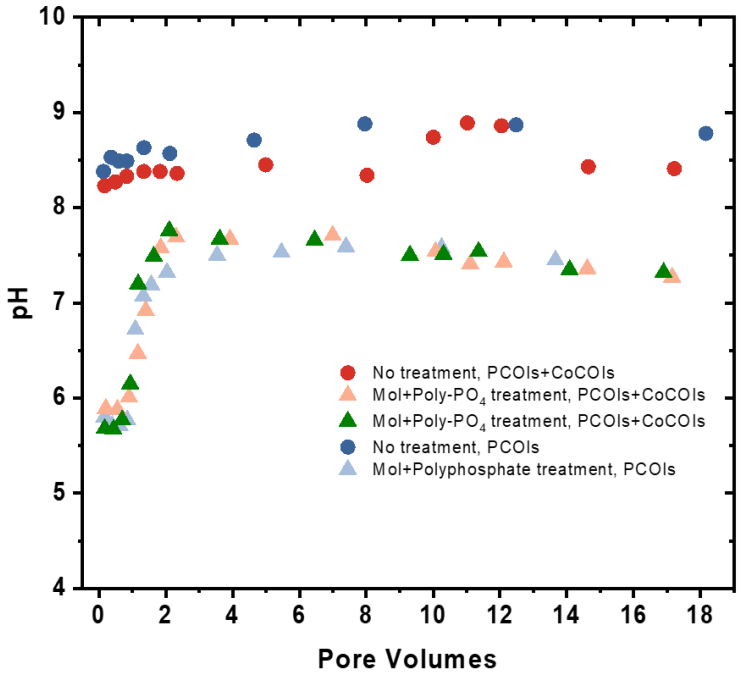

Figure K.21. Effluent pH in water-saturated columns for BY Cribs groundwater conditions with (*triangle)* or without *(circle)* molasses+Poly-PO_4 treatment. Experiments were performed with either PCOIs (Tc and U) or PCOIs and CoCOIs (NO_3^-, Cr, Sr, and IO_3^-).

K.4.5 Bromide Tracer Breakthrough

A bromide solution (with a concentration of 66 mg/L) was injected at the end of the leaching phase in each column to evaluate physical transport through sediments. Overall, the bromide breakthrough curves were similar in all conditions tested (Figure K.22). Bromide breakthrough curves are fit for dispersion and compared across all technologies in Appendix A, Section A.3.2.

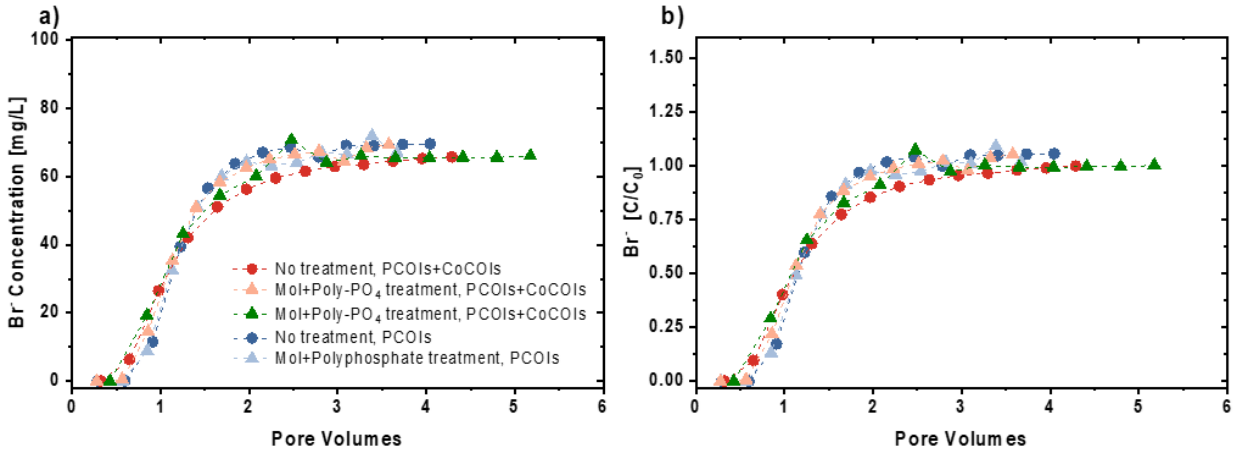

Figure K.22. Effluent concentration (a) and fraction of the concentration in effluent over the concentration of the influent solution (C/C_0) (b) of bromide (Br^-) in saturated columns for BY Cribs groundwater conditions with (*triangles)* and without (*circles)* molasses+Poly-PO_4 treatment. The Br^- tracer test was performed at the end of the leaching phase for all sediment columns.

K.4.6 Microbial Characterization

Analysis of sequencing data at the phylum level revealed microbial community shifts under varying conditions, including the addition of water, contaminants, and treatments. Dominant bacterial populations identified in samples may exhibit resistance to heavy metals and a potential for bioremediation. These findings suggest that bioremediation may be an effective strategy for addressing PCOIs and CoCOIs. The addition of water and/or carbon sources increased biodiversity, suggesting that sediments supplemented with water and organic carbon may exhibit an enhanced capacity for bioreduction.

Sequencing results from the untreated CCug sediment showed a microbiological composition consisting of nearly 70% Proteobacteria, approximately 30% Actinobacteriota (also known as Actinomycetota or Actinobacteria), and minimal amounts of Firmicutes (Figure K.23). Proteobacteria, Actinobacteriota, and Firmicutes are commonly abundant in soils contaminated by heavy metals (Bai et al. 2023; Zhang et al. 2021). Proteobacteria exhibit metal resistance and Actinobacteriota and Firmicutes have previously displayed Cr(VI) reducing capabilities (Bai et al. 2023; Xu et al. 2024; Emenike et al. 2023). Additionally, Actinobacteriota may play a large role in the N cycle in Cr stressed soils (Bai et al. 2023).

Batch studies demonstrated improved biodiversity, with the emulsified oil substrate (EOS) additions increasing Bacteroidota, Acidobacteriota, and Gemmatimonadota populations. Molasses additions significantly increased Firmicutes, although their abundance decreased slightly with addition of Poly-PO_4 but remained higher than the initial sediment (Figure K.23 and Figure K.24). Column studies also demonstrated notable microbial shifts, mirroring batch study trends where molasses enriched Firmicutes and EOS enhanced Gemmatimonadota. Untreated samples also exhibited microbial community changes driven by water additions alone (Figure K.25). Post-leaching column studies aligned with pre-leaching trends, indicating Firmicutes enrichment by molasses, while untreated samples showed increased biodiversity, specifically Gemmatimonadota, Acidobacteriota, and Bacteroidota (Figure K.26). Proteobacteria populations had a higher abundance in PCOIs compared to CoCOIs, likely due to their capability of heavy metal resistance (Figure K.26). Enhanced biodiversity can significantly improve the capability of microbial communities to remediate contaminants in the subsurface more rapidly and efficiently.

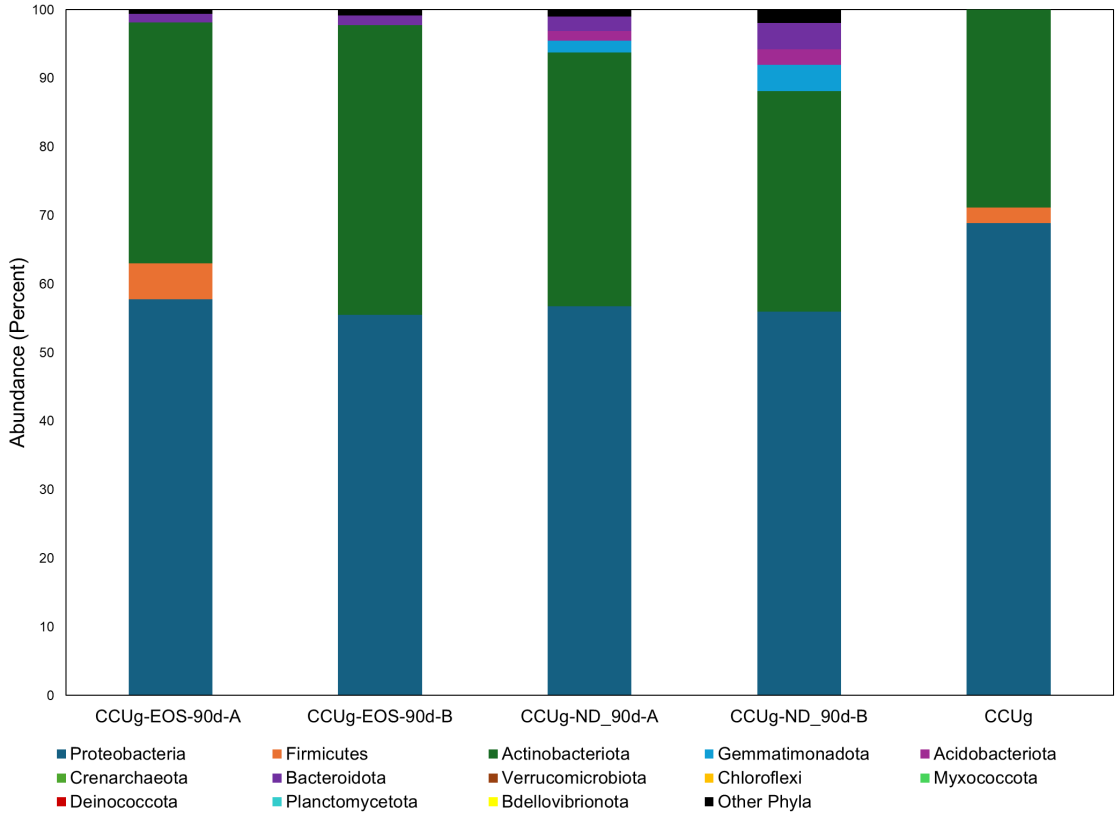

Figure K.23. Community composition of EOS batch studies. Sequencing analyses were conducted at the phylum level to evaluate microbial community composition. Batch studies using EOS as a carbon source revealed additional phyla, including Bacteroidota, Acidobacteriota, and Gemmatimonadota. These data are For Information Only (FIO).

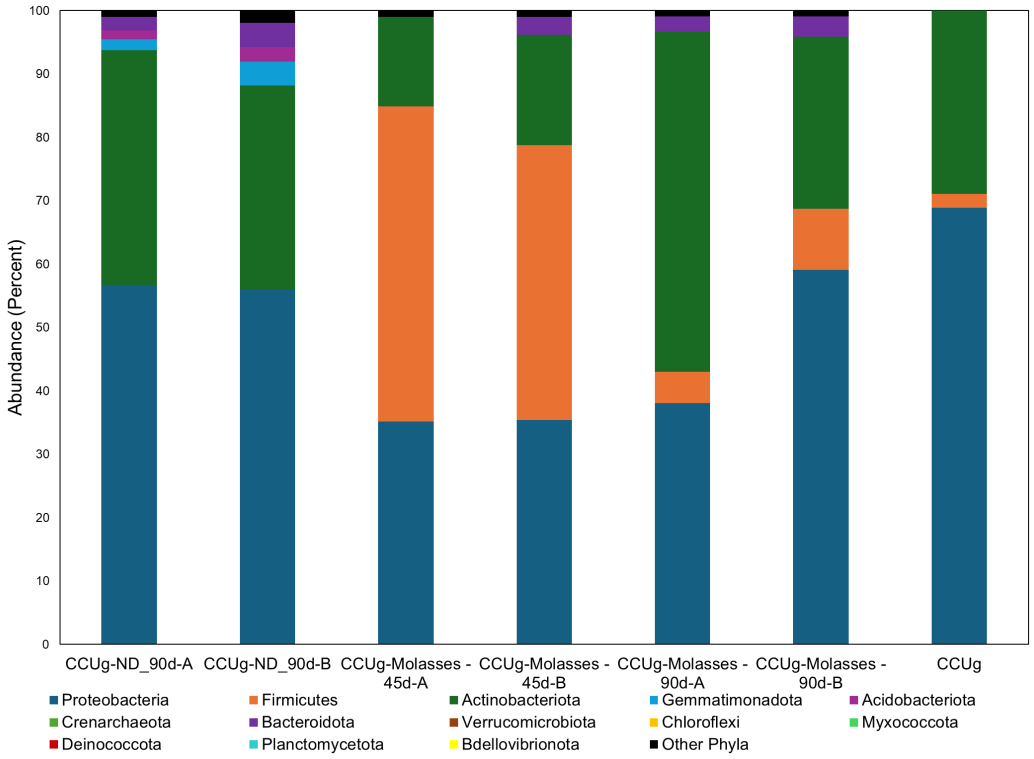

Figure K.24. Community composition of molasses batch studies. The addition of molasses increased the abundance of Firmicutes, which decreased with the addition of contaminant but remained higher than in the untreated sediment. These data are FIO.

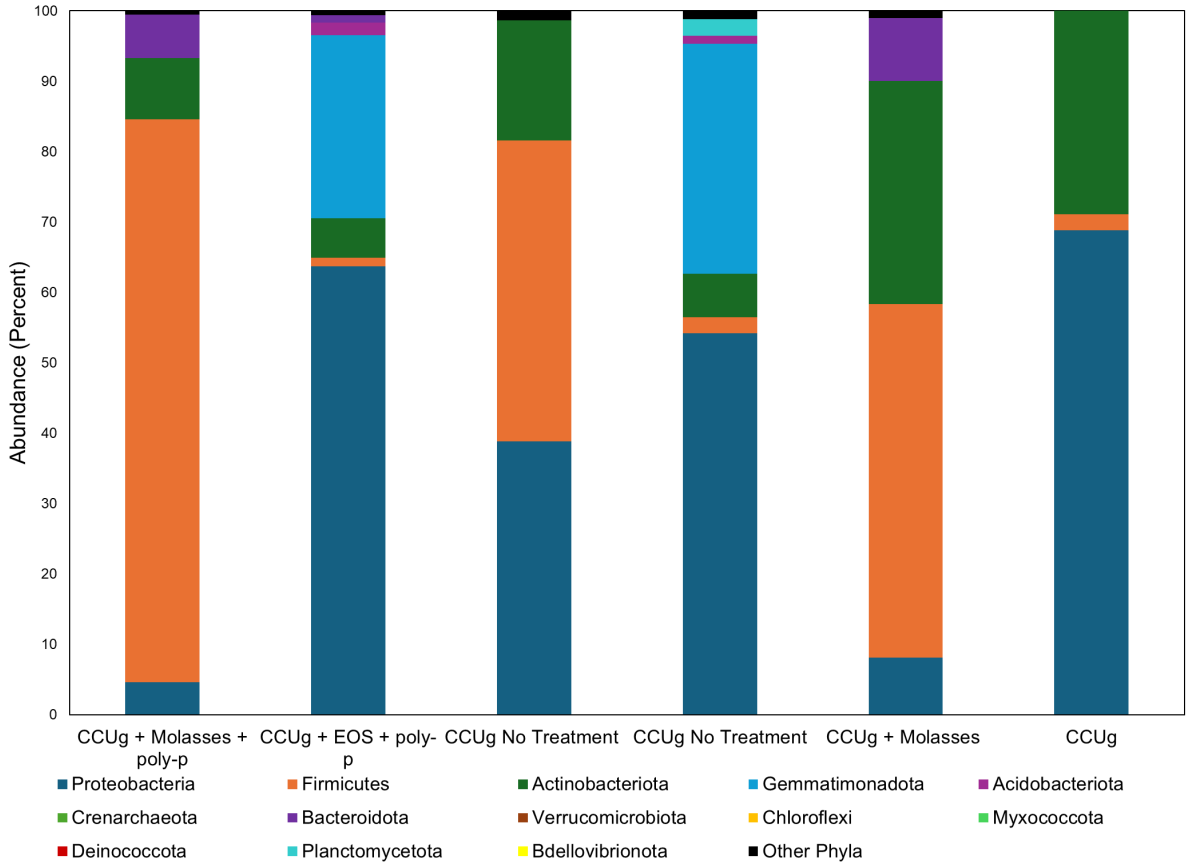

Figure K.25. Community composition of column studies pre-leach. Column studies revealed significant shifts in microbial communities. Similar to the findings in the batch studies, molasses additions increased Firmicutes populations, while EOS enhanced Gemmatimonadota populations. Interestingly, samples without treatment also exhibited microbial community changes, indicating the influence of water additions on sediment. These data are FIO.

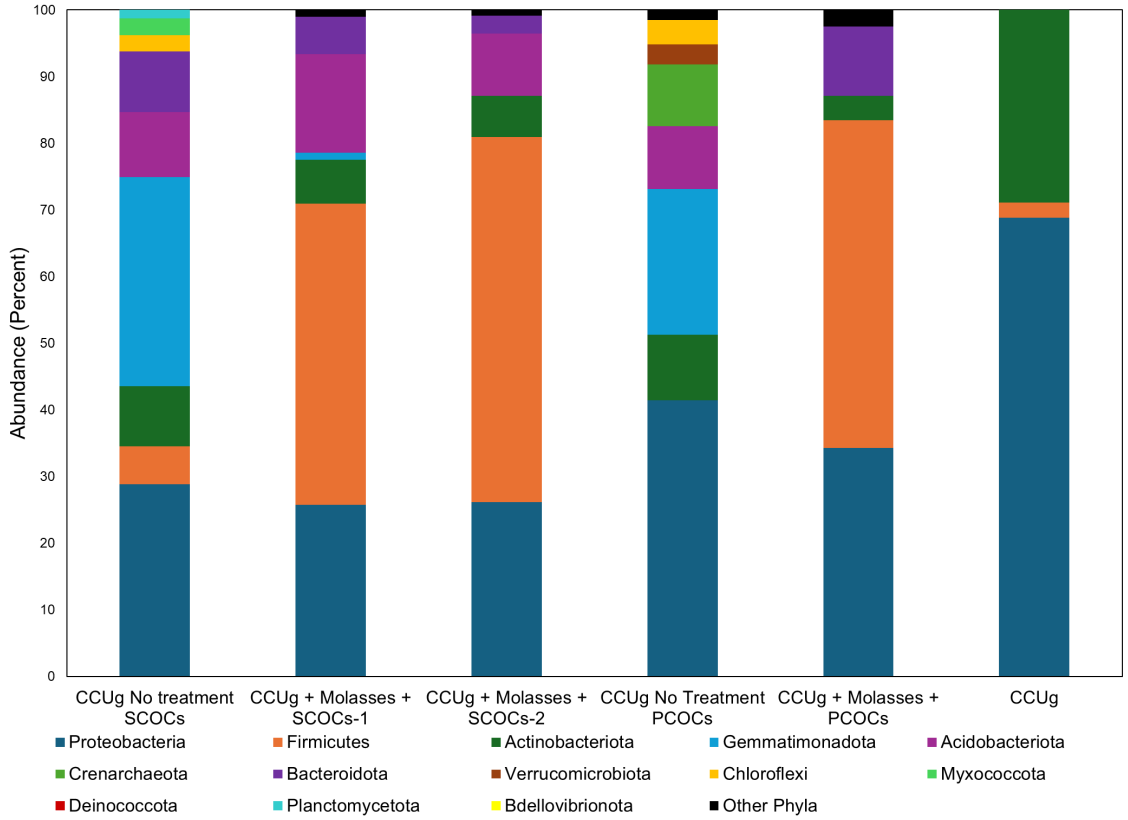

Figure K.26. Community composition of column studies after leaching. Column studies conducted after leaching exhibited trends consistent with the batch studies and pre-leaching column studies. Molasses additions significantly increased the presence of Firmicutes, while untreated samples also demonstrated increases in biodiversity, including higher abundance of Gemmatimonadota, Acidobacteriota, and Bacteriodata. These data are FIO.

K.5 Summary of Performance of Molasses and Polyphosphate for Groundwater

K.5.1 Perched Water Conditions

For the static batch studies, PZsd sediments were (1) artificially contaminated with PCOIs (Tc, U, and nitrate), then (2) treated with molasses and subsampled between 0 to 75 days, and then (3) treated with Poly-PO_4 solution at 75 days post-molasses treatment and subsampled between 83 to 138 days. Molasses was added to the sediments at a targeted TOC concentration of 1.09 g/L. This resulted in significantly higher nitrate reduction rates (between 0 to 75 days post-molasses treatment), and the addition of Poly-PO_4 at 75 days appeared to increase nitrate reduction as well. Tc-99 reduction rates were increased with the addition of molasses when compared to the no-treatment control; however, the amount of Tc-99 sequestered in molasses+Poly-PO_4 sediments at 138 days was close to the amount of Tc-99 sequestered by PZsd sediment alone. Also, treatment did not result in a considerable decrease in Tc-99 mobility relative to the no-treatment control. U reduction rates were not improved with the addition of molasses during the first 75 days of testing. The addition of Poly-PO_4 after 75 days did increase the mass fraction of U sequestered, as expected.

For the 1-D column leaching studies, PZsd sediments were artificially contaminated with PCOIs and treated with molasses+Poly-PO_4 similarly to the sediments used in the static batch studies. Sediments were then packed into columns and leached with aerated SPW through 100 PVs with stop flow events to evaluate end-product stability for sequestered PCOIs. Sediment columns with treatment leached significantly less nitrate compared to the no-treatment controls, indicating that more nitrate reduction had occurred with treatment during the equilibration period. Treatment with molasses+Poly-PO_4 did not improve Tc-99 and U sequestration, and both followed the same leaching behavior observed for the no-treatment control. This indicates that neither Tc-99 nor U were reduced/sequestered during the equilibration period, likely due to the high concentration of nitrate remaining in the sediment.

The amount of molasses added to both static batch and column sediments resulted in the reduction of approximately half of the nitrate inventory in sediment. This means that approximately 800 µg/g nitrate remained in the sediment to compete with U (132 µg/g) and Tc-99 (0.19 µg/g) as a more energetically favorable electron acceptor (Istok et al. 2004). The limited amount of molasses used provided energy (i.e., electrons) to sediment microbes and likely resulted in the observed limited reduction of nitrate, Tc, and U. However, it is likely that the reduction potential was not enough to reduce all contaminants present. Nitrate is the most favorable electron acceptor in the system. Nitrate reduction to nitrite has a Gibbs free energy of -140 kJ/mol, making it the most energetically favorable of the possible electron acceptors. This implies that because not all the nitrate was reduced, there were not enough electrons donated to the system from the molasses, suggesting that the limiting factor in these experiments was the carbon source. However, this limitation could be addressed by adding more molasses to stimulate the complete reduction of nitrate and allow for the reduction of Tc-99 and U.

Microbial reduction is constrained by the number of electrons available to fully balance the reactions that are driven by cellular processes, often with the primary goal of energy gains and proliferation. In this system, the available organic carbon serves not only as a growth substrate but also as the primary electron donor. When carbon is scarce, the total number of electrons available for transfer is limited. This imbalance slows reactions rates and can lead to the accumulation of intermediary compounds and shift microbial metabolism toward other, more favorable pathways. Based on calculations using the total available organic carbon in the system and making several assumptions based on the likely availability of reduced electrons, there was not enough to fully reduce the nitrate in the system, indicating that other microbial processes were underway and that not enough carbon was available within the system.

K.5.2 BY Cribs Groundwater Conditions

Molasses+Poly-PO_4 amended CCug sediments were used to simulate the reaction of PCOIs (Tc and U) with a permeable reactive barrier in a column. During the loading phase, SGW with PCOIs or PCOIs + CoCOIs (NO_3^-, Cr, Sr, and IO_3^-) was injected into sediment columns through 100 PVs to determine sequestration rates for Tc-99 and U. Next, in the leaching phase, aerated SGW was injected into sediment columns through 100 PVs with stop flow events to quantify end-product stability for sequestered Tc-99 and U. In addition, analysis of sequencing data at the phylum level (FIO) for evaluation of microbial shifts was performed on CCug sediments before and after treatment with molasses+Poly-PO_4, and on column sediments at the end of the loading phase.

There was a considerable improvement in performance with treatment using molasses+Poly-PO_4 for both Tc-99 and U. Both contaminants were entirely removed from SGW influent solutions (with Tc-99 and U influent concentrations of 86 and 812 µg/L, respectively) through 100 PVs. This complete removal from the influent solution resulted in a higher mass fraction of Tc-99 and U sequestration in sediments. Leaching with aerated SGW resulted in Tc-99 and U leaching from treated sediments; however, the mass fraction of Tc-99 and U remained higher compared to the no-treatment control. The presence of CoCOIs decreased the ability for molasses+Poly-PO_4 amended sediments to sequester Tc-99 to the same extent as

in tests with PCOIs only. Despite this decrease, Tc-99 sequestration with CoCOIs was still considerably higher than the no-treatment controls, and normalized release rates before and after stop flows were lower than in tests with PCOIs only. For U, the presence of CoCOIs did not impact the mass fraction sequestered by treated sediments, and normalized release rates before stop flows were lower compared to tests with PCOIs only. However, nearly half of the U that was sequestered during the loading phase was leached by the end of the leaching phase, irrespective of PCOIs vs. PCOIs+CoCOIs present.

The coloration of the sediments with molasses+Poly-PO_4 treatment was used as a qualitative indicator of redox conditions in the columns. Injection of SGW solutions with PCOIs and CoCOIs led to a gradual change in sediment color from dark grey (reducing conditions) to tan (oxidizing conditions), starting from the influent end of the columns. This observation was not noted with columns being injected with PCOIs only. As a result of observable shifting conditions from reducing to oxidizing in the presence of CoCOIs, Tc-99 and U sequestration was lower in comparison to columns injected with PCOIs only. In support of the visual loss of reducing conditions with time, nitrate reduction and nitrite formation ceases, and Tc-99 and Cr breakthrough (where the effluent concentration equals the influent concentration) happen at around the same time at 40 PVs.

It is not confirmed that the improvement in Tc-99 and U sequestration with molasses+Poly-PO_4 was a result of biotic or abiotic processes, although simultaneous microbial reduction of nitrate and Tc-99 and U has been reported (Istok et al. 2004; Lee et al. 2015). FIO results for bacterial populations in CCug sediments alone may indicate resistance to heavy metals and a potential for bioremediation. Also, the addition of treatment appeared to diversify the microbial community, as seen in post-leached sediment samples from columns.

Appendix L – Cross-Technology Cyanide Testing

This laboratory work focused on evaluating the impact of select remediation technologies on cyanide species mobilization in the 200-DV-1 Operable Unit. Cyanide is found in Hanford Site groundwater primarily from historical discharges and unplanned releases of waste in the 1950s (WHC-2433-FP). Cyanide was added to a scavenging solution to decrease cesium-127 (Cs-127) in aqueous nitrate containing wastes to free up additional waste storage space. The Cs-127 was scavenged by adding sodium or potassium ferrocyanide, $[Fe(CN)_6]^{-4}$, and nickel sulfate, which precipitated cesium nickel ferrocyanide $[NiCs_2Fe(CN)_6]$. However, strontium-90 (Sr-90) was also scavenged. The removal of Cs-127 and Sr-90 allowed the supernatant to be transferred to disposal cribs on the Hanford Site. As a result, groundwater cyanide contamination is generally considered to be in the form of an $[Fe(CN)_6]^{-4}$ complex (PNL-21497). In EPA 815-B-16-012, *Cyanide Clarification of Free and Total Cyanide Analysis for Safe Drinking Water Act (SDWA) Compliance*, the U.S. Environmental Protection Agency clarifies that total cyanide methods are allowed, but cyanide is regulated as free cyanide (CN^-).

Batch and column experiments evaluated whether select technologies have the potential to mobilize free cyanide from either free or complexed cyanide that has either sorbed to sediment or precipitated as a solid phase. Previous experiments demonstrated that these technologies performed well in batch and column experiments for primary and some co-contaminants of interest. However, because these technologies rely on changing physiochemical parameters, the potential for mobilization of cyanide may exist. The studies described here were conducted to fill critical data gaps about cyanide fate and transport and to provide additional lines of information needed to advance DV-1 technology recommendations.

Note that in strongly oxidative environments that are neutral or acidic, Fe(II) may be oxidized, which could decompose the complex releasing CN^-. However, as none of the DV-1 technologies are oxidative, this is unlikely to occur in any of the experiments herein (Meeussen et al. 1992). An increase in the chances of ligand dissociation is likely in highly alkaline conditions, which would lead to increases in free cyanide; however, at high pH levels, this may force precipitation reactions that would remove the cyanide from solution in a stable form.

L.1 Supplemental Methods

L.1.1 Scoping – Batch Methods

Scoping static batch tests were used to screen technologies (Table L.1) for their possible effects on total cyanide and free cyanide in solution when cyanide was added either as ferrocyanide, ferricyanide, or free cyanide. The batch tests were performed in one of three solutions [ultrapure water, synthetic groundwater (SGW), or synthetic perched water (SPW)] based on the overall area of interest for application of each technology and the parameters used in each treatment.

Additional static batch tests with 0.7 and 1.05 g of calcium polysulfide (CPS) and 7 mmol of Poly-PO_4 in 100 mL of SGW were prepared with 1,500 µg/L cyanide added as potassium ferricyanide or potassium ferrocyanide or 100 µg/L free cyanide. These batch tests were prepared without sediment and incubated on a shaker at 125 rpm and at room temperature for 3 days.

Table L.1. Batch matrix/matrices for each technology, along with constituents added from technologies.

Technology	Matrices	Saturated	N_2 Degas	Technology Constituents
SMI	SGW	Yes	Yes	0.7 wt% in sediments for SMI followed by 24 mmol/L total PO_4 as Poly-PO_4
CPS	SGW	Yes	Yes	0.725 vol% CPS in SGW followed by 35 mmol/L total PO_4 as Poly-PO_4
Ca-Cit-PO_4	SGW	Yes	Yes	35 mmol/L total PO_4 as Ca-Cit-PO_4
Sn(II)-PO_4	SGW	Yes	Yes	3.0 wt% Sn(II)-PO_4 in sediments
BSN	SGW	Yes	No	1.5 wt% BSN in sediments
C_2H_6	Ultrapure water	No	With ethane	~20-100% headspace C_2H_6, balance N_2
Molasses	SPW	Yes	Yes	0.625 g/L molasses followed by 24 mmol/L total PO_4 as Poly-PO_4
Poly-PO_4	SGW	Yes	No	35 mmol/L PO_4 as total Poly-PO_4
Control	SGW, SPW, ultrapure water	Yes/No	Yes	No treatment

To reduce potential interactions with other contaminants, batch experiments used sediments that had not been exposed to waste solutions and/or contaminants previously, i.e., Hanford formation (Hf) sediments, as described in Section 3.1 of the Phase 1 report (PNNL-35432). The sediments chosen are colloquially known as the "Pasco gravels" and are the principal sediments of the Hf.

Batch experiments were doped with one of three cyanide compounds: potassium ferrocyanide, potassium ferricyanide, or potassium cyanide (KCN). For saturated batch experiments using iron cyanide complexes, samples were prepared using a 1:2 wt/wt sediment-to-solution ratio in glass serum bottles with 30 g of sediment and 60 mL of SGW or SPW as appropriate for each technology. Similarly, for unsaturated technologies, a sealable vial was amended with 35 g of wet sediment at ambient water content (approximately 11%). Cyanide was added as an iron cyanide complex, either potassium ferricyanide ($K_3[Fe(CN)_6$) or potassium ferrocyanide ($K_4[Fe(CN)_6]\cdot 3H_2O$). The iron cyanide complexes were added individually to vials to give a final concentration of 1,500 µg/L, or for unsaturated, a final concentration of 1,500 µg/L as if 60 mL of water had been added. Immediately after cyanide addition, the appropriate aqueous matrix was added (i.e., SGW or SPW for the saturated technologies), followed by the technology. After the addition of all constituents, the samples were degassed with 100% N_2, where appropriate (see Table L.1).

Saturated samples were placed on their sides, wrapped in foil, and shaken at room temperature at 75 rpm until sampling. Unsaturated samples were incubated on their sides in the dark at room temperature, without shaking. At select time points, the samples were collected, preserved, and analyzed for free and total cyanide (see Appendix A, Section A.1.1.8). Batch experiments using CN^- were prepared in the same manner as the iron cyanide treatments, except that CN^- was added as KCN in ultrapure water to vials for a final concentration of 800 µg/L CN^- (after water was added as extractant at the end of the incubation, for the unsaturated technologies). All technologies were set up in replicates of four. For all technologies except bismuth subnitrate (BSN) and Sn(II)-PO_4, the replicates were sacrificially sampled at a single end point. However, for BSN and Sn(II)-PO_4, two replicates were sampled at two different time points, approximately 90 days apart.

At each termination point, samples were sacrificially sampled by removing stoppers and decanting into 50-mL centrifugation tubes. Samples were centrifuged at 6,000 × g for 10 minutes and the supernatant solution was then filtered through a 0.2-µm syringe filter [25 mm (0.98 in.) Acrodisc, Supor membrane, Pall-Gellman]. Column samples did not require additional filtration as part of the column setup includes an inline 0.5-µm filter that prevents particulates from entering the line. Samples were measured for pH using either a Horiba LAQUAtwin pH-22 or an Orion Versa star benchtop pH meter equipped with a

Thermo Scientific Orion 8302BNUMD ROSS Ultra Glass Triode, and select samples were checked for free sulfide using a commercial kit for sulfide detection, as high levels of free sulfide can interfere with cyanide analysis.

L.1.2 Column Methods

Column leach tests were prepared to determine whether, after incubation of selected technologies in the presence of ferrocyanide, measurable quantities of free cyanide were formed and/or mobilized. Technologies were selected for testing based on batch results and included sulfur modified iron (SMI) with the addition of Poly-PO_4, Sn(II)-PO_4, and BSN, as summarized in Table L.2. A column with no technology was also prepared and run. An additional batch test was performed using CPS with calcium polyphosphate to determine if the reagents interacted individually with cyanide in place of a column.

Table L.2. Column matrix/matrices for each treatment, along with constituents added from treatments.

Technology	Leachant	Technology Constituents
Sn(II)-PO_4	SGW	3.0 wt% Sn(II)-PO_4 in sediments
BSN	SGW	1.5 wt% BSN in sediments
SMI	SGW	0.7 wt% in sediments followed by 35 mmol/L total PO_4 as Poly-PO_4
Control	SGW	No treatment

Columns mimicked the contaminant concentrations used in BY Cribs groundwater testing conditions (Section 2.4.2). Nitrate and strontium were added to sediments at concentrations of 100 and 50 µg/g sediment, respectively (Table L.3). After adding additional constituents, presented in Table L.3, ferrocyanide was added to total 10 µg CN/g sediment. Following this, each DV-1 technology was added as appropriate, per Table L.2. Sediments targeted a water content below saturation (e.g., 25 wt%). Then, treated sediments were packed into individual 1-D columns (e.g., 1-in. inner diameter and 6-in. length). Columns were then sealed and wrapped in foil prior to the leach. Columns were leached for approximately 20 pore volumes, as cyanide species were expected to be relatively mobile. Selected samples were analyzed for pH and free and total cyanide as described in Table L.4, Figure L.1 and Figure L.2, respectively.

Table L.3. Targeted column sediment addition concentrations.

Contaminant	(µg/g sediment)	To Be Added As
Water Table Conditions		
Sr-88	50	$Sr(NO_3)_2$
NO_3^-	100	$NaNO_3$ and $Sr(NO_3)_2$
CN^-	10	$K_4[Fe(CN)_6]$

L.2 Batch Results

Samples with potassium salts of ferrocyanide, ferricyanide, and cyanide were prepared in batch and incubated for at least 60 days. The average pH levels and standard deviations are presented in Table L.4. The pH values of the SGW and SPW are buffered to 7.8 and 8.2, respectively. The average pH of deionized (DI) water is approximately 6; however, DI water is known to be difficult to measure due to the lack of ions in solution. The pH levels of several solutions increased (both the treated bio experimental and control, the no technology SGW, the SMI, and the CPS) while the others (no technology SPW and liquid bio with molasses, Ca-Cit-PO_4, BSN, Sn(II)-PO_4, and Poly-PO_4) decreased. The pH of a solution is critical in understanding the potential transformations of cyanide complexes, as the pH influences the stability and dissociation behavior of metal-cyanide complexes.

The pH levels of the solutions in Table L.4 and the reductive nature of these techniques suggest that any free cyanide generated would be technology specific and would not be generated by the general alterations to soil and ground water chemistry.

Table L.4. Average batch pH levels after incubation with DV-1 technologies and cyanide amendments.

DV-1 Technology	Average pH	Matrix
No technology control for gas bio (DI)	9.27 ±0.03	Ultrapure water
Gas bio	9.24 ±0.06	Ultrapure water
No technology control of liq bio (SPW)	7.73 ±0.06	SPW
Liq bio	7.39 ±0.03	SPW
No technology control for saturated technologies (SGW)	8.28 ±0.05	SGW
Ca-Cit-PO_4	7.08 ±0.18	SGW
BSN	7.15 ±0.75	SGW
Sn(II)-PO_4	7.55 ±0.16	SGW
SMI	9.06 ±0.09	SGW
CPS	9.14 ±0.11	SGW
Poly-PO_4	6.76 ±0.06	SGW

Figure L.1 and Figure L.2 show the total and free cyanide results along with the corresponding no-technology controls. There is variability in the recovery, likely due to sorption to both the sediments and solid phase technologies, precipitation with cations in solution, and complexation with organics (in the case of liquid biological technology). Most significantly, few technologies showed a large increase in free cyanide, with the notable exception of Poly-PO_4, which also showed the largest decrease in pH. Both systems that contain reduced sulfur (SMI, CPS) also showed an increase in free cyanide; however, sulfide is known to increase the measurement of free cyanide. The SMI and CPS samples were tested for sulfide using lead acetate test strips, and while they did not test positive, there may have been interferences from other reduced sulfide compounds besides S^{2-}(aq). Overall, these batch studies suggest that there is minimal risk of generating free cyanide using the technologies. However, additional follow-up studies examined several of these technologies in 1-D column flow experiments, and a discussion on the Poly-PO_4 system follows.

The method used for analysis of free cyanide is based on the pyridine-barbituric acid method. This method is based on the formation of chloramine-T, which then reacts with free cyanide to form cyanogen chloride, which then complexes with pyridine and barbituric acid to form a violet-colored solution that is measured spectrophotometrically at a maxima of ~578 nm. Poly-PO_4 can chelate iron, which may affect the overall concentration of free cyanide in solution by freeing the cyanide by taking up the $Fe^{2+/3+}$. It is more likely that the high concentration of Poly-PO_4 caused a small amount of turbidity within the sample over time as the Poly-PO_4 slowly polymerized, which could increase the overall recoveries by interfering with the spectrophotometric analysis. It is also possible that the Poly-PO_4 hydrolyzed into orthophosphate, which may have affected the overall stability of the cyanogen chloride intermediate or interfered with the chromogenic reaction with the pyridine/barbituric acid reaction. Due to these potential interferences, it is unlikely that the results indicate the generation of free cyanide, especially given the pH of the samples (~6.8). However, additional studies should be considered in light of these data.

These data do, however, agree with the kinetic and thermodynamic literature suggesting that KCN is indeed a direct source of free cyanide and can readily evolve hydrogen cyanide (HCN) in acidic conditions. Ferrocyanide is highly stable with minimal toxicity, with tightly bound octahedral coordinated CN^-, which is not easily released or evolved into HCN. Ferricyanide is more reactive and slightly toxic as it is a mild eye and skin irritant, when compared to ferrocyanide, but still does not easily release CN^- unless under direct light or in strongly acidic conditions.

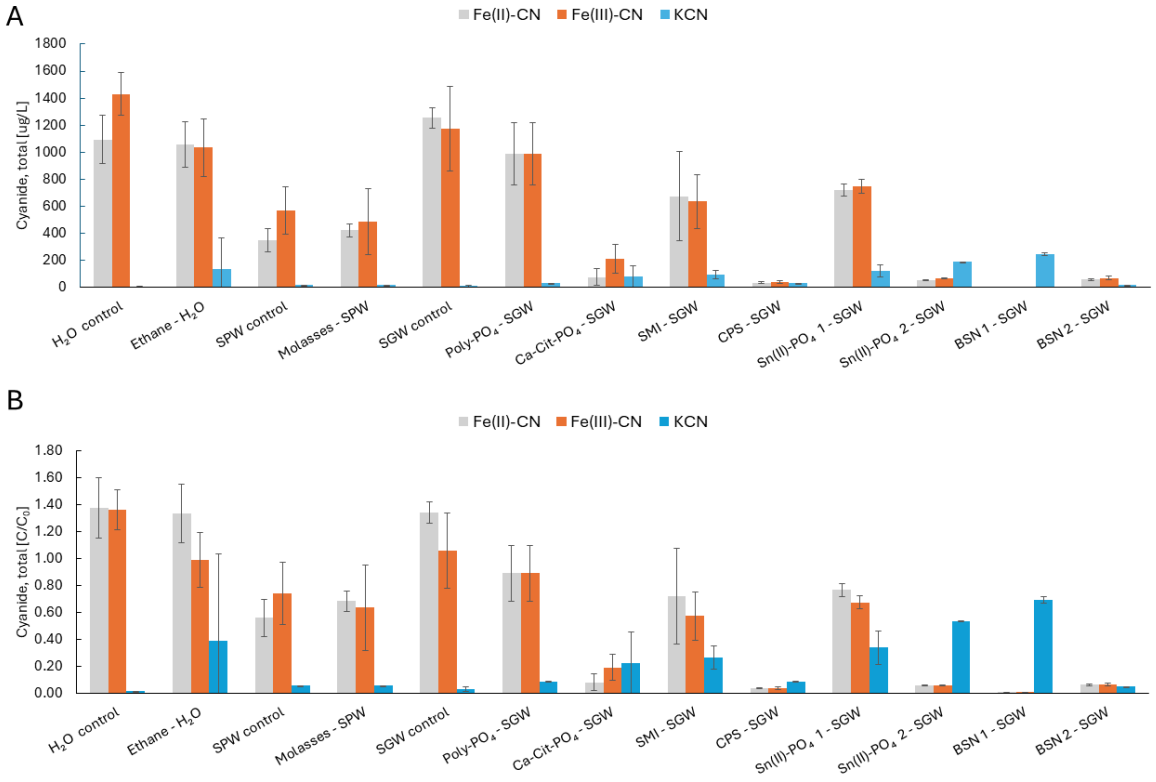

Figure L.1. Averages and standard deviations of the batch samples for total cyanide after incubation with DV-1 technologies and corresponding no-technology controls for each of the three cyanide technologies: (A) total cyanide in µg/L, (B) total cyanide as C/C_0. The 1 and 2 with respect to Sn(II)-apatite and BSN refer to time points 1 and 2.

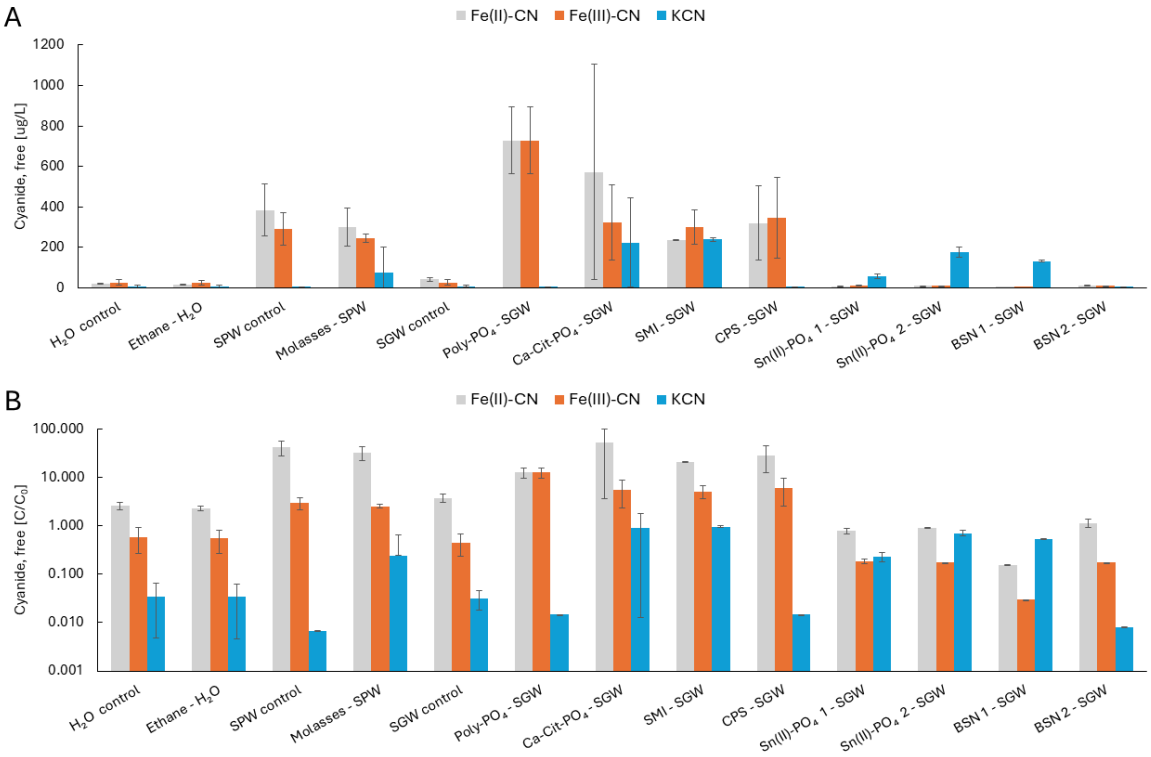

Figure L.2. Averages and standard deviations of the batch samples for free cyanide after incubation with DV-1 technologies and corresponding no-technology controls for each of the three cyanide technologies: (A) free cyanide in µg/L, (B) free cyanide as C/C_0, where C_0 is total cyanide added at time zero. The 1 and 2 with respect to Sn(II)-apatite and BSN refer to time points 1 and 2.

In addition to columns, an additional batch experiment, without sediment, was performed using CPS+Poly-PO_4. This experiment was used to determine if there was interference in the original Poly-PO_4 measurements in the batch tests. These additional batch tests used two concentrations of CPS, a no-treatment control (without Poly-PO_4) and one concentration of Poly-PO_4. Results indicated that both can significantly interfere with the measurements for the cyanide, which is most notable in the measurements for free cyanide. However, discrepancies can also be seen in the total cyanide measurements (Figure L.3a). The total cyanide measurements are significantly lower than the control. This could be for several reasons, though as no precipitates were seen during the analysis, the most likely cause for this is error in analytical methodology. For free cyanide in all instances except for the ferricyanide sample with high CPS, free cyanide was measured over double the concentration, which was added, as shown by the cyanide control (Figure L.3b). Additionally, the standard deviations were often greater than half the measurement, indicating a considerable lack of reproducibility in these analyses.

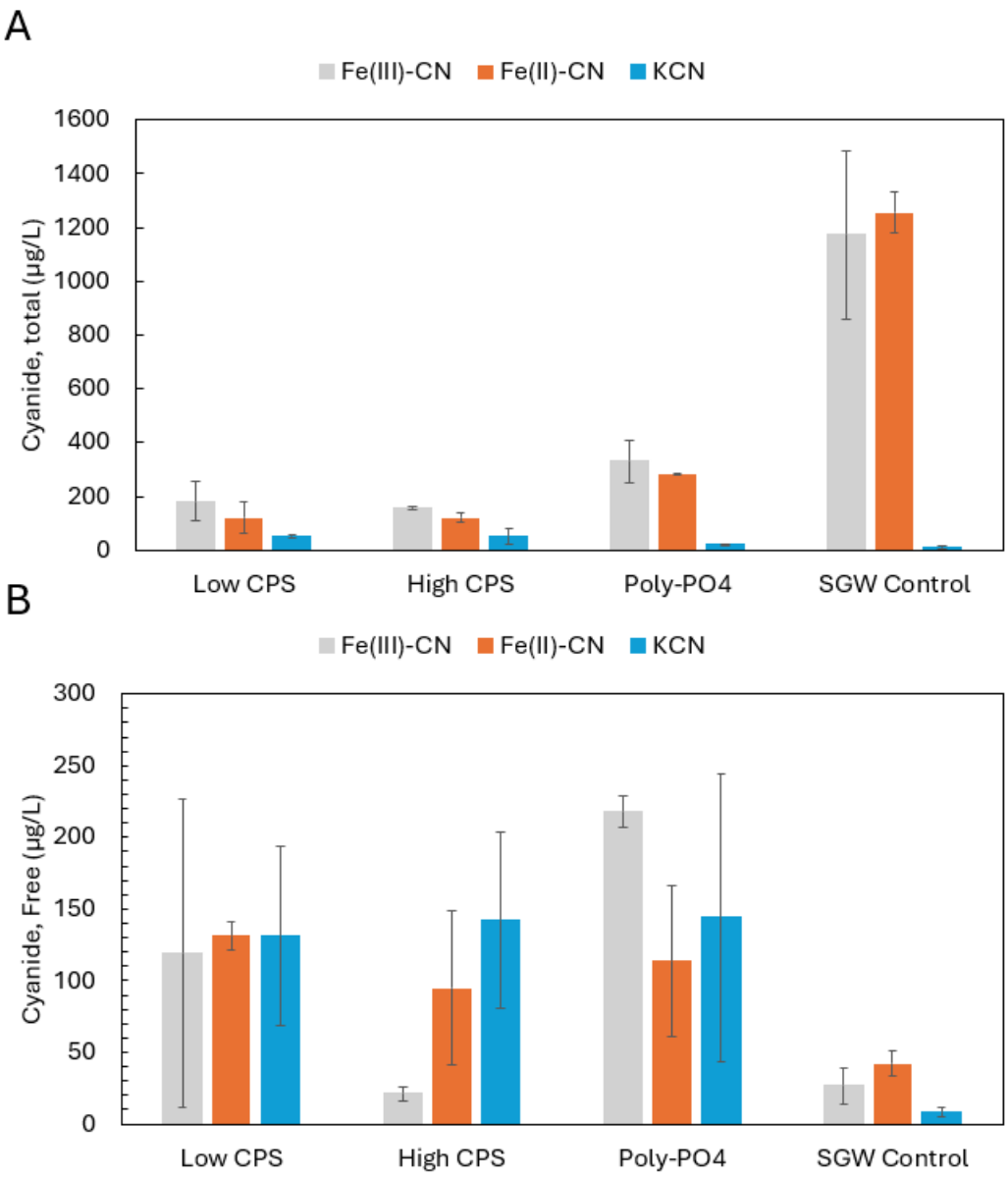

Figure L.3. Without the addition of sediment, SGW shows the added amount of total cyanide in (A). However, the CPS+Poly-PO_4 concentrations are noticeably suppressed, though the exact mechanism is unknown. In (B) the addition of sediment SGW shows a low amount of free cyanide while CPS+Poly-PO_4 shows significant increases and high variability with large deviations, suggesting that CPS+Poly-PO_4 interferes with measurements.

Pacific Northwest National Laboratory

902 Battelle Boulevard
P.O. Box 999
Richland, WA 99354

1-888-375-PNNL (7665)

www.pnnl.gov